760

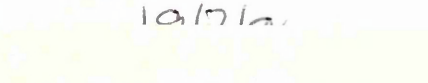

15.4
19.39.

3/6/96
16.59

THE QUENCHING CHARACTERISTICS OF SODIUM POLYACRYLATE SOLUTIONS

BY

W. D. GRIFFITHS

A THESIS SUBMITTED TO THE COUNCIL FOR NATIONAL ACADEMIC AWARDS IN PARTIAL FULFILMENT FOR THE DEGREE OF DOCTOR OF PHILOSOPHY

SPONSORING ESTABLISHMENT;

Department of Metals and Materials Engineering,

Sheffield City Polytechnic,

Sheffield,

United Kingdom.

COLLABORATING ESTABLISHMENT;

Edgar Vaughn & Co. Limited,

Legge Street,

Birmingham,

United Kingdom.

OCTOBER 1989

PREFACE

The work presented in this thesis was carried out in the Department of Metals and Materials Engineering at Sheffield City Polytechnic during the period of October 1986 to September 1989 while the candidate was registered with the Council for National Academic Awards for a higher degree. During this period the candidate has not been registered for any other CNAA award or university degree.

The research reported here is, as far as can be ascertained, original except where due reference has been made to previous work.

In accordance with the requirements of the Total Technology PhD in Industrial Metallurgy the following elements of an MSc in Metallurgical Process Management were taken;

MODULE ONE

Process Metallurgy

Mechanical Metallurgy

Applied Thermodynamics

MODULE TWO

Economics

Accounting Principles

Numerical Methods and Programming

MODULE THREE

Refractories Technology

Quality Assurance

Metals and Competitive Materials

Corrosion and Heat Resistant Materials

Heat Treatment and Transformations

Automation and Process Control

MODULE FOUR

This consisted of three techno-economic case studies in the following areas;

Quality Assurance

Martempering

Polymer Quenchants

The latter case study has been included in this thesis in Appendix A.

The candidates performance on these courses was monitored by examination and continuous assessment.

In addition the candidate presented a paper at the 2nd International Conference on Residual Stresses held at Nancy, France on the 23-25 November, 1988. This paper has been included at the back of the thesis.

ACKNOWLEDGEMENTS

I would like to express my grateful thanks to Dr. A J Fletcher to whom I am greatly indebted for his patient supervision and encouragement. It would not be an exageration to say that without the experience and skill of Dr. Fletcher this work would not have been completed.

I would also like to acknowledge the assistance of members of Edgar Vaughn UK Ltd., the collaborating establishment. Dr. R von Bergen, Mr. D Moore and Mr. J Smith have provided invaluable discussion in addition to materials necessary for the performance of the work.

Many of the technical staff of Sheffield City Polytechnic have been of great assistance but I would like to single out for special thanks Mr. D Latimer, Mr. B Palmer, Mr. B Taylor, Mr. M Muldownie, Mr. P Fisher, Mr. M Jackson, Mr. R Day and Mr. P Fletcher. Of the academic staff Mr. A Battye has also been of material assistance.

I would like to thank Professor A W D Hills for providing me with the opportunity to carry out this research at Sheffield City Polytechnic and I would also like to thank the Science and Engineering Research Council for providing me with funds for the previous three years.

Finally I would like to acknowledge the encouragement, support and sheer endurance of my mother, sister and Andrea.

THIS THESIS IS DEDICATED TO THE

MEMORY OF MY FATHER AND ALSO TO

MY MOTHER, SISTER AND TO ANDREA

THE QUENCHING CHARACTERISTICS OF SODIUM POLYACRYLATE SOLUTIONS

W D GRIFFITHS

The quenching characteristics of a range of concentrations of sodium polyacrylate, a commercially available polymer quenchant, have been studied. These solutions showed a stable film boiling stage the duration of which increased with increasing concentration. The maximum surface heat transfer coefficients were significantly below those recorded in water or polyalkylene glycol solutions and decreased with increasing concentration. Just after the passage of this maximum the surface heat transfer coefficient declined rapidly to reach values, at a surface temperature of about 300^{o}C, equivalent to those recorded in the film boiling stage. Photography showed that this was associated with a decline in the mobility of the vapour bubbles formed in this stage.

The surface heat transfer coefficients were used to calculate the stress and strain generated during quenching using a visco-elasticplastic model of an infinite plate of a low alloy steel. Comparisons of the predicted residual stresses in the case of the sodium polyacrylate solutions with residual stresses predicted in the case of other quenchants indicated that sodium polyacrylate solutions were capable of producing residual stress distributions similar to that produced by a medium speed quenching oil and greatly below those produced in the case of polyalkylene glycol solutions. This was achieved by a decline in the temperature gradient in the specimen before transformation to martensite began associated with the rapid reduction in surface heat transfer coefficient caused by the loss of mobility of the vapour at these surface temperatures. The predicted residual stresses and strains were also compared to experimentally measured residual stresses and strains to validate the model used.

Three boundary layer theory models of film boiling were evaluated in the case of quenching in both water and a sodium polyacrylate solution and the predicted surface heat transfer coefficients compared to experimentally obtained values. None of the models produced a close agreement therefore a modification has been proposed to allow the inclusion of a turbulent interface in the models.

NOMENCLATURE

The symbols given below are those used in the text except where locally redefined.

A	area
Bi	Biot number
C_p	specific heat capacity
c	similarity transformation variable
E	Youngs Modulus
Fo	Fourier number
f	dimensionless stream function
G	Shear Modulus
Gr	Grashof number
g	acceleration due to gravity
h	surface heat transfer coefficient
h_{co}	conduction surface heat transfer coefficient
h_{rad}	radiation surface heat transfer coefficient
j	position of node (section 5.2.1)
K,k	constant
K	number of nodes in specimen (section 5.2)
L	characteristic length
l	latent heat of vapourisation
M_f	martensite transformaton finish temperature
M_s	martensite transformation start temperature
m	volume fraction of martensite (section 3.3)
m	similarity transformation variable (after reference 112)
m	mass
Nu	Nusselt number
n	position of node (section 5.2.2)

Pr	Prandtl number
P	pressure
q	heat flux
Re	Reynolds number
Re_{crit}	Reynolds number for the transition from laminar to turbulent flow
r	radius
Sc	dimensionless liquid subcooling
Sc	Schmidt number
Sp	dimensionless vapour superheating
s_{ij}	deviatoric stress tensor
T	temperature
T_∞	bulk liquid temperature
t	time
u,U	velocity
u	displacement
u_s	velocity of the liquid/vapour interface
u_∞	velocity of the bulk liquid
v,V	velocity
v, V	volume
v	displacement
w	displacement
x	cartesian coordinate
x	distance from leading edge
x	distance between nodes (section 5.2)
Y	yield stress
y	cartesian coordinate
y	boundary layer thickness

z	cartesian coordinate

superscripts

a	ambient temperature
i	initial (section 5.2.1)
s	surface
TC	thermocouple
tp	transformation plasticity

subscripts

c	thermodynamic critical temperature
crit	critical
E	experimental
e	elastic
i	interface
ij	tensorial notation
L	liquid
mfb	minimum film boiling point
n	time interval (section 6.2.1)
s,sat	saturation temperature
t	time
tp	transformation plasticity
v	vapour
w	wall
x,y,z	cartesian coordinates
∞	infinity, ie, bulk liquid properties

Greek letters

α	coefficient of linear expansion

α thermal diffusivity

β coefficient of volumetric expansion

γ surface tension

δ boundary layer thickness (after reference 112)

δ_{ij} Kroneckers delta

ξ dimensionless concentration

ϵ, ξ strain

ϵ emissivity

η dimensionless boundary layer thickness

θ temperature

λ thermal conductivity

ψ stream function

μ dynamic viscosity

ν kinematic viscosity

ν Poissons ratio

ρ density

σ stress

σ_e effective stress = $(1.5 s_{ij} s_{ij})$

σ_m mean stress = $(\sigma_r + \sigma_\theta + \sigma_z)/3$

σ_o initial stress

σ_r radial stress

σ_s threshold stress

σ_z longitudinal stress

σ_θ axial stress

σ Stefan-Boltzmann constant

ϕ similarity transformation variable (after reference 111)

CONTENTS

Chapter	page no.
1.0 INTRODUCTION	16
2.0 POLYMER QUENCHANTS	20
2.1 The Characterisation Of Polymer Quenchants	21
2.2 Polyvinyl Alcohol (PVA)	23
2.3 Polyalkylene Glycol (PAG)	25
2.4 Polyvinylpyrrolidone (PVP)	32
2.5 Sodium Polyacrylate (ACR/SPA)	34
2.6 Other Polymer Quenchants	39
2.7 The Control Of Polymer Quenchants	44
3.0 THE PREDICTION OF THERMAL STRESS AND STRAIN	46
3.1 Analytical Studies	48
3.2 Early Numerical Models	51
3.3 The Interaction Of Transformation And Stress: Transformation Plasticity	58
3.4 The Interaction Of Transformation And Stress: The Effect Of Stress On The Transformation Kinetics	65
3.5 The Introduction Of Visco-Elastoplasticity	71
4.0 BOILING HEAT TRANSFER	74
4.1 Film Boiling Heat Transfer	76
4.2 Film Boiling Heat Transfer By Boundary Layer Theory	83
4.3 The Vapour Transport Stage	94

5.0 EXPERIMENTAL PROCEDURE 102

5.1 Quenching And Related Experimental Procedures 102

5.1.1 The Determination Of The Surface Heat Transfer Coefficient 102

5.1.2 Photography Of The Plate Surface During Quenching 105

5.1.3 Quenching Procedure For The Determination Of Residual Stress And Strain 106

5.1.4 Experimental Determination Of Residual Strain 107

5.1.5 Experimental Determination Of Residual Stress 108

5.1.6 Determination Of The Kinematic Viscosity Of The Sodium Polyacrylate Solutions 109

5.1.7 The Determination Of The Surface Tension Of The Sodium Polyacrylate Solutions 110

5.2 Calculation Of The Surface Heat Transfer Coefficient And The Prediction Of The Generation Of Thermal Stress And Strain During The Quenching Of A Steel Plate 112

5.2.1 Calculation Of the Surface Heat Transfer Coefficient Of A Steel Plate During Quenching 112

5.2.2 The Generation Of Thermal Stress And Strain In A Steel Plate During Quenching 116

5.3 Calculation Of The Film Boiling Surface Heat Transfer Coefficient During Quenching Of A Steel Plate 122

5.3.1 The Model Of Cess And Sparrow 123

5.3.2 The Model Of Nishikawa And Ito 132

5.3.3 The Model Of Nishikawa, Ito And Matsumoto 138

5.3.4 Calculation Of The Film Boiling Surface Heat Transfer Coefficient Assuming A Turbulent Interface 144

6.0 RESULTS 149

6.1 Relationships Between Time And Temperature During The Quenching Of The Steel Plate 150

6.2 Surface Heat Transfer Coefficients 153

6.3 Results Obtained From The Water Quenches 155

6.4 Still Photography Of The Quenching Process 156

6.5 Cine Photography 164

6.6 The Results Of The Stress And Strain Calculations 165

6.6.1 The Calculated Residual Stresses In Plates Quenched In Sodium Polyacrylate Solutions 166

6.6.2 The Calculated Residual Strain In Plates Quenched In Sodium Polyacrylate Solutions 167

6.7 The Generation Of Thermal Stress And Strain During Quenching In Sodium Polyacrylate Solutions 168

6.7.1 The Generation Of Thermal Stress And Strain During Quenching In A Solution Of 20% Aquaquench ACR 169

6.7.2 The Generation Of Thermal Stress And Strain During Quenching In A Solution Of 5% Aquaquench ACR 173

6.7.3 Characteristics Of The Generation Of Thermal Stress And Strain In Sodium Polyacrylate Solutions 175

6.8 Experimental Measurements Of Residual Stress 177

6.9 Experimental Measurements Of Residual Strain 179

6.10 Viscosity And Density Of The Sodium Polyacrylate Solutions 180

6.11 Surface Tension In Sodium Polyacrylate Solutions 181

6.12 The Viscosity Of A Liquid Extracted From The Vicinity Of The Plate Surface 182

6.13 Differential Thermogravimetric Analysis 183

6.14 Scanning Electron Micrographical Examination Of The Surface Of A Quenched Plate 184

6.15 Film Boiling Heat Transfer Models 185

6.15.1 The Film Boiling Heat Transfer Model Of Cess And Sparrow 186

6.15.2 The Film Boiling Heat Transfer Model Of Nishikawa And Ito 189

6.15.3 The Film Boiling Heat Transfer Model Of Nishikawa, Ito And Matsumoto 191

6.15.4 Film Boiling with a Turbulent Interface 192

6.16 The Application Of Film Boiling Models To Surface Temperatures Of Below 420°C 194

7.0 DISCUSSION OF RESULTS 196

7.1 The Quenching Characteristics Of Sodium Polyacrylate Solutions 197

7.1.1 Film Boiling 197

7.1.2 The Vapour Transport Stage 199

7.2 The Generation Of Thermal Stress And Strain During Quenching In Sodium Polyacrylate Solutions 208

7.3 Comparison Of The Predicted And Experimental Residual Stresses And Strains 212

7.4 Modelling Of Film Boiling Heat Transfer 216

7.5 The Turbulent Interface Film Boiling Model 220

7.6 The Conductive Cooling Stage And Its Relationship With Film Boiling Heat Transfer 226

8.0 CONCLUSIONS 228

9.0 RECOMMENDATIONS FOR FURTHER WORK 233

10.0 REFERENCES 236

TABLES 247

FIGURES 270

PLATES 371

APPENDIX A 385

APPENDIX B 411

PUBLISHED MATERIAL 413

1.0 INTRODUCTION

Quenching is a widely practised process used to obtain a required structure and desirable mechanical properties in metal parts. A well-known example of this is the use of quenching to produce a martensitic structure in steel in order to obtain a material with a high hardness and high yield stress. This structure and its properties is of great importance in engineering. It is accomplished by heating a steel of suitable composition into the austenitic region of the iron-iron carbide phase diagram, soaking it at this temperature for a period of time, (to allow the material to fully austenitise), and then rapidly cooling the material by quenching into a liquid.

Austenite is a high temperature allotrope of iron with a face centre cubic crystal structure which can contain a relatively large amount of carbon in solution. With equilibrium cooling this structure undergoes a diffusion transformation to ferrite and carbide, (known as pearlite).

If the material is cooled rapidly from the austenitic stage there is not sufficient time for the diffusion transformations to occur and martensite, a tetragonal structure supersaturated with carbon, is the result. This effect can be enhanced by the addition of alloying elements to the steel which increase the amount of time required for the diffusion transformations to occur.

A commonly used quenching medium for the production of a martensitic structure has been water. This produced the required rapid cooling rate in the metal part, and therefore achieved the

required structure, but also caused a high level of internal stress. This can lead to cracking of the quenched component or an unacceptable level of distortion. Mineral oils produced a lower cooling rate and therefore reduced these dangers, (at the expense of some reduction in hardenability), but their use has environmental and safety problems. Quenching in oil produces fume and there is also a fire risk as the combustible oil may ignite. These risks can be reduced but only at the cost of installing extra equipment.

Recently another range of quenchants consisting of aqueous solutions of polymers has become available to the user. These have been shown to produce a less severe quench than water and, since the solutions are water based, there is no fire hazard and therefore environmental, health and safety costs may be significantly reduced.

The quenching characteristics of polymer solutions have been previously investigated using comparative techniques such as the determination of the cooling curve by standard tests and observation of the effects of quenching, (for example, the amount of distortion produced), on standard samples. The results of these tests have indicated that some polymer solutions may be feasible alternatives to some quenching oils, particularly the faster, accelerated oils. One of the most recently invented polymer solutions - sodium polyacrylate - has been shown to be one of the slowest of the new quenchants and therefore one of the most likely candidates as a potential replacement for mineral oil quenchants.

The empirical tests applied previously have, however, provided

little information about the quenching mechanism of the solutions though various explanations have been proposed. These explanations have been largely unsupported by experimental evidence.

The purpose of this investigation was to determine the quenching characteristics of sodium polyacrylate solutions by measuring the surface heat transfer coefficient and its relationship with surface temperature during quenching while examining the heat transfer mechanism at the surface of a steel plate by photography.

An important feature of quenching is the level of residual stress and strain induced in the material by the process. The prediction of the generation of thermal stress and strain during heat treatment is an area of research which has received much attention by many groups throughout the world in the last few decades and a fairly complete description of the phenomena occurring during quenching has been achieved.

One model has been developed in the United Kingdom which incorporates, using a numerical method, the important features of the quenching of a high hardenability steel, namely, the generation of thermal stress and strain, the effect of the martensitic transformation including transformation plasticity and creep and stress relaxation.

This model was used to examine the generation of thermal stress and strain during quenching in solutions of sodium polyacrylate and also to calculate the level of residual stress and strain for comparison with the levels produced in other

quenchants.

Heat transfer by boiling has also received attention from modellers with film boiling, the most stable process, receiving the most attention. These models have not previously been applied to the quenching process. Sodium polyacrylate solutions are characterised by a long stable film boiling stage so the most rigorous of the film boiling models, which utilise boundary layer theory, have been applied to the film boiling stage in both water and a sodium polyacrylate solution.

The research was therefore aimed at increasing the understanding of a recently introduced product with commercial potential.

2.0 POLYMER QUENCHANTS

The use of aqueous solutions of polymers as quenchants offer immediate advantages to manufacturers in that they promise a method of producing the required structure in quenched parts with no risk of fire. Also, health and safety disadvantages associated with the use of quenching oils, (for example, fume produced during quenching and dangers due to spillage), may be eliminated. In quenching severity they appear to lie approximately between water and oil and therefore increase the options available to the user.

Many water soluble polymers have been produced with these factors in mind and these fall naturally into two groups - those that have been produced commercially and those that have not. The polymer quenchants that have become commercially available are, in order of patent date, aqueous solutions of polyvinyl alcohol, polyalkylene glycol, polyvinylpyrrolidone and sodium polyacrylate. The structures of the polymer molecules have been given in figure 1. These solutions are predominantly produced for use as bulk quenchants and are sold as liquid concentrates containing various proprietary packages of rust inhibitors and biocides. The precise concentration of dissolved polymer in the concentrate and its molecular weight distribution is regarded as commercially sensitive information and is therefore not revealed.

The second group of polymer solutions includes those which have been invented but ignored commercially, polymer quenchants popular only in Eastern Europe and also polymer solutions which have been patented recently and are undergoing development.

Quenchants consisting of aqueous solutions of polymers require control over the variables which affect the quenching severity of the solutions. These variables include concentration, molecular weight distribution and level of contamination.

The quenching mechanisms of the polymer solutions have not yet been studied in detail. Commercial interests have dictated that research has been directed toward providing comparative measures of quenching severity in order to demonstrate that the offered product is suitable for the proposed market. Also, much published work has been carried out by the retailers of the products and this has largely been confined to comparisons between their product and that of commercial rivals. Similarly, research into the control and effect of the quenching variables listed above has been largely limited to investigating tests such as cooling curve tests which provide qualitative evidence of the quenchant performance.

2.1 The Characterisation Of Polymer Quenchants

The quenching characteristics of polymer quenchants have been investigated by a wide range of techniques which can be classified as follows.

1. Determination of the cooling curves at the centre of a standard probe. This is the simplest method and the most widely used but authors have preferred to use their own probes which have consisted of many different geometries and have been constructed of different materials. Test conditions have also been different; agitation was used inconsistently and quenchant

temperature also varied. As a result the information produced by different tests has generally not been comparable.

2. The observation of the effect of quenching on standard samples. For example, Irani and Hayes[1] used standard Navy "C" samples to determine the amount of distortion caused by quenching in different types of polymer solutions. Other tests have depended on hardness profiles or hardness measurements at set depths in quenched standard specimens to provide a comparison.

3. Determination of cooling rates from standard probes. Cooling rates at temperatures of metallurgical significance can be examined by this test. However, it has suffered from the same disadvantages as the first method in that standard conditions were frequently not used. Further, the cooling rate at the centre of an arbitrary probe is not necessarily applicable to a complex part, probably of a different material, and neither does it take into account the thermal gradient between the centre and the surface.

4. Determination of surface heat transfer coefficients. These tests have provided information on the surface cooling phenomena which occur during quenching. This information was generally obscured by temperature gradients in the cooling rate tests. However, the values reported are only true for the conditions under which the test was carried out with concentration, quenchant temperature, surface finish and agitation all affecting the surface heat transfer coefficient.

5. Differential thermogravimetry.[2] A sample of a concentrated aqueous solution of polymer was heated in air at a constant rate and its changes in mass with temperature, and temperature with

time, recorded and related to changes in cooling rate during quenching. It was assumed that the polymer was deposited onto the metal surface being quenched where it underwent fusion, dissociation, crystallisation, etc., or reacted with the metal surface or any scale present; these reactions being either exothermic or endothermic. The former would reduce the surface cooling rate while the latter would increase it. As a result additions may be made to the concentrate with the intention of raising or lowering the temperature or suppressing or expanding those quenching phenomena deemed desirable or otherwise. However the initial assumption did not take into account that cooling during quenching is as likely to be affected by solution viscosity as changes in chemical structure.

2.2 Polyvinyl Alcohol (PVA)

Polyvinyl alcohol was patented in 1952 as an additive to modify the cooling rate of water to provide a quenchant with a hardening ability between that of water and oil. Polyvinyl alcohol was produced by the hydrolysis of polyvinyl acetate[3] [4] and solubility depended on the molecular weight and the amount of residual polyvinyl acetate.[5] The molecular structure of polyvinyl alcohol is given in figure 1.

The earliest description of the cooling mechanism of a polymer quenchant was based on polyvinyl alcohol and was as follows.[6] A viscous gel formed around the vapour envelope of the film boiling stage which slowed cooling. When the vapour envelope collapsed the hot metal was wetted, nucleate boiling occurred and rapid

cooling took place, (the gel presumably was dispersed). During what was described as the "last quenching stage" the gel reformed but redissolved on completion of cooling. A protective thin vinyl film or lacquer remained to coat the part; this was claimed to retard rust formation. This explanation was unsatisfactory as it was not based on experimentally obtained cooling curves but inferred from observation of the cooling of a standard piece and the hardness results obtained from end quench tests. It was not clear what was meant by the "last quenching stage" which can be taken to mean either the convective cooling stage or the vapour transport stage. There was no indication that the boiling point of the quenchant was different from that of water and therefore the reformation of the viscous gel during the convective cooling stage would have been of little significance.

Polyvinyl alcohol is rarely used at present since very fine control over concentration is required for successful quenching. This is partly due to the low concentration of polymer used, (0.05-0.3% polyvinyl alcohol), and partly due to a tendency for residues to form on exposed metal surfaces. In addition equipment or fittings with exposed surfaces with temperatures above about 80^{o}C, for example, heat exchangers, acquired an insoluble varnish-like coating. Figure 2 demonstrates how only small additions of the polymer affected the cooling characteristics of water, (giving marked reductions in the cooling rate), and hence the need for fine concentration control.[3] [5] Losses of polymer from the bath due to high drag-outs, (polymer removed with the quenched part), was another disadvantage.[7]

2.3 Polyalkylene Glycol (PAG)

Polyalkylene glycols are produced by the random polymerisation of ethylene and propylene oxides[3]. Polyalkylene glycols are unusual in that they exhibit inverse solubility, that is, upon reaching a certain temperature bulk precipitation of the polymer occurs. This is due to the amphipathic nature of the polyalkylene glycol molecule which contains both hydrophilic oxyethylene sections and hydrophobic hydrocarbon sections. The polyalkylene glycol molecule dissolves in water by the hydration of the oxyethylene section but at the inversion temperature the "hydration sheaf" is broken and the hydrocarbon sections render the polymer insoluble.[5] The temperature at which this occurs can vary from 63°C to 88°C depending on the molecular weight distribution, (which may be up to 40,000[8]), and the ratio of hydrophilic and hydrophobic units. The molecular structure of polyalkylene glycol is given in figure 1.

This inverse solubility can be both an advantage in that it controls the cooling rate of the quenched part and a disadvantage in that it occurs in the possible operating temperature range of some quenching baths.

These quenchants were patented by Blackwood and Cheesman in 1965[8] who proposed that after inversion of the solution a thermally conducting layer of polyalkylene glycol formed which lay on the metal surface and reduced heat transfer by preventing contact between the surface and the bulk liquid.

Allen, Fletcher and King[9] produced a study of a commercial polyalkylene glycol solution, (Aquaquench 1250), and determined

the quenching characteristics and surface heat transfer coefficients in solutions of varying concentration.

Comparisons were made with the quenching characteristics of water. The addition of 5% Aquaquench 1250 to water eliminated the film boiling stage which did not reappear until the concentration was raised to 20%. A subsequent increase in concentration to 25% extended the duration of the film boiling stage.

The addition of polyalkylene glycol to water caused a marked decrease in surface heat transfer coefficients compared to those observed in a water quench. A maximum of about 4300 $W.m^{-2}.K^{-1}$ was reported during the vapour transport stage in a 5% Aquaquench 1250 solution. This value was largely unaffected by further increases in concentration and remained about one-third the value reported in water, (see figure 3).

Photography revealed that the surface of the vapour blanket contained waves, (described as Taylor waves), which moved in both vertical and horizontal directions. The amplitude of the waves increased with increased distance from the bottom edge of the plate while the speed of the liquid/vapour interface during film boiling was deduced to be about 1.5 $m.s^{-1}$. The vapour blanket persisted longest in the lower half of the plate probably being fed by vapour from the base.

A similar phenomenom to the vertical waves described as Taylor waves above may be seen in published photographs of the film boiling stage surrounding vertically quenched cylinders though no lateral waves in the interface were detected.[10] [11]

Allen et alia[9] reported that the stage after the collapse of the vapour film was characterised by the production of coarse

bubbles, (about 5 mm in diameter), which travelled up the face of the plate at a speed initially of the same order as the liquid/vapour interface during film boiling. The bubbles were observed to rotate and coalesce while the associated heat transfer rate was lower than that observed in the vapour transport stage of a water quench. The hot liquid surrounding the bubbles was reported to be laden with polymer. It was pointed out that it was not apparent how, if heat transfer was reduced by the deposition of polymer onto the surface of the metal, (as has been claimed[12]), the polymer molecules were able to withstand the temperatures involved.

As the temperature fell the bubble size became smaller and their speed decreased by about an order of magnitude. As the polymer concentration increased bubble size was also observed to increase. The effect of agitation was not readily apparent probably due to the small amount of agitation applied.

However, Mason and Capewell[13] showed that increasing agitation increased the maximum cooling rate in solutions of 20% Aquaquench 1250 but had a negligible effect on the cooling rate at 300°C. The measured hardness of quenched standard steel samples was also increased by agitation.

Hilder[14] found that, while the effects of agitation were negligible, increasing the concentration consistently increased film boiling duration, (therefore making polyalkylene glycol solutions similar in this respect to other polymer quenchants). The reason for the discrepancy between these results and those of Allen, Fletcher and King[9] probably lay in the former where the

initial wetting stage was mistaken for a short film boiling stage in the 5% solution. A close examination of the data of Allen, Fletcher and King[9] suggested that there was no film boiling stage in the 5% solution either.

Hilder[14] noted various phenomena during quenching in solutions of polyalkylene glycol, polyvinylpyrrolidone and sodium polyacrylate which were explained by suggesting the formation of a stable polymer-rich film, which occurred after the higher rates of cooling by nucleate boiling. The description was confused but the author was apparently suggesting that cooling was controlled by the presence of an encasing gel which formed shortly after the peak heat flux. This gel reduced the mobility of the vapour bubbles. Bubbles encapsulated in polymer were observed to be released from the surface during this stage. This mechanism was deduced from the observation of quenching in a polyalkylene glycol solution only and bears similarities with the description of Allen, Fletcher and King.[9] However, evidence for either the presence or the effect of this viscous gel was not presented and to state that this is the quenching mechanism that occurs in all polymer quenchants, is therefore unsubstantiated. Other polymer quenchants must be examined in greater detail than that undertaken by Hilder[14] before a general explanation of the quenching mechanisms in polymer solutions can be made.

The polyalkylene glycol concentrate used by Hilder[14] contained 60% by mass of solid but this figure may be in error since the residue was not described as a solid but as a viscous liquid.

An analysis has been made[15] of the generation of thermal stress and strain occurring in a low alloy steel plate, (835M30),

quenched in a 25% Aquaquench 1250 solution. The following table shows the maximum calculated residual stress and strain for this solution compared with a water and an oil quench, (RDN175), under identical, (unagitated), conditions;

QUENCHANT	STRESS (MPa)	STRAIN (%)
Water	460±60	0.63±0.05
Oil	-220±5	0.17±0.005
25% Aquaquench 1250	370±10	0.43±0.005

The predicted residual stress and strain for the polymer solution was less than that predicted in the case of the water quench but the polymer solution produced a tensile residual stress at the surface, (thus encouraging surface crack propagation), and a compressive stress at the centre, the reverse of that observed in oil.

A more recent analysis[16] which used a more accurate model of the generation of thermal stress and strain during quenching predicted a maximum residual stress of 210 MPa and a maximum residual strain of 0.20%. These were closely in agreement with experimentally determined residual stresses and strains.

An examination of the ageing characteristics of polyalkylene glycol solutions has been performed[17] which concluded that quenching speed, and therefore cracking, increased with use. The increase in cooling rate occurred most rapidly in the convective cooling stage and the vapour transport stage, (the film boiling stage being hardly affected), and was considered to be due to depolymerisation, oxidation and contamination.

A study,[18] using cooling curves, of polyalkylene glycol solutions contaminated with a range of industrial substances revealed varying effects. Stable film boiling was extended with even small additions of oil, (0.03% by mass), and in general, increasing contamination decreased the overall cooling rate. Contamination with a grinding fluid appeared to have no effect, even in concentrations of 10%. Sodium hydroxide, (which may be added to impart corrosion protection by increasing the pH of the solution), caused a rapid acceleration in cooling rate. Ammonia and both carbon monoxide and carbon dioxide encouraged the formation of stable vapour films which decreased cooling rates at the higher temperature ranges and gave non-uniform hardening. However it was pointed out that the solubilty of both carbon monoxide and carbon dioxide in aqueous polymer solutions was limited.

Hilder,[14] in a comparison of polyvinylpyrrolidone, polyalkylene glycol, and sodium polyacrylate quenchants with concentration, temperature and fluid agitation as variables derived several relationships to predict cooling rates, (Table 1). The cooling rate at 300^{o}C was chosen as a parameter as it represented the rate of heat abstraction at approximately the beginning of the martensitic transformation stage.

This work reported a reduction in the maximum cooling rate in polyalkylene glycol solutions when the solution was contaminated by oil and ammonia though the cooling rate at 300^{o}C was unaffected. Salt contamination rapidly increased the overall cooling rate. For example, a 30% solution which contained 5% salt

showed the cooling characteristics of water; that is, no advantage over water was obtained at this level of contamination.

Restoring the quality of the bath may be done by ultrafiltration[19] or by thermal separation.[20] When a bath became contaminated by a salt, heating above the inversion temperature caused the precipitated polymer to separate from an aqueous salt rich phase which rested on the top of the tank due to a diffeence in density. With increasing salt contamination the inversion temperature was lowered and the density of the salt-rich phase increased to above that of the polymer-rich phase. At high levels of contamination the tank was easily inverted at a low temperature and the salt-rich phase drained from the bottom of the tank.

Contamination by biological activity may be a problem though polyalkylene glycol quenchants are naturally bioresistant in that they contain no available source of nutrient for the bacterium. In addition the repeated thermal shock suffered by the tank is usually sufficient to inhibit bacterial growth. However, contamination may occur depending on the cleanliness or otherwise of the user. In concentrations above 20% Quendila PA, (a polyalkylene glycol solution produced by British Petroleum), osmotic pressure prevents bacterial growth.[21] In lower concentrations, when the tank is allowed to remain idle, aerobic bacteria may deplete the surface layers of oxygen and promote conditions for anaerobic bacteria to flourish in the bulk of the bath. These are responsible for offensive odours by the production of hydrogen sulphide and are avoided by occasionally agitating the bath.

Blackwood et alia[22] published the results of three years of biological monitoring, using agar coated slides, of the polyalkylene glycol quenching tanks of customers and showed that 80% of the tanks contained bacteria though only a small percentage required additions of a biocide.

Applications of polyalkylene glycols are numerous and particular attention has been paid to their use with aluminium alloys.[23] [24] [25] Too fast a quench produced distortion or residual stresses sufficiently high to cause cracking but sufficient quenching speed was required to prevent the decomposition of solid solution phases and to give the required mechanical properties. Polymer quenchants in general are advantageous here conferring an intermediate quench between that obtainable with hot water and oil.

Disadvantages exist, however. Archambault et alia[26] noted that polyalkylene glycol solutions are inefficient in any application when very irregularly shaped pieces are quenched because of high drag-out losses.

2.4 Polyvinylpyrrolidone (PVP)

Polyvinylpyrrolidone was patented as a quenchant in 1975 by Meszaros.[27] It was derived from the polymerisation of N-vinyl-2-pyrrolidone with product variations offered on the basis of different molecular weights distributions.[3] [4] The molecular structure of polyvinylpyrrolidone is given in figure 1.

Foreman and Meszaros[28] claimed advantages for polyvinylpyrrolidone solutions over polyalkylene glycols in that

they have a longer film boiling stage and a slower convective cooling stage, features more typical of quenching oils.

Hilder reported[14] some unusual characteristics of polyvinylpyrrolidone solutions including a rapid drop in the cooling rate at 300°C when the quenchant temperature was raised to 50°C and an approximately three-fold increase in the cooling rate at 300°C when the solution was agitated, (see figures 4 and 5). The concentrate used by Hilder[14] contained 10% by mass of solid, the lowest concentration of the three tested.

Hilder[14] showed that polyvinylpyrrolidone was unusual in that oil and ammonia contamination lowered the cooling rate at 300°C. This was attributed to the formation of a stable polymer rich film. Film boiling, not previously encountered in these tests in polyvinylpyrrolidone solutions, was observed with an addition of 5% by mass of ammonia.

The use of this polymer quenchant has been facilitated by an ultrafiltration method that removes insoluble contaminants and lower-molecular weight constituents without interrupting the quenching process. Other benefits associated with the use of polyvinylpyrrolidone include a tolerance of rust inhibitor additions of up to 2% before the quenching characteristics are significantly affected, low fume production from burnt off polymer residues, (compared to polyalkylene glycols), and lower dragouts than either polyalkylene glycols or polyacrylates. In addition polyvinylpyrrolidone has been claimed to be non-toxic and slowly biodegradable.[27] It is interesting that no such claim has been made for the use of polyalkylene glycol although no

statement to the contrary has been made either.

Moreaux et alia[29 30] investigated the stability of the film boiling stage in polyvinylpyrrolidone solutions by liquid injection to examine the possibility of replacing the unstable film boiling stage with nucleate boiling and therefore create a more reproducible quench. The film boiling stability diagram for polyvinylpyrrolidone is shown in figure 6. This approach showed that this polymer quenchant had characteristics common to both an oil and a water quench with a stable film boiling stage which limited the cooling power of the solution, (as in oil), and a low temperature for the onset of the convective cooling stage, (as in water). This implied an undesirably large temperature gradient during the martensitic transformation temperature range of most steels. The effects of an additive were also reported that, in low concentrations, destabilised the film boiling stage and raised the onset of the convective cooling stage to 330°C. The benefits of this quenchant were demonstrated by quenching three steel cylinders in water at 20°C, a mineral oil at 50°C and a solution of polyvinylpyrrolidone with the additive. The latter produced a compressive surface tangential stress whereas the oil and water quenches produced a tensile surface stress in the cylinders. In addition some of the cylinders quenched in the polymer solution showed the least distortion of all.

2.5 Sodium Polyacrylate (ACR/SPA)

Sodium polyacrylate solutions were patented in 1978 by Kopietz and Munjat[31] who proposed a quenchant which consisted of an

aqueous solution of a water soluble salt of polyacrylic acid, the sodium salt being preferred. The alkali metal salt, ie, of sodium, conferred solubility. The sodium may ionise in aqueous solution and hence it is sensitive to hard water which implies that changes in viscosity may occur which render concentration control more difficult.[3] [5] Since acrylates are ionic in nature it was suspected[4] that this may provide different quenching characteristics to other polymer quenchants.The molecular structure of sodium polyacrylate is given in figure 1.

Aqueous solutions of sodium polyacrylate are characterised by a lengthy and stable film boiling stage and a slow cooling rate in the martensitic transformation region though the patent[31] did not explain how this was achieved. Figure 7 shows the duration of the film boiling stage against solution viscosity, the latter being related to the molecular weight distribution of the polymer.

Removal of the article from the bath before the collapse of the vapour film prevented the adherence of any polymer to the part. However, should adherence occur it may be removed by washing in hot or cold water, the resultant wastes being biodegradable. Alternatively the residue may be burnt off completely at temperatures above 400^{o}C though this is probably not a feasible alternative for steel since it is above the temperature of the start of the martensitic transformation in many steels. It was claimed that the shelf life of the polymer was unlimited and that freezing and rethawing would not affect quenching characteristics.[10]

Segerberg claimed[7] that the quenching mechanism was dependant

on a thick, high viscosity film which formed on the surface of the quenched part and which produced low cooling rates. The film was considered to be vulnerable to agitation and temperature and that therefore irregular parts, surrounded by varying liquid velocities and temperatures, may suffer from non-uniform hardness and distortion.

Hilder showed[14] that sodium polyacrylate solutions produced much lower cooling rates than either polyalkylene glycol or polyvinylpyrrolidone solutions. (It has been claimed that a 5-10% solution would be comparable to an oil quench.[7 32]) Increasing the concentration increased the duration of the film boiling stage and decreased the maximum cooling rate. The cooling rate at 300°C was also decreased while the temperature at which the maximum cooling rate occurred was reduced. Raising the quenchant temperature decreased the maximum cooling rate while the cooling rate at 300°C decreased markedly. Agitation greatly increased the maximum cooling rate and also increased the cooling rate at 300°C. These results are shown in figure 8. Ageing tests showed that sodium polyacrylate solutions aged much more rapidly than polyalkylene glycol or polyvinylpyrrolidone but still maintained lower cooling rates. Kinematic viscosity initially decreased markedly with ageing but then the effects became more uniform. A 50% decrease was reOorded for a comparatively low quench loading, (20 $kg.l^{-1}$). This was reflected by a rapid rise in maximum cooling rate with increased quench loading due to changes in the molecular weight distribution caused by thermal degradation. This indicated that concentration control problems would not

necessarily be solved with the application of kinematic viscosity testing.

Dragout tests showed[7] that sodium polyacrylate had the highest dragouts of the three polymer quenchants tested, approximately twice that of polyalkylene glycol and four times that of polyvinylpyrrolidone. Dragouts were less than in oils, for a solution of similar quenching capacity, as was the case for all of the polymer quenchants.

From hardness measurements and measurements of the surface tangential residual stress by an X-ray diffraction method Hilder[14] concluded that unagitated sodium polyacrylate quenchants were capable of producing lower residual stresses during quenching than either polyalkylene glycol or polyvinylpyrrolidone solutions. For this reason the quenching characteristics of sodium polyacrylate solutions have been widely hailed as bearing favourable comparison with quenching oils and heat treatment plants have been reported to be changing to this quenchant from both oil and polyalkylene glycol solutions.[33] However, as Hilder[14] pointed out, hardness measurements alone are insufficient and the same objection can be levelled at surface measurements of residual stress since they reveal nothing about levels of residual strain or about the residual stress at points inside a specimen. For example, it cannot be assumed that the residual stress is a maximum at the surface.

The concentrate examined by Hilder[14] contained 23% by mass of solid. Of the three polymer quenchants tested sodium polyacrylate solutions produced the least severe quench but the polyalkylene glycol concentrate contained the most polymer in solution, (60%

by mass). However the polyalkylene glycol molecule is relatively simple compared to the sodium polyacrylate molecule and therefore one would expect the latter to produce a more viscous solution, and therefore slower quenching characteristics, than the former. The polyvinylpyrrolidone molecule was the most complex of the three but the concentrate tested contained the least solid matter of all, (10% by mass), and produced quenching characteristics closer to polyalkylene glycol solutions than to sodium polyacrylate solutions. A complete explanation of the relationship between quenching severity, concentration and molecular structure would require a knowledge of the molecular weight distribution also but this is information which has been regarded as commercially important and is therefore rarely revealed.

Patenting using polymer quenchants has also received particular attention. Patenting depends on slow cooling rates to achieve a fine pearlite structure and therefore a ductile material. Such slow cooling rates were typically achieved in the extended film boiling stage of high concentration sodium polyacrylate solutions. Therefore Mason and Griffiths[34] tested 30-40% solutions of Aquaquench 110 for suitability for patenting and found that the resultant mechanical properties were comparable to those achieved using lead baths though without the attendant health hazards and for a much reduced cost. However the stability of the vapour blanket, and therefore the success of the operation, was vulnerable to mechanical vibration.

Sodium polyacrylate has been stated to be quite safe as a

quenchant though it can be an eye irritant. Also, when heated to the decomposition temperature, acrid smoke and Na_2O fumes may be produced.[35]

2.6 Other Polymer Quenchants

Polyacrylamide quenchants, (PAA), are aqueous solutions of the iron salt of polyacrylic acid, (feracryl), with additions of sodium hydroxide sufficient to render them alkali, (pH 7-12).

These quenchants are, at the time of writing, restricted to Eastern Europe where there they are the most widely used of the aqueous polymer solutions available. Their cooling mechanism has been explained[36] in terms of a film which forms around the part early in the quench and which stabilises the film boiling stage. Upon subsequent cooling the film settles onto the surface of the part and further slows the cooling rate in the lower temperature range. An objection to this explanation is that it seems unlikely that the polymer molecule would not be decomposed at the surface temperatures involved. It was claimed that solutions of polyacrylamide, in concentrations of 0.2-0.5%, are suitable for spray quenching but are not suitable for immersion quenching since they produced an unacceptable rate of cracking.

Goryushin and Kobasko[37] examined PK-2, a 0.5-2.5% polyacrylamide solution, and concluded that certain concentrations and temperatures are suitable for quenching. A 1-1.25% PK-2 solution produced results comparable to a quenching oil.

Approximate confirmation of this was given by Levina et alia[38]

who showed that 0.005-0.01% polyacrylamide solution produced a faster cooling rate than water, (presumably due to enhanced wetting), 0.025% polyacrylamide solution produced a quench approximately equal in severity to water while 0.05% gave cooling rates markedly lower than water. Optimum mechanical properties after quenching were achieved with a 0.01-0.025% solution.

There was therefore an apparent contradiction between these results and the results of other workers. Zakamaldin et alia[36] suggested that 0.2-0.5% polyacrylamide produced too severe a quench while Levina et alia[38] suggested that a solution of 0.05% produced a quenching severity below that of water. Goryushin and Kobasko[37] suggested that low concentrations of polyacrylamide, (0.005-0.03%), produced a quench approximately equal to an oil in severity. Hilder[14] showed that increasing the concentration of solutions of polyalkylene glycol, sodium polyacrylate and polyvinylpyrrolidone decreased the quenching severity of the solutions while the results of the above workers[36 37 38] apparently demonstrated the reverse, ie, that increasing the concentration of polyacrylamide solutions increased the quenching severity of the solution. An explanation for this discrepancy probably lies in the different molecular weight distributions of the polyacrylamide solutions tested by different workers. This information is usually not revealed but it is known[39] that cooling rates during quenching are related to solution viscosity which is a function of not only solution concentration but also the molecular weight distribution of the solute.

One may only conclude that low concentrations of polyacrylamide are suitable as a quenchant but then the control

of such small concentrations as are required would probably cause problems, as would the enhancement of the effects of contamination.

Kobasko et alia[40] determined the surface heat transfer coefficient during quenching in a 1% polyacrylamide solution over a range of solution temperatures. Maximum values were found to occur at relatively low surface temperatures, around 120°C. These ranged from 6.8 $kW.m^{-2}.K^{-1}$ with a solution temperature of 23°C to 10.0 $kW.m^{-2}.K^{-1}$ at 80°C. The value of the maximum therefore increased with increasing solution temperature and also occurred within the martensitic transformation temperature range of most high hardenability steels, (figure 9); this would tend to produce large residual stresses.

Photographic studies of this quenchant were also performed[41] in which the various boiling regimes were identified and their progression on the surface of a cylindrical specimen quenched in 0.44% polyacrylamide solution noted. Film boiling, the vapour transport stage and convective cooling appeared on the surface of the cylinder at the same time at one point in the quench, (in that order from the top of the cylinder). These regions of cooling were propagated upwards at a velocity of about 7 to 8 $mm.s^{-1}$. The film boiling interface showed no wave formations.

Polyethylene oxide, (PEO), was patented as a quenchant by Chase and Ewing[42] who stated that cooling rates were dependent on a combination of molecular weight and concentration - the lower the average molecular weight of the solution, then the higher the concentration that must be employed to achieve the same quench

severity. Konyukhov et alia[43] tested the suitability of polyethylene oxide solutions for the quenching of aluminium alloys and showed that, though some reduction was experienced, mechanical properties were not greatly inferior to those achieved in water. Some decomposition of the solid solution was detected in the heavier sections, this effect being exacerbated by increasing the concentration, (and therefore decreasing the cooling rate), of the quenchant.

Warchol[44] recommended the use of solutions of nonionic substituted oxazoline polymers, polyoxazoline, (POE), in concentrations of 0.5-5.0%. The severity of this quenchant was claimed to be equal to a polyalkylene glycol solution of two to three times the concentration. This resulted in not only lower quenchant costs but also savings in waste disposal and, since polyoxazolines have a lower viscosity, lower dragout costs. These polymer quenchants show a short film boiling stage and a long convective cooling stage, unlike, for example, sodium polyacrylate.

More recently a mixture of polymer quenchants has been patented[45] consisting of polyoxazolines combined with polyvinylpyrrolidone in concentrations of 25-75%. Again, the quenching characteristics were claimed to be similar to oils but the added polyvinylpyrrolidone lowered the cost and gave a slower cooling rate at the temperature of the start of the martensitic transformation than either of the two constituents alone. In tests it was considered unnecessary to use a greater total concentration than 2% and in a novel approach cooling rates were varied by manipulating the molecular weights of the added

polymers. However, due to the low concentration used and the difficulty of the determination of the concentration of a mixture of two branched copolymers by viscosity measurement alone the problems of control would be great.

It has been proposed[46] that aqueous solutions of 5-20% polyalkylene glycol, (molecular weight 10,000-20,000), and 0.5-2% polyoxazoline, (molecular weight 5,000-1,000,000), produced a slower quench than solutions of the individual constituents. In addition the viscosity of this mixture was also reduced which means that drag-outs would also be reduced.

Carboxy methyl cellulose, (CMC), was patented in 1956 by Gordon[47] who recommended a 1.0-1.25% addition of the sodium salt of carboxy methyl cellulose: the sodium carboxy methyl radical rendered the polymer soluble. This quenchant has been commercially exploited in Eastern Europe with additions of up to 10% sodium chloride.[48]

Used exclusively in Eastern Europe, sulfite liquor and sulfite yeast mash, (SYM), are produced as residues from the paper and pulp industries and are therefore very cheap and readily available. As quenchants they have slow cooling rates during the martensitic transformation which may be further reduced by the addition of 0.5-1.0% sodium or potassium hydroxide. This also increased the cooling rate during the pearlitic transformation.[44] Zakamaldin et alia[36] stated that the quenching mechanism in these solutions depended upon a colloidal coagulant which formed around the hot metal when in contact with the solution. This caused the cooling rate to decrease sharply. The colloidal film deposited on

the metal surface and did not return into solution. Again, no evidence for this explanation was produced.

2.7 The Control Of Polymer Quenchants

When polymer quenchants were first introduced it was believed that their concentration could be controlled by monitoring the refractive index of the solution on a regular basis. Tests on the effects of ageing[17] and contamination[18] of the quenchants indicated that while a relationship exists between solution concentration and refractive index which was valid in the laboratory a divergence from this relationship occurred with commercial use. It became apparent that the refractive index of a polymer quenchant was as dependent upon temperature, molecular weight distribution, degree of use and degree of contamination as it was on concentration. More recently the refractive index method has been largely abandoned in favour of a much heavier reliance upon measurements of kinematic viscosity.

The kinematic viscosity of a polymer solution is a function of shear rate. It is also dependent on molecular weight distribution as well as concentration. An examination[39] of the effect of solution viscosity of polymer quenchants using cooling capacity tests showed that polymer solutions of the same concentration but different molecular weight, (and therefore different viscosity), gave different cooling curves. However, the cooling curves for solutions of different concentration but the same viscosity were largely identical. This suggested that the quenching characteristics of a polymer quenchant were governed by the

viscosity of the solution rather than its concentration. However the concentration of a bath is easier to adjust than its viscosity. Therefore more reliance has been placed on the measurement of cooling curves obtained under standard conditions and their comparison with those of the initially pure solution. For example, the recent introduction of the Wolfson Group Engineering Test.[14]

It has also been necessary to maintain control over the level of rust inhibitors and biocides in the solution and the level of biological contamination. The corrosion inhibitors included in the commercially available concentrates may be tested using various titration techniques.[21] while biological contamination may be assessed by using agar coated Petri dishes or agar coated dipsticks.[22] However, there is no evidence that bacterial growth affects the quenching characteristics of any polymer quenchant and therefore no real incentive to test for it.

Other tests which may be carried out include the determination of the pH of the solution to detect changes in alkalinity and the determination of conductivity to ascertain the degree of salt contamination. In polyalkylene glycol quenchants the latter may also be determined by measuring the temperature at which inversion occurs.

3.0 THE PREDICTION OF THERMAL STRESS AND STRAIN

The prediction of the generation of thermal stress and strain during heat treatment evolved through sevaral stages as more accurate models were sought. Analytical techniques were first explored but this approach was only capable of achieving solutions for simple geometries and required the problems to be considerably simplified. The text of Boley and Weiner[50] is a good example of the limits to which classical stress analysis could be applied to this problem. In this work elastic, elastic-plastic and visco-elastic models were derived but their application was confined to simple structures such as plates, beams and rings and their accuracy was limited by the assumption that the physical and mechanical properties of the material were independent of temperature. In addition the process of transformation could not be easily included in the analyses.

The inclusion of the effects of transformation on the generation of thermal stress and strain was accomplished using numerical techniques facilitated by the use of digital computers. Many models have been produced of heat treatment processes, (for example, quenching, induction hardening and carburising), and applied to simple geometries such as plates and cylinders. More complex geometries, as are encountered in practice, may be dealt with by using the finite element method. (Space does not allow the finite element method to be dealt with adequately in the present work; the reader is referred to the many specialist texts in the field, for example, Desai and Abel.[51]) The models of quenching have most often used the martensitic transformation by

applying relationships between temperature and structure obtained empirically or by using theoretical models of the transformation process that involved experimentally determined constants.

A further advance was made when other aspects of thermo-mechanical coupling were considered. Thermo-mechanical coupling relates the interaction of the thermal processes with the generation of stress and strain as follows, (see figure 10);

1. A decrease in temperature causes transformation but the latent heat of transformation thus evolved raises the temperature of the material.

2. The progress of transformation causes stress but the presence of the stress affects the progress of the transformation.

3. A decrease in temperature causes thermal stress and strain but deformation produces heat and therefore alters the temperature distribution in the material.

The relative importance of the couplings has been explored, mostly, but not exclusively, for steels transforming to martensite. It has become apparent that the interaction of major importance is that referred to as transformation plasticity. This relates to the plastic deformation which occurs when a transformation takes place under the influence of a stress even though the stress is below the yield stress of the material. The inclusion of transformation plasticity has been the last major advance in the field of the calculation of thermal stress and strain.

The most recent review of the subject at the time of writing has been published by Fletcher.[52]

The prediction of the generation of thermal stress and strain

during heat treatment requires a knowledge of the temperature distribution in a body during the process. The methods of calculating this are not dealt with here; the reader is referred to the many specialist texts on the subject, for example, Arpaci[53] or Adams and Rogers.[54]

3.1 Analytical Studies

Boley and Weiner[50] examined a completely elastic material for which a nonuniform temperature distribution was known and which was independent of deformation, that is, there was no thermo-mechanical coupling. The stress-strain relationships for an elastic solid are;

$$\epsilon_{xx} = \frac{1}{E}[\sigma_{xx} - \nu(\sigma_{yy}+\sigma_{zz})]+\alpha\theta$$

$$\epsilon_{yy} = \frac{1}{E}[\sigma_{yy} - \nu(\sigma_{zz}+\sigma_{xx})]+\alpha\theta$$

$$\epsilon_{zz} = \frac{1}{E}[\sigma_{zz} - \nu(\sigma_{xx}+\sigma_{yy})]+\alpha\theta$$

$$\epsilon_{xy} = \frac{1}{2G}\sigma_{xy}$$

$$\epsilon_{yz} = \frac{1}{2G}\sigma_{yz}$$

$$\epsilon_{zx} = \frac{1}{2G}\sigma_{zx}$$

where ν = Poisson's ratio

α = coefficient of linear expansion

θ = temperature

E = Youngs Modulus

G = shear modulus = $\dfrac{E}{2(1+\nu)}$

The body was assumed to be in a state of equilibrium which gave the following relationships between the stress components;

$$\frac{\partial \sigma_{xx}}{\partial x} + \frac{\partial \sigma_{xy}}{\partial y} + \frac{\partial \sigma_{xz}}{\partial z} + X = 0$$

$$\frac{\partial \sigma_{xy}}{\partial x} + \frac{\partial \sigma_{yy}}{\partial y} + \frac{\partial \sigma_{yz}}{\partial z} + Y = 0$$

$$\frac{\partial \sigma_{xz}}{\partial x} + \frac{\partial \sigma_{yz}}{\partial y} + \frac{\partial \sigma_{zz}}{\partial z} + Z = 0$$

where X, Y and Z = the components of the body forces.

The relationships between strain and the displacements u, v and w are;

$$\epsilon_{xx} = \frac{\partial u}{\partial x}$$

$$\epsilon_{yy} = \frac{\partial v}{\partial y}$$

$$\epsilon_{zz} = \frac{\partial w}{\partial z}$$

$$\epsilon_{xy} = \frac{1}{2}\left(\frac{\partial u}{\partial y} + \frac{\partial v}{\partial x}\right)$$

$$\epsilon_{yz} = \frac{1}{2}\left(\frac{\partial v}{\partial z} + \frac{\partial w}{\partial y}\right)$$

$$\epsilon_{zx} = \frac{1}{2}\left(\frac{\partial w}{\partial x} + \frac{\partial u}{\partial z}\right)$$

The problem has been solved when the 6 stress components, 6 strain components and the 3 displacement components u, v and w have been determined from the above. The problem also has to satisfy certain boundary conditions. Since heat treated parts generally have surfaces which are not subject to loads the components x, y and z of the surface stress are zero;

$$\sigma_{xx}n_x + \sigma_{xy}n_y + \sigma_{xz}n_z = 0$$

$$\sigma_{yx}n_x + \sigma_{yy}n_y + \sigma_{yz}n_z = 0$$

$$\sigma_{zx}n_x + \sigma_{zy}n_y + \sigma_{zz}n_z = 0$$

where n_x, n_y and n_z = the direction cosines normal to the surface

These problems may be further simplified by assuming plane stress or plane strain conditions. Boley and Weiner[50] presented solutions for thermoelastic stresses in infinite plates and cylinders and beams and rings.

Boley and Weiner[50] also presented a visco-elastic solution for a free plate subject to a temperature distribution through the

thickness only. This approach utilised the Maxwell body as a model of the behaviour of a visco-elastic material.

Subsequently an elastic-plastic model of the free plate was developed which used a temperature independent von Mises yield criterion. This was extended to include a temperature dependent yield stress and viscoelasticity. Finally, elastic-plastic analyses were performed for cylinders using both the Tresca and von Mises yield criterion.

Calculations were performed for some of the analyses mentioned above and figure 11 shows an example of the residual stresses calculated for a viscoelastic-plastic model of a free plate cooled symmetrically in air. A temperature dependent yield stress was employed but in all other respects the physical and mechanical properties of the material were assumed to be independent of temperature. The surface heat transfer coefficient was also assumed to be constant. No experimental measurements of the residual stress in such a plate were performed so it was not possible to check the accuracy of the calculation but measurements of the residual stress performed to check the elastic-plastic cylinder models produced an impressive level of agreement.

3.2 Early Numerical Models

For the inclusion of more complex phenomena in the models such as an accurate representation of transformation and the large variation in surface heat transfer coefficient observed during quenching, it was necessary to use more sophisticated models.

These involved a solution using numerical methods, which required the use of a digital computer.

Chevrier[55] performed an analysis of a quenched cylinder of an aluminium alloy, (which did not undergo a transformation), with the relationships between the physical and mechanical properties and temperature determined experimentally. The rate at which the material work hardened was assumed to be constant as was Poisson's ratio and the coefficient of thermal expansion. However, after the application of the yield criterion when plastic deformation occurred the stresses were not rebalanced across the section of the cylinder.

Toshioka et alia[56] formulated a method to predict the residual stresses in quenched cylinders of varying dimensions. The temperature distribution in the cylinder was obtained experimentally in both an oil and a water quench and expressed as a temperature gradient coefficient, A. A mean value of A, obtained from the whole quench, (which implied a constant temperature gradient), was used in both cases. The progress of transformation in the model was approximated by a quadratic relationship though this was not a good fit to the progress of transformation measured experimentally. A description of transformation to martensite and bainite was also included. The yield stress of the material was assumed to be zero in the austenitic stage and was also assumed to be proportional to the progress of transformation. The coefficient of expansion, Poissons' ratio and Young's Modulus were assumed to be constant and independent of temperature.

The residual stresses in a steel cylinder quenched in oil to give a completely martensitic structure were predicted to be tensile at the surface and compressive at the centre. Increasing the temperature gradient in the cylinder to simulate a water quench reversed this predicted distribution. Simulating a quench which produced a combination of bainite and martensite led to complex distributions of residual stress depending upon the temperature gradient chosen and the distribution of bainite and martensite produced.

The simplifications introduced into this model inevitably reduced the accuracy of the results. For example, a constant temperature gradient is not representative of heat transfer during quenching. In addition, M_s was set to 300°C and M_f to 250°C, but during calculation of the progress of transformation M_f was displaced upwards to 275°C for convenience. Also, the yield strength of martensite was assumed to be 294 MPa which was low for a medium carbon steel.

Spektor and Stepanova[57] calculated the residual stress and strain in infinite steel plates of a high hardenability steel of thickness 10 and 20 mm quenched in mineral oils of varying viscosity. The model incorporated the variation of surface heat flux with surface temperature, (obtained from experimental determination of the cooling curves), and also the temperature dependence of the thermal conductivity, coefficient of expansion and yield strength of the material. A mean value for Young's Modulus was used based on values for the entire plate at one time.

The results suggested that the first stage of quenching,

(where heat transfer was rising to a maximum), produced tensile surface stresses and compressive centre stresses. After the peak heat flux passed this stress distribution reversed. The transformation to martensite began at 200°C and as this progressed the surface stress again became tensile and the centre stress again became compressive. The tensile surface stress peaked at 150°C and then declined. Maximum stresses were reported during transformation and were related to the temperature gradient in the plate during this period which in turn was related to the temperature at which the maximum surface heat flux occurred.

One of the first finite element applications was carried out by Inoue and Tanaka[58] who studied a 60 mm diameter medium carbon steel cylinder water quenched to produce a martensitic structure. Though some assumptions were made with regard to the properties of the material the coefficient of expansion was made dependent on temperature and also, unusually, cooling rate. Very good agreement was obtained with experimental measurements of the residual stress made by Sachs' method.

Fujio, in a series of reports,[59 60 61 62] examined, using the finite element method, the residual stresses and distortions created during the case hardening of gear teeth. This required the introduction of composition, ie, the variation in carbon content, as a variable in the thermo-mechanically coupled model which had a considerable effect on the physical properties of the material and the resulting structure. In general, good agreement was obtained between the calculated and experimentally obtained

results when an X-ray method was used to measure residual stresses but not when a layer removal method was used. The reason for this was assumed to lie in the latter test.

Fletcher[63] considered the problem of quenching of infinite plate of a low alloy steel which transformed fully to martensite. Plane stress conditions were assumed and therefore only the stress and strain in the thickness of the plate were considered. The model assumed that temperature distribution and stress and strain were symmetrical about the centre-line of the plate. One half of the plate was split into 41 elements for the calculation of the temperature distribution and 10 elements for the calculation of thermal stress and strain. The temperature distribution was determined by a finite difference solution of Ficks Law of transient heat conduction.

The change in dimension of each element due to the change in temperature which occurred during the passage of a specific time interval was used to calculate the elastic stress increment. Between M_s and M_f the elastic stress increment due to the progress of transformation was also determined. Values of the elastic stress calculated for each element in excess of the yield stress were corrected to equal the yield stress. The section of the plate was required to have no net force acting upon it so the stresses were balanced across the plate section. The von Mises yield criterion was applied and this procedure repeated until the net force on the section was deemed negligible. The new strain values were then determined assuming that any elastic stress increment produced a strain increment in accordance with Hookes Law.

Surface heat transfer coefficients were either assumed constant or varied with surface temperature according to data obtained from the literature but the physical properties of the material were assumed to be independent of temperature. The relationship between austenite yield strength and temperature was derived from experimental data.

An extension of this model[15] utilised precise relationships between surface heat transfer coefficient and surface temperature obtained from previous work.[64] The effect of work hardening on the yield stress was introduced as was the temperature dependence of the coefficient of expansion, Young's Modulus and Poissons ratio.

This model[15] was applied to the problem of quenching of 20 mm low alloy steel plates in water, oil and a polymer quenchant, (25% Aquaquench 1250, a polyalkylene glycol solution in water). All three calculations predicted plastic deformation during the first stage of the quench while the surface heat transfer coefficient was rising to its maximum. This was greatest in the water quench and least in the oil quench calculation. The tensile stress that accompanied this plastic deformation unloaded as the maximum surface heat transfer coefficient passed and a compressive loading was subsequently predicted in all three cases. The extent of this loading was a minimum in the oil quench calculation. The calculated stresses then unloaded once more to become more tensile.

The predicted residual stresses for the water quench calculation were an approximately stress free surface with a

large tensile peak just below the surface and a compressive centre stress. The oil quench calculation predicted a compressive surface residual stress which rose to a tensile centre residual stress. The polymer quench calculation predicted a residual stress distribution similar to that in the water quench with a low value of tensile surface residual stress, a tensile peak just below the surface and a compressive residual stress at the centre.

A fair agreement between calculated and measured, (using a layer removal method), residual stresses in water and the polyalkylene glycol solution was obtained but agreement between the calculated and measured residual stresses in the oil quench was poor. Also, the agreement between the calculated and measured residual strains was good in the case of a water quench calculation but poor for the oil and polymer quench calculations.

Archambault et alia[65] used the finite element method to study a precipitation hardened aluminium alloy in an attempt to obtain an optimum condition with a high strength, created by quenching, but low residual stress, to avoid cracking. A "quench window" was defined on the basis of the results but the required rate of cooling was so fast as to be generally unobtainable except by coating the part to accelerate quenching.

Yu and Macherauch[66] presented a finite element program to calculate the residual stresses in welds and quenched cylinders with and without the effects of transformation. The authors produced plots of the state of stress of the cylinder at certain times and in a novel approach these were translated onto 16 mm film in order to produce a cine film which showed the development

of stress and strain during the entire quench.

The type of model which was developed in the manner related in the foregoing and which included only the dominant interactions of thermo-mechanical coupling has been used widely with useful results obtained.

For example, Burnett[67] presented a finite element method program to calculate the generation of stresses during the carburising and quenching of steel cylinders.

Jeanmart and Bouvaist[68] performed a finite element analysis, using the MARC finite element package, of the stresses generated in hot and cold water quenched and mechanically stress relieved plates of a high strength aluminium alloy. This was aimed at a reduction in the distortion during machining of aluminium parts for the aircraft industry and an impressive agreement with experimentally determined residual stresses was obtained.

Fujio and Sakota[69] extended the finite element model of the residual stresses in case hardened gears[59 60 61 62] to include the effects of different depths of case and obtained a similar good agreement with experimental results as before. An optimum case thickness was discovered with maximum residual stress at the root fillet of the gear tooth and therefore maximum fatigue life.

3.3 The Interaction Of Transformation And Stress: Transformation Plasticity

While previous work concentrated on the introduction of phase transformations into models for the prediction of stress and strain attention then turned to the interaction of internal

stress and transformation. This is complex but may be considered to be split into two parts, namely, transformation plasticity and the effect of stress on the kinetics of transformation. Work on these aspects was generally reported simultaneously but for the sake of clarity the phenomena will be dealt with in two separate sections, beginning with transformation plasticity.

Transformation plasticity is observed when a transformation occurs under the influence of a stress. Though the stress is less than the yield stress of the material involved a permanent deformation occurs, (see figure 12). Many explanations have been proposed for this phenomenom. It has been suggested that the atoms in the lattice of the material temporarily lose their cohesion as they undergo transformation. Alternatively the yield stress of the material may be locally exceeded by the combination of an internal stress with the stress created by the transformation. It has been attributed to slip at the interface between the phases or the preferred orientation of the phase produced by the transformation. Transformation plasticity has also been attributed to the acceleration of creep processes by the formation of point defects.

Greenwood and Johnson[70] examined transformation plasticity in uranium, titanium, zirconium and iron and proposed the following relationship;

$$\epsilon = \frac{5\sigma_z(\Delta V/V)}{6Y}$$

where σ_z = applied stress

$\Delta V/V$ = volume dilation

Y = the yield stress of the weaker phase

This was based on the assessment of the relative contribution to plastic deformation of the processes occurring during transformation such as creep and stress relaxation and anisotropy of thermal expansion. These factors were shown to produce only a small amount of deformation during transformation and could therefore be neglected; the relationship given above was derived from a consideration of a plastic material which deformed when the applied stress caused the yield stress of the weaker phase to be locally exceeeded with the effect of the orientation of the transformation product being negligible. This approach has been the most popular method of introducing transformation plasticity into models of the generation of thermal stress and strain.

Desalos[71] proposed an incremental relationship for transformation plasticity;

$$\frac{d\xi_{ij}}{dt} = 3K(1-m)s_{ij}\frac{dy}{dt}$$

where K = constant

m = volume fraction of martensite

s_{ij} = deviatoric stress tensor

y = volume of transformation product formed

One of the first models of the generation of thermal stress and strain to incorporate transformation plasticity was that of Denis et alia[72] who proposed a model of the quenching in water at 80°C of a steel cylinder which transformed completely to

martensite. This model also incorporated the effects of stress on the kinetics of the martensite transformation. These latter effects will be discussed in the next section.

A plastic modulus was defined to describe plastic deformation at up to 0.5%. This, together with the Youngs Modulus of the material, gave two linear relationships which described the stress/strain behaviour in both elastic and plastic regions. Their intersection defined an apparent yield stress, (see figure 13).

Transformation plasticity was introduced by assuming a temporary reduction in the apparent yield stress to achieve plastic deformation during transformation. The effect of this was to produce a tensile surface and a compressive centre longitudinal residual stress; the reverse was observed in a model in which transformation plasticity was ignored. In addition, with the introduction of transformation plasticity, the levels of absolute residual stress and total plastic deformation were significantly increased.

It was argued that this method of modelling transformation plasticity, (using a reduction of the yield stress during transformation), was unsatisfactory since it meant that the amount of plastic deformation predicted was not related to the progress of transformation as experimental evidence suggested but was dependent upon the level of the applied stress only. In addition there was no experimental evidence for a reduction in the yield stress during transformation.

In a finite element treatment of the stresses generated during

the water quenching of steel cylinders Sjostrom[73] compared the effects of including transformation plasticity by a reduced yield stress method and by a rate type equation after Desalos;[71]

$$\frac{d\xi^{tp}_{ij}}{dt} = 3K(1-v_6)\frac{dv_6}{dt}(\sigma_{ij} - \frac{1}{3}\delta_{ij}\sigma_{mm})$$

where K = constant

v_6 = the volume fraction of martensite

δ_{ij} = Kronecker's delta

A calculation was also performed in which transformation plasticity was ignored. All three types of calculation, (performed for different grades of steel cylinders of different diameters quenched into water under varying conditions), produced a good agreement with experimentally determined stresses except in the case of the smallest diameter cylinder, (17 mm). In this case the introduction of transformation plasticity by the Desalos-type formulation significantly improved the agreement with the experimentally determined residual stress and as a consequence a preference for the modelling of transformation plasticity by this method was expressed.

Denis et alia[74] subsequently formulated a method where deformation was treated as an additional plastic strain related to an empirical constant, the stress state and the volume of transformation product. The constant was derived from uniaxial tensile tests and was applied to the multiaxial problem which existed in the cylinder by assuming that transformation plasticity behaved like classical plasticity and that the

deformation was oriented in the direction of the applied stress;

$$d\xi^{tp}_{ij} = \frac{3}{2} \frac{d\xi^{tp}_{e} s_{ij}}{\sigma_e}$$

where $d\xi^{tp}_{e} = 2k\sigma_e(1-m)dm$

k = constant = 5.2×10^{-5} MPa^{-1}

This approach to the inclusion of transformation plasticity in the model led to a significant reduction in the absolute level of residual stress predicted compared to that produced by the reduction in yield stress model.[72] The modelling of transformation plasticity as an additional strain has since remained the most widely used method.

Abbasi and Fletcher[75] also investigated the modelling of transformation plasticity using the reduced yield stress, additional elastic strain and additional plastic strain methods. This work was based on dilatometer tests carried out with both applied tensile and compressive stresses. The results indicated no transformation plasticity when the applied stress was below 40 MPa. The different methods were introduced into a visco-elasticplastic model of the generation of thermal stress and strain in low alloy steel plates quenched in water and oil. The additional strain methods introduced transformation plasticity by a series of quadratic relationships between plastic strain and temperature.[76] A comparison with experimentally determined residual stresses and strains showed that the introduction of transformation plasticity as an additional plastic strain showed greatest agreement.

However, the quadratic relationships used produced instability in the stress calculation at temperatures close to M_s and they were therefore replaced[77] by a linear relationship which operated between 300°C and 260°C thus;

$$\xi_{tp} = 6.25\text{x}10^{-7}(\sigma\text{-}40)(300\text{-}\theta)$$

Denis et alia[78] extensively reviewed the literature dealing with transformation plasticity before presenting a model which incorporated it as an additional plastic strain where;

$$\xi^{tp} = k\sigma f(m)$$

where $k = 5.2 \times 10^{-4}$ MPa^{-1}

σ = uniaxial stress

$f(m) = (2\text{-}m)m$

m = volume fraction of martensite according to the Koistinen and Marburger relationship

This was used in the multiaxial problem as before, (note the change in the value of the constant). No threshold stress was used. The effect of the introduction of transformation plasticity by this method was as described above, (when transformation plasticity was incorporated as a reduction in the yield stress[72]); The predicted residual stress distribution was reversed compared to that obtained by the model in which transformation plasticity was ignored. This new distibution agreed well with that determined experimentally by the Sachs method.

Transformation plasticity was also applied[79 80 81] to the

modelling of a quenched eutectoid carbon steel cylinder;

$$\xi^{tp} = k(\sigma-\sigma_s)y$$

where y = volume fraction of pearlite formed

$k = 1.7\text{x}10^{-4}$ MPa^{-1}

σ_s = threshold stress

The constant k was the slope of the transformation strain vs applied tensile stress relationship obtained from dilatometer tests. This slope was linear and highly temperature dependent. The constant given above related to a transformation that began at 663°C; increasing the temperature by 20°C decreased this constant by 30% to $1.3\text{x}10^{-4}$. A threshold stress, σ_s, of 10 MPa was observed. Compared to the results obtained when this effect was neglected, the introduction of transformation plasticity in the eutectoid steel model resulted in reduced stress levels during transformation. The introduction of transformation plasticity also increased the absolute residual stress and strain at a particular point in the specimen and reversed the sense of the residual stress.

3.4 The Interaction Of Stress And Transformation: The Effect Of Stress On The Transformation Kinetics

Dilatometry tests with an applied tensile stress indicated that as the applied stress was increased the temperature of the start of the martensitic transformation increased. The total transformation strain also increased, (transformation

plasticity).

Denis et alia[72] examined the effect of stress on the kinetics of the martensite transformation by using two models of a water quenched tool steel cylinder. One model assumed that no stress-transformation interaction occurred while the second model assumed that the effect of the internal stress created by the cooling of the specimen during the earlier stages of the quench was to increase M_s by 15°C. From the results it was concluded that the differences in residual stress distribution that occurred as a result of including the effect of stress on the martensite transformation kinetics in the model were of a small magnitude.

Inoue and Wang[82] applied an elastic-plastic analysis using the finite element method to the quenching of a steel cylinder. The problem was considered to be fully thermo-mechanically coupled though transformation plasticity was not included. The effect of stress on the austenite-pearlite reaction and also on the austenite-martensite reaction was incoporated.

It was concluded that the inclusion of the effect of stress on the transformation kinetics was important if an accurate prediction of the residual stress was to be obtained. Very good agreement with experimentally determined stresses was claimed despite the absence of transformation plasticity in the model, (though these measurements were all carried out close to the surface of the cylinder).

Denis et alia[74] subsequently modified their procedure. Experimental data suggested that M_s was raised 0.05°C for every 1 MPa of applied tensile stress in the case of the steel used and

the authors reviewed work which suggested, (for a steel of similar composition), that M_s fell by a similar amount when subjected to a hydrostatic stress. The model had previously used the Koistinen and Marburger equation to describe the formation of martensite with decreasing temperature;

$$m = 1 - \exp[-k(M_s - \sigma)]$$

where k = an empirical constant

σ = applied stress

This was modified, in the manner after Inoue,[82] to account for the change in M_s with internal stress;

$$M_s = M_{so} - \Delta M_s$$

where $\Delta M_s = (A\sigma_m + B\sigma_e)/k$

where M_{so} = martensite start temperature under zero stress

σ_m = mean stress = $(\sigma_r + \sigma_\theta + \sigma_z)/3$

σ_e = effective stress = $(1.5 s_{ij} s_{ij})^{0.5}$

A and B = constants

The effect of uniaxial stress on the transformation kinetics for which data was available was therefore adapted to the multiaxial case by using the mean and effective stresses and two experimentally determined constants, A and B.

This procedure was applied to a finite element model of a water quenched tool steel cylinder. The generation of stress was shown to affect the progress of transformation markedly. As the transformation temperature at the surface was approached the

surface was in a state of tensile stress which raised the temperature of M_s, (by 38°C in the example given). As transformation began at the surface the tensile stress decreased due to the formation of martensite. This caused a compressive loading of the surface as the expansion there was restrained by the centre. M_s also therefore decreased until it fell below the surface temperature. Transformation was then halted until the surface temperature fell below the new M_s temperature whereupon transformation continued. This behaviour occurred in all of the elements from the surface to the centre of the cylinder with one or more halts in the model of the progress of transformation.

The results of this model again suggested that the effect of stress on the kinetics of the martensite transformation had little effect on the residual stress distribution.

A subsequent publication,[78] accompanied by a thorough review of the effect of stress on transformation kinetics, simplified the method by which ΔM_s was calculated to exclude the constant k such that;

$$\Delta M_s = A\sigma_m + B\sigma_e$$

(This increased the magnitude of the constants A and B by approximately a hundredfold but, since these constants were empirical, did not affect the conclusions drawn). Calculations using the MARC finite element package indicated that if the effect of stress on the kinetics of the martensite transformation was included in this manner the result was higher compressive stresses at the surface of the cylinder and lower tensile

stresses at the centre but again these effects were deemed slight.

The incremental approach to the calculation of thermal stress and strain has been clearly presented by Sjostrom[83] where the total strain, and therefore stress, was described as consisting of several parts due to elastic, plastic, thermal, transformation and transformation plasticity strain. In modelling the quenching of steel cylinders in water at $0^{o}C$, (iced water), $20^{o}C$ and oil at $60^{o}C$ it was concluded that the effect of stress on transformation kinetics was negligible but that much experimental data remained to be collected for accurate calculations to be made. (This was evident in the heat flux data used where the peak heat flux for iced water was reported to be four times that of water at $20^{o}C$ while the latter was reported to be only slightly higher than that in oil at $60^{o}C$. These figures appear unrealistic in the light of other research.[64] [84] Errors in the calculated temperature distribution introduced in this fashion would have affected the calculated thermal stress and strain considerably.)

Denis et alia applied their approach to investigate thermo-mechanical couplings in a eutectoid steel.[79] [80] [81] A review of the literature showed that diffusional transformations, (particularly the pearlite reaction in steel), were more strongly affected by the application of stress than shear transformations and therefore an investigation was carried out to assess the effect of stress on the reaction kinetics of an eutectoid steel. The latent heat evolved during transformation was also shown to be considerable, (see figure 14). Experimental work indicated that the effect of hydrostatic stresses was negligible while both

compressive and tensile stresses accelerated the reaction, (that is, the isothermal transformation curves were shifted to shorter times). The effect of the internal stress present during the decomposition of the austenite was to decrease the length of time before transformation began and to accelerate the rate at which it occurred. The effect of stress on the transformation was modelled on the basis of uniaxial tensile test results only. The shift in the isothermal transformation curve created by the application of a stress was based on the value of the effective stress, σ_e, which existed at the beginning of the transformation. This displacement was assumed to remain constant throughout the transformation.

This model also incorporated transformation plasticity and the interaction between transformation plasticity and the effect of stress on the transformation kinetics was noted. Due to the latter the plastic deformation produced by transformation was increased. In addition, since the transformation occurred at an earlier time the stress unloading associated with it also occurred earlier. The net effect was to substantially increase absolute stress levels though the type of distribution remained qualitatively similar with a tensile surface and a compressive centre axial residual stress. Quantitative agreement with experimentally determined residual stresses was not good.

A calculation was also performed which used the current state of stress during transformation to calculate the rate of transformation rather than using the stress level at the beginning of the transformation and treating it as a constant.

This caused the progress of transformation to be slowed and reduced the discrepancy between the calculated and measured stresses.

Inoue and Wang[85] studied thermo-mechanical coupling in an elastic-plastic formulation for quenching and a visco-plastic formulation for welding using a finite element method and concluded, in contradiction to the above, that the effect of stress on the kinetics of transformation was important but that the production of latent heat was not.

3.5 The Introduction Of Visco-Elastoplasticity

Viscous processes, (creep and stress relaxation), have generally been ignored in models for the generation of thermal stress and strain during quenching on the grounds that the time scales involved were too short for these to have a significant effect. It was argued by Abbasi and Fletcher[86] that this was not always so, particularly with an oil quench. Isothermal creep and stress relaxation tests were modelled using the standard linear solid and several methods proposed by which the isothermal data could be used to represent the real situation that applied during quenching.

Model 1 proposed that the stress relaxation rate at one temperature was equal to that obtained at zero time from the tests. Model 2 proposed that the stress relaxation rate at any one temperature and time was represented by the mean of the results over a representative period of time from the correct temperature test. Model 3 proposed that the stress relaxation

rate was represented by Model 2 for the first 20 seconds but thereafter remained constant at the value for 20 seconds. Model 4 proposed that the stress relaxation rate at one particular temperature and time was represented by that rate obtained at that time from the isothermal tests. Each proposal therefore represented elements of the viscous processes which would be expected to occur during quenching but when these models were introduced into the elastic-plastic model already formulated, (in which transformation plasticity was absent), agreement with experimentally determined data improved but significant discrepancies remained. A better fit was obtained when it was assumed that stress relaxation at any one temperature was represented by the stress relaxation rate at zero time at the relevant temperature isothermal test, (Model 1), but that no stress relaxation occurred below 230^{o}C. This gave high rates of stress relaxation at high temperatures but none at low temperatures as one would expect. For example, at the beginning of the martensite transformation high levels of stress were generated which was expected to cause significant stress relaxation as indeed this approach predicted.

A variation of this model,[87] (which included transformation plasticity), was used to examine martempering. Here the stress relaxation at one time or temperature was obtained from the relevant isothermal test for the first 20 s of the test, (Model 2), and thereafter the stress relaxation rate was assumed to be dependent on temperature only. The calculated residual stress distribution was close to the experimentally determined residual stress distribution when stress relaxation was included in the

model and a divergence occurred when stress relaxation effects were removed. The residual strains were not largely affected by the inclusion of viscous processes.

Subsequently the effect of initial stress on the stress relaxation rates was introduced into the model[88] to improve further the agreement with experimentally obtained data.

4.0 Boiling Heat Transfer

The majority of the heat transferred from a metal part quenched in a vapourisable liquid from a sufficiently high temperature is associated with boiling of the liquid at the metal surface. Four distinct stages are discernible during quenching, being, in the order of which they occur;

1. the initial wetting stage,
2. the film boiling stage,
3. the vapour transport stage,
4. the convective cooling stage.

When the metal part is quenched in the liquid the liquid adjacent to the surface is heated and vapourised. In the very early stages a large amount of heat is extracted as the heat transfer processes at the surface move through the stages of convective cooling, the vapour transport stage and perhaps, (depending on the initial surface temperature, the temperature of the quenchant, the amount of quenchant agitation and the amount of heat extracted by the earlier stages), the film boiling stage. This whole process is termed the initial wetting stage and it may be accompanied by an observable decrease in the radiation emitted by the surface. For example, a metal part quenched from 850^{o}C will be red hot at the point of immersion but the surface may temporarily blacken when wetted by the liquid. The red appearance of the surface returns because the rate of heat transfer at the surface is subsequently diminished by the formation of a vapour film. This initial wetting stage lasts for only a fraction of a second.

If the conditions are favourable a continuous or semi-continuous vapour blanket may form around the part, (the film boiling stage). Heat transfer is low in this stage as the vapour blanket insulates the hot surface from the cold liquid and takes place mainly by conduction through the vapour and convection in the liquid. Unless the surface temperature is very high, (ie, above usual austenitising temperatures), the heat transferred by radiation is negligible. When the surface temperature has fallen sufficiently the amount of vapour formed at the vapour/liquid interface is insufficient to maintain the vapour film. It collapses and the surface is wetted by the liquid. This is known as the minimum film boiling point.

When the surface has been wetted by the liquid the latter is vapourised to form bubbles. This stage persists until the surface temperature falls below the boiling point of the liquid. At that point no more bubbles can be created and heat transfer by vapour transport has ended. This stage has universally been considered to consist of two sections, (for example see reference 89 and figure 15). Transition boiling is used to describe boiling after the collapse of the vapour blanket when the rate of heat transfer from the surface rises as the surface temperature falls. It has been suggested that the vapour blanket may locally reform in this stage but it is also characterised by the formation of many small bubbles. Any partial reformation of a vapour film would be highly unstable. It has been suggested[89] that the frequency with which the film reforms is reduced to zero when the point of maximum heat transfer is reached. This maximum is described as the critical heat flux. After this point heat transfer rates fall

with decreasing surface temperature in what is termed the nucleate boiling stage.

Heat transfer in the vapour transport stage is dependent on many factors including the latent heat of vapourisation, extracted as a bubble is formed, and a "microconvection" term which has been used[90] to describe the bringing of cold liquid to the hot surface as a bubble is released. Heat transfer is therefore dependent on factors which govern the nucleation and growth of bubbles such as surface condition and the contact angle and surface tension of the liquid.

When the surface temperature has fallen below the boiling point of the liquid then boiling is halted and cooling occurs by convection in the liquid. This stage is important in quenchants with high boiling points such as mineral oils.

The study of boiling heat transfer has largely been motivated by the recent investment in nuclear reactor technology. In contrast its application to other processes, such as quenching, has been limited.

4.1 Film Boiling Heat Transfer

Several approaches to the modelling of film boiling have been studied depending upon the authors opinion as to the most significant points of the process. The most ambitious models have generally used boundary layer theory in which the process was viewed as two parallel fluid layers in laminar flow. The solution of the boundary layer equations may be performed by many techniques but they may be broadly split into two types -

solution by similarity transformation or by the integral profile method. Three reviews of film boiling have been performed in recent years. The review of Jordan[91] dealt with explanantions of the early attempts of mathematical models of film boiling heat transfer. Boundary layer theory models were neglected though sevaral had appeared by the date of the publication of the review. Clements and Colver[92] presented a detailed review of film boiling data and commented on the models produced. Again boundary layer theory models were hardly touched. Kalinin et alia[93] referred to the models produced up to that date including boundary layer theory models but there was hardly any discussion.

The first model of film boiling heat transfer was due to Bromley[94] who modified an analysis of film condensation by Nusselt to calculate the heat transfer coefficient from horizontal and vertical tubes and plates in a saturated liquid. Bromley[94] assumed that the vapour interface was smooth and continuous and that heat transfer was by conduction only through the vapour. Inertia in the vapour film was ignored. This might have incorporated an unnacceptable error into the theory but for the use of an experimentally determined constant which was dependent on the shear stress at the interface.

Bromley[94] also proposed a method of including radiation heat transfer into the the conduction heat transfer coefficient;

$$h = h_{co}\left(\frac{h_{co}}{h}\right)^{1/3} + h_{rad}$$

where h = total surface heat transfer coefficient

h_{co} = surface heat transfer coefficient due to

conduction only

h_{rad} = surface heat transfer coefficient due to radiation only

This was derived intuitively but later Lubin[95] derived the same expression analytically to confirm the relationship.

Hsu and Westwater[96] examined saturated film boiling on varying lengths of vertical tube for a range of liquids and compared the results to the predictions of Bromley.[94] In general the agreement was poor. Photography of the test piece during film boiling showed that the liquid/vapour interface was highly irregular. This turbulence at the interface was associated with heat transfer coefficients two or three times that predicted and Reynolds numbers of above 2000.

As a result Hsu and Westwater[97] presented a model for saturated film boiling on a vertical surface which took into account the presence of a turbulent vapour/liquid interface, (see figure 16). It was assumed that a laminar vapour layer existed at short distances from the leading edge only. At a certain critical height and thickness the interface became turbulent and, as height increased, the thickness of the turbulent zone increased and the thickness of the laminar layer of vapour beneath decreased. Heat transfer in the lower, laminar portion of the film was assumed to be as predicted by Bromley.[94] The Prandtl-Nikuradse universal velocity profile was used to determine the critical Reynolds number for transition from laminar to turbulent flow, (which was found to be 100). A force balance on the turbulent zone was performed, together with a heat balance, to

give the conduction heat transfer coefficient across the laminar layer. The turbulent interface was assumed to have no effect on the heat transfer from the surface. This method gave an accuracy of ±32% when compared to experimental data.

Berenson[98] examined saturated film boiling from a horizontal surface in the light of Taylor-Helmhotz hydrodynamic instability. Taylor[99] studied an accelerated interface between two fluids and, supported by experimental work, (Lewis[100]), concluded that when an interface containing an initial disturbance was accelerated perpendicularly from the direction of the lighter fluid to the heavier one then the disturbance would grow exponentially to become unstable. This was precisely the case in film boiling on a horizontal surface where the lighter fluid, (vapour), lay beneath the heavier fluid, (liquid), and the interface was accelerated perpendicularly by gravity. It was accepted that heat transfer from horizontal surfaces was controlled by bubble release as the vapour at a particular point in the interface formed a bubble which then departed. The pattern and periodicity of this bubble release had a regular appearance and Berenson[98] proposed that it was governed by hydrodynamic instability. While the interface would contain oscillations of many different wavelengths, all with greater or lesser potentials for growth, the instability which controlled the rate of bubble release was assumed to be governed by one wavelength which gave the maximum rate of interface growth. In n-pentane it was shown that all disturbances with wavelengths greater than 1.55 mm would create an unstable interface. However, the disturbance which controlled film boiling heat transfer was given by that wavelength which maximised the

term that controlled the growth rate of the interface, b. This was shown to have a wavelength of approximately 2.7 mm, (see figure 17). An equation predicting the surface heat flux was proposed on this basis. The results agreed with experimental data to ±10% but it was pointed out that this analysis was only correct for the region of film boiling just above the minimum film boiling point as increasing the surface temperature decreased the value of the dominant or "most dangerous" wavelength which controlled the periodicity of the interface.

The effect of subcooling on film boiling was examined by Tachibana and Fukui[101] who proposed an integral profile method in their model. Their experimental work demonstrated that increasing the subcooling of the bulk liquid increased the film boiling heat transfer coefficient. Nishikawa et alia[102] carried out similar experiments and concluded that the interval between bubble release during film boiling on small diameter horizontal wires was smaller than that suggested by Taylor Instability theory and that the heat transfer coefficient increased as the wire diameter increased.

Coury and Dukler[103] proposed a model which included the effect of the turbulent interface on film boiling heat transfer from a vertical surface. Photography revealed that the interface contained two types of motion - small ripples passing upwards in the direction of the vapour flow and large, low frequency fluctuations in the vapour film thickness created by waves. A diagram showing their model is given in figure 18. This model therefore incorporated a pressure gradient which existed inside the vapour layer as a result of the behaviour of the interface.

Their experimental results revealed small surface temperature fluctuations, (0.5 to 1.5°C), but large variations in the surface heat flux, varying from +450% to -120% of the mean value. That is, the surface heat flux occasionally declined to below the rate of heat transfer from the interior to the surface of the specimen resulting in a net increase in the surface temperature. These effects were correlated with the behaviour of the large scale wave formations. Though this model predicted film boiling heat transfer, (both saturated and subcooled), with an accuracy no better than previous models it was concluded that the behaviour of the interface controlled the calculation of heat transfer to an extent that had been previously ignored.

Greitzer and Abernathy[104] presented a model for free convection saturated film boiling on a vertical surface, (see figure 19), in which it was assumed that the majority of heat transfer took place in that region of the vapour film that was thinnest and which lay between two vapour protusions. These protusions acted as reservoirs for the vapour created at the thinnest regions. This model therefore assumed no turbulence. A good agreement with experimental results was claimed for the theory for free convection film boiling for both saturated and subcooled liquids but the maximum subcooling for which comparison was made was only 22°C. More importantly it was noted that the film boiling heat transfer coefficient measured experimentally was apparently affected by surface condition. It was dependent on the temperature at which the test piece was cleaned and, once cleaned, on the length of time elapsed since the first test. This therefore must cast doubt on the results obtained since this

suggested that some surface contact occurred during the test and that the entire surface of the specimen was not therefore in film boiling.

Dhir and Lienhard[105] examined Taylor Instability in horizontal film boiling in a viscous liquid, (cyclohexane), and concluded that increasing viscosity damped the disturbances in the interface to increase the size of the "most dangerous" wavelength but this data was not applied to calculate the heat transfer rate.

Up to this point in time most film boiling data had been obtained for either saturated liquids or for cases of only small amounts of subcooling. To correct this Ede and Siviour[106] obtained data for film boiling heat flux for water and ethanol from horizontal cylinders of varying dimensions, (3, 6 and 13 mm), at three surface temperatures over a wide range of subcooling, (up to 80^{o}C). The results indicated that as subcooling increased the heat flux rose; as the cylinder diameter increased the heat flux decreased; and as the surface temperature rose, the heat flux increased.

These results were in contradiction to the results of Tachibana and Fukui,[101] (figure 20), who suggested that as subcooling increased the nature of the relationship between the heat transfer coefficient and temperature changed. At zero or low degrees of subcooling their results suggested that heat flux increased with increased surface temperature, (this agreed with Ede and Siviour[106]), but at high degrees of subcooling this trend was apparently reversed and the heat flux decreased as surface temperature increased. However the results of Ede and Siviour[106]

showed that the minimum film boiling point increased as the degree of liquid subcooling increased and it would appear that Tachibana and Fukui[101] failed to take this into account and unwittingly included portions of the transition boiling curve in their results in the case of large degrees of subcooling.

The results of Ede and Siviour[106] showed that the relationship between heat flux and subcooling was of an approximately linear form in both liquids, (see figure 21). As an example of their results the surface heat transfer coefficient at a surface temperature of 878°C with a 6 mm cylinder in water at 20°C was approximately 525 $W.m^{-2}.K^{-1}$. It was also reported that with an increase in subcooling the interfacial oscillations were damped down and the rate of bubble release from the top of the cylinder reduced. It was reported that a point was reached in water where the degree of subcooling was such that the release of bubbles ceased and the vapour/liquid interface became completely smooth.

Finally Seki et alia[107] studied film boiling heat transfer from a circular plate facing both upwards and downwards in a refrigerant, (R-11). The film boiling surface heat transfer coefficient for the upward facing side was found to be several times that of the downward facing side.

4.2 Film Boiling Heat Transfer By Boundary Layer Theory

Two methods of predicting fiim boiling heat transfer by boundary layer theory have been widely used - a similarity transformation where velocity profiles in the boundary layers are assumed to be similar with increasing distance from the leading

edge and the integral method where the velocity profile in the boundary layers is assumed by the use of a polynomial relationship between velocity and distance from the wall.

The first boundary layer treatment of film boiling heat transfer was performed by McFadden and Grosh[108] who used a similarity transformation to treat saturated film boiling on a vertical isothermal surface and a horizontal cylinder. Film boiling in this model, (and indeed all similarity transformation models), was considered as two contiguous laminar layers - one consisting of vapour, the other of liquid. The temperature of the interface was assumed to be that of the saturated liquid. The velocity of the liquid, and therefore of the vapour/liquid interface, was assumed to be zero.

The starting point of the similarity transformation models were the laws of conservation of mass, momentum and energy for both fluids. In this instance the physical properties of the fluids, viscosity and thermal conductivity, were assumed to be constant across the layer but the specific heat capacity and density were varied. The former properties were assumed to change negligibly with temperature across the boundary layer. It was also assumed that all of the heat conducted through the interface was used to vapourise liquid.

A stream function was defined which satisfied the law of conservation of mass. Similarity variables for both the vapour and liquid layers were defined and the insertion of these into the equations for the conservation of energy and momentum produced two sets of ordinary differential equations, one for the vapour layer and one for the liquid layer. The boundary

conditions were treated in the same manner to produce a two point boundary value problem which could be solved by numerical integration techniques. Since a detailed treatment of this model is relevant to the work in this thesis this procedure will be presented in more detail when the Cess and Sparrow[109] model is discussed below.

The model of McFadden and Grosh[108] was used to compare calculations with and without the use of variable physical properties and to determine the effects of pressure on the film boiling surface heat transfer coefficient for a vertical surface. It was concluded that it was necessary to include variable physical properties in the prediction of film boiling heat transfer only when the pressure was high, but no comparison with experimental data was made.

By contrast Tachibana and Fukui[101] presented an integral profile method of determining the heat transfer in subcooled film boiling. In this type of analysis one boundary layer was assumed to exist which contained the vapour film and which reached far enough into the liquid to obey the criterion that the velocity of the liquid at infinity should be negligible, (see figure 22). The problem with this type of analysis is the requirement for an accurate velocity profile. In this model liquid and vapour velocities were assumed to be determined by;

$$u_v = 4U\left(\frac{Y}{\delta_v} - \frac{Y^3}{\delta_v^3}\right) + \frac{u_s Y}{\delta_v}$$

$$u_L = u_s\left(\frac{1-3Y' + 1\,Y'^3}{2\delta_L\ 2\ \delta_L^3}\right)$$

where u_v = velocity of the vapour

U = the maximum velocity of the vapour when the liquid/vapour interface is stationary

Y = the distance from the wall

δ_v = the thickness of the vapour film

u_s = the velocity of the liquid/vapour interface

u_L = the velocity of the liquid

δ_L = the thickness of the liquid layer

Y' = the distance from the interface

The authors compared the predictions of this model with experimental data but were obliged to multiply the latter by a factor of 0.75 to obtain reasonable agreement.

Koh[110] performed a similarity transformation in the case of saturated laminar film boiling on a vertical surface with fixed physical properties. It was assumed that the interface was not stationary but travelled upwards and the continuity of mass transfer, velocity and shear stress was therefore related at the interface. Since the liquid was saturated no heat transfer in the liquid layer was considered; all the heat conducted through the vapour was assumed to vapourise liquid. This model was therefore less complex than the model of McFadden and Grosh[108] in that fixed physical properties were used allowing a simplification of the mathematical treatment of the boundary layer equations. Also, since the continuity of velocity and shear stress at the interface was taken into account this rendered the model closer to the observed process of film boiling, (ie, a moving vapour/liquid interface). No comparison was made with

experimentally derived data though it was claimed that the laminar film boiling problem had been "solved exactly".

Cess and Sparrow[109] addressed the case of subcooled film boiling from a vertical surface using a similarity transformation. As with previous similarity transformation models the vapour film was assumed to behave as one boundary layer while the bulk liquid was assumed to behave as another, (see figure 23). Since the liquid was subcooled heat and mass transfer across the interface and in the liquid layer were considered but the interface velocity, and therefore shear stress, were assumed to be zero. The analysis began with the statement of the steady state equations of conservation of mass, momentum and energy for an incompressible fluid for both vapour and liquid. These are, for the vapour, respectively;

$$\frac{\partial u}{\partial x} + \frac{\partial v}{\partial y} = 0$$

$$u\frac{\partial u}{\partial x} + v\frac{\partial u}{\partial y} = \frac{g(\rho_L - \rho_v)}{\rho_v} + \nu_v\frac{\partial^2 u}{\partial y^2}$$

$$u\frac{\partial T}{\partial x} + v\frac{\partial T}{\partial y} = \left(\frac{\lambda}{\rho C_p}\right)_v \frac{\partial^2 T}{\partial y^2}$$

and for the liquid;

$$\frac{\partial u}{\partial x} + \frac{\partial v}{\partial y} = 0$$

$$u\frac{\partial u}{\partial x} + v\frac{\partial u}{\partial y} = g\beta_L(T - T_\infty) + \nu_L\frac{\partial^2 u}{\partial y^2}$$

$$u\frac{\partial T}{\partial x} + v\frac{\partial T}{\partial y} = \left(\frac{\lambda}{\rho C_p}\right)_L \frac{\partial^2 T}{\partial y^2}$$

The term $g(\rho_L - \rho_v)$ described buoyancy in the vapour layer while convection in the liquid layer was described by $g\beta_L(T-T_\infty)$. The physical properties of the fluids were assumed to be constant across the boundary layers and, where required, were evaluated at the mean temperature of the layer. The term for viscous dissipation was omitted from the conservation equations under the assumption that it would be negligible at the low velocities considered. This is usual in this type of analysis.

A stream function, ψ, was defined such that;

$$u = \frac{\partial \psi}{\partial y}$$

$$v = -\frac{\partial \psi}{\partial x}$$

Inserting these expressions into the conservation equations eliminated the equation for the continuity of mass. Inserting the stream function into the equation of continuity of momentum in the vapour layer produced;

$$\frac{\partial \psi}{\partial y}\frac{\partial^2 \psi}{\partial x \partial y} - \frac{\partial \psi}{\partial x}\frac{\partial^2 \psi}{\partial y^2} = \frac{g(\rho_L - \rho_v)}{\rho_v} + \nu_v \frac{\partial^3 \psi}{\partial y^3}$$

Inserting the stream function into the equation for the continuity of energy in the vapour layer produced;

$$\frac{\partial\psi}{\partial y}\frac{\partial T}{\partial x} - \frac{\partial\psi}{\partial x}\frac{\partial T}{\partial y} = \left(\frac{\lambda}{\rho C_p}\right)_v \frac{\partial^3 T}{\partial y^2}$$

Performing the same process for the conservation equations in the liquid layer also eliminated the equation for the conservation of mass and produced similar equations to those given above in the case of the vapour layer.

The original solution of the boundary layer problem by this method was due to Blasius, (for example, see reference 111). In the problem considered by Blasius, (forced convection on a flat plate), a similarity variable, ϕ, was defined such that;

$$\frac{u}{u_\infty} = \phi\,\frac{y}{\delta}$$

and, therefore, from the assumption that the boundary layer thickness was approximated by $\delta \simeq x^{1/4}$;

$$\frac{u}{u_\infty} = \phi\,\frac{y}{x^{1/4}}$$

This states that the velocity, expressed non-dimensionally as u/u_∞ is equal to the boundary layer thickness, (also expressed non-dimensionally as $y/x^{1/4}$), multiplied by some constant. Thus, as the distance from the leading edge increased and the boundary layer thickness increased the dimensionless velocity at any one point in the boundary layer remained constant and therefore the velocity profile in the boundary layer remained unchanged.

By analogy, Cess and Sparrow[109] defined similarity variables for film boiling as follows;

$$\eta_v = c_v \frac{y}{x^{1/4}}$$

where c_v = the constant of similarity in the vapour layer

$$= \left(\frac{g(\rho_L - \rho_v)}{4\nu_v^2 \rho_v} \right)^{1/4}$$

Finally the dimensionless stream function was defined as;

$$f_v(\eta) = \frac{\psi_v}{4\nu_v c_v x^{3/4}}$$

and the dimensionless temperature was defined as;

$$\theta_v(\eta_v) = \frac{T - T_{sat}}{T_w - T_{sat}}$$

Using these variables the equations relating to the vapour layer were reduced to;

$$f_v''' + 3f_v f_v'' - 2(f_v')^2 + 1 = 0$$

$$\theta_v'' + 3Pr_v f_v \theta_v' = 0$$

The primes indicate differentiation with respect to dimensionless distance, η. Carrying out a similar exercise for the liquid layer equations gave the following ordinary differential equations;

$$f_L''' + 3f_L f_L'' - 2(f_L')^2 + \theta_L = 0$$

$$\theta_L'' + 3Pr_L f_L \theta_L' = 0$$

Treating the boundary conditions in the same manner gave;

at the wall; $f_v(0) = f_v'(0) = 0$; $\theta_v(0) = 1$

at the interface; $f_v'(\eta_v) = 0$; $\theta_v(\eta_v) = 0$; $f_L'(0) = 0$; $\theta_L(0) = 1$

at infinity; $f_L'(\infty) = 0$; $\theta_L(\infty) = 0$

In addition the requirement of continuity of mass and heat transfer at the interface was introduced. Since the bulk liquid was subcooled the heat transferred across the interface not only vapourised liquid but also raised the temperature of the bulk liquid.

The ordinary differential equations thus derived were capable of solution using numerical integration techniques using the boundary conditions stated. The development of the Cess and Sparrow model[109] has been presented in some detail as an example of the method of the similarity transformation on which many of the film boiling models were based.

The next development was performed by Nishikawa and Ito,[112] who used the same boundary layer equations as Cess and Sparrow[109] but used the interface conditions of Koh,[110] to derive a model for subcooled film boiling on an isothermal vertical surface in which the mass transfer, velocity, shear stress and heat transfer were matched across the interface. That is, the liquid/vapour interface was assumed to move upwards but at an unknown velocity. A relationship applicable to horizontal cylinders was also derived. No comparison between predicted and experimentally determined values for heat transfer was made.

Yue and Weber[113] applied two phase boundary layer theory to the film boiling of a saturated binary mixture of two organic liquids on a vertical surface. This required diffusion in the liquid layer to be included in the analysis and this was derived from the law of conservation of the diffusion of species. Whereas the vapour layer equations were the same as for the Cess and Sparrow[109] analysis the ordinary differential equations for the liquid layer became;

$$f_L''' + 3f_L f_L'' - 2(f_L')^2 + \theta_L = 0$$

$$\theta_L'' + 3Pr_L f_L \theta_L' = 0$$

$$\xi_L'' + 3Sc_L f_L \xi_L' = 0$$

where ξ = dimensionless concentration

Sc = the Schmidt number

The interface temperature was not known a priori and had to be determined as a consequence of the liquid composition as described by the last equation above. Very good agreement was obtained with experimental data.

Nishikawa, Ito and Matsumoto[114] extended the analysis of subcooled film boiling to account for the variation of physical properties across the boundary layers. Whereas McFadden and Grosh[108] varied density and specific heat capacity only this model[114] varied the thermal conductivity and viscosity also. This model showed, as McFadden and Grosh[108] concluded, that the effect of varying physical properties was important at high pressures. Nishikawa et alia[114] noted that the difference between analyses

with constant and varying physical properties increased as pressure increased but their results also showed that the difference increased as wall superheat increased, (see figure 24).

A new method of solving the boundary layer equations for film boiling was presented by Farahat and Madbouly[115] who used an explicit finite difference technique to model saturated film boiling heat transfer for a downward facing flat plate. Unfortunately very poor agreement with experimental data was obtained.

Marschall and Moresco[116] also performed an analysis of film boiling of binary liquid mixtures but felt it unneccessary to include the energy equation in the liquid layer, thus simplifying the matter considerably. The value of this approach over that adopted by Yue and Weber[113], (who included the liquid energy equation), was difficult to assess since Marschall and Moresco[116] produced no experimental data for comparison, although reference to the performance of experimental work was made. Since no justification for the absence of a comparison between predicted and experimental results was made the method used by Yue and Weber[113] in the case of film boiling in binary liquids might appear prefarable.

Though Nishikawa, with co-workers,[112 114] initially used a similarity transformation for the analysis of free convection film boiling this approach was later abandoned. In the case of forced convection film boiling on a horizontal cylinder Nishikawa et alia[117 118] used an integral method. However, a similarity transformation has been performed to produce the ordinary

differential equations for forced convection film boiling[93] though they have not been used to calculate heat transfer.

Finally, the most recent analysis at the time of writing, (1989), was performed by Nakayama and Koyama[119] who used an integral method to model film boiling heat transfer from elliptical cylinders.

4.3 The Vapour Transport Stage

As noted above the vapour transport stage may be subdivided into two stages, namely, transition and nucleate boiling. The point of incipient nucleate boiling separates the nucleate boiling stage and the convective cooling stage and is approximately equal to the boiling point of the liquid. Nucleate boiling refers to the heat transfer processes which occur at temperatures above convective cooling and up to the point of maximum heat flux while after this and up to the minimum film boiling point is referred to as transition boiling.

Despite the title of the review by Jordan[91] - "Film and Transition Boiling", the minimum film boiling point was hardly discussed. Berensons' work[98] on the film boiling heat flux close to the minimum point was reiterated and some experimental data for organic liquids reported.

Winterton,[89] in his review of transition boiling, reviewed two models for the minimum film boiling point. The Taylor Instability model described the minimum film boiling heat flux as that heat flux at which the rate of release of bubbles, controlled by Taylor Instability, is such that the vapour film can not be

supported. Taylor Instability at the minimum film boiling point was first applied by Zuber[120] who proposed;

$$\frac{q}{A} = \frac{\pi}{24} x\rho_v \left(\frac{\gamma g(\rho_L-\rho_v)}{(\rho_L+\rho_v)^2}\right)^{1/4}$$

The homogeneous nucleation model related the temperature of the minimum film boiling point to that surface temperature at which the liquid temperature was sufficiently high for vapour embryos to nucleate homogeneously in the liquid and therefore create a continuous vapour phase. The theory of homogeneous nucleation led to a simple relationship between the temperature of the minimum point and the thermodynamic critical temperature of the liquid;

$$T_{mfb} = 0.9\ T_c$$

This, however, gave the temperature of the liquid rather than the surface temperature. The latter must be obtained, from a knowledge of the liquid temperature, using Berensons[98] work;

$$\frac{T_{mfb}-T_B}{T_B-T_b} = 0.42\left(\left(\frac{\lambda_L\rho_L C_{pL}}{\lambda_w\rho_w C_{pw}}\right)^{1/2} \frac{1}{C_{pw}\Delta T_B}\right)^{0.6}$$

where T_{mfb} = temperature of the minimum film boiling point

T_B = minimum film boiling point predicted by Berenson[98]

T_b = bulk liquid temperature

$\Delta T_B = T_{mfb} - T_B$

A new approach to the determination of the minimum film

boiling point was proposed by Segev and Bankoff[121] who suggested that, if the surface temperature were sufficiently low, a thin layer of non-evaporating liquid would be adsorbed onto the metal surface. This adsorbed layer would act as a precursor to the spreading liquid behind and promote the wetting of the surface. This theory might therefore describe the processes that operate at the edge of a vapour blanket as it retreated across a cooling surface. The temperature of the minimum film boiling point was given by;

$$T_{mfb} = \frac{T_w + \beta T_L}{1 + \beta}$$

$$\text{where } \beta = \left(\frac{(\lambda \rho C_p)_L}{(\lambda \rho C_p)_w} \right)^{1/2}$$

The implication of this theory for quenching is that since the surface physical properties are involved in the expression liquids do not have one set minimum film boiling point. This may be considered confirmation of the work of Sato,[122] Cowley[123] and Moreaux et alia[124] who demonstrated that the film boiling stage may be broken down by coating a metal surface with a low thermal conductivity material.

Yue and Weber[125] explored the minimum film boiling heat flux for binary mixtures but confined their investigation to volatile organic liquids.

Transition boiling has been thoroughly reviewed by Winterton[89] who characterised it as that portion of the boiling curve in

which heat flux declined with increased surface temperature, (see figure 15). Heat transfer during transition boiling has been described by empirical or semi-empirical relationships produced by the nuclear engineering industry to whom this process has been of great interest.

Much debate has centred around the possibility of liquid contact during this stage. One of the earliest photographic studies, by Westwater and Santangelo,[126] suggested that no surface contact occurred. Berenson[127] disputed this and produced boiling curves in which the transition boiling stage was clearly affected by surface conditions which indicated surface contact. Berenson[127] carried out experiments on the pool boiling heat transfer of n-pentane and concluded that the transition boiling heat flux, when plotted on log-log graph paper, lay on a straight line connecting the minimum film boiling point to the critical heat flux, (for example see figure 25). The mechanism of transition boiling was explained as a combination of unstable nucleate boiling and unstable film boiling as follows. The surface temperature during this stage was sufficiently high for large amounts of vapour to be generated. The volume of vapour was too great to be carried away by processes which occurred during nucleate boiling so that a vapour film temporarily formed. However the surface temperature was not sufficiently high to produce sufficient vapour generation at the interface to maintain the vapour film and it collapsed. The surface was rewetted and the process repeated. Therefore at any point on the surface nucleate boiling and film boiling replaced each other alternately.

This approach has recently been confirmed by two studies of the amount of liquid/solid contact that occurred during transition boiling. Dhuga and Winterton[128] measured the impedance between a metal probe and the boiling liquid and concluded that the surface was alternately subject to nucleate and film boiling and that the fraction of film boiling that occurred increased as surface temperature rose toward the minimum film boiling point.

Lee et alia[129] reached the same conclusion using surface mounted thermocouples and showed that the liquid/solid contacts occurred at very high frequencies. The frequency of liquid contact was a maximum at about 50 s^{-1} and decreased to about 30 s^{-1} as the critical heat flux was approached. The duration of the contacts was of the order of about 4 ms and decreased as surface temperature increased. These results can however indicate either the rapid reformation and dispersal of the vapour blanket or the formation and liberation of the fine bubbles by which transition boiling is characterised. The authors suggested that repeated liquid/solid contacts may be the dominant energy transfer mechanism in this stage.

The critical heat flux has been recently reviewed by Katto.[130] This review revealed that the majority of work on this phenomenom has been carried out with nuclear reactors in mind as most of the work reviewed related to forced convection flows in specific geometries and the prediction of the critical heat flux by empirical means. This phenomenom represents the limit of nucleate boiling and is characterised by a certain bubble shape, (see figure 26). During nucleate boiling bubbles form at nucleation

sites on the metal surface and are released into the bulk liquid. The frequency of bubble nucleation and release during this stage increased with increasing surface temperature until the bubbles coalesced to form a stem of vapour. At a certain height above the surface the vapour stems coalesced to form a larger bubble adjacent to the metal surface.

Zuber[120] also dealt with the critical heat flux as well as the minimum film boiling point in terms of hydrodynamic instability.

Berenson[127] claimed that his results showed that the value of the critical heat flux was constant for a particular liquid. This was consistent with the Zuber[120] theory where the maximum heat flux was limited by hydrodynamic considerations which were independent of surface conditions. Berensons data[127] showed a constant value of the critical heat flux to within ±10%, a level which was considered to be approximately the limits of accuracy for the apparatus. The surface temperature at which it occurred varied according to surface condition. This trend was not confirmed by other workers who gave marked deviations in the value of the critical heat flux but it was noted that these results consistently gave values that were less than those predicted by Zuber.[120] Berenson[127] pointed out that the results of other workers were taken from experiments where the average critical heat flux was measured, (ie, from the total surface area of the specimen). It was proposed that due to local variations in conditions the true local critical heat flux values occurred at different surface temperatures at different points on the specimen which were then averaged to give an apparently low value

of the critical heat flux that was subject to considerable variation.

The nucleate boiling portion of the boiling curve has recently been the subject of sevaral reviews.[89] [131] [132] [133] Work has concentrated on two areas - the study of the nucleation and growth of a bubble and the characterisation of nucleation sites on the boiling surface.

The problem of interest in nucleate boiling is that of heterogeneous nucleation from a cavity. The cavity has generally been assumed to have been filled by a gas or vapour phase, possibly left behind by a departing bubble. Theory and experimental evidence have shown that nucleation was most favoured by a vapour filled cavity. Nucleation was therefore shown to be dependent on the contact angle of the liquid and the angle of the cavity, (termed wedge angle, see figure 27). If an advancing liquid has a contact angle greater than the wedge angle then the liquid front will strike the far wall of the cavity before it reaches the bottom. That is, not all of the vapour will be displaced from the cavity but some will be entrapped to act as a nucleus to form a new bubble. If the contact angle is less than the wedge angle then the vapour will be displaced. In a similar fashion an advancing gas/liquid interface may or may not sweep liquid from a cavity depending on the contact angle of the liquid and the geometry of the cavity. Well wetted cavities which trap liquid were shown to be poor nucleation sites.

It was then possible to calculate the heat transfer for a growing single bubble which emerged from a cavity into a liquid

thermal layer of known temperature distribution and reached a critical radius corresponding to its maximum curvature. The nucleation ability of a surface was shown to be characterised by a single dimension which described the cavity size; the size of the cavities being normally distributed on a surface. However, the application of the heat transfer calculations for a single bubble to the prediction of nucleate boiling heat transfer from a surface would require a knowledge of the number of nucleation sites active at any one time and their mean radius and size distribution.

This problem would be complicated by the probability that nucleation sites are not stable. Once a bubble departs from a cavity cold liquid would rewet the surface and penetrate the cavity. Some condensation of the vapour inside the cavity would occur. If the condensation of the vapour inside the cavity was complete then the cavity would have changed from a poorly wetted favourable nucleation site to a fully wetted unfavourable site.

Nucleate boiling is the most complicated stage in boiling heat transfer and presents considerable difficulties in modelling as outlined above. At a period of time when it is not possible to say that even a stable process such as film boiling can be modelled successfully it is not surprising that, while certain characteristics of nucleate boiling have been investigated and understood, much work remains to be performed.

5.0 EXPERIMENTAL PROCEDURE

5.1 Quenching And Related Experimental Procedures

The relationships between time and temperature and surface heat transfer coefficient were determined during the quenching of a stainless steel plate into aqueous solutions of various concentrations of sodium polyacrylate. Simultaneously still and cine photography of the surface of the cooling plate was carried out. The surface heat transfer coefficients thus obtained were used to predict the generation of thermal stress and strain in plates of a low alloy steel. The residual stress and strain present in plates of this material quenched in a range of sodium polyacrylate solutions was also measured.

5.1.1 The Determination Of The Surface Heat Transfer Coefficient

The procedure for the determination of the surface heat transfer coefficient during quenching in solutions of sodium polyacrylate was the same as that described by Price and Fletcher[64] and is outlined below.

The specimen used was a plate of grade 316 stainless steel of dimensions 120 mm x 120 mm x 20 mm. The chemical composition and physical properties of the material are given in table 2. Manipulation of the plate was performed by a handle, 12 mm in diameter, which was welded into a shallow hole at the centre of one edge of the plate. This edge of the plate therefore became the top of the specimen while it was in the quenching tank. Three thermocouple holes, 1.5 mm in diameter and 60 mm deep were spark

eroded at points on the upper edge of the plate. Figure 28 shows the construction of the plate and the arrangement of the thermocouples. The axes of the three spark eroded holes lay in one line across the thickness of the plate and as close to the centre of the upper edge of the plate section as the presence of the handle would allow. The middle one of the three thermocouples lay on the central axis of the upper edge of the plate which ran parallel to the two faces of the plate. The other two thermocouples lay at an equal distance either side of the middle thermocouple and their axes were positioned at a depth of 1.5 mm from either face.

The quenching tank had dimensions 894 mm x 246 mm and was filled to a depth of 300 mm with solutions of 5,10,15,20 and 25% Aquaquench ACR in water. Aquaquench ACR is a concentrated solution of sodium polyacrylate containing proprietary rust inhibitors produced by Edgar Vaughan UK. The concentration of the bath was checked periodically by the determination of the kinematic viscosity of the contents; adjustments being made to maintain the concentration to within 7.5% of that required. Before each quench the tank was thoroughly stirred to ensure homogeneity of composition and temperature. The required temperature of the bulk quenchant was $20^{o}C \pm 2^{o}$, which was maintained throughout the quench.

Prior to heat treatment the plate was shot blasted to remove any surface oxide remaining from the previous quench and then abraded with 400 grade paper in a circular motion to establish a reproducible surface finish.

The thermocouples were inserted and then connected to an Orion

Datalogger capable of recording each thermocouple temperature at time intervals of a minimum of 0.1s. A fourth thermocouple was suspended in the quenching tank to monitor the quenchant temperature.

The plate was placed in a muffle furnace at 860^{o}C until the central thermocouple recorded that temperature - a process that took some 35-40 minutes. In order to preserve the surface from excessive oxidation an argon atmosphere was supplied to the furnace at a pressure of 0.1 bar.

Upon reaching 860^{o}C the plate was removed from the furnace and suspended over the tank for the short period of time necessary for one of the thermocouples to record a temperature of 850^{o}C whereupon the plate was immersed in the tank. This ensured a constant and reproducible initial condition for each quench. The position and depth of immersion was controlled by the presence of guide rails with slots within which the plate handle rested. After immersion the upper edge of the plate was 65 mm from the surface of the bath.

The Orion Datalogger recorded the temperature of each thermocouple with a variety of frequencies depending upon requirements. Ideally an interval between measurements of 2 s was required during film boiling, 0.1 s during the first part of the vapour transport stage and 5 s during the final stages of the quench. This maximised the efficiency with which the data was collected and enabled this data to be used to determine the surface heat transfer coefficient directly rather than by using information obtained by interpolation from more widely spaced data.

The effects of agitation were determined using two rotors at a speed of 400 ±10 rpm. These were positioned either side of the plate at a distance of 24 cm and operated at a depth of 18 cm. When in use the rotors were set to sweep liquid against both faces of the plate in the same direction.

For each concentration at least three quenches were carried out in a still bath and one quench, at least, but generally two, was carried out in an agitated bath. A total of 30 quenches were performed for the purpose of determining the surface heat transfer coefficients in the five concentrations examined.

5.1.2 Photography Of The Plate Surface During Quenching

Photography of the plate surface required the plate to be positioned closer to the side of the tank, (at a distance of 13.5 cm), but in all other respects the procedure was identical to that described above.

Still photography was carried out using a 35mm Nikon f3 with motor drive fitted with a 55mm f3.5 micro-Nikkor lens at f8. The film used was a Kodak Tri-X negative, rated at 200 ASA and was processed in Microsol-X. Lighting was provided by two flash guns positioned to the left and right of the visible face of the plate and at the same level and were at an angle of approximately 45^{o} to an axis between the camera and the centre of the plate face. The flashes were controlled by a computer setting on 200 ASA at f8.

The cine film was made using a Beaulieu R16 with a 25mm, f1.4, Cine-Xenon lens. The film used was a Kodak 4X negative rated at

400 ASA, frames being taken at 64 per second at f11-16. Two floodlights were used to light the surface of the plate.

5.1.3 Quenching Procedure For The Determination Of Residual Stress And Strain

The experimental determination of residual stress and strain was carried out using a low alloy steel plate, (835M30), of the same dimensions as the plate used for the determination of the surface heat transfer coefficients. The composition and physical properties of the low alloy steel are given in table 3. Manipulation was also performed using a 12 mm diameter handle but this was attached using a screw-thread so that the handle could be removed to allow the measurement of the residual stress and strain.

The plate was plated with nickel to reduce the oxidation of the surface by the following heat treatments. The thickness of the nickel plating varied in response to conditions but did not exceed 50 microns which represented 0.5% of the total thickness of the plate section. After plating the plate surfaces were abraded with 400 grade paper in a manner similar to that applied to the stainless steel plate in order to duplicate the surface conditions under which the surface heat transfer coefficients were determined.

The plate was stress relieved at 630^{o}C for 2 hours and then allowed to cool to ambient temperature within the furnace; this operation took place under an atmosphere of argon supplied to the furnace at a pressure of 0.1 bar.

Before quenching the plate was austenitised for 1.5 hours at 850°C. In all but the first two tests the edges of the stress relieved plate were covered with a 10 mm layer of "Kaowool" which was kept in position by a metal strip. The insulating "Kaowool" ensured that the majority of the heat transfer occurred through the plate faces and therefore simulated an infinite plate condition.

Two plates were quenched, without an insulating layer, in solutions of 15% and 25% Aquaquench ACR respectively. A further six low alloy steel plates, with an insulating layer at the edge, were quenched; two each in solutions of 5%, 15% and 25% Aquaquench ACR respectively.

5.1.4 Experimental Determination Of Residual Strain

To allow the stress relieved plate to acclimatise it was allowed to stand in the metrology laboratory, a temperature and humidity controlled room, for 24 hours. The breadth, length and thickness of the plate were then measured at the points indicated in figure 29 using a Ferranti Merlin 750 Accurate Measuring System. The accuracy of this apparatus was estimated at ±5 microns.

After quenching the plate was again allowed to acclimatise for 24 hours in the laboratory before it was remeasured at the same points. This provided a measure of the longitudinal residual strain at depths of 1 mm, 4.5 mm, 10 mm, 14.5 mm and 19 mm below the plate surface and also the lateral residual strain at the centre of the plate face.

To compare the experimentally determined strains obtained by measurements of the plate length with those obtained by calculation it was necessary to multiply the former by a factor to correct for the effect of the free edge. A factor of 1.2, derived from Saint-Venant's Principle, was applied. This assumed that the effect of the free edge was such that the stress in the plane of the plate rose from zero at the edge of the plate to a value unaffected by the presence of the edge, (ie, associated with an infinite plate), within a distance of one plate thickness. It was also assumed that a linear relationship between stress and strain existed in this region.

5.1.5 Experimental Determination Of Residual Stress

In order to determine the residual stress in a quenched plate a layer removal method was employed as detailed by Fletcher and Price.[15] After the residual strain was determined a strain gauge rosette, (type FRA-6-11 manufactured by Tokyo Sokki Kenkyujo Co. Ltd.), was attached to the centre of the plate while another was attached within the recess of a cast iron supporting plate. The latter recess was filled with wax to prevent the gauges coming into contact with the cooling fluid. This assembly was then allowed to acclimatise in the laboratory for 12 hours. A diagram showing the arrangement of the 835M30 plate and the cast iron supporting plate is given in figure 30. The layer removal process used was that given by Treuting and Read[134] as modified by Andrews[135] and Price.[136] 1 mm layers were removed by a precision grinder in 15 layers of 50 microns and then 10 layers of 25

microns each. This reduced grinding stresses to negligible amounts. After a 1 mm layer had been removed the plate was allowed to rest for 15 minutes before each gauge was read four times by the Orion Datalogger. The rosette on the supporting plate recorded the zero drift induced in the gauges on the 835M30 plate by the magnetic field of the chuck. The residual stresses were calculated from an average of the four readings of the plate rosette less the average of the four readings from the central gauge of the supporting plate rosette using the method given by Price,[136] (see Appendix B).

The residual stresses determined by this method were balanced across the half section of the plate and then corrected for the effect of the free edge using the factor of 1.2 derived from Saint-Venant's Principle. (The assumptions on which this was based have been given in section 5.1.4.) Comparison with the calculated residual stresses was then possible.

5.1.6 Determination Of The Kinematic Viscosity Of The Sodium Polyacrylate Solutions

The determination of the kinematic viscosity of solutions of sodium polyacrylate was carried out using an Ostwald viscometer.[137] Solutions of 5,10,15,20 and 25% Aquaquench ACR in distilled water were tested.

The Ostwald viscometer consisted of a U-tube with two reservoirs, one on either arm, connected by a capillary tube. The viscosity of the liquid depended upon the length of time required for the liquid to flow from one reservoir through the capillary

tube into the other; the passage of the liquid meniscus from one fixed point to another was used as a reference. This procedure was repeated five times for each sample to achieve an accuracy in excess of that demanded by BS188:1977.[138] By comparing the passage time of a liquid of known kinematic viscosity, (in this case an approximately 60% glycerol solution), with the passage time of the sodium polyacrylate solution at the same temperature the kinematic viscosity of the latter at 20.2°C was obtained. The density of the glycerol solution was measured in order to obtain an accurate value for its concentration.

The apparatus constant, c, was determined from the relationship $\nu = ct$ and this allowed the kinematic viscosity of the sodium polyacrylate solutions to be determined at higher temperatures.

The solution viscosities were determined at 20.2, 40.0, 60.0 and 80.0°C for each concentration. Temperature control was exercised to ±0.2°C.

The densities of the sodium polyacrylate solutions were also determined, at the same concentrations and temperatures, using S.G. bottles. Dividing the kinematic viscosity by the density gave the dynamic viscosity.

5.1.7 The Determination Of The Surface Tension Of The Sodium Polyacrylate Solutions

The surface tension of the polymer solutions was determined using Sugden's version of Jaeger's maximum bubble pressure method.[137] Two jets, one having a large and the other a small

orifice, (1-2mm and about 0.1mm respectively), were immersed to the same depth in a solution which, in its turn, was immersed in a water bath. Air was forced through either jet to form bubbles by the use of a dropping funnel, (see diagram, figure 31). A micromanometer was used to measure the pressure required to form a bubble at either orifice. The pressure in the system was increased slowly in order to reduce the formation of bubbles to the rate of about one a second.

The diameter of the larger orifice was ascertained and the apparatus constant was then determined as a function of solution temperature against the known values of the surface tension of water. The following empirical equation was used;

$$\gamma = A(P_1-P_2)\left(1+0.69r_2\frac{\rho_L g}{(P_1-P_2)}\right)$$

where γ = surface tension

A = apparatus constant

P_1 = the pressure required to form a bubble at the smaller orifice

P_2 = the pressure required to form a bubble at the larger orifice

r_2 = the radius of the larger orifice

The surface tension of 5,10,15,20 and 25% Aquaquench ACR solutions were determined in each case at approximately 20,40,60 and 70°C, the temperature of the solution being maintained at ±0.2°C. The degree of error in the measurements was calculated to be 3% at 20°C, 5% at 40°C, 7% at 60°C and 9% at 80°C. The

measurements were performed twice using different solutions. The surface tension of the polymer quenchant was then determined at 20.0, 40.0, 60.0, and 80.0°C by interpolation from both sets of results in order to obtain values at the same temperatures as the viscosity and density measurements.

5.2 Calculation Of The Surface Heat Transfer Coefficient And The Prediction Of The Generation Of Thermal Stress And Strain During The Quenching Of A Steel Plate

The surface heat transfer coefficient during quenching was obtained from the sub-surface time/temperature relationships using a finite difference technique. This information was then used as input data to a viscoelastic-plastic model of the generation of thermal stress and strain during quenching. Accurate data for the surface heat transfer coefficient was required in order to obtain a more accurate prediction of the residual stress and strain from the model.

5.2.1 Calculation Of The Surface Heat Transfer Coefficient Of A Steel Plate During Quenching

The surface heat transfer coefficient was determined from the time and temperature relationships obtained during quenching by the use of an inverse solution to the explicit finite difference formulation of the transient heat conduction equation, as detailed by Price and Fletcher.[15] This procedure, which used a method of successive approximations, is shown by a flow diagram in figure 32.

This required a knowledge of the thermal conductivity, thermal diffusivity and specific heat capacity of the material, (grade 316 stainless steel), and their relationships with temperature.[139]

The temperature distribution and heat transfer was assumed to be symmetrical about the centre-line of the plate so the 20 mm plate was split into two half-plate sections each 10 mm thick. The surface heat transfer coefficient was calculated for each half of the plate separately from the data obtained from each of the thermocouples placed just below the surface at the approximate centre of each face. The half section was divided into 15 elements.

The data used in the calculation was a series of pairs of time and temperature values, at approximately 30 K intervals, obtained by the thermocouples referred to above.

The time step for the calculation was calculated from the following stability criterion;

$$\Delta Fo < \frac{1}{2 + \Delta Bi}$$

$$\text{where } \Delta Fo = \frac{\alpha \Delta t}{(\Delta x)^2}$$

$$\Delta Bi = \frac{h \Delta x}{\lambda}$$

The physical properties of the material involved in this criterion were evaluated to ensure stability throughout the entire temperature range of the quench; that is, the thermal

diffusivity used was the value for 900°C, the surface heat transfer coefficient was assumed to be 10 $kW.m^{-2}.K^{-1}$, (greatly in excess of the maximum calculated in the case of the sodium polyacrylate solutions), and the thermal conductivity used was the value for 20°C. However, this required the use of a very small value for the time step, Δt, (0.029 s in a 2 cm thick plate with 15 elements). This time step was so small that accurate information for the change in temperature at the thermocouple position for this increment was not obtainable. A larger time interval, $p.\Delta t$, was used such that $p.\Delta t$ represented the time interval between two measurements of temperature at the thermocouple position. The surface heat transfer coefficient was therefore assumed to be constant over the time step $p.\Delta t$ and is therefore an approximate value for the temperature range which occurred during that time.

The position of the thermocouple was then established with regard to the position of the nodes at which the temperature distribution in the plate was calculated.

The initial temperature distribution was given by;

$$\theta_1^j = \theta^i; \text{ for } j = 2,K$$

where θ = temperature of the node

and the central boundary condition was given by;

$$\theta_n^{K+1}; \text{ for } n = 1,L$$

K represented the number of nodes in the plate while L represented the number of time intervals used.

An initial estimate of the surface heat transfer coefficient

was then performed;

$$h = \frac{mC_p}{p\Delta tA} \ln\left(\frac{\theta^a - (\theta_n{}^{TC})_E}{\theta^a - (\theta_{n+p}{}^{TC})_E}\right)$$

This estimated value was then used in a forward difference solution to the transient heat conduction equation. The temperature of the first element was given by;

$$\theta_n{}^1 = \theta_n{}^3 - \frac{2h\Delta x(\theta_n{}^2 - \theta^a)}{\lambda}$$

The remaining nodal temperatures were then given by;

$$\theta_{n+1}{}^j = \theta_n{}^j + \frac{\alpha\Delta t}{(\Delta x)^2}(\theta_n{}^{j+1} - 2\theta_n{}^j + \theta_n{}^{j-1})$$

for $j = 2,K$; $n = 1,L$

This allowed estimates of $\theta_{n+1}{}^j$ to be found and gave a calculated temperature distribution in the plate which was compared to the experimentally measured thermocouple temperature, at the thermocouple position, at the relevant time. The thermocouple position did not lie on a node so it was necessary to obtain an interpolated value for its temperature from the temperatures of the nodes on either side. This was performed using Bessel's Interpolating Polynomial. The error in the two temperatures was due to the difference in the estimated surface heat transfer coefficient compared to the true surface heat transfer coefficient. This difference, Δh, was calculated by;

$$\Delta h = \frac{mC_p}{p\Delta tA}\left(\ln\left(\frac{\theta^a-(\theta_n{}^{TC})_E}{\theta^a-(\theta_{n+p}{}^{TC})}\right) - \ln\left(\frac{\theta^a-(\theta_n{}^{TC})_E}{\theta^a-(\theta_{n+p}{}^{TC})_E}\right)\right)$$

The change in surface heat transfer coefficient, Δh, was added to the previous estimated surface heat transfer coefficient and the calculation of the temperature distribution of the plate repeated. This procedure occasionally led to a diverging set of temperatures when that part of the quench was reached where rapid temperature changes occurred, (the beginning of the vapour transport stage). This led to an endless loop being formed in the computer program but when a diverging series was detected the Δh value was reduced by 1% and the temperature distribution calculation repeated until a converging series was obtained.

The calculation was repeated until the experimentally determined thermocouple temperature and the calculated thermocouple temperature lay within 1 K.

This procedure produced not only values for the surface heat transfer coefficient but also the temperature distribution throughout the plate and therefore the surface temperature to which the surface heat transfer coefficient was related.

5.2.2 The Generation Of Thermal Stress And Strain In A Steel Plate During Quenching

The calculation of the generation of thermal stress and strain during the quenching of a low alloy steel plate required a knowledge of the temperature distribution within the plate and the change in volume with change in temperature. A knowledge of the differential rates of contraction which occurred in the

presence of a temperature gradient allowed a calculation of the thermal stress and strain. Since the material was a high hardenability steel the effects of the transformation from austenite to martensite had also to be taken into account.

An accurate knowledge of both the variation of surface heat transfer coefficient with surface temperature, (obtained by the method outlined in the previous sections), and also the temperature dependence of the physical and mechanical properties of the material was required. Plane stress conditions were assumed, (see figure 33). This model also incorporated the effect of work hardening on the yield stress and creep and stress relaxation and also transformation plasticity.

The model was not fully thermo-mechanically coupled but neglected the effect of stress on the kinetics of the martensitic transformation and the effects of the evolution of heat during transformation and deformation on the temperature distribution. These effects have been shown to be very small in the case of a steel transforming to martensite, by Denis and co-workers.[74] [78] [79] A flow diagram showing the calculation procedure is given in figure 34.

The temperature distribution in the plate was calculated using a finite difference solution to Fick's Law of transient heat conduction. The half-plate was divided into 41 elements, (according to the stability criterion, $\lambda/h > \Delta x$), which gave the time step, Δt, according to the Schmidt construction parameter;

$$\frac{\lambda \Delta t}{(\Delta x)^2} < \frac{1}{2}$$

It was therefore possible to state;

$$\theta_{t+1}^{n} = \frac{\theta_{t}^{n+1} + \theta_{t}^{n-1}}{2}; \text{ for } n = 2,J$$

The surface temperature was calculated by assuming a constant temperature gradient from the surface into the bulk liquid which gave;

$$h(\theta^{\infty}-\theta_{0}^{s}) = \frac{2\lambda(\theta_{0}^{1}-\theta_{0}^{s})}{\Delta x}$$

However, only the initial surface temperature was known. For values of time greater than zero the surface temperature was approximated by making the assumption that a constant temperature gradient existed from the surface element into the bulk liquid, (Arparci's method);[53]

$$\theta_{t+1}^{1} = \left((\theta_{t}^{2}-\theta^{\infty})\left(\frac{\lambda}{h} - \frac{\Delta x}{2}\right)\right)\Big/\left(\left(\frac{\lambda}{h} + \frac{\Delta x}{2}\right)\right) + \theta^{\infty}$$

The temperature gradient at the centre of the plate was assumed to be zero.

The number of elements was reduced from the 41 required for the calculation of the temperature distribution to 10 for the calculation of the stress and strain. With the passage of a set time interval, Δt, the change in dimension of each element caused by the falling temperature and, between 300°C and 90°C, (M_s and M_f respectively), the progress of transformation from austenite to martensite, was calculated from the relationship between

temperature and dilatation obtained from a dilatometer curve. The elastic stress this dilatation caused in each element during each time interval was then determined using the assumption that each element was completely restrained;

$$\Delta\sigma_{t+1}^{n} = \frac{E\alpha(\theta_{t+1}^{n}-\theta_{t}^{n})}{1-\nu} \quad ; \text{ for } n = 2,K$$

where ν = Poissons ratio

This change in stress was then added to the value of stress obtained at the end of the previous time interval;

$$\sigma_{t+1}^{n} = \sigma_{t}^{n} + \Delta\sigma_{t+1}^{n}; \text{ for } n = 2,K$$

The values of stress thus calculated were then modified by taking into account the effects of creep and stress relaxation and transformation plasticity. The assumption of an external restraint was then replaced by the criterion that the forces created perpendicular to a transverse section through the plate were balanced, ie, there was no net force on the plate section. This was achieved by making a uniform adjustment to the values of stress in each element until the balance was obtained.

The von Mises criterion was used to determine the elements in which plastic flow has occurred. Where the stress in any element exceeded the yield stress it was corrected to the value of the yield stress. This then disturbed the value of the net force on the section of the plate and therefore the stresses of the elastic regions of the plate. The plate section was then rebalanced; the change in the force on the section of the plate

caused by the application of the yield criterion was divided by the number of elements disturbed in this way. This gave a value of stress which was used to change the values of stress in each element. The application of the von Mises criterion and the rebalancing of the plate was repeated until no values of stress were greater than the yield stress and, simultaneously, the requirement of zero net force across the transverse section of the plate was obeyed.

Since plastic deformation had occurred the yield stress was subject to work hardening. It was therefore corrected by a temperature dependent strain hardening coefficient. Two such coefficients were determined from experimental data depending upon the strain history of the material. One operated for values of plastic deformation between 0 and 0.5% while the other operated at values of plastic deformation of 0.5 to 1.0%.

The value of elastic strain calculated at the beginning of the time interval was then modified to include the changes in the elastic stress brought about by the application of the yield criterion.

The effect of strain rate on the yield stress and the work hardening coefficents had been examined experimentally but it was assumed that the effects were not sufficiently important to justify inclusion in the model and a constant strain rate was therefore assumed, (5.8×10^{-3} s^{-1}).

Viscous processes, (creep and stress relaxation), were described by the standard linear solid. For example, stress relaxation was described by;

$$\frac{\sigma}{\sigma_o} = (1-A)e^{-Bxt} + A$$

and creep was described by;

$$\xi_{creep} = \frac{\sigma_o}{E}\left(\frac{1}{A} - 1\right)(1-e^{-ABt})$$

where A and B = constants dependent upon temperature and stress

Stress relaxation was assumed not to occur below 230°C and above this temperature it was assumed that the stress relaxation parameters were independent of time though dependent on temperature. The A and B parameters of the standard linear solid model were also regarded as dependent on stress on the basis of data obtained from isothermal stress relaxation tests carried out at various temperatures. The effects of the viscous processes were included in the model after the addition of the elastic stress to the previously calculated stress and before the iteration to achieve a zero net force over the plate section.

Transformation plasticity was modelled as an additional plastic strain proportional to the amount of absolute stress greater than 40 MPa up to an upper limit of 160 MPa. 160 MPa was approximately the yield stress of austenite at M_s in this steel. This was based on experimental data;

$$\xi_{tp} = 6.25x10^{-7}(\sigma-40)(300-\theta)$$

The results indicated that transformation plasticity did not occur below a threshold stress of ±40 MPa and was confined to

between 300°C and 260°C. A linear relationship between experimental stress and transformation plasticity results produced as good a fit as more complex polynomial relationships used in an earlier work but without the problems of instability introduced by the use of the latter. The effects of transformation plasticity were included in the model after the addition of the elastic stress to the previously calculated stress and before the inclusion of the effects of creep and stress relaxation.

The values of predicted residual strain did not take into account the volume change associated with the change in structure from ferrite and pearlite to martensite which occurred during heat treatment of the low alloy steel. This has been measured as 0.127%.[136] Consequently this value was added to the predicted residual strains to ennable a comparison with the experimentally determined residual strains.

5.3 Calculation Of The Film Boiling Surface Heat Transfer Coefficient During Quenching Of A Steel Plate

Three mathematical models which adopted a similarity transformation to calculate the surface heat transfer coefficient during film boiling were examined. Each model assumed that laminar flow occurred. The first model, due to Cess and Sparrow,[109] assumed constant physical properties across the boundary layer and a stationary liquid/vapour interface. The second, Nishikawa and Ito,[112] assumed constant physical properties across the boundary layers and an interface that moved

upwards at an unknown velocity. The third, Nishikawa, Ito and Matsumoto[114] assumed temperature dependent physical properties across the boundary layers and a moving interface. All of the models assumed that film boiling was a steady state process.

These three models were evaluated for the case of film boiling during a water quench and during a 25% Aquaquench ACR quench. The surface heat transfer coefficient predicted by these models was then compared to experimentally determined values for both quenchants in order to assess the accuracy of each model. As a result a fourth model has been proposed which incorporated a turbulent interface.

5.3.1 Model Of Cess and Sparrow (1962)

Using a similarity transformation as outlined in the literature survey Cess and Sparrow[109] defined the following differential equations to describe the behaviour of the vapour and liquid during film boiling, (the primes denote differentiation with respect to dimensionless boundary layer thickness η_v or η_L). For the vapour layer;

$$f_v''' + 3f_v f_v'' - 2(f_v')^2 + 1 = 0 \; ; \quad \text{velocity equation}$$

$$\theta_v'' + 3Pr_v f_v \theta_v' = 0 \; ; \quad \text{energy equation}$$

where f = dimensionless stream function

θ = dimensionless temperature

with the following boundary conditions;

at the wall; $f_v(0) = f_v'(0) = 0$; $\theta_v(0) = 1$

at the interface; $f_v'(\eta) = 0$; $\theta_v(\eta) = 0$

and similarly for the liquid layer;

$$f_L''' + 3f_Lf_L'' - 2(f_L')^2 + \theta_L = 0 \; ; \quad \text{velocity equation}$$

$$\theta_L'' + 3Pr_Lf_L\theta_L' = 0 \; ; \quad \text{energy equation}$$

with boundary conditions;

at the interface; $f_L'(0) = 0$; $\theta_L(0) = 1$

at infinity; $f_L'(\infty) = 0$; $\theta_L(\infty) = 0$

The four differential equations, (two each for the vapour and liquid boundary layers respectively), describe the velocity and temperature profiles in both layers. The dimensionless velocity is described by f' while the dimensionless temperature is described by θ. The velocity equation for the vapour layer does not contain a dimensionless temperature term and therefore the vapour equations are said to be uncoupled - that is, the velocity and energy equations may be solved separately if required. The velocity equation for the liquid layer does, however, contain a dimensionless temperature term. The liquid layer equations are therefore coupled and must be solved simultaneously.

The boundary conditions given by Cess and Sparrow[109] state that the velocity at the wall is zero; $f_v'(0) = 0$; while the dimensionless temperature at the wall is one, ie, the wall temperature; $\theta_v(0) = 1$. The velocity at the interface is zero; $f_v'(\eta) = 0$; while the dimensionless temperature is also zero, ie, the interface temperature; $\theta_v(\eta) = 0$. The zero interfacial

velocity also gives $f_L'(0) = 0$; while the temperature of the interface, expressed non-dimensionally in terms of liquid temperature variables is 1; $\theta_L(0) = 1$. The bulk liquid is stationary; $f_L'(\infty) = 0$; while the dimensionless temperature is equal to the bulk liquid temperature; $\theta_L(\infty) = 0$.

The physical properties used in this model were calculated at the mean temperatures of the respective boundary layers. For example, if the wall temperature was 850°C, the boiling point of the quenchant 100°C and the bulk quenchant temperature 20°C then the Prandtl numbers used in the energy equations would be evaluated at 450°C in the vapour layer and 60°C in the liquid layer.

To solve these two sets of fifth order equations it was first necessary to reduce them to a set of five, first order equations.[140] For the vapour layer;

$$Y1' = f_v'$$

$$Y2' = f_v''$$

$$Y3' = f_v''' = -3f_v f_v'' + 2(f_v')^2 - 1$$

$$Y4' = \theta_v'$$

$$Y5' = -3Pr_v f_v \theta_v'$$

where $Y1 = f_v$

$Y2 = f_v'$

$Y3 = f_v''$

$Y4 = \theta_v$

$Y5 = \theta_v''$

for the liquid layer;

$$Y1' = f_L'$$

$$Y2' = f_L''$$

$$Y3' = f_L''' = -3f_L f_L'' + 2(f_L')^2 - \theta_L$$

$$Y4' = \Gamma_L'$$

$$Y5' = \theta_L'' = -3Pr_L f_L \theta_L'$$

where $Y1 = f_L$

$Y2 = f_L''$

$Y3 = f_L''$

$Y4 = \theta_L$

$Y5 = \theta_L'$

All physical properties for the solution of the equations were taken from either steam tables[141] or the Chemists Handbook,[142] or, in the case of the viscosity and density of the polymer solution, obtained experimentally. Where information for the polymer solution was not available, for example, thermal conductivity, specific heat capacity and coefficient of expansion, then values for water were used, (see table 4). Similarly, the boiling point of the polymer solution was assumed to be 100°C. The physical properties of the vapour at a temperature greater than 800°C were not obtainable. Therefore it was necessary to extrapolate this information from the data for lower temperatures.

The solution of the differential equations was essentially a boundary value problem with an unknown range. Solution was achieved using a NAG, (Numerical Algorithms Group), routine.[143] This involved a numerical integration technique which used a Runge-Kutta method.

In addition to the boundary conditions stated the solution must also obey the law of conservation of mass across the interface which was stated as;

$$f_L(0) = \frac{R}{\left(\frac{C_{pL}(T_{sat}-T_\infty)}{l}\right)^{1/4}} f_v(\eta)$$

$$\text{where } R = \left(\frac{(\rho\mu)_v}{(\rho\mu)_L}\right)^{1/2}\left(\frac{\rho_L-\rho_v}{\rho_v}\right)^{1/4}\left(\frac{C_{pL}}{\beta_L l}\right)^{1/4}$$

and the law of conservation of energy across the interface stated as;

$$\frac{C_{pv}(T_w-T_{sat})}{lPr_v} = \frac{3f_v(\eta)}{-\theta_v'(\eta)} + \left(\frac{C_{pL}(T_{sat}-T_\infty)}{l}\right)^{5/4} \frac{\theta_L'(0)/\theta_v'(\eta)}{RPr_L}$$

Five boundary conditions are required to solve a fifth order differential equation. Five boundary conditions were known for the vapour layer but only four boundary conditions were known in the case of the liquid layer and it was necessary to obtain a fifth boundary condition, $f_L(0)$, by evaluating the equation defining the conservation of mass using the value for $f_v(\eta)$ obtained from solution of the vapour layer equations. This allowed the liquid layer equations to be integrated.

The liquid layer equations were integrated over the range zero to infinity, (the unknown boundary conditions again being estimated). Infinity was assumed to be that distance, (expressed non-dimensionally as η_L), at which $\theta_L'(\infty)$ fell below -1×10^{-6} and did not vary once set. That is, that distance from the interface

where the variation in temperature with change in distance became vanishingly small. A lower value of η_L, the distance from the interface to infinity, may have meant that the behaviour of the temperature profile at infinity may not have been correctly represented. A higher value of η_L would have increased computing time but with little compensating increase in accuracy.

The objective of the analysis was to obtain a correct value for $\theta_v'(0)$ from which the surface heat transfer coefficient could be calculated. $\theta_v'(0)$ described the behaviour of the temperature profile at the wall. The method by which this was obtained from the above information is given in the following algorithm and is also presented in a flow chart in figure 35.

1. The relationships between the physical properties of the vapour and liquid and temperature were expressed. The temperature of the liquid/vapour interface was set to the boiling point of the quenchant, ($100^{o}C$), and the bulk quenchant temperature, (the temperature of the liquid at infinity), was set to $20^{o}C$.

2. The wall temperature for which the surface heat transfer coefficient was required was set.

3. The dimensionless thickness of the vapour layer, (the thickness of the vapour blanket), was set to 1.0. The dimensionless thickness of the liquid layer, (the distance from the liquid/vapour interface to infinity), was set to 2.0. A variable specifying by how much the thickness of the dimensionless vapour thickness shall vary, ($\Delta\eta$), was set to 0.2.

4. The mean temperatures of the vapour and liquid layers were determined and the values of the respective Prandtl numbers, (for use in the differential equations), calculated at these

temperatures.

5. The known boundary conditions for the vapour layer were set. The unknown boundary conditions were estimated to be zero.

6. The vapour layer differential equations were integrated using the NAG routine D02HAF. This routine integrated the differential equations over the given range, (the dimensionless thickness of the vapour layer), using a shooting and matching technique by varying the unknown boundary conditions until the known boundary conditions were obeyed. This gave new estimates of the unknown boundary conditions which were correct for the integration range used.

7. The boundary condition $f_L(0)$ was evaluated from the equation governing the conservation of mass across the interface. This gave five known boundary conditions for the liquid layer. However, of the five known boundary conditions, $f_L(0)$ was incorrect due to the error in the initial estimate of the vapour layer thickness.

8. The known boundary conditions for the liquid layer, (including $f_L(0)$), were set. The unknown boundary conditions were estimated to be zero.

9. The liquid layer differential equations were integrated using the NAG routine D02HAF. The integration range used was equal to the dimensionless thickness of the liquid layer.

10. The equation governing the conservation of energy across the interface was evaluated and both sides compared. If the two sides were not equal, (to within ±2%), the thickness of the vapour layer was altered by the amount $\Delta\eta$. The variable $\Delta\eta$ was

then reduced and steps 5-10 repeated until the two sides of the equation agreed.

When the two sides of the energy equation agreed then the thickness of the vapour layer was known to be correct. That is, the solution of the differential equations governing the behaviour of the vapour and liquid in the boundary layers obeyed the known boundary conditions and also the requirements of conservation of mass and energy across the liquid/vapour interface. The final estimates of the unknown boundary conditions, including $\theta_v'(0)$, were therefore established as correct for the chosen wall temperature. The Nusselt number and subsequently the convective heat transfer coefficient, h_{co}, was then obtained by;[109]

$$Nu = \frac{-\theta_v'(0)}{\left(\frac{4\nu_v^2\rho_v}{g(\rho_L-\rho_v)x^3}\right)^{1/4}}$$

where x = distance from the leading edge of the plate

$$h_{co} = \frac{Nu\lambda_{vw}}{x}$$

h_{co} was calculated using the value of the vapour thermal conductivity expressed at the wall temperature, (λ_{vw}), rather than at the mean temperature of the vapour layer. The distance from the leading edge of the plate, x, was taken to be equal to the distance from the bottom of the plate to the position of the hot junction of the thermocouple from which the experimental

surface heat transfer coefficients were obtained, (ie, 0.06 m).

The radiative heat transfer coefficient, h_{rad}, was then evaluated;

$$h_{rad} = \frac{\sigma\epsilon(T_w^4 - T_\infty^4)}{T_w - T_\infty}$$

where σ = Stefan-Boltzmann constant

ϵ = emissivity ($\simeq$ 0.85)

T = temperature

The value for the emissivity of the surface of the stainless steel plate was obtained from the Chemists Handbook.[142] The total surface heat transfer coefficient was then calculated according to the method of Bromley[94] and Lubin;[95]

$$h = h_{co}\left(\frac{h_{co}}{h}\right)^{1/3} + h_{rad}$$

The thickness of the vapour layer was obtained from the dimensionless vapour layer thickness, η_v;

$$y = \frac{\eta_v x^{1/4}}{c_v}$$

where c_v = the similarity transformation variable

Cess and Sparrow[109] adopted a different approach to the solution of the differential equations using a McLaurin expansion to solve the vapour layer equations and a Runge-Kutta numerical integration to solve the liquid layer equations.

5.3.2 The Model Of Nishikawa And Ito (1966)

The model of Nishikawa and Ito[112] utilised the same boundary layer equations as Cess and Sparrow[109] but rejected the assumption of zero interfacial velocity. This reduced the number of boundary conditions available for solution which became, in the vapour layer;

at the wall; $f_v(0) = f_v'(0) = 0$; $\theta_v(0) = 1$

at the interface; $\theta_v(\eta) = 1$

In the liquid layer;

at the interface; $\theta_L(0) = 1$

at infinity; $f_L'(\eta) = 0$; $\theta_L = 0$

Cess and Sparrow[109] assumed that the vapour/liquid interface was stationary and therefore required the solution of the differential equations to obey the relationships of continuity of mass and energy across the interface only. Nishikawa and Ito[112] assumed that the interface moved upwards but at an unknown velocity and therefore required the solution to obey, in addition to the continuity of mass and energy, the relationships governing the continuity of velocity and shear stress at the interface also. The problem was also phrased slightly differently in terms of dimensionless groupings thus;

$$A = Sc^{-0.25}.V$$

$$B = R^{-2}.Sc^{-0.5}.V^2$$

$$C = A.B$$

$$D = Pr_L^{-1}.Sc^{1.25}.V^{-1}$$

where $Sc = \dfrac{C_{pl}(T_{sat}-T_{\infty})}{lPr_L}$

$$V = R\left(\frac{\rho_v}{\rho_L}\right)^{-1/4}\left(\frac{C_{pL}}{\beta_L l}\right)^{1/4}$$

$$R = \left(\frac{(\rho\mu)_v}{(\rho\mu)_L}\right)^{1/2}$$

$$Pr_L = \frac{C_{pL}\mu_L}{\lambda_L}$$

The physical properties were again evaluated at the arithmetic mean temperature of the boundary layer. The dimensionless values A,B,C and D were used to describe the interface matching conditions as follows;

Continuity of mass transfer : $f_L(0) = A.f_v(\eta)$

No slip in tangential velocity : $f_L'(0) = B.f_v'(\eta)$

Equal tangential shear stress : $f_L''(0) = C.f_v''(\eta)$

Continuity of heat transfer : $Sp = -3f_v(\eta) + D\theta_L'(0)$

$$\theta_v'(\eta) \qquad \theta_v'(\eta)$$

where $Sp = \dfrac{C_{pv}(T_w-T_{sat})}{lPr_v}$

Since the specified boundary conditions at the interface were less complete in this model the solution of this problem was more arduous. In the case of Cess and Sparrow[109] $f_v'(\eta) = f_L'(0) = 0$, (that is, the velocity of the interface was equal to zero), whereas here these boundary conditions were specified in the

interfacial matching condition relating to an unknown interface velocity. Since only four boundary conditions were known for the vapour layers, but five were required to solve the differential equations, a fifth was estimated and temporarily assumed to be correct for the purpose of obtaining a solution. The boundary condition $f_v''(0)$ was arbitrarily selected.

The final value for $f_v''(0)$ was obtained by reference to the liquid layer equations via the requirement of continuity of shear stress at the interface. (Nishikawa and Ito[112] used a finite difference approximation of the ordinary differential equations to obtain a solution).

Setting the unknown boundary conditions to zero as in the Cess and Sparrow[109] model failed to give a convergence. Closer approximations to the final values had to be made for the initial estimates. Therefore estimates, which gave convergence, for the ten unknown boundary conditions were obtained by a process of trial and error. Estimates for the dimensionless thiknesses of the vapour and liquid layers were also obtained in this manner.

The algorithm for the numerical integration procedure was as follows, (figure 36 shows a flowchart for the calculation);

1. The physical properties of the liquid and vapour and their relationships with temperature were expressed. The interface temperature was set equal to the boiling point of the quenchant, ($100^{o}C$), and the temperature of the bulk quenchant was set equal to $20^{o}C$.

2. The dimensionless thicknesses of the vapour and liquid layers were set. The wall temperature was set to the required

value as was a variable, $\Delta\eta$, which was used to change the dimensionless vapour thickness.

3. Using the vapour and liquid physical properties expressed at the mean temperatures of the boundary layers, the vapour and liquid Prandtl numbers, the parameters R,V,Sc,Sp and hence A,B,C and D were calculated.

4. A parameter, Δ, with which the unknown boundary condition, $f_v''(0)$, was varied was set to an arbitrary value, (0.1).

5. The known boundary conditions and the estimates of the unknown boundary conditions were expressed.

6. The vapour layer differential equations were integrated using the NAG numerical integration routine, D02HAF, with the dimensionless thickness of the vapour layer as the integration range.

7. The three known boundary conditions in the liquid layer were set. Two further boundary conditions were obtained from the equations governing the continuity of mass transfer and velocity at the interface, ie, $f_L(0) = A.f_v(\eta)$ and $f_L(0)' = B.f_v'(\eta)$.

8. The liquid layer differential equations were integrated using the NAG numerical integration routine, D02HAF, with the dimensionless thickness of the liquid layer as the integration range.

9. The equation governing the continuity of shear stress at the interface, $f_L''(0) = C._v''(\eta)$, was evaluated and the two sides compared. The two sides of this equation would not be equal due to the error in the initial estimate of the unknown boundary condition $f_v''(0)$. Therefore the value of the initial estimate of

$f_v''(0)$ was altered by the increment Δ. The variable Δ was then reduced to ensure that converging estimates of $f_v''(0)$ were obtained.

10. Steps 5-9 were then repeated using the new estimate of $f_v''(0)$. This procedure was repeated until a value of $f_v''(0)$ was obtained which meant that the equation governing the continuity of shear stress at the interface was obeyed.

11. The equation governing the continuity of heat transfer at the interface was then evaluated and both sides compared. The two sides of the equation would not be equal due to the error in the initial estimate of the dimensionless vapour layer thickness. This was therefore altered by the amount $\Delta\eta$ and the variable $\Delta\eta$ was reduced to ensure converging estimates of the dimensionless vapour layer thickness.

12. Steps 4-11 were repeated using new estimates of the dimensionless vapour layer thickness until a value was obtained which meant that the equation governing the continuity of heat transfer at the interface was obeyed.

When this was achieved the solution obeyed the known boundary conditions and the laws of continuity of mass, velocity, shear stress and heat transfer at the interface. The boundary conditions were then used to calculate the velocity of both the vapour and the liquid at the interface and their associated Reynolds numbers and the surface heat transfer coefficient at the specified wall temperature.

The relationship between $\theta_v'(0)$ and the surface heat transfer coefficient was given by;[112]

$$Nu = \left(\frac{Gr}{4}\right) - \theta_v'(0)$$

where Gr = Grashof number

$$h_{co} = \frac{Nu\lambda_{vw}}{x}$$

The radiative heat transfer coefficient was added in the same manner as before, (section 5.3.1).

The vapour film thickness was calculated by;[112]

$$y = \frac{\eta_v}{c_v x^{-1/4}}$$

where c_v = the similarity transformation variable for the vapour layer

Nishikawa and Ito[112] did not present velocity expressions therefore the velocity of the liquid and vapour at the interface was calculated using expressions derived from Cess and Sparrow[109] who stated;

$$u = 4cx^{1/2} f'\nu$$

The following expressions were therefore used to describe the velocity of the vapour and liquid at the interface in the model of Nishikawa and Ito,[112] (the subscript i denotes the interfacial value);

$$u_{vi} = f_v'(\eta) 4c_v \nu_{vs} x^{1/2}$$
$$u_{Li} = f_L(0)' 4c_L \nu_{Ls} x^{1/2}$$

However, all three of these expressions were dimensionally incorrect and therefore produced incorrect values for the velocity of the interface. This did not affect the accuracy of the solution since this was performed using variables expressed non-dimensionally but did affect the value of the interface velocity when it was converted from a dimensionless variable. The correct expression for the interface velocity will be presented in section 5.3.4 when its importance becomes apparent.

5.3.3 The Model Of Nishikawa, Ito And Matsumoto (1976)

This model was formulated to account for the variation of the physical properties with temperature when the boundary layer equations were derived but otherwise it was similar to the Nishikawa and Ito[112] model in that the interface was assumed to be moving. However, the interfacial matching conditions were expressed differently to allow for the fact that the physical properties of the fluid were varied across the boundary layers.

The differential equations describing the velocity and temperature profiles in the vapour and liquid layers were defined, for the vapour layer, as follows. As before the primes denote differentiation with respect to η;

$$\left(\frac{(\rho\mu)_v}{(\rho\mu)_{vs}} f_v''\right)' - 2(f_v')^2 + 3f_v f_v'' + \frac{((\rho_{L\infty}-\rho)/\rho)_v}{((\rho_{L\infty}-\rho)/\rho)_{vs}} = 0$$

$$\left(\frac{(\rho\lambda)_v}{(\rho\lambda)_{vs}} \theta_v'\right)' + 3Pr_{vs}\frac{C_{pv}}{C_{pvs}} f_v \theta_v' = 0$$

and for the liquid layer;

$$\left(\frac{(\rho\mu)_L\, f_L''}{(\rho\mu)_{Ls}}\right)' - 2(f_L')^2 + 3f_L f_L'' + \frac{((\rho_{L\infty}-\rho)/\rho)_L}{((\rho_{L\infty}-\rho)/\rho)_{Ls}} = 0$$

$$\left(\frac{(\rho\lambda)_L\, \theta_L'}{(\rho\lambda)_{Ls}}\right)' + 3Pr_{Ls}\frac{C_{pL}}{C_{pLs}} f_L \theta_L' = 0$$

To facilitate solution the following variables were defined;

$$d_1 = \frac{(\rho\mu)_v}{(\rho\mu)_s}$$

$$d_2 = \frac{((\rho_{L\infty}-\rho)/\rho)_v}{((\rho_{L\infty}-\rho)/\rho)_{vs}}$$

$$d_3 = \frac{(\rho\lambda)_v}{(\rho\lambda)_{vs}}$$

$$d_4 = \frac{C_{pv}}{C_{pvs}}$$

$$d_5 = \frac{(\rho\mu)_L}{(\rho\mu)_{Ls}}$$

$$d_6 = \frac{((\rho_{L\infty}-\rho)/\rho)_L}{((\rho_{L\infty}-\rho)/\rho)_{Ls}}$$

$$d_7 = \frac{(\rho\lambda)_L}{(\rho\lambda)_{Ls}}$$

$$d_8 = \frac{C_{pL}}{C_{pLs}}$$

Inserting these parameters in the equations and simplifying using the function of a function rule gave, for the vapour layer;

$$d_1 f_v''' + d_1' f_v'' - 2(f_v')^2 + 3 f_v f_v'' + d_2 = 0$$

$$d_3 \theta_v'' + d_3' \theta_v'' + 3 Pr_{vs} d_4 f_v \theta_v' = 0$$

and for the liquid layer;

$$d_5 f_L''' + d_5' f_L'' - 2(f_L')^2 + 3 f_L f_L'' + d_6 = 0$$

$$d_7 \theta_v'' + d_7' \theta_v'' + 3 Pr_{Ls} d_8 f_L \theta_L' = 0$$

Reducing these equations to a system of five, first order differential equations gave, for the vapour layer;

$$Y1' = f_v'$$

$$Y2' = f_v''$$

$$Y3'' = f_v''' = (2(f_v')^2 - d_1' f_v'' - 3 f_v f_v'' - d_2)/d_1$$

$$Y4' = \theta_v'$$

$$Y5' = (-3 Pr_{vs} d_4 f_v \theta_v' - d_3' \theta_v'')/d_3$$

where $Y1 = f_v$

$Y2 = f_v'$

$Y3 = f_v''$

$Y4 = \theta_v$

$Y5 = \theta_v'$

and for the liquid layer;

$$Y1' = f_L'$$

$$Y2' = f_L''$$

$$Y3' = f_L''' = (2(f_L')^2 - d_5' f_L'' - 3 f_L f_L'' - d_6)/d_5$$

$$Y4' = \theta_L'$$

$$Y5' = \theta_L'' = (-3Pr_{Ls} d_8 f_L \theta_L' - d_7' \theta_L'')/d_7$$

where $Y1 = f_L$

$Y2 = f_L'$

$Y3 = f_L''$

$Y4 = \theta_L$

$Y5 = \theta_L'$

The differential equations required the physical properties of the vapour and liquid in the boundary layers to be known but it was not possible to determine the physical properties exactly since they were dependent on the temperature profile in the boundary layer, (which in turn was dependent on the physical properties). Only the temperature at the point $\eta = 0$ in the boundary layer was known exactly, (as $\theta = 1$). However, the step length used by the integration procedure was very small so a good estimate of the temperature at any point in a boundary layer was obtained from a knowledge of the dimensionless temperature, θ, at the end of the calculation of the previous step. This estimate was used to determine the physical properties which were used to calculate the variables d_1 to d_8 to allow the formulation of the differential equations for solution by the Runge-Kutta routine. The incremental change in d_1, d_3, d_5 and d_7 divided by the incremental change in η was used to estimate d_1', d_3', d_5' and d_7'. When η was equal to zero d_1', d_3', d_5' and d_7' were assumed to be zero also.

The interfacial matching conditions were expressed as;

Continuity of mass transfer; $f_L(0) = A.f_v(\eta)$

Continuity of velocity; $f_L'(0) = B.f_v'(\eta)$

Continuity of shear stress; $f_L''(0) = C.f_L''(\eta)$

Continuity of heat transfer;

$$Sp = -3(f_v(\eta)/\theta_v'(\eta)) - D(\theta_L'(0)/\theta_v'(\eta))Sc$$

where $A = KR$

$B = K^2$

$C = K^3R$

$D = 1/KR$

and $$Sp = C_{pvs}(T_w - T_{sat})/lPr_{vs}$$

$$Sc = C_{pLs}(T_{sat} - T_\infty)/lPr_{Ls}$$

$$R = ((\rho\mu)_{vs}/(\rho\mu)_{Ls}))^{1/2}$$

$$K = \left(\frac{((\rho_{L\infty} - \rho)/\rho)_{vs}}{((\rho_{L\infty} - \rho)/\rho)_{Ls}}\right)^{1/4}$$

The solution proceeded in an identical manner to that used to solve the model of Nishikawa and Ito,[112] (see section 5.3.2). The variable $f_v''(0)$ was obtained by iterating against the requirement of continuity of shear stress at the interface. The dimensionless thickness of the vapour film was obtained by iterating against the requirement of continuity of heat transfer at the interface. The upper limit of integration for the liquid layer was fixed according to the criterion that at infinity $\theta_L' < -1 \times 10^{-6}$.

(The authors adopted a finite difference approximation of the

differential equations to obtain a solution as before).

The value of the film thickness was calculated from;[114]

$$\eta_v = \frac{c_v}{x^{1/4}} \int_0^y \frac{\rho_v dy}{\rho_{vs}}$$

with the similarity transformation variable being expressed using values for the physical properties at the interface temperature. The integral term was approximated by a finite difference term using the Trapezoidal Rule for one panel. The film thickness, y, was then the step length;

$$y = \frac{\eta_v x^{1/4}}{c_v} \left(\frac{1}{2} \left(\frac{\rho_{vw}+1}{\rho_{vs}} \right) \right)$$

The conduction heat transfer coefficient, h_{co}, was calculated from;

$$Nu = \frac{-(\rho\lambda)_{vw} \theta_v'(0)}{(\rho\lambda)_{vs}} \left(\frac{Gr}{4} \right)^{1/4}$$

$$h = \frac{Nu\lambda_{vs}}{x}$$

the radiative heat transfer being added as before.

Nishikawa, Ito and Matsumoto[114] did not present relationships for the velocity therefore the velocity of the vapour and liquid at the interface was obtained using relationships stated by Cess and Sparrow[109] but expressed using interfacial values;

$$u_{vi} = 4.c_v.\nu_{vs}.x^{1/2}.f_{vi}'$$
$$u_{Li} = 4.c_L.\nu_{Ls}.x^{1/2}.f_{Li}'$$

These expressions were also dimensionally incorrect.

5.3.4 Calculation Of The Film Boiling Surface Heat Transfer Coefficient Assuming A Turbulent Interface

The three previous models all assumed that film boiling was associated with laminar flow. Experimental evidence presented in this work and reported by others suggested that film boiling may be accompanied by turbulent flow at the vapour/liquid interface. Therefore a model has been developed in the present work for film boiling on an isothermal vertical plate which incorporated a turbulent interface.

The values of interfacial velocity predicted by the models that assumed a moving interface, (Nishikawa and Ito[112] and Nishikawa, Ito and Matsumoto[114]), were examined to see whether these models predicted values of Reynolds numbers at the interface which would indicate that the interface was moving at a sufficient velocity that turbulence could be inferred. Initial results suggested that this was not the case but, as mentioned above, the values for velocity were subject to doubt since the expressions used were not dimensionally correct. The correct expression for the velocity in a boundary layer has been given by Koh[110] and Schlichting;[111]

$$u = 4c^2 \nu x^{1/2} f',$$

where c = similarity variable

ν = kinematic viscosity

x = distance from leading edge

f' = dimensionless velocity

The use of this expression indicated that the Reynolds numbers at the interface were sufficiently high as to suggest turbulent flow.

The physical model proposed is shown in figure 37. The existence of a laminar vapour layer adjacent to the wall was assumed together with a laminar liquid layer which extended into the bulk liquid. The turbulent interface was assumed to consist of a mixture of the fluids in laminar flow on either side. The reasoning which led to this model is given in section 7.5.

The assumption of turbulence at the interface provided new boundary conditions with which the equations describing laminar flow, and which were assumed to apply either side of the interface, were solved. The fixed property differential equations used by Cess and Sparrow[109] and Nishikawa and Ito[112] were employed to describe the laminar boundary layers.

The critical Reynolds number for transition from laminar to turbulent flow was not known a priori so therefore a series of critical Reynolds numbers were assumed. The predicted surface heat transfer coefficients obtained using the assumed critical Reynolds numbers were then compared with experimentally obtained values. This was performed in the case of film boiling in both water and for a 25% Aquaquench ACR solution.

The same critical Reynolds number at the point of transition from laminar to turbulent flow was assumed to apply at both the vapour and liquid sides of the interface. Since the temperature of the interface was known, (from the assumption that it was at

the boiling point of the quenchant, 100°C), this gave the kinematic viscosity and therefore allowed the velocity to be calculated from the Reynolds number at both these points. This gave values for the boundary conditions $f_v'(\eta)$ and $f_L'(0)$ and provided five known boundary conditions for each set of differential equations so that a solution could be obtained.

These boundary conditions are set out below;

at the wall; $f_v(0) = f_v'(0) = 0$; $\theta_v(0) = 1$

at the interface; $\theta_v(\eta) = 0$; $\theta_L(0) = 1$

$$Re_{vi} = Re_{Li} = Re_{crit} ;$$

$$u_{vi} = \frac{Re_{crit}\mu_{vs}}{\rho_{vi}x} ; \quad u_{Li} = \frac{Re_{crit}\mu_{Ls}}{\rho_{Li}x} ;$$

$$f_v'(\eta) = 4c_v{}^2x^{1/2}u_{vi}\nu_{vs} ; \quad f_L'(0) = 4c_L{}^2x^{1/2}u_{Li}\nu_{Ls}$$

where c_v and c_L are the similarity transformation variables described by Cess and Sparrow[109] and Nishikawa and Ito.[112]

$f_L(0)$ was obtained from the relationship for the continuity of mass transfer at the interface as defined by Cess and Sparrow.[109]

at infinity ; $f_L'(\infty) = 0$; $\theta_L'(\infty) = 0$

Sufficient boundary conditions were therefore known to enable $f_v''(0)$ to be obtained by the integration of the vapour layer equations directly rather than by using the liquid layer equations as was done in the Nishikawa and Ito[112] and Nishikawa,

Ito and Matsumoto[114] models. The correct value for the dimensionless film thickness was obtained by iteration against the requirement of continuity of heat transfer at the interface. The procedure for the solution of the differential equations was therefore identical to that adopted for the Cess and Sparrow[109] model and required that the solution obey the relationships governing the continuity of heat and mass transfer at the interface as expressed by them.

The physical properties used in the boundary layer equations and the interfacial matching conditions were evaluated at the arithmetic mean temperature of the boundary layers except that the surface heat transfer coefficient was calculated using the wall temperature value for the thermal conductivity of the vapour. (This was the procedure adopted in the solution of the previous models).

The vapour layer thickness was calculated by the same method as used in the Cess and Sparrow[109] model.

The velocity profile in this model therefore was as follows. The velocity was zero at the wall and then rose in the laminar vapour layer until it reached a value associated with the critical Reynolds number at the boundary of the laminar vapour layer and the turbulent interface. The same critical Reynolds number was assumed to occur at the point of transition from laminar to turbulent flow in the liquid layer also. The velocity profile therefore declined across the turbulent layer as the physical properties of the turbulent layer changed, (see figure 37). The velocity then further declined from the value associated with the critical Reynolds number in the liquid layer until it

reached zero in the bulk liquid. Therefore, whereas previous models assumed that the the velocity was continuous across the interface, this model assumed that the Reynolds number was continuous across the interface and was equal to the critical Reynolds number for transition from laminar to turbulent flow.

The temperature profile behaved as follows. The temperature of the vapour at the wall was equivalent to the surface temperature. With increasing distance normal to the surface the temperature of the vapour declined until it reached the boiling point of the quenchant at the turbulent interface. The interface was considered to be sufficiently mixed that the velocity profile in the turbulent layer was flat until the laminar liquid layer was reached whereupon the temperature again declined until it reached ambient at a point equivalent to infinity in the bulk liquid.

6.0 RESULTS

The relationships between time and temperature during quenching were determined at both the approximate centre and at points just below either face of a stainless steel plate. The latter information was used to calculate the surface heat transfer coefficient and its relationship with surface temperature during the quench. The appearance of the plate surface during quenching was also recorded by still and cine photography and related to the surface temperature and surface heat transfer coefficient in order to determine the quenching characteristics of the solutions.

(The surface heat transfer coefficient during quenching in water has also been measured but comparison between these results and those obtained for the sodium polyacrylate solutions can only be limited since the former were obtained by quenching from 1000°C, (to obtain film boiling data), 150°C higher than the latter.)

The surface heat transfer coefficients were then used to calculate the thermal stress and strain generated during quenching in infinite plates of a low alloy steel. The relationship between surface temperature and surface heat transfer coefficient has a considerable effect on the generation of thermal stress and strain. The calculated generation of thermal stress and strain during quenching in sodium polyacrylate solutions was compared to the calculated quenching histories and residual stresses and strains for other liquids with different quenching characteristics, (water, oil and a polyalkylene glycol

solution), in order to identify the positions of these solutions within the context of the more commonly used quenchants.

Experimental measurements of the residual stresses and strains in a range of sodium polyacrylate solutions were then performed and comparisons with the calculated residual stresses and strains made in order to assess the accuracy of the mathematical model.

The understanding of the quenching characteristics of the polymer solutions was further increased by differential thermogravimetric analysis of the initial, as-suplied concentrate, determination of the viscosity of a sample of liquid extracted from the vicinity of the plate face during cooling and by a scanning electron microscopy examination of the plate after quenching. The physical properties of solutions of sodium polyacrylate of varying concentrations were also determined.

Three models of heat transfer during film boiling were evaluated and their predictions of the surface heat transfer coefficient compared with experimental results derived from quenching in water and a solution of sodium polyacrylate. As a result of these comparisons a modification to the film boiling models was proposed which allowed the inclusion of a turbulent liquid/vapour interface.

6.1 Relationships Between Time And Temperature During The Quenching Of The Steel PLate

The relationships between time and temperature in figure 38 relate to quenches carried out in unagitated aqueous solutions of 5,10,15,20 and 25% Aquaquench ACR. The relationships presented

are between time and the calculated surface temperature obtained from the calculation of the surface heat transfer coefficient. Figure 39 shows corresponding relationships for quenches performed in agitated solutions of the same composition.

Increasing the polymer concentration decreased the surface cooling rate in all stages of the quench while agitation of the bath tended to increase it. The film boiling stage, (denoted by A in figure 38), occurred in each test except that carried out in the 5% agitated solution. This stage produced a relatively slow rate of cooling. (Estimates of the cooling rates for the different stages in the cooling curves are presented in table 5). The duration of the film boiling stage increased substantially as the concentration of polymer was increased while the surface temperature at which the film boiling stage ceased, (the minimum film boiling point, B in figure 38), simultaneously decreased. Table 6 shows that this temperature fell from 769^{o}C in 5% Aquaquench ACR, unagitated, to 592^{o}C in 25% Aquaquench ACR, unagitated.

After the end of the film boiling stage the first part of the vapour transport stage, termed transition boiling, began, (denoted by C in figure 38). This was marked by a rapid increase in the rate of cooling of the plate with cooling rates in this stage estimated to be about an order of magnitude higher than in the film boiling stage. The effects of agitation on cooling rate in this stage were, however, contradictory since the results of the 20 and 25% solutions suggested that agitation increased surface cooling rate but the results for the 5,10 and 15% solutions indicated the reverse.

The cooling curve in the later part of the vapour transport stage underwent a sudden reduction in gradient which corresponded to a rapid decrease in cooling rate, (denoted by D in figure 38). The temperature, (on average), at which this occurred tended to decrease with increasing concentration of sodium polyacrylate though the result obtained from the 5% Aquaquench ACR solution was anomalous in this respect. The agitated results behaved similarly but in this case both the 5 and 10% Aquaquench ACR results were anomalous. No relationship between agitation and this temperature was apparent.

The cooling curve associated with the later part of the vapour transport stage, that is, after point D in figure 38, frequently exhibited another change in gradient which is denoted E in figure 38. This was observed in all concentrations of the polymer quenchant and in both agitated and unagitated tests, though with varying degrees of clarity. It is most clearly shown in the cooling curve for the 25% Aquaquench ACR solution in figure 38. The variation in the surface temperature of the occurrence of the change in gradient is recorded in table 7. This shows that the mean temperature in both agitated and unagitated results was 424^{o}C with the mean temperature of the results for any one concentration showing little variation from this.

The latter part of the vapour transport stage, (denoted by F in figure 38), was associated with cooling rates which were of the same order as those produced by the film boiling stage. For example, the surface cooling rate in this stage in a 25% Aquaquench ACR solution was estimated to be approximately 2^{o}C.s^{-1}.

As was observed in the boiling regimes that occurred at higher temperatures the cooling rate decreased with increasing concentration but agitation had little effect in this stage.

6.2 Surface Heat Transfer Coefficients

The relationships between surface heat transfer coefficient and surface temperature were calculated from the data obtained from quenching by the method explained in section 5.2.1. Figures 40 and 41 show the mean surface heat transfer coefficients obtained in each concentration of sodium polyacrylate examined while figures 42 to 46 show the range recorded in each concentration, (unagitated solutions only), and hence the reproducibility of the quenching procedure.

Each curve followed the same general path with the surface heat transfer coefficient rising from a low value at the beginning of the quench to a peak as stable film boiling was established, (figure 40). This was not so pronounced in the case of the lower concentrations of the agitated quenches which suggested that the film boiling stage was absent in those solutions. As the temperature fell the surface heat transfer coefficient declined slightly until the temperature associated with the minimum film boiling point was reached, whereupon it rose rapidly to a peak value associated with the critical heat flux. This stage, at higher surface temperatures than those associated with the maximum surface heat transfer coefficient but below the minimum film boiling point, was associated with the region of transition between film and nucleate boiling.

After the passage of the maximum, in all concentrations of sodium polyacrylate examined, the surface heat transfer coefficient fell very rapidly with decreasing surface temperature and quickly reached values of the order of those associated with the film boiling stage. This was followed by a slight rise in the surface heat transfer coefficient towards the end of the quench.

The 5% Aquaquench ACR solution was an exception here since the surface heat transfer coefficient fell by only a limited amount after the passage of the maximum and subsequently rose significantly as the surface temperature continued to fall before declining again toward the end of the quench.

The value of the surface heat transfer coefficient in the film boiling stage was of the order of 3-400 $W.m^{-2}.K^{-1}$ with the values associated with the agitated solutions at the higher end of the range. As the surface temperature fell the surface heat transfer coefficient in this stage tended to fall also. The value of the surface heat transfer coefficient at the minimum film boiling point fell with increased concentration from 420 $W.m^{-2}.K^{-1}$ in 5% Aquaquench ACR unagitated to 300 $W.m^{-2}.K^{-1}$ in 25% Aquaquench ACR unagitated. Agitation increased the value of the surface heat transfer coefficient at this point.

The mean maximum surface heat transfer coefficent decreased with increased concentration of sodium polyacrylate from about 4275 $w.m^{-2}.K^{-1}$ in 5% Aquaquench ACR, unagitated, to 1807 $W.m^{-2}.K^{-1}$ in 25% Aquaquench ACR, unagitated. The effect of agitation on the magnitude of the maximum surface heat transfer coefficient was not apparent.

The value of the surface heat transfer coefficient dropped

rapidly after it reached a maximum compared to its behaviour in water. The range of surface temperatures over which this fall occurred included the mean surface temperature at which a change in gradient in the cooling curve, (at 424^{o}C), was noted. In sodium polyacrylate solutions greater than 10% Aquaquench ACR the surface heat transfer coefficient reached a value at 300^{o}C only slightly higher than the values associated with the film boiling stage. The surface heat transfer coefficient at 300^{o}C also decreased further with increased concentration of sodium polyacrylate.

The exception was the 5% Aquaquench ACR solution which, in the unagitated test, fell to just below 2.0 kW.m^{-2}.K^{-1} at 350^{o}C but then rose to just over 2.5 kW.m^{-2}.K^{-1} at 200^{o}C before it fell again. The agitated solution behaved similarly but exhibited higher values of the surface heat transfer coefficient.

The extent of the various boiling phases and their dependence on concentration as reported in this section are summarised in figure 47.

6.3 Results Obtained From The Water Quenches

The relationships between time and temperature during quenching in still water displayed most of the characteristics of the polymer quenchant cooling curves with a film boiling stage followed by a vapour transport stage characterised by a rapid decrease in surface temperature followed by a region of slower cooling, (figure 48).

The minimum film boiling point occurred at a mean surface

temperature of 809°C after a film boiling stage which was characterised by surface heat transfer coefficients which reached a maximum, on average, of about 690 $W.m^{-2}.K^{-1}$. As the surface temperature fell the value of the surface heat transfer coefficient during film boiling also fell, reaching 430 $W.m^{-2}.K^{-1}$ at the temperature of the minimum film boiling point.

The transition boiling stage then replaced the film boiling stage and the surface temperature rapidly decreased down to about 200-300°C whereupon the surface of the plate was subject to a period of slower cooling.

The mean maximum surface heat transfer coefficient in water was 12910 $W.m^{-2}.K^{-1}$, (three times that recorded in a 5% Aquaquench ACR solution), and the mean temperature at which it occurred was 318°C, well below that recorded in the polymer quenchant, (figure 49). Hereafter the surface heat transfer coefficient fell rapidly until boiling ceased. (Substantial scatter, about ±25%, was observed in both the values of the maximum surface heat transfer coefficient and the temperature at which it occurred, as it was in the polymer quenchant results).

6.4 Still Photography Of The Quenching Process

Still photography allowed the surface boiling phenomena which accompanied the quenching of the plate to be recorded and examined. Since the time at which each photograph was taken was known this enabled it to be related to the surface temperature and surface heat transfer coefficient which existed at that time. It should be borne in mind however that the temperature was not

constant at all points of the plate face so that the observations involving surface temperature and surface heat transfer coefficient properly relate only to that portion of the surface adjacent to the hot junction of the thermocouple, (ie, the centre of the plate face).

The entire quenching process in a solution of 10% Aquaquench ACR is shown in plates 1 to 12. The first two photographs, (plates 1 and 2), show the film boiling stage. This was characterised by a bright reflection by the vapour/liquid interface and relatively low values of the surface heat transfer coefficient. The uneveness of the reflection suggested that the interface was not smooth but consisted of peaks and troughs. In both plates the surface was partially obscured by white clouds. In plate 1, showing the surface of the plate after 2 s, the white cloud appeared to emanate from most of the plate face excepting a narrow region around the bottom and sides of the face. Two seconds later, (plate 2), the region from which the white cloud was produced had contracted towards the centre of the plate face. Despite the presence of these clouds it is still possible to see, in plate 2, the liberation of a large bubble, some 5-6 mm in diameter, from the upper left-hand edge of the plate.

A much clearer presentation of the appearance of the surface of the vapour blanket is supplied by plate 13 which relates to a quench in 5% Aquaquench ACR. The surface has a high reflectivity and is irregular in appearance with a network of narrow troughs that isolate the thicker parts of the film as distinct protuberances. No less than five large bubbles are observed

leaving the upper edge of the plate in this photograph. These are of approximately the same size as the protuberances in the vapour blanket on the face of the plate.

Plates 14 and 15 show photographs of the edges of a plate quenched in 20% Aquaquench ACR, (which had a more stable film boiling stage), and clearly show that the variation in thickness of the vapour blanket may be regular, to give a wave-like appearance, similar to Taylor waves. The wave formations here have a wavelength of about 8-9 mm but the wavelength increased with increasing height and decreased with increasing time. Although not shown so clearly as in plates 14 and 15, plates 1 and 2 show that these periodic variations in film thickness were not confined to any one concentration of Aquaquench ACR.

To return to the 10% Aquaquench ACR quench, photographs of the plate face when the surface heat transfer coefficient at the centre of the plate face rose from the value associated with the minimum film boiling point to a maximum were obscured by the fine white cloud noted earlier. A series of high speed photographs were taken to examine this stage and an example is given in plate 3. This showed that the white cloud was the characteristic form of boiling when the surface temperature was associated with the transition stage between film and nucleate boiling. These photographs show the interior of the plate face liberating a white mist which probably consisted of fine bubbles.

This is also illustrated by plate 16 taken in a 5% solution which showed the last remnants of the film boiling stage in the upper region of the plate face with the white cloud generated in the surrounding region.

This photograph shows four distinct features existing on the surface of the plate at the same time. The film boiling stage is present over a small region of the upper surface of the plate immediately below the handle and this is therefore the hottest portion of the plate surface. Surrounding this is a large region of white cloud which has been shown to be associated with the commencement of the vapour transport stage and, more particularly, that region between the film boiling stage and the maximum surface heat transfer coefficient. At the bottom edge of the plate face, and therefore at a lower surface temperature, are features which are dendritic in appearance. These merge imperceptibly into a feature having the appearance of a fine froth which lines the extreme sides and bottom edge of the plate face. This latter feature was therefore associated with the lowest surface temperature of the four features observed.

A fine white cloud was also physically observed to form around the plate upon first placing it into the quenching bath. In addition a number of audible reports also occurred which were confined to the earlier stages of the quench. These increased in number with increased concentration and increased in frequency with agitation and were probably associated with the collapse of the vapour blanket on the plate.

At 14s the surface heat transfer coefficient was approximately at its peak at the centre of the face of a plate quenched in a 10% Aquaquench ACR solution, (plate 4). The central region was dominated by the white cloud but around this was an annular region which contained isolated oblate features some 7-8 mm in diameter. Two seconds later, (plate 5), the surface heat transfer

coefficient has declined and the oblate features have diminished in size.

One feature of both photographs is the one-sided illumination of the oblate structures indicating that the flashguns used on either side of the plate were not completely synchronised. This one-sided illumination indicated that the oblate features were either raised features illuminated from the left, (bubbles), or depressions illuminated from the right, (troughs), depending on the direction of strongest illumination. The photographs show that the plate face was illuminated more strongly from the left which indicated that the former deduction was correct.

As the quench proceeded and the surface heat transfer coefficient decreased further the features previously noted at the edges of the plate face in plate 16 became more widespread. The interior of the plate face became covered with dark dendritic markings, (plates 6 and 7), while the regions adjacent to the plate sides and bottom edge became covered with a white froth. (These are most clearly illustrated in the 5% solution, (plates 17 and 18). At this point the position of the sub-surface thermocouple in the plate was revealed as the linear structure reaching from the upper edge down towards the centre of the plate face. The reason for this appears to be that the face immediately adjacent to the thermocouple has protruded very slightly, presumably as a consequence of the machining of the hole into which the thermocouple had been placed. It is interesting that the appearance of the liquid in contact with this part of the face was characterised by features present on the periphery of the plate face, (where the temperature was lower).

The same reasoning as regards the one-sided illumination was applied to plates 6 and 7. The linear reflection that this created lay consistently to the left of the dark dendritic markings which indicated that these were elongated protrusions of vapour. In plates 17 and 18, taken during a 5% Aquaquench ACR quench, the illumination of the flash was strongest from the right hand side of the quenched plate. The linear reflection now lay consistently to the right of the dark dendritic markings which confirmed the deduction made above.

With increasing time the area dominated by the dendritic features contracted towards the centre of the plate face while the area dominated by the froth simultaneously expanded. (Compare plate 6 to plate 7 and plate 17 to plate 18). The white interdendritic areas merged imperceptibly into the white froth of the periphery and were therefore presumed to be the same phenomenom. The surface heat transfer coefficients calculated during the period when the central area of the plate face showed the "dendritic" stage was low - of the order of those calculated in the film boiling stage.

The photograph of the transition boiling stage in 10% Aquaquench ACR referred to above, (plate 3), showed a white mist liberated from the central areas of the plate face. The edge of the plate face showed a white froth while separating the two phenomena was an annulus of oblate structures. In these photographs the dendritic structures, which one would expect to appear between the froth and the oblate structures, have not yet formed.

As the quench in the 10% Aquaquench ACR solution proceeded the

white froth at the periphery of the plate face encroached on the dendritic central region while the interdendritic spacing was simultaneously reduced. The appearance of the white froth was visible to an observer during the quench and the bubbles of which it comprised appeared to be confined to the surface of the plate. Eventually the dendritic region was completely consumed. As the surface temperature of the plate fell toward ambient the bubbles of which the white froth consisted shrank in diameter. However, the largest bubbles of those existing at any one period were always those at the centre of the plate face. The average diameter of these bubbles was of the order of 0.5 - 3.0 mm. These effects are illustrated in plates 8 to 10.

The foregoing descriptions apply equally well to quenches performed in solutions of both 5% and 10% Aquaquench ACR. Despite the difference in behaviour of the surface heat transfer coefficient no difference in boiling phenomena was detected by still photography.

In the very late stages of the quench, when the froth was confined to the central region of the plate face the presence of a viscous gel was revealed in silhouette, (plates 11 and 12). This structure had hitherto not been detected but was now noticeable as it lifted away from the top edge of the plate.

This viscous gel was observed to have formed around the plate during quenching in concentrations of 10% Aquaquench ACR and greater. (In 5% Aquaquench ACR the viscous gel was occasionally observed to have formed at the corners of the faces of the plate). At the end of the quench, when the plate had reached ambient temperature, the viscous gel separated itself from the

plate and floated on the surface of the bath. Bubbles were observed to be entrapped in the gel. It was not possible to discern the precise time of the formation of the viscous gel as it was colourless and therefore not easy to distinguish against a background of either the bulk quenchant or the liquid boiling on the surface of the plate. It was not observed to form in agitated quenches. A sample of the gel removed from the bath returned into solution over a period of approximately eighteen months.

Plates 11 and 12 also show that as the white froth retreated from the periphery of the plate face, presumably as the surface temperature fell below the boiling point of the liquid, black linear features had formed on the plate surface. These are most visible in the upper left hand corner of the plate face.

The surface of the plate after removal from the bath was only slightly oxidised and was covered with these black markings. Two forms were distinguishable. The first form was linear, (about 5 cm in length), ran approximately parallel to the plate edges, and was confined to the areas adjacent to the plate edges. The second form appeared as a broken ring, about 3 mm in diameter, and was confined to the central region of the plate face. As the concentration of sodium polyacrylate increased the area of the plate covered by the linear structures increased at the expense of the central area covered by the ring-shaped structures. Plates 19 to 22 show examples of these structures in two different concentrations of the polymer quenchant. The linear structures also appeared on the plate edges and base where the ring-shaped structures were largely absent.

6.5 Cine Photography

Three cine films were made of quenches performed in sodium polyacrylate solutions, (two were carried out in 10% Aquaquench ACR and one in 15% Aquaquench ACR). On the whole the quality of the cine films was poor but it was possible to relate the phenomena shown by the cine film to the surface temperature and the surface heat transfer coefficient calculated for the centre of the plate face in the same manner as for the still photographs, (figure 50).

The photographs, (plates 23 to 25), and the accompanying descriptions, refer to a quench performed in a 10% Aquaquench ACR solution.

The film boiling stage was shown to be very unstable and to contain a series of waves which followed the contour of the edge of the plate and quickly moved inwards from the edge to the centre of the plate in rapid succession. These first occurred after about 6 s in 10% Aquaquench ACR. Plate 23 shows a photograph of the plate face, (taken from a cine film), at 14.75 s when the surface temperature and surface heat transfer coefficient calculated at the centre of the plate face showed that a vapour blanket existed at this time. This photograph shows the vapour blanket confined to the upper centre of the plate face where it has the appearance of being split into a light irregular centre set in a dark rectangle. The remainder of the plate face extending to the edge was cooler and in the vapour transport stage and therefore produced the fine white cloud of bubbles noted earlier. The variation in contrast of the appearance of the

vapour blanket was probably due to variations in thickness as observed in the still photographs.

Plate 24 shows the plate face after the maximum surface heat transfer coefficient had passed at the centre. At this point in the quench the plate face contained the dendritic features noted earlier in the central region of the plate face surrounded by a white froth which extended to the edge of the plate.

The dendritic markings, which still photography had revealed to be elongated protusions of vapour, were shown to consist of individual bubbles, which were of the same width as the dendrites, and which travelled upwards rapidly. The white froth was shown to consist of discrete stationary bubbles. As the quench progressed and the surface heat transfer coefficient declined, (plate 25), the area of white froth expanded inwards and the dendritic area contracted. The net effect was a reduction in the mean velocity of the bubbles on the plate face.

6.6 The Results Of The Stress And Strain Calculations

The relationships between stress and strain produced during quenching were calculated for a low alloy steel using the infinite plate model given in section 5.2.2. Calculations were performed for specimens quenched in solutions of 5, 10, 15, 20 and 25% Aquaquench ACR, both still and agitated, and also for water, a medium speed quenching oil and a polyalkylene glycol solution.

6.6.1 The Calculated Residual Stresses In Plates Quenched In Sodium Polyacrylate Solutions

The maximum residual stress predicted in plates quenched in both still and agitated solutions of 10,15,20 and 25% Aquaquench ACR consistently occurred at the surface but this was not the case for the calculations performed in the case of plates quenched in 5% Aquaquench ACR, (figures 51 and 52). The predicted maximum residual stress for a plate quenched in the latter solution occurred at a depth of 1.5 mm below the plate face while for an agitated solution the maximum predicted residual stress occurred at 2.5 mm below the plate face. (A similar effect was observed in calculations performed for plates quenched in water, (figure 53), and 25% Aquaquench 1250, (figure 54)).

As the concentration of sodium polyacrylate increased the level of the predicted absolute residual stress in the quenched plates decreased. This trend occurred in calculations for both still and agitated solutions though it was not so marked in the latter case, (figures 51 and 52).

The calculation for the unagitated 5% solution produced a predicted maximum residual stress of 227 MPa, 24% below that predicted for a water quench, while the predicted centre residual stress was -183 MPa, comparable to that predicted for a water quench. In comparison to the calculation performed for the 25% Aquaquench 1250 solution the maximum predicted residual stress was 6% higher while the predicted residual stress at the centre of the plate was approximately the same in both cases, (figure 55).

The calculation for a quench carried out in a 15% Aquaquench ACR solution predicted residual stress levels that bore a close resemblance to those predicted by the calculation performed for the medium speed oil quench, (see figure 56). The maximum predicted residual stress at the surface was, in the case of the sodium polyacrylate solution, 145 MPa, (compared to 146 MPa obtained from the oil quench calculation), while the predicted residual stress at the centre was -96 MPa, (compared to -100 MPa).

6.6.2 The Calculated Residual Strains In Plates Quenched In Sodium Polyacrylate Solutions

The predicted residual strain for plates quenched in concentrations of sodium polyacrylate of 10% Aquaquench ACR and greater followed the same trend with the maximum predicted residual strain at the surface and the minimum at the centre, (figures 57 and 58). In contrast the predicted residual strain in the case of a plate quenched in a solution of 5% Aquaquench ACR was a minimum at the surface, rose to a maximum at a depth of 1.5 mm and then declined as the centre of the plate was approached.

The predicted residual strain was tensile in all parts of the plate in all quenchants for which calculations were performed.

No clear relationships between concentration, agitation and absolute residual strain were apparent from the results but there was a tendency for the difference between minimum and maximum predicted residual strain to decrease with increasing concentration.

The predicted residual strains obtained from calculations for plates quenched in the sodium polyacrylate solutions were in all cases lower than that predicted for a water quench while the calculation for the 25% Aquaquench 1250 solution predicted a greater surface residual strain but also a lower centre residual strain. The predicted residual strain for a plate quenched in the medium speed quenching oil was of approximately the same magnitude as the predicted residual strains for the sodium polyacrylate solutions. These comparisons are shown in figure 59.

6.7 The Generation Of Thermal Stress And Strain During Quenching In Sodium Polyacrylate Solutions

The generation of stress and strain during the quenching of an infinite plate of a low alloy steel was calculated for both still and agitated solutions of 5,10,15,20 and 25% Aquaquench ACR using the relationships for surface temperature and surface heat transfer coefficient obtained by this work. The relationships between stress and strain during quenching thus obtained are presented in figures 60 to 69.

The results for the higher concentrations of sodium polyacrylate examined, (that is, greater than 10% Aquaquench ACR), bore strong similarities to each other and therefore one calculation only, that for quenching in a still solution of 20% Aquaquench ACR, has been selected and described in detail. The calculation performed for quenching in 5% Aquaquench ACR solutions showed a marked difference to the results obtained for the solutions with higher concentrations and therefore this has

been described separately in section 6.7.2.

Comparisons between the results of these calculations and those performed for other popular quenchants, (namely water, a medium speed quenching oil and a polyalkylene glycol solution), using surface heat transfer coefficient data obtained by other workers, are made in 6.7.3.

6.7.1 The Generation Of Thermal Stress And Strain During Quenching In A Solution Of 20% Aquaquench ACR

The relationship between calculated stress and strain during quenching in this solution is shown in figure 63. At the point of immersion the surface heat transfer coefficient rose from zero as the vapour blanket became established. Due to the falling temperature at the surface this part of the plate contracted but was restrained by the centre of the plate which, due to its higher temperature, was contracting at a lower rate. The net effect was that the surface was restrained in its contraction by the centre which caused a tensile stress at the surface while the centre was forced to contract by the surface which in turn created a compressive stress at the centre.

In the early part of the quench the surface heat transfer coefficient rose to a small peak as the film boiling stage was established, (figure 44). This caused the initial tensile stress at the surface and the compressive stress at the centre. These stresses rose until the yield stress of the material was reached, (which was relatively low at this temperature), and thereafter plastic deformation was produced. The value of the stresses at

the surface and centre then followed the value of the yield stress as it rose with decreasing temperature and as it was affected by work hardening.

When the vapour blanket was established in this solution the surface heat transfer coefficient began to decline as the surface temperature fell. The cooling rate at the surface fell to below the cooling rate at the centre. The latter was driven by the temperature gradient between the surface and centre created by the rising surface heat transfer coefficient at the start of the quench. As the centre cooling rate rose above that of the surface the relative restraints of the surface and centre were reversed. The centre now began to exert a compressive force on the surface as it tried to contract at a faster rate than the surface. This is shown in figure 63 as the unloading of the surface element at 782^{o}C and the centre element at 832^{o}C. With the declining surface heat transfer coefficient as film boiling progressed the surface stress became more compressive and the centre stress more tensile.

This continued until the vapour blanket collapsed and the vapour transport stage began at a mean surface temperature of 636^{o}C in this solution. Surface cooling rates again rose to above those of the centre as the surface heat transfer coefficient increased towards its maximum. The stresses in the surface and centre elements therefore reloaded once more, at 680^{o}C and 724^{o}C respectively.

With the rapid rise in surface heat transfer coefficient produced by the first part of the vapour transport stage the surface stress quickly became more tensile until the yield stress

was again reached. This part of the quench therefore produced substantial plastic deformation at the surface with smaller amounts of plastic deformation produced at the centre.

The maximum surface heat transfer coefficient occurred at a mean surface temperature of 450°C in this solution. After this had passed the surface cooling rate fell rapidly to below that of the centre which caused an unloading of the surface stress at 478°C and an unloading of the centre stress at 611°C.

As the vapour transport stage continued at the surface the tensile stress declined until it became compressive at 410°C. It then became increasingly more compressive until the yield point was reached. This period of the quench was associated with the rapid decline in the surface heat transfer coefficient from its value at the maximum. Shortly afterwards the stress unloaded once more at 344°C.

This reversal at 344°C had two causes. Firstly, the surface cooling rate had now declined considerably from its value at the maximum surface heat transfer coefficient though it had not yet become equal to that of the centre. Secondly, the stress relaxation rate at the surface was sufficiently large, despite the relatively low temperature, to accomplish a significant reduction in surface stress. That stress relaxation played a part in this unloading was shown by the fact that a reversal in the generation of stress was observed but with no accompanying reversal in the generation of strain. In short, this reversal, and the associated reversal in the centre at 356°C, was caused by a reduction in the cooling rate at the surface to a degree that

the rate of increase in stress caused by differential contraction fell below the rate of decrease in stress caused by stress relaxation.

Shortly thereafter transformation began in the surface element, (at 300°C), and transformation plasticity began to operate. This had the effect of increasing the surface stress to -40 MPa and produced a plastic deformation plateau between 300°C and 260°C. A similar process, though smaller in extent, occurred at the centre. Upon the cessation of transformation plasticity the surface stress experienced a tensile loading.

This tensile loading was due to the low temperature gradient which existed in the plate at this time. By the time transformation plasticity had ceased at the surface the transformation front had reached sufficiently far into the interior that expansion there exerted a tensile force on the surface and also offset any expansion caused by the ongoing transformation, which was more advanced, at the surface. After the centre reached a temperature of 260°C and transformation plasticity ceased the expansion created by the ongoing transformation was restrained by the surface and caused a compressive loading at the centre following completion of the martensite transformation.

Subsequently, both surface and centre subsequently experienced a slight unloading as the temperature gradient in the specimen was finally eliminated.

At ambient temperature the residual stress was therefore tensile at the surface of the plate and compressive at the centre. The residual strain was tensile throughout the thickness

of the plate and was at its maximum at the surface and its minimum at the centre.

6.7.2 The Generation Of Thermal Stress And Strain During Quenching In A Solution Of 5% Aquaquench ACR

Upon being quenched in an unagitated 5% Aquaquench ACR solution, (see figure 60), the surface initially experienced a tensile loading and the centre a compressive loading as is normal in any quenching operation. The tensile stress rose at the surface until the elastic limit was exceeded and plastic deformation commenced. There was a slight film boiling stage in this solution and the surface heat transfer coefficient passed through a maximum value before declining slightly just before the onset of the vapour transport stage. This decline gave rise to the unloading of the surface tensile stress at 815^{o}C. The tensile stress at the surface was reduced as surface cooling rates declined until the minimum film boiling point was passed. Surface cooling rates then rose rapidly and caused the tensile loading at 784^{o}C. The tensile stress at the surface increased and plastic deformation again occurred. This tensile loading was maintained until the attainment of the maximum surface heat transfer coefficient. The subsequent reduction in the surface heat transfer coefficient produced the unloading of the surface stress at 507^{o}C. These unloadings at the surface were reflected with unloadings at the centre at 847^{o}C, 821^{o}C and 722^{o}C respectively.

The tensile stress at the surface decreased under the influence of the compression exerted by the centre until it

reversed completely and became compressive. This compressive stress then increased until the yield point was again reached but shortly after the surface stress unloaded at 351°C and became less compressive. Within a short space of time the centre stress also unloaded.

The unloadings at 351°C at the surface and 458°C at the centre were absent in the calculations performed for the higher concentration solutions of sodium polyacrylate. In 5% Aquaquench ACR solution the surface heat transfer coefficient rose again at a surface temperature of about 350°C, (see figure 41), and again produced higher surface than centre cooling rates. This caused the surface tensile loading at 351°C. There was no unloading of the stress significantly influenced by stress relaxation as occurred with the higher concentrations examined.

Almost immediately afterwards M_s was reached at the surface. The transformation caused this part of the plate to expand and caused a tensile loading of the centre. Transformation plasticity began to operate at the surface and produced the plastic deformation plateau observed at -40 MPa. At the end of transformation plasticity the surface experienced a large compressive loading. This was due to the expansion caused by transformation being restrained by the interior of the specimen, to which the transformation front had not yet reached. (The reverse occurred, with a tensile loading of the surface at the end of transformation plasticity, in the results of the calculations for the higher concentrations of sodium polyacrylate). The compressive loading continued until the

surface stress reached -609 MPa at 228°C whereupon it unloaded as the transformation front progressed into the interior. The tensile loading of the surface after 228°C continued until the surface stress reversed and created a tensile residual stress at ambient temperature.

After M_s was reached at the surface the centre stress continued to become more tensile until the yield point was reached and substantial plastic deformation occurred at this point in the plate. The transformation front then moved inwards until it reached the centre so that the stress at this point fell to -40 MPa where it remained until transformation plasticity was complete. Subsequently, the centre stress became more compressive with the progression of transformation. In consequence a compressive residual stress existed at the centre at ambient temperature.

The predicted residual strain was tensile throughout the plate but was a minimum at the surface and a maximum at a depth of 1.5 mm.

The foregoing description is also applicable to the generation of thermal stress and strain in an agitated solution of 5% Aquaquench ACR, figure 65.

6.7.3 Characteristics Of The Generation Of Thermal Stress And Strain In Sodium Polyacrylate Solutions

The temperatures at which the unloadings occurred during the generation of thermal stress and strain are given in table 8, together with their attributed causes. Tables 9 and 10 give the stress and strain values, respectively, associated with each of

these unloadings. Values for the whole range of Aquaquench ACR solutions examined and also values for a quench in water, oil and a polyalkylene glycol solution are given. The relationships between stress and strain from which this information was derived are presented in figures 60 to 68 in the case of the sodium polyacrylate solutions and figures 70, 71 and 72 in the case of water, a medium speed quenching oil and a polyalkylene glycol solution respectively.

As the concentration of sodium polyacrylate was increased the temperatures at which each of the unloadings occurred tended to decrease. Only the unloading caused by the passage of the maximum surface heat coefficient was clearly affected by the agitation of the bath. This tended to cause a slight increase in the temperature of its occurrence.

The stress and strain values associated with the changes in loading were largely independent of concentration and agitation though some isolated trends were observed. For example, the surface stress values for the start of the stress unloading associated with the maximum film boiling surface heat transfer coefficient tended to increase with increased concentration. The stress values for the unloading associated with the passage of the maximum surface heat transfer coefficient tended to increase with increased concentration while the strain value decreased.

Both stress and strain values at the onset of the unloading associated with the decline in surface cooling rates, (unloading 4 in tables 8, 9 and 10), tended to decrease with increased concentration of sodium polyacrylate.

6.8 Experimental Measurements Of Residual Stress

The first experimental determinations of residual stress were carried out on plates quenched in solutions of 15% and 25% Aquaquench ACR without the use of an insulating Kaowool blanket at the plate edges. These results are given in figures 73 and 74 respectively with comparisons with the predicted residual stress in each case. The experimentally determined residual stresses given in this section were corrected to account for the effect of the free edge by applying a factor derived from Saint-Venants' Principle, (see section 5.1.5).

Qualitative agreement between the calculated and measured residual stresses was obtained. The experimental values of residual stress obtained from a plate quenched in 15% Aquaquench ACR were significantly higher than the corresponding calculated values at both the surface and centre. The residual stress at the surface of the plate was 2.4 times the value of the calculated residual stress while at the centre it was 1.8 times the value predicted.

The experimentally determined residual stress obtained using the 25% solution, figure 74, again showed qualitative agreement with the calculated values in that the surface stress was tensile and the centre stress compressive but quantitative agreement was again poor. The experimental residual stress was 1.2 times the value of the predicted residual stress at the surface but it then rose to a maximum at a depth of 1.5 mm. (This maximum was a feature observed in the predicted stresses only with the more severe quenchants such as water or the dilute sodium polyacrylate

solution, 5% Aquaquench ACR). At the centre the absolute experimental residual stress was 3.0 times the value of the calculated residual stress.

The remaining measurements were performed on plates with an insulating Kaowool layer around the edge; two tests being carried out in each solution examined. Generally the results showed slightly better agreement with the calculated values than those obtained from plates not insulated in this way.

In 5% Aquaquench ACR, (figure 75), the mean experimental surface residual stress was 1.2 times, and the mean experimental centre residual stress 1.4 times, the values predicted. Both experimental measurements of residual stress displayed a rise from the surface value to a maximum at a depth of 2 mm in common with the calculated residual stress.

The experimentally determined residual stresses in specimens quenched in 15% Aquaquench ACR are shown in figure 76. The mean surface stress was within 0.5 MPa of that calculated but the centre residual stress was 1.9 times the predicted value. These results demonstrated well the level of reproducibility which may be attained with this experimental procedure.

In 25% Aquaquench ACR the mean surface experimental residual stress was only 0.4 times the calculated value while the centre residual stress was 2.9 times the calculated value, (figure 77). This poor agreement was due to the fact that both experimental measurements of residual stress in this solution showed a marked rise in residual stress, which was absent in the calculations, from the stress measured at the surface to a maximum stress recorded at a depth of 2mm.

6.9 Experimental Measurements Of Residual Strain

The experimentally measured residual strains given in this section were also corrected, using Saint-Venants Principle, to allow a comparison with the predicted residual strains, (see section 5.1.4).

The experimentally measured residual strain in a plate quenched in a 15% Aquaquench ACR solution is given in figure 78. This plate was not insulated at the edge. At a depth of 1 mm the measured residual strain was approximately equal to the value of the calculated residual strain but with increasing depth below the plate face the measured residual strain increased to reach a maximum as the further face of the plate was reached. In contrast the calculated residual strain declined from the surface value to reach a minimum at the centre and then rose again to produce a strain distribution that was symmetrical about the centre. This symmetry was a consequence of the assumption that temperature distribution, and therefore the calculated stress and strain, were symmetrical about the centre-line of the plate.

The lack of symmetry in the measured residual strain was due to the plate bending during the quenching process. This occurred in all of the specimens examined. The bending would also influence the level of agreement between the measured and calculated residual strain at the centre of the plate face. Therefore the only meaningful comparisons that could be drawn from these results were those between an average of the calculated and an average of the measured strain. These results are shown in figure 79.

Adopting this procedure the mean measured residual strain for the uninsulated plate quenched in a 15% Aquaquench ACR solution was 1.6 times greater than the mean calculated residual strain while the measured residual strain at the centre of the plate face was 4.2 times the calculated value.

The mean measured residual strain for an uninsulated plate quenched in a 25% Aquaquench ACR solution was 1.2 times the mean calculated value while the measured strain at the centre of the plate face was 1.5 times the calculated value.

The remaining measurements were carried out on plates that had insulated edges, (in order to better simulate the infinite geometry assumed by the model); two plates each being quenched in solutions of 5, 15 and 25% Aquaquench ACR. (Figures 80, 81 and 82 show the results obtained from each of these quenches to demonstrate the level of reproducibility of the experiment). These results show mean measured residual strains that were below the mean calculated values, in contrast to the results obtained from the uninsulated plates, being 0.3, 0.7 and 0.4 times the mean calculated values respectively. The measured strains at the centre of the plate face were, respectively, 3.4, 2.0 and 1.3 times the calculated values. Therefore the effect of the insulating layer around the plate edge was to reduce the mean experimentally measured residual strain from above to below calculated values.

6.10 Viscosity And Density Of The Sodium Polyacrylate Solutions

The kinematic viscosities of the sodium polyacrylate solutions

are given in figure 83 and table 11 with data for water from the Chemists Handbook[142] included for comparison. These results showed that as the concentration of sodium polyacrylate was increased the kinematic viscosity increased while an increase in the temperature of the solution reduced the kinematic viscosity. At room temperature a 25% Aquaquench ACR solution had a kinematic viscosity of about forty times that of water.

The density of the sodium polyacrylate solutions similarly increased with increased concentration and decreased with increased temperature, (table 12), but in the former case the increase was slight. The density of a 25% Aquaquench ACR solution was between 2.0 and 2.5% greater than water at all the temperatures examined.

The dynamic viscosity of the solutions, (table 13), duplicated the trends observed in the kinematic viscosity results.

6.11 Surface Tension In Sodium Polyacrylate Solutions

The results of the surface tension tests are given in figure 84 together with values for water as a comparison. The addition of sodium polyacrylate to water, (equivalent to concentrations of 25% Aquaquench ACR and lower), produced changes in surface tension which were of the order of the accuracy of the experiment.

An increase in the concentration of sodium polyacrylate and an increase in the temperature of the solution both reduced the surface tension of the quenchant. The effects of increased polymer concentration on surface tension became smaller as the

temperature of the solution was increased, (for example, 25% Aquaquench ACR had a surface tension 10% below that of water at 20°C but only 4% below at 80°C).

6.12 The Viscosity Of A Liquid Extracted From The Vicinity Of The Plate Surface

Still photography and personal inspection showed that when the temperature of the surface of the centre of the plate was below about 420°C the mobility of the bubbles on the plate surface was greatly reduced. The calculated surface heat transfer coefficient below this surface temperature was also very low being about the order of the values determined for the film boiling stage. This suggested the hypothesis that the mobility of the bubbles was restricted by the presence of a viscous phase which had formed in the vicinity of the plate surface. This would have accounted for the reduced surface heat transfer coefficient.

The viscosities of three 8 ml samples of the polymer quenchant were measured. One sample was taken, using a syringe, from the immediate vicinity of the centre of the plate face just after the surface temperature in this area had fallen to below approximately 420°C. Another sample was taken from the bulk of the bath before the quench began while the third was removed, again using a syringe, from below the viscous gel as it floated on the surface of the bath above the plate at the end of the quench.

Very similar results, (table 14), were obtained from all three samples. This suggested that the liquid at the plate face

associated with the reduction in surface heat transfer coeffient and the liquid associated with the viscous gel at the end of the quench were no more viscous than the bulk quenchant itself.

6.13 Differential Thermogravimetric Analysis

In order to examine the response of the polymer to heat differential thermogravimetric tests were performed on samples of the Aquaquench ACR concentrate. This involved heating the sample in an inert atmosphere, at a predetermined rate, over the required temperature range while recording its mass. From this the relationships between mass and temperature and rate of mass loss and temperature were determined.

A test performed over the range 35-850^{o}C showed three regions in which the rate of mass loss was greater than average, (figure 85). The first region reached a maximum at 140^{o}C and was probably due to the water being driven off from the concentrate. The second region was spread over a wide range of temperature, (from about 200^{o}C to about 530^{o}C), and showed a maximum rate of mass loss at about 430^{o}C, although the magnitude of this effect was not large. The third region showed a maximum rate of mass loss of about half that recorded at 430^{o}C over a temperature range of 750-800^{o}C.

A test was performed over the temperature range 360-540^{o}C to investigate the region where the maximum rate of mass loss occurred at about 430^{o}C, figure 86. (This was also approximately the temperature at which the surface heat transfer coefficient declined rapidly after reaching a maximum in the vapour transport

stage). However, the results showed only a gradual weight loss over the entire range.

These tests suggested that the value of the results was reduced by the presence of comparatively large amounts of water in the concentrate. Therefore, this was removed by evaporation from the sample and a test performed on the residue. A differential thermogravimetric test on this sample produced different results, (figure 87), to those above which suggested that the polymer had been damaged in some way by the evaporative treatment despite the low temperature. However, the first test did at least suggest a change in the structure of the polymer molecule at approximately the temperature at which the surface heat transfer coefficient experienced a rapid decline.

6.14 Scanning Electron Micrographical Examination Of The Surface Of A Quenched Plate

An examination of the surface of a quenched plate was performed using a scanning electron microscope. Two areas on the base of a stainless steel plate quenched in 15% Aquaquench ACR were examined. One area lay approximately in the centre of one of the black linear structures, (these are illustrated in plate 25, for example), while the other lay approximately halfway between two such structures.

An analysis of the chemical composition of the two areas, figure 88, revealed that both areas contained considerably more carbon than the material from which the plate was made, a grade 316 stainless steel which had a specification of 0.08% carbon,

and that the surface of the black linear structure or dark band contained more carbon than the surface of the area between the bands. (This was a qualitative assessment only since precise measurements of composition were not possible). A reduction in the quantity of oxygen in the surface of the dark band was also noted.

Both areas contained approximately the same amount of sodium.

Micrographs of both areas displayed a marked difference. The surface between the dark bands, (plate 26), appeared rough in comparison to the surface within the dark bands, (plate 27), probably due to the increased deposition of carbon-rich material which had occurred at the latter position.

6.15 Film Boiling Heat Transfer Models

Three boundary layer models of subcooled film boiling heat transfer were evaluated as explained in section 5.3. The first model, by Cess and Sparrow,[109] assumed that the film boiling interface was stationary while the second model, by Nishikawa and Ito,[112] assumed that it was moving upwards but at an unknown velocity. Both models assumed that the physical properties of the liquid and vapour could be represented by their values at the mean temperatures of the boundary layers. The third model, by Nishikawa, Ito and Matsumoto,[114] also assumed a moving interface but in addition assumed that the physical properties of the liquid and vapour were represented at their values at the temperature appropiate to their distance from the hot surface.

The surface heat transfer coefficients predicted by these

models were compared to experimental data obtained from quenching in water and a 25% Aquaquench ACR solution, (figures 89 and 90). As a result of these comparisons a further model was proposed which incorporated a turbulent interface.

6.15.1 The Film Boiling Heat Transfer Model Of Cess And Sparrow

The film boiling surface heat transfer coefficients predicted by the model of Cess and Sparrow[109] are given in figure 89 in the case of water and figure 90 in the case of a solution of 25% Aquaquench ACR. They are compared with experimental data for the surface heat transfer coefficient derived from the information obtained during quenching. Tables 15 and 16 give further data predicted by this model for water and the polymer solution respectively.

Both sets of experimental data displayed a form which was not duplicated by any of the calculated results. In water the experimental surface heat transfer coefficient rose initially to a peak of nearly 800 $W.m^{-2}.K^{-1}$ before it declined to below 500 $W.m^{-2}.K^{-1}$. Thereafter the surface heat transfer coefficient rose and fell once more before rising rapidly as the film boiling stage ended and transition boiling began. The experimental data obtained using the 25% Aquaquench ACR solution behaved similarly. The surface heat transfer coefficient rose from zero to a peak at about 390 $W.m^{-2}.K^{-1}$ before falling to a low of about 300 $W.m^{-2}.K^{-1}$. Thereafter it oscillated twice between about 305 $W.m^{-2}.K^{-1}$ and 375 $W.m^{-2}.K^{-1}$ before transition boiling began.

The data for the two quenchants are not strictly comparable

with each other since they occur at different surface temperatures; thus the vapour transport stage began, in the case of water, at about 850°C while in the 25% Aquaquench ACR solution it began at about 590°C. The specimen was quenched from a temperature of 1000°C in the case of water while the polymer quench began at 850°C. Nevertheless it was possible to deduce from the data that the film boiling surface heat transfer coefficient in water tended to rise with decreasing surface temperature while in the case of the sodium polyacrylate solution it remained approximately constant.

Mean surface heat transfer coefficients in the film boiling stage were about 500 $W.m^{-2}.K^{-1}$ in the case of water and about 325 $W.m^{-2}.K^{-1}$ in the case of 25% Aquaquench ACR.

The film boiling heat transfer model of Cess and Sparrow[109] predicted surface heat transfer coefficients that were lower than the corresponding experimental values for both quenchants. Also, a gradual rise in surface heat transfer coefficient with increasing surface temperature, (ie, the opposite trend to that observed experimentally), was predicted in the case of both water and the sodium polyacrylate solution. In water the mean of these values, (from 850°C to 1000°C), was 284 $W.m^{-2}.K^{-1}$, 57% of the mean experimental values while in 25% Aquaquench ACR solution the model predicted a mean, (from 600°C to 850°C), of 224 $W.m^{-2}.K^{-1}$, 69% of that measured experimentally. No oscillations such as those recorded in the experimental data were predicted.

Both the experimental and calculated values of surface heat transfer coefficient referred to above contained a contribution from the effects of radiation. The mathematical model of Cess and

Sparrow predicted the conduction heat transfer coefficient, h_{co}, only.

In water the calculated conduction heat transfer coefficient, h_{co}, did not behave in the same manner as the calculated total surface heat transfer coefficient, h. Whereas the latter rose consistently with increased surface temperature the former fell from its value at 700°C to a minimum at 850°C before rising as surface temperature increased. (The overall rise in the total calculated surface heat transfer coefficient was therefore caused by the contribution of the radiation heat transfer coefficient which increased as surface temperatures increased). The temperature of the minimum film boiling point of water was found to be approximately 850°C from the time/temperature relationships presented in section 6.1. However, a proposal that this model predicted the minimum film boiling point is not well founded as the conduction heat transfer coefficient in the sodium polyacrylate solution was observed to rise continuously with increasing surface temperature, passing through the surface temperature where the minimum film boiling point would be expected.

The thickness of the vapour film predicted by this model, in the case of water, increased with increased surface temperature from 0.37 mm at 700°C to 0.56 mm at 1000°C. In the sodium polyacrylate solution it increased from 0.37 mm at 550°C to 0.55 mm at 850°C. Therefore, at the same surface temperature, the vapour film was thicker in the polymer solution than in water, (for example, at 800°C the thickness of the vapour film was

0.43 mm in water but 0.53 mm in the sodium polyacrylate solution). It would be expected that an increased thickness in the vapour film would give an increased resistance to heat transfer which would account for the reduced predicted surface heat transfer coefficient in the case of the polymer quenchant compared to water.

6.15.2 The Film Boiling Heat Transfer Model Of Nishikawa And Ito

The model formulated by Nishikawa and Ito,[112] (which assumed that the liquid/vapour interface was moving rather than stationary as was assumed by Cess and Sparrow[109]), predicted higher film boiling surface heat transfer coefficients in water than did the latter model. These results are shown in figure 89 and table 17. In the case of water the mean calculated surface heat transfer coefficient over the range of surface temperatures 850-1000^{o}C was 330 $W.m^{-2}.K^{-1}$, 66% of that determined experimentally. The total surface heat transfer coefficient again rose gradually with increased surface temperature but so did the conduction heat transfer coefficient; it did not fall to a minimum and then rise again as was observed in the previous model.

This model reduced the predicted film boiling surface heat transfer coefficient in the case of 25% Aquaquench ACR to a mean, over the range of surface temperatures 600-850^{o}C, of 199 $W.m^{-2}.K^{-1}$, which was about 61% of that recorded experimentally, (see figure 90 and table 18).

The predicted thickness of the vapour film was accordingly

increased with this model in the case of the polymer quenchant but decreased in the case of water compared to the values predicted by the model of Cess and Sparrow.[109] At 800°C the calculated thickness of the vapour film was 0.36 mm in water and 0.60 mm in 25% Aquaquench ACR.

The interfacial velocities predicted by this model gave rise to some uncertainty since clearly the condition that the velocity of the vapour should equal the velocity of the liquid at the interface was not obeyed. For example, in 25% Aquaquench ACR, at a surface temperature of 750°C, the calculated velocity of the vapour at the interface was of the order of 0.1 $mm.s^{-1}$ but the calculated velocity of the liquid at the interface was 9.0 $mm.s^{-1}$. The values of the Reynolds number of the vapour and liquid at the interface given in tables 17 and 18 were calculated from this data. In both quenchants the predicted velocity of the vapour and liquid at the interface rose as the surface temperature of the plate increased, as did the associated Reynolds numbers.

The Reynolds numbers for the vapour at the interface were low; of the order of 1.5 in the case of water and 0.3 in the case of the sodium polyacrylate solution. The Reynolds numbers for the liquid increased from about 170 to 220 over the range of the calculations in the case of water but were substantially lower in the case of the polymer solution ranging from 39 to 49. If 100 be taken as the critical Reynolds number for the transition from laminar to turbulent flow then film boiling in water would be accompanied by a turbulent interface whereas film boiling in a 25% Aquaquench ACR solution would be accompanied by a laminar interface.

6.15.3 The Film Boiling Heat Transfer Model Of Nishikawa, Ito And Matsumoto

The model of Nishikawa, Ito and Matsumoto[114] also predicted surface heat transfer coefficients that were lower than the values obtained experimentally with mean values of 326 $W.m^{-2}.K^{-1}$ in the case of water and 211 $W.m^{-2}.K^{-1}$ in the case of the 25% Aquaquench ACR solution. These values were both about 65% of those measured experimentally. (See figures 89 and 90 and tables 19 and 20 respectively).

The trend observed in the previous two models with respect to the effect of temperature on the surface heat transfer coefficient was reversed in this model. The conduction heat transfer coefficient decreased with increased surface temperature and, as a result, so did the total surface heat transfer coefficient. This was the trend observed in the experiments carried out in water. The calculated vapour film thickness again increased with increased surface temperature though it showed a reduction in values from the previous two models. For example, it ranged from, in the case of water, 0.12 mm at 700°C to 0.18 mm at 1000°C and in the case of the 25% Aquaquench ACR solution from 0.17 mm at 550°C to 0.26 mm at 850°C.

The velocity of the vapour and liquid at the interface again increased with increased surface temperature but was substantially reduced compared to the values predicted by the model of Nishikawa and Ito.[112] The values of the associated Reynolds numbers were correspondingly reduced. Again the condition that the velocity of the vapour should equal the

velocity of the liquid at the interface was not obeyed. In the case of both quenchants the maximum Reynolds number now calculated was 131 in water at the liquid side of the interface at a surface temperature of 1000°C which may indicate that some turbulent flow may be expected.

However, the expressions for obtaining the velocity at the interface from the dimensionless velocity, based on expressions given by Cess and Sparrow,[109] were found to be in error as revealed by the inaccuracy of the dimensions they produced. Correct expressions were obtained from Koh[110] and Schlichting,[111] (section 5.3.4), and the condition that the velocity of the vapour and the liquid at the interface should equal one another was now met. This produced the results in table 21 from the model with varying physical properties in the boundary layers.[114] In the case of water the interfacial velocity was now predicted to be, for example, (at a surface temperature of 950°C), of the order of 0.6 $m.s^{-1}$ with correspondingly increased values of the Reynolds number of about 1760 for the vapour at the interface and about 132,700 for the liquid at the interface. In 25% Aquaquench ACR, at a surface temperature of 750°C, the interfacial velocity now became 0.109 $m.s^{-1}$ with vapour and liquid Reynolds numbers of 317 and 576 respectively. Turbulent flow in film boiling during quenching, in both water and the sodium polyacrylate solution, would therefore be indicated by these high values of the Reynolds number.

6.15.4 Film Boiling With A Turbulent Interface

The solution of the previous models had shown that the

assumption of film boiling as a process involving only laminar flow produced predicted surface heat transfer coefficients which were not in close agreement with experimentally measured values.

Therefore the assumption was made, as outlined in the procedure, (section 5.3.4), that the film boiling interface was turbulent and that the Reynolds numbers of the vapour and liquid at the interface were equal. The fixed physical property differential equations, (that is, the equations used by Cess and Sparrow[109] and Nishikawa and Ito[112]), were then used to calculate the film boiling surface heat transfer coefficient with different critical Reynolds numbers assumed for the interface.

It was not possible to obtain experimentally determined values for the velocity of the interface in either quenchant. No values could be measured from the cine films due to their poor quality. Hsu and Westwater[97] based their model of film boiling in a saturated liquid on a critical Reynolds number of 100 but experimental work previously presented by them[96] suggested that the transition from laminar to turbulent flow of the interface was associated with Reynolds numbers of about 2000. Coury and Dukler[103] presented a model for subcooled film boiling with a turbulent interface which assumed a critical Reynolds number of 35. However, the assumption of values of 35 and 100 for the critical Reynolds number in this model did not significantly improve the agreement between predicted and experimental surface heat transfer coefficient.

Therefore, since the critical Reynolds number for the transition from laminar to turbulent flow was not known beforehand various Reynolds numbers for the interface were

assumed and the predicted surface heat transfer coefficients compared to those obtained experimentally. A good agreement with the experimentally measured surface heat transfer coefficient was obtained when values of the interfacial Reynolds numbers of 22,500, in the case of water, and 250, in the case of the 25% Aquaquench ACR solution, were employed. The results of these calculations are shown in figures 91 and 92 and tables 22 and 23.

Assuming a critical Reynolds number of 22,500 in the case of water produced values for the velocity of the vapour at the interface of 7.76 $m.s^{-1}$ and for the velocity of the liquid at the interface of 0.103 $m.s^{-1}$. The predicted thickness of the vapour blanket varied from 0.19 mm to 0.31 mm over the range of surface temperatures from 700°C to 1000°C.

Assuming a critical Reynolds number of 250 in the case of the 25% Aquaquench ACR solution produced values for the velocity of the vapour at the interface of 0.086 $m.s^{-1}$ and for the velocity of the liquid at the interface of 0.047 $m.s^{-1}$. The predicted thickness of the vapour blanket varied from 0.21 mm at 550°C to 0.40 mm at 850°C.

6.16 The Application Of Film Boiling Models To Surface Temperatures Of Below 420°C

In the later stages of the quench, when the white froth had formed on the plate surface, the surface heat transfer coefficient was of the same order as that recorded during film boiling. In both cases it was recognised that heat transfer might be dependent upon the presence of the vapour adjacent to the

plate surface. This suggested that film boiling models might be capable of predicting the surface heat transfer coefficient at surface temperatures associated with the presence of the white froth.

Therefore the two types of differential equations previously presented, one using fixed boundary layer properties, (Cess and Sparrow[109] and Nishikawa and Ito[112]), and one using variable boundary layer properties, (Nishikawa, Ito and Matsumoto[114]), were used to predict the surface heat transfer coefficients at surface temperatures of 420°C and below in the case of a 25% Aquaquench ACR solution. Since the cine film and personal observation had shown that the bubbles of which the white froth was composed were stationary, the boundary conditions of Cess and Sparrow[109] were used. That is, the velocity of the vapour/liquid interface was assumed to be zero.

The results are shown in figure 93. Both models produced order of magnitude agreement with the experimentally measured surface heat transfer coefficient in the case of the 25% Aquaquench ACR solution. However, the experimental values fell rapidly from the maximum surface heat transfer coefficient to a minimum but then rose again as the boiling point of the quenchant was approached. The predicted results, using the fixed property differential equations, rose from their values at 420°C until they exceeded the experimental results while the values predicted by the variable property differential equations fell slightly from their value at 420°C before rising again slightly to exceed the experimental values. The latter produced higher predicted values of the surface heat transfer coefficient than the former.

7.0 DISCUSSION OF RESULTS

The results given in the previous section show that while sodium polyacrylate solutions have some characteristics in common with other quenchants there are also marked differences.

The discussion of the results in section 7.1 deals with the quenching characteristics of the polymer solutions as revealed by the time and temperature relationships and the surface heat transfer coefficients in conjunction with the appearance of the plate surface during quenching, as revealed by photography. The earlier stages of the quench, (film boiling and the early part of the vapour transport stage), bore most resemblance to previously encountered quenching phenomena and these are explored first. However, as the vapour transport stage in the polymer solutions progressed marked deviations from the boiling processes normally encountered, ie, in a water or an oil quench, were observed. The film boiling stage is therefore discussed in section 7.1.1 while the remainder of the quench is discussed separately in section 7.1.2.

The predicted residual stress and strain, and the calculated relationship between stress and strain during quenching produced by solutions of sodium polyacrylate are discussed in 7.2 with explanations of the results being sought in terms of the behaviour of the surface heat transfer coefficient and the photographed surface boiling phenomena. The calculated stress and strain levels during quenching in the case of these solutions have also been compared with the results obtained in the case of other quenchants, (namely, water, a medium speed quenching oil

and a polyalkylene glycol solution). Section 7.3 discusses comparisons between the predicted and experimentally determined residual stresses and strains and explores criticisms of the mathematical model and the experimental method implied by these results.

The results obtained from the solution of previously formulated film boiling models are discussed in section 7.4 together with the results obtained by a model which incorporated the concept of a turbulent interface, (7.5). Finally, the application of film boiling models to the later stages of quenching in solutions of sodium polyacrylate is examined in 7.6.

7.1 The Quenching Characteristics Of Sodium Polyacrylate Solutions

7.1.1 Film Boiling

An increase in the concentration of sodium polyacrylate caused an increase in the duration of the film boiling stage while the minimum film boiling point was simultaneously displaced to lower temperatures, (figure 40). This has been attributed to the formation of a viscous gel in this stage which contained and stabilised the vapour film[14] but photography of the film boiling stage failed to produce any evidence for the formation or presence of any such structure. Plates 2 and 13 show bubbles being released from the upper edge of the plate which would not be possible if a restraining structure surrounded the vapour blanket. An explanation for the increased stability of the film boiling stage was therefore sought in the heat transfer

characteristics of the vapour layer and their relationship with the physical properties of the polymer solution.

The collapse of the film boiling stage has been shown to be governed by the rate of removal of the vapour and the rate of evaporation of the liquid at the interface.[89 91] The surface heat transfer coefficient in the film boiling stage decreased slightly as the concentration of sodium polyacrylate increased, (figure 40). Since heat was mainly transferred by conduction through the vapour film[94 97 109] a reduction in the surface heat transfer coefficient required an increase in the vapour film thickness. This was demonstrated by the results of the calculation of the film boiling surface heat transfer coefficient in section 6.15. The calculated values for the more viscous, (compared to water), sodium polyacrylate solutions were associated with a thicker vapour blanket. An increase in the concentration of sodium polyacrylate in solution increased the viscosity of the solution, (table 11). Vapour escaped from the vapour blanket by travelling up the face of the plate and was released from the top of the plate by a process probably controlled by Taylor Instability. This process has been shown to be reduced by an increase in viscosity.[105] Increasing the concentration of sodium polyacrylate therefore reduced the rate of removal of vapour and caused the thickness of the vapour film to be increased. The net effect was to delay the collapse of the vapour film and to displace this event to a later time and a lower temperature.

The still photographs revealed that the vapour/liquid interface contained periodic oscillations, (plates 13 and 15).

These oscillations have been described as Taylor waves[9 84] though their presence on a vertically oriented surface suggests that their behaviour may not be truly described by a strict application of Taylor Instability theory. However, the term Taylor Waves has been retained in this report as a convenient term to describe all interfacial waves observed during film boiling.

The cine films showed that this stage was unstable and indicated turbulent flow. A series of wave-like structures that moved inwards with the line of the wave parallel to the edge of the plate face was also observed. This phenomenom was apparently absent in the still photographs while the Taylor waves observed in the latter were apparently absent in the cine film. It is difficult to reconcile the appearances of the two formations and it is therefore unlikely that they are two representations, one moving, one still, of the same process. The quality of the cine film was such, however, that it is probable that details recorded by still photography, (such as the Taylor waves), would not be recorded by the cine photography. It is possible that the moving waves represented large-scale variations in the vapour film thickness due to the vapour blanket being unstable in its nature and which were revealed in the cine film by their contrast and movement but which were invisible in the 10% Aquaquench ACR still photographs.

7.1.2 The Vapour Transport Stage

After the collapse of the vapour blanket the surface heat

transfer coefficient rose rapidly, (figures 40 and 41), while photography revealed the presence of many fine bubbles formed at the surface of the plate, (plate 3). The size of the bubbles was so small that collectively they bore the appearance of a white mist, (plates 4 and 16 for example). Their appearance was associated with a rise in the surface heat transfer coefficient from its value at the minimum film boiling point to its maximum. The white mist may have contained precipitated polymer but only a fine effervescence was observed on the surface of the bath above the plate during this time.

The collapse of the film boiling stage in these solutions therefore gave rise to a mode of boiling similar to that observed during water quenching - the removal of heat by the formation of many small bubbles.

Plate 4 shows the appearance of the plate when the surface heat transfer coefficient in the centre of the plate face was approaching the maximum. The centre of the plate face, to which the values of surface temperature and surface heat transfer coefficient related, was producing the white mist of bubbles associated with the part of the vapour transport stage characterised by a rapidly rising surface heat transfer coefficient while the adjacent areas of the plate, which were cooler, showed oblate bubbles or blisters. A photograph taken two seconds later, (plate 5), shows the surface of the plate when the surface heat transfer coefficient in the centre of the plate face was 3010 $W.m^{2}.K^{-1}$ and had just started to decline. The centre of the plate face to which the surface heat transfer coefficient referred appears to show a mixture of the blister structures,

(though they are smaller in appearance than those associated with cooler areas of the plate face), with some fine bubbles as well. Therefore, the fine mist of bubbles noted earlier produced a rising surface heat transfer coefficient which reached a peak and then began to decline as they gave way to the oblate, blister-type bubbles.

The surface heat transfer coefficient then declined rapidly with decreasing surface temperature until, at about 300°C, values equivalent to those recorded in the film boiling stage were reached. This occurred with both still and agitated solutions and in all concentrations examined except that of 5% Aquaquench ACR, (figures 40 and 41). In the latter case the surface heat transfer coefficient still fell rapidly after the passage of the maximum but did not fall so far before rising once again.

By comparison the surface heat transfer coefficients in water, (figure 49), quenching oils[84] and polyalkylene glycol solutions,[9] (figure 3), tended to fall in a more gradual fashion, from their maximums, until values associated with convection cooling were reached.

The still photographs of the plate quenched in 5 and 10% Aquaquench ACR showed that the latter stages of the quench, which were associated with the rapid decline in surface heat transfer coefficient, were characterised by two formations, (see plate 18 for example). These photographs showed a central region which consisted of dendritic features surrounded by a region of froth which extended to the edge of the plate. Since the central region of the plate was the hottest the former feature, the "dendritic"

stage, was associated with a higher surface temperature than the "frothy" stage. The dendritic stage consisted of alternate dark and light markings, the latter having the same appearance as the frothy stage. No boundary between the frothy stage and the light areas of the dendritic stage was observed and therefore the two phenomena appeared to be one and the same.

This was also shown by the cine photography which showed, in addition, bubbles which rose upwards in the paths between the white froth. The latter consisted of stationary bubbles. These results indicated a rapid decrease in the mobility of the bubbles adjacent to the surface of the plate and a consequent reduction in the surface heat flux. The decrease in bubble mobility was probably caused by an increase in the viscosity of the medium through which they were passing. This reduced the ability of bubbles to escape from the surface of the plate and they were therefore confined to its surface and forced to travel adjacent to it, in the interdendritic spacings within the white froth, to escape, finally, at the top edge. Surface roughness would cause the bubble paths to coalesce and split and therefore might be responsible for the unusual dendritic appearance of this stage.

An analagous, but reversed, situation is observed when condensation, in the form of drops, occurs on a cold, vertical surface, for example, a window pane. Under the influence of gravity the condensate flows downwards in paths that coalesce and divide to create a similar appearance.

Towards the end of the quench a viscous gel was observed to have formed around the plate in concentrations of 10,15,20 and 25% Aquaquench ACR. This structure can be seen, in silhouette, in

plates 11 and 12. Its presence was only detected very late in the quenching process when the gel separated from the plate and it was not possible to determine the precise time of its formation. It may therefore have formed at an earlier point in the quench but remained undetected as it lay adjacent to the surface of the specimen. Its presence would be expected to restrict the mobility of the vapour bubbles and this viscous gel can therefore be considered a candidate for the cause of the rapidly declining surface heat transfer coefficient and the formation of the dendritic and frothy stages of the quench.

However, other possibilities exist - a viscous liquid would have the same effects. The viscous gel observed at the later stage may have occurred as a byproduct of the formation of this viscous liquid or the viscous liquid may have become the viscous gel as its temperature fell as the quench progressed.

Tests on the viscosity of a sample of liquid extracted from a position adjacent to the centre of the plate face at a time when the dendritic stage formed were inconclusive. The results showed no difference in viscosity, measured at ambient temperature, between the sample extracted and the bulk quenchant. This implied that any viscous medium responsible for the decline in surface heat transfer coefficient existed in a thin layer close to the plate surface and that the sample extracted therefore consisted mostly of the bulk quenchant. There remains the possibility, however, that the viscosity of the extracted liquid behaved differently, compared to the bulk liquid, at higher temperatures.

Evidence exists of a change in the molecular structure of the

polymer at elevated temperatures. Differential thermogravimetric tests, (figure 85), indicated that sodium polyacrylate underwent a reaction over a temperature range of 300°C to 500°C and which reached a peak at about 430°C. This was approximately the temperature range over which the surface heat transfer coefficient fell rapidly. It was not possible to determine the nature of the reaction or the composition of the viscous gel but a possible reaction would be decomposition to polyacrylic acid. It is probable, therefore, that the reaction detected by differential thermogravimetry was associated with the change in appearance of the vapour on the surface of the plate and the associated decline in surface heat transfer coefficient.

The viscous gel was not observed to form when the quench was performed in an agitated bath yet the cooling curves and surface heat transfer coefficients in agitated quenches, (figures 39 and 41), showed the same characteristics as those obtained in unagitated quenches. These results indicated that the absence of the viscous gel, during agitation, did not greatly increase the value of the surface heat transfer coefficient above what could be attributed to the effects of agitation alone. This suggested that a viscous liquid, rather than the viscous gel observed later in the quench, was responsible for the behaviour of the vapour and therefore the surface heat transfer coefficient.

In the dendritic stage values of the surface heat transfer coefficient of the order of those determined during the film boiling stage were obtained. For example at 300°C, the temperature of M_s in the steel for which thermal stress and strain calculations were performed, the mean surface heat

transfer coefficient in solutions of 25% Aquaquench ACR was 345 $W.m^{-2}.K^{-1}$. By comparison the surface heat transfer coefficient in both water and RDN175, (a medium speed quenching oil), decreased at a slower rate from the value of maximum surface heat transfer coefficient to the boiling point of the quenchant. In water the maximum surface heat transfer coefficient occurred at about 300°C, (approximately 11.25 $W.m^{-2}K^{-1}$ in figure 49), while in RDN 175, a medium speed quenching oil, though the surface had entered the convective cooling stage by 300°C, the surface heat transfer coefficient[15] was still higher than that recorded in all concentrations of Aquaquench ACR greater than 10% being approximately 500 $W.m^{-2}K^{-1}$. Hence, the 25% Aquaquench ACR solution produced the lowest rate of heat transfer in the temperature range where the martensite transformation occurred.

As the quench progressed the central area of the dendritic stage shrank while the peripheral area of the frothy stage expanded. (Compare plate 6 to plate 10). Simultaneously the width of the dark dendrites shrank and the width of the white interdendritic spacings increased. Therefore as the plate cooled the dendritic feature vanished from the surface of the plate to be replaced by the frothy feature. This was associated with a slight increase in the surface heat transfer coefficient which began at a surface temperature of about 300°C, (figure 40). The reason for this is not apparent since the moving bubbles of which the dendrites consisted would be expected to produce a higher heat transfer rate than that obtained with the stationary bubbles of the froth.

Below the temperature of the maximum surface heat transfer coefficient the solution of 5% Aquaquench ACR produced surface heat transfer coefficients which were different from those produced in concentrations of 10% Aquaquench ACR and greater, (figures 40 and 41). However, some similarity in the results to those obtained in the case of higher concentrations was observed. Namely, the surface heat transfer coefficient declined rapidly after the passage of the first maximum, and still photography indicated the formation of a dendritic stage, (plate 17). But the surface heat transfer coefficient then rose to another peak, lower than the first, as the surface temperature fell further. In this solution no viscous gel was observed at ambient temperature. These results also disagreed with the hypothesis that the rapid decline in surface heat transfer coefficient was caused by the formation of a viscous gel as there was no evidence for its existence at any point in the quench but still the surface heat transfer coefficient declined sharply after passing the maximum.

If, therefore, the rapid decline in surface heat transfer coefficient can be attributed to the formation of a viscous liquid rather than a viscous gel the subsequent large rise in surface heat transfer coefficient in 5% Aquaquench ACR can be attributed to the partial or total removal of this viscous liquid. One explanation would be its removal by the convection of the bulk liquid. It is possible that the viscosity of the liquid and the ability of a viscous gel to be subsequently formed was related to the concentration of the polymer solution and that at low concentrations it was vulnerable to either free or forced convection.

A parallel to the results for the 5% Aquaquench ACR solution, where a double peak was observed in the surface heat transfer coefficient during quenching in a polyalkylene glycol solution, was reported by Fletcher and Price.[64] A change in gradient in that part of the cooling curve that related to the vapour transport stage, (figure 94), was also reported. This was attributed to a deposition of polymer onto the surface though no evidence to support this hypothesis was produced. (A similar change in gradient was detected in this work, (section 6.1)).

The rapid reduction in bubble mobility and consequent reduction in surface heat transfer coefficient in solutions of sodium polyacrylate, attributed to the formation of a viscous second phase, presents a new phenomenom not previously reported in relation to the quenching process. The temperature of the surface during which these effects occurred has been generally associated with the vapour transport stage in aqueous solutions but since, in sodium polyacrylate solutions, bubble mobility, (and hence vapour transport), is limited the application of this term to this stage can be considered a misnomer. Heat transfer would be expected to be mainly by conduction through the layer of vapour adjacent to the surface which largely consisted of discrete stationary bubbles. Therefore a convenient term to describe this phase is suggested, namely, the conductive cooling stage - where heat transfer is dependent upon conduction through a largely stationary vapour layer to a convecting liquid.

The surface of the plate at the end of the quench showed dark

markings (for example, see plates 19 to 22). A scanning electron microscopy examination of the surface revealed a high concentration of carbon on the surface as a whole, (higher than the chemical composition of the material), which was greatest at the position of the dark bands, (figure 88). A probable source of carbon for the material of the formations was the polymer molecule which suggests that during the quenching process the polymer solutions came into contact with the surface of the plate which caused the degradation of the polymer molecule. The film boiling stage suggests itself as the point at which the linear structures were formed on account of the presence of the Taylor waves in the liquid/vapour interface while the broken-ring structures were similar in size, and may therefore have been formed by, the oblate blisters observed just after the maximum surface heat transfer coefficient had passed.

7.2 The Generation Of Thermal Stress And Strain During Quenching in Sodium Polyacrylate Solutions

The sodium polyacrylate solutions differed from water and polyalkylene glycol solutions in having a prolonged film boiling stage. Despite the low value of the surface heat transfer coefficient in this stage variations with surface temperature produced a relatively complex loading pattern. Initially the surface experienced a tensile stress while the centre experienced a compressive stress but as the surface heat transfer coefficient reached a maximum with the establishment of the film boiling stage an unloading occurred at both the surface and centre. This

was also observed in an oil quench calculation, (RDN 175), performed using the data of Price and Fletcher,[15] (see figure 71), and was reported by Allen.[84] In contrast, the film boiling stage was virtually absent in water and solutions of polyalklyene glycol and the steadily increasing surface heat transfer coefficient during transition boiling produced surface and centre stresses that rose without interruption. Increasing the concentration of sodium polyacrylate increased the stability of the film boiling stage and also therefore the magnitude of the effects caused by its formation and collapse. Therefore the more concentrated sodium polyacrylate solutions displayed relationships between stress and strain, during the film boiling stage, which were similar to those calculated in the case of the RDN 175 quenching oil. With the collapse of the vapour blanket transition boiling began and the associated rising surface heat transfer coefficient produced a pattern of stress generation that was also observed in the case of other quenchants such as water, oil and polyalkylene glycol, (figures 70, 71 and 72 respectively). The surface and centre stresses reloaded and the surface stress rapidly became more tensile and the centre stress rapidly more compressive.

Since the yield stress of austenite at this temperature was relatively low substantial plastic deformation occurred between the end of the film boiling stage and the point at which the maximum surface heat transfer coefficient occurred. Increasing the concentration of sodium polyacrylate decreased the value of the maximum surface heat transfer coefficient, (figures 40 and

41), and also tended to slightly decrease the surface temperature at which it occurred, (table 8). The net effect was to diminish the amount of plastic deformation that occurred in the early parts of the quench, (table 10). Table 10 also shows that the calculated plastic deformation in the case of a quench in a RDN175 quenching oil was similar to values calculated in the case of quenches in 20% and 25% Aquaquench ACR.

After the passage of the maximum surface heat transfer coefficient the stresses unloaded and reversed their sense becoming compressive at the surface and tensile at the centre, (figures 60 to 69). This behaviour was also observed in calculations performed for quenches in the case of water, a quenching oil and a polyalkylene glycol solution, (figures 70, 71 and 72 respectively).

In sodium polyacrylate solutions this part of the quench was associated with a rapid decline in the surface heat transfer coefficent and the formation of the dendritic and frothy stages. In these solutions the compressive surface stress reached the level of the yield stress and some plastic deformation, though now compressive, again occurred. This was most marked in solutions of 10% and 15% Aquaquench ACR, (figures 61 and 62). In concentrations of 10% Aquaquench ACR and greater the rapid decline in surface heat transfer coefficient produced a situation where the surface cooling rate and the generation of thermal stress and strain became sufficiently slow that the effects of stress relaxation became significant and produced a net decrease in the absolute level of stress, (referred to as unloading 4 in tables 8, 9 and 10), but without a corresponding unloading in the

level of strain. This was a phenomenom hitherto unreported in the generation of thermal stress and strain during quenching.

Just after this unloading the M_s temperature was reached at the surface of the specimen and the associated transformation plasticity altered the stress at this point to -40 MPa. The associated plastic deformation occurring at the surface between 300°C and 260°C was reduced with increasing concentration of sodium polyacrylate from -0.17% in 5% Aquaquench ACR to -0.08% in 25% Aquaquench ACR.

With solutions of 10% Aquaquench ACR and greater the surface experienced a tensile loading as transformation plasticity ended. In water, by contrast, after transformation plasticity ceased at 260°C, a large compressive loading was experienced since the temperature gradient at this point was sufficiently high that the transformation was confined to the surface layers whose expansion was constrained by the centre, (figure 70). A similar effect was observed in the calculated stress/strain histories for the 25% Aquaquench 1250 and both still and agitated 5% Aquaquench ACR solutions, (figures 72, 60 and 65 respectively). In solutions of sodium polyacrylate of 10% Aquaquench ACR and greater, in which a relatively low temperature gradient existed at M_s, the transformation front had reached well into the interior of the specimen by the time the surface had reached a temperature of 260°C. The transformation of the interior at this time caused a tensile loading of the surface. The RDN175 oil quench calculation also predicted a tensile loading at the end of transformation plasticity, (figure 71).

The net effect of the rapid reduction in surface heat transfer coefficient was to produce a calculated residual stress which was of the order of that predicted by the oil quench calculation. The 15% Aquaquench ACR solution produced a residual stress distribution comparable to that produced by the oil quench, (figure 56), while the calculated 5% Aquaquench ACR stress distribution was comparable to that calculated for a 25% Aquaquench 1250 solution, (figure 55).

The calculated relationships between stress and strain histories may be conveniently divided into two categories on the basis of the effect of the temperature gradient at M_s. A "water-like" category typified by water, 25% Aquaquench 1250 and 5% Aquaquench ACR in which the surface experienced a compressive loading after transformation plasticity and which produced a relatively high level of predicted residual stress and an "oil-like" category in which the surface experienced a tensile loading after transformation plasticity and which produced a relatively low level of predicted residual stress. Solutions of 10% Aquaquench ACR and greater belonged to the "oil-like" category by virtue of the reduction in vapour mobility after the maximum surface heat transfer coefficient.

7.3 Comparison Of The Predicted And Experimental Residual Stresses And Strains

The agreement between the calculated and experimentally determined residual stresses and strains has been shown in sections 6.7 and 6.8 respectively. In general, a fair agreement

between the two was observed with the relationships between residual stress and strain and depth from the plate face being reproduced by the experimental measurements. However, there were some discrepancies between the precise values of the predicted and experimental results. The differences in the two sets of results can be attributed to two causes - those inherent in the experimental method and those inherent in the mathematical model.

The first measurements of residual stress and strain were performed on plates which were not insulated at their edges but the results obtained did not compare very well with the results predicted by the infinite plate model. Therefore the edges of the plates were insulated in order to reduce the amount of heat flow parallel to the surface of the plate and therefore to better duplicate the conditions of the infinite plate model. This would be expected to improve the level of agreement between calculated and experimentally determined results.

The reproducibility of the experimental method was determined by repeating the experimental measurement of the residual stress and strain on low alloy plates, (with insulated edges), quenched in unagitated solutions of 5%, 15% and 25% Aquaquench ACR, (figures 75, 76 and 77 respectively). The level of reproducibility was good. The discrepancies between the predicted and mean experimental results were larger than the differences obtained between the measured results in individual tests carried out in the same concentration. Hence experimental error was not wholly responsible for the reported discrepancies.

One reason for the discrepancies between the predicted and

experimental results may lie in the application of a factor to the experimental measurements to account for the effect of the free edge on the finite plate. A factor of 1.2, derived from Saint-Venants Principle, was used in this work. This assumed that the residual stress in the plane of the plate fell linearly to zero within one plate thickness of the edge. However, the level of agreement between the calculated and predicted residual stress varied with the distance from the plate face which suggested that the correction factor for the effect of the free edge was a function of the depth of the stress measurement from the face of the plate. Therefore the use of a constant factor, independent of the depth of the measurement as given by Saint-Venants Principle, may not be correct. (A study has been performed on the effect of the free edge but this has yet to be published.[144])

Further reasons for the differences in the predicted and measured residual stress and strain may be sought in the mathematical model used. Several simplifying assumptions were made by the model such as the neglect of the effect of stress on the martensite transformation kinetics and the effect of deformation and latent heat of transformation on the temperature distribution. However, as outlined in the literature survey, the effects of these relationships has been demonstrated, in the particular case of a steel transforming completely to martensite, to be negligible.[72 73 77] Therefore the model used incorporated the dominant thermo-mechanical couplings and these additional refinements are unlikely to significantly increase the accuracy of the model.

The model assumed that the temperature distribution, and therefore the generation of thermal stress and strain, was symmetrical about the centre-line of the plate. (This has been demonstrated, in one case, by experimental measurement of the residual stress through the majority of the plate thickness[15]). The simultaneous experimental measurement of the sub-surface temperature below both faces of the plate during quenching showed that this was not always the case. For example, figure 95 shows the cooling curve for an unagitated quench in 15% Aquaquench ACR. A surface to surface temperature difference of about 120°C existed at about 20 s though this difference was later greatly reduced as the surface heat transfer coefficient declined. A lack of symmetry in the temperature distribution in the plate would cause a similar lack of symmetry in the distribution of stress and strain.

The calculation procedure was based upon the assumption that no net force existed on the half-section of the plate. However, measurements of the residual strain distribution were rendered inaccurate by the fact that the plate had bent during the quenching process and this demonstrated that a force, due to the nonsymmetry of the stresses about the centreline of the plate, had existed at some point during quenching. This was additional evidence for a lack of symmetry in the temperature distribution in the specimen.

Finally, the initial wetting stage of the quenching process had not been taken into account. The surface heat transfer coefficient appeared to indicate that, upon immersion the surface heat transfer coefficient rose gradually, from approximately

zero, to a peak associated with stable film boiling, (figure 40). However when the film boiling stage was examined more closely and the surface heat transfer coefficient calculated using smaller time steps it was observed that, in both water and 25% Aquaquench ACR, the surface heat transfer coefficient rose from approximately zero to a small peak before declining to values associated with film boiling, (figures 89 and 90 respectively). For the surface to reach the film boiling stage the boiling curve must have been traversed upwards to pass through the vapour transport stage. Therefore the initial peak observed may correspond to the maximum surface heat transfer coefficient in the vapour transport stage of the initial wetting stage.

The magnitude of this peak is such that one would not expect it to have a large effect on the temperature distribution, and hence generation of thermal stress and strain, in the specimen. However, it has been remarked that upon immersion a specimen can temporarily lose its red appearance as it is wetted by the quenchant. If this be taken to be equivalent to a drop in surface temperature of from 850^{o}C to 550^{o}C in 0.2 s then there would exist, presumably caused by conduction to the liquid, a surface heat transfer coefficient of the order of 10^{5} W.m^{2}.K^{-1}. This might well have a significant effect on the temperature distribution and the generation of thermal stress and strain within the plate.

7.4 Modelling Of Film Boiling Heat Transfer

The prediction of the surface heat transfer coefficient during

film boiling by the model of Cess and Sparrow[109] predicted results that were significantly lower than those obtained by experiment, (figures 89 and 90), being an average of 57% in water and 69% in 25% Aquaquench ACR. Five assumptions made by Cess and Sparrow[109] did not agree with the situation pertaining to quenching under which the experimental results were obtained. These were as follows;

1. The assumption of a stationary vapour/liquid interface.

2. The assumption that the physical properties of the vapour and liquid were represented by their values expressed at the arithmetic mean temperature of the boundary layer.

3. The assumption that the liquid and vapour layers were laminar.

4. The assumption that the vertical surface was isothermal.

5. The assumption that the contribution of radiation to the surface heat transfer coefficient was negligible.

The last assumption was corrected and all of the predicted surface heat transfer coefficients given in this work include the contribution from radiation heat transfer. The importance of this greatly depended on surface temperature but was significant at high temperatures. For example, in film boiling in the case of water at a surface temperature of 1000^{o}C radiation contributed about 15% of the total surface heat transfer coefficient.

The assumption of a stationary interface was contradicted, in the case of water, by other work,[89 90 91 92] and, in the case of the sodium polyacrylate solutions, by still and cine photography in the present investigation. Plate 15, for example, shows Taylor

waves, associated with a moving interface, in a 20% Aquaquench ACR solution and, though photography was not possible at any higher concentration, it was considered unlikely that the interface in a 25% solution would be stationary.

The model of Nishikawa and Ito[112] made assumptions identical to the model of Cess and Sparrow[109] except that the interface was assumed to move upwards at an unknown velocity. This increased the predicted surface heat transfer coefficient, compared to the model of Cess and Sparrow,[109] by about 16% in the case of water, but, for an unknown reason, reduced the predicted surface heat transfer coefficient by about 13% in the case of the sodium polyacrylate solution. The values predicted by this model were therefore still significantly below the experimental values, (being, on average, 66% in the case of water and 61% in the case of 25% Aquaquench ACR), but the results indicated that the assumption of a stationary interface, at least in the case of water, introduced a significant inaccuracy into the calculation.

The model of Nishikawa, Ito and Matsumoto[114] included a moving interface and also discarded the assumption of constant physical properties, (ie, evaluated at their mean temperatures), in the boundary layers. The density, viscosity, specific heat capacity and thermal conductivity of both the vapour and liquid were varied with temperature in both boundary layers. However, this model also predicted surface heat transfer coefficients which were below those experimentally obtained, (being 65% of experimental values in vboth cases).

In comparison with the model of Nishikawa and Ito[112] the use of variable physical properties slightly decreased the predicted

surface heat transfer coefficients in the case of water and increased them by about 6% in the case of the sodium polyacrylate solution. These results showed that the introduction of variable physical properties into a model which included a moving interface did not greatly affect the predicted surface heat transfer coefficient in the case of water but an improvement was obtained in the case of the sodium polyacrylate solution. However, in the latter case the validity of this improvement can be questioned in view of the fact that the inclusion of a moving interface reduced the predicted surface heat transfer coefficient.

These results showed that none of the three models accurately predicted film boiling heat transfer in either quenchant. Therefore the effect of the introduction of turbulent flow was considered while retaining the assumption, (the last of the original five), of an isothermal vertical surface.

An additional reason for the lack of agreement between the experimental and predicted results in the case of the 25% Aquaquench ACR solution may be noted. Diffusion of sodium polyacrylate in the liquid may occur during the film boiling stage and this factor may affect the physical properties, and therefore the amount of heat transferred by convection, in the liquid. The effect of diffusion could be introduced into the models in the same manner employed by Marschall and Moresco[116] or Yue and Weber[113] but before this could be examined a film boiling model capable of predicting the surface heat transfer coefficient in a single phase liquid, (ie, water), should be established.

7.5 The Turbulent Interface Film Boiling Model

All the boundary layer theory models considered above made the assumption that the vapour film was laminar. This has been replaced by an assumption of turbulent flow in some models based on the direct observation of turbulent behaviour of the vapour/liquid interface by photography.[97 103] A knowledge of the critical Reynolds number for the transition from laminar to turbulent flow allowed the critical velocity at this transition to be obtained. For example, Hsu and Westwater,[97] modelled saturated film boiling heat transfer in water and assumed a critical Reynolds number of 100, (the value assumed at the transition point in an enclosed pipe). Their model divided the vapour blanket into a laminar layer next to the wall and a turbulent sub-layer between this and the saturated liquid, (figure 16). The turbulent layer was assumed to offer no resistance to heat transfer and to have no variation in the velocity profile. Coury and Dukler[103] modelled film boiling heat transfer with an assumed critical Reynolds number of 35. Their model was similar in construction but also included the effect of large scale oscillations in vapour thickness, (Taylor waves).

Photography of similar specimens to those used in this investigation quenched in water indicated that a turbulent interface did exist.[84] Evidence reported above in the present work indicated that turbulence occurred in sodium polyacrylate solutions though it was a more viscous liquid. As a first step to the introduction of turbulence into the laminar models, the velocity of the interface was calculated in those models which

assumed a moving interface.[112 114] The results suggested that these models predicted very low Reynolds numbers for the interface - so low that there was little justification for including turbulence in the model, (tables 17 to 20). However an examination of the method of calculating the velocity of the interface revealed that the method produced a velocity that was dimensionally incorrect. Cess and Sparrow[109] stated;

$$u = 4cx^{1/2}f'\nu$$

where c = the similarity variable (units ≡ $m^{-3/4}$)

x = distance from leading edge (units ≡ m)

f' = dimensionless velocity

ν = kinematic viscosity (units ≡ $m^2.s^{-1}$)

This expression produces u with units of $m^{1.75}.s^{-1}$ which is incorrect. The expression used to derive the interface velocity from the dimensionless velocity in the model of Nishikawa and Ito[112] was based on this;

$$u_i = 4.m.x^{1/2}.f'_i.\nu_s$$

where m = the similarity variable (units ≡ $m^{-3/4}$)

This also was dimensionally incorrect. The velocity of the interface in the model of Nishikawa, Ito and Matsumoto[114] was calculated by a similar expression;

$$u_i = 4.c.x^{1/2}.f'_i.\nu_s$$

This was also dimensionally incorrect. This meant that the expression of continuity of velocity across the interface; u_{vi} =

u_{Li}; was not obeyed, (tables 17 to 20). These errors did not affect the accuracy of the calculations of the surface heat transfer coefficient since the ordinary differential equations were solved using variables which were expressed non-dimensionally and therefore the incorrect expressions noted above were not involved. Rather, an error was introduced when the velocity at the interface was obtained from the dimensionless velocity using these expressions, to obtain values for the Reynolds number at the interface.

The correct expression for the relationship between the dimensionless velocity and the actual velocity of the fluid has been given by Schlichting[111] and has been used by Koh,[110] (one of the first workers to use boundary layer theory to model saturated film boiling from a vertical surface);

$$u = 4.c^2.\nu.x^{1/2}.f' \quad ; \quad (\text{units} \equiv m.s^{-1})$$

It appears that the error in the dimensions of u lay originally with Cess and Sparrow[109] who neglected to square the similarity variable. Once the correct expression for the interface velocity was inserted into the models the criterion of continuity of velocity across the interface; $u_{vi} = u_{Li}$; was obeyed. This confirmed that the formulation of the velocity expression was correct.

These new calculated velocities gave Reynolds numbers at the interface which were much higher, particularly in the case of water, and which were above any previously assumed critical Reynolds numbers for the transition from laminar to turbulent

flow.

Therefore, a model is proposed in which the interface is assumed to have a velocity above that required for turbulence to occur. The vapour layer adjacent to the vertical wall is assumed to behave as a laminar fluid as is the bulk liquid on the opposite side of the interface. The velocity of the vapour is zero at the wall and rises as the distance perpendicular to the wall increases. At some point the velocity of the vapour reaches an assumed critical value, associated with the assumed critical Reynolds number, and the flow becomes turbulent. The temperature of the vapour is assumed to be a maximum at the wall and to decline as the distance from the wall increases. A diagram of this model is given in figure 37. The model, in common with all previously produced models, is based upon the assumption that the vertical surface is isothermal.

The model of Hsu and Westwater,[96] (figure 16), assumed that the turbulence existed wholly in the vapour layer and that the velocity remained constant across the turbulent core. This approach cannot be adopted in a subcooled liquid since this would require the velocity of the liquid in the laminar layer adjacent to the turbulent vapour to be the same as the velocity of the laminar vapour layer as the latter reached the critical velocity for turbulence. Since, at an equal velocity and at the saturation temperature the kinematic viscosity of a liquid is greater than that of its vapour this would mean that the Reynolds number of the liquid, assumed to be in laminar flow, would be greater than the critical Reynolds number of the transition from laminar to turbulent flow of the vapour.

This model therefore assumed a constant Reynolds number, equal to the critical value, within the turbulent layer. This therefore gave the velocities of the vapour and liquid adjacent to the turbulent layer and hence the boundary conditions related to the dimensionless velocity at these points. This allowed the solution of the differential equations governing the behaviour of the laminar boundary layers. The temperature profile in the turbulent layer was assumed to be constant and to be equal to the saturation temperature of the liquid, 100°C, due to the turbulence of the interface. That is, the turbulent interface offers no resistance to heat transfer.

It was not found possible to solve the ordinary differential equations governing heat and mass flow when the physical properties were made dependent on temperature in the laminar vapour and liquid layers, (ie, when the differential equations of Nishikawa, Ito and Matsumoto[114] were employed). Therefore the physical properties in the boundary layers were assumed constant, that is, the differential equations of Cess and Sparrow[109] and Nishikawa and Ito[112] were used to obtain the surface heat transfer coefficients associated with the assumed critical Reynolds Numbers.

When the critical Reynolds assumed by other workers, namely, 35[103] and 100,[97] were used in this model the predicted surface heat transfer coefficients were increased only very slightly compared to the values predicted by the original Cess and Sparrow[109] model. This indicated that closer agreement with experimental results would be obtained if the critical Reynolds

number were higher. It was not possible to determine experimentally the Reynolds number for the transition from laminar to turbulent flow in film boiling therefore increasing values of Reynolds numbers were assumed and the surface heat transfer coefficients predicted using these compared to the experimental values. The critical Reynolds numbers required to give a good agreement with the experimentally determined surface heat transfer coefficients were found to be 22,500 in the case of water and 250 in the case of 25% Aquaquench ACR solution, (figures 91 and 92).

The critical Reynolds numbers required to produce good agreement between the experimental and calculated surface heat transfer coefficients are greatly in excess of any that have been previously used in analyses of film boiling incorporating turbulence. However, there are examples of transition from laminar to turbulent flow occurring at much higher values of the Reynolds number. For example, Schlichting[111] quotes reports of flow over a flat plate in which critical Reynolds numbers of 350,000 to 3,500,000, (depending upon the amount of turbulence already in the fluid), were observed. Also, the velocities associated with these critical Reynolds numbers reported here do not appear to be unreasonably high. In the case of water the velocity of the liquid at the interface would be 0.1 $m.s^{-1}$ with a vapour blanket thickness of about 0.2-0.3 mm, (table 22), while in the case of the 25% Aquaquench ACR solution the corresponding velocity would be 0.047 $m.s^{-1}$ with a vapour blanket thickness of about 0.2 to 0.4 mm. However, the validation of this turbulent interface model must depend upon experimental verification of

these predicted values.

Of the five assumptions made by Cess and Sparrow[109] there therefore remains only the assumption of an isothermal surface which might significantly affect the accuracy of the model. An anisothermal surface would be expected to increase the value of the predicted surface heat transfer coefficient by reducing both the thickness and the distance to the edge of the vapour blanket. The inclusion of these effects would probably increase the accuracy of the model.

7.6 The Conductive Cooling Stage And Its Relationship With Film Boiling Heat Transfer

It was recognised that what has been previously described as the conductive cooling stage during quenching in sodium polyacrylate solutions, (section 7.1.2), had some similarity to the film boiling stage in that heat transfer in both regimes takes place through vapour adjacent to the vertical surface. In the conductive cooling stage a layer of bubbles, which were mostly stationary, became established on the surface of the plate. (Some vapour movement occurred in the dendritic spacings). Figure 93 shows the application of two of the film boiling models at surface temperatures of 420^{o}C and below with a zero interfacial velocity. Both models, (one assuming fixed and the other variable physical properties), produced surface heat transfer coefficients that were within an order of magnitude of the experimental results. With both models there was one temperature at which the two values were identical.

This suggested that the mechanism of heat transfer in the conductive cooling stage may have some similarities with that found in the film boiling stage. In both cases a layer of vapour insulated the surface from the bulk liquid although this layer was probably incomplete in the case of the conductive cooling stage. It is probable that heat transfer in both stages is largely by conduction through the vapour which would account for the level of agreement between the film boiling models and the experimental results in this stage, and also for the similarity in the values of surface heat transfer coefficient determined in this stage and the film boiling stage. The values in the conductive cooling stage were greatly below those observed in other aqueous based quenchants at these surface temperatures.

8.0 CONCLUSIONS

1. Solutions of sodium polyacrylate in water produce a pronounced film boiling stage. An increase in the concentration of the polymer increased the duration of the film boiling stage while the temperature of the minimum film boiling point was simultaneously decreased. Taylor waves were observed in the liquid/vapour interface.

2. After the collapse of the vapour blanket the surface heat transfer coefficient rose rapidly to a maximum value. This was associated with the formation of many small bubbles at the surface of the specimen.

3. The fine bubbles gave way to the formation of larger, oblate, vapour "blisters" as the surface heat transfer coefficient passed its maximum value.

4. The value of the maximum surface heat transfer coefficient in aqueous solutions of sodium polyacrylate was significantly below the values observed in water or polyalkylene glycol solutions. The surface temperature at which the maximum occurred was significantly higher than observed in water. Increasing the concentration of sodium polyacrylate in solution decreased the value of the maximum surface heat transfer coefficient.

5. After the passage of the maximum, in concentrations of sodium polyacrylate of 10% Aquaquench ACR and greater, the surface heat transfer coefficient declined rapidly to reach values, at about 300^{o}C, equivalent to those measured in the film boiling stage.

These values were also similar to those observed in a medium speed quenching oil at this surface temperature.

6. The decline in surface heat transfer coefficient was accompanied by the formation of an unusual vapour pattern on the surface of the specimen. This had the appearance of dendrites of vapour, (which lay within the hotter, central area of the specimen), and which contained bubbles moving upwards, within a matrix of stationary bubbles. As surface temperatures fell the area of the dendritic stage shrank while the area of the stationary bubbles expanded. The formation of these vapour patterns and the accompanying decline in surface heat transfer coefficients occurred over a temperature range that was associated with a change in molecular structure indicated by differential thermogravimetry.

7. The region of the boiling curve, after the passage of the maximum surface heat transfer coefficient, would normally be described as the vapour transport stage but, in solutions of sodium polyacrylate examined, it was associated with stationary bubbles and some narrow dendrites containing moving vapour. Therefore a new description of this region was proposed - the conductive cooling stage - based on the possibility that the heat transfer mechanisms of this stage and the film boiling stage may have some features in common.

8. Below a surface temperature of about 300^{o}C the surface heat transfer coefficient rose slightly as the end of the quench was approached. An exception to this was observed in the lowest

concentration solution examined, 5% Aquaquench ACR. In this solution the surface heat transfer coefficient fell only slightly after reaching a maxiumum before rising again to a second, but lower, peak. The surface heat transfer coefficient then fell as the end of the quench was approached. However, no difference in the appearance of the vapour patterns on the surface of the specimen was detected.

9. At ambient temperature a viscous gel was observed to have formed except in quenches carried out in still baths except in the case of the least concentrated solutions which contained 5% Aquaquench ACR. The viscous gel was not observed to form in quenches carried out in agitated baths of any concentration.

10. After quenching the surface of the specimens exhibited deposits of carbon-rich material in the form of linear features, (at the periphery), or broken-ring structures, (in the centre of the face of the specimen). As the concentration of sodium polyacrylate increased the area covered by the linear structures increased at the expense of the area covered by the broken ring structures.

11. Increasing the concentration of sodium polyacrylate in solution decreased the absolute residual stress at any point in the specimen. The corresponding residual strains, on the other hand were increased.

12. The rapid decline in surface heat transfer coefficient after the maximum passed reduced the temperature gradient in the specimen at temperatures close to M_s. In concentrations of sodium

polyacrylate of 10% Aquaquench ACR and greater this caused a tensile loading of the surface at the end of transformation plasticity and a relatively low level of residual stress similar to that observed in the case of a medium speed quenching oil.

13. In water, 25% Aquaquench 1250, (a polyalkylene glycol solution), and 5% Aquaquench ACR the temperature gradient was higher as the transformation began and this caused a compressive loading of the surface after the end of transformation plasticity and relatively higher residual stresses.

14. The predicted residual stresses and strains have been shown to be in qualitative agreement with measured values. Quantitative agreement was affected by the lack of a completely satisfactory means to correct for the effect of the free edge. A lack of symmetry in the temperature distribution of the specimen was also observed in contradiction to the assumptions made by the visco-elasticplastic model.

15. The film boiling model of Cess and Sparrow,[109] which assumed a stationary interface and constant physical properties, predicted surface heat transfer coefficients which were significantly below those measured experimentally in the case of both water and a 25% Aquaquench ACR solution.

16. The inclusion of a moving interface in the model, (Nishikawa and Ito[112]), significantly increased the predicted surface heat transfer coefficient in the case of water but decreased it in the case of the sodium polyacrylate solution. (This latter effect was

tentatively attributed to the inability of the model to account for diffusion in the liquid).

17. The assumption of variable physical properties in the model, (Nishikawa, Ito and Matsumoto[114]), had little effect on the predicted surface heat transfer coefficient in the case of water but slightly increased its value in the case of the sodium polyacrylate solution.

18. A method of incorporating a turbulent interface in film boiling models was proposed which required the assumption of critical Reynolds numbers for the transition from laminar to turbulent flow. The critical Reynolds numbers required to successfully predict film boiling heat transfer were 22,500 in the case of water and 250 in the case of 25% Aquaquench ACR solution. These values suggested that this model may not be a complete description of the film boiling process and that further refinements should be considered.

19. The film boiling models were applied to the conductive cooling stage during quenching in a 25% Aquaquench ACR solution and predicted surface heat transfer coefficients that were within an order of magnitude of the experimentally measured values.

9.0 RECOMMENDATIONS FOR FURTHER WORK

1. The surface temperature at which the viscous gel formed should be measured in order to determine if this structure is responsible for the reduction in surface heat transfer coefficients associated with the formation of the dendritic stage.

2. The molecular structure and viscosity of the viscous gel should be determined in order to assess the effect of its formation on the quenching process.

3. Parallel results in other polymer quenchants, specifically, polyalkylene glycol solutions, should be explored to examine the hypothesis that polymer quenchants have a common cooling mechanism.

4. Other recently patented polymer quenchants, for example, polyethyloxazoline and mixtures of polyethyoxazoline and polyvinylpyrrolidone and polyethyloxazoline and polyalkylene glycol, show slow cooling rates. The quenching characteristics of these solutions should be determined in order to assess their usefulness as commercially attractive replacements for quenching oils.

5. The relationships between stress, strain and distance from the free edge should be determined in the case of quenched plates in order to provide a method for accurately comparing the results of the visco-elasticplastic model to experimentally measured values.

6. The surface heat transfer coefficient should be determined for

the period of the initial wetting stage during quenching. This stage of quenching has been hitherto neglected. The stress and strain generated in this stage should be determined and its contribution to levels of residual stress and strain assessed.

7. The effect of the lack of symmetry of the temperature distribution in the specimen and hence its effect on the generation of thermal stress and strain should be determined. This would further improve the accuracy of the visco-elasticplastic model.

8. The visco-elasticplastic model should be extended for use in predicting the generation of thermal stress and strain in the case of a steel undergoing the pearlite transformation. This would involve the incorporation into the model of the effect of stress on the transformation kinetics and the inclusion of the generation of latent heat during transformation.

9. The visco-elasticplastic model should be applied to structures of more complex geometry such as occur in industrial applications.

10. The critical Reynolds numbers for transition from laminar to turbulent flow in the case of film boiling in water and polymer solutions should be calculated and compared to experimentally measured values. These Reynolds numbers may then be used in the film boiling models to determine the increase in accuracy given by the inclusion of a turbulent interface.

11. Oil quenchants also show a stable film boiling stage. The

prediction of the surface heat transfer coefficient should therefore be extended to film boiling during oil quenching. Boundary layer theory can also be used to model the important convective cooling stage in oil quenching.

12. The effect of diffusion in the liquid should be included in film boiling models of quenching in polymer solutions in order to increase the accuracy of the application of these models for these quenchants.

13. There is a strong probability that the inclusion of the effect of an anisothermal surface and changes in the extent of the vapour blanket would greatly increase the accuracy of the film boiling models. Therefore a relationship between surface temperature and the extent of the vapour blanket should be determined and included in the models.

10.0 REFERENCES

1. Irani, RS and Hayes, DM, "Integrity Of Gas Containers: Material Technology", National Physical Laboratory, 1984, 90-106.
2. Bannykh, OA, Bozkho, GT, Gedberg, MG and Tropkina, MN, Met. Sci. Heat Treat. (USSR), May-June, 1984, 26, (5-6), 445-449.
3. Mueller, ER, Heat Treat., Oct., 1980, 30-33.
4. Metals Handbook, 9th Edition, American Society of Metals, 1981.
5. Hilder, NA, Heat Treat. Met., 13, (1), 1986, 15-26.
6. Cary, PE, Magnus, EO and Herring, WE, Met. Prog., Mar., 1958, 79-81.
7. Segerberg, S, proc.conf., 4th International Congress on Heat Treatment of Materials, vol. 2, Federal Republic of Germany, 3-7 June, 1985, Institut fur Treatment Werkstofftechnik TU Berlin, 1254-1265.
8. Blackwood, RR and Cheesman, WD, US patent no. 3,220,893, November 30, 1965.
9. Allen, FS ,Fletcher, AJ and King, S, Mat. Sci. Eng., 95, 1988, 247-257.
10. "Quenching Principles and Practice", pamphlet, Edgar Vaughn Uk plc.
11. Hasson, JA, Met. Prog., Sep. 1985, 128, (4), 67,69-70,72.
12. Steel Times, Jan. 1985, 213, (1), 37.
13. Mason, KJ and Capewell, I, Heat Treat. Met., 1986.4, 99-103.
14. Hilder, NA, Heat Treat. Met., 1987.2, 31-46.
15. Fletcher, AJ and Price, RF, Met. Technol., Nov. 1981, 8,

(11), 427-446.

16. Fletcher, AJ and Soomro, AB, Mat. Sci. Eng., 91, 1987, 153-160.
17. Kopietz, k-H, Heat Treat., Sep. 1984, 16, (9), 20-24,26.
18. Burgdorf, EH, Ind. Heat., Oct. 1981, 18-25.
19. Anderson, K, Croucher, T and Butler, D, Met. Prog., May 1983, 37-40.
20. Croucher, T, Heat Treat., Sep. 1984, 27-30.
21. Technical Information, BP Lubricants plc.
22. Blackwood, RR, Lorbach, MM and Mueller, ER, Heat Treat, July 1985, 17, (7), 40-42.
23. Croucher, T, Heat Treat., Nov. 192, 14, (11), 18-19.
24. Creal, R, Heat Treat., Dec. 1985, 17, (12), 18-21.
25. Creal, R, Heat Treat., Dec. 1986, 18, (12), 27-29.
26. Archambault, P, Chevrier, JC and Beck, G, Mat. Sci. Eng., 1980, 43, 1-6.
27. Meszoros, AG, US patent no. 3,902,929, September 2, 1975.
28. Foreman, RW and Meszaros, A, Ind. Heat., Jan. 1984, 22-29.
29. Moreaux, F, Naud, JM, Beck, G and Olivier, J, proc. conf., Heat Treatment '84, London, England, 2-4 May 1984, Institute of Metals, 18.1-18.5.
30. Moreaux, F and Beck, G, proc. conf., 8th International Heat Transfer Conference, San Fransisco, USA, 17-22 Aug. 1986, 1-5.
31. Kopietz, k-H and Munjat, FS, US patent no. 4087290, 2 May 1978.
32. Segerberg, S and Bodin, J, Metallurgia, Sep. 1986, 53, (9), 425-426.

33. von Bergen, RT, proc. conf., Heat Treatment '84, London, England, 2-4 May 1984, Institute of Metals, 17.1-17.4.

34. Mason, KJ and Griffin T, Heat Treat. Met., 1982.3, 77-83.

35. "Dangerous Properties of Industrial Materials", 6th Edition, N Irving Sax, Van Nostrand Reinhold Co. Inc., 1984.

36. Zakamaldin, AA, Kochurkina, Yu I and Tikhonov, GI, Met. Sci. Heat Treat. (USSR), Jan-Feb. 1983, 25, (1-2), 13-18.

37. Goryushin, VV and Kobasko, NI, Met. Sci. Heat Treat. (USSR), Jul.-Aug. 1984, 26, (7-8), 516-520.

38. Levina, MKh, Zaitsev, VV, Grachev, VI, Andreichenko, KG and Goncharenko, NF, Met. Sci. Heat Treat. (USSR), May-Jun. 1984, 26, (5-6), 438-440.

39. Bozkho, GT, Bannykh, OA, Tropkina, MN, Manikhin, PI and Popov, AV, Met. Sci. Heat Treat. (USSR), Nov.-Dec. 1983, 25, (11-12), 810-813.

40. Kobasko, NI, Shvets, Yu I, Fialko, NM, Meranova, NO and Nikolaev, ED, Met. Sci. Heat Treat. (USSR), Sep.-Oct. 1985, 27, (9-10), 639-643.

41. Kobasko, Ni and Timchenko, NP, Met. Sci. Heat Treat. (USSR), Sep.-Oct. 1986, 28, (9-10), 729-734.

42. Chase, FL and Ewing, CW, US patent no. 3022205, 20th Feb. 1962.

43. Konyukhov, GP, Bedarev, AS, Beloborodov, GI, Il'yushko, EG, Murav'ev, VV and Sharko, AV, Met. Sci. Heat Treat. (USSR), Sep.-Oct. 1980, 22, (9-10), 731-736.

44. Warchol, JF, US patent no. 4486246, 4th Dec. 1984.

45. Warchol, JF, US patent no. 4528044, 9th July 1985.

46. Lakin, JJ, European patent no. 0196836, March 21, 1986.

47. Gordon M, US patent no. 2770564, 13th Nov. 1956.

48. Loshkarev, VE and Kolpishon, E Yu, Met. Sci. Heat Treat. (USSR), Sep.-Oct. 1986, 28, (9-10), 746-749.

49. Tolstousov, AV and Bannykh, OA, Met. Sci. Heat Treat. (USSR), May-Jun. 1984, 26, (5-6), 435-437.

50. Boley AB and Weiner, JH, "Theory of Thermal Stresses", John Wiley and Sons, Inc., 1960.

51. Desai, CS and Abel, JF, "Introduction to the Finite Element Method", van Nostrand, New York, 1972.

52. "The Generation of Thermal Stress and Strain During Heat Treatment", Fletcher, AJ, Elseviers Publishing Corporation, 1989.

53. Arpaci, VS, "Conduction Heat Transfer", Addison Wesley, 1966.

54. Adams, JA and Rogers, DF, "Computer Aided Heat Transfer Analysis", McGraw-Hill, 1973.

55. Chevrier, JC, Moreaux F, Beck, G and Bouvaist J, 15th Colloque International Pour L'Etude des Traitements Thermique, Societe Francaise de Metallurgie, Caen, France, May, 1974.

56. Toshioka, Y, Fukugawa, M and Saiga, Y, Trans. Iron Steel Inst. Jap., 172, 12, (1), 6-15.

57. Spektor, AG and Stepanova, NI, Met. Sci. Heat Treat., Mar.-Apr. 1975, 17, (3-4), 282-286.

58. Inoue, T and Tanaka, K, Int. J. Mech. Sci., 1975, 17, 361-367.

59. Fujio, H, Aida, T and Masumoto, Y, Bull. J.M.S.E., 1977, 20, 146, 1051-1058.

60. Fujio, H, Aida, T and Masumoto, Y, Bull. J.S.M.E., 1977, 20, 150, 1655-1662.

61. Fujio, H, Aida, T, Masumoto, Y and Tswuki, T, Bull. J.S.M.E., 1979, 22, 169, 1001-1008.

62. Fujio, H, Aida, T and Akizono, J, Bull. J.S.M.E., 1979, 22, 169, 1009-1016.

63. Fletcher, AJ, Met. Technol., 6, 1977, 307-316.

64. Price, RF and Fletcher, AJ, Met. Technol., May 1980, 203-211.

65. Archembault, P, Chevrier, JC and Beck, G, Mat. Sci. Eng., 1980, 43, 1-6.

66. Yu, HJ and Macherauch, E, proc. conf., 28th Sagamore Army Materials Conference, 1982, 484-501.

67. Burnett, JA, Mater. Sci. Technol., Oct. 1985, 1, (10), 863-871.

68. Jeanmart, P and Bouvaist, J, Mater. Sci. Technol., Oct. 1985, 1, (10), 754-764.

69. Fujio, H and Sakota, M, Bull. J.S.M.E., sep. 1984, 27, (231), 2045-2052.

70. Greenwood, GW and Johnson, RM, Proc. Roy.Soc., 283A, 1965, 403-422.

71. Desalos, Y, Giusti, J, and Guinsberg, F, Report no. 902, IRSID, St. Germain-en-Laye, 1982.

72. Denis, S, Simon, A and Beck, G, Trans. Iron Steel Inst. Jpn., Jul. 1982, 22, (7), 504-513.

73. Sjostrom, S, "The Calculation of Quench Stresses in Steel", Dissertation no. 84, Linkoping, 1982.

74. Denis, S, Simon, A and Beck, G, proc. conf., Heat Treatment

Shanghai '83: 3rd International Congress on Heat Treatment of Materials, Shanghai, China, 7-11 Nov. 1983, The Metals Society, London, England, 1984, 5.68-5.79.

75. Abbasi, F and Fletcher, AJ, Mat. Sci. Technol., Oct. 1985, 830-837.
76. Abbasi, F, PhD thesis, Sheffield City Polytechnic, 1983.
77. Soomro, AB, PhD thesis, Sheffield City Polytechnic, 1986.
78. Denis, S, Gautier, E, Simon, A and Beck, G, Mater. Sci. Technol., Oct. 1985, 1, (10), 805-814.
79. Denis, S, Sjostrom, S and Simon, A, Metall. Trans., Jul. 1987, 18A, (7), 1203-1212.
80. Denis, S, Sjostrom, S and Simon, A, proc. conf., International Conference on Residual Stresses, (FRG), Deutsche Gesellschaft fur Metallkunde, 17-21 Oct., 1986, vol. 2, 595-602.
81. Denis, S, Gautier, E, Sjostrom, S and Simon, A, Acta Metall., 1987, 35, (7), 1621-1632.
82. Inoue, T and Wang, Z, proc. conf., Numerical Methods in Industrial Forming Processes, United Kingdom, 12-16 July 1982, Pineridge Press Ltd., 1982, 391-400.
83. Sjostrom, S, Mater. Sci. Technol., Oct. 1985, 1, (10), 823-829.
84. Allen, FS, PhD Thesis, Sheffield City Polytechnic, 1987.
85. Inoue, T and Wang, Z, Mater. Sci. Technol., Oct. 1985, 1, (10), 845-850.
86. Abbasi, F and Fletcher, AJ, Mat. Sci. Technol., Oct. 1985, 770-779.
87. Abbasi, F, Fletcher, AJ and Soomro, AB, proc. conf., Advances

in Manufacturing Technology: Proceedings of the 1st Conference on Production Research, Nottingham, Sep. 1985, 320-328.

88. Fletcher, AJ, Soomro, AB, Mat. Sci. Eng., 82, 1986, 101-115.
89. Winterton, RHS, "Transition Boiling", Safety and Engineering Science Division, AEE Winfrith, Aug. 1982.
90. "Boiling", Leppert, G and Pitts, CC, Advances in Heat Transfer, Ed. Irvine, TF and Hartnett, JP, Academic Press Ltd., 1965.
91. "Film and Transition Boiling", Jordan, DP, Advances in Heat Transfer, Ed. Irvine, TF and Hartnett, JP, Academic Press Ltd., 1969.
92. Clements, LD and Colver, CP, Ind. Eng. Chem., 1970, 62, 26-46.
93. "Film-Boiling Heat Transfer", Kalinin, EK, Berlin, II and Kostyuk, VV, Advances in Heat Transfer, Ed. Irvine, TF and Hartnett, JP, Academic Press Ltd., 1975.
94. Bromley, LA, Chem. Eng. Prog., 1950, 46, (5), 221-227.
95. Lubin, BT, J. Heat Trans., 1969, 8, 452-453.
96. Hsu, YY and Westwater, JW, A.I.Ch.E.J., 1958, 4, 58-62.
97. Hsu, YY and Westwater, JW, Chem. Eng. Progr. Symp. Ser., 1960, 30, 56, 15-24.
98. Berenson, PJ, J. Heat Trans., 1961, 83, 351-358.
99. Taylor, GI, Proc. Roy. Soc., 1950, 201A, 192-196.
100. Lewis, DJ, Proc. Roy. Soc., 1951, 202A, 81-96.
101. Tachibana, F and Fukui, S, "International Developments in Heat Transfer", 1961, American Society of Mechanical

Engineers, New York, 219-223.

102. Nishikawa, K, Shimomura, R, Hatano, M and Nagatomo, H, J.S.M.E., 1967, 10, (37), 123-131.

103. Coury, GE and Dukler, AE, proc. conf. Heat Transfer 1970, 4th International Conference, Paris-Versailles, 1970, Elsevier Publishing Company, Amsterdam, 1970, vol. 5, B3.6.

104. Greitzer, EM and Abernathy, FH, Int. J. Heat Mass Trans., 1972, 15, 475-491.

105. Dhir, VK and Lienhard, RH, Int. J. Heat Mass Trans., 1973, 16, 2097-2109.

106. Ede, AJ and Siviour, JB, Int. J. Heat Mass Trans., 1975, 18, 737-742.

107. Seki, N, Fukusako, S and Torikoshi, K, Trans, A.S.M.E., Nov. 1978, 100, 624-628.

108. McFadden, PW and Grosh, RJ, Int. J. Heat Mass Trans., 1961, 1, 325-335.

109. Sparrow, EM and Cess, RD, J. Heat Trans., May 1962, 149-155.

110. Koh, JCY, J. Heat Trans., Feb. 1962, 55-62.

111. Schlichting, H, "Boundary Layer Theory", trans. Kestin, J, McGraw-Hill, 1979.

112. Nishikawa, K and Ito, T, Int. J. Heat Mass Trans., 1966, 9, 103-115.

113. Yue, PL and Weber, ME, Trans. Inst. Chem. Eng., 1974, 52, 217-221.

114. Nishikawa, K, Ito, T and Matsumoto, K, Int. J. Heat Mass Trans., 1976, 19, 1173-1182.

115. Farahat, MM and Madbouly, EE, Int. J. Heat Mass Trans., 1977, 20, 269-277.

116. Marschall, E and Moresco, LL, Int. J. Heat Mass Trans., 1977, 20, 1013-1018.

117. Ito, T, Nishikawa, K and Shigechi, T, Bull. J.S.M.E., Dec. 1981, 198, 24, 2107-2114.

118. Shigechi, T, Ito, T and Nishikawa K, Bull. J.S.M.E., Apr. 1983, 214, 26, 554-561.

119. Nakayama, A and Koyama, H, J. Heat Trans., 1986, 108, 490-493.

120. Zuber, N, Trans. A.S.M.E., Apr. 1958, 711-720.

121. Segev, A and Bankoff, SG, J. Heat Trans., Nov. 1978, 100, 624-628.

122. Sato, S, Sci. Rep. Tohoku Imp. Univ., 1932, 564-574.

123. Cowley, CW, I and EC Process Design and Development, Apr. 1962, 1, 2, 81-84.

124. Moreaux, F, Chevrier, JC and Beck, G, Int. J. Multiphase Flow, 1975, 2, 183-190.

125. Yue, PL and Weber, ME, Int. J. Heat Mass Transfer, 1973, 16, 1877-1888.

126. Westwater, JW and Santangelo, JG, Ind. Eng. Chem., 1955, 8, 47, 1605-1610.

127. Berenson, PJ, Int. J. Heat Mass Trans, 1962, 5, 985-999.

128. Dhuga, DS and Winterton, RHS, Int. J. Heat Mass Trans., 1985, (10), 28, 1869-1879.

129. Lee, LYW, Chen, JC and Nelson, RA, Int. J. Heat Mass Trans., 1985, (8), 28, 1415-1423.

130. "Critical Heat Flux", Katto, Y, Advances in Heat Transfer, vol. 17, ed. Irvine, TF and Hartnett, JP, Academic Press

Ltd., 1985.

131. "Boiling Nucleation", Cole, R, Advances in Heat Transfer, vol. 10, ed. Irvine, F and Hartnett, JP, Academic Press Ltd., 1974.

132. "Heat Flow Rates in Saturated Nucleate Boiling - A Wide-Ranging Examination Using Reduced Properties", Cooper, MG, Advances in Heat Transfer, vol. 16, ed. Irvine, TF and Hartnett, JP, Academic Press Ltd., 1984.

133. "Boiling Liquid Superheat", Afgan, NH, Advances in Heat Transfer, vol. 11, ed. Irvine, TF and Hartnett, JP, Academic Press Ltd., 1975.

134. Treuting, RG and Read, WT, J. Appl. Physics, Feb., 1951, (22), 2, 130-134.

135. Andrews, KW, "Physical Metallurgy: Techniques and Applications", vol. 2, George Allen and Unwin Ltd., London, 1973.

136. Price, RF, PhD thesis, Sheffield City Polytechnic, 1980.

137. "Findlays Practical Physical Chemistry", 9th edition, ed. Levitt, BP, Longman.

138. BS188:1977

139. BSC Swinden Laboratories: private communication.

140. "Modern Numerical Methods for Ordinary Differential Equations", edited by Hall, G and Watt, JM, Clarendon Press, Oxford, 1976.

141. Haywood RW, "Thermodynamic Tables in SI (Metric) Units", 2nd edition, Cambridge University Press, 1972.

142. "Handbook of Chemistry and Physics", 53rd edition, CRC Press Inc, USA, 1972-1973.

143. "The Numerical Algorithms Group Fortran Library Manual - Mark 12", Numerical Algorithms Group, March 1987.

144. Lewis, C, unpublished work.

TABLE 1: COOLING RATES IN POLYMER SOLUTIONS DERIVED BY HILDER[14]

Polyalkylene glycol	MR = 244.7 - 4.3C - 1.7T + 47.2V R_{300} = 83 - 1.68C - 0.36T + 14.1V
Polyvinyll-pyrollidone	MR = 223.7 - 2.94C - 1.9T + 71.9V R_{300} = 96.3 - 1.8C - 1.02T + 37.68V
Sodium polyacrylate	MR = 160.59 - 5.63C - 1.10T + 114.8V R_{300} = 58.6 - 2.5C - 0.57T + 43.4V

where MR = maximum rate of cooling ($^{o}C.s^{-1}$)

R_{300} = rate of cooling at 300^{o}C ($^{o}C.s^{-1}$)

C = concentration (%)

T = temperature of quenchant (^{o}C)

V = velocity of quenchant ($m.s^{-1}$)

TABLE 2: THE CHEMICAL SPECIFICATION AND PHYSICAL PROPERTIES OF GRADE 316 STAINLESS STEEL

C	Mn	P	S	Si	Cr	Ni	Mo
0.08%	2.0%	0.045%	0.03%	1.0%	16-18%	10-14%	2-3%

THERMAL CONDUCTIVITY	$14.5744 + 0.0164T$ $(W.m^{-2}.K^{-1})$
THERMAL DIFFUSIVITY	$3.912 \times 10^{-6} + 2.6255 \times 10^{-9}T$ $(m^2.s^{-1})$
SPECIFIC HEAT CAPACITY	$458.25 + 0.2488T - 1.3773 \times 10^{-4}T^2$ $(J.kg^{-1}.K^{-1})$

TABLE 3: THE CHEMICAL SPECIFICATION AND PHYSICAL PROPERTIES OF GRADE 835M30 STEEL

C	Si	Mn	Ni	Cr	Mo
0.26-0.34%	0.1-0.35%	0.4-0.6%	3.9-4.3%	1.1-1.4%	0.2-0.4%

Thermal diffusivity ($mm^{-2}.s^{-1}$)	$T > 355^{o}C$	$4.0698 + 1.7802 \times 10^{-3}T$
	$355-286^{o}C$	$0.03762T - 8.668$
	$286-265^{o}C$	2.1
	$265-164^{o}C$	$11.769 - 0.03644T$
	$164-20^{o}C$	$7.357 - 0.00722T$
Thermal conductivity ($W.m^{-1}.K^{-1}$)	$T > 328^{o}C$	$20.1 + 8.29 \times 10^{-3}T$
	$328-223^{o}C$	$33.152 - 3.143 \times 10^{-2}$
	$223-20^{o}C$	$25.521 - 2.726 \times 10^{-3}T$
Yield stress (MPa); austenite	$T > 850^{o}C$	40
	$850-400^{o}C$	$257.2 - 0.02556T$
	$T < 400^{o}C$	155
martensite	$300-90^{o}C$	$\sigma_f = V(\sigma_f)_{\alpha'} + V(\sigma_f)_{\gamma}$
	$T < 90^{o}C$	1600
Work hardening coefficients (MPa)	W_1; $T > 600^{o}C$	$8950 - 7.75T$
	W_1; $T < 600^{o}C$	4300
	W_2; $T > 600^{o}C$	$10600 - 11.5T$
	W_2; $T < 600^{o}C$	3700
$E/(1-\nu)$ (MPa)	$850-90^{o}C$	$2.935 \times 10^{-5} - 141.77T$
Transformation plasticity strain	$300-260^{o}C$	$6.25 \times 10^{-7}(\sigma-40)(300-T)$

TABLE 4: PHYSICAL PROPERTY DATA USED IN THE CALCULATION OF THE SURFACE HEAT TRANSFER COEFFICIENT DURING FILM BOILING

Water vapour	
Specific heat capacity	$2065.0 - 0.72312T + 2.2179\times10^{-3}T^2 - 1.0993\times10^{-6}T^3$ $(J.kg^{-1}.K^{-1})$
Dynamic viscosity	$8.16\times10^{-6} + 4.0827\times10^{-8}T$ $(kg.m^{-1}.s^{-1})$
Thermal conductivity	$0.0151 + 8.358\times10^{-5}T + 4.1136\times10^{-8}T^2$ $(W.m^{-1}.K^{-1})$
Density	$0.74041 - 1.67\times10^{-3}T + 1.8874\times10^{-6}T^2 - 7.8684\times10^{-10}T^3$ $(kg.m^{-3})$
Water	
Specific heat capacity	$4214.6 - 2.2T + 0.03716T^2 - 1.5228\times10^{-4}T^3$ $(J.kg^{-1}.K)$
Dynamic viscosity	$1.759\times10^{-3} - 4.729\times10^{-5}T + 5.818\times10^{-7}T^2 - 2.585\times10^{-9}T^3$ $(kg.m^{-1}.s^{-1})$
Thermal conductivity	$0.5608 + 1.986\times10^{-3}T - 7.765\times10^{-6}T^2$ $(W.m^{-2}.K^{-1})$
Density	$1000.54 - 0.06902T - 3.5735\times10^{-3}T^2$ $(kg.m^{-3})$
Coefficient of cubic expansion	$-4.223\times10^{-5} + 1.24086\times10^{-5}T - 4.6558\times10^{-8}T^2$ (K^{-1})
25% Aquaquench ACR	
Dynamic viscosity	$7.03085\times10^{-2} - 1.649412\times10^{-3}T + 1.59586\times10^{-5}T^2 - 5.3742\times10^{-8}T^3$ $(kg.m^{-1}.s^{-1})$
Density	$1025.95 - 0.2512T - 1.6555\times10^{-3}T^2$ $(kg.m^{-3})$

TABLE 5: COOLING RATES DURING QUENCHING IN SODIUM POLYACRYLATE SOLUTIONS

Concentration of Aquaquench ACR	Film boiling stage	Cooling rates ($^{o}C.s^{-1}$) Vapour Transport Stage	
		1st part	2nd part
5% Unagitated	8.5	203.1	8.2
10% "	8.6	68.1	3.5
15% "	6.0	55.7	2.7
20% "	6.2	50.7	2.5
25% "	4.8	35.4	2.2
5% Agitated	-	111.6	7.0
10% "	8.3	62.2	3.5
15% "	9.6	50.2	2.7
20% "	7.3	69.0	2.7
25% "	6.6	61.9	2.4

TABLE 6: QUENCHING CHARACTERISTICS OF SODIUM POLYACRYLATE SOLUTIONS

Concentration of Aquaquench ACR	Film Boiling Duration (s)	T(mfb) (^{o}C)	T(hmax) (^{o}C)	h(max) ($W.m^{-2}.K^{-1}$)
5% Unagitated	5.7	769	438	4275
10% "	11.8	740	519	3405
15% "	15.0	720	490	3115
20% "	33.0	636	450	2219
25% "	48.1	592	429	1807
5% Agitated	-	-	431	4260
10% "	4.5	744	482	3320
15% "	11.5	726	527	2957
20% "	25.1	666	440	2335
25% "	40.5	574	436	2118

where T(mfb) = temperature at which the minimum film boiling point occurred

T(hmax) = temperature at which the maximum surface heat transfer coefficient occurred

h(max) = value of the maximum surface heat transfer coefficient

TABLE 7: MINIMUM AND MAXIMUM SURFACE TEMPERATURES AT WHICH THE CHANGE IN GRADIENT OCCURRED

Concentration of Aquaquench ACR	Minimum (^{o}C)	Maximum (^{o}C)	Mean (^{o}C)
5% Unagitated	385	473	421
10% "	403	435	424
15% "	395	445	420
20% "	405	443	426
25% "	393	445	413
5% Agitated	423	438	430
10% "	400	430	421
15% "	388	415	403
20% "	400	465	439
25% "	393	483	438
Mean	399	449	424

TABLE 8: TEMPERATURES AT WHICH THE UNLOADINGS IN THE GENERATION OF THERMAL STRESS OCCURRED (^{o}C)

Quenchant	1	2	3	4	5	6	7
Surface loadings							
Water	-	-	352	-	-	260	211
RDN175	752	555	440	-	300	-	-
25% 1250	-	-	567	-	-	260	223
5% ACR U	815	784	507	351	-	260	229
10% ACR U	816	773	505	341	-	-	-
15% ACR U	792	754	514	343	-	-	-
20% ACR U	782	680	478	344	-	-	-
25% ACR U	781	645	451	325	-	-	-
5% ACR A	-	-	488	-	300	260	218
10% ACR A	807	779	491	345	-	-	-
15% ACR A	810	867	516	348	-	-	-
20% ACR A	760	675	479	349	-	-	-
25% ACR A	767	640	469	347	-	-	-
Centre loadings							
Water	-	-	722	-	-	-	-
RDN175	828	605	550	-	300	-	-
25% 1250	-	-	742	-	-	-	-
5% ACR U	847	821	722	458	-	-	-
10% ACR U	847	791	690	378	-	-	-
15% ACR U	843	808	702	381	-	-	-
20% ACR U	832	724	611	356	-	-	-
25% ACR U	837	682	551	328	-	-	-
5% ACR A	-	-	721	-	300	-	-
10% ACR A	845	822	704	380	-	-	-
15% ACR A	846	792	691	377	-	-	-
20% ACR A	829	743	621	369	-	-	-
25% ACR A	830	691	579	362	-	-	-

KEY; 1 - caused by surface heat transfer coefficient reaching maximum in film boiling stage
2 - caused by collapse of vapour blanket
3 - caused by passage of maximum surface heat transfer coefficient
4 - caused by decline in surface cooling rate coupled with the effect of stress relaxation
5 - caused by beginning of martensitic transformation
6 - caused by progression of transformation front into interior

TABLE 9: STRESS VALUES AT WHICH THE UNLOADINGS IN THE GENERATION OF THERMAL STRESS OCCURRED (MPa)

Quenchant	1	2	3	4	5	6	7
Surface loadings							
Water	-	-	174	-	-	-33	-856
RDN175	66	-35	147	-	121	-	-
25% 1250	-	-	119	-	-	-55	-636
5% ACR U	49	25	136	-165	-	-267	-609
10% ACR U	49	-12	135	-167	-	-	-
15% ACR U	55	35	133	-166	-	-	-
20% ACR U	56	18	138	-159	-	-	-
25% ACR U	58	-5	143	-112	-	-	-
5% ACR A	-	-	140	-	-154	-11	-464
10% ACR A	51	45	139	-168	-	-	-
15% ACR A	50	-6	132	-165	-	-	-
20% ACR A	64	39	138	-160	-	-	-
25% ACR A	61	6	139	-138	-	-	-
Centre loadings							
Water	-	-	-83	-	-	-	-
RDN175	-45	16	-97	-	69	-	-
25% 1250	-	-	-68	-	-	-	-
5% ACR U	-37	-22	-75	86	-	-	-
10% ACR U	-37	2	-83	134	-	-	-
15% ACR U	-42	-28	-80	127	-	-	-
20% ACR U	-38	-13	-102	84	-	-	-
25% ACR U	-43	-1	-101	56	-	-	-
5% ACR A	-	-	-76	146	-	-	-
10% ACR A	-40	-33	-80	147	-	-	-
15% ACR A	-39	-2	-82	124	-	-	-
20% ACR A	-45	-28	-99	95	-	-	-
25% ACR A	-44	-8	-102	67	-	-	-

KEY; 1 - caused by surface heat transfer coefficient reaching maximum in film boiling stage
2 - caused by collapse of vapour blanket
3 - caused by passage of maximum surface heat transfer coefficient
4 - caused by decline in surface cooling rate coupled with the effect of stress relaxation
5 - caused by beginning of martensitic transformation
6 - caused by progression of transformation front into interior

TABLE 10: STRAIN S AT WHICH THE UNLOADINGS IN THE GENERATION OF THERMAL STRESS OCCURRED

Quenchant	1	2	3	4	5	6	7
Surface loadings							
Water	-	-	0.605	-	-	0.189	-0.144
RDN175	0.126	0.089	0.192	-	0.080	-	-
25% 1250	-	-	0.427	-	-	0.025	-0.208
5% ACR U	0.055	0.056	0.358	0.221	-	-0.021	-0.351
10% ACR U	0.056	0.034	0.313	0.091	-	-	-
15% ACR U	0.087	0.087	0.314	0.092	-	-	-
20% ACR U	0.068	0.064	0.218	0.076	-	-	-
25% ACR U	0.079	0.063	0.164	0.056	-	-	-
5% ACR A	-	-	0.374	-	0.249	-0.105	-0.284
10% ACR A	0.063	0.072	0.341	0.086	-	-	-
15% ACR A	0.061	0.042	0.299	0.087	-	-	-
20% ACR A	0.108	0.112	0.227	0.076	-	-	-
25% ACR A	0.095	0.083	0.184	0.065	-	-	-
Centre loadings							
Water	-	-	-0.429	-	-	-	-
RDN175	-0.066	-0.047	-0.104	-	-0.033	-	-
25% 1250	-	-	-0.318	-	-	-	-
5% ACR U	-0.026	-0.028	-0.224	-0.146	-	-	-
10% ACR U	-0.026	-0.014	-0.181	-0.065	-	-	-
15% ACR U	-0.040	-0.045	-0.180	-0.064	-	-	-
20% ACR U	-0.035	-0.036	-0.112	-0.028	-	-	-
25% ACR U	-0.038	-0.033	-0.089	-0.023	-	-	-
5% ACR A	-	-	-0.242	-	0.087	-	-
10% ACR A	-0.030	-0.038	-0.208	-0.080	-	-	-
15% ACR A	-0.028	-0.019	-0.164	-0.052	-	-	-
20% ACR A	-0.055	-0.061	-0.120	-0.033	-	-	-
25% ACR A	0.048	-0.044	-0.098	-0.027	-	-	-

KEY; 1 - caused by surface heat transfer coefficient reaching maximum in film boiling stage
2 - caused by collapse of vapour blanket
3 - caused by passage of maximum surface heat transfer coefficient
4 - caused by decline in surface cooling rate coupled with the effect of stress relaxation
5 - caused by beginning of martensitic transformation
6 - caused by progression of transformation front into interior

TABLE 11: KINEMATIC VISCOSITY OF SODIUM POLYACRYLATE SOLUTIONS AT VARIOUS TEMPERATURES ($mm^2.s^{-1}$)

Concentration of Aquaquench ACR	Temperature (°C) 20.2	40.0	60.0	80.0
0 %	1.00	0.66	0.48	0.37
5 %	9.62	6.35	4.27	2.96
10 %	15.63	10.44	7.20	4.77
15 %	22.76	14.66	10.01	9.97
20 %	32.27	20.09	13.63	9.59
25 %	42.32	26.46	17.85	12.57

TABLE 12: DENSITY OF SODIUM POLYACRYLATE SOLUTIONS AT VARIOUS TEMPERATURES ($kg.m^{-3}$)

Concentration of Aquaquench ACR	Temperature (°C)			
	20.2	40.0	60.0	80.0
0 %	998.2	992.2	983.2	971.8
5 %	1002.6	996.9	990.9	986.8
10 %	1007.2	1002.0	995.8	983.3
15 %	1011.5	1005.1	1002.8	993.3
20 %	1015.5	1010.9	1003.4	997.8
25 %	1019.7	1014.8	1003.4	995.8

TABLE 13: DYNAMIC VISCOSITY OF SODIUM POLYACRYLATE SOLUTIONS AT VARIOUS TEMPERATURES (mPa.s)

Concentration of Aquaquench ACR	Temperature (°C)			
	20.2	40.0	60.0	80.0
0 %	1.00	0.65	0.47	0.36
5 %	9.65	6.37	4.31	3.00
10 %	15.75	10.42	7.23	4.86
15 %	23.02	14.58	9.98	7.01
20 %	32.77	19.87	13.59	9.61
25 %	43.15	26.07	17.72	12.62

TABLE 14: VISCOSITY OF LIQUIDS EXTRACTED DURING QUENCHING IN 10% AQUAQUENCH ACR SOLUTION

Source of liquid	Kinematic viscosity at 40°C ($mm^2.s^{-1}$)	Concentration (% Aquaquench ACR)
Bulk liquid; extracted before the quench	12.6	9.8
Plate face; extracted during the quench	12.6	9.8
Viscous gel; extracted after the quench	12.2	9.3

TABLE 15: RESULTS OF CESS AND SPARROW[109] MODEL OF FILM BOILING

(WATER)

Wall temperature (^{o}C)	700.0	750.0	800.0	850.0	900.0	950.0	1000.0
Conduction surface heat transfer coefficient ($W.m^{-2}.K^{-1}$)	256.3	255.7	254.5	253.0	253.5	254.4	258.7
Radiation surface heat transfer coefficient ($W.m^{-2}.K^{-1}$)	17.0	20.9	25.3	30.3	35.9	42.2	49.2
Total surface heat transfer coefficient ($W.m^{-2}.K^{-1}$)	269.0	271.3	273.5	275.7	280.4	286.1	295.5
Dimensionless vapour layer thickness	0.800	0.838	0.877	0.922	0.962	1.000	1.022
Dimensionless liquid layer thickness	6.0	6.0	6.0	6.0	6.0	6.0	6.0
Thickness of vapour blanket (mm)	0.371	0.400	0.431	0.466	0.500	0.533	0.558

TABLE 16: RESULTS OF CESS AND SPARROW[109] MODEL OF FILM BOILING

(25% AQUAQUENCH ACR SOLUTION)

Wall temperature (^{o}C)	550.0	600.0	650.0	700.0	750.0	800.0	850.0
Conduction surface heat transfer coefficient ($W.m^{-2}.K^{-1}$)	200.9	202.8	204.0	207.8	210.3	213.0	218.2
Radiation surface heat transfer coefficient ($W.m^{-2}.K^{-1}$)	8.3	10.8	13.7	17.0	20.9	25.3	30.3
Total surface heat transfer coefficient ($W.m^{-2}.K^{-1}$)	207.2	210.9	214.2	220.6	225.9	232.0	240.9
Dimensionless vapour layer thickness	0.892	0.938	0.978	1.006	1.050	1.078	1.103
Dimensionless liquid layer thickness	2.0	2.0	2.0	2.0	2.0	2.0	2.0
Thickness of vapour blanket (mm)	0.372	0.405	0.437	0.464	0.499	0.528	0.555

TABLE 17: RESULTS OF NISHIKWAWA AND ITO[112] MODEL OF FILM BOILING

(WATER)

Wall temperature (^{o}C)	700.0	750.0	800.0	850.0	900.0	950.0	1000.0
Conduction surface heat transfer coefficient ($W.m^{-2}.K^{-1}$)	301.6	304.5	303.2	301.2	298.8	300.5	300.6
Radiation surface heat transfer coefficient ($W.m^{-2}.K^{-1}$)	17.0	20.9	25.3	30.3	35.9	42.2	49.2
Total surface heat transfer coefficient ($W.m^{-2}.K^{-1}$)	314.5	320.3	322.4	324.3	326.1	332.7	338.2
Dimensionless vapour layer thickness	0.674	0.698	0.732	0.769	0.803	0.835	0.866
Dimensionless liquid layer thickness	2.0	2.0	2.0	2.0	2.0	2.0	2.0
Thickness of vapour blanket (mm)	0.312	0.334	0.360	0.389	0.417	0.445	0.473
Vapour velocity at interface ($mm.s^{-1}$)	0.356	0.388	0.420	0.452	0.480	0.522	0.546
Liquid velocity at interface ($mm.s^{-1}$)	0.780	0.825	0.868	0.908	0.938	0.995	1.016
Vapour Reynolds Number at interface	1.031	1.125	1.219	1.310	1.391	1.513	1.583
Liquid Reynolds Number at interface	170.6	180.5	190.0	198.7	205.2	217.7	222.2

TABLE 18: RESULTS OF FILM BOILING MODEL OF NISHIKAWA AND ITO[112]

(25% AQUAQUENCH ACR SOLUTION)

Wall temperature (^{o}C)	550.0	600.0	650.0	700.0	750.0	800.0	850.0
Conduction surface heat transfer coefficient ($W.m^{-2}.K^{-1}$)	166.6	172.1	176.5	181.3	186.7	191.3	197.0
Radiation surface heat transfer coefficient ($W.m^{-2}.K^{-1}$)	8.3	10.8	13.7	17.0	20.9	25.3	30.3
Total surface heat transfer coefficient ($W.m^{-2}.K^{-1}$)	172.9	180.3	186.9	194.2	202.6	210.6	220.1
Dimensionless vapour layer thickness	1.103	1.131	1.159	1.187	1.212	1.236	1.261
Dimensionless liquid layer thickness	0.16	0.16	0.16	0.16	0.16	0.16	0.16
Thickness of vapour blanket (mm)	0.460	0.488	0.517	0.547	0.576	0.605	0.635
Vapour velocity at interface ($mm.s^{-1}$)	0.081	0.089	0.096	0.103	0.112	0.118	0.124
Liquid velocity at interface ($m.s^{-1}$)	7.325	7.770	8.067	8.414	8.909	9.156	9.305
Vapour Reynolds Number at interface	0.234	0.257	0.277	0.297	0.325	0.343	0.359
Liquid Reynolds Number at interface	38.57	40.92	42.62	44.25	47.00	48.11	49.00

TABLE 19: RESULTS OF NISHIKAWA, ITO AND MATSUMOTO[114] MODEL OF FILM BOILING (WATER)

Wall temperature (^{o}C)	700.0	750.0	800.0	850.0	900.0	950.0	1000.0
Conduction surface heat transfer coefficient ($W.m^{-2}.K^{-1}$)	352.1	336.6	323.0	310.7	300.4	290.8	283.6
Radiation surface heat transfer coefficient ($W.m^{-2}.K^{-1}$)	17.0	20.9	25.3	30.3	35.9	42.2	49.2
Total surface heat transfer coefficient ($W.m^{-2}.K^{-1}$)	364.9	352.3	342.3	333.7	327.7	323.0	321.3
Dimensionless vapour layer thickness	0.305	0.325	0.344	0.363	0.382	0.401	0.417
Dimensionless liquid layer thickness	3.50	3.50	3.50	3.50	3.50	3.50	3.50
Thickness of vapour blanket (mm)	0.124	0.133	0.143	0.152	0.162	0.172	0.182
Vapour velocity at interface ($mm.s^{-1}$)	0.263	0.275	0.294	0.310	0.327	0.344	0.366
Liquid velocity at interface ($m.s^{-1}$)	0.428	0.450	0.479	0.506	0.534	0.562	0.597
Vapour Reynolds Number at interface	0.759	0.798	0.851	0.898	0.948	0.998	1.060
Liquid Reynolds Number at interface	93.57	98.40	104.9	110.8	117.0	123.0	130.7

TABLE 20: RESULTS OF NISHIKAWA, ITO AND MATSUMOTO[114] MODEL OF FILM BOILING (25% AQUAQUENCH ACR SOLUTION)

Wall temperature (°C)	550.0	650.0	750.0	850.0
Conduction surface heat transfer coefficient ($W.m^{-2}.K^{-1}$)	229.9	206.9	193.7	184.2
Radiation surface heat transfer coefficient ($W.m^{-2}.K^{-1}$)	8.3	13.7	20.9	30.3
Total surface heat transfer coefficient ($W.m^{-2}.K^{-1}$)	236.2	217.2	209.6	207.4
Dimensionless vapour layer thickness	0.450	0.516	0.570	0.620
Dimensionless liquid layer thickness	1.0	1.0	1.0	1.0
Thickness of vapour blanket (mm)	0.174	0.206	0.233	0.258
Vapour velocity at interface ($m.s^{-1}$)	0.047	0.055	0.063	0.069
Liquid velocity at interface ($m.s^{-1}$)	0.511	0.060	0.071	0.754
Vapour Reynolds Number at interface	0.136	0.160	0.182	0.200
Liquid Reynolds Number at interface	2.695	3.182	3.615	3.968

TABLE 21: CALCULATED[114] PROPERTIES IN THE FILM BOILING INTERFACE FOR WATER AND 25% AQUAQUENCH ACR SOLUTION

Surface Temperature (^{o}C)	Interface Velocity ($m.s^{-1}$)	Vapour Reynolds Number	Liquid Reynolds Number
Water;			
850	0.5465	1584	119,598
900	0.5781	1676	126,490
950	0.6064	1758	132,691
1000	0.6443	1868	140,989
25% Aquaquench ACR;			
550	0.0836	242	440
650	0.0962	279	507
750	0.1093	317	576
850	0.1200	348	632

TABLE 22: RESULTS OF THE TURBULENT INTERFACE MODEL (WATER)

Wall temperature (^{o}C)	700.0	750.0	800.0	850.0	900.0	950.0	1000.0
Conduction surface heat transfer coefficient ($W.m^{-2}.K^{-1}$)	498.5	486.1	472.9	465.4	465.7	465.1	456.7
Radiation surface heat transfer coefficient ($W.m^{-2}.K^{-1}$)	17.0	20.9	25.3	30.3	35.9	42.2	49.2
Total surface heat transfer coefficient ($W.m^{-2}.K^{-1}$)	511.3	501.8	491.8	488.1	492.7	496.7	493.6
Dimensionless vapour layer thickness	0.408	0.437	0.469	0.498	0.516	0.538	0.570
Dimensionless liquid layer thickness	5.0	5.0	5.0	5.0	5.0	5.0	5.0
Thickness of vapour blanket (mm)	0.189	0.209	0.231	0.252	0.268	0.287	0.312
Vapour velocity at interface ($m.s^{-1}$)	7.762						
Liquid velocity at interface ($m.s^{-1}$)	0.103						
Vapour Reynolds Number at interface	22,500						
Liquid Reynolds Number at interface	22,500						

TABLE 23: RESULTS OF TURBULENT INTERFACE MODEL (25% AQUAQUENCH ACR SOLUTION)

Wall temperature (^{o}C)	550.0	600.0	650.0	700.0	750.0	800.0	850.0
Conduction surface heat transfer coefficient ($W.m^{-2}.K^{-1}$)	354.1	332.2	321.2	307.9	304.5	292.4	291.6
Radiation surface heat transfer coefficient ($W.m^{-2}.K^{-1}$)	8.3	10.8	13.7	17.0	20.9	25.3	30.3
Total surface heat transfer coefficient ($W.m^{-2}.K^{-1}$)	360.3	340.3	331.4	320.6	320.1	311.4	314.3
Dimensionless vapour layer thickness	0.498	0.559	0.606	0.662	0.703	0.763	0.800
Dimensionless liquid layer thickness	1.0	1.0	1.0	1.0	1.0	1.0	1.0
Thickness of vapour blanket (mm)	0.208	0.241	0.271	0.305	0.334	0.373	0.403
Vapour velocity at interface ($m.s^{-1}$)	0.086						
Liquid velocity at interface ($m.s^{-1}$)	0.047						
Vapour Reynolds Number at interface	250						
Liquid Reynolds Number at interface	250						

FIGURE 1: Molecular structure of the polymer quenchants;

a) polyvinyl alcohol,

b) polyalkylene glycol,

c) polyvinylpyrrolidone,

d) sodium polyacrylate,

(after Hilder[14]).

a) 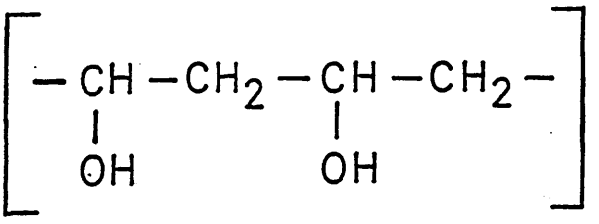

b) 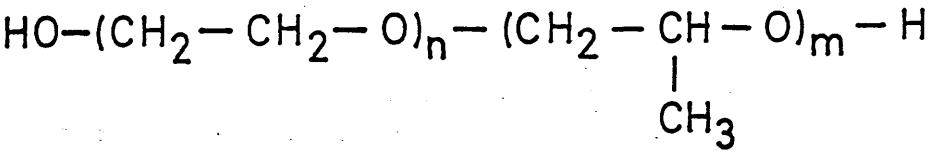

c) 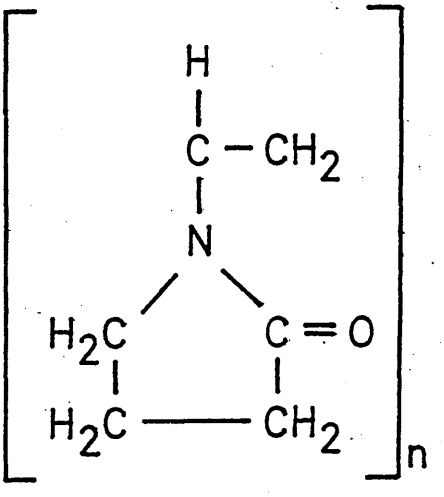

d) 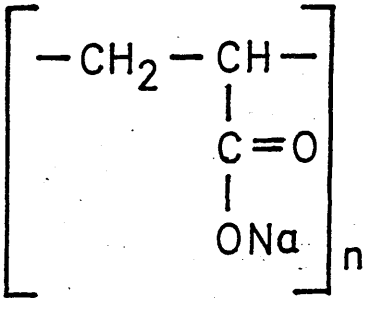

FIGURE 2: Effect of concentration of polyvinyl alcohol in water on quenching severity, solution temperature 25°C, (after Hilder[14]).

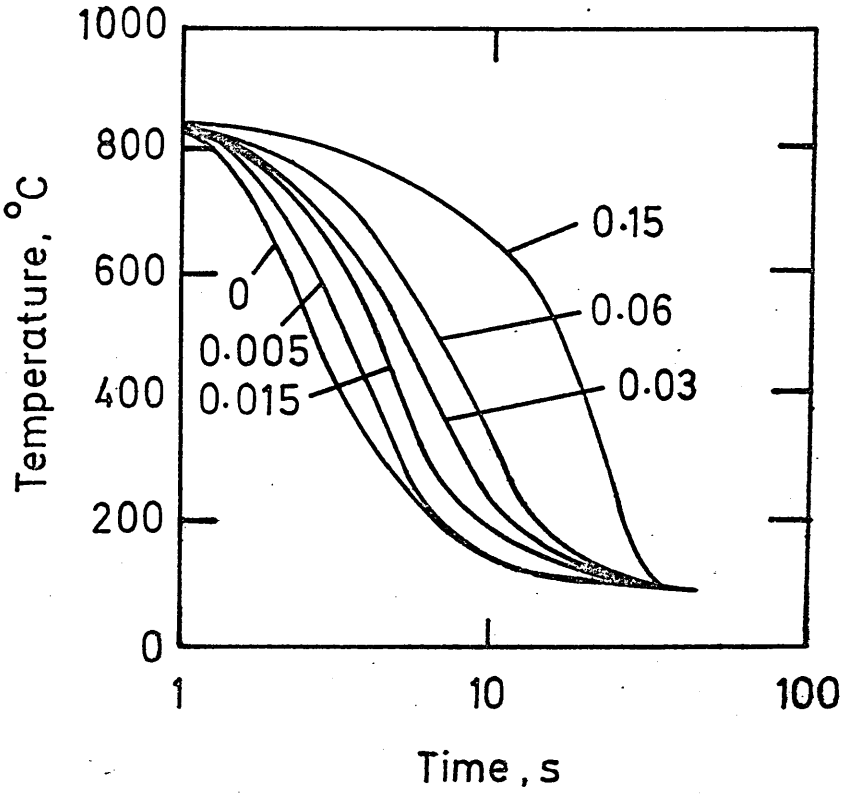
1000
800
600
400
200
0
Temperature, °C
0
0·005
0·015
0·03
0·06
0·15
1
10
100
Time , s

FIGURE 3: Surface heat transfer coefficients measured in solutions of 5-25% Aquaquench 1250 in water, (after Allen, Fletcher and King[9].

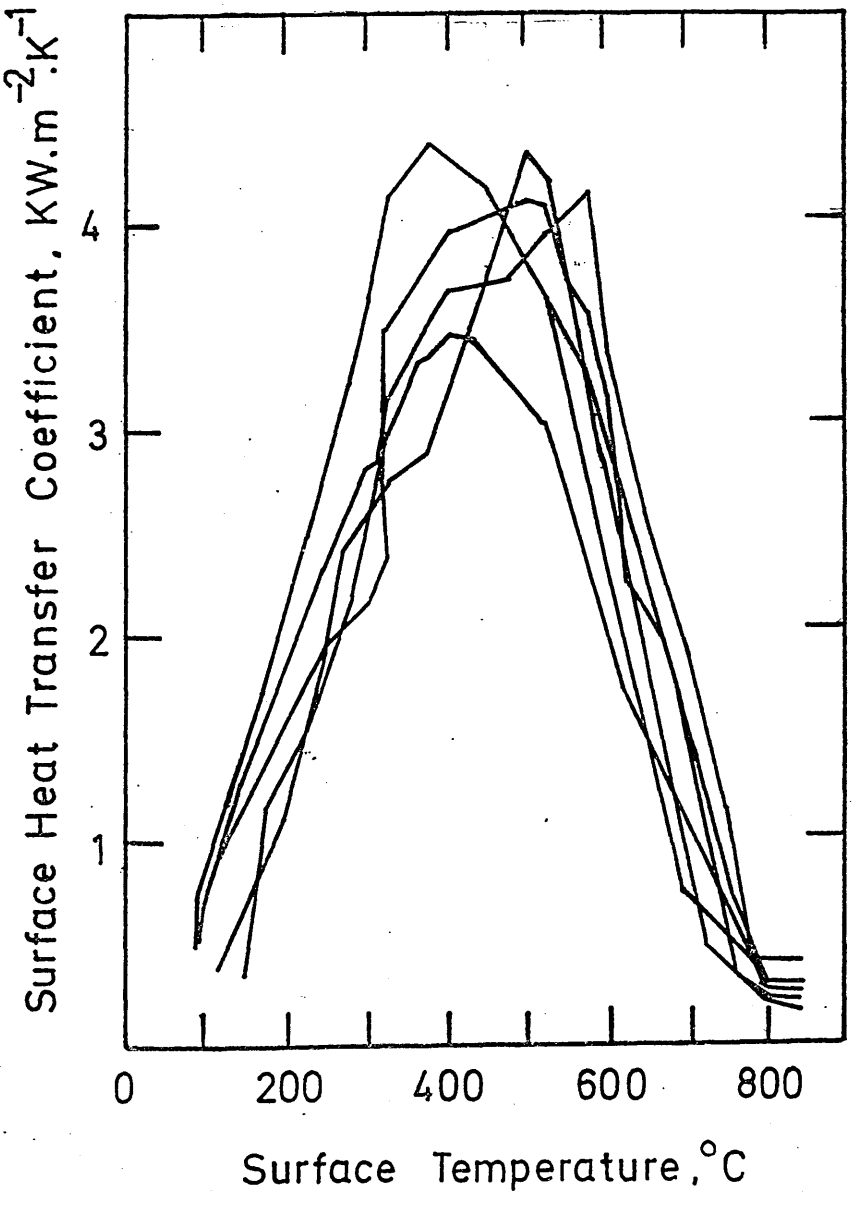
Surface Heat Transfer Coefficient, KW.m^{-2}.K^{-1}
4
3
2
1
0
200
400
600
800
Surface Temperature, °C

FIGURE 4: Effect of polymer solution temperature on cooling rate, (after Hilder[14]).

a) Maximum cooling rate

b) Cooling rate at 300°C

FIGURE 5: Effect of agitation of polymer solution on cooling rate, (after Hilder[14]).

a) Maximum cooling rate

b) Cooling rate at 300°C

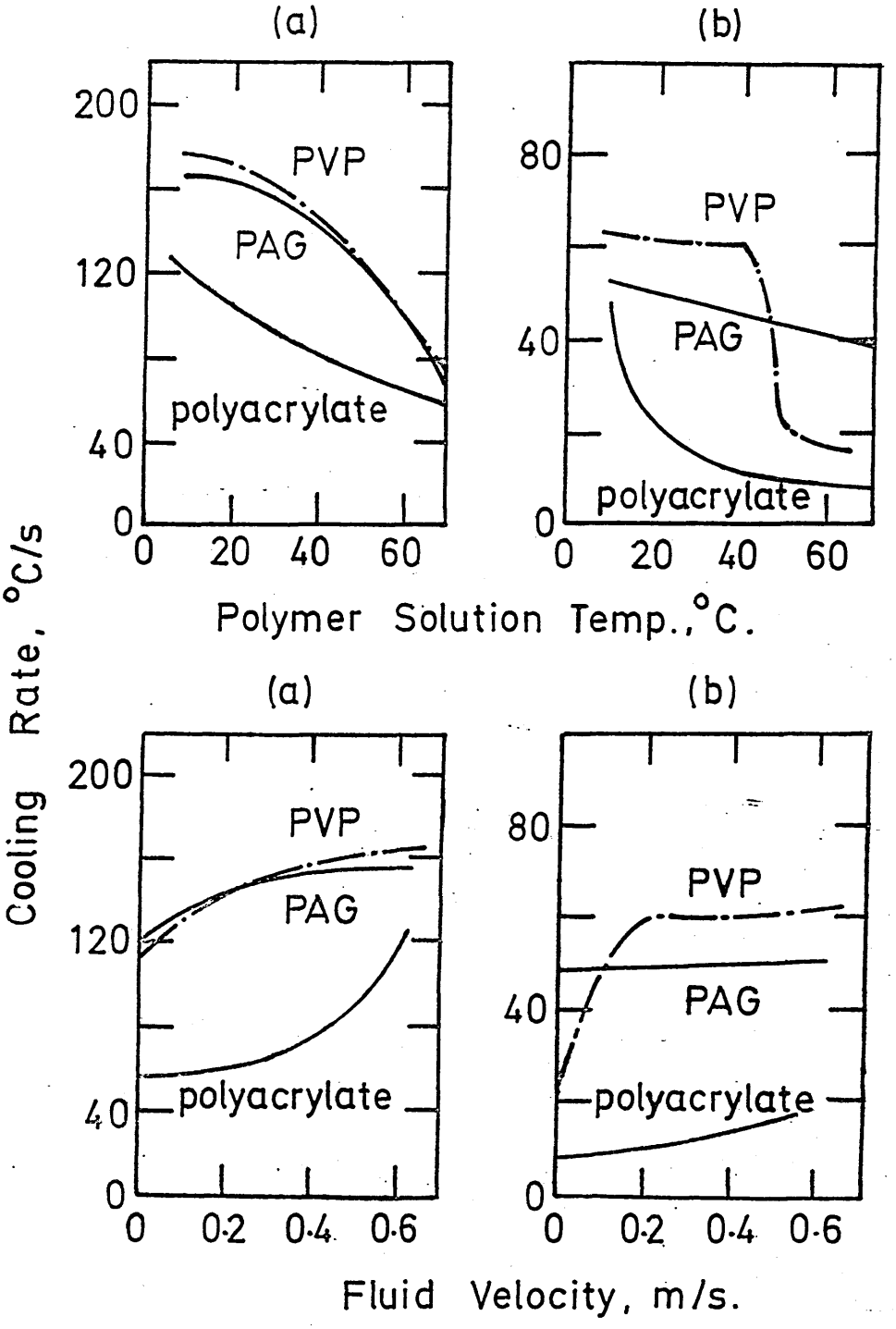
(a)
(b)
200
120
40
0
80
40
0
PVP
PAG
polyacrylate
0 20 40 60
Polymer Solution Temp., °C.
Cooling Rate, °C/s
0 0·2 0·4 0·6
Fluid Velocity, m/s.

FIGURE 6: Boiling stability diagram for solutions of polyvinylpyrrolidone in water, (after Moreaux et alia[29 30]).

θ_s = surface temperature

θ_L = liquid temperature

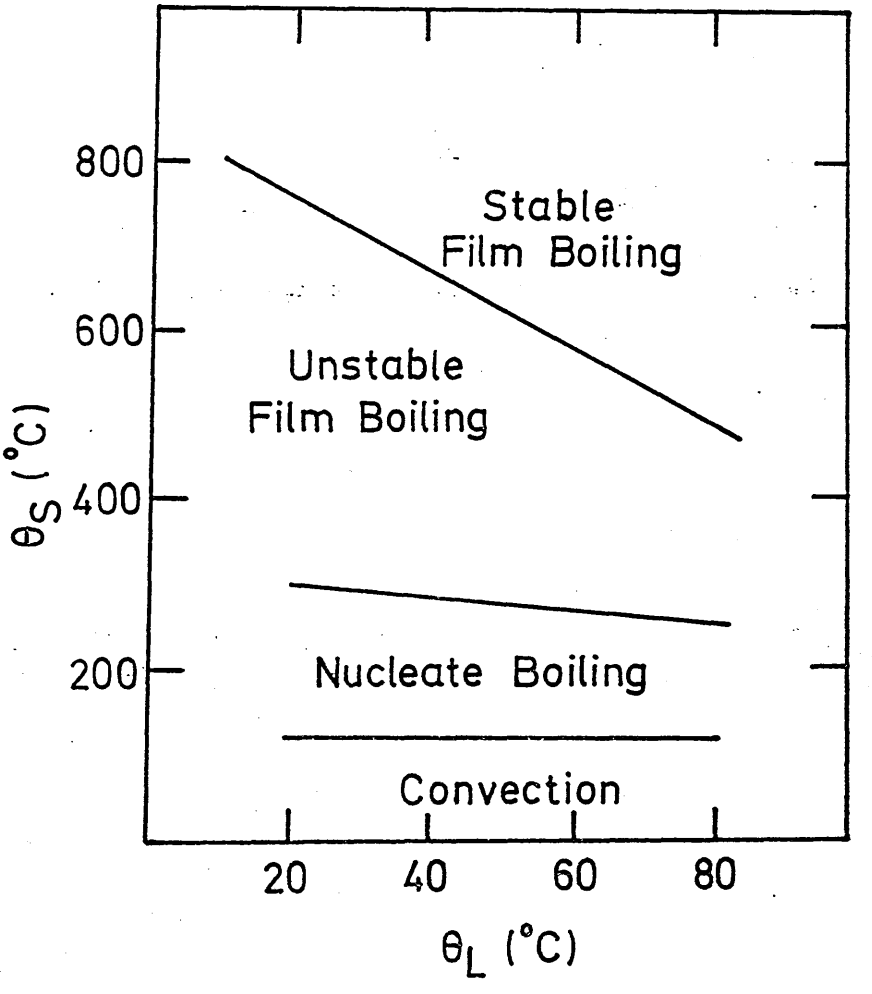
800
600
400
200
Stable
Film Boiling
Unstable
Film Boiling
Nucleate Boiling
Convection
θS (°C)
20
40
60
80
θL (°C)

FIGURE 7: The effect of viscosity on the duration of the film boiling stage in aqueous solutions of sodium polyacrylate, (after Kopietz and Munjat[31]).

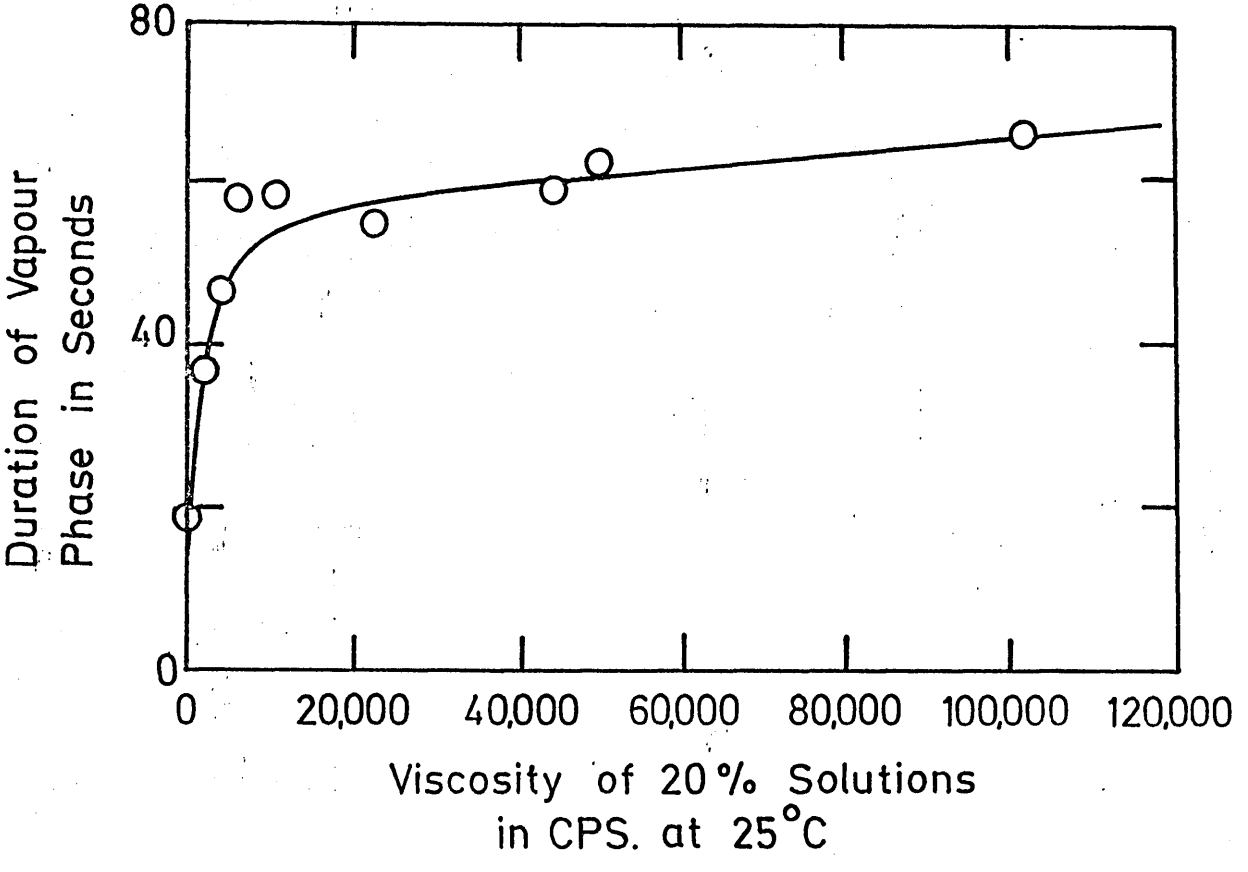
80
40
0
Duration of Vapour Phase in Seconds
0
20,000
40,000
60,000
80,000
100,000
120,000
Viscosity of 20% Solutions in CPS. at 25°C

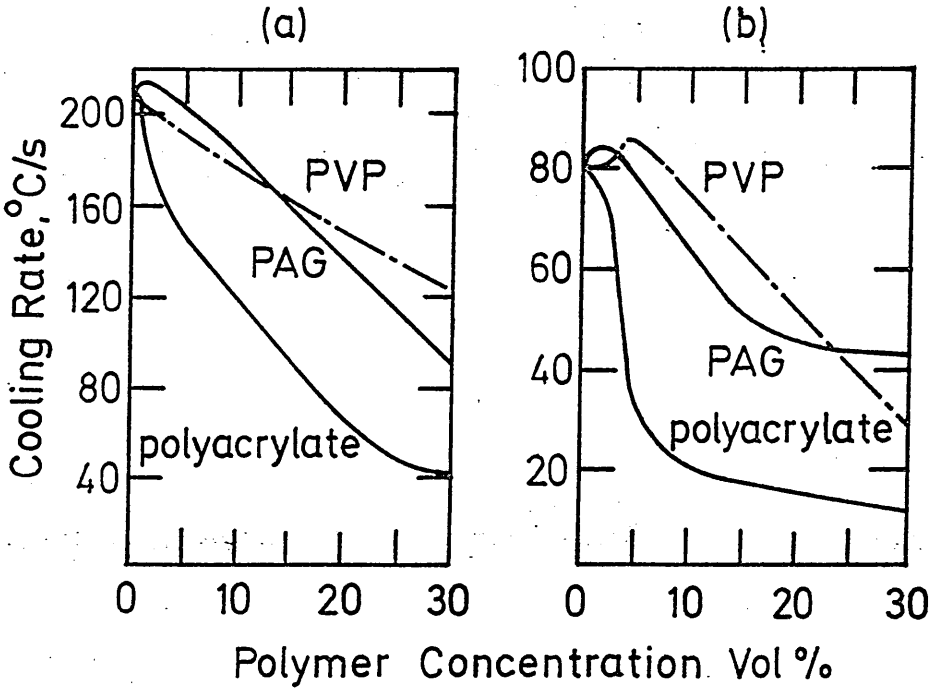
(a)
(b)
Cooling Rate, °C/s
200
160
120
80
40
100
80
60
40
20
PVP
PAG
polyacrylate
0
10
20
30
Polymer Concentration Vol %

FIGURE 8: Effect of polymer concentration on cooling rate, (after Hilder[14]).

a) Maximum cooling rate

b) Cooling rate at 300°C

FIGURE 9: Surface heat transfer coefficients measured in aqueous solutions of 1% PK-2, (a polyacrylamide solution), at various solution temperatures;

a) 23°C b) 60°C c) 80°C

T_I = surface temperature

(after Kobasko et alia[40]).

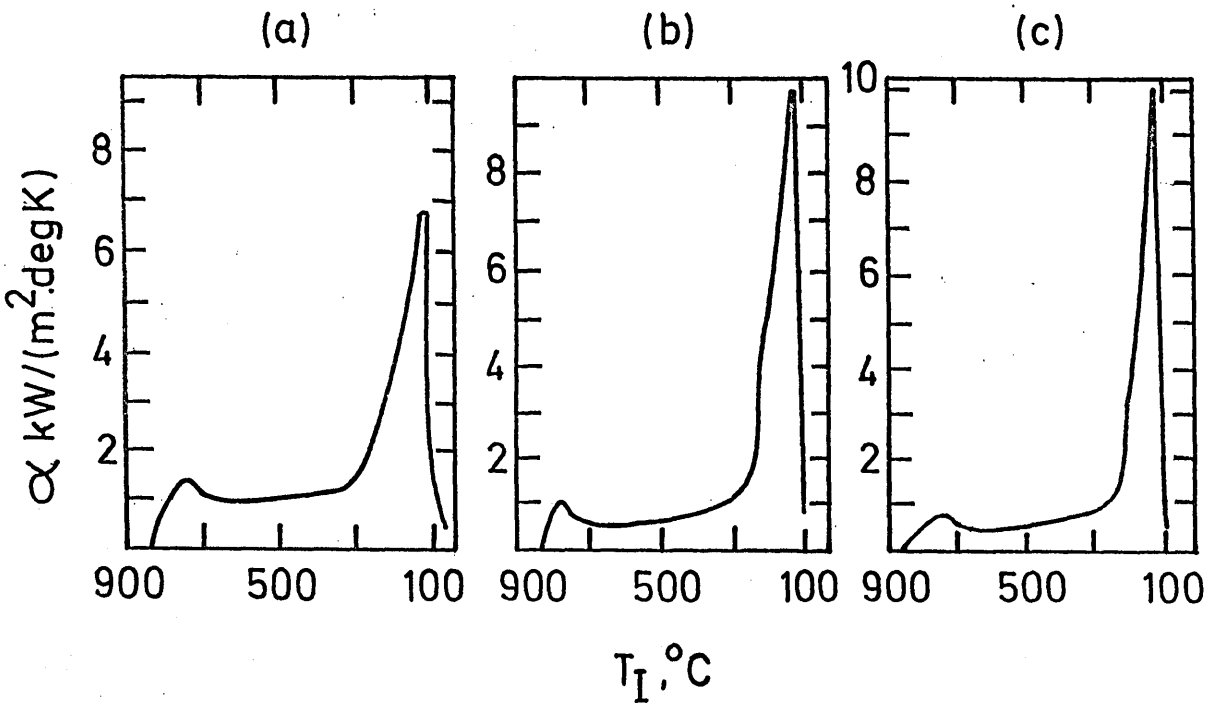
(a)
(b)
(c)
α kW/(m².degK)
2
4
6
8
10
900
500
100
T_I, °C

FIGURE 10: Thermo-mechanical coupling, (after Inoue and Wang[85])

(1) Thermal stress

(2) Temperature-dependent phase temperature

(3) Transformation stress

(4) Heat generation due to mechanical work

(5) Stress-induced transformation

(6) Latent heat

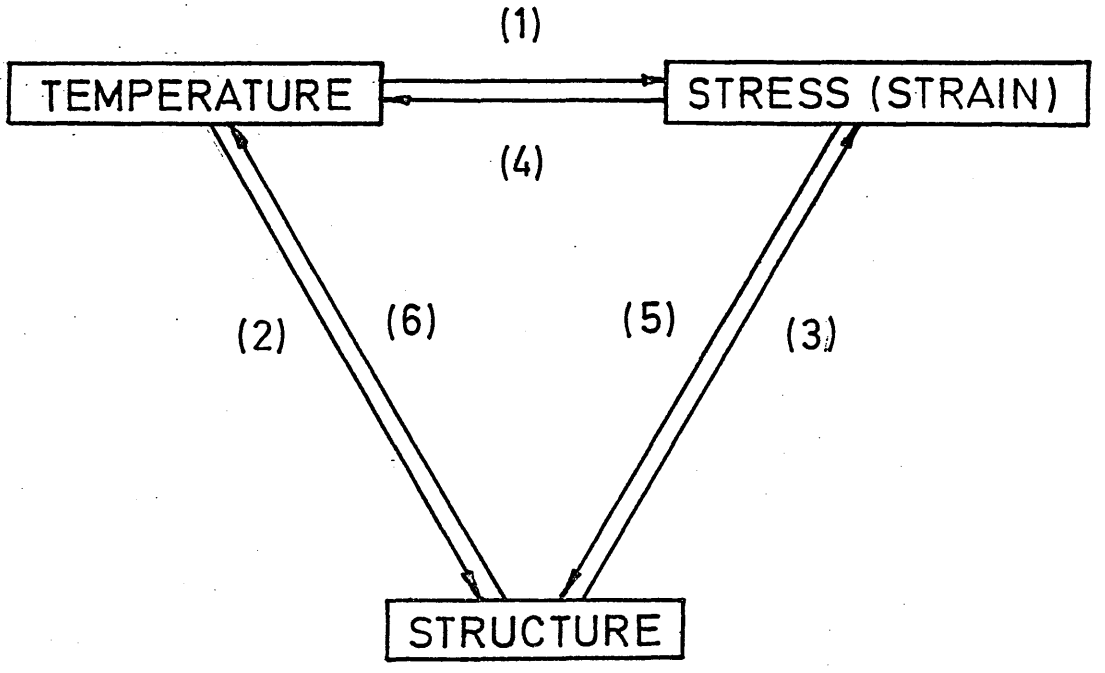
(1)
TEMPERATURE
STRESS (STRAIN)
(4)
(2)
(6)
(5)
(3)
STRUCTURE

FIGURE 11: Residual stresses predicted in the case of an air-cooled plate, (after Boley and Weiner[50]). Temperatures refer to initial temperature of plate.

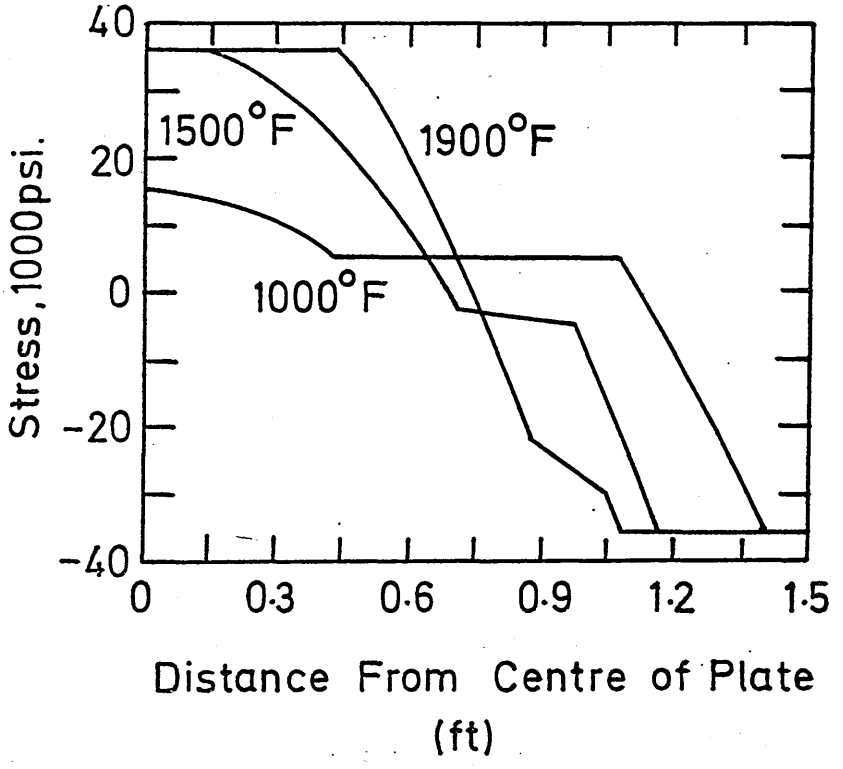
40
20
0
-20
-40
Stress, 1000psi.
1500°F
1900°F
1000°F
0
0·3
0·6
0·9
1·2
1·5
Distance From Centre of Plate
(ft)

FIGURE 12: Dilatometer curves showing transformation plasticity; figures refer to applied tensile stress in MPa, after Denis et alia[74]).

FIGURE 13: Elastic and plastic relationships between stress and strain used by Denis et alia;[72]

E_p = plastic Modulus

σ_{Eap} = apparent yield stress

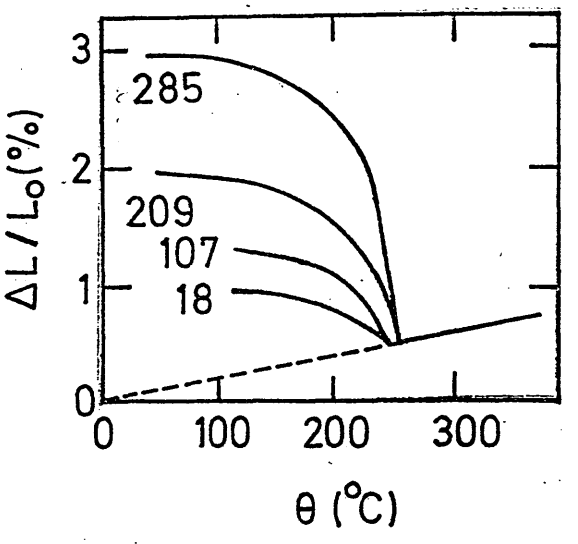
3
2
1
0
285
209
107
18
ΔL / L₀(%)
0
100
200
300
θ (°C)

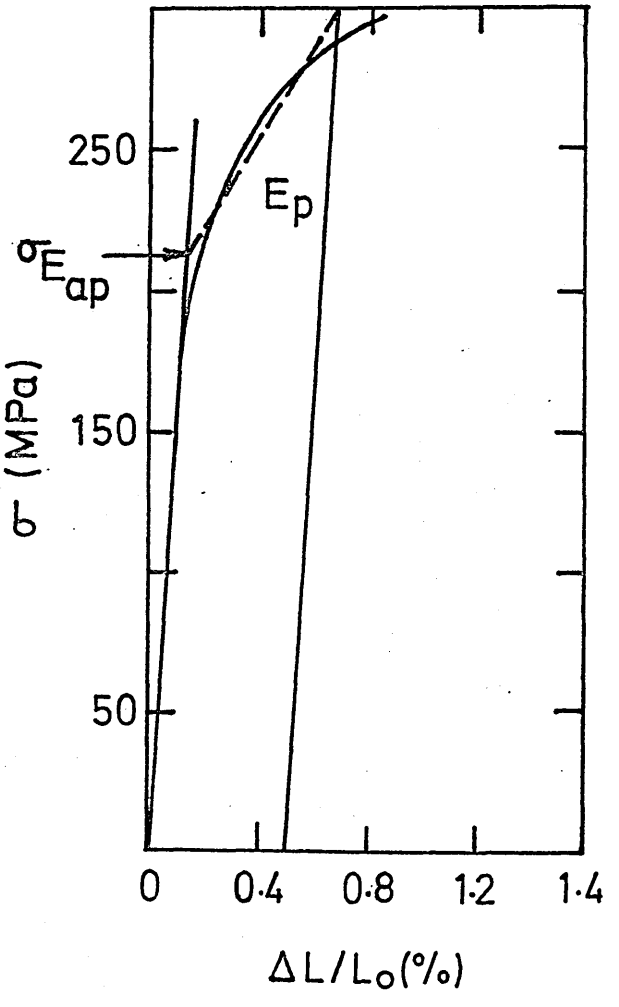
250
150
50
σ (MPa)
σ Eap
Ep
0
0·4
0·8
1·2
1·4
ΔL/L₀(%)

FIGURE 14: Comparison of experimentally measured and calculated cooling curves at the centre of a cylinder of a eutectoid steel, (after Denis et alia[80]).

FIGURE 15: The boiling curve, (after Winterton[89]).

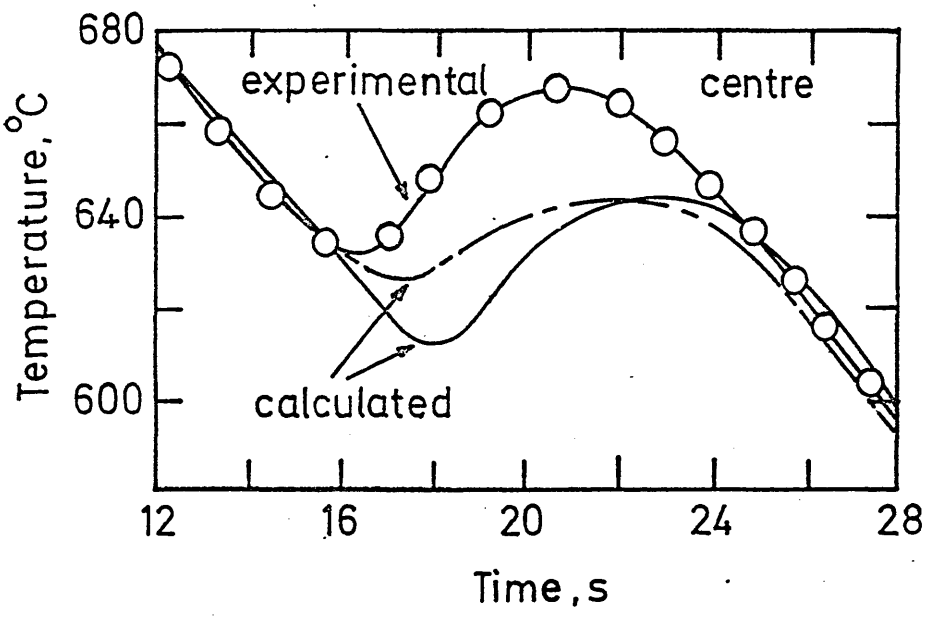
680
640
600
Temperature, °C
experimental
centre
calculated
12
16
20
24
28
Time, s

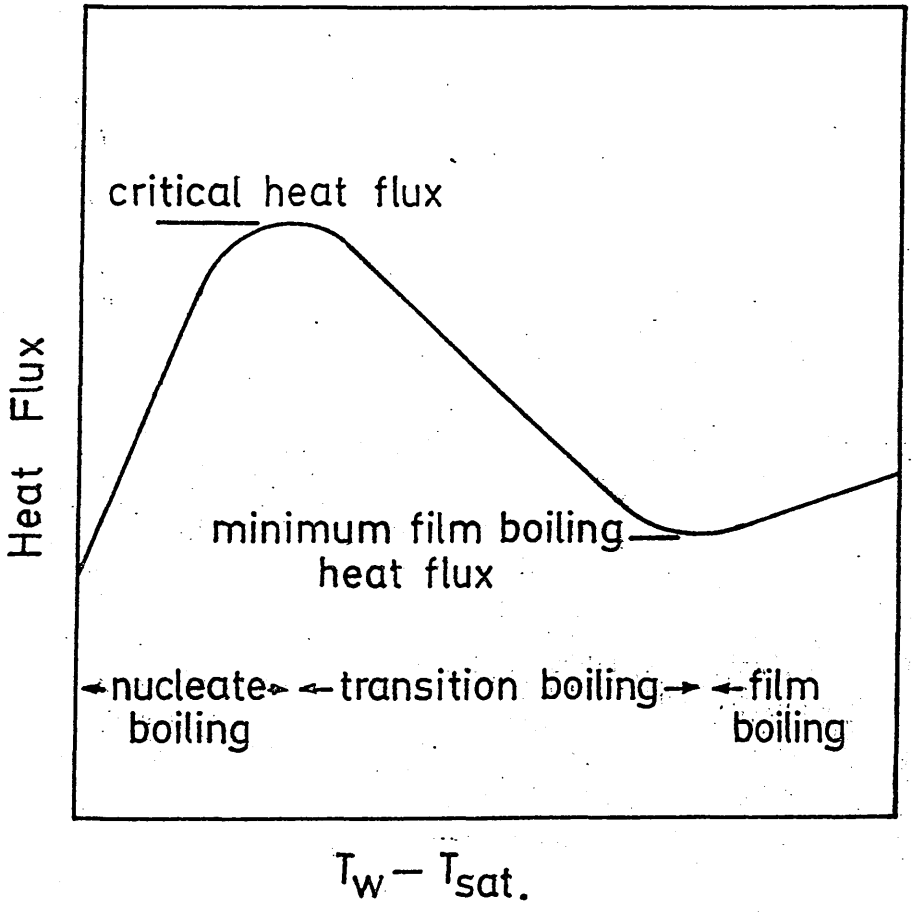
critical heat flux
Heat Flux
minimum film boiling
heat flux
nucleate
boiling
transition boiling
film
boiling
$T_w - T_{sat.}$

FIGURE 16: The film boiling model of Hsu and Westwater[97].

FIGURE 17: The potential for growth of an oscillation in an interface accelerated perpendicularly, (after Berenson[98]).

b = a coefficient describing the rate of growth of a disturbance in the interface

m = the wave number, related to the wavelength by;

$m = (2\pi)/\lambda$ where λ = wavelength

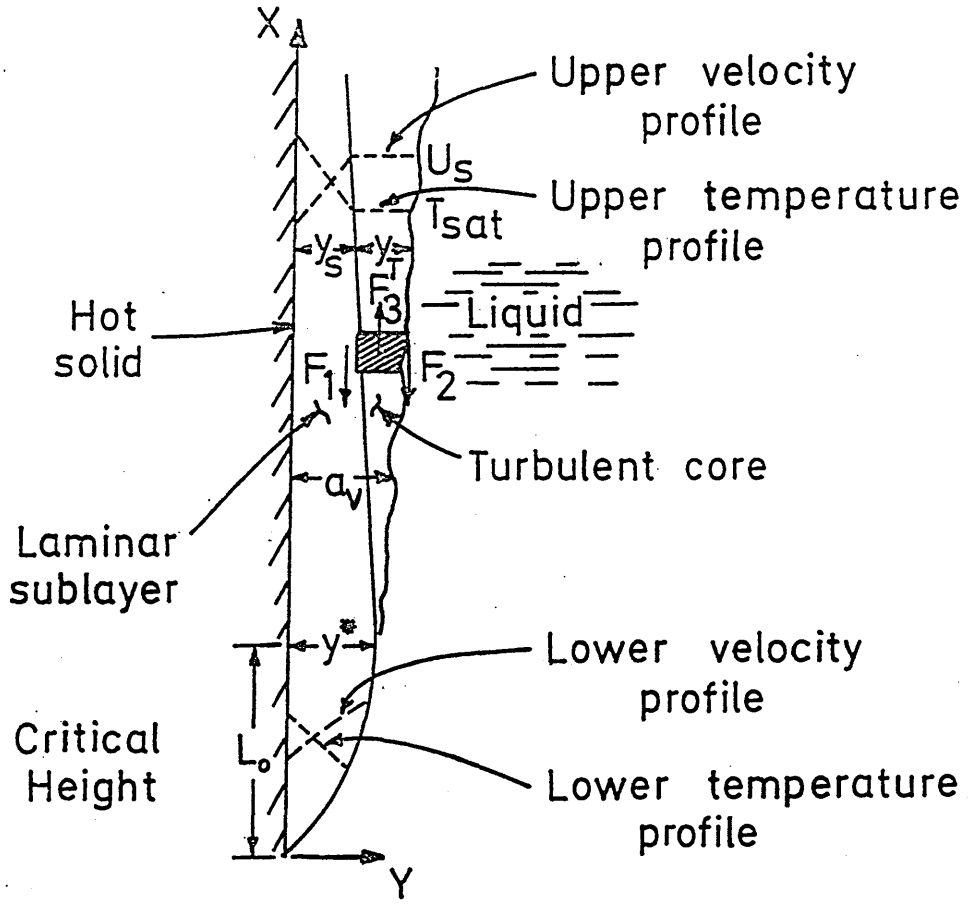
X
Upper velocity profile
U_s
Upper temperature profile
T_{sat}
y_s
y_T
F_3
Liquid
Hot solid
F_1
F_2
Turbulent core
a_v
Laminar sublayer
y^*
Lower velocity profile
Critical Height
L_o
Lower temperature profile
Y

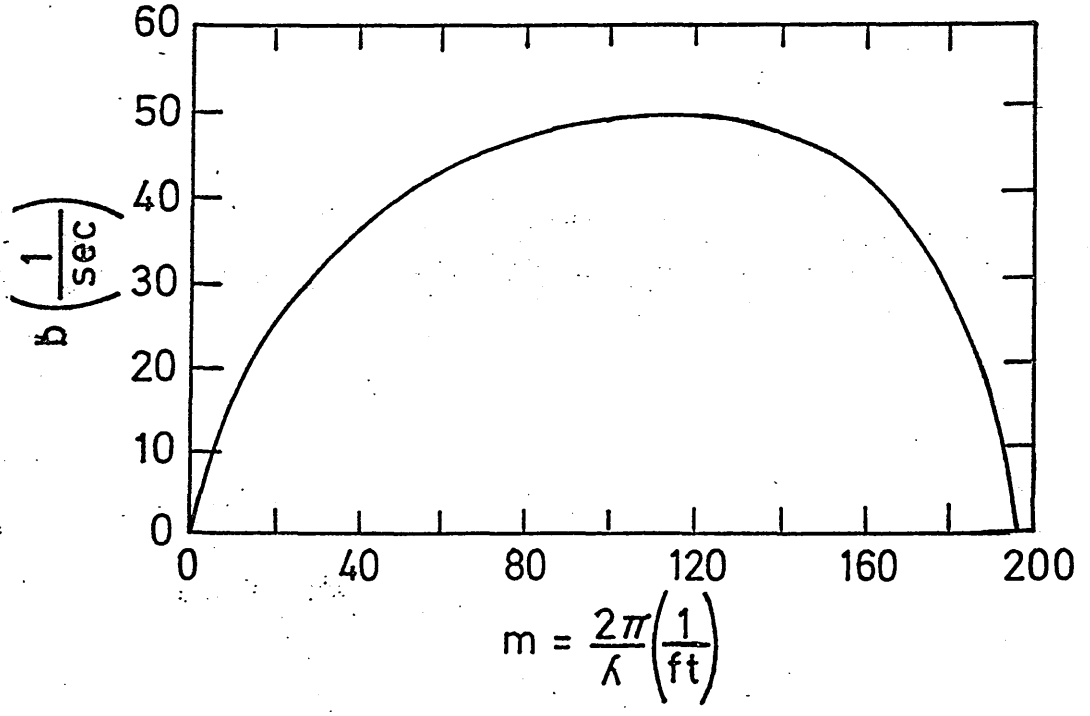
60
50
40
30
20
10
0
$b\left(\frac{1}{sec}\right)$
0
40
80
120
160
200
$m = \frac{2\pi}{\lambda}\left(\frac{1}{ft}\right)$

FIGURE 18: The film boiling model of Coury and Dukler[103].

U = velocity
T = temperature
W = wall
M = mean
I = interface
L = liquid

FIGURE 19: The film boiling model of Greitzer and Abernathy[104]

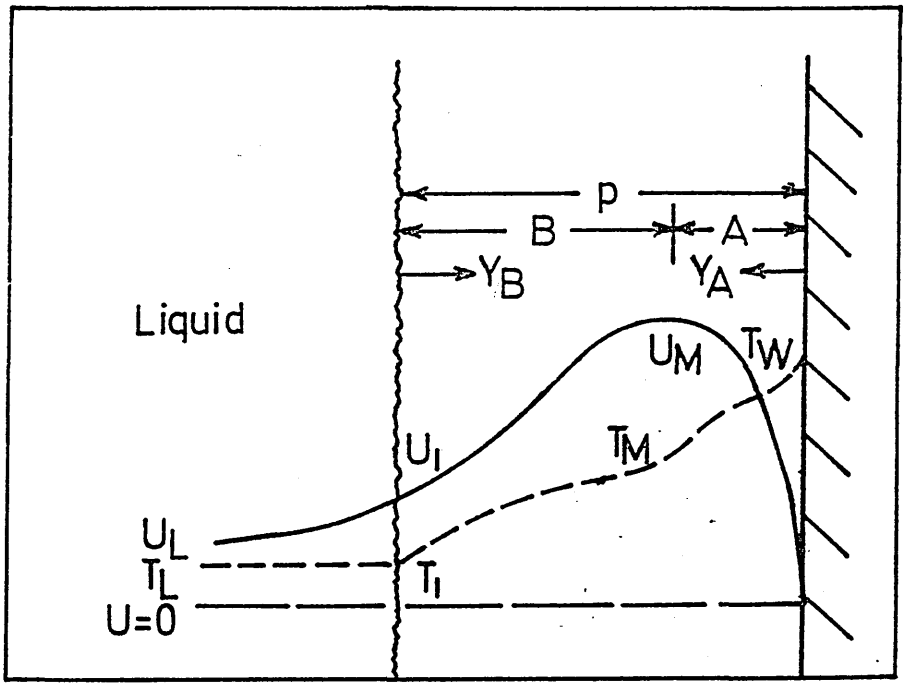
p
B
A
Y_B
Y_A
Liquid
U_M
T_W
U_I
T_M
U_L
T_L
T_I
U=0

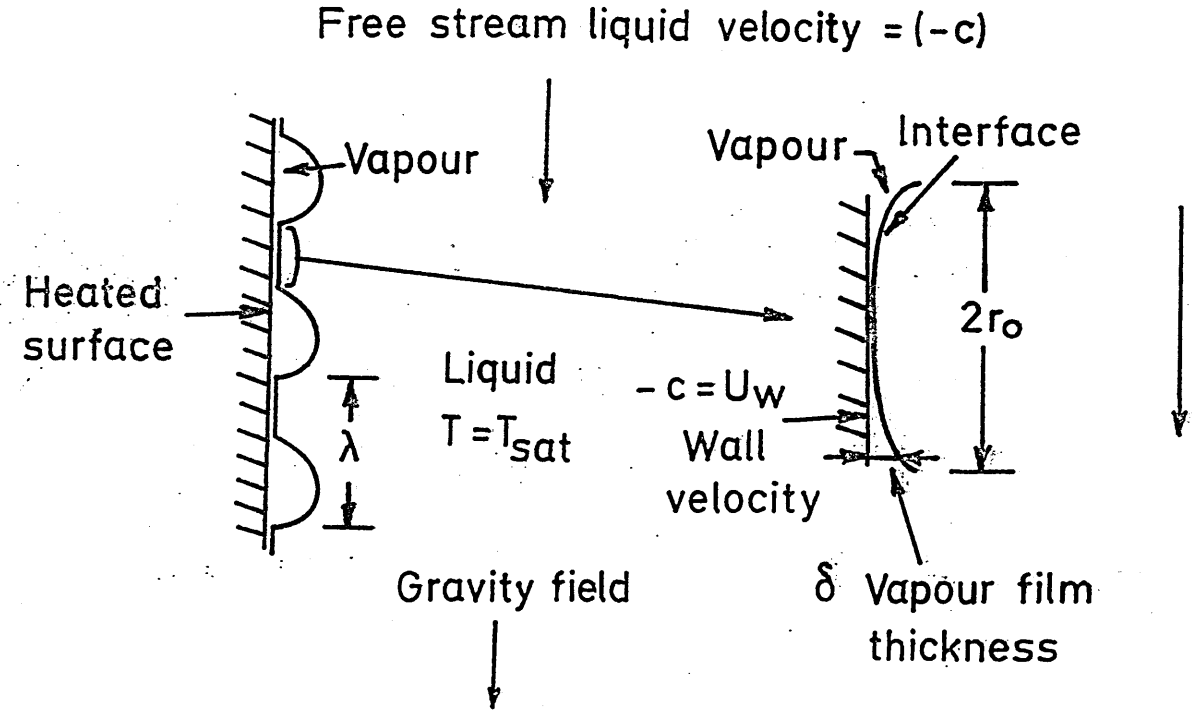
Free stream liquid velocity = (-c)
Vapour
Vapour
Interface
Heated surface
$2r_o$
Liquid
$T = T_{sat}$
$-c = U_W$
Wall velocity
λ
Gravity field
δ Vapour film thickness

FIGURE 20: The surface heat transfer coefficient during film boiling measured by Tachibana and Fukui.[101] Figures refer to amount of liquid subcooling, (^{o}F).

t_w = wall temperature, (^{o})

t_s = saturation temperature, (^{o}F)

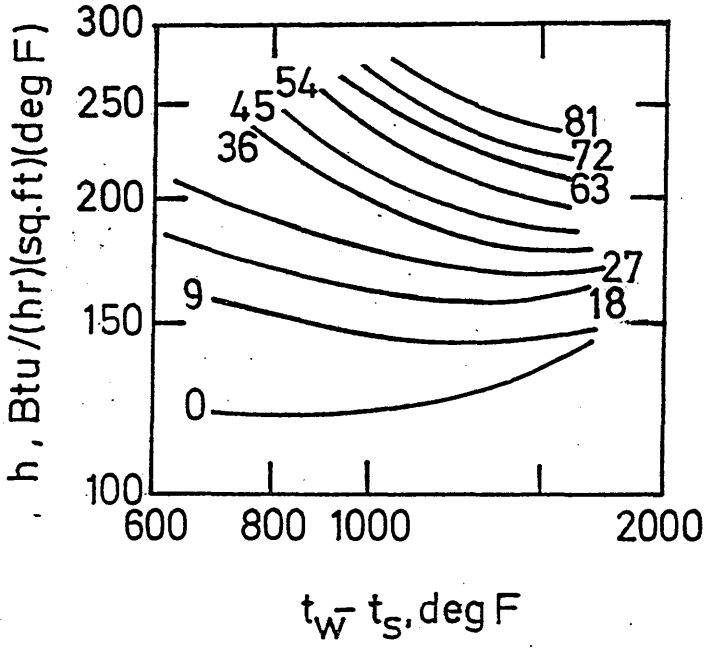
h, Btu/(hr)(sq.ft)(deg F)
300
250
200
150
100
600
800
1000
2000
$t_w - t_s$, deg F
54
45
36
81
72
63
27
18
9
0

FIGURE 21: Film boiling heat flux measurements obtained by Ede and Siviour[106] in the case of an isothermal horizontal cylinder in water; from top to bottom, 3, 6 and 13 mm diameter respectively.

Temperatures denote surface temperatures.

κ denotes degree of liquid subcooling in ^{o}C.

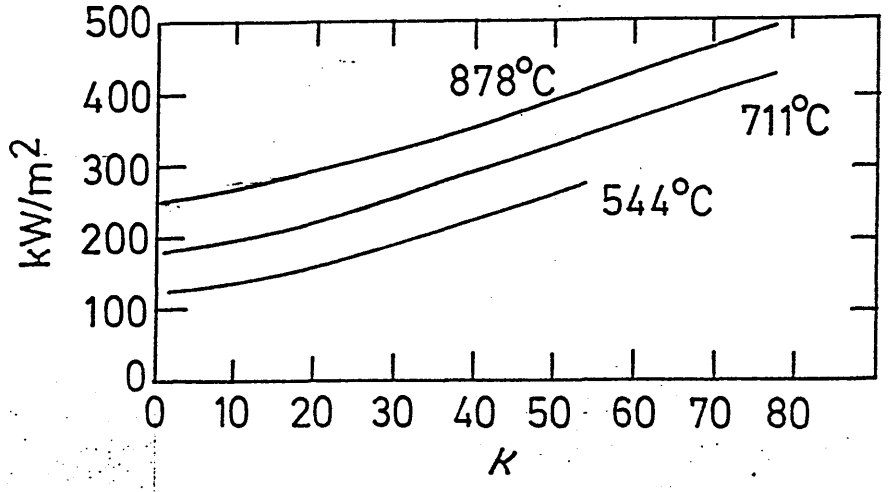
500
400
300
200
100
0
kW/m2
878°C
711°C
544°C
0 10 20 30 40 50 60 70 80
K

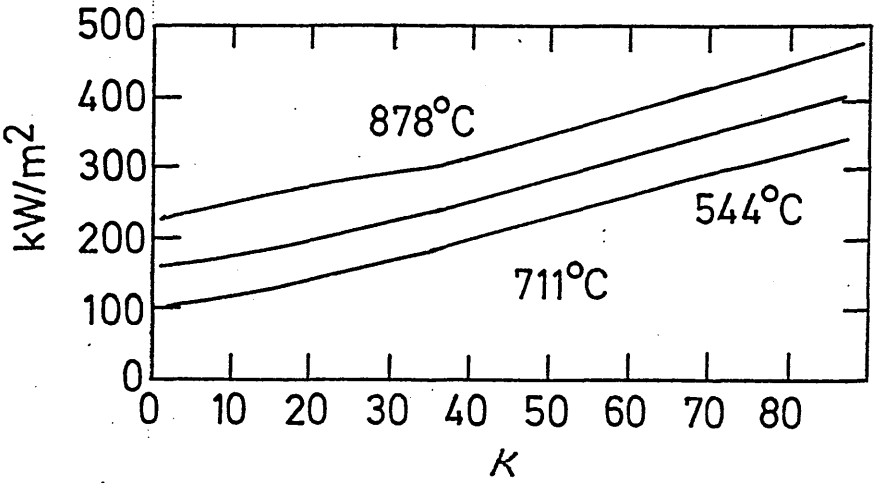
500
400
300
200
100
0
kW/m2
878°C
544°C
711°C
0 10 20 30 40 50 60 70 80
K

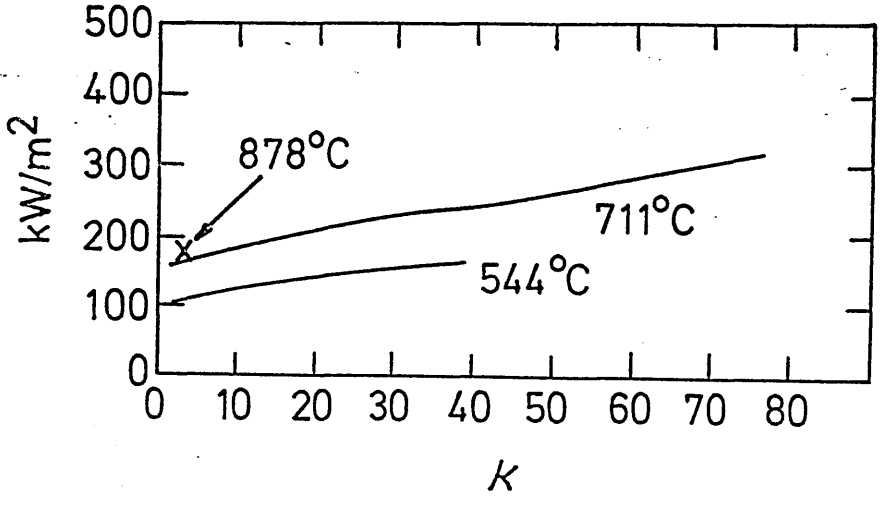
500
400
300
200
100
0
kW/m2
878°C
711°C
544°C
0 10 20 30 40 50 60 70 80
K

FIGURE 22: The film boiling model of Tachibana and Fukui[101].

t_w = wall temperature
t_s = saturation temperature
t_o = liquid temperature
U_v = vapour velocity
U_e = liquid velocity
δ_v = vapour layer thickness
δ_e = liquid velocity boundary layer thickness
δ_t = liquid thermal boundary layer thickness

FIGURE 23: The film boiling model of Cess and Sparrow[109].

V = vapour ; L = liquid

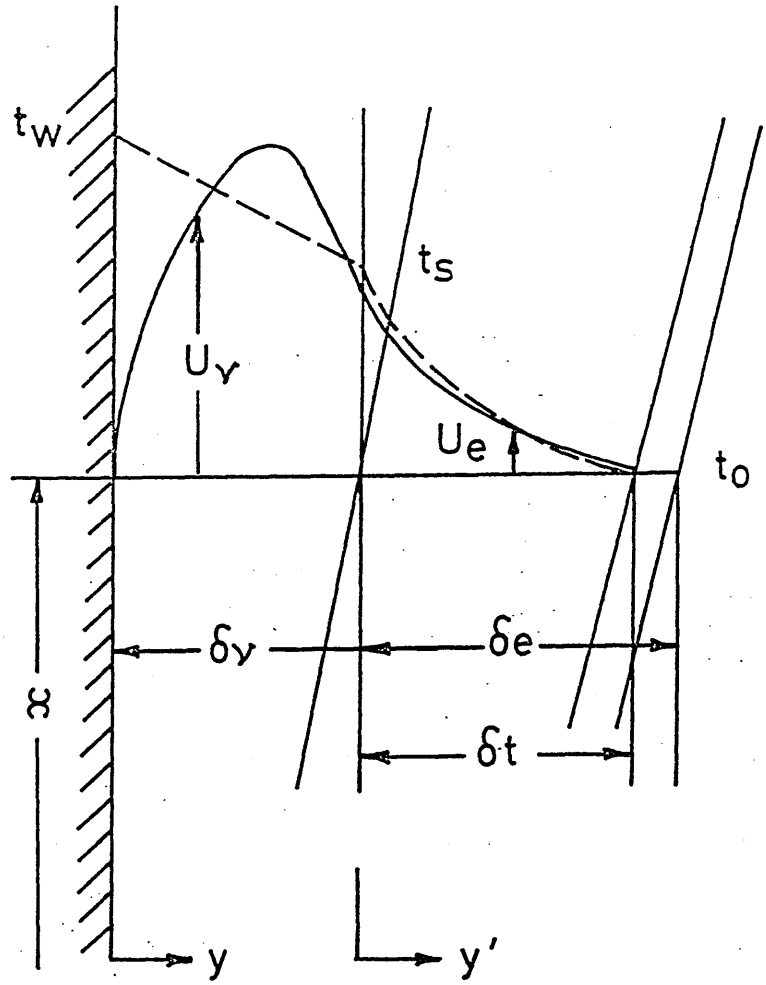
t_w
t_s
U_v
U_e
t_o
δ_v
δ_e
δ_t
x
y
y'

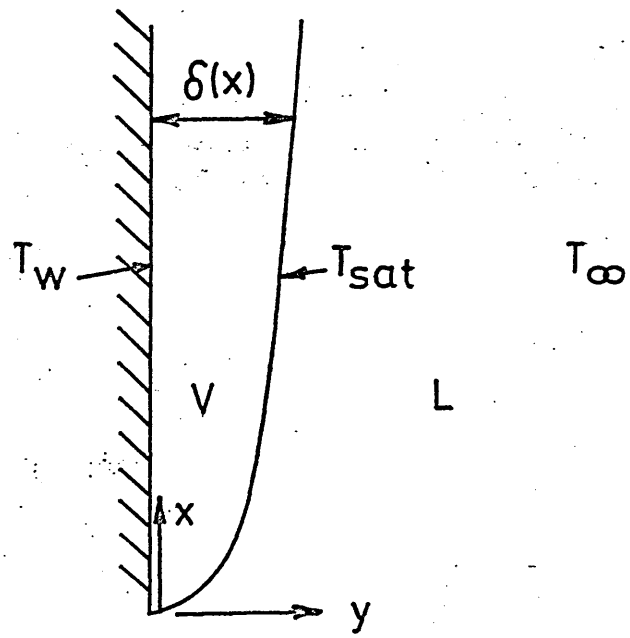
δ(x)
T_w
T_{sat}
T_∞
V
L
x
y

FIGURE 24: Surface heat transfer coefficients predicted by Nishikawa, Ito and Matsumoto[114].

$\Delta T_v = T_w - T_{sat}$

$\Delta T_L = T_{sat} - T_\infty$

FIGURE 25: An example of the transition boiling heat flux data obtained by Berenson[127], (n-pentane boiling on a copper surface).

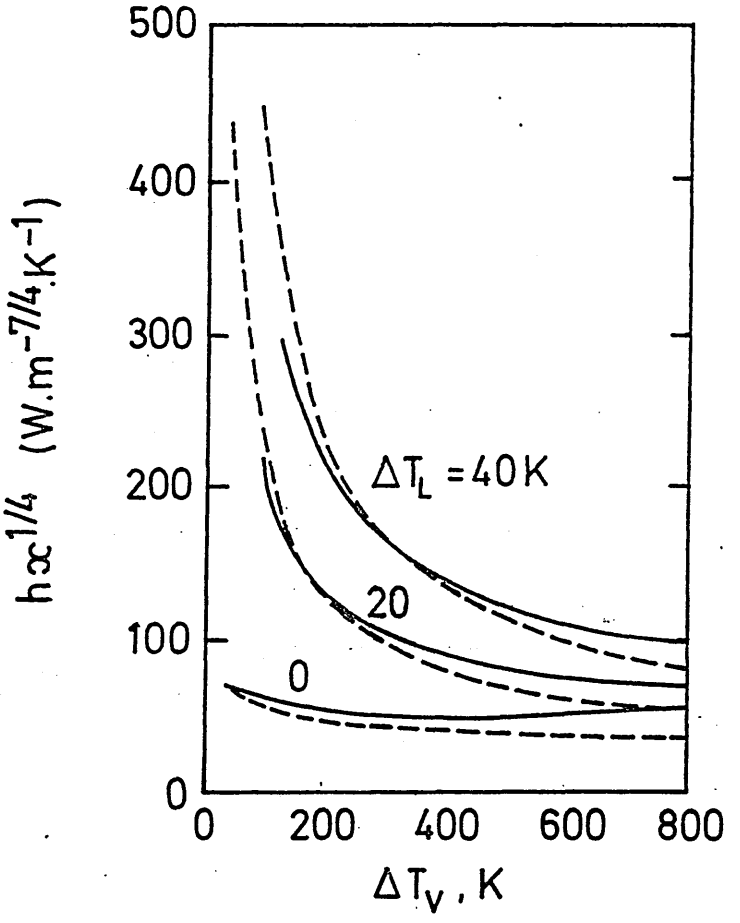
500
400
300
200
100
0
0
200
400
600
800
$h x^{1/4}$ (W.m$^{-7/4}$.K^{-1})
ΔT_L = 40 K
20
0
ΔT_V, K

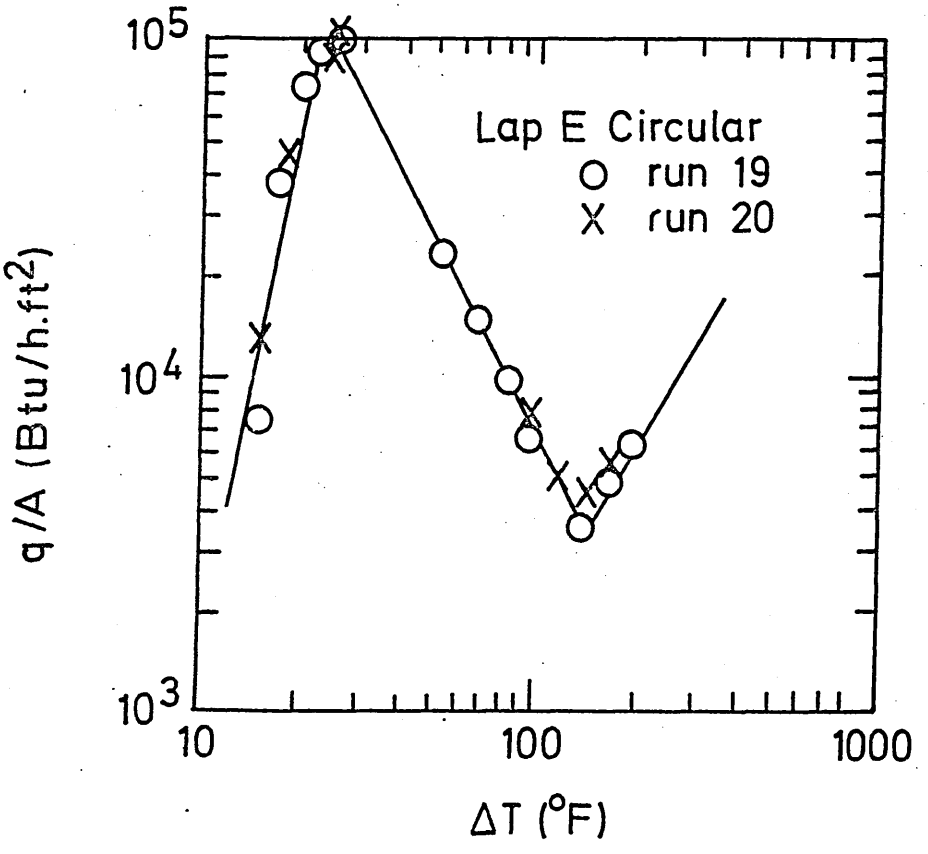
10^5
10^4
10^3
10
100
1000
q/A (Btu/h.ft^2)
Lap E Circular
O run 19
X run 20
ΔT (°F)

FIGURE 26: Typical vapour formations at the critical heat flux, (after Katto[130]).

d = diameter of hot surface

FIGURE 27: Advancing vapour/liquid interfaces and their effects on gas and liquid filled cavities, (after Cole[131]).

θ = liquid/vapour contact angle

ϕ = wedge angle of cavity

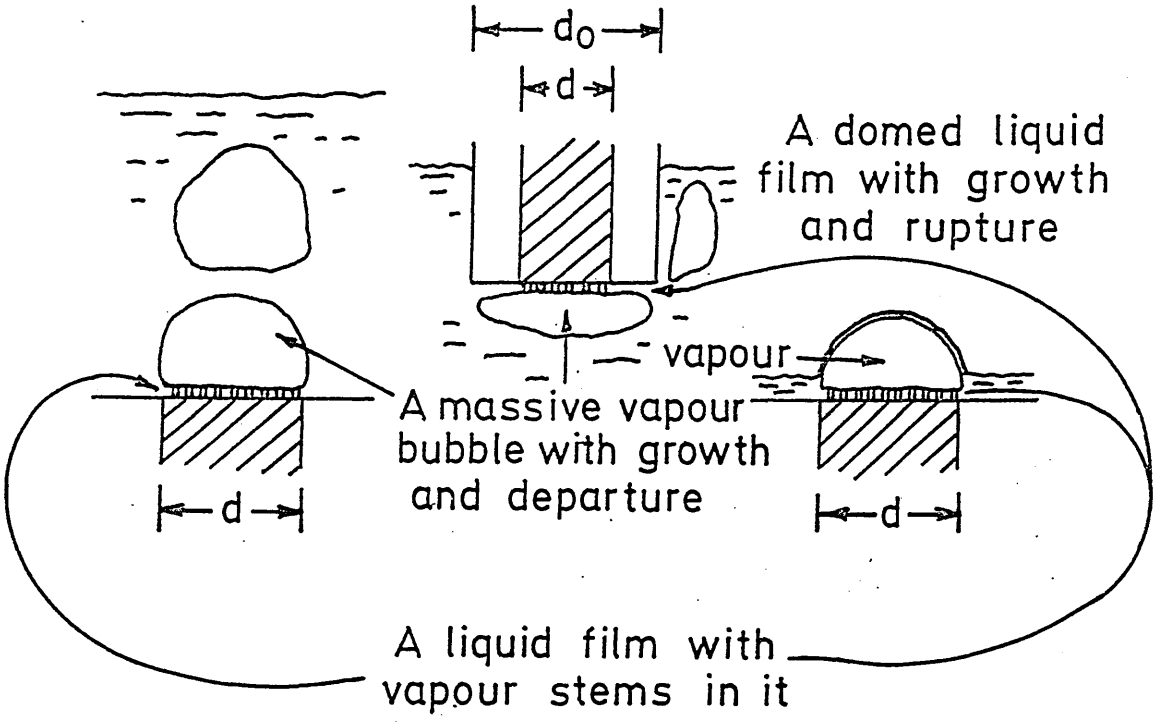
d_o
d
A domed liquid film with growth and rupture
vapour
A massive vapour bubble with growth and departure
d
d
A liquid film with vapour stems in it

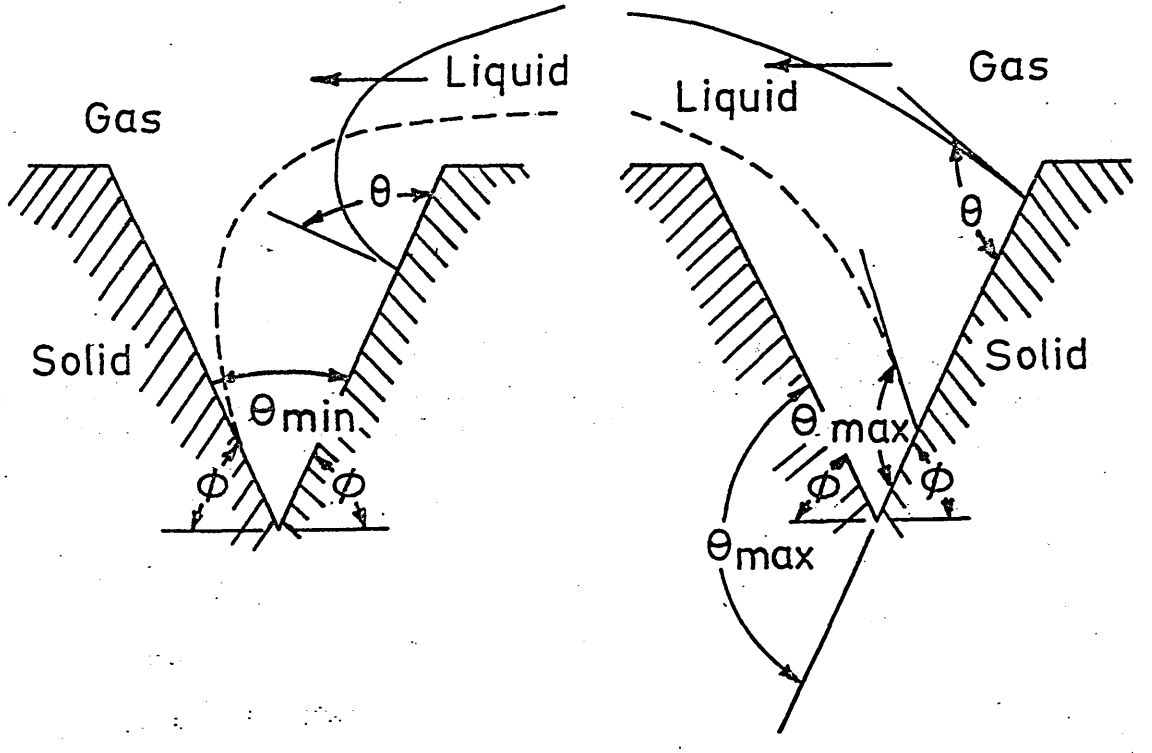
Liquid
Gas
θ
Solid
θmin
Φ
Φ
Liquid
Gas
θ
Solid
θmax
Φ
Φ
θmax

FIGURE 28: The construction of the stainless steel plate, (grade 316), used to measure the surface heat transfer coefficient during quenching.
Dimensions in millimetres.

FIGURE 29: The measurement points on the low alloy steel plate from which the residual strain was determined.

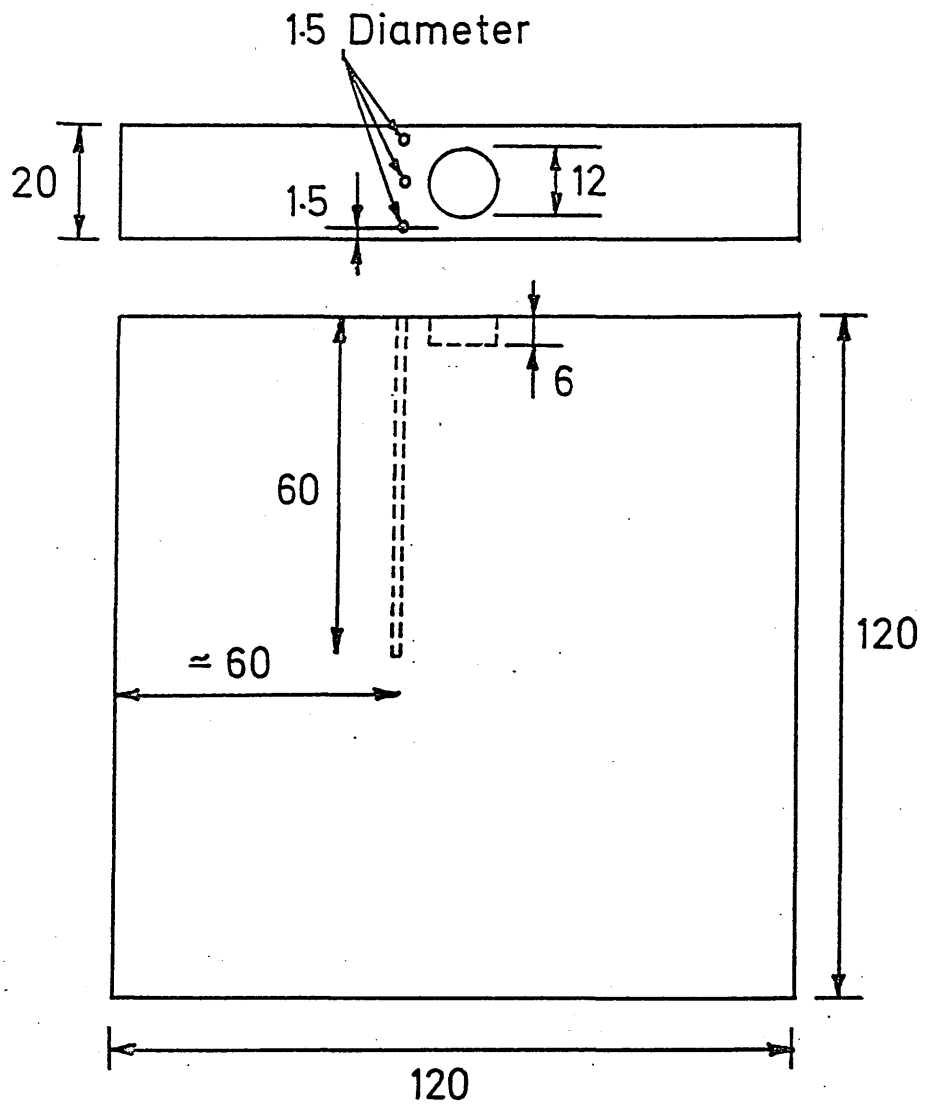
1·5 Diameter
20
1·5
12
6
60
120
≃ 60
120

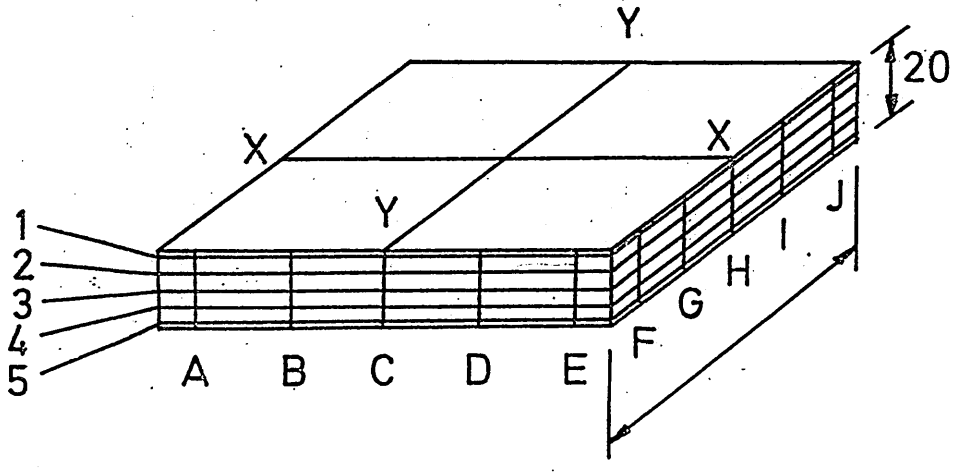
Y
20
X
X
Y
J
I
H
G
F
1
2
3
4
5
A
B
C
D
E

FIGURE 30: Arrangement of the quenched low alloy steel plate, (grade 835M30), and the cast iron supporting plate during the measurement of residual stress.

FIGURE 31: Apparatus used for the measurement of the surface tension of the polymer solutions.

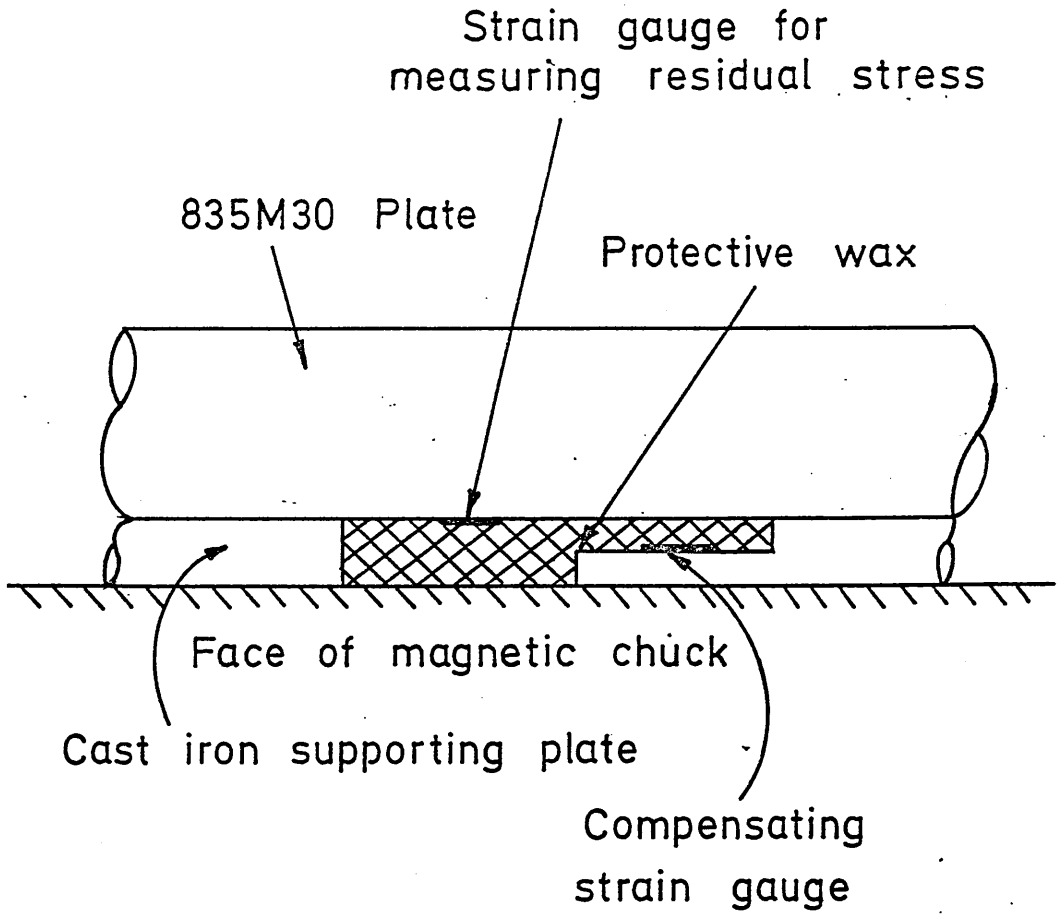
Strain gauge for
measuring residual stress
835M30 Plate
Protective wax
Face of magnetic chuck
Cast iron supporting plate
Compensating
strain gauge

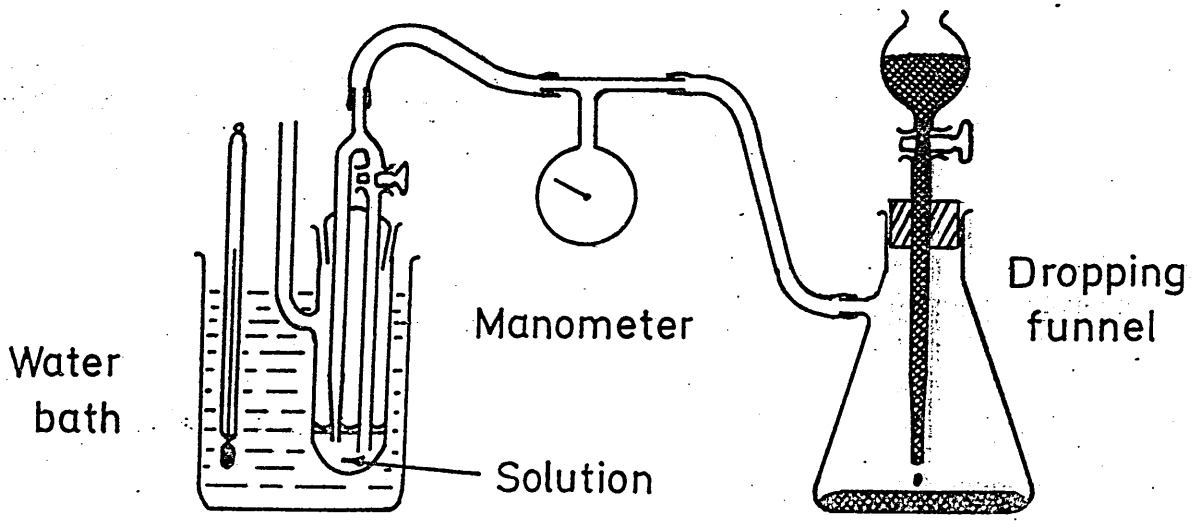
Water
bath
Manometer
Dropping
funnel
Solution

FIGURE 32: Flow diagram of the procedure for the calculation of the surface heat tranfer coefficient during quenching.

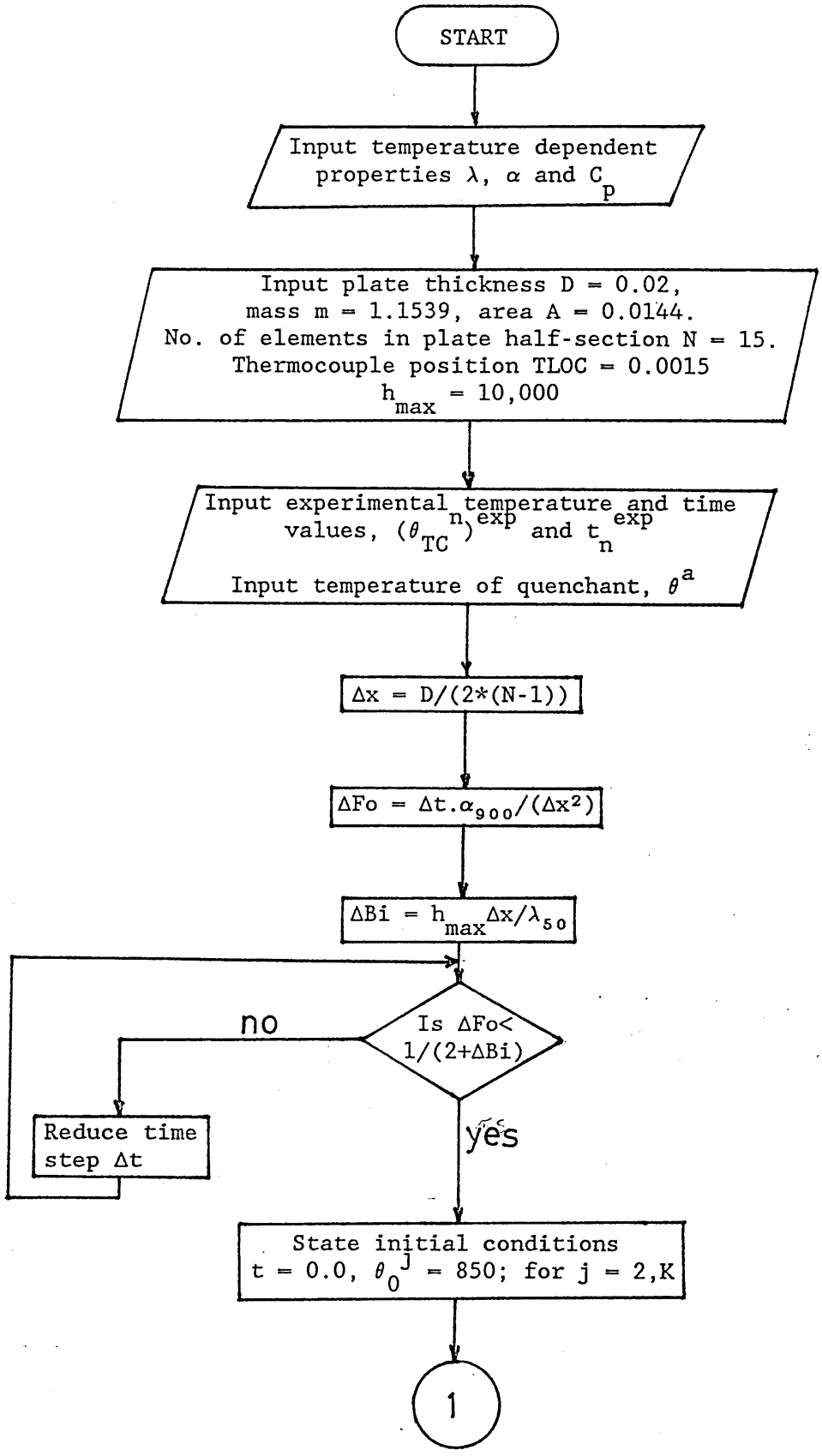
START
Input temperature dependent properties λ, α and C_p
Input plate thickness D = 0.02,
mass m = 1.1539, area A = 0.0144.
No. of elements in plate half-section N = 15.
Thermocouple position TLOC = 0.0015
h_{max} = 10,000
Input experimental temperature and time values, $(\theta_{TC}^{n})^{exp}$ and t_n^{exp}
Input temperature of quenchant, θ^a
Δx = D/(2*(N-1))
$\Delta Fo = \Delta t.\alpha_{900}/(\Delta x^2)$
$\Delta Bi = h_{max}\Delta x/\lambda_{50}$
Is ΔFo< 1/(2+ΔBi)
no
yes
Reduce time step Δt
State initial conditions
t = 0.0, θ_0^j = 850; for j = 2,K
1

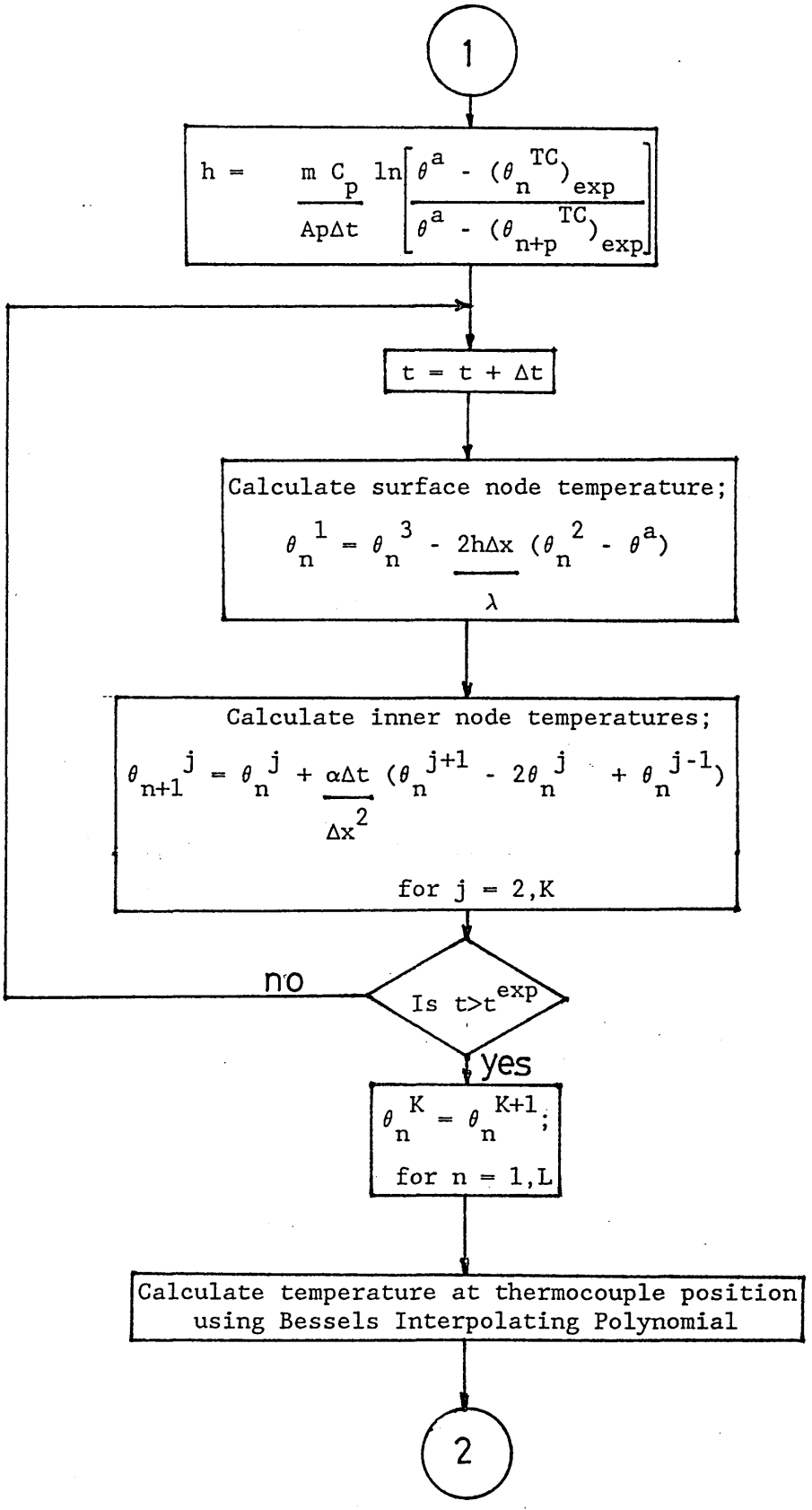
1
$h = \frac{m C_p}{Ap\Delta t} \ln\left[\frac{\theta^a - (\theta_n^{TC})_{exp}}{\theta^a - (\theta_{n+p}^{TC})_{exp}}\right]$
$t = t + \Delta t$
Calculate surface node temperature;
$\theta_n^1 = \theta_n^3 - \frac{2h\Delta x}{\lambda}(\theta_n^2 - \theta^a)$
Calculate inner node temperatures;
$\theta_{n+1}^j = \theta_n^j + \frac{\alpha\Delta t}{\Delta x^2}(\theta_n^{j+1} - 2\theta_n^j + \theta_n^{j-1})$
for j = 2,K
Is $t>t^{exp}$
no
yes
$\theta_n^K = \theta_n^{K+1}$;
for n = 1,L
Calculate temperature at thermocouple position using Bessels Interpolating Polynomial
2

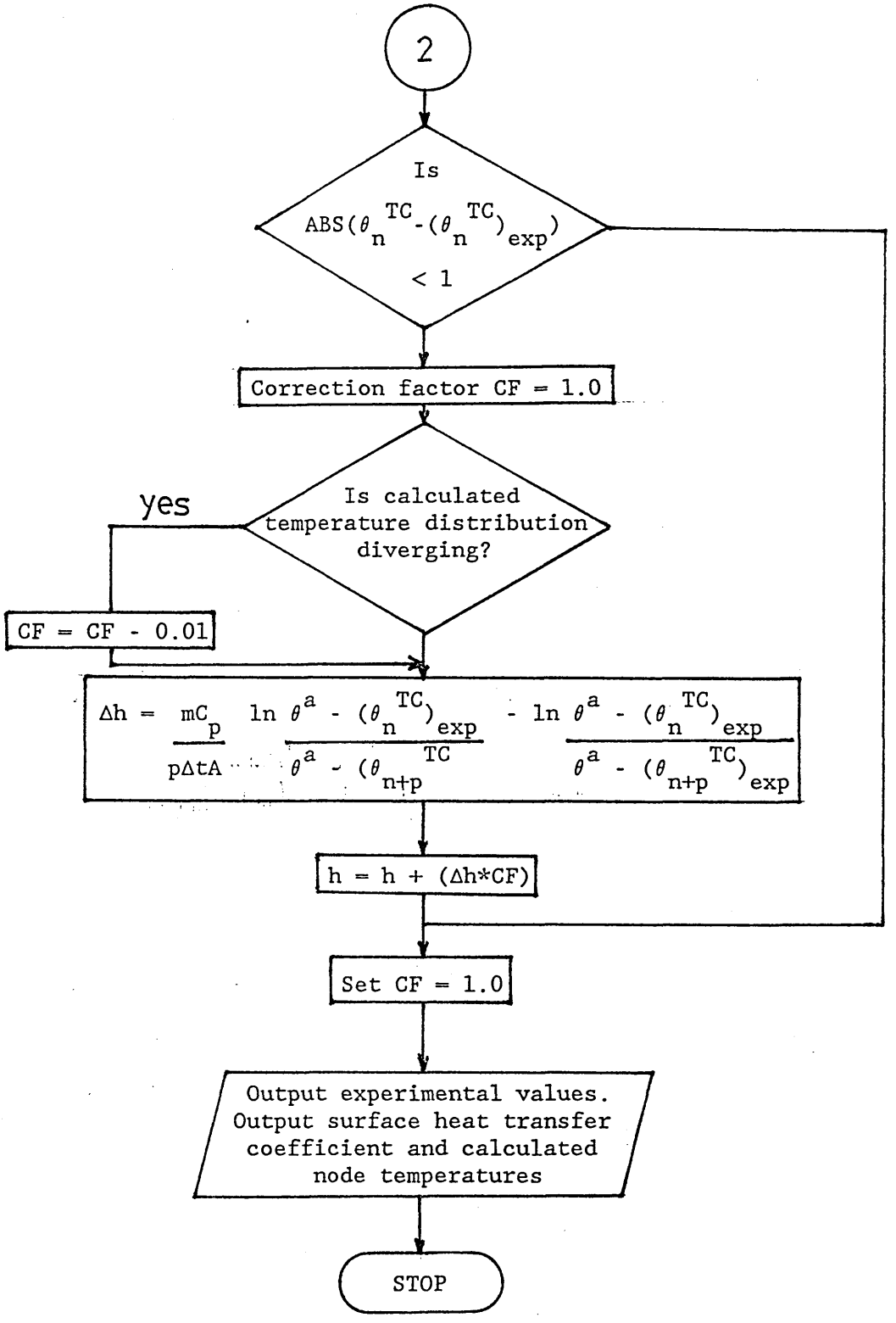
2
Is
ABS(θ_n^{TC}-(θ_n^{TC})$_{exp}$)
< 1
Correction factor CF = 1.0
yes
Is calculated temperature distribution diverging?
CF = CF - 0.01
$\Delta h = \frac{mC_p}{p\Delta tA} \ln \frac{\theta^a - (\theta_n^{TC})_{exp}}{\theta^a - (\theta_{n+p}^{TC})} - \ln \frac{\theta^a - (\theta_n^{TC})_{exp}}{\theta^a - (\theta_{n+p}^{TC})_{exp}}$
h = h + (Δh*CF)
Set CF = 1.0
Output experimental values. Output surface heat transfer coefficient and calculated node temperatures
STOP

FIGURE 33: The plane stress conditions assumed in the case of the visco-elasticplastic model for the calculation of thermal stress and strain during quenching of an infinite plate.

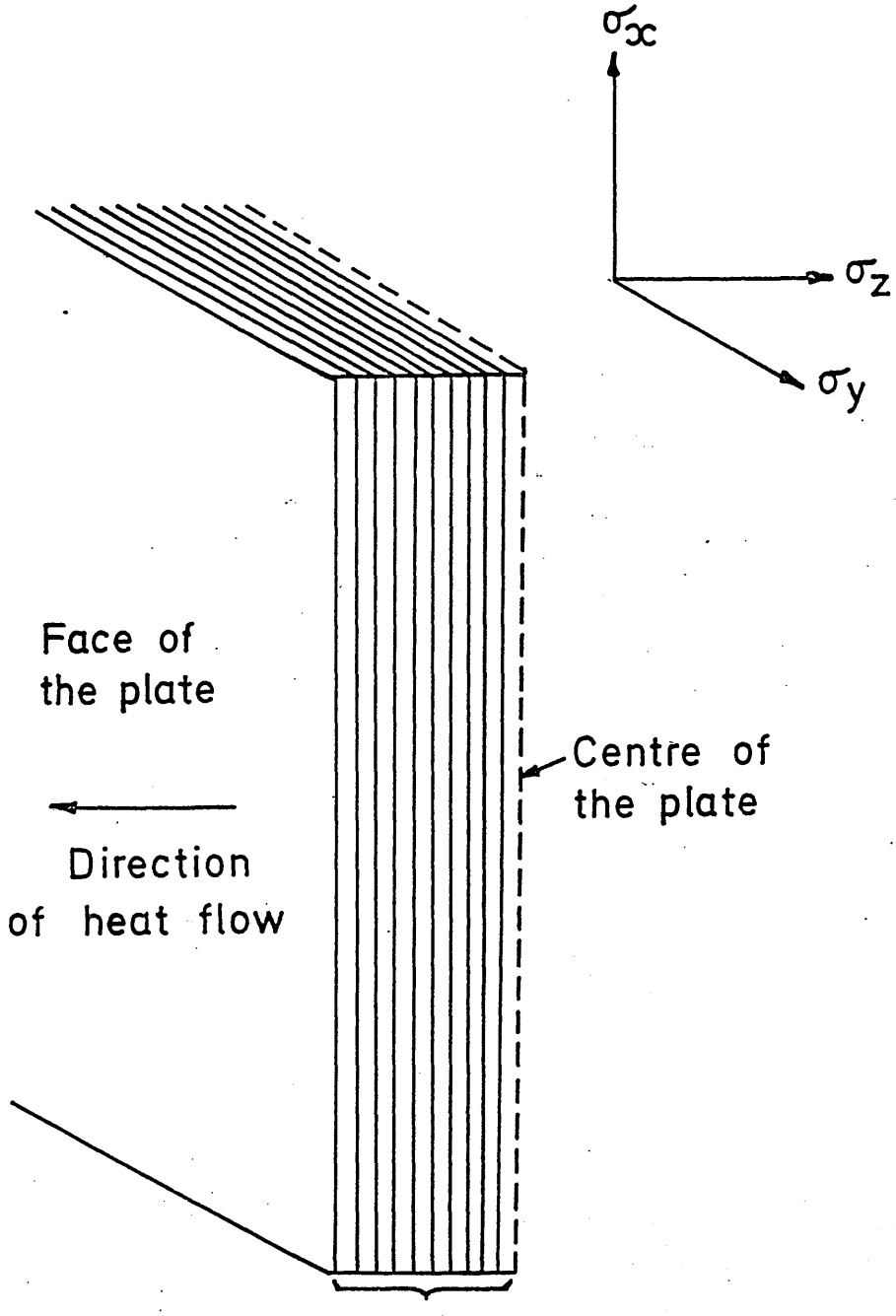

$$\sigma = \sigma_x = \sigma_y$$

$$\sigma_{xy} = \sigma_{yz} = \sigma_{zx} = 0$$

$$\sigma_z = 0$$

FIGURE 34: Flow diagram of the procedure for the calculation of thermal stress and strain generated during quenching.

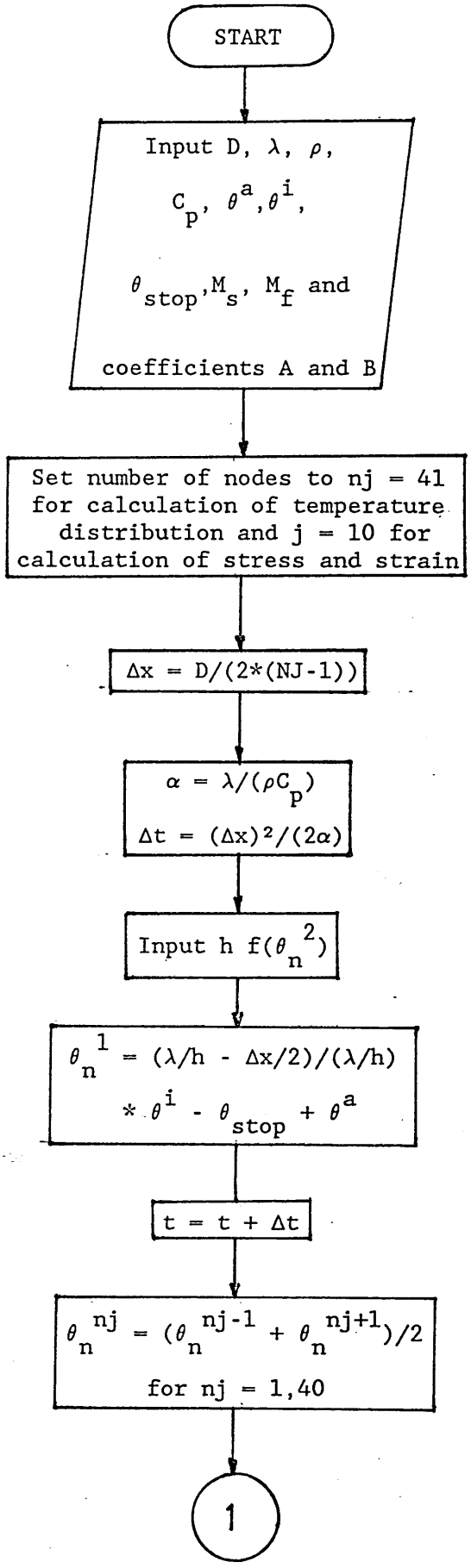
START
Input D, λ, ρ,
C_p, θ^a, θ^i,
θ_{stop}, M_s, M_f and
coefficients A and B
Set number of nodes to nj = 41 for calculation of temperature distribution and j = 10 for calculation of stress and strain
Δx = D/(2*(NJ-1))
$\alpha = \lambda/(\rho C_p)$
$\Delta t = (\Delta x)^2/(2\alpha)$
Input h $f(\theta_n^2)$
$\theta_n^1 = (\lambda/h - \Delta x/2)/(\lambda/h) * \theta^i - \theta_{stop} + \theta^a$
t = t + Δt
$\theta_n^{nj} = (\theta_n^{nj-1} + \theta_n^{nj+1})/2$
for nj = 1,40
1

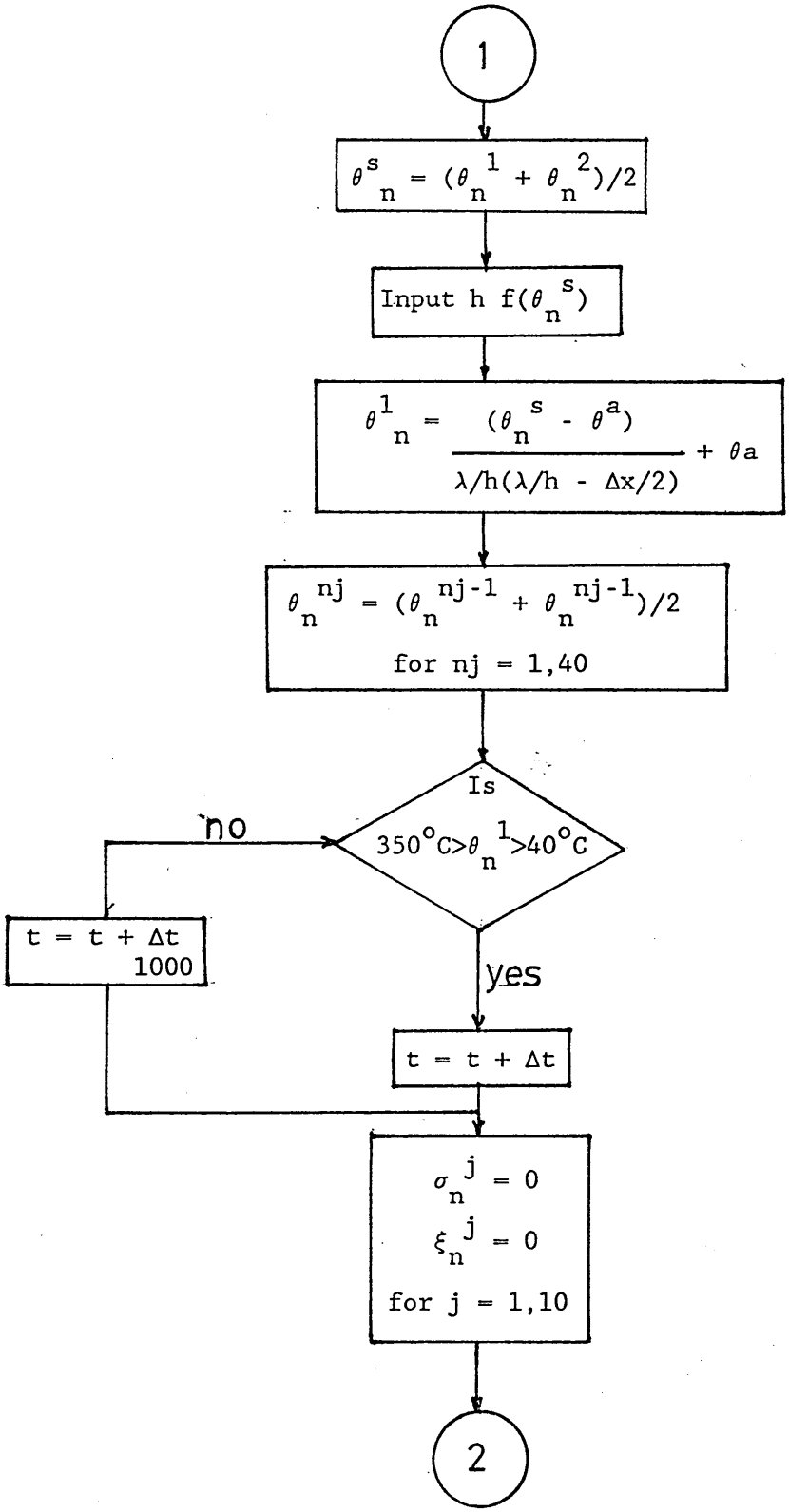
1
$\theta^s_n = (\theta_n^1 + \theta_n^2)/2$
Input h $f(\theta_n^s)$
$\theta^1_n = \frac{(\theta_n^s - \theta^a)}{\lambda/h(\lambda/h - \Delta x/2)} + \theta a$
$\theta_n^{nj} = (\theta_n^{nj-1} + \theta_n^{nj-1})/2$
for nj = 1,40
Is
$350^oC > \theta_n^1 > 40^oC$
no
yes
t = t + Δt
1000
t = t + Δt
$\sigma_n^j = 0$
$\xi_n^j = 0$
for j = 1,10
2

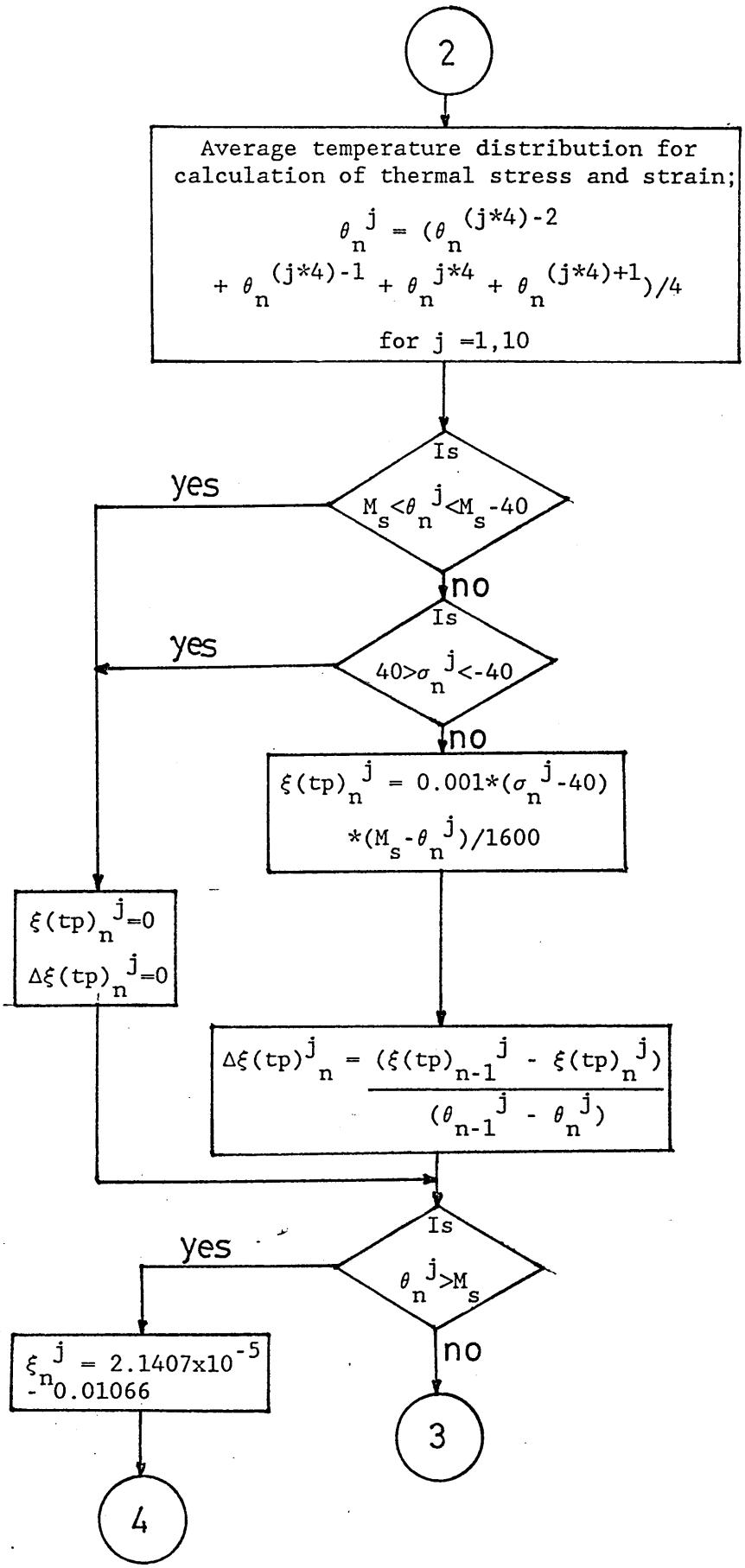
2
Average temperature distribution for calculation of thermal stress and strain;
$\theta_n^j = (\theta_n^{(j*4)-2} + \theta_n^{(j*4)-1} + \theta_n^{j*4} + \theta_n^{(j*4)+1})/4$
for j =1,10
Is
$M_s<\theta_n^j<M_s-40$
yes
no
Is
$40>\sigma_n^j<-40$
yes
no
$\xi(tp)_n^j = 0.001*(\sigma_n^j-40)*(M_s-\theta_n^j)/1600$
$\xi(tp)_n^j=0$
$\Delta\xi(tp)_n^j=0$
$\Delta\xi(tp)^j_n = \frac{(\xi(tp)_{n-1}^j - \xi(tp)_n^j)}{(\theta_{n-1}^j - \theta_n^j)}$
Is
$\theta_n^j>M_s$
yes
no
$\xi_n^j = 2.1407x10^{-5}$
-0.01066
3
4

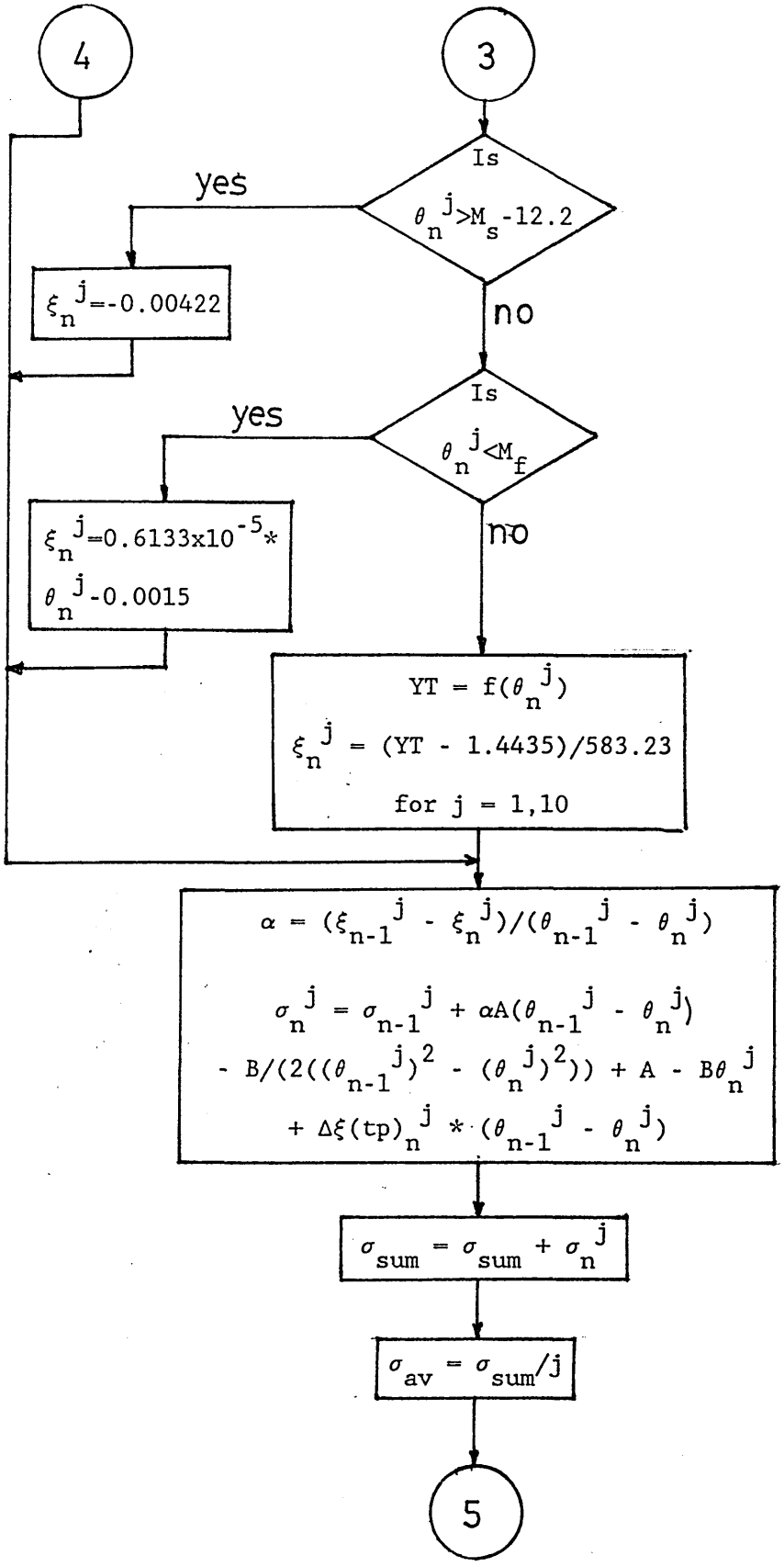
4
3
Is
$\theta_n^j > M_s - 12.2$
yes
no
$\xi_n^j = -0.00422$
Is
$\theta_n^j < M_f$
yes
no
$\xi_n^j = 0.6133 \times 10^{-5} * \theta_n^j - 0.0015$
$YT = f(\theta_n^j)$
$\xi_n^j = (YT - 1.4435)/583.23$
for j = 1,10
$\alpha = (\xi_{n-1}^j - \xi_n^j)/(\theta_{n-1}^j - \theta_n^j)$
$\sigma_n^j = \sigma_{n-1}^j + \alpha A(\theta_{n-1}^j - \theta_n^j)$
$- B/(2((\theta_{n-1}^j)^2 - (\theta_n^j)^2)) + A - B\theta_n^j$
$+ \Delta\xi(tp)_n^j * (\theta_{n-1}^j - \theta_n^j)$
$\sigma_{sum} = \sigma_{sum} + \sigma_n^j$
$\sigma_{av} = \sigma_{sum}/j$
5

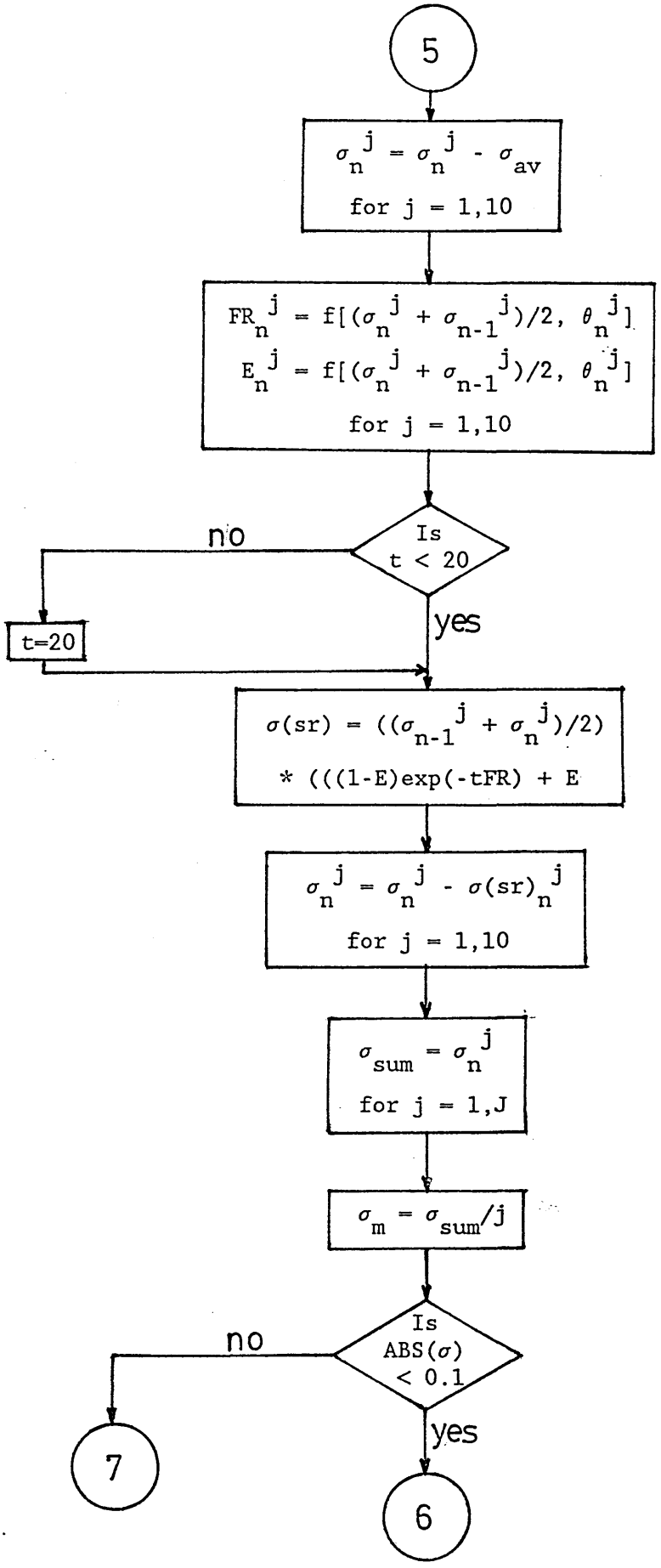
5
$\sigma_n^j = \sigma_n^j - \sigma_{av}$
for j = 1,10
$FR_n^j = f[(\sigma_n^j + \sigma_{n-1}^j)/2, \theta_n^j]$
$E_n^j = f[(\sigma_n^j + \sigma_{n-1}^j)/2, \theta_n^j]$
for j = 1,10
Is t < 20
no
yes
t=20
$\sigma(sr) = ((\sigma_{n-1}^j + \sigma_n^j)/2)$
* (((1-E)exp(-tFR) + E
$\sigma_n^j = \sigma_n^j - \sigma(sr)_n^j$
for j = 1,10
$\sigma_{sum} = \sigma_n^j$
for j = 1,J
$\sigma_m = \sigma_{sum}/j$
Is ABS(σ) < 0.1
no
yes
7
6

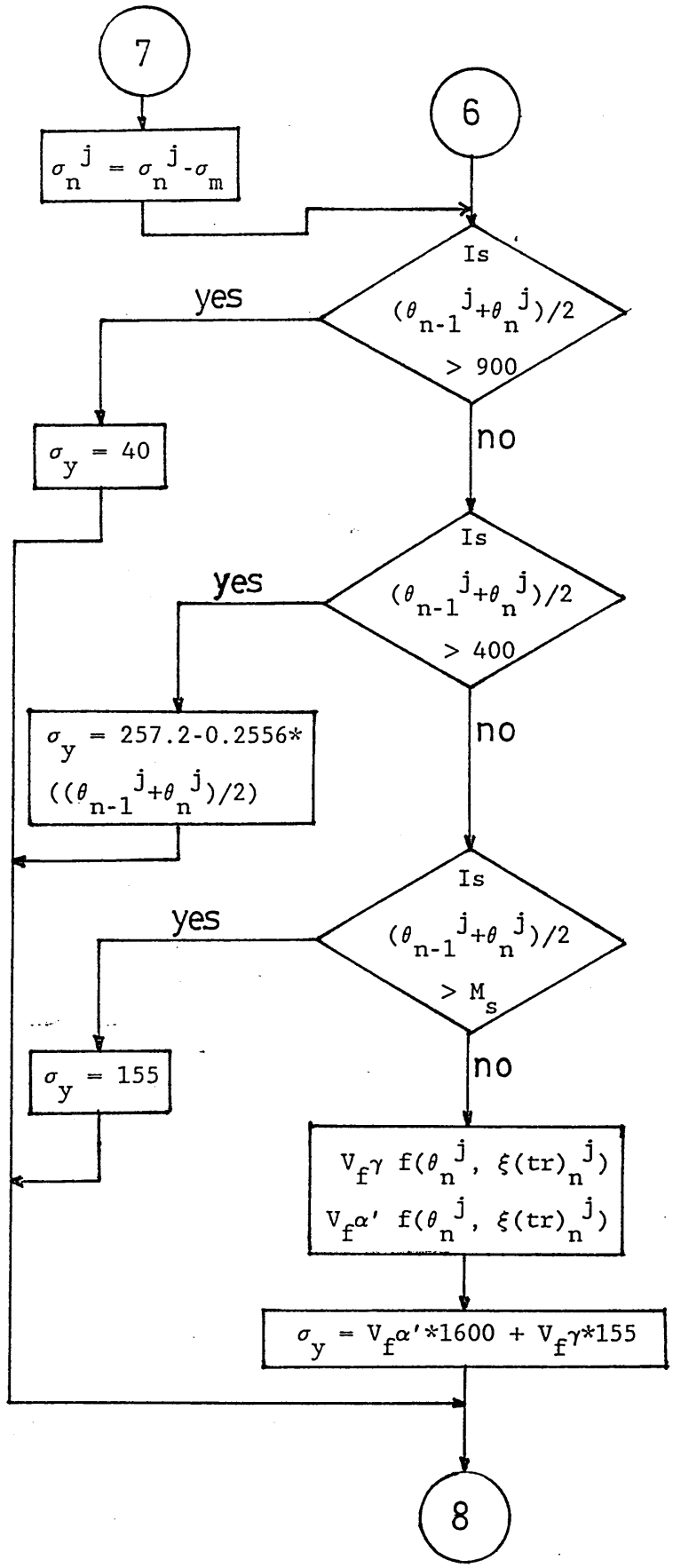
7
6
$\sigma_n^j = \sigma_n^j - \sigma_m$
Is
$(\theta_{n-1}^j + \theta_n^j)/2$
> 900
yes
no
σ_y = 40
Is
$(\theta_{n-1}^j + \theta_n^j)/2$
> 400
yes
no
σ_y = 257.2-0.2556*
$((\theta_{n-1}^j + \theta_n^j)/2)$
Is
$(\theta_{n-1}^j + \theta_n^j)/2$
> M_s
yes
no
σ_y = 155
$V_f\gamma\ f(\theta_n^j, \xi(tr)_n^j)$
$V_f\alpha'\ f(\theta_n^j, \xi(tr)_n^j)$
$\sigma_y = V_f\alpha' * 1600 + V_f\gamma * 155$
8

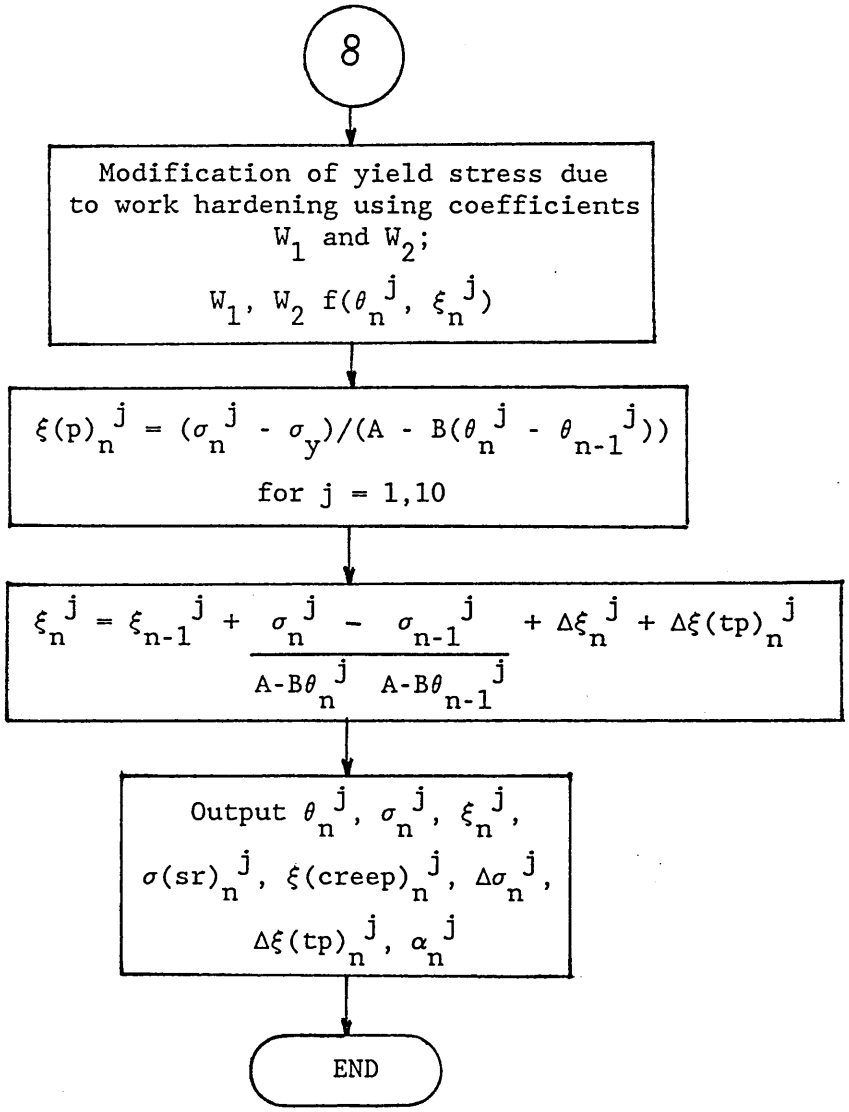
8
Modification of yield stress due to work hardening using coefficients W_1 and W_2;
W_1, W_2 $f(\theta_n^j, \xi_n^j)$
$\xi(p)_n^j = (\sigma_n^j - \sigma_y)/(A - B(\theta_n^j - \theta_{n-1}^j))$
for j = 1,10
$\xi_n^j = \xi_{n-1}^j + \frac{\sigma_n^j - \sigma_{n-1}^j}{A-B\theta_n^j \quad A-B\theta_{n-1}^j} + \Delta\xi_n^j + \Delta\xi(tp)_n^j$
Output θ_n^j, σ_n^j, ξ_n^j, $\sigma(sr)_n^j$, $\xi(creep)_n^j$, $\Delta\sigma_n^j$, $\Delta\xi(tp)_n^j$, α_n^j
END

FIGURE 35: Flow diagram of the procedure for the calculation of the surface heat transfer coefficient during film boiling using the model of Cess and Sparrow[109].

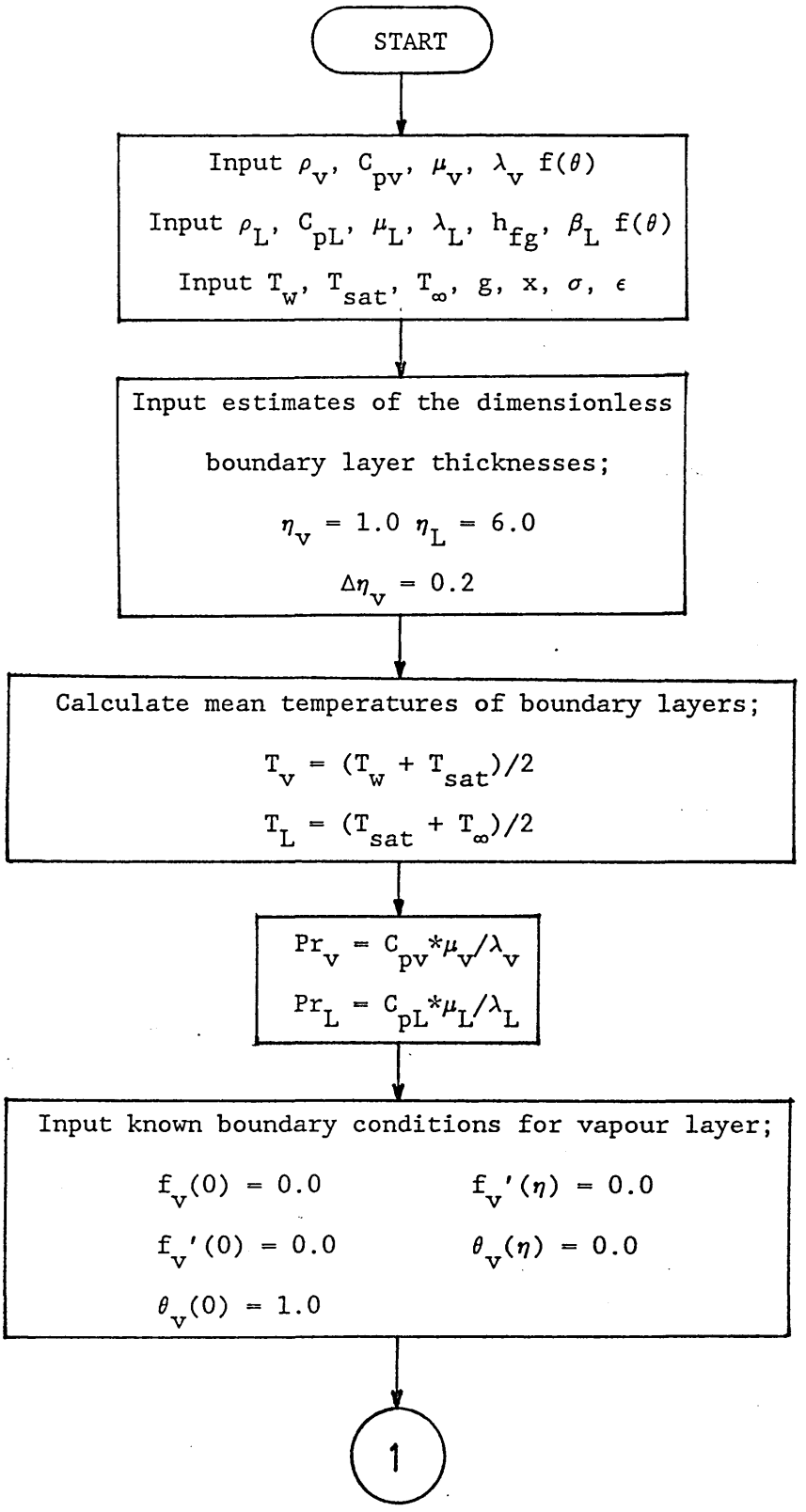
START
Input ρ_v, C_{pv}, μ_v, λ_v $f(\theta)$
Input ρ_L, C_{pL}, μ_L, λ_L, h_{fg}, β_L $f(\theta)$
Input T_w, T_{sat}, T_∞, g, x, σ, ϵ
Input estimates of the dimensionless boundary layer thicknesses;
$\eta_v = 1.0$ $\eta_L = 6.0$
$\Delta\eta_v = 0.2$
Calculate mean temperatures of boundary layers;
$T_v = (T_w + T_{sat})/2$
$T_L = (T_{sat} + T_\infty)/2$
$Pr_v = C_{pv}*\mu_v/\lambda_v$
$Pr_L = C_{pL}*\mu_L/\lambda_L$
Input known boundary conditions for vapour layer;
$f_v(0) = 0.0$
$f_v'(\eta) = 0.0$
$f_v'(0) = 0.0$
$\theta_v(\eta) = 0.0$
$\theta_v(0) = 1.0$
1

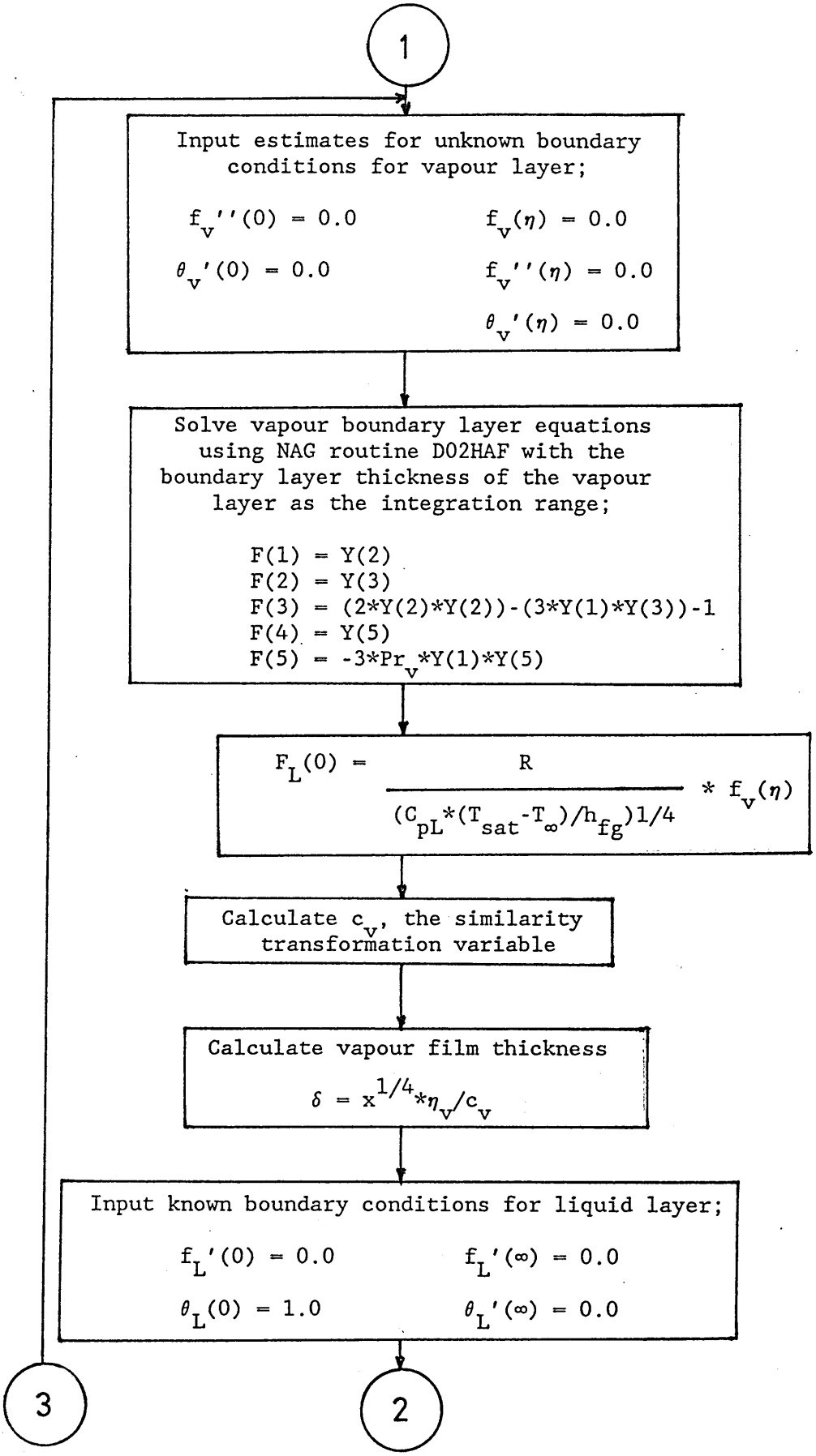
1
Input estimates for unknown boundary conditions for vapour layer;
$f_v''(0) = 0.0$
$f_v(\eta) = 0.0$
$\theta_v'(0) = 0.0$
$f_v''(\eta) = 0.0$
$\theta_v'(\eta) = 0.0$
Solve vapour boundary layer equations using NAG routine D02HAF with the boundary layer thickness of the vapour layer as the integration range;
F(1) = Y(2)
F(2) = Y(3)
F(3) = (2*Y(2)*Y(2))-(3*Y(1)*Y(3))-1
F(4) = Y(5)
F(5) = -3*Pr_v*Y(1)*Y(5)
$F_L(0) = \frac{R}{(C_{pL}*(T_{sat}-T_\infty)/h_{fg})1/4} * f_v(\eta)$
Calculate c_v, the similarity transformation variable
Calculate vapour film thickness
$\delta = x^{1/4}*\eta_v/c_v$
Input known boundary conditions for liquid layer;
$f_L'(0) = 0.0$
$f_L'(\infty) = 0.0$
$\theta_L(0) = 1.0$
$\theta_L'(\infty) = 0.0$
3
2

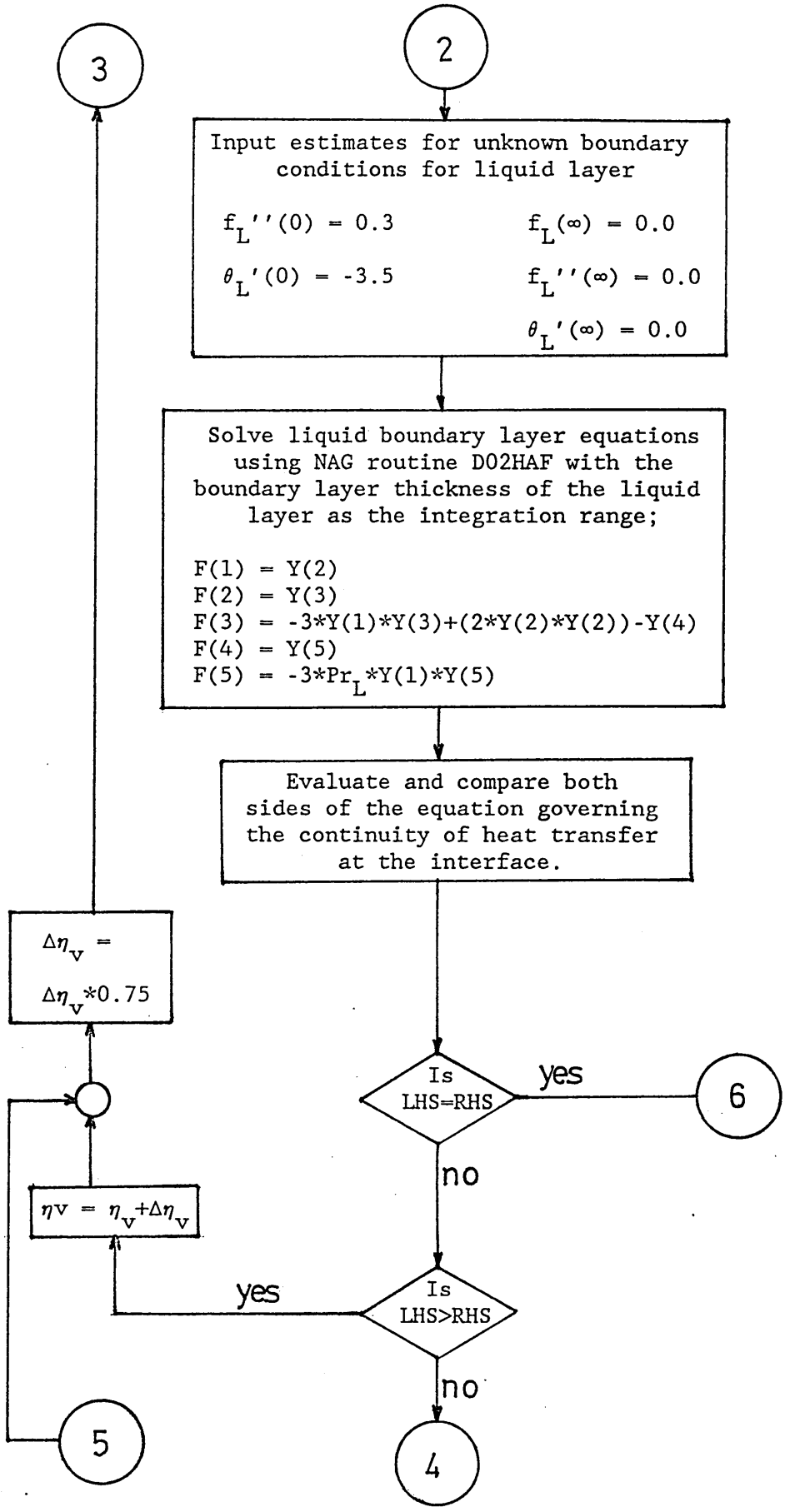
3
2
Input estimates for unknown boundary conditions for liquid layer
$f_L''(0) = 0.3$
$f_L(\infty) = 0.0$
$\theta_L'(0) = -3.5$
$f_L''(\infty) = 0.0$
$\theta_L'(\infty) = 0.0$
Solve liquid boundary layer equations using NAG routine D02HAF with the boundary layer thickness of the liquid layer as the integration range;
F(1) = Y(2)
F(2) = Y(3)
F(3) = -3*Y(1)*Y(3)+(2*Y(2)*Y(2))-Y(4)
F(4) = Y(5)
F(5) = -3*Pr_L*Y(1)*Y(5)
Evaluate and compare both sides of the equation governing the continuity of heat transfer at the interface.
$\Delta\eta_v$ = $\Delta\eta_v$*0.75
Is LHS=RHS
yes
6
no
$\eta v = \eta_v + \Delta\eta_v$
yes
Is LHS>RHS
no
5
4

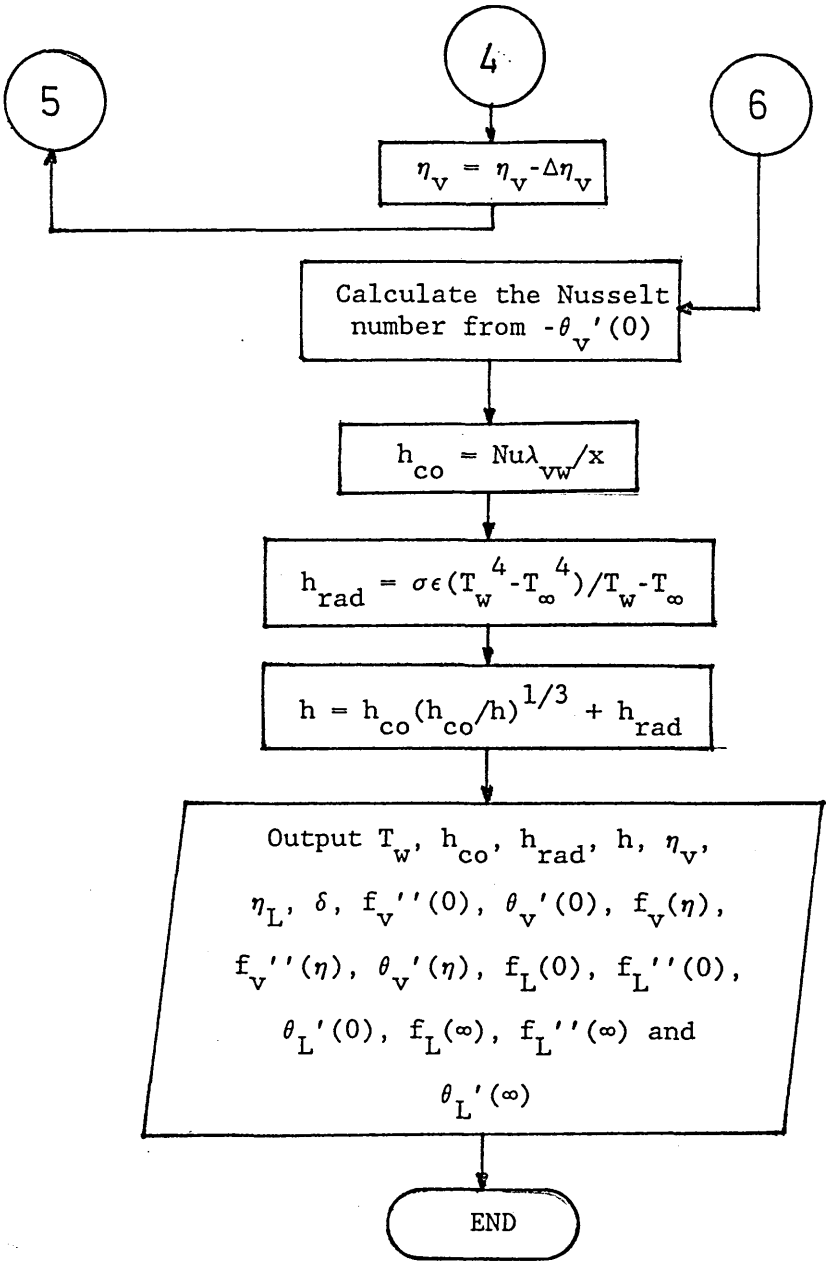
4
5
6
$\eta_v = \eta_v - \Delta\eta_v$
Calculate the Nusselt number from $-\theta_v'(0)$
$h_{co} = Nu\lambda_{vw}/x$
$h_{rad} = \sigma\epsilon(T_w^4 - T_\infty^4)/T_w - T_\infty$
$h = h_{co}(h_{co}/h)^{1/3} + h_{rad}$
Output T_w, h_{co}, h_{rad}, h, η_v, η_L, δ, $f_v''(0)$, $\theta_v'(0)$, $f_v(\eta)$, $f_v''(\eta)$, $\theta_v'(\eta)$, $f_L(0)$, $f_L''(0)$, $\theta_L'(0)$, $f_L(\infty)$, $f_L''(\infty)$ and $\theta_L'(\infty)$
END

FIGURE 36: Flow diagram of the procedure for the calculation of the surface heat transfer coefficient during film boiling using the model of Nishikawa and Ito[112].

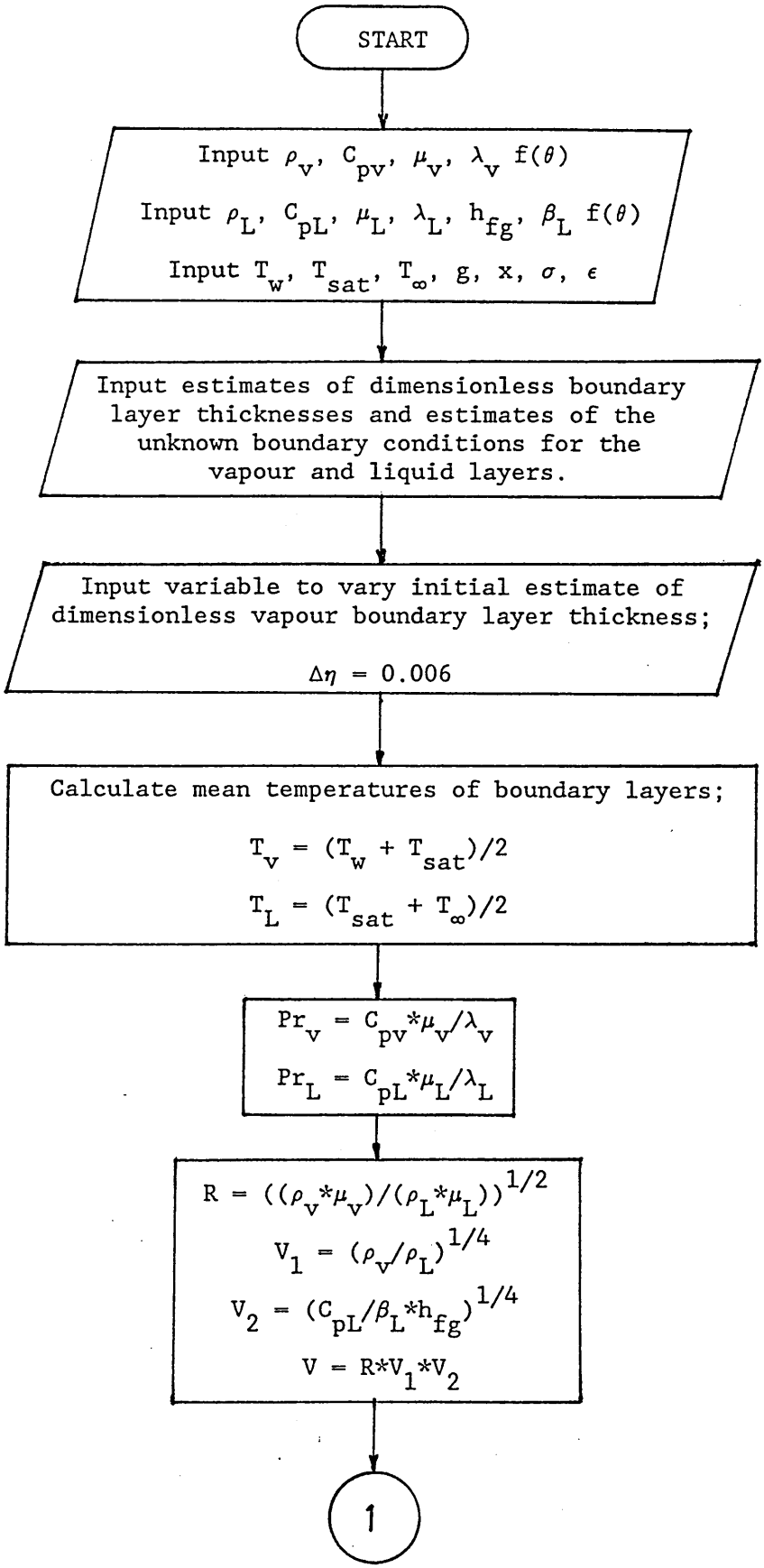
START
Input ρ_v, C_{pv}, μ_v, λ_v $f(\theta)$
Input ρ_L, C_{pL}, μ_L, λ_L, h_{fg}, β_L $f(\theta)$
Input T_w, T_{sat}, T_∞, g, x, σ, ϵ
Input estimates of dimensionless boundary layer thicknesses and estimates of the unknown boundary conditions for the vapour and liquid layers.
Input variable to vary initial estimate of dimensionless vapour boundary layer thickness;
$\Delta\eta = 0.006$
Calculate mean temperatures of boundary layers;
$T_v = (T_w + T_{sat})/2$
$T_L = (T_{sat} + T_\infty)/2$
$Pr_v = C_{pv}*\mu_v/\lambda_v$
$Pr_L = C_{pL}*\mu_L/\lambda_L$
$R = ((\rho_v*\mu_v)/(\rho_L*\mu_L))^{1/2}$
$V_1 = (\rho_v/\rho_L)^{1/4}$
$V_2 = (C_{pL}/\beta_L*h_{fg})^{1/4}$
$V = R*V_1*V_2$
1

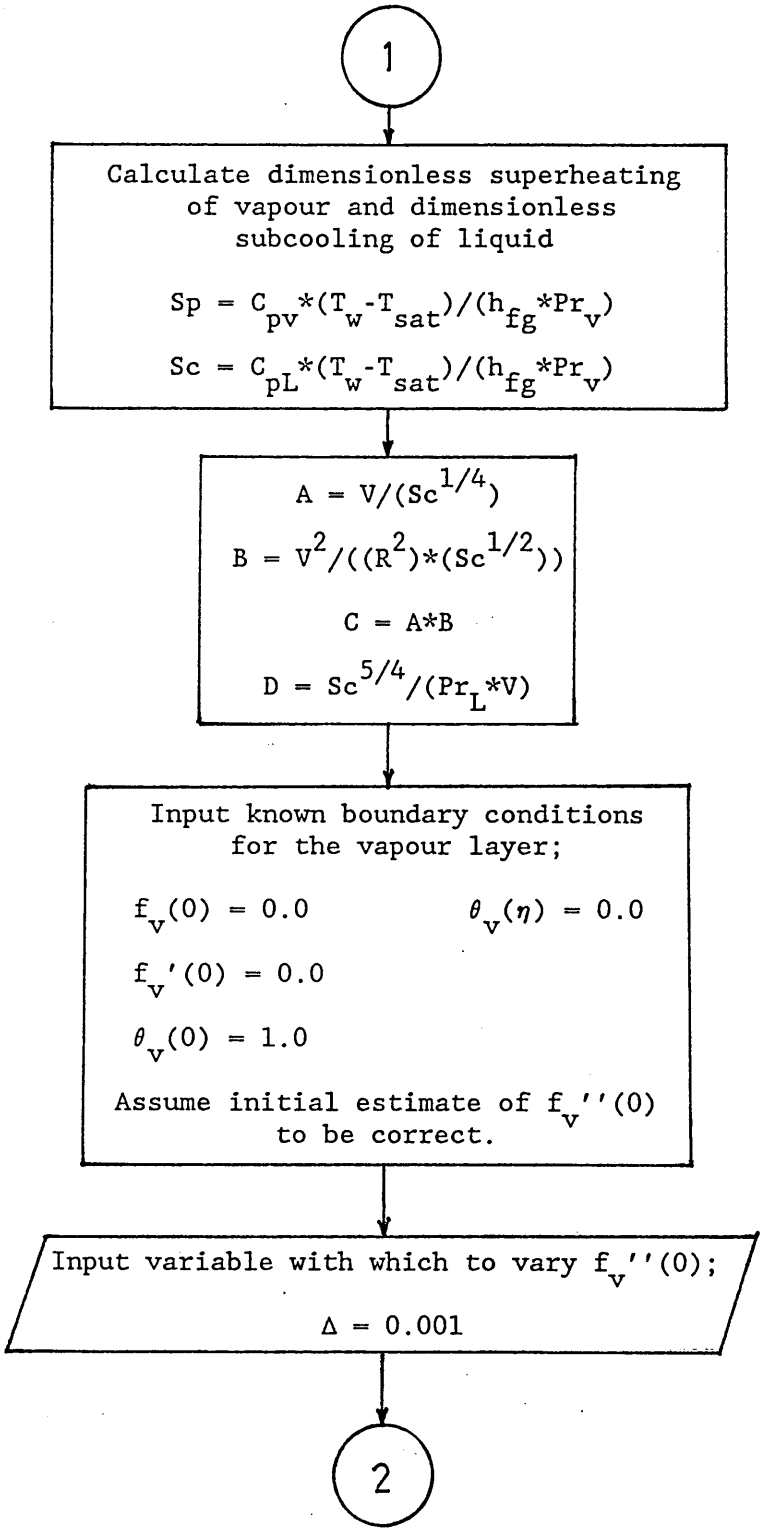
1
Calculate dimensionless superheating of vapour and dimensionless subcooling of liquid
Sp = C_pv*(T_w-T_sat)/(h_fg*Pr_v)
Sc = C_pL*(T_w-T_sat)/(h_fg*Pr_v)
A = V/(Sc^1/4)
B = V^2/((R^2)*(Sc^1/2))
C = A*B
D = Sc^5/4/(Pr_L*V)
Input known boundary conditions for the vapour layer;
f_v(0) = 0.0
θ_v(η) = 0.0
f_v'(0) = 0.0
θ_v(0) = 1.0
Assume initial estimate of f_v''(0) to be correct.
Input variable with which to vary f_v''(0);
Δ = 0.001
2

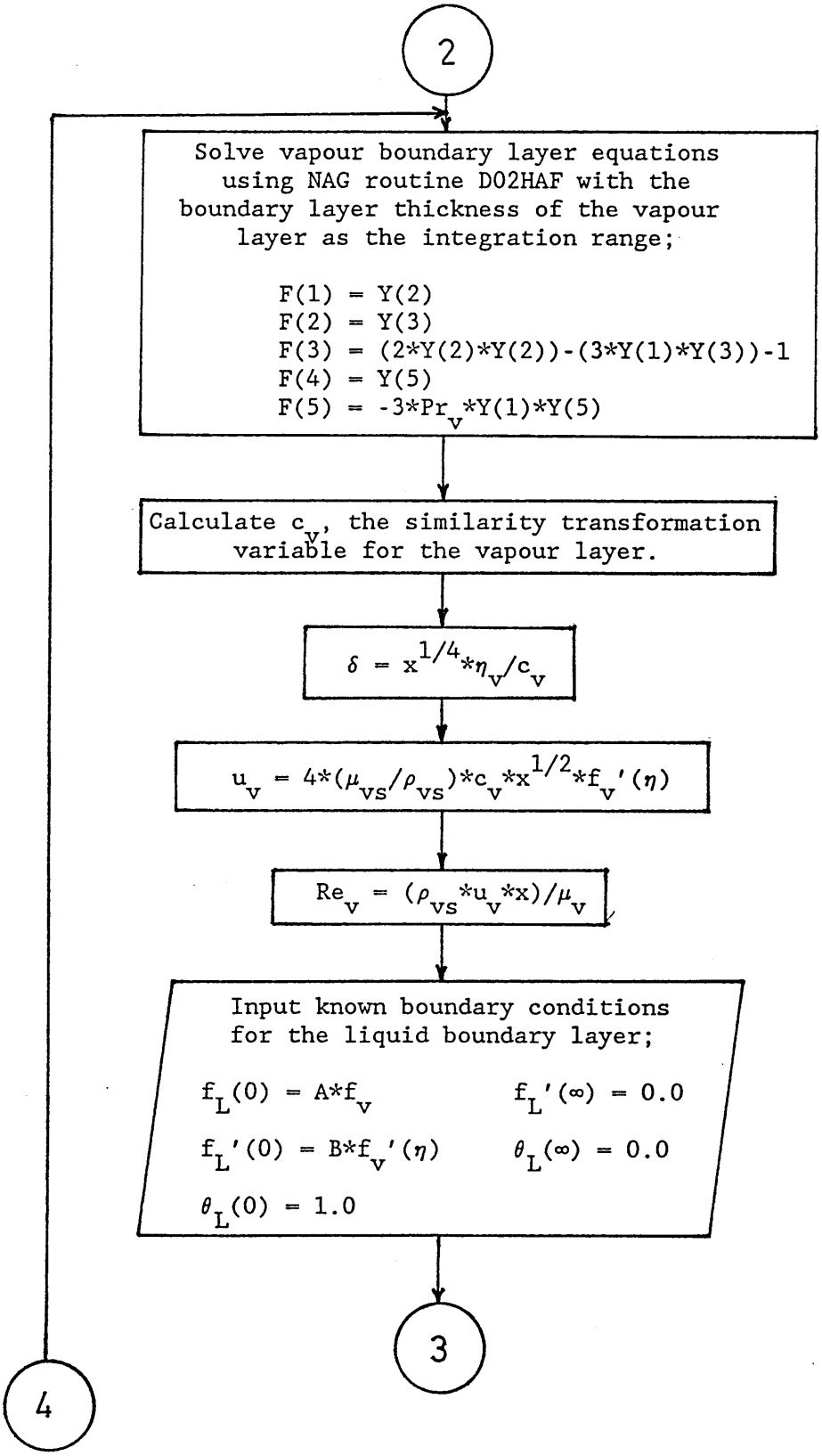
2
Solve vapour boundary layer equations using NAG routine D02HAF with the boundary layer thickness of the vapour layer as the integration range;
F(1) = Y(2)
F(2) = Y(3)
F(3) = (2*Y(2)*Y(2))-(3*Y(1)*Y(3))-1
F(4) = Y(5)
F(5) = -3*Pr_v*Y(1)*Y(5)
Calculate c_v, the similarity transformation variable for the vapour layer.
δ = x^1/4*η_v/c_v
u_v = 4*(μ_vs/ρ_vs)*c_v*x^1/2*f_v'(η)
Re_v = (ρ_vs*u_v*x)/μ_v
Input known boundary conditions for the liquid boundary layer;
f_L(0) = A*f_v
f_L'(∞) = 0.0
f_L'(0) = B*f_v'(η)
θ_L(∞) = 0.0
θ_L(0) = 1.0
3
4

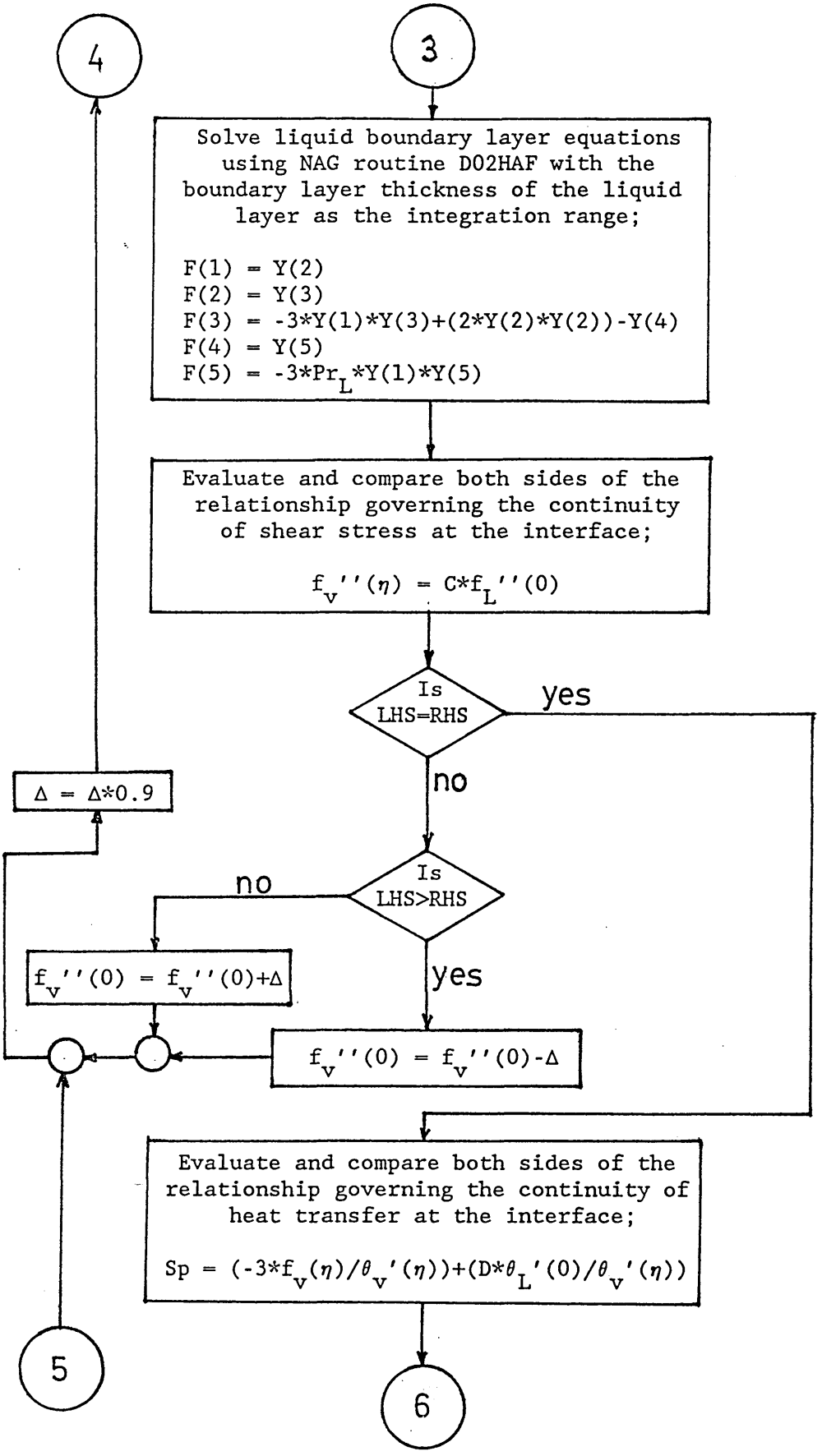
4
3
Solve liquid boundary layer equations using NAG routine D02HAF with the boundary layer thickness of the liquid layer as the integration range;
F(1) = Y(2)
F(2) = Y(3)
F(3) = -3*Y(1)*Y(3)+(2*Y(2)*Y(2))-Y(4)
F(4) = Y(5)
F(5) = -3*Pr_L*Y(1)*Y(5)
Evaluate and compare both sides of the relationship governing the continuity of shear stress at the interface;
f_v''(η) = C*f_L''(0)
Is LHS=RHS
yes
no
Δ = Δ*0.9
Is LHS>RHS
no
yes
f_v''(0) = f_v''(0)+Δ
f_v''(0) = f_v''(0)-Δ
Evaluate and compare both sides of the relationship governing the continuity of heat transfer at the interface;
Sp = (-3*f_v(η)/θ_v'(η))+(D*θ_L'(0)/θ_v'(η))
5
6

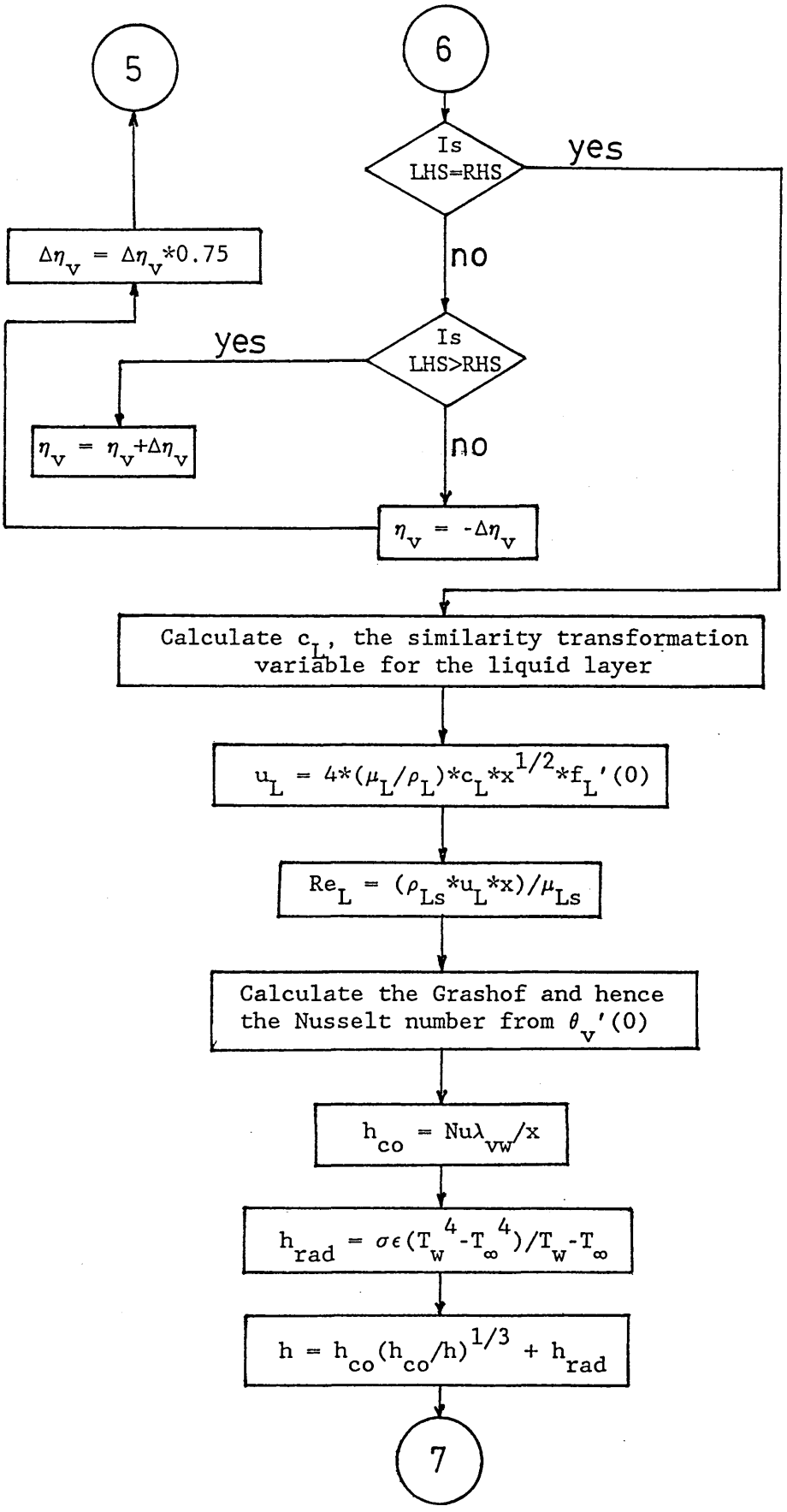
5
6
Is LHS=RHS
yes
no
$\Delta\eta_v = \Delta\eta_v * 0.75$
yes
Is LHS>RHS
$\eta_v = \eta_v + \Delta\eta_v$
no
$\eta_v = -\Delta\eta_v$
Calculate c_L, the similarity transformation variable for the liquid layer
$u_L = 4*(\mu_L/\rho_L)*c_L*x^{1/2}*f_L'(0)$
$Re_L = (\rho_{Ls}*u_L*x)/\mu_{Ls}$
Calculate the Grashof and hence the Nusselt number from $\theta_v'(0)$
$h_{co} = Nu\lambda_{vw}/x$
$h_{rad} = \sigma\epsilon(T_w^4 - T_\infty^4)/T_w - T_\infty$
$h = h_{co}(h_{co}/h)^{1/3} + h_{rad}$
7

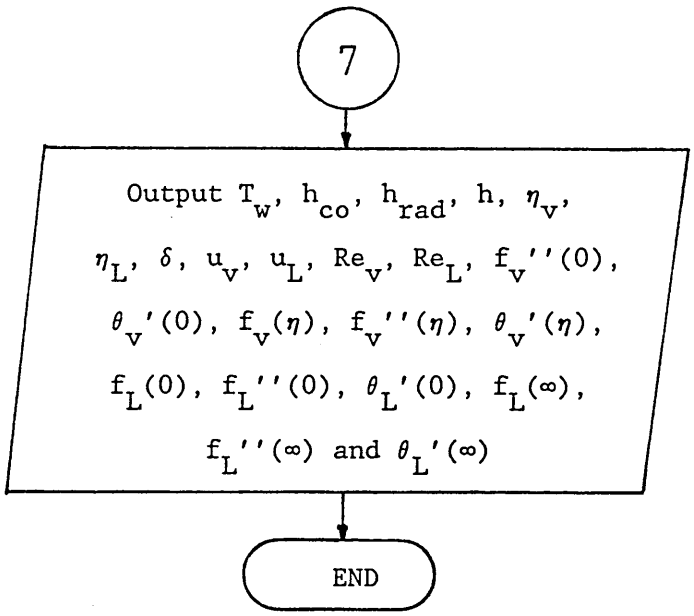
7
Output T_w, h_{co}, h_{rad}, h, η_v,
η_L, δ, u_v, u_L, Re_v, Re_L, $f_v''(0)$,
$\theta_v'(0)$, $f_v(\eta)$, $f_v''(\eta)$, $\theta_v'(\eta)$,
$f_L(0)$, $f_L''(0)$, $\theta_L'(0)$, $f_L(\infty)$,
$f_L''(\infty)$ and $\theta_L'(\infty)$
END

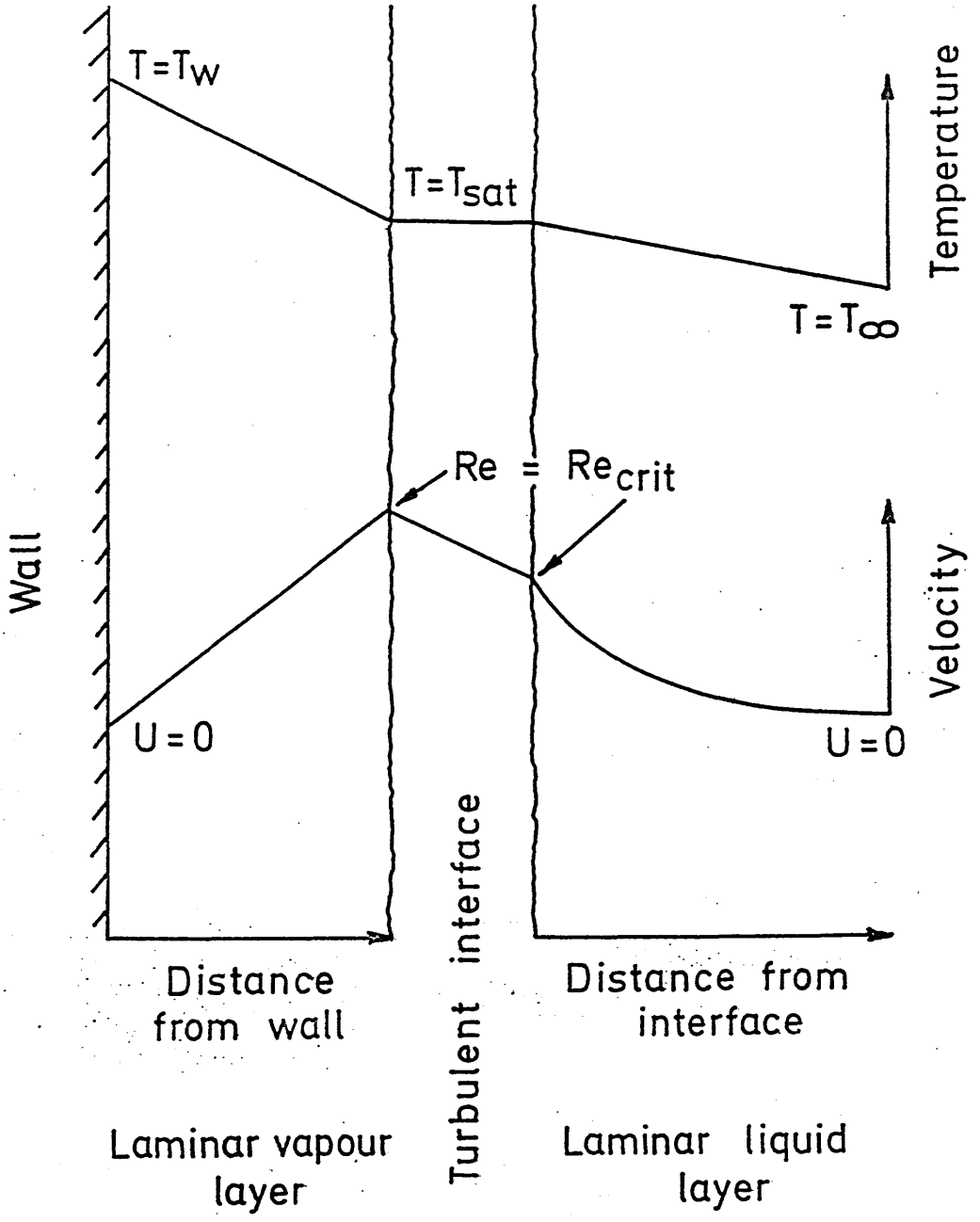
T=Tw
T=Tsat
T=T∞
Temperature
Re = Recrit
Wall
U=0
U=0
Velocity
Distance from wall
Turbulent interface
Distance from interface
Laminar vapour layer
Laminar liquid layer

FIGURE 38: Relationships between time and temperature at the surface of stainless steel plates quenched in a range of unagitated sodium polyacrylate solutions. (Figures refer to concentration of Aquaquench ACR in water).

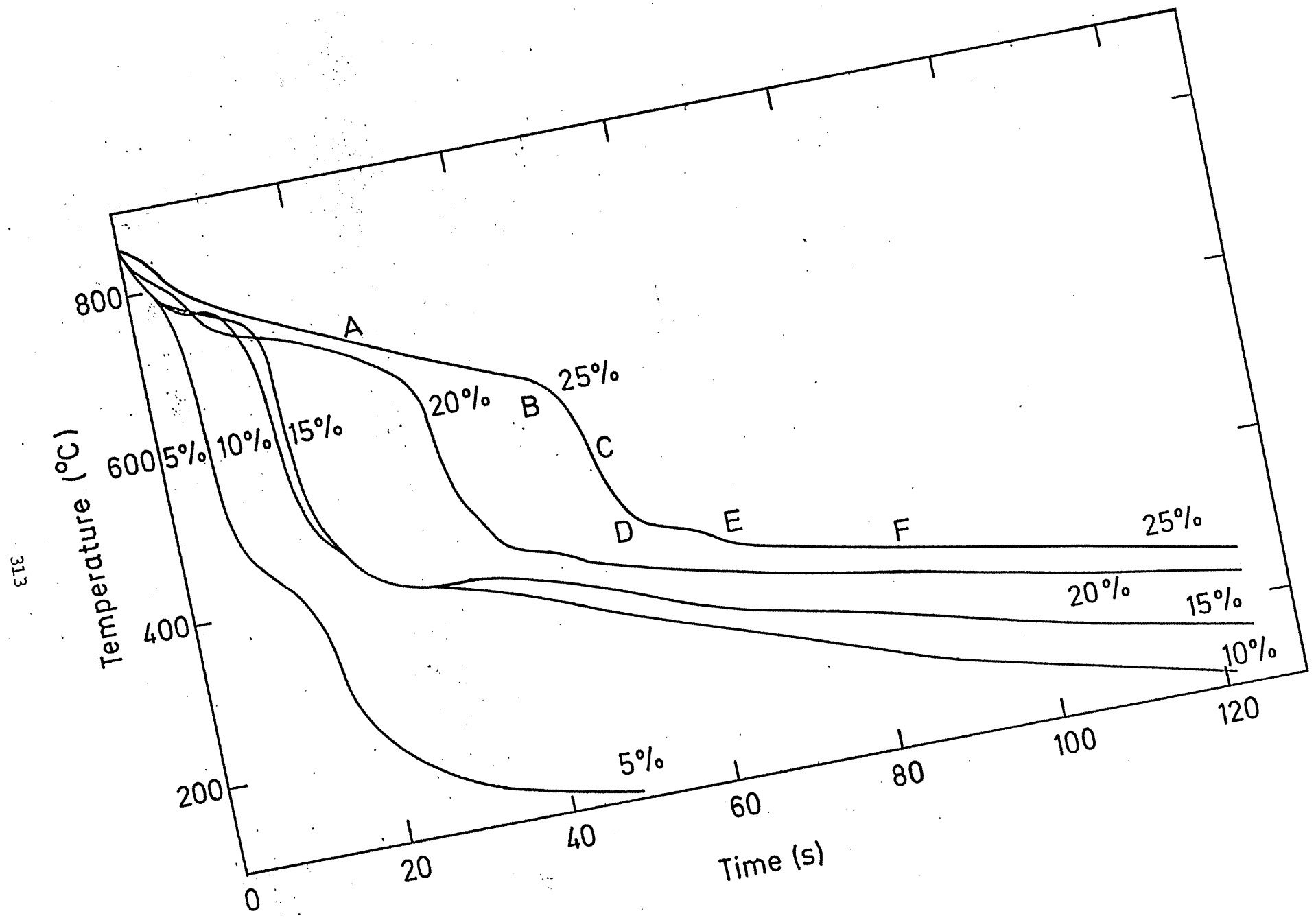
800
600
400
200
0
Temperature (°C)
20
40
60
80
100
120
Time (s)
A
B
C
D
E
F
5%
10%
15%
20%
25%
25%
20%
15%
10%
5%

FIGURE 39: Relationships between time and temperature at the surface of stainless steel plates quenched in a range of agitated sodium polyacrylate solutions. (Figures refer to concentration of Aquaquench ACR in water).

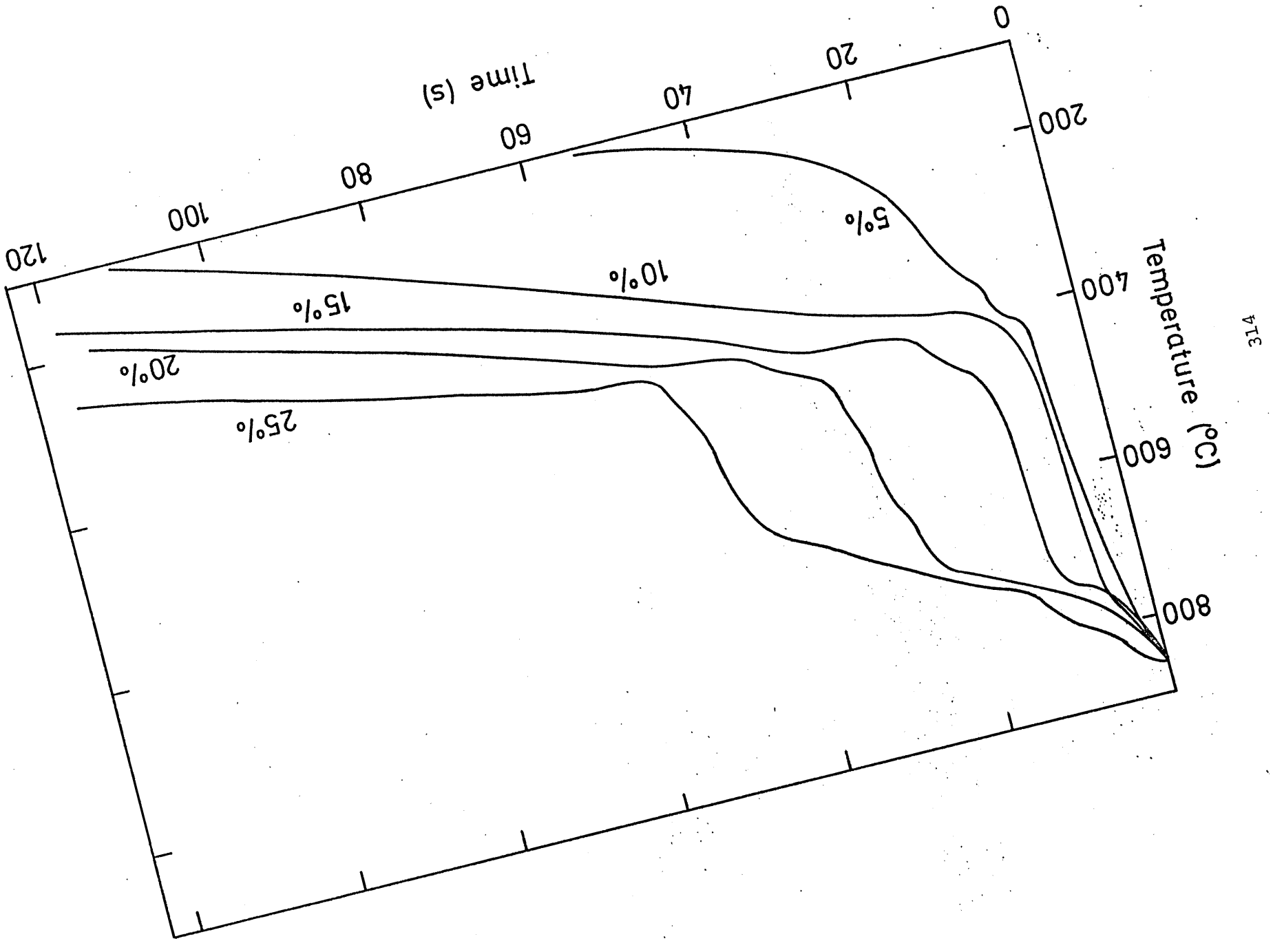
Time (s)
0
20
40
60
80
100
120
Temperature (°C)
200
400
600
800
5%
10%
15%
20%
25%

FIGURE 40: Relationships between surface temperature and mean surface heat transfer coefficients measured during quenching in a range of unagitated sodium polyacrylate solutions. (Figures refer to concentration of Aquaquench ACR in water).

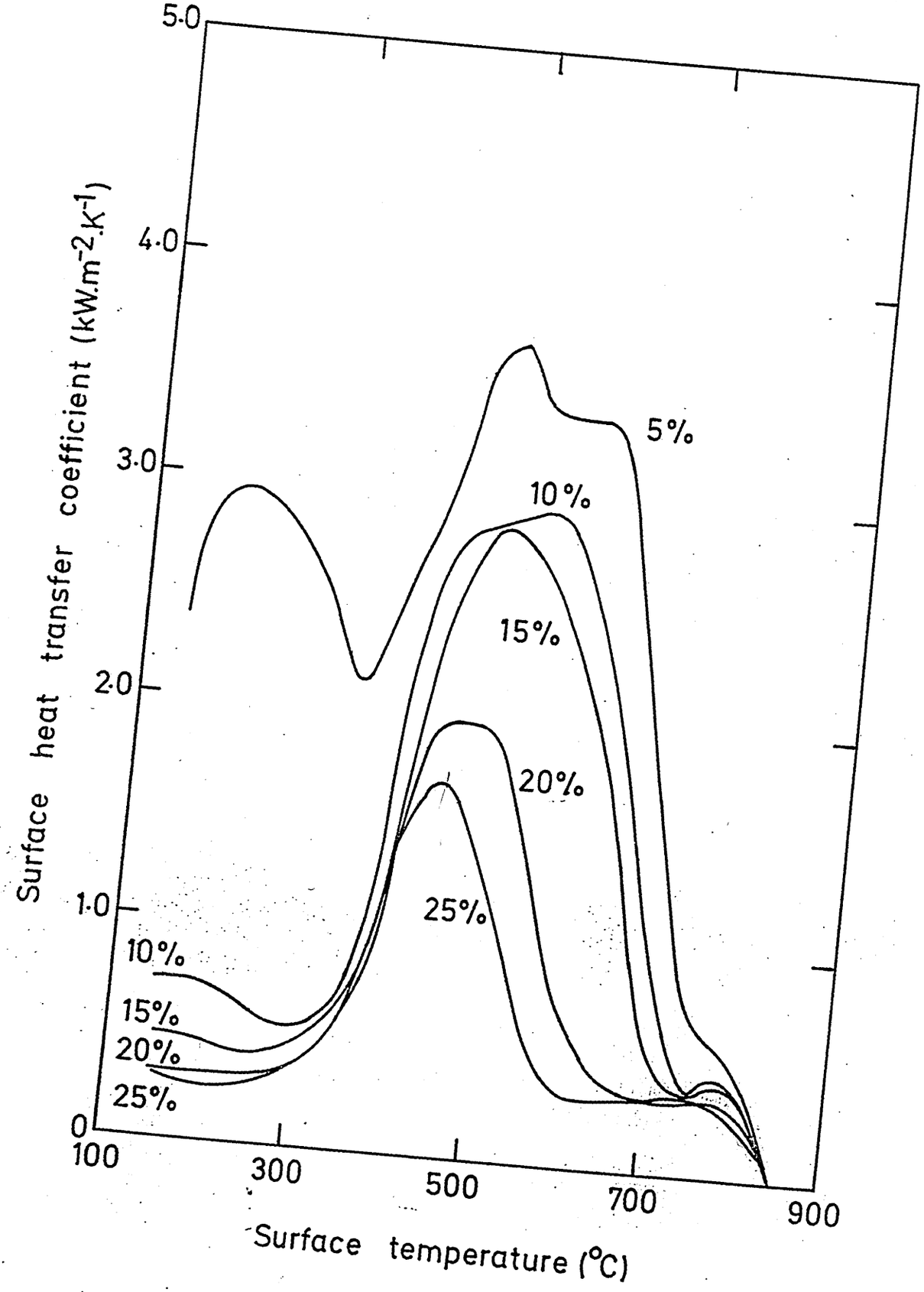
5·0
4·0
3·0
2·0
1·0
0
Surface heat transfer coefficient (kW.m⁻².K⁻¹)
5%
10%
15%
20%
25%
10%
15%
20%
25%
100
300
500
700
900
Surface temperature (°C)

FIGURE 41: Relationships between surface temperature and mean surface heat transfer coefficients measured during quenching in a range of agitated sodium polyacrylate solutions. (Figures refer to concentration of Aquaquench ACR in water).

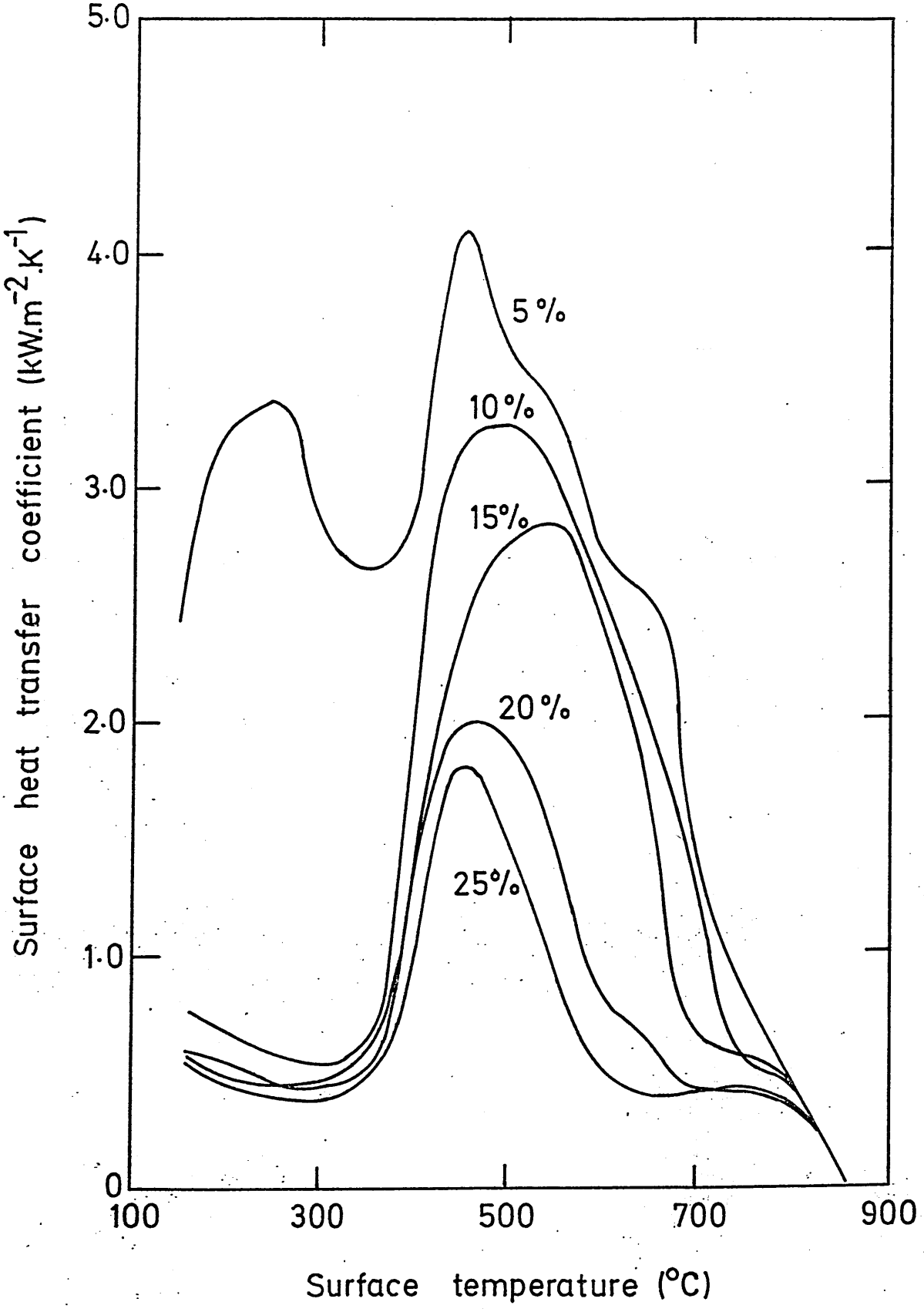
5·0
4·0
3·0
2·0
1·0
0
100
300
500
700
900
5 %
10 %
15%
20 %
25%
Surface heat transfer coefficient (kW.m^{-2}.K^{-1})
Surface temperature (°C)

FIGURE 42: The range of surface heat transfer coefficients measured during quenching in unagitated solutions of 5% Aquaquench ACR in water.

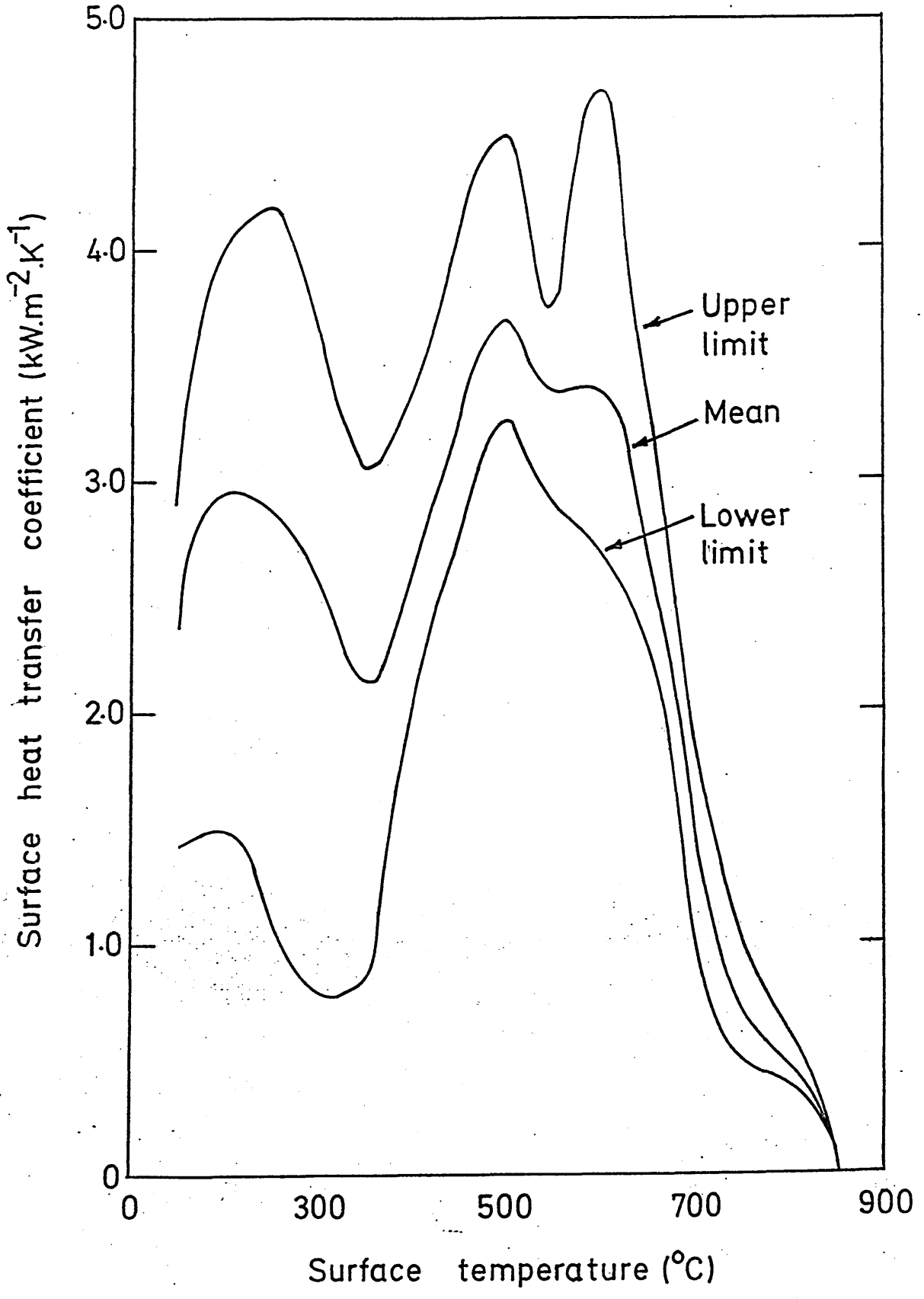
5·0
4·0
3·0
2·0
1·0
0
Surface heat transfer coefficient (kW.m^{-2}.K^{-1})
Upper limit
Mean
Lower limit
0
300
500
700
900
Surface temperature (°C)

FIGURE 43: The range of surface heat transfer coefficients measured during quenching in unagitated solutions of 10% Aquaquench ACR in water.

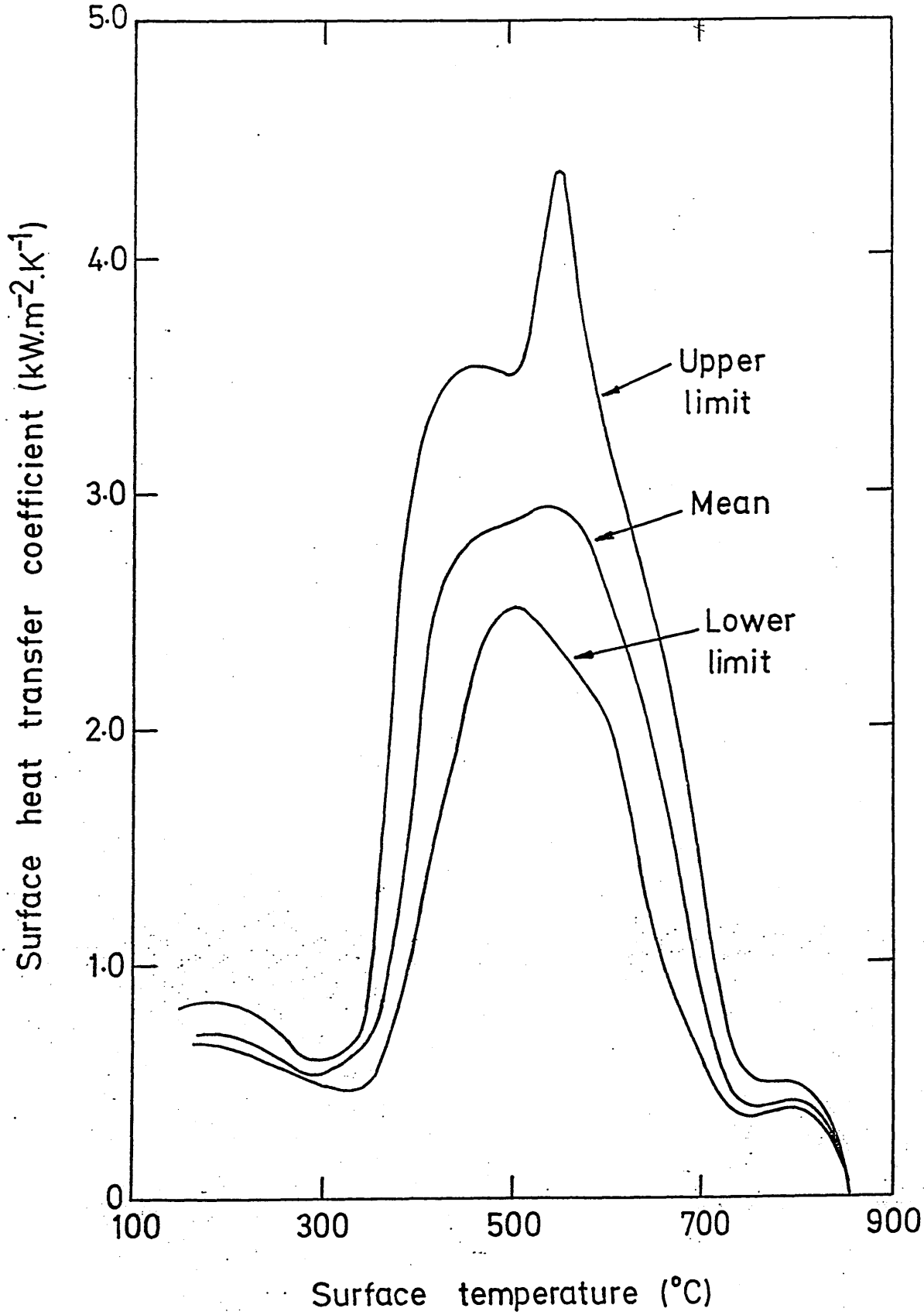
5·0
4·0
3·0
2·0
1·0
0
100
300
500
700
900
Surface heat transfer coefficient (kW.m^{-2}.K^{-1})
Surface temperature (°C)
Upper limit
Mean
Lower limit

FIGURE 44: The range of surface heat transfer coefficients measured during quenching in unagitated solutions of 15% Aquaquench ACR in water.

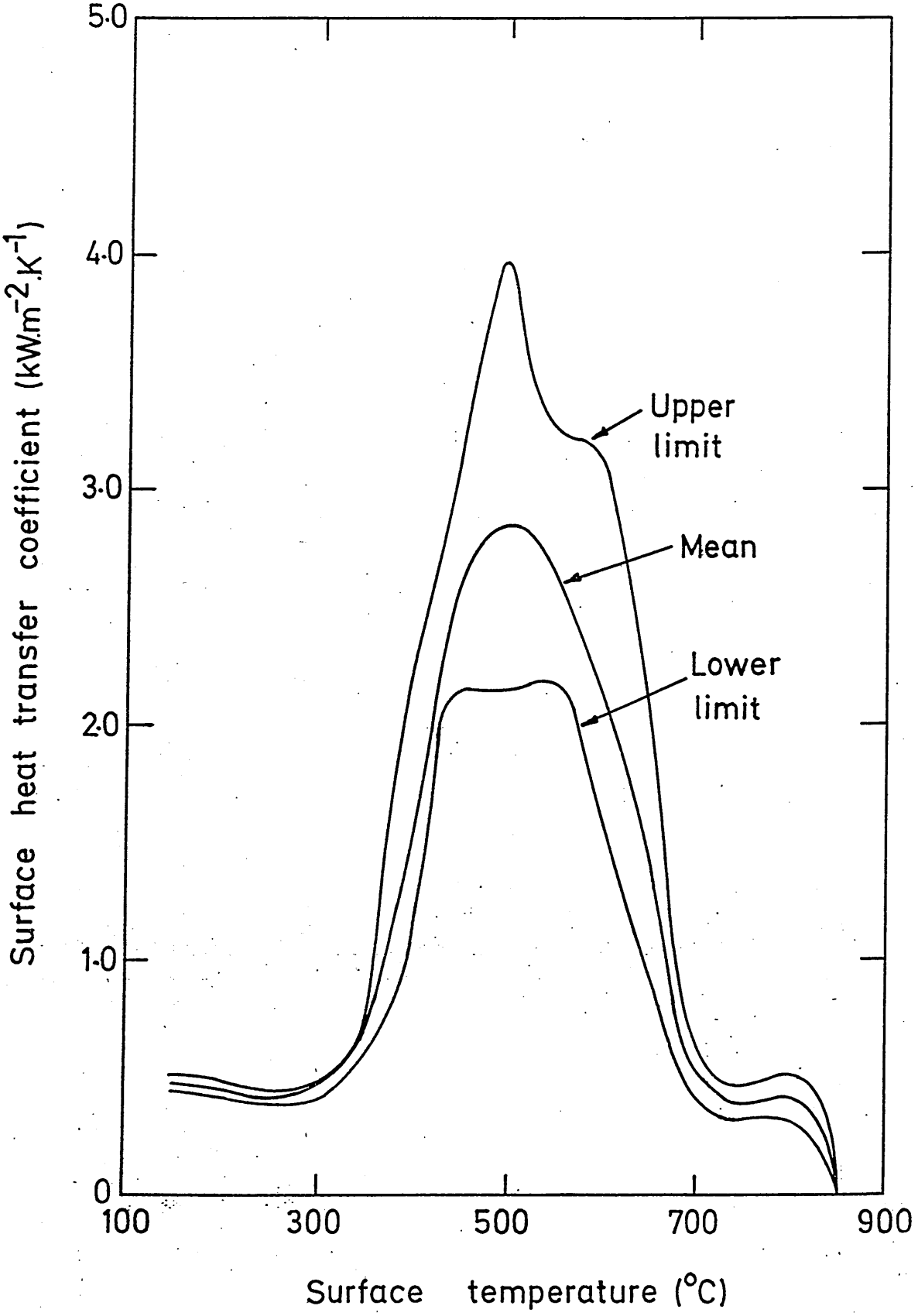
5·0
4·0
3·0
2·0
1·0
0
100
300
500
700
900
Surface heat transfer coefficient (kW.m^{-2}.K^{-1})
Surface temperature (°C)
Upper limit
Mean
Lower limit

FIGURE 45: The range of surface heat transfer coefficients measured during quenching in unagitated solutions of 20% Aquaquench ACR in water.

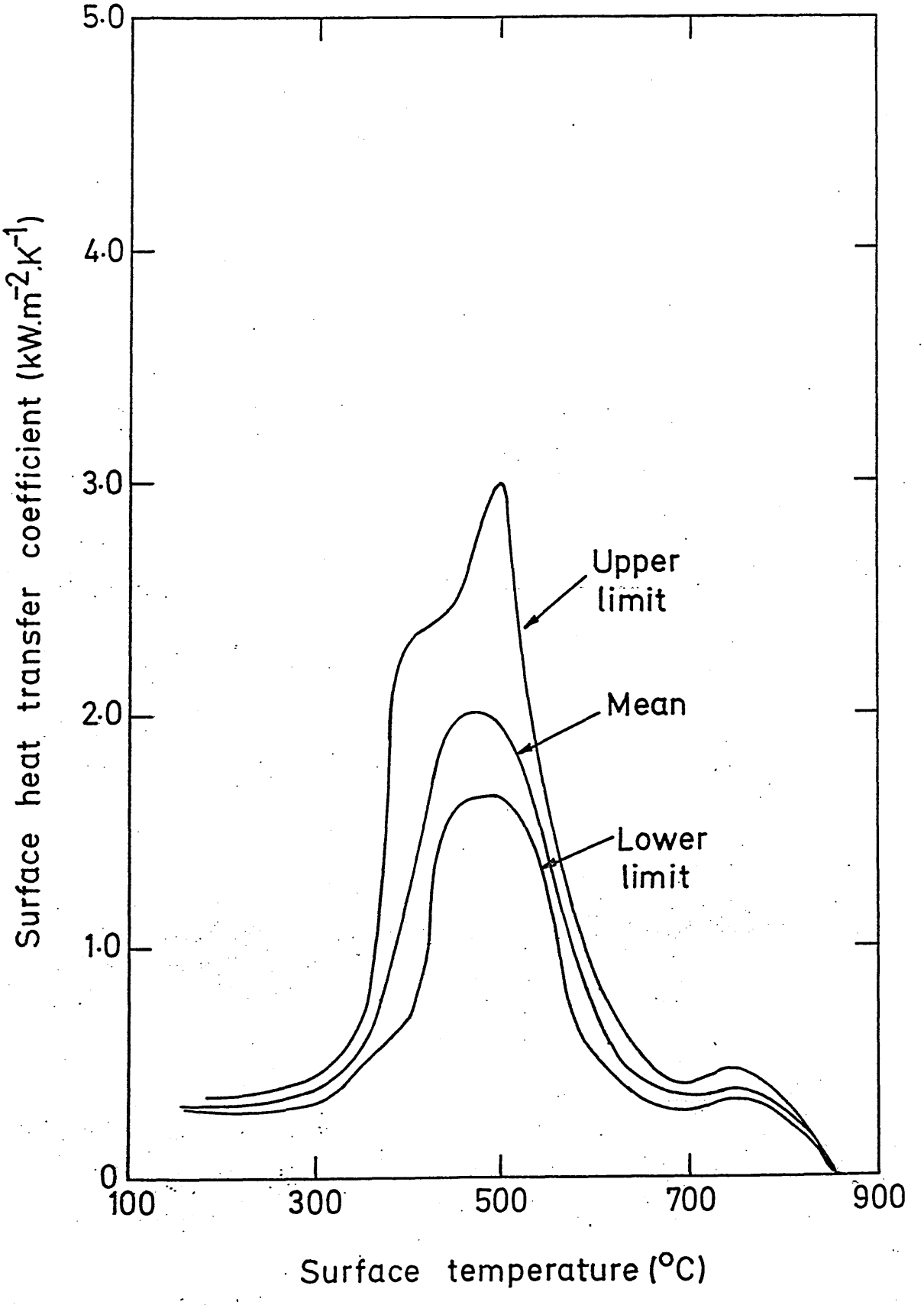
5·0
4·0
3·0
2·0
1·0
0
100
300
500
700
900
Surface heat transfer coefficient (kW.m^{-2}.K^{-1})
Surface temperature (°C)
Upper limit
Mean
Lower limit

FIGURE 46: The range of surface heat transfer coefficients measured during quenching in unagitated solutions of 25% Aquaquench ACR in water.

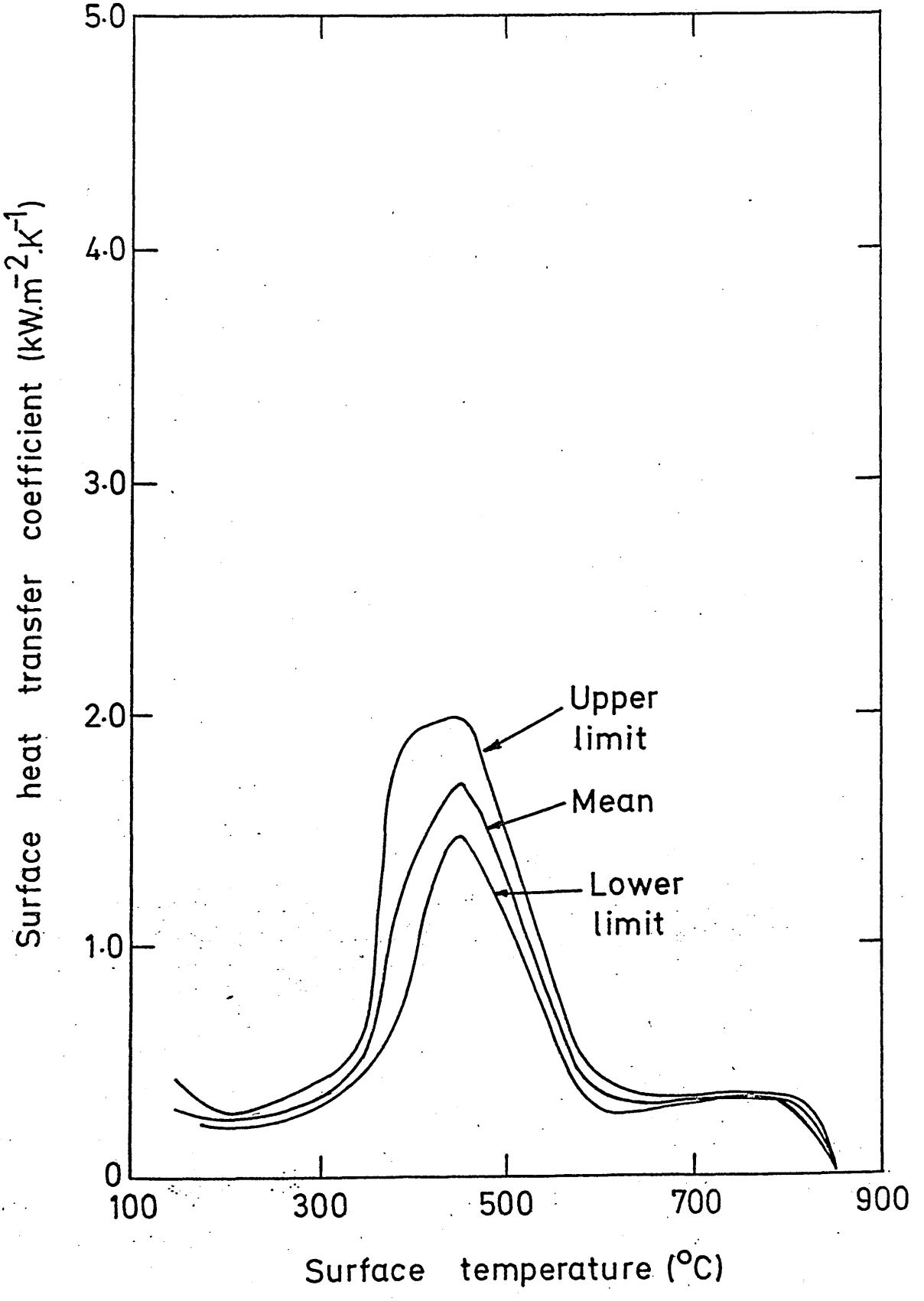
5·0
4·0
3·0
2·0
1·0
0
100
300
500
700
900
Surface heat transfer coefficient (kW.m⁻².K⁻¹)
Surface temperature (°C)
Upper limit
Mean
Lower limit

FIGURE 47: The boiling regimes produced in aqueous solutions of sodium polyacrylate.

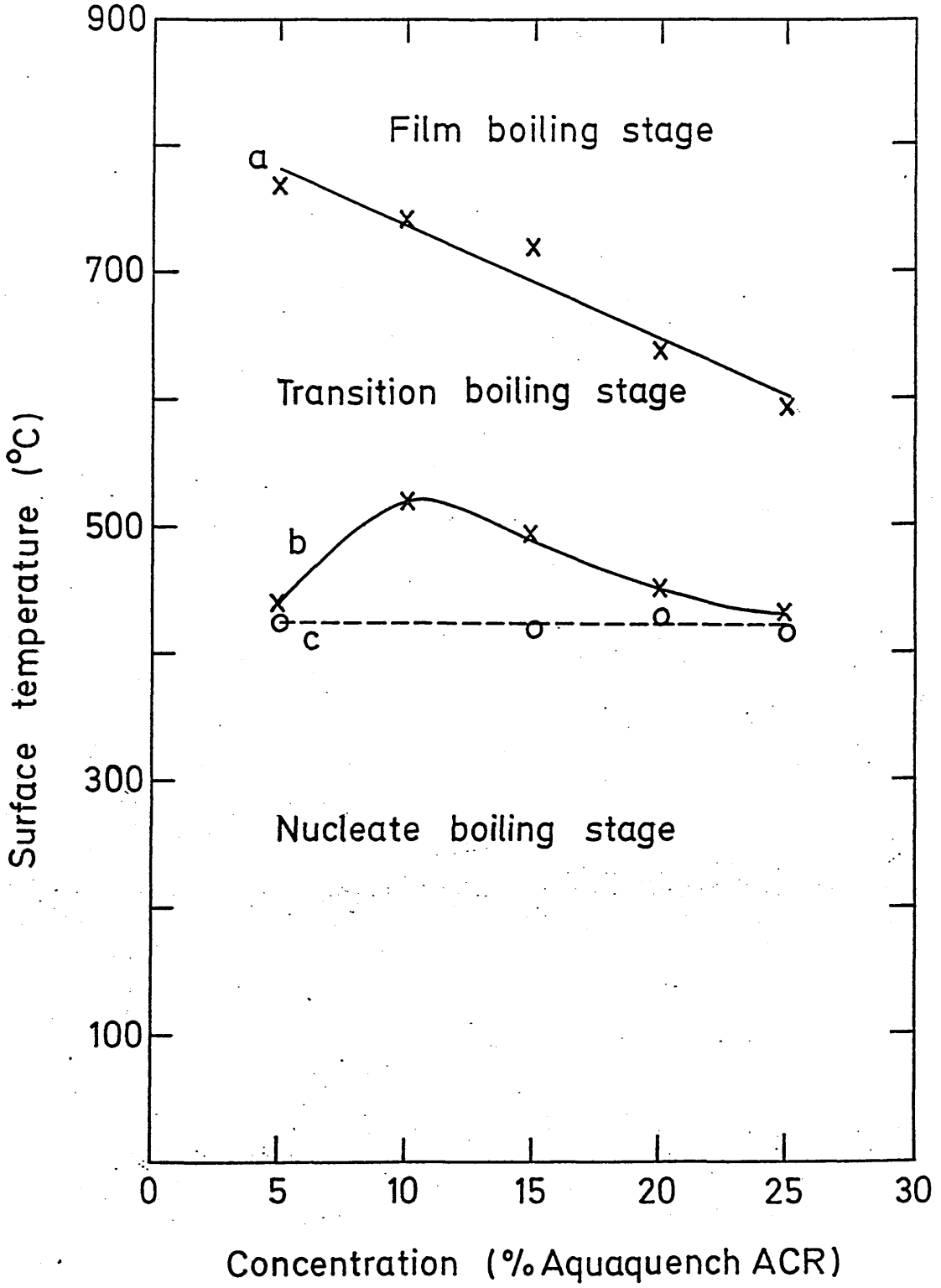
900
700
500
300
100
Film boiling stage
Transition boiling stage
Nucleate boiling stage
a
b
c
Surface temperature (°C)
0
5
10
15
20
25
30
Concentration (% Aquaquench ACR)

FIGURE 48: Relationships between time and temperature measured during quenching a stainless steel plate in water.

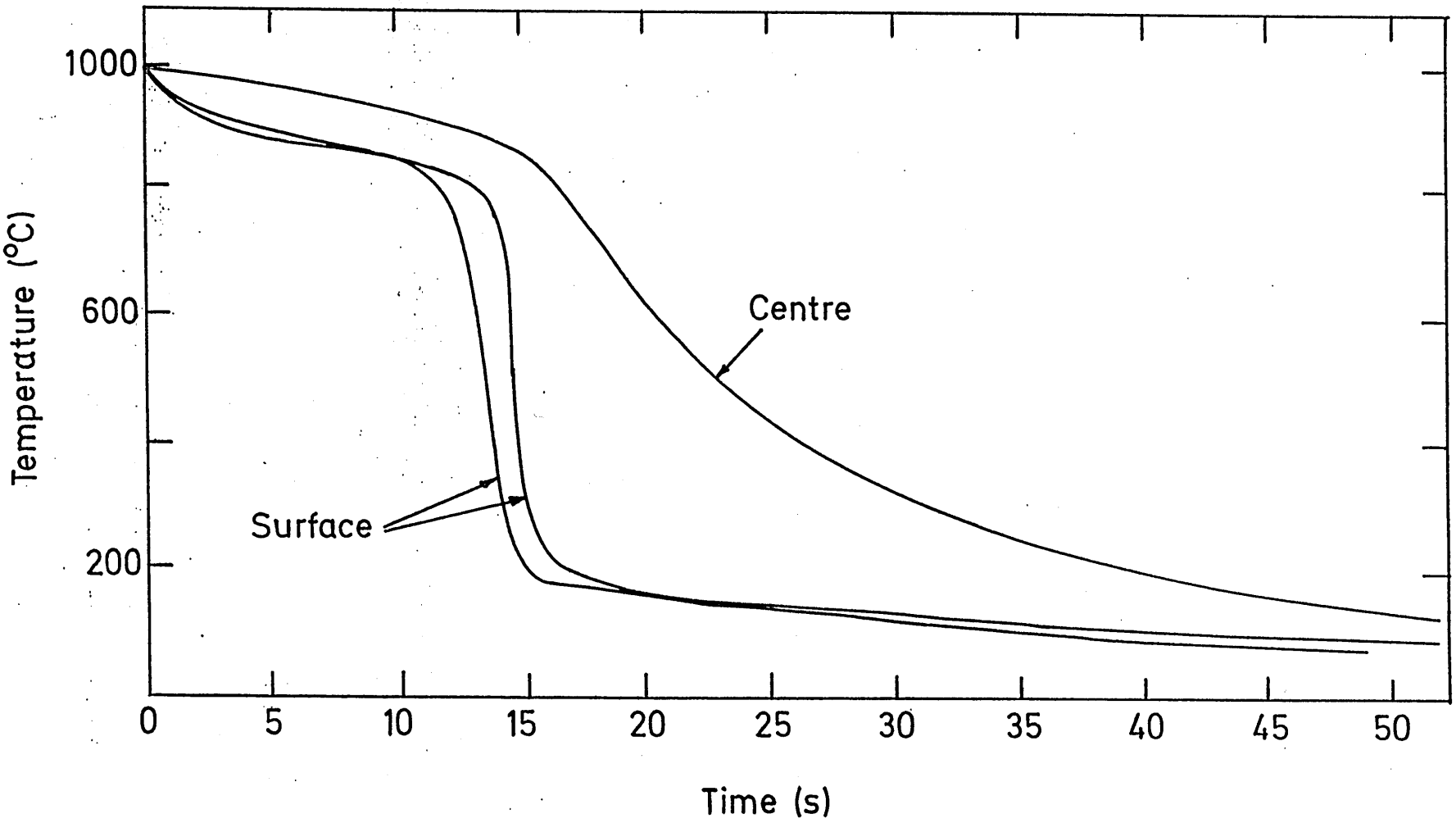
1000
600
200
Temperature (°C)
Centre
Surface
0
5
10
15
20
25
30
35
40
45
50
Time (s)

FIGURE 49: Mean surface heat transfer coefficient measured during quenching in water.

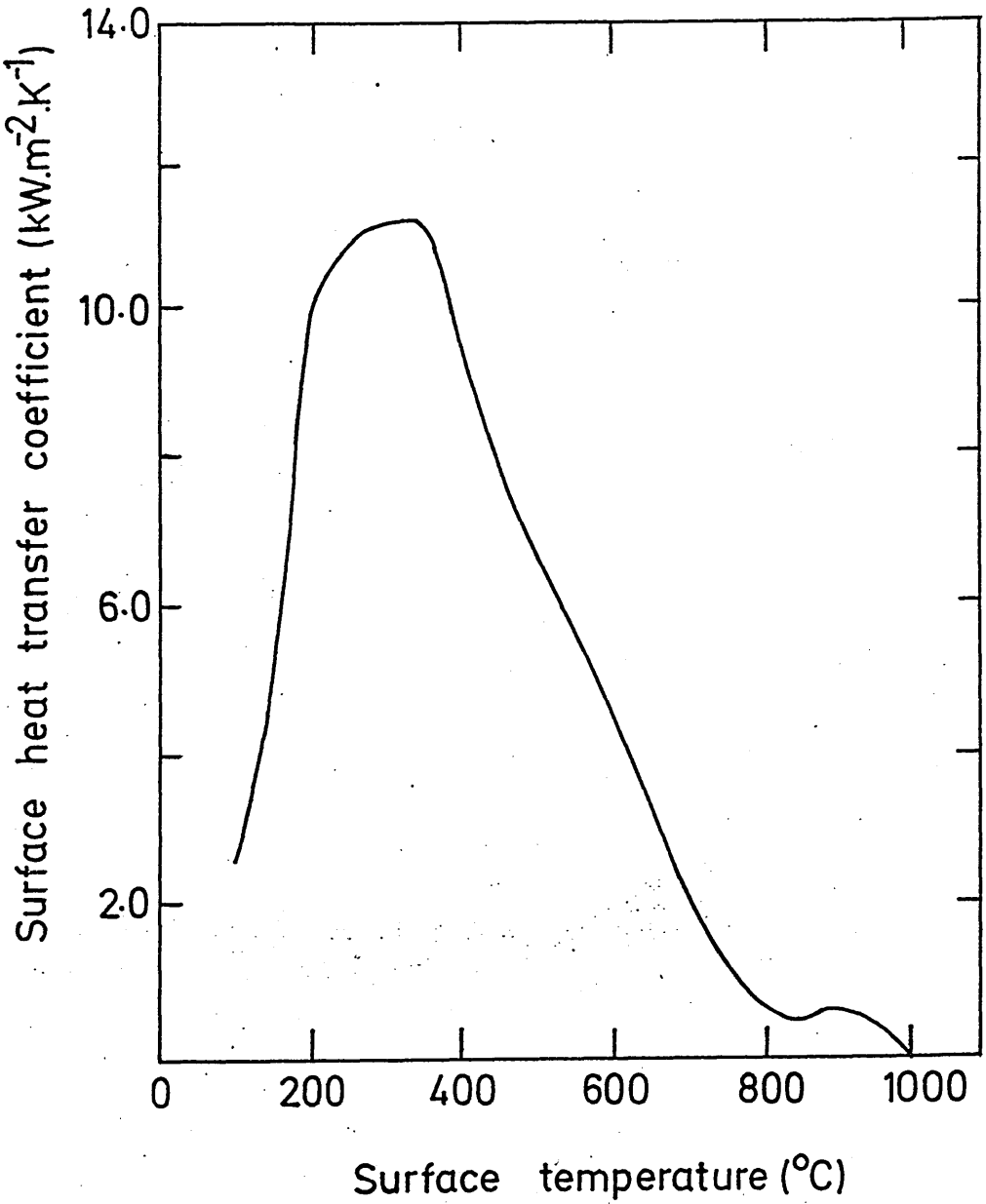
14·0
10·0
6·0
2·0
Surface heat transfer coefficient (kW.m^{-2}.K^{-1})
0
200
400
600
800
1000
Surface temperature (°C)

FIGURE 50: Relationship between time, temperature and surface heat transfer coefficient measured during quenching in an unagitated solution of 10% Aquaquench ACR. (This quench was cine filmed).

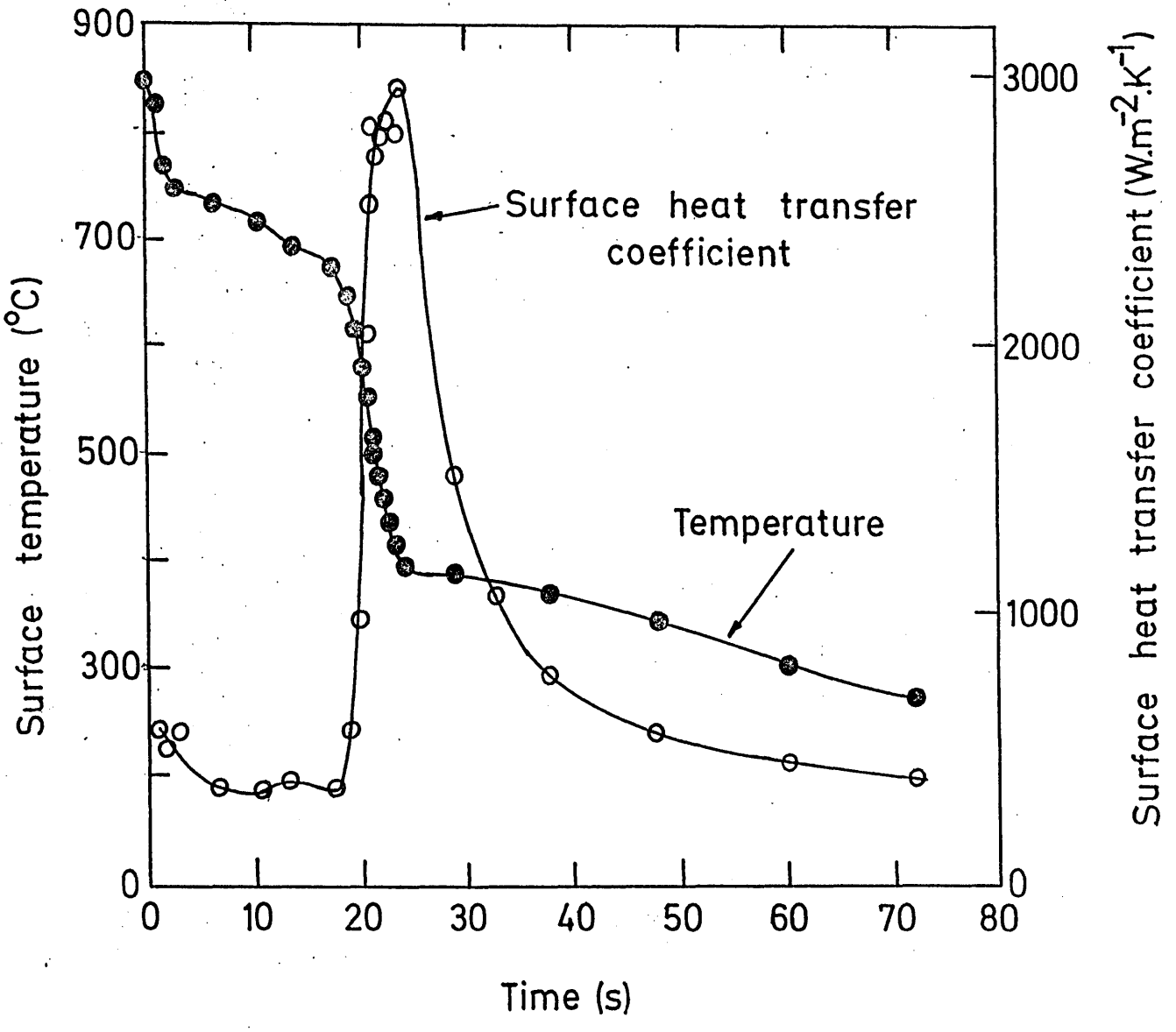
900
700
500
300
0
0
10
20
30
40
50
60
70
80
Time (s)
Surface temperature (°C)
3000
2000
1000
0
Surface heat transfer coefficient (W.m^{-2}.K^{-1})
Surface heat transfer coefficient
Temperature

FIGURE 51: Calculated residual stresses in low alloy steel plates quenched in unagitated aqueous solutions of sodium polyacrylate. (Figures refer to concentration of Aquaquench ACR).

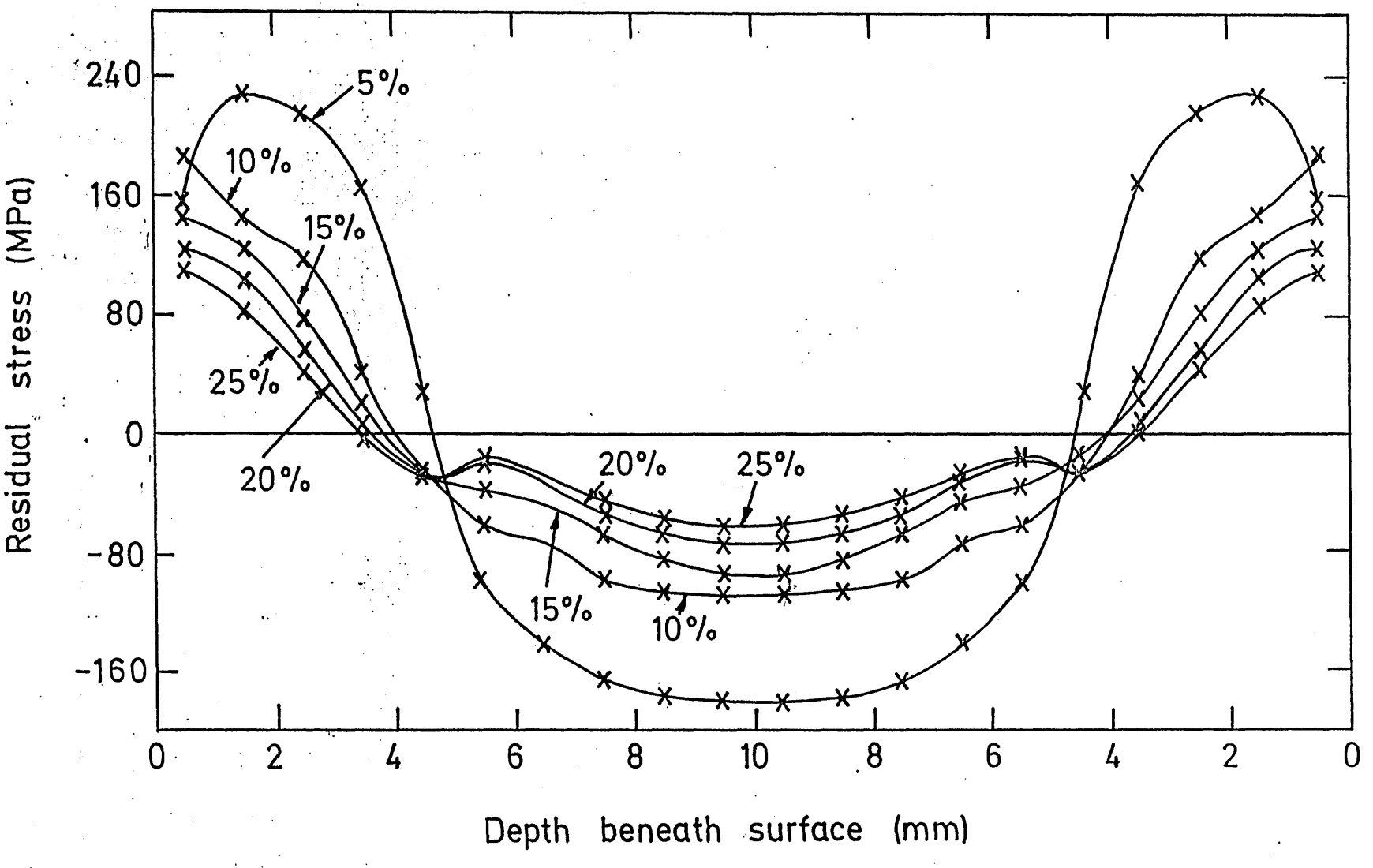
Residual stress (MPa)
240
160
80
0
-80
-160
5%
10%
15%
25%
20%
20%
25%
15%
10%
0
2
4
6
8
10
8
6
4
2
0
Depth beneath surface (mm)

FIGURE 52: Calculated residual stresses in low alloy steel plates quenched in agitated solutions of sodium polyacrylate. (Figures refer to concentration of Aquaquench ACR).

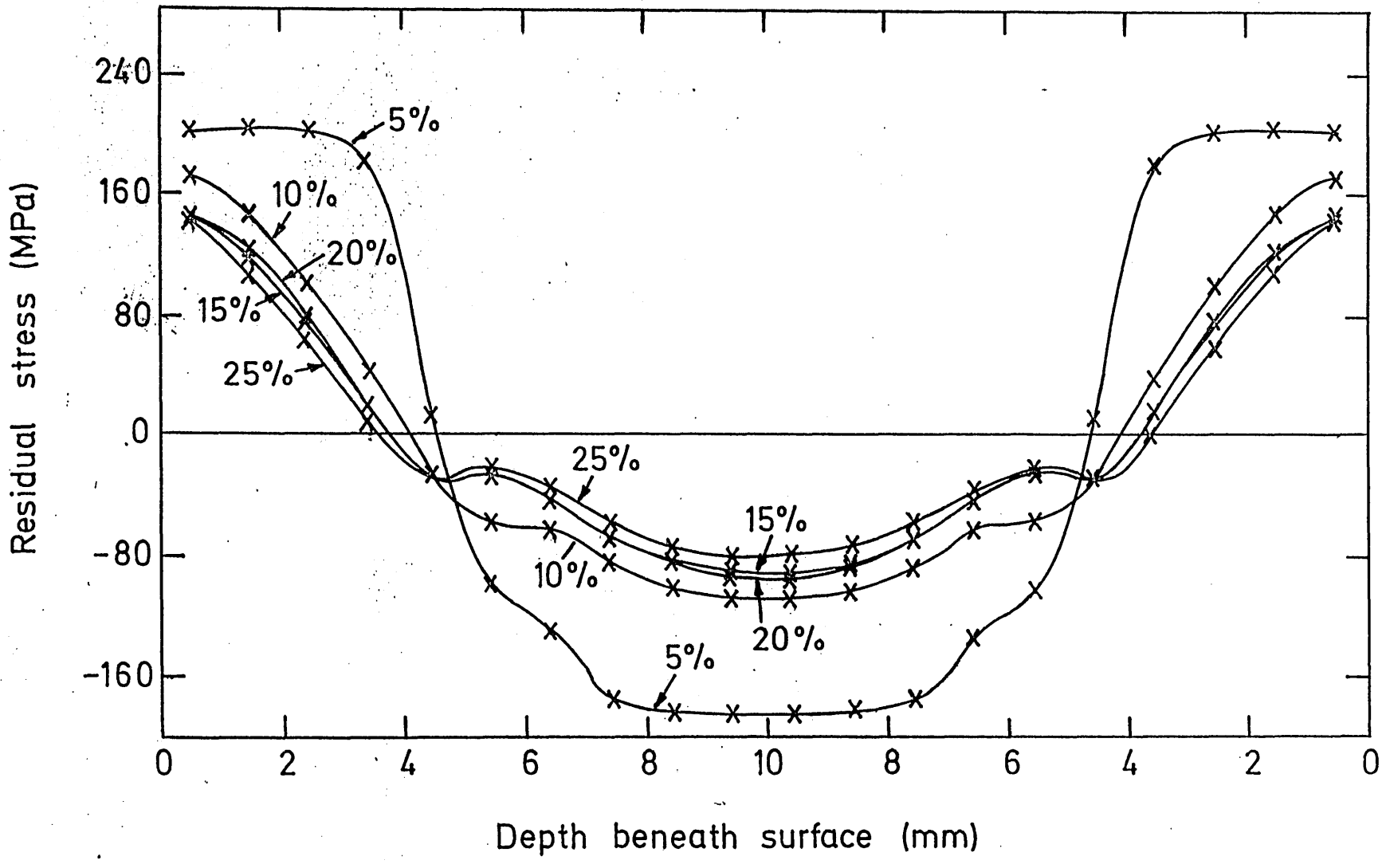
Residual stress (MPa)
240
160
80
0
-80
-160
5%
10%
20%
15%
25%
25%
15%
10%
20%
5%
0
2
4
6
8
10
8
6
4
2
0
Depth beneath surface (mm)

FIGURE 53: Calculated residual stress in a low alloy steel plate quenched in water.

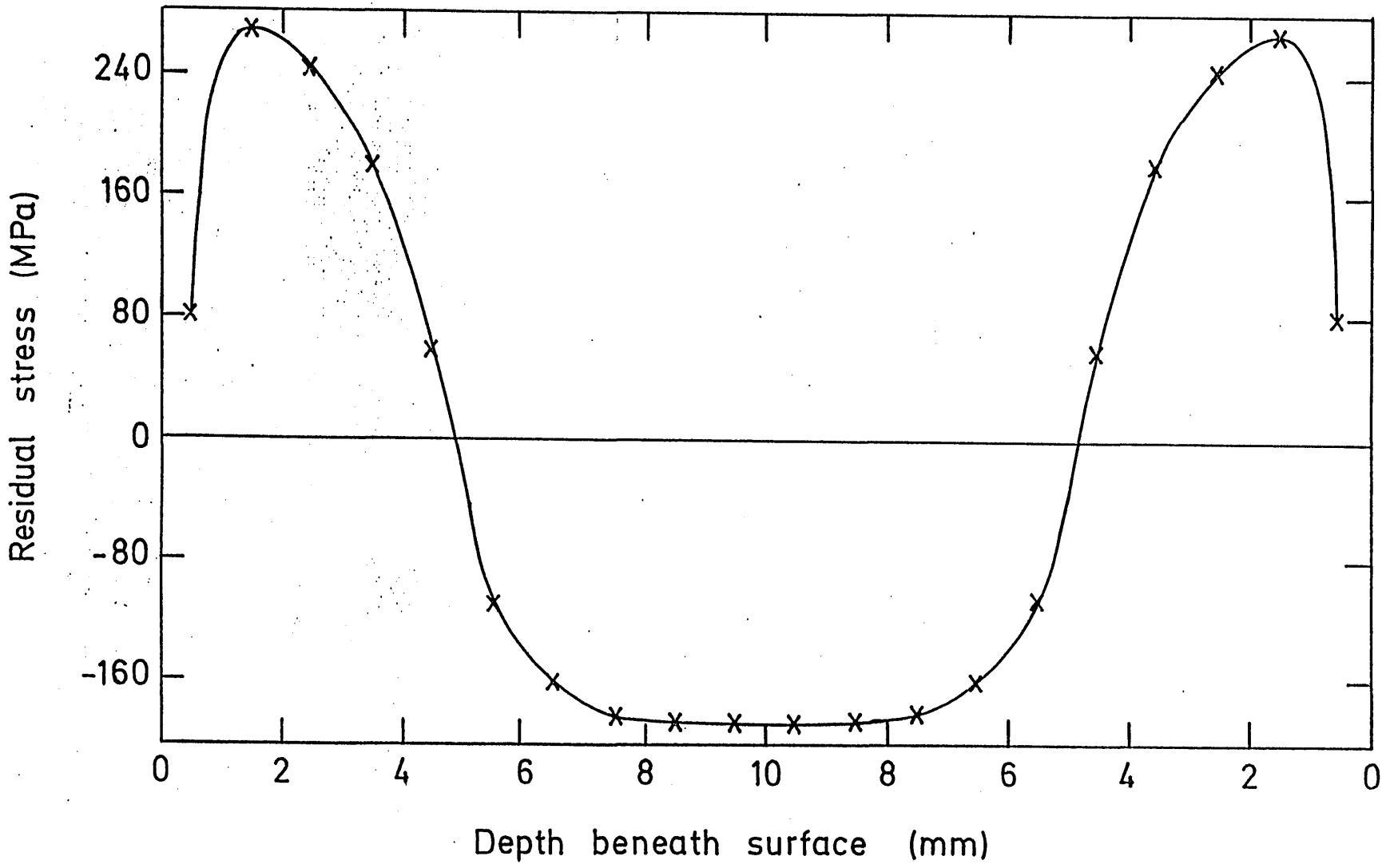
Residual stress (MPa)
240
160
80
0
-80
-160
0
2
4
6
8
10
8
6
4
2
0
Depth beneath surface (mm)

FIGURE 54: Calculated residual stress in a low alloy steel plate quenched in an aqueous solution of polyalkylene glycol, (25% Aquaquench 1250).

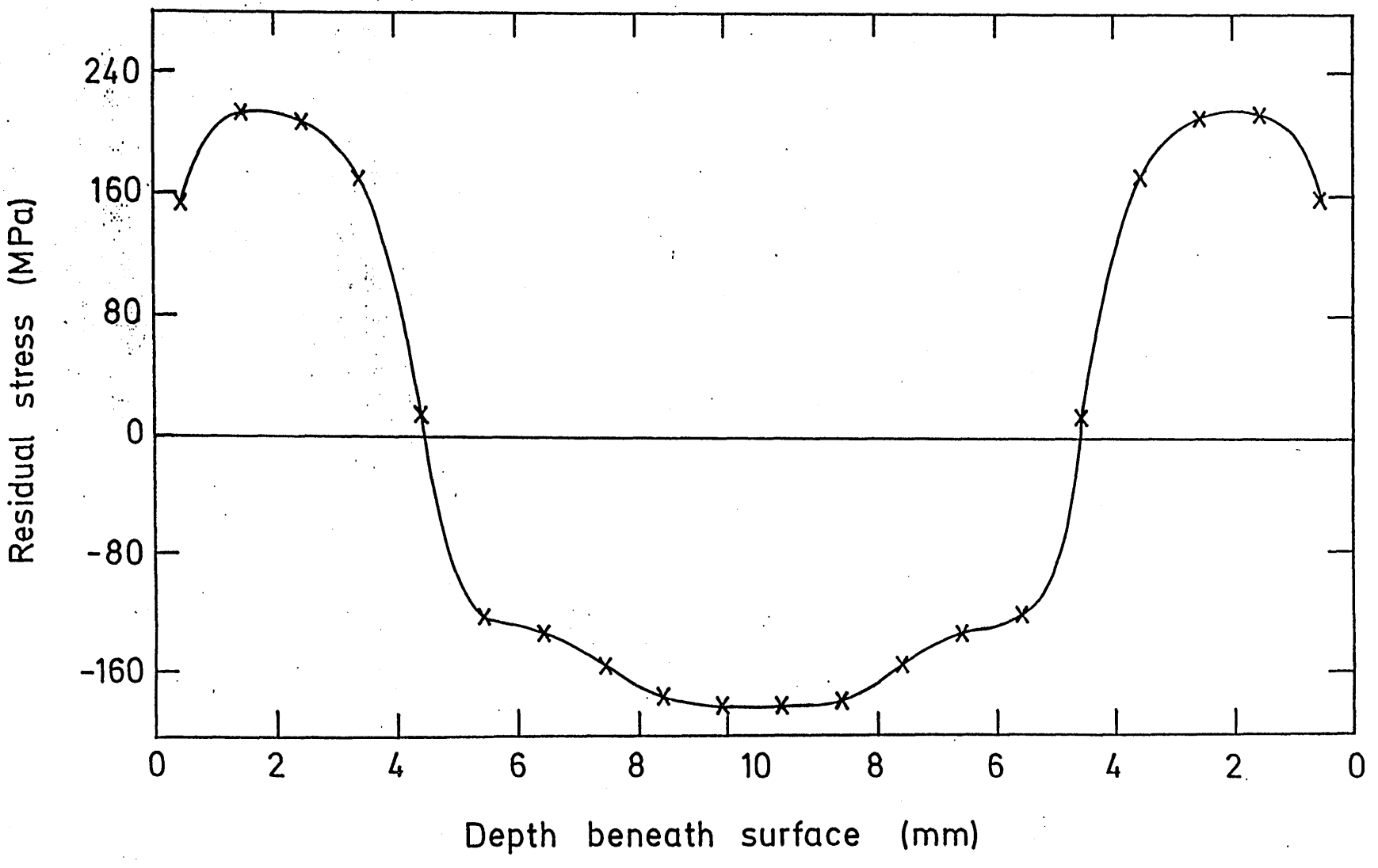
240
160
80
0
-80
-160
Residual stress (MPa)
0
2
4
6
8
10
8
6
4
2
0
Depth beneath surface (mm)

FIGURE 55: Comparison of calculated residual stresses in low alloy steel plates quenched in water, a 25% Aquaquench 1250 solution and a 5% Aquaquench ACR solution.

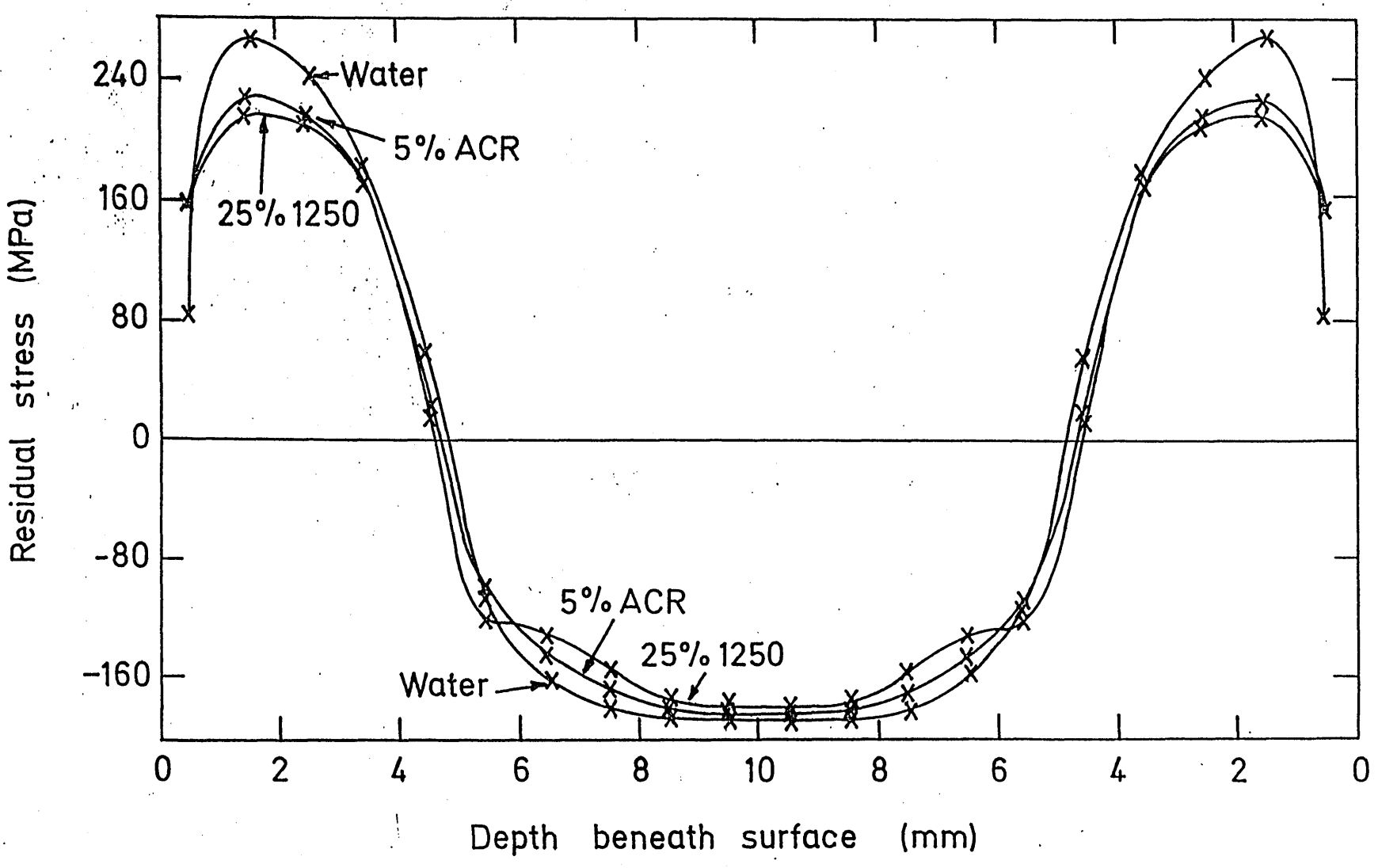
Residual stress (MPa)
240
160
80
0
-80
-160
Water
5% ACR
25% 1250
5% ACR
25% 1250
Water
0
2
4
6
8
10
8
6
4
2
0
Depth beneath surface (mm)

FIGURE 56: Comparison of calculated residual stresses in low alloy steel plates quenched in a medium speed quenching oil, (RDN175), and an aqueous solution of 15% Aquaquench ACR.

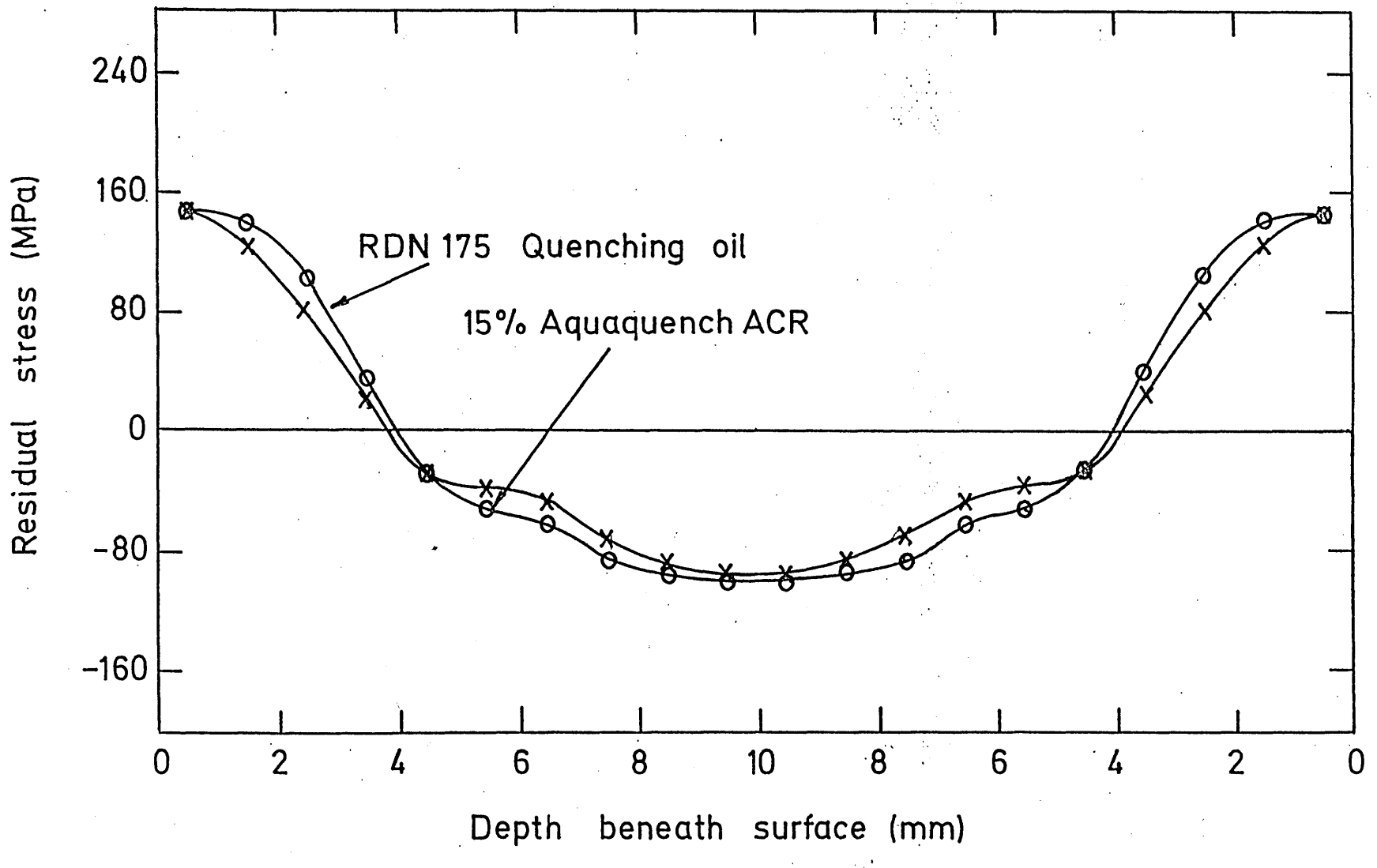
240
160
80
0
-80
-160
Residual stress (MPa)
RDN 175 Quenching oil
15% Aquaquench ACR
0
2
4
6
8
10
8
6
4
2
0
Depth beneath surface (mm)

FIGURE 57: Calculated residual strains in low alloy steel plates quenched in unagitated solutions of sodium polyacrylate. (Figures refer to concentration of Aquaquench ACR).

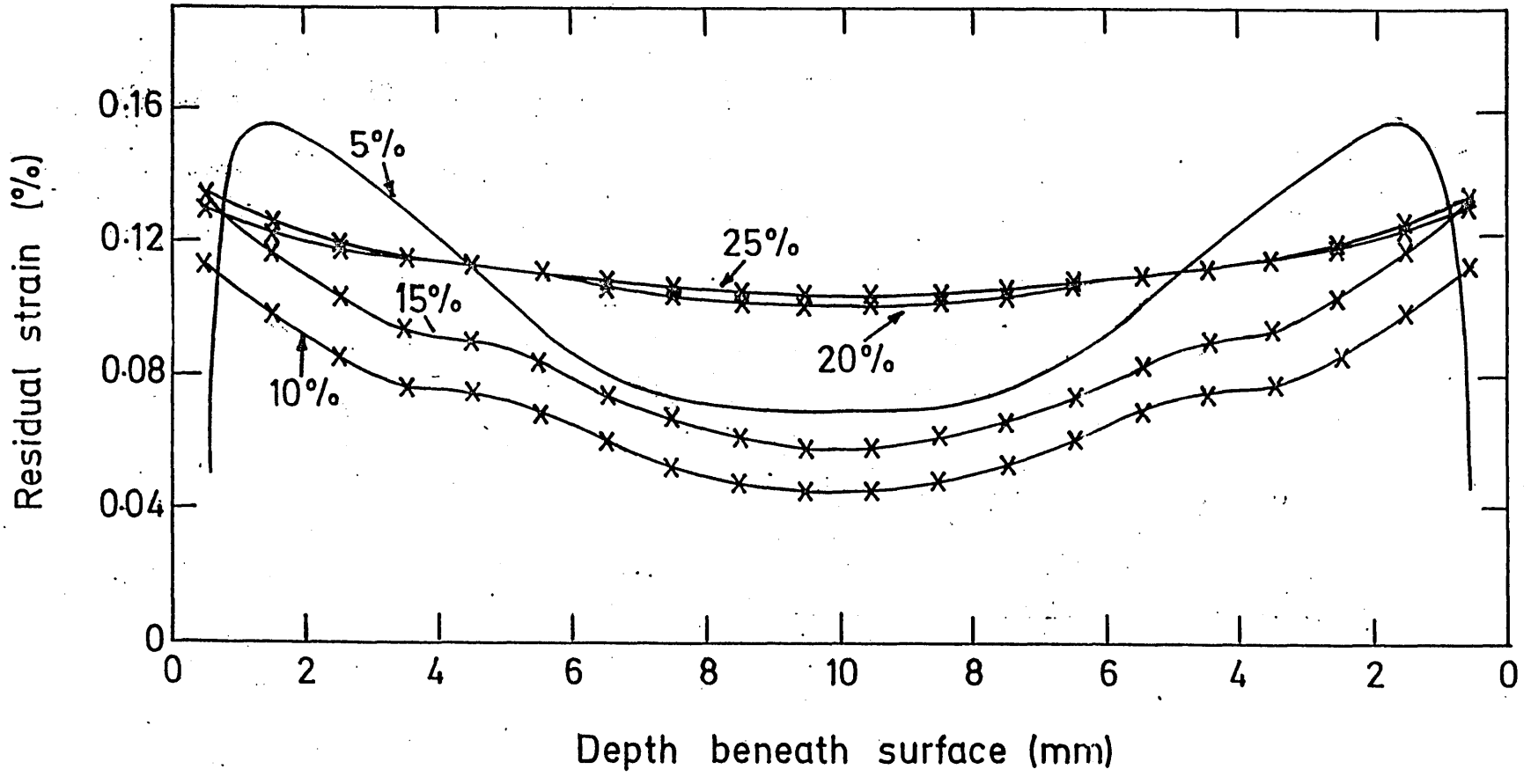
Residual strain (%)
0·16
0·12
0·08
0·04
0
5%
25%
15%
20%
10%
0
2
4
6
8
10
8
6
4
2
0
Depth beneath surface (mm)

FIGURE 58: Calculated residual strains in low alloy steel plates quenched in agitated solutions of sodium polyacrylate. (Figures refer to concentration of Aquaquench ACR).

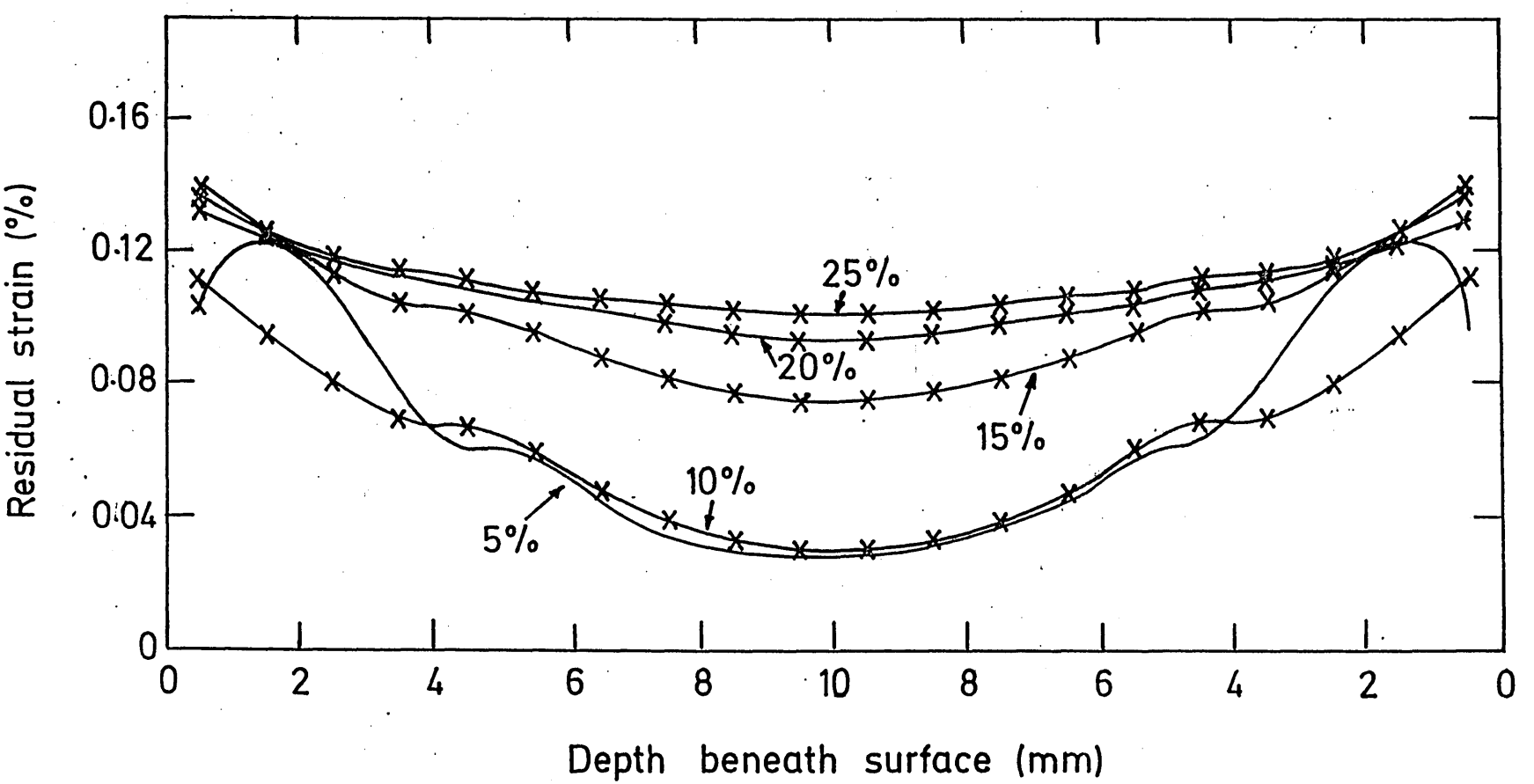
Residual strain (%)
0·16
0·12
0·08
0·04
0
25%
20%
15%
10%
5%
0
2
4
6
8
10
8
6
4
2
0
Depth beneath surface (mm)

FIGURE 59: Comparison of calculated residual strains in low alloy steel plates quenched in water, a medium speed quenching oil, (RDN175), a polyalkylene glycol solution, (25% Aquaquench 1250), and an unagitated solution of 15% Aquaquench ACR.

(a) 25% Aquaquench 1250

(b) 15% Aquaquench ACR

(c) RDN175

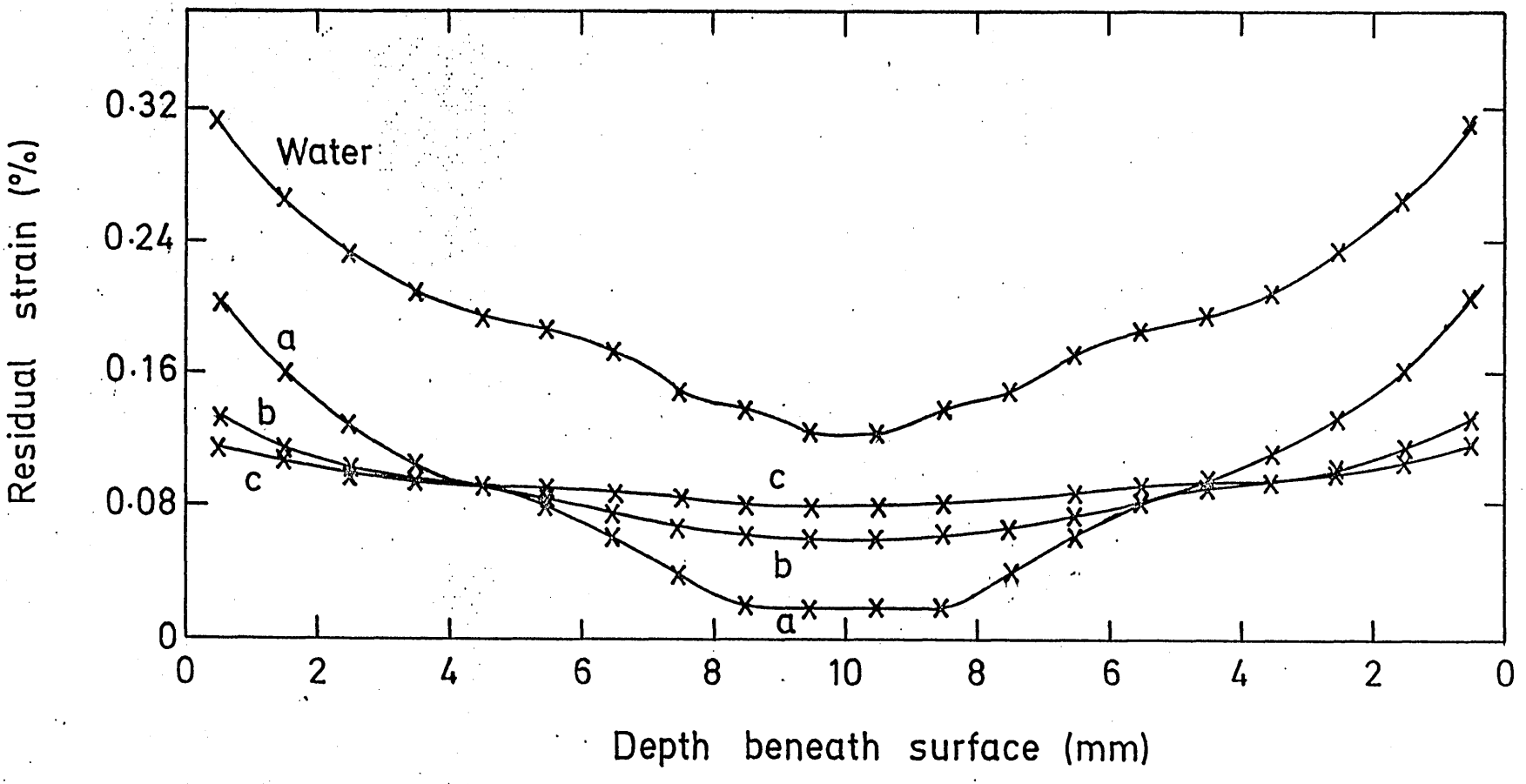
Residual strain (%)
0·32
0·24
0·16
0·08
0
Water
a
b
c
c
b
a
0
2
4
6
8
10
8
6
4
2
0
Depth beneath surface (mm)

FIGURE 60: The calculated relationships between stress and strain during quenching at the surface, (solid line), and centre, (broken line), of a low alloy steel plate quenched in an unagitated solution of 5% Aquaquench ACR. Figures indicate temperatures in ^{o}C.

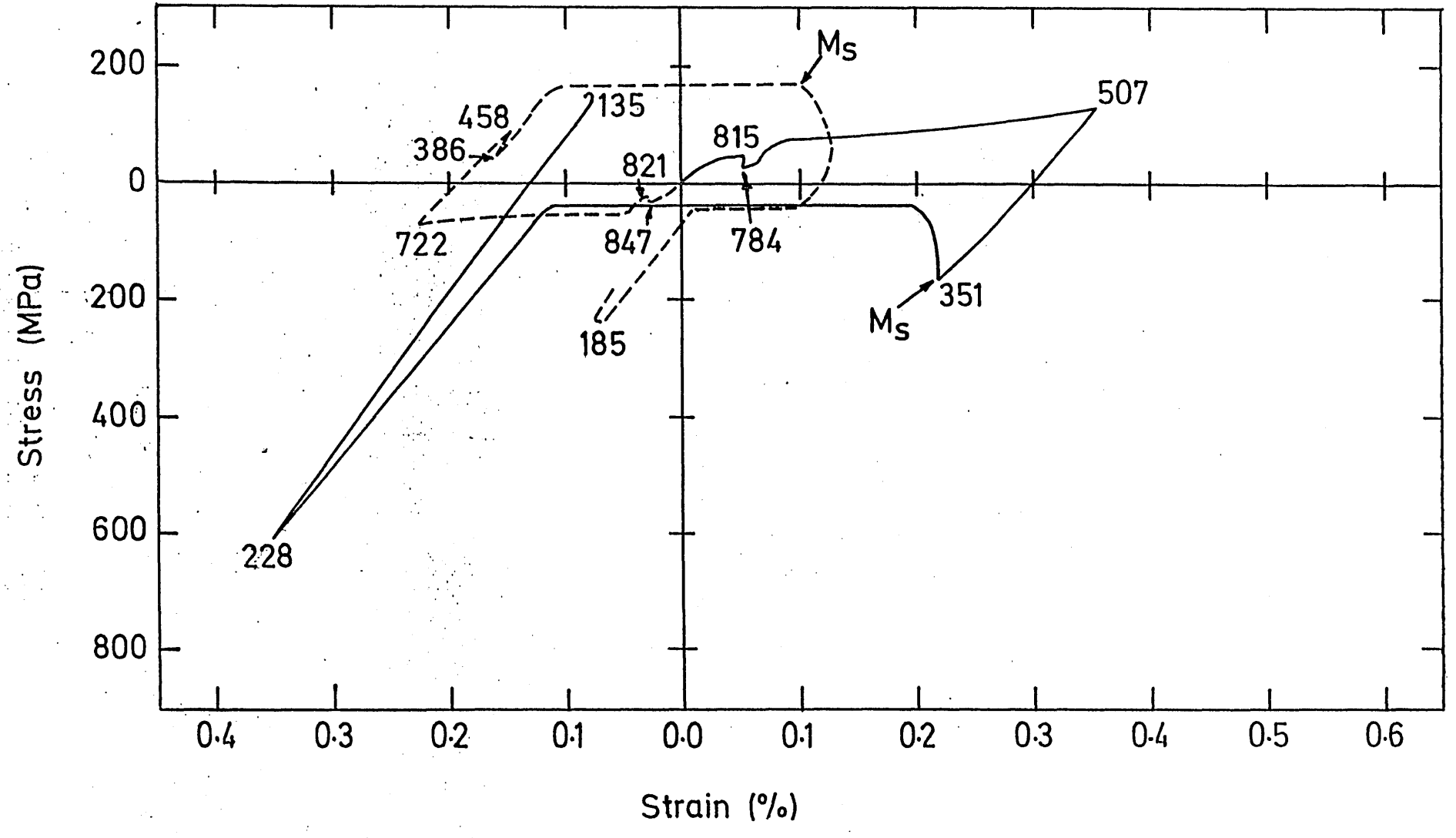
Stress (MPa)
200
0
200
400
600
800
0·4
0·3
0·2
0·1
0·0
0·1
0·2
0·3
0·4
0·5
0·6
Strain (%)
Ms
507
135
458
386
815
821
722
847
784
185
351
Ms
228

FIGURE 61: The calculated relationships between stress and strain during quenching at the surface, (solid line), and centre, (broken line), of a low alloy steel plate quenched in an unagitated solution of 10% Aquaquench ACR. Figures indicate temperatures in ^{o}C.

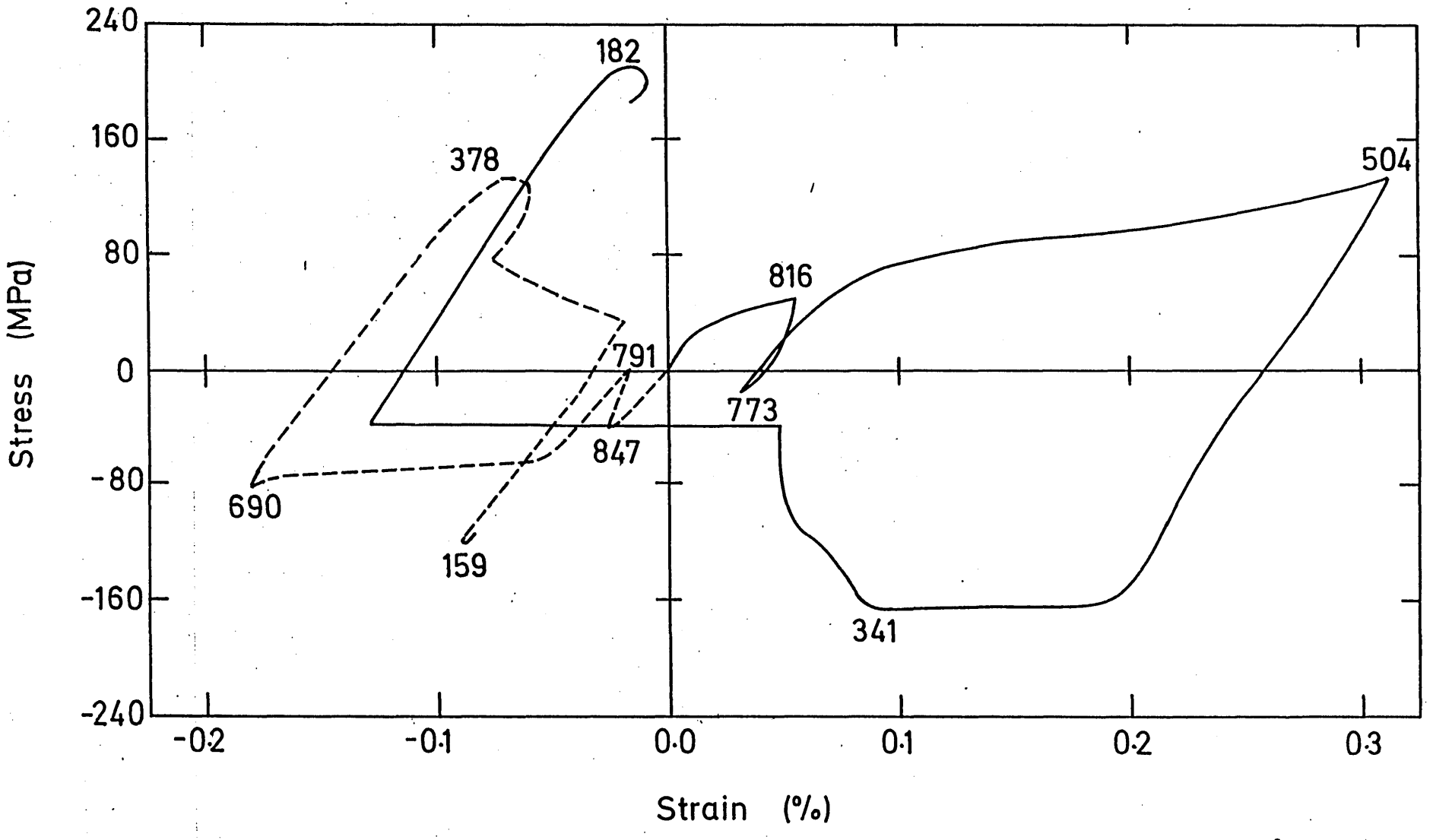
240
160
80
0
-80
-160
-240
Stress (MPa)
-0·2
-0·1
0·0
0·1
0·2
0·3
Strain (%)
182
378
504
816
791
773
847
690
159
341

FIGURE 62: The calculated relationships between stress and strain during quenching at the surface, (solid line), and centre, (broken line), of a low alloy steel plate quenched in an unagitated solution of 15% Aquaquench ACR. Figures indicate temperatures in ^{o}C.

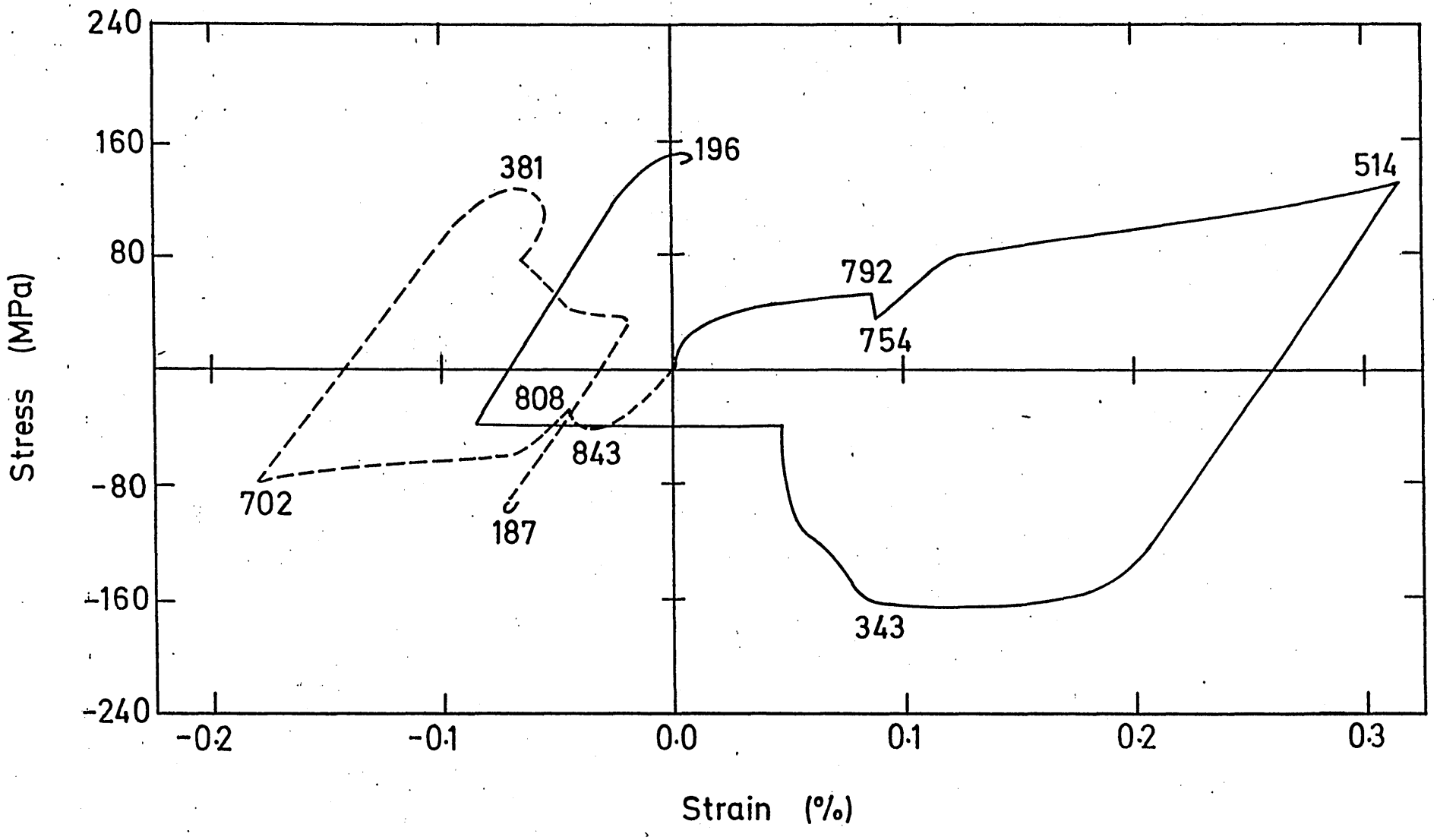
240
160
80
-80
-160
-240
-0·2
-0·1
0·0
0·1
0·2
0·3
Stress (MPa)
Strain (%)
381
196
514
792
754
808
843
702
187
343

FIGURE 63: The calculated relationships between stress and strain during quenching at the surface, (solid line), and centre, (broken line), of a low alloy steel plate quenched in an unagitated solution of 20% Aquaquench ACR. Figures indicate temperatures in ^{o}C.

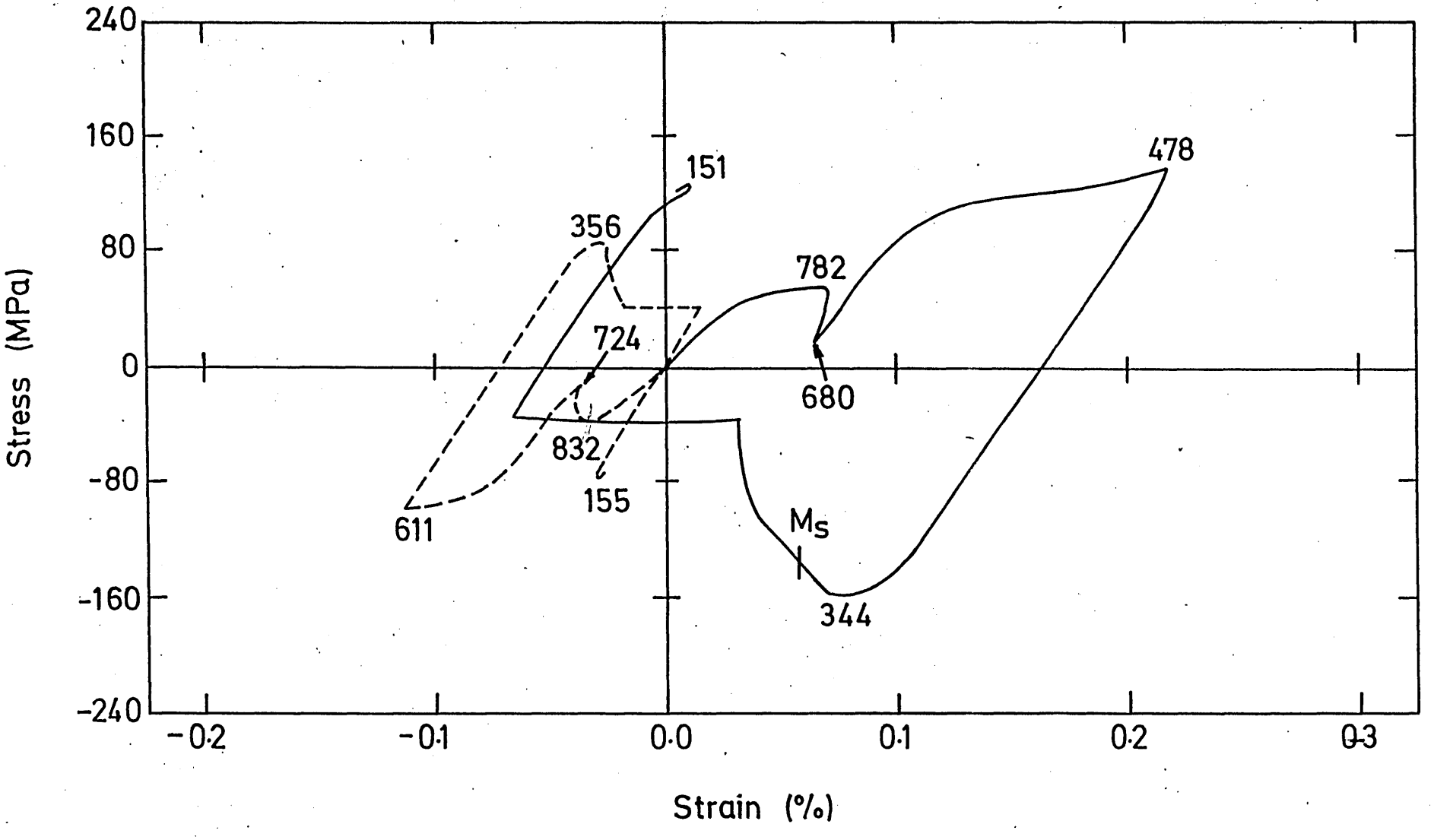
240
160
80
0
-80
-160
-240
-0·2
-0·1
0·0
0·1
0·2
0·3
Stress (MPa)
Strain (%)
151
356
478
782
724
680
832
155
611
Ms
344

FIGURE 64: The calculated relationships between stress and strain during quenching at the surface, (solid line), and centre, (broken line), of a low alloy steel plate quenched in an unagitated solution of 25% Aquaquench ACR. Figures indicate temperatures in ^{o}C.

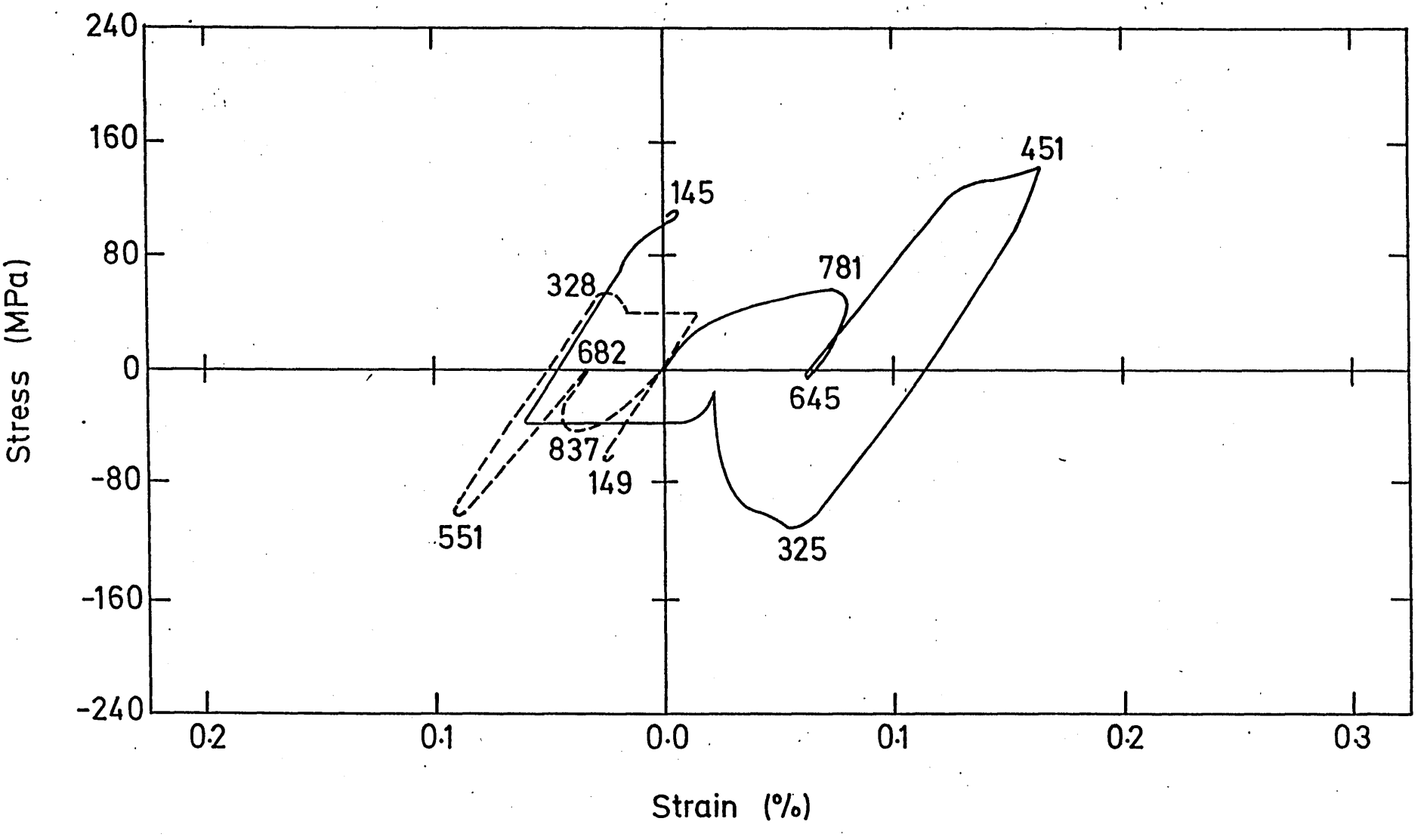
240
160
80
0
-80
-160
-240
Stress (MPa)
0·2
0·1
0·0
0·1
0·2
0·3
Strain (%)
145
451
328
781
682
645
837
149
551
325

FIGURE 65: The calculated relationships between stress and strain during quenching at the surface, (solid line), and centre, (broken line), of a low steel plate quenched in an agitated solution of 5% Aquaquench ACR. Figures indicate temperatures in ^{o}C.

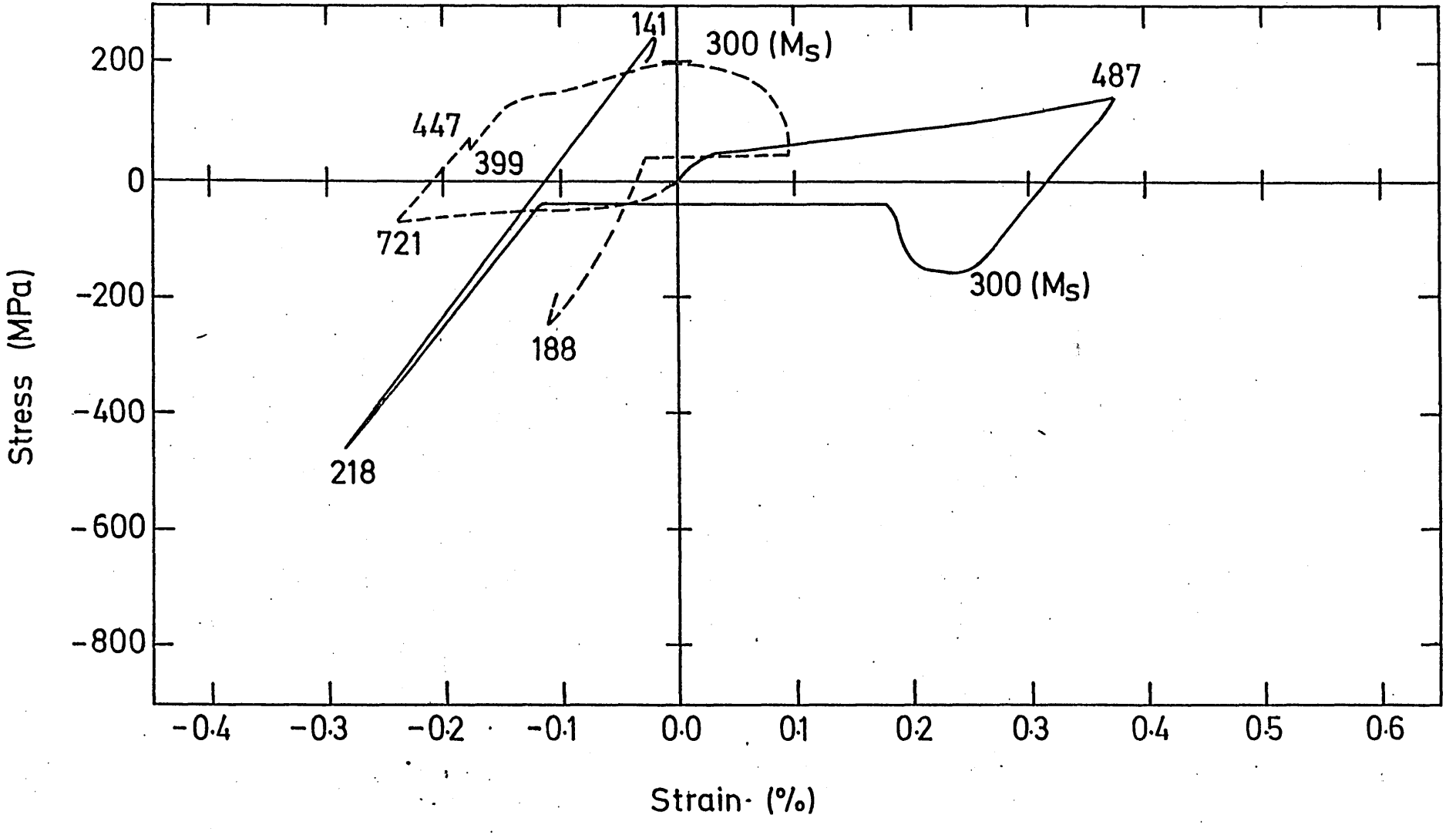
141
300 (Ms)
487
447
399
721
188
218
300 (Ms)
200
0
-200
-400
-600
-800
-0·4
-0·3
-0·2
-0·1
0·0
0·1
0·2
0·3
0·4
0·5
0·6
Stress (MPa)
Strain· (%)

FIGURE 66: The calculated relationships between stress and strain during quenching at the surface, (solid line), and centre, (broken line), of a low alloy steel plate quenched in an agitated solution of 10% Aquaquench ACR. Figures indicate temperatures in ^{o}C.

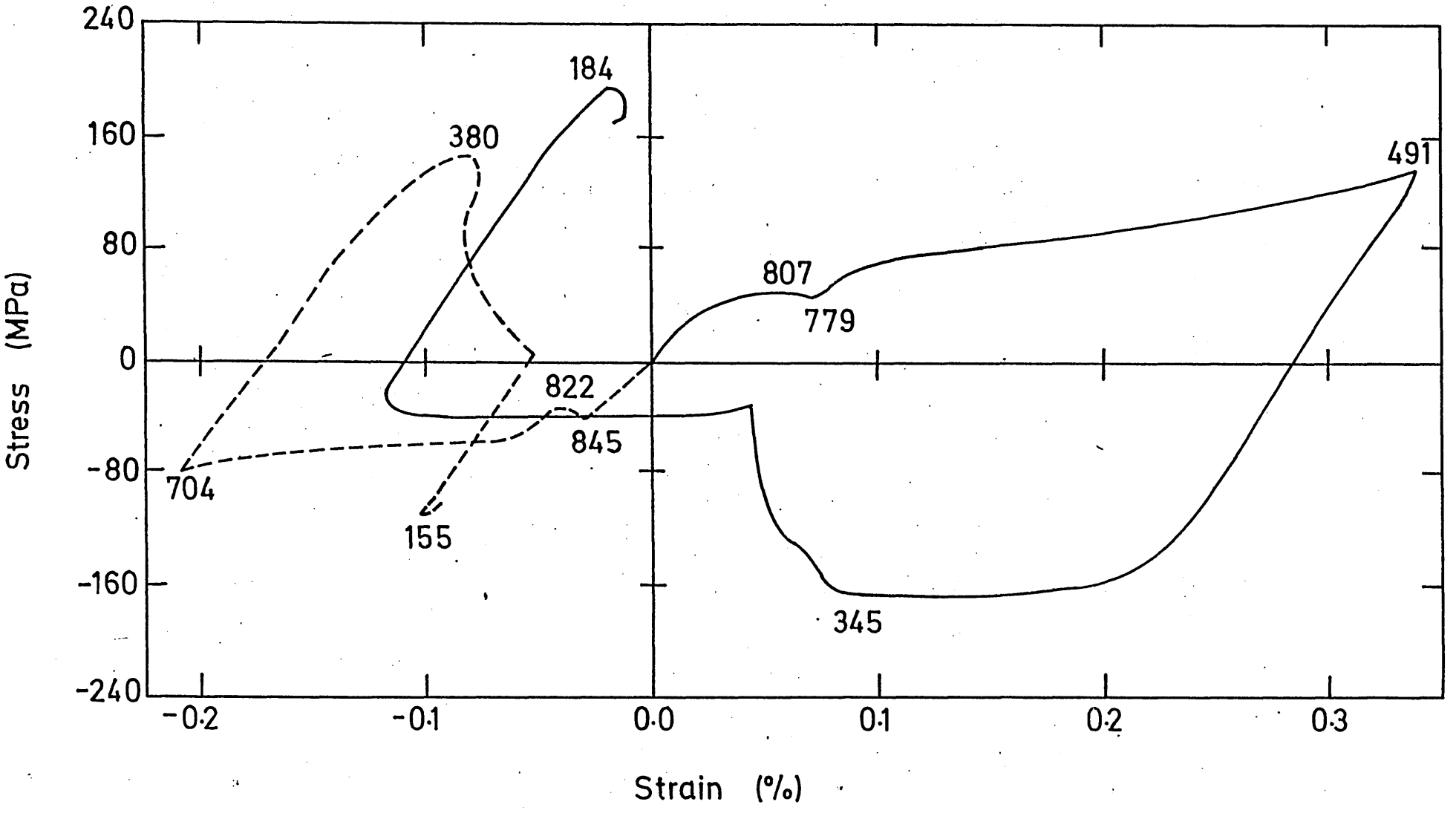
240
160
80
0
-80
-160
-240
Stress (MPa)
-0·2
-0·1
0·0
0·1
0·2
0·3
Strain (%)
184
380
491
807
779
822
845
704
155
345

FIGURE 67: The calculated relationships between stress and strain during quenching at the surface, (solid line), and centre, (broken line), of a low alloy steel plate quenched in an agitated solution of 15% Aquaquench ACR. Figures indicate temperatures in ^{o}C.

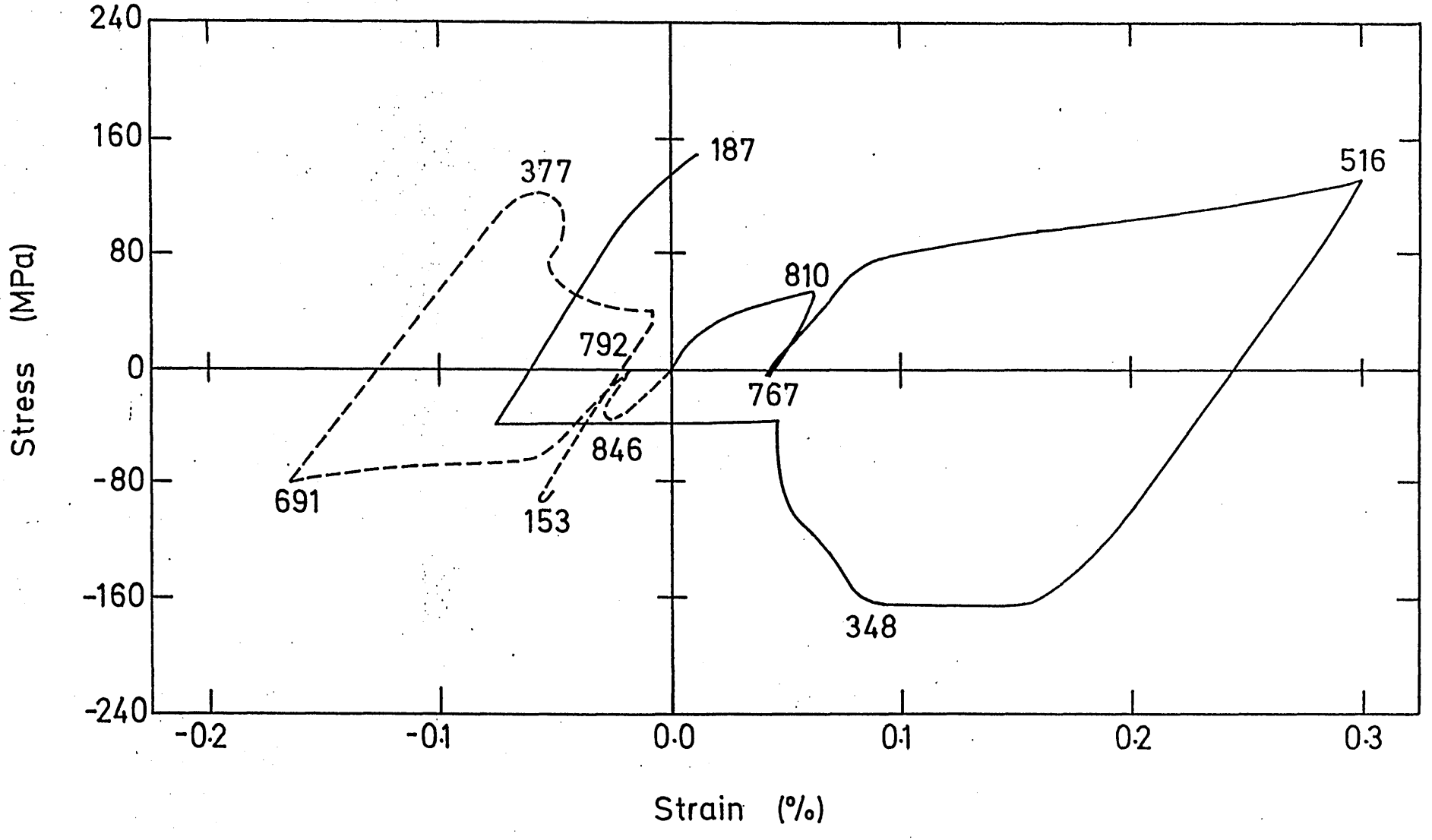
240
160
80
0
-80
-160
-240
-0·2
-0·1
0·0
0·1
0·2
0·3
Stress (MPa)
Strain (%)
187
377
516
810
792
767
846
691
153
348

FIGURE 68: The calculated relationships between stress and strain during quenching at the surface, (solid line), and centre, (broken line), of a low alloy steel plate quenched in an agitated solution of 20% Aquaquench ACR. Figures indicate temperatures in ^{o}C.

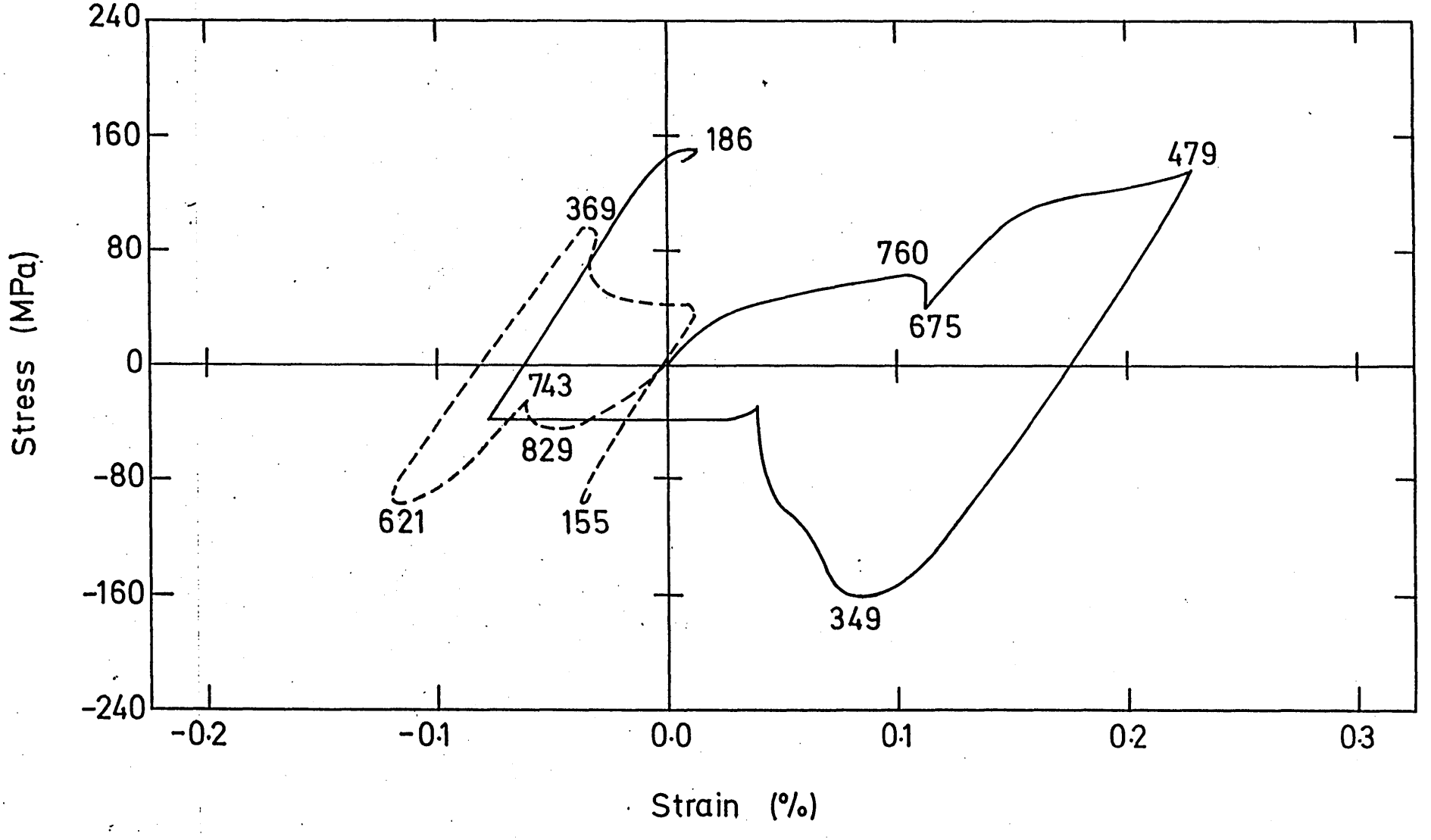
240
160
80
0
-80
-160
-240
-0·2
-0·1
0·0
0·1
0·2
0·3
Stress (MPa)
Strain (%)
186
369
760
479
675
743
829
621
155
349

FIGURE 69: The calculated relationships between stress and strain during quenching at the surface, (solid line), and centre, (broken line), of a low alloy steel plate quenched in an agitated solution of 25% Aquaquench ACR. Figures indicate temperatures in ^{o}C.

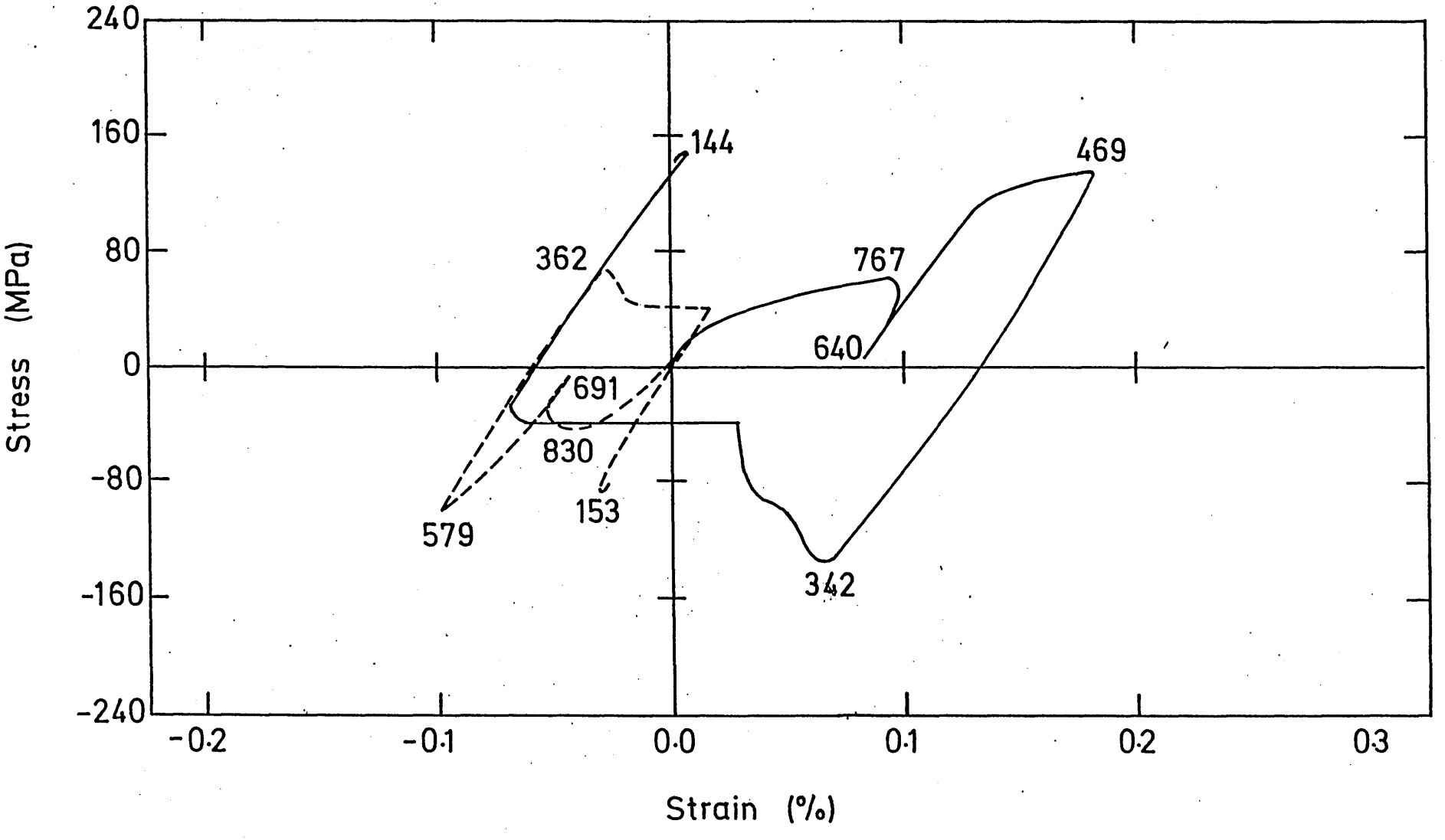
240
160
80
0
-80
-160
-240
-0·2
-0·1
0·0
0·1
0·2
0·3
Stress (MPa)
Strain (%)
144
469
362
767
640
691
830
153
579
342

FIGURE 70: The calculated relationships between stress and strain during quenching at the surface, (solid line), and centre, (broken line), of a low alloy steel plate quenched in water.

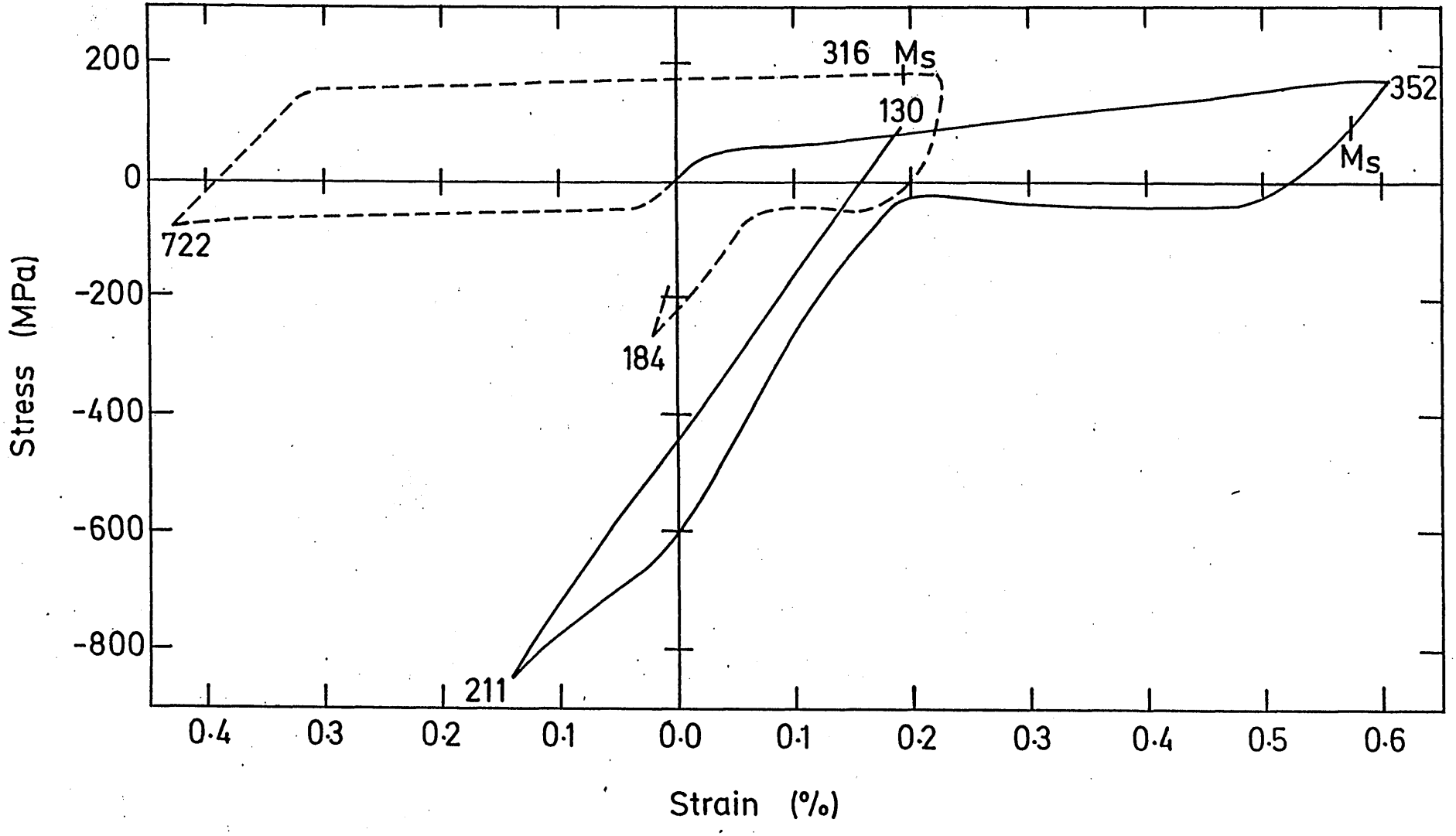
200
0
-200
-400
-600
-800
Stress (MPa)
316 Ms
130
352
Ms
722
184
211
0·4
0·3
0·2
0·1
0·0
0·1
0·2
0·3
0·4
0·5
0·6
Strain (%)

FIGURE 71: The calculated relationships between stress and strain during quenching at the surface, (solid line), and centre, (broken line), of a low alloy steel plate quenched in a medium speed quenching oil, (RDN175).

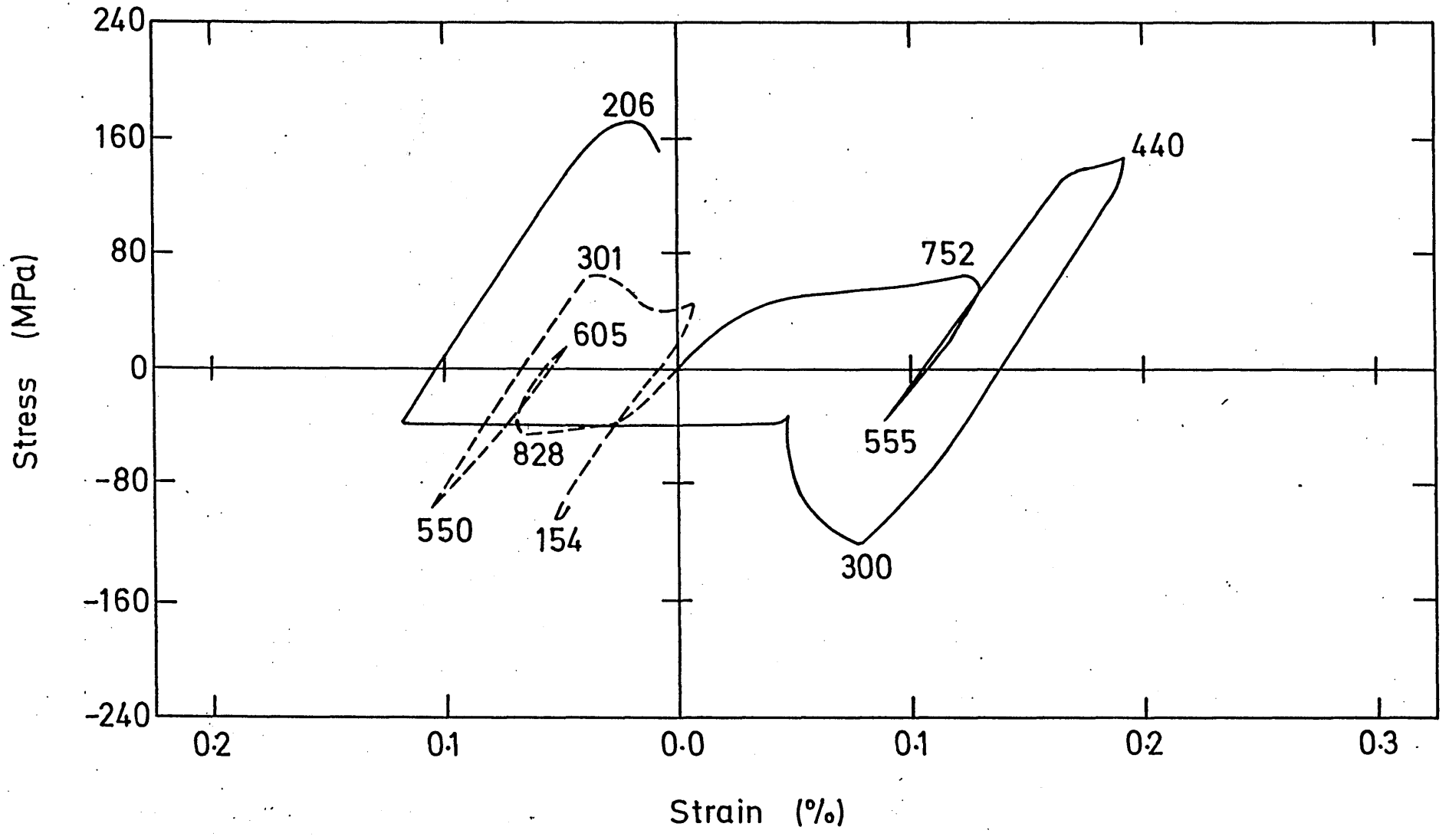
240
160
80
0
-80
-160
-240
Stress (MPa)
206
440
301
752
605
828
555
550
154
300
0·2
0·1
0·0
0·1
0·2
0·3
Strain (%)

FIGURE 72: The calculated relationships between stress and strain during quenching at the surface, (solid line), and centre, (broken line), of a low alloy steel plate quenched in a polyalkylene glycol solution, (25% Aquaquench 1250).

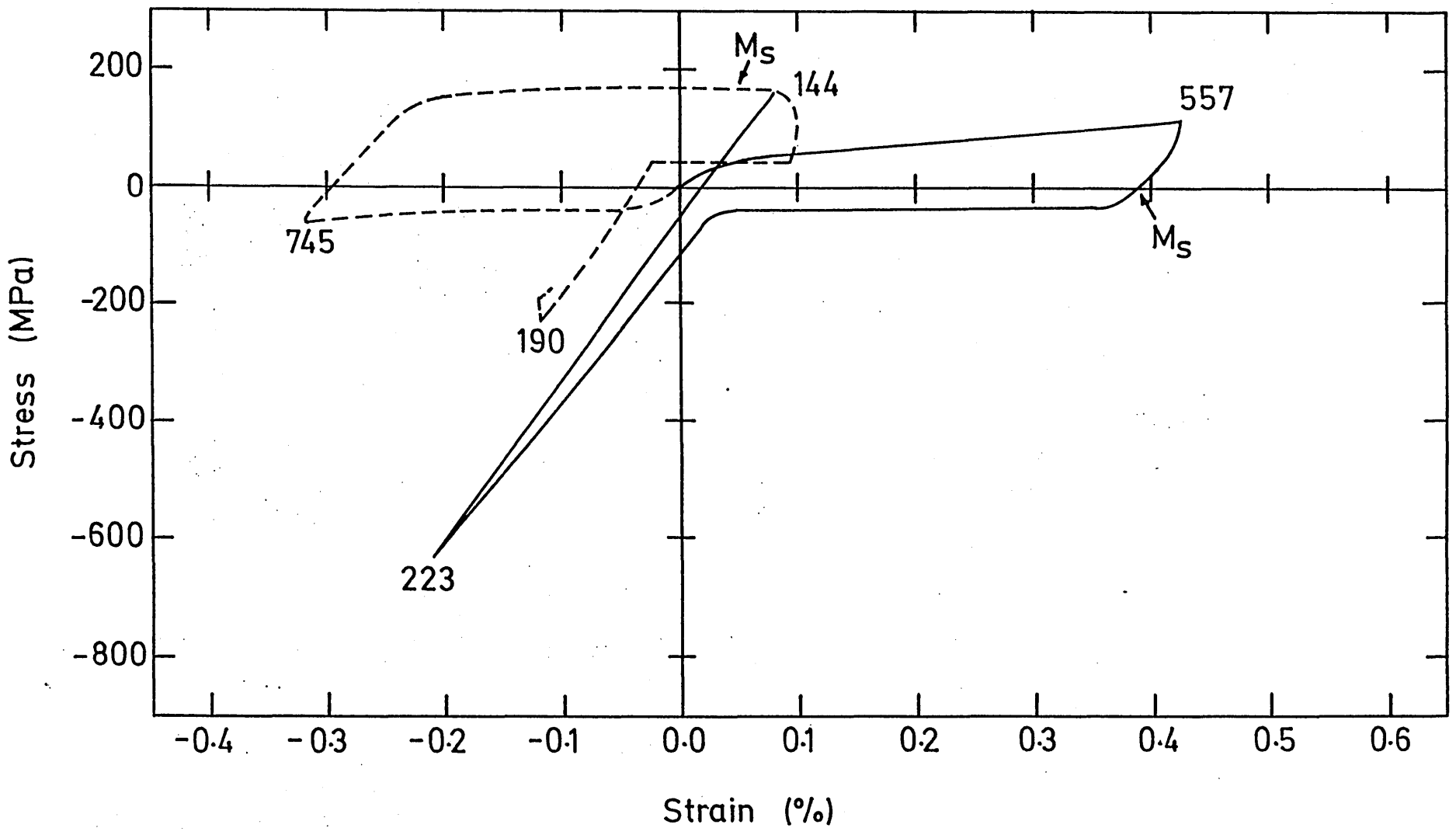
200
0
-200
-400
-600
-800
Stress (MPa)
-0·4
-0·3
-0·2
-0·1
0·0
0·1
0·2
0·3
0·4
0·5
0·6
Strain (%)
Ms
144
557
745
190
223
Ms

FIGURE 73: Comparison of calculated and experimentally measured residual stresses in a low alloy steel plate quenched in an unagitated solution of 15% Aquaquench ACR, (uninsulated edge).

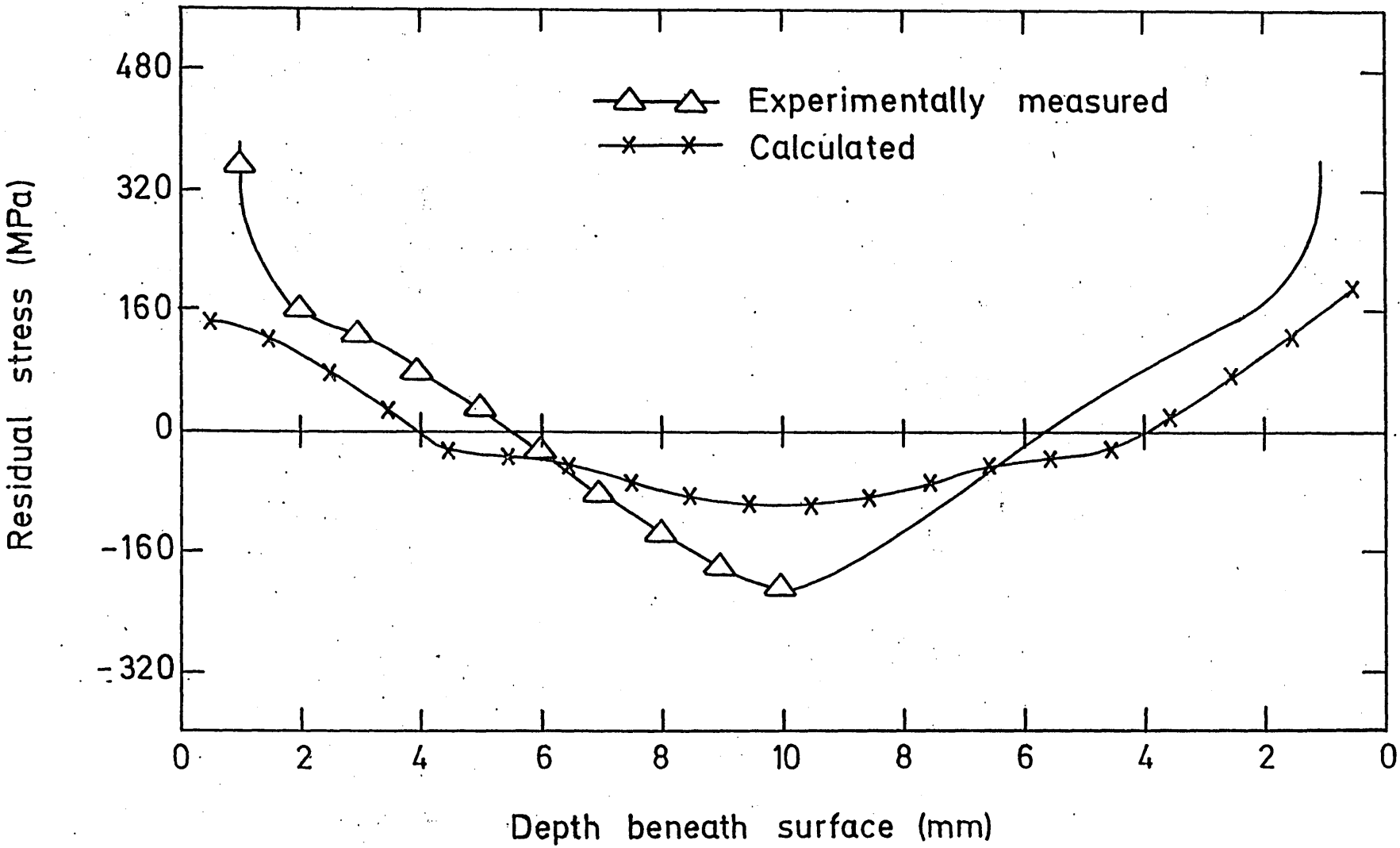
480
320
160
0
-160
-320
Residual stress (MPa)
Experimentally measured
Calculated
0
2
4
6
8
10
8
6
4
2
0
Depth beneath surface (mm)

FIGURE 74: Comparison of calculated and experimentally measured residual stresses in a low alloy steel plate quenched in an unagitated solution of 25% Aquaquench ACR, (uninsulated edge).

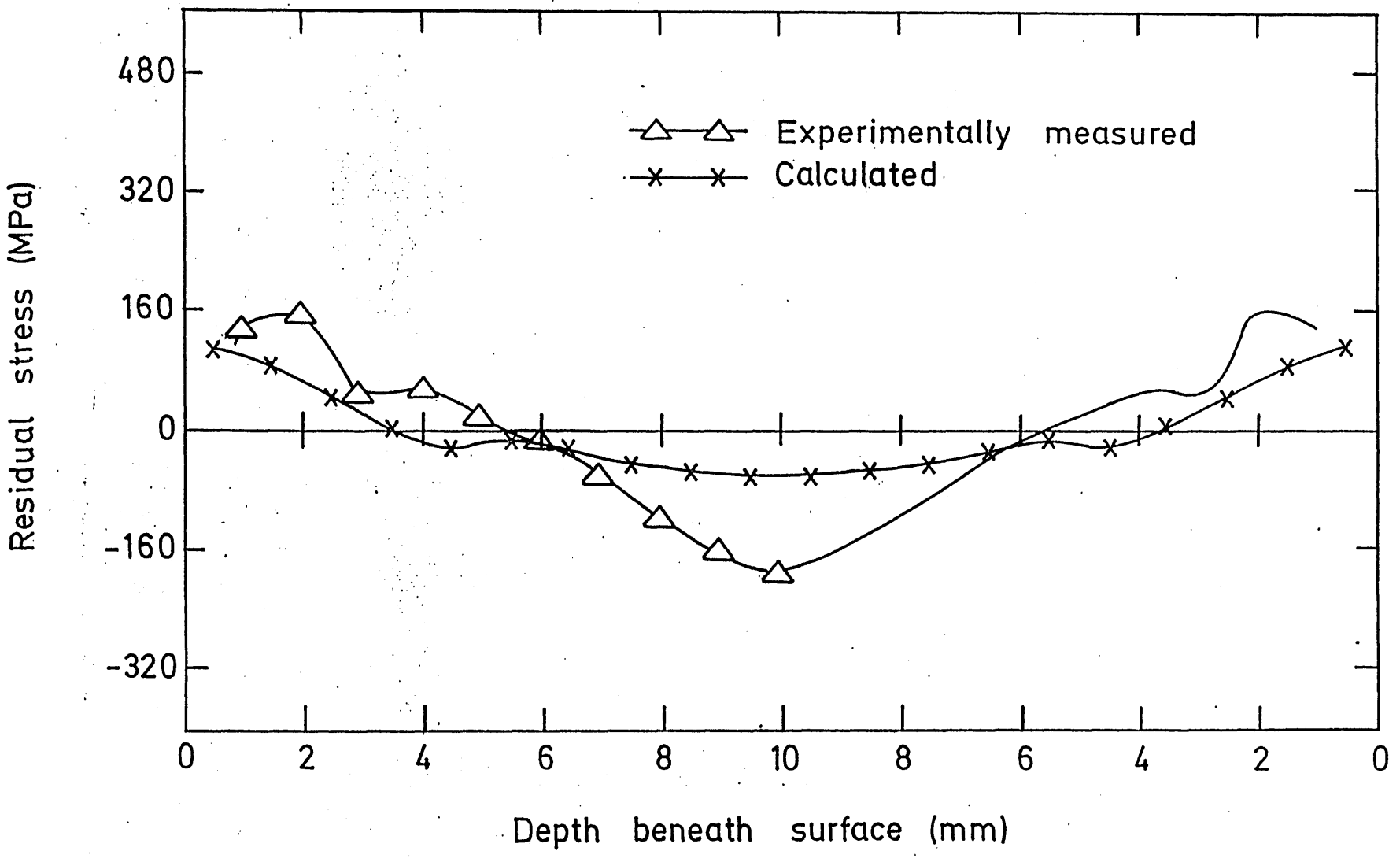
480
320
160
0
-160
-320
Residual stress (MPa)
Experimentally measured
Calculated
0
2
4
6
8
10
8
6
4
2
0
Depth beneath surface (mm)

FIGURE 75: Comparison of calculated and experimentally measured residual stresses in low alloy steel plates quenched in unagitated solutions of 5% Aquaquench ACR, (insulated edge).

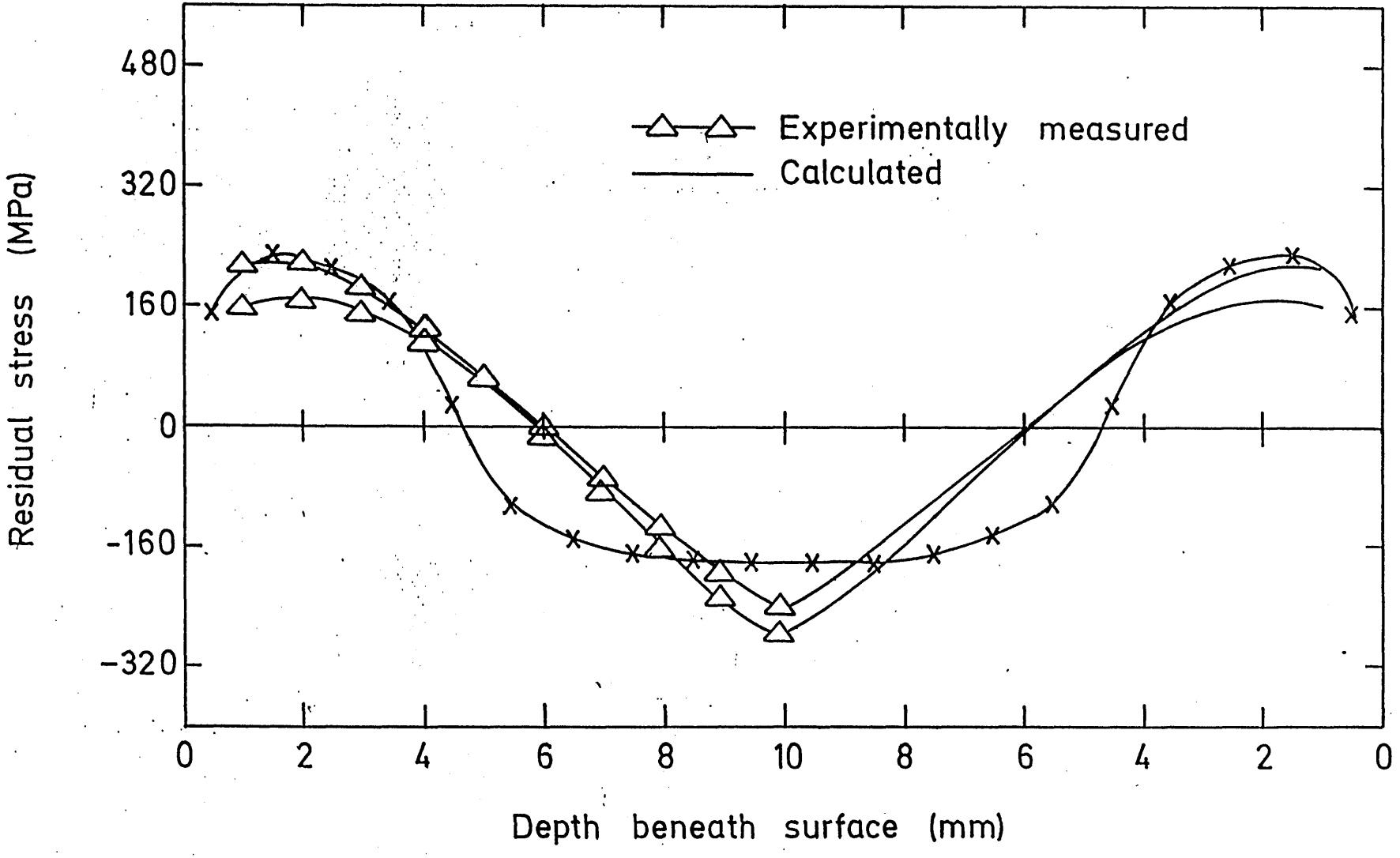
480
320
160
0
-160
-320
Residual stress (MPa)
Experimentally measured
Calculated
0
2
4
6
8
10
8
6
4
2
0
Depth beneath surface (mm)

FIGURE 76: Comparison of calculated and experimentally measured residual stresses in low alloy steel plates quenched in unagitated solutions of 15% Aquaquench ACR, (insulated edge).

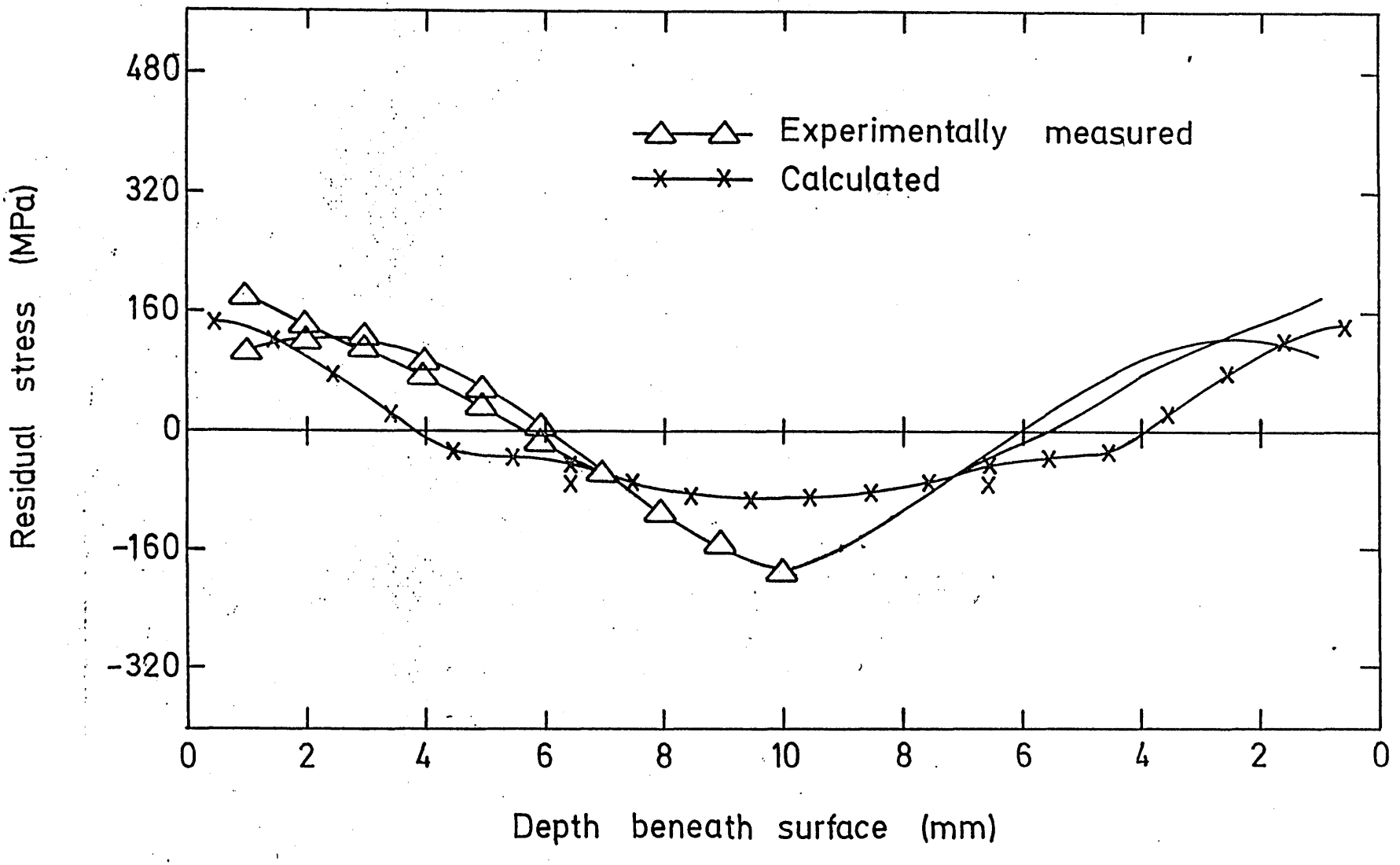
480
320
160
0
-160
-320
Residual stress (MPa)
Experimentally measured
Calculated
0
2
4
6
8
10
8
6
4
2
0
Depth beneath surface (mm)

FIGURE 77: Comparison of calculated and experimentally measured residual stresses in low alloy steel plates quenched in unagitated solutions of 25% Aquaquench ACR, (insulated edge).

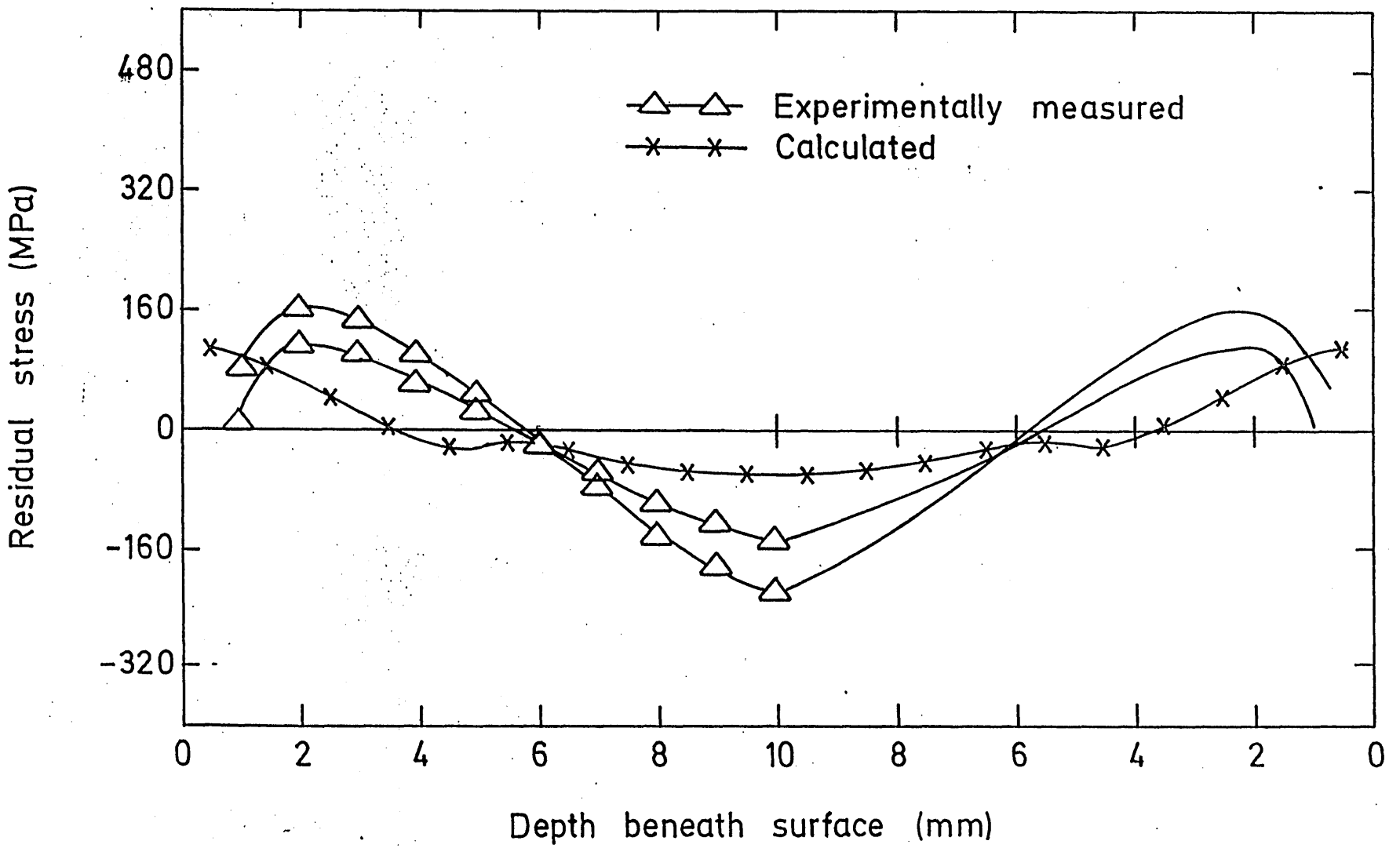
Experimentally measured
Calculated
Residual stress (MPa)
480
320
160
0
-160
-320
0
2
4
6
8
10
8
6
4
2
0
Depth beneath surface (mm)

FIGURE 78: Comparison of calculated and experimentally measured residual strains in a low alloy steel plate quenched in an unagitated solution of 15% Aquaquench ACR, (uninsulated edge).

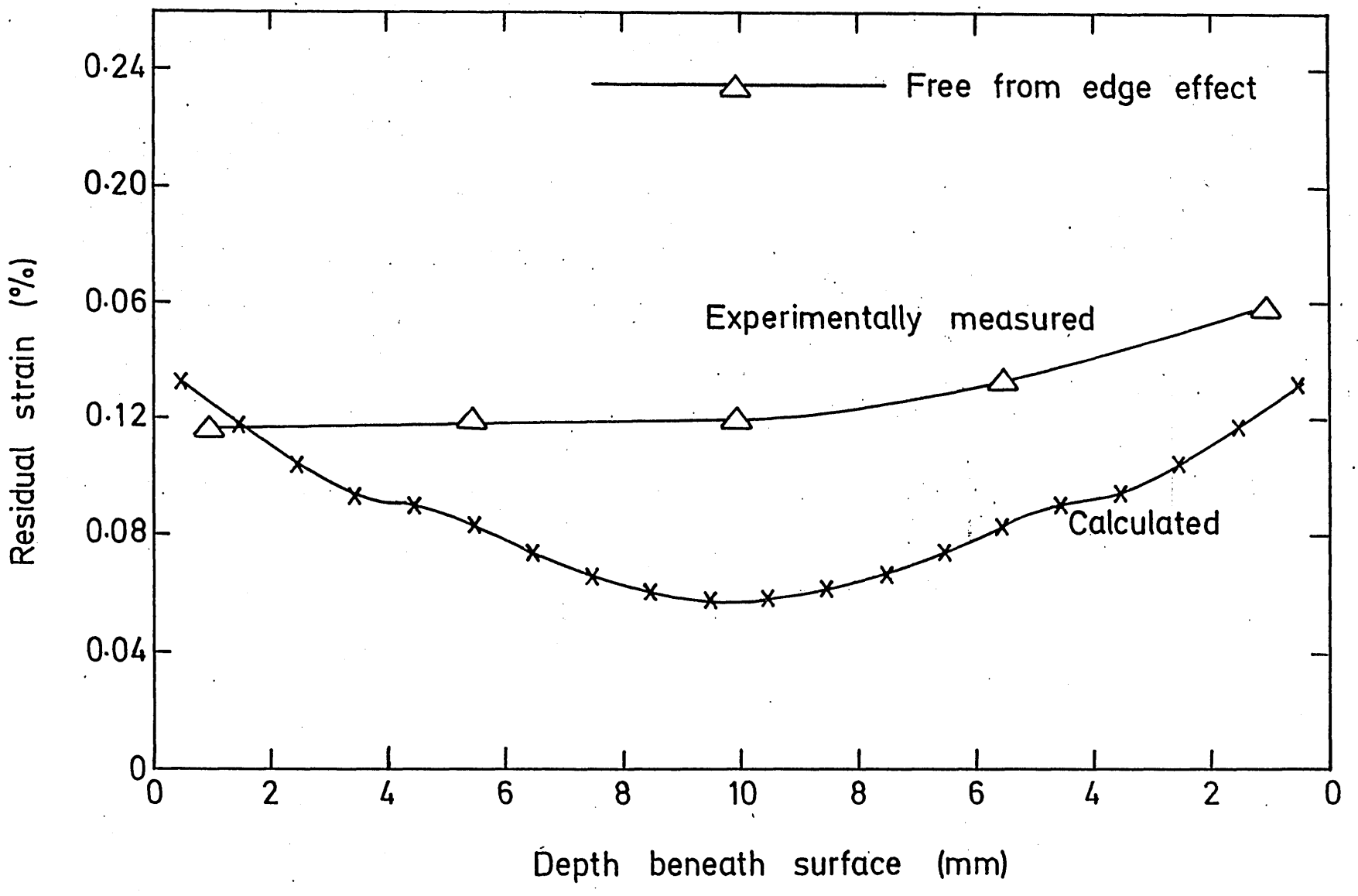
Free from edge effect
Experimentally measured
Calculated
Residual strain (%)
0·24
0·20
0·06
0·12
0·08
0·04
0
0 2 4 6 8 10 8 6 4 2 0
Depth beneath surface (mm)

FIGURE 79: Comparison of mean values of the calculated and experimentally measured residual strains in low alloy steel plates quenched in a range of unagitated sodium polyacrylate solutions.

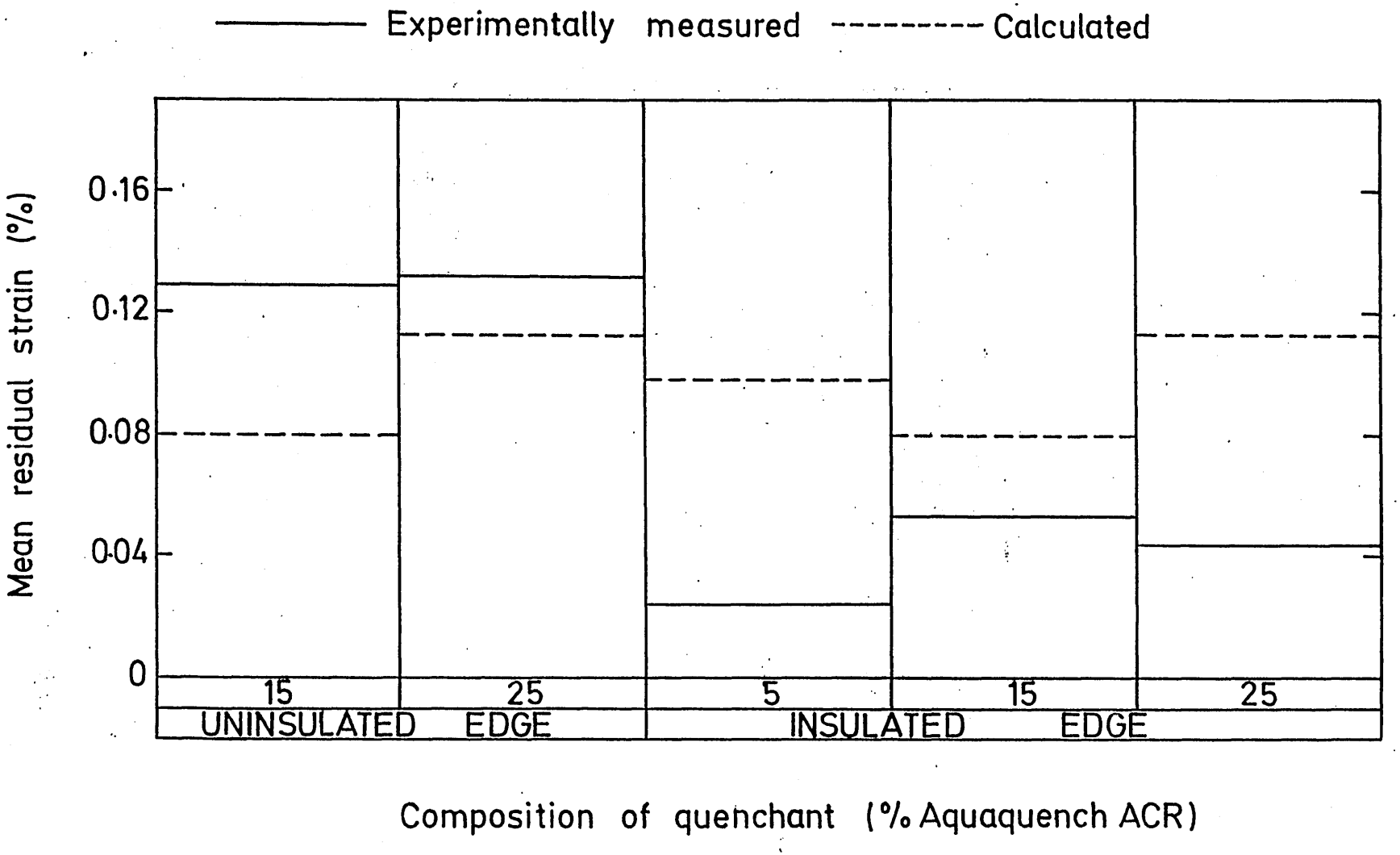
Experimentally measured
Calculated
Mean residual strain (%)
0·16
0·12
0·08
0·04
0
15
25
5
15
25
UNINSULATED EDGE
INSULATED EDGE
Composition of quenchant (% Aquaquench ACR)

FIGURE 80: Comparison of calculated and experimentally measured residual strains in low alloy steel plates quenched in unagitated solutions of 5% Aquaquench ACR, (insulated edge).

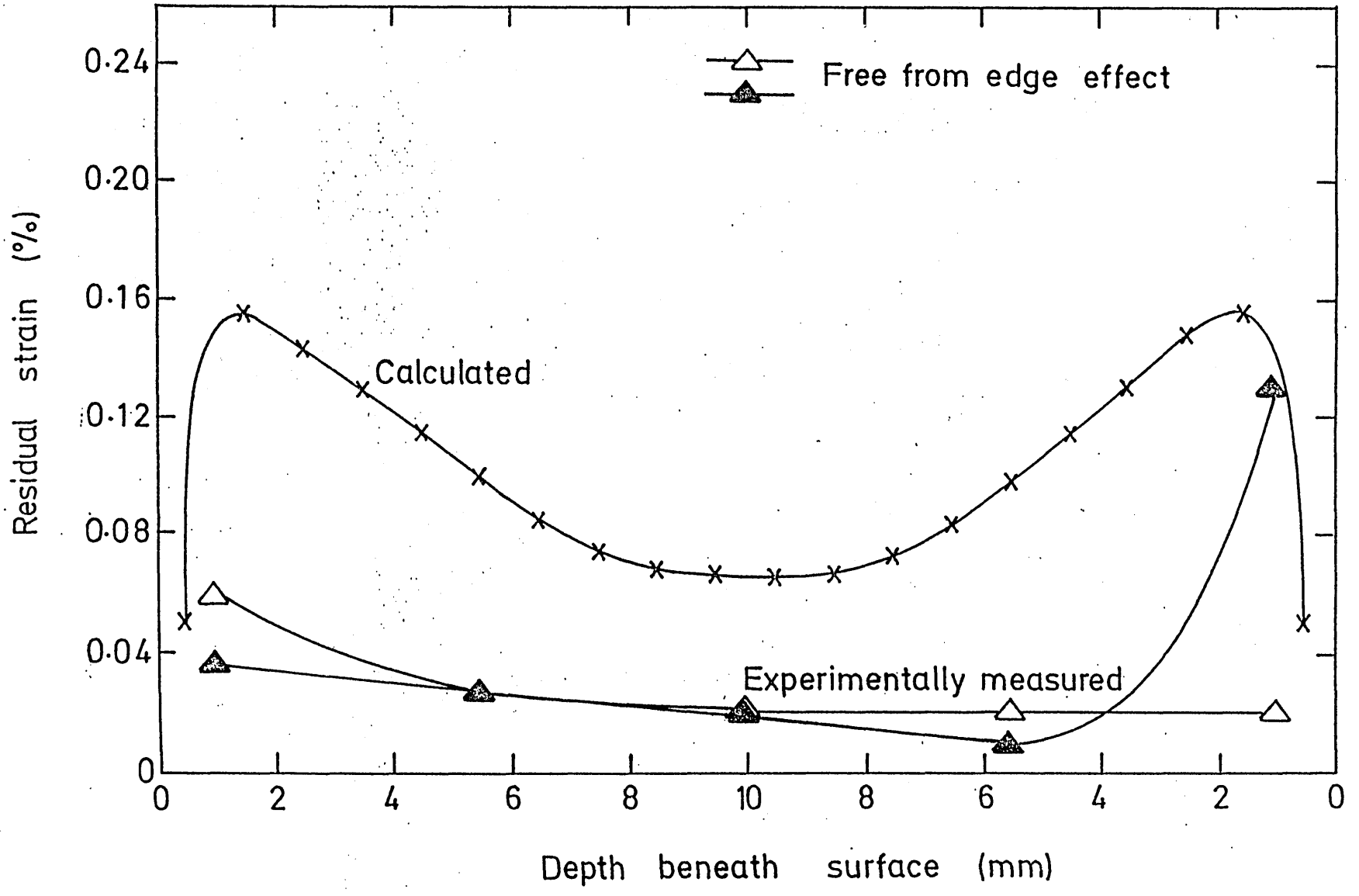
Free from edge effect
Calculated
Experimentally measured
Residual strain (%)
0·24
0·20
0·16
0·12
0·08
0·04
0
0
2
4
6
8
10
8
6
4
2
0
Depth beneath surface (mm)

FIGURE 81: Comparison of calculated and experimentally measured residual strains in low alloy steel plates quenched in unagitated solutions of 15% Aquaquench ACR, (insulated edge).

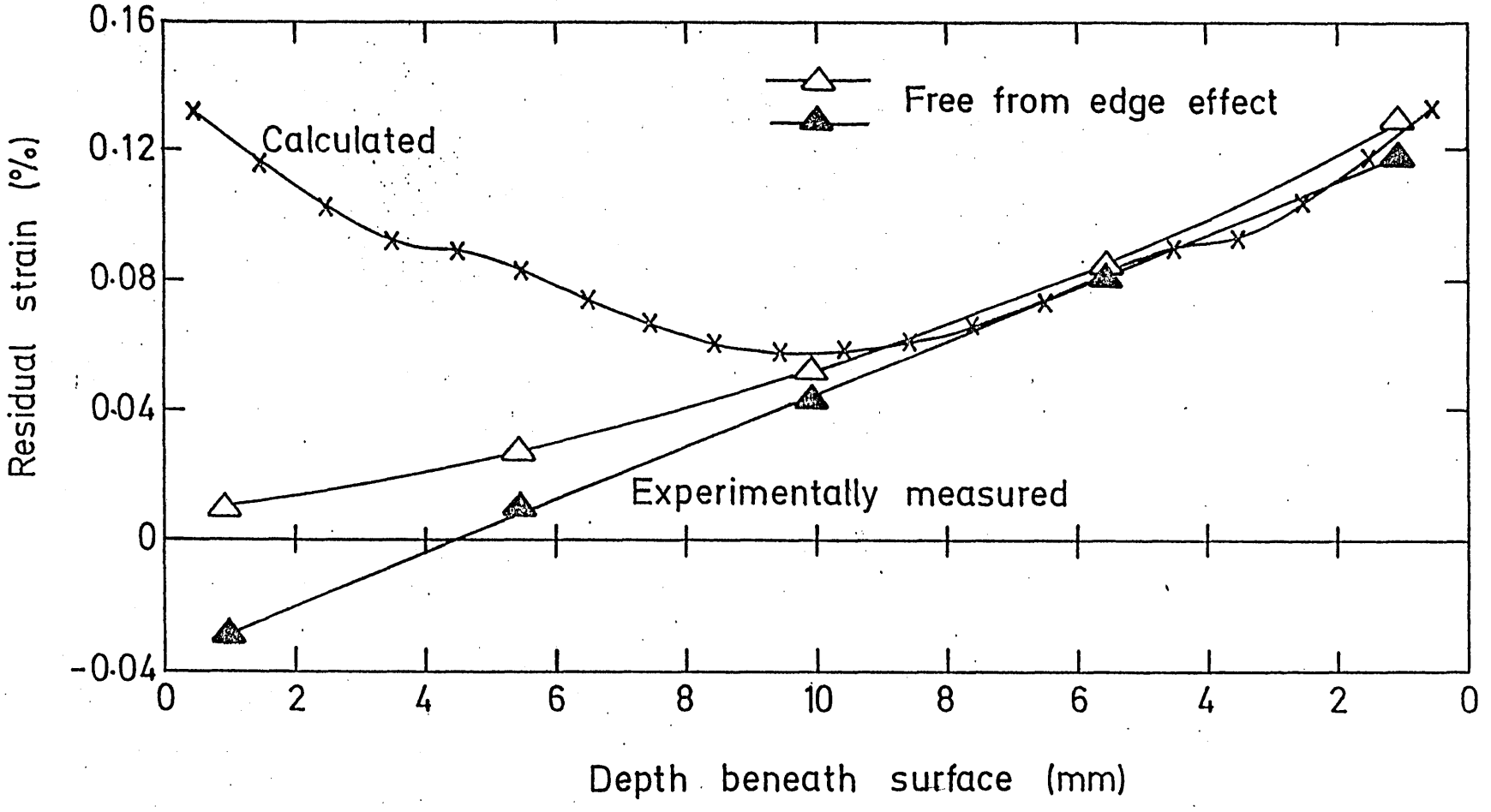
0·16
0·12
0·08
0·04
0
-0·04
Residual strain (%)
Calculated
Free from edge effect
Experimentally measured
0
2
4
6
8
10
8
6
4
2
0
Depth beneath surface (mm)

FIGURE 82: Comparison of calculated and experimentally measured residual strains in a low alloy steel plate quenched in an unagitated solution of 25% Aquaquench ACR, (insulated edge).

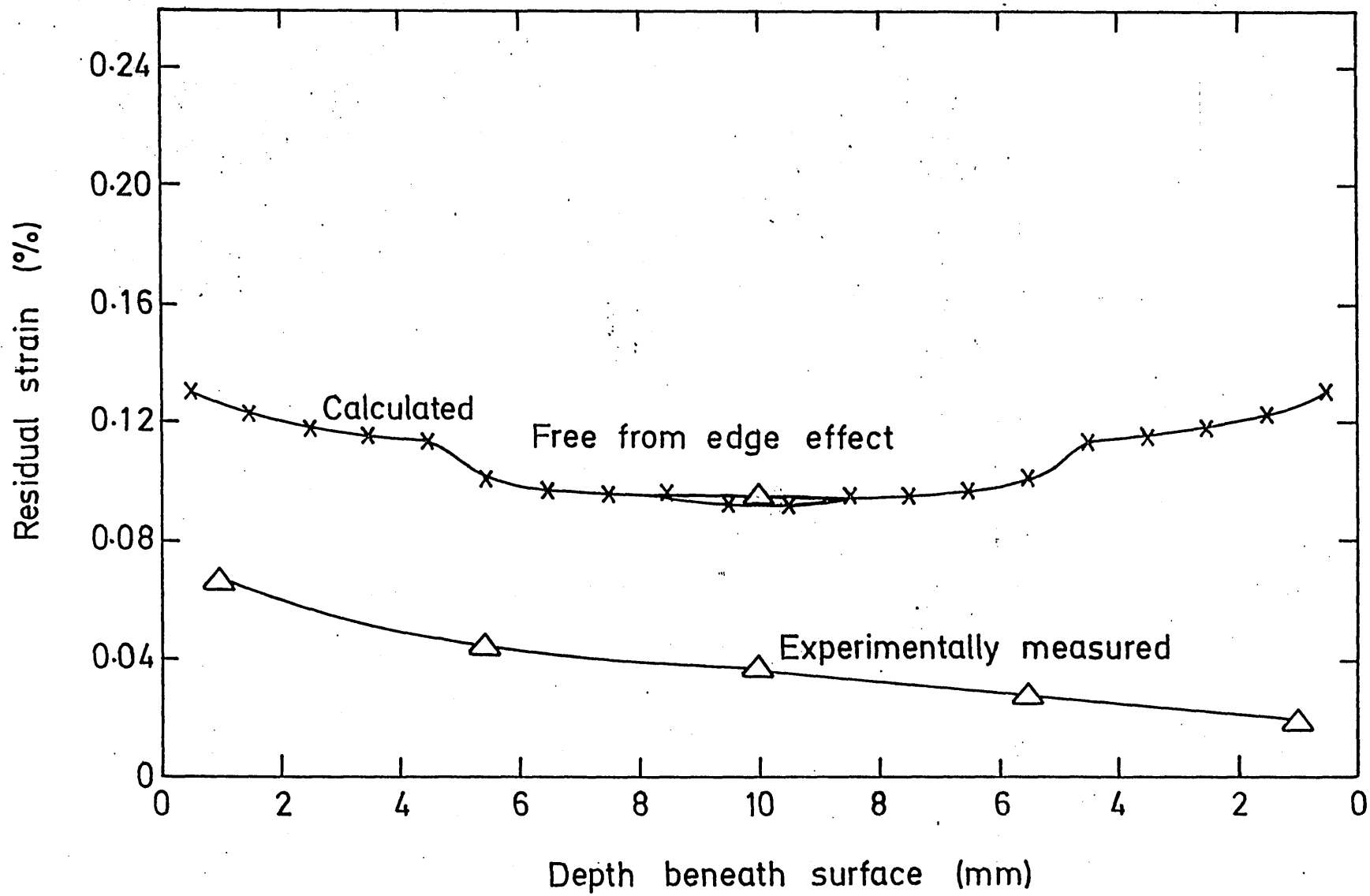
0·24
0·20
0·16
0·12
0·08
0·04
0
Residual strain (%)
Calculated
Free from edge effect
Experimentally measured
0
2
4
6
8
10
8
6
4
2
0
Depth beneath surface (mm)

FIGURE 83: Experimentally measured relationships between kinematic viscosity and solution temperature in sodium polyacrylate solutions. Figures refer to concentration of Aquaquench ACR.

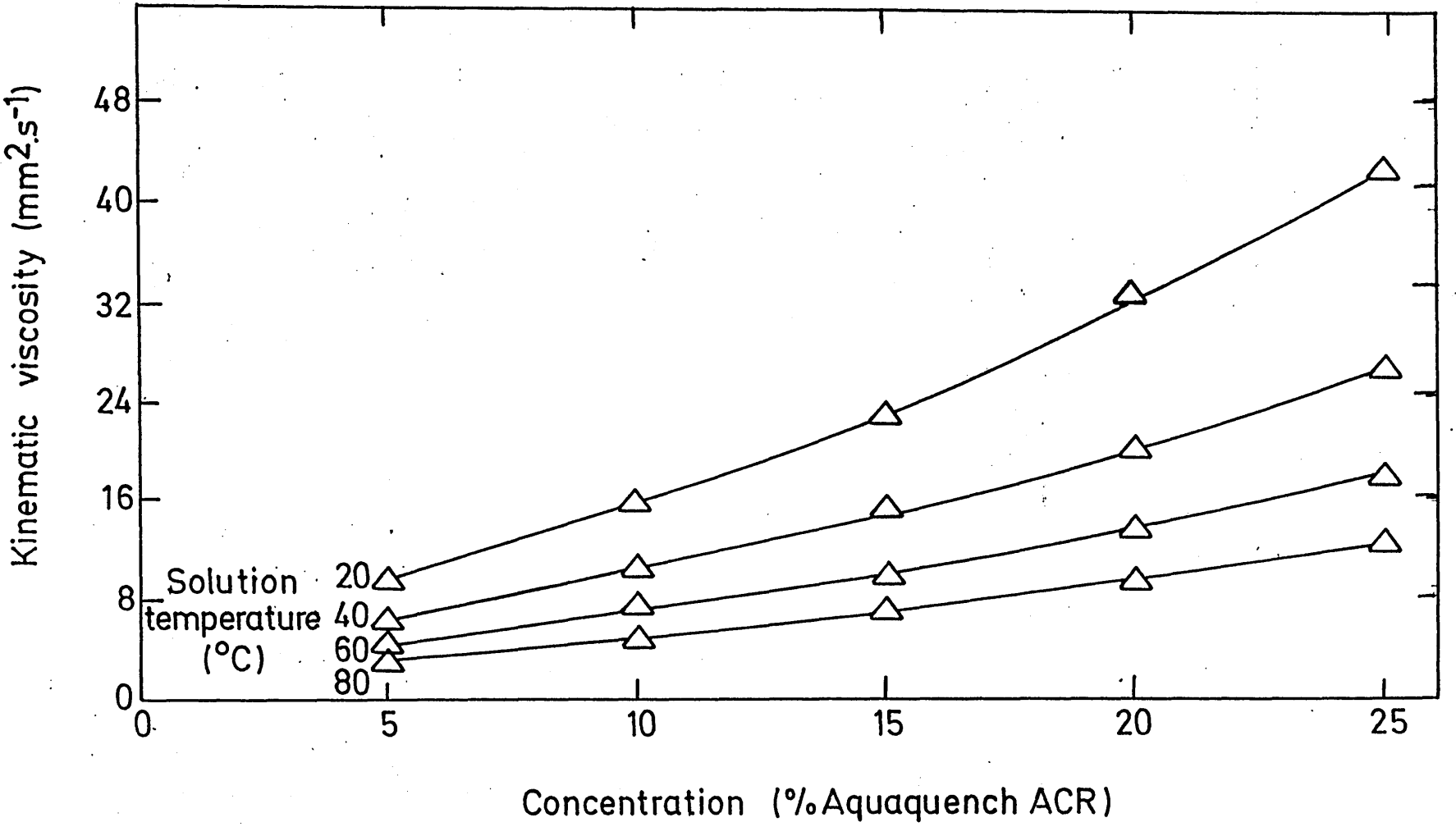
Kinematic viscosity (mm2.s-1)
48
40
32
24
16
8
0
0
5
10
15
20
25
Solution temperature (°C)
20
40
60
80
Concentration (% Aquaquench ACR)

FIGURE 84: Experimentally measured relationships between surface tension and solution temperature in sodium polyacrylate solutions. Figures refer to concentration of Aquaquench ACR.

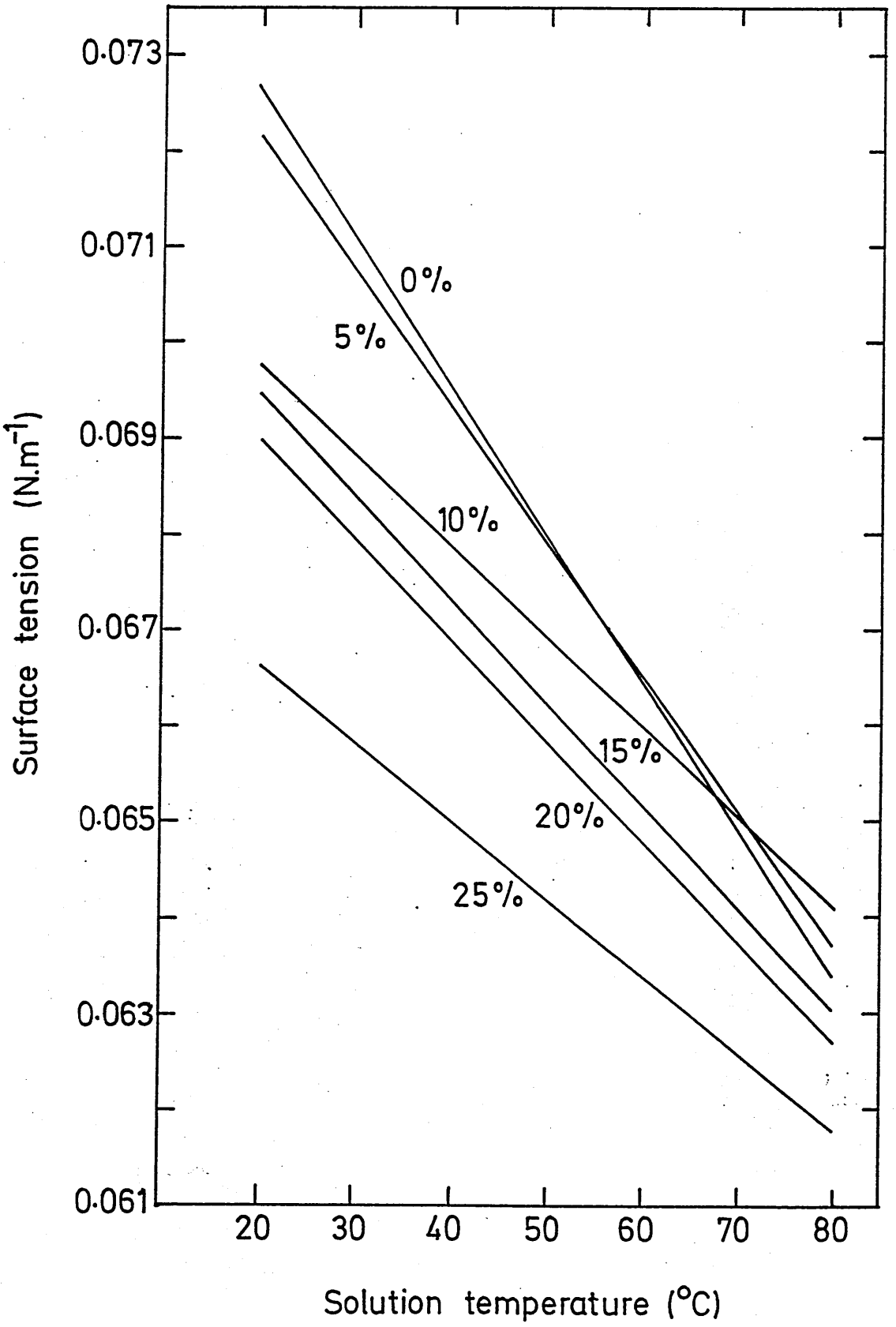
0·073
0·071
0·069
0·067
0·065
0·063
0·061
Surface tension (N.m⁻¹)
0%
5%
10%
15%
20%
25%
20
30
40
50
60
70
80
Solution temperature (°C)

FIGURE 85: Results of a differential thermogravimetric analysis of the Aquaquench ACR concentrate over the temperature range 35-850°C. Upper scale: relationship between temperature and sample mass. Lower scale: relationship between temperature and rate of mass loss.

Mass (mg)
36
24
12
0
Rate of mass loss (mg.s⁻¹)
0.023
0.046
0.069
0
100
200
300
400
500
600
700
800
900
Temperature (°C)

FIGURE 86: Results of a differential thermogravimetric analysis of the Aquaquench ACR concentrate over the temperature range 360-540°C. Upper scale: relationship between temperature and sample mass. Lower scale: relationship between temperature and rate of mass loss.

Mass (mg)
3
2
1
0
Rate of mass loss
(x10⁻⁴mg.s⁻¹)
-6
-12
-18
360
420
480
540
Temperature (°C)

FIGURE 87: Results of a differential thermogravimetric analysis of the evaporite from the Aquaquench ACR concentrate over the temperature range 35-850°C. Upper scale: relationship between temperature and sample mass. Lower scale: relationship between temperature and rate of mass loss.

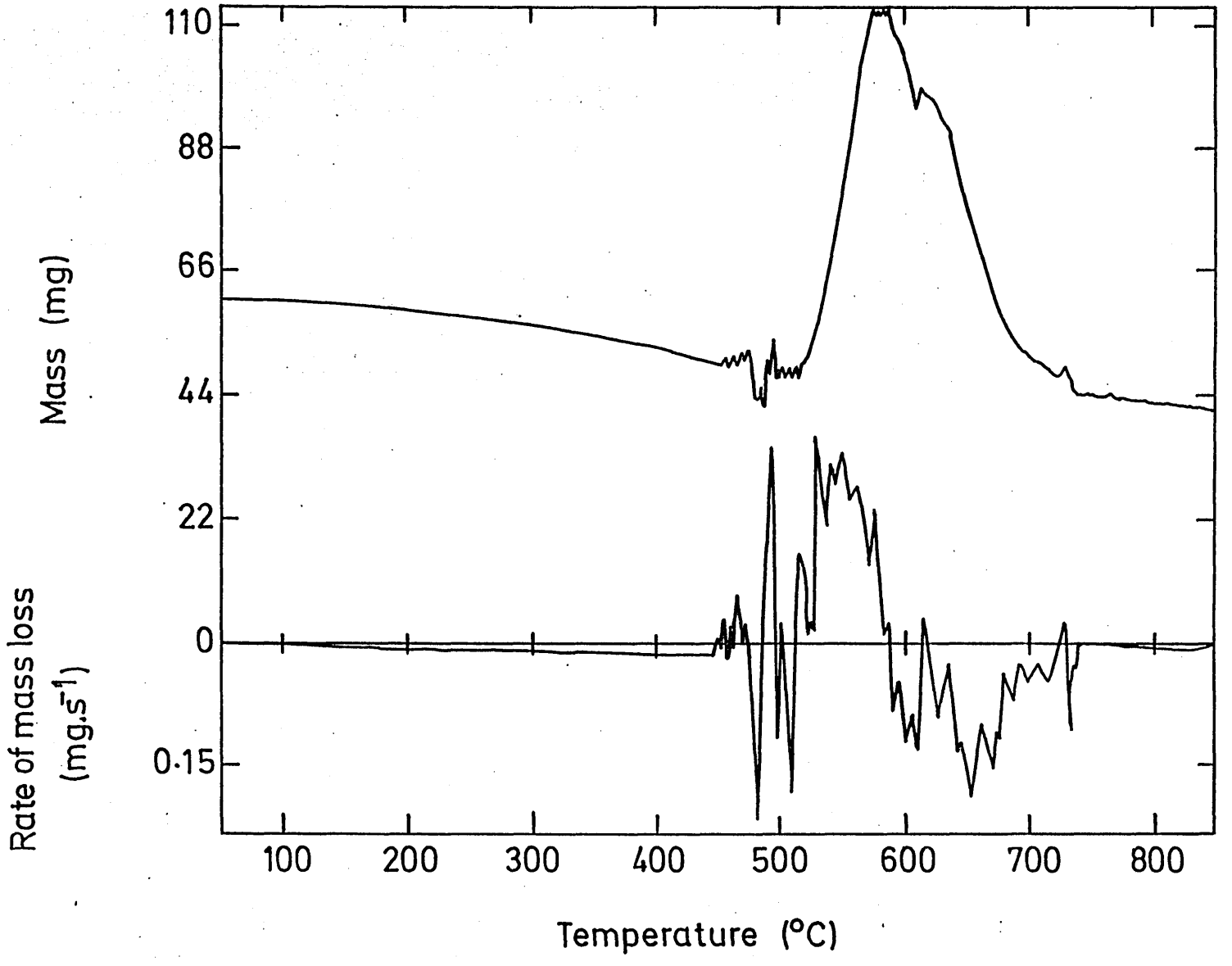
110
88
66
44
22
0
0·15
Mass (mg)
Rate of mass loss
(mg.s⁻¹)
100
200
300
400
500
600
700
800
Temperature (°C)

FIGURE 88: Comparison of the composition of the surface of a quenched plate at a black marking with an adjacent, lighter, area. Stainless steel plate quenched in an unagitated solution of 15% Aquaquench ACR.

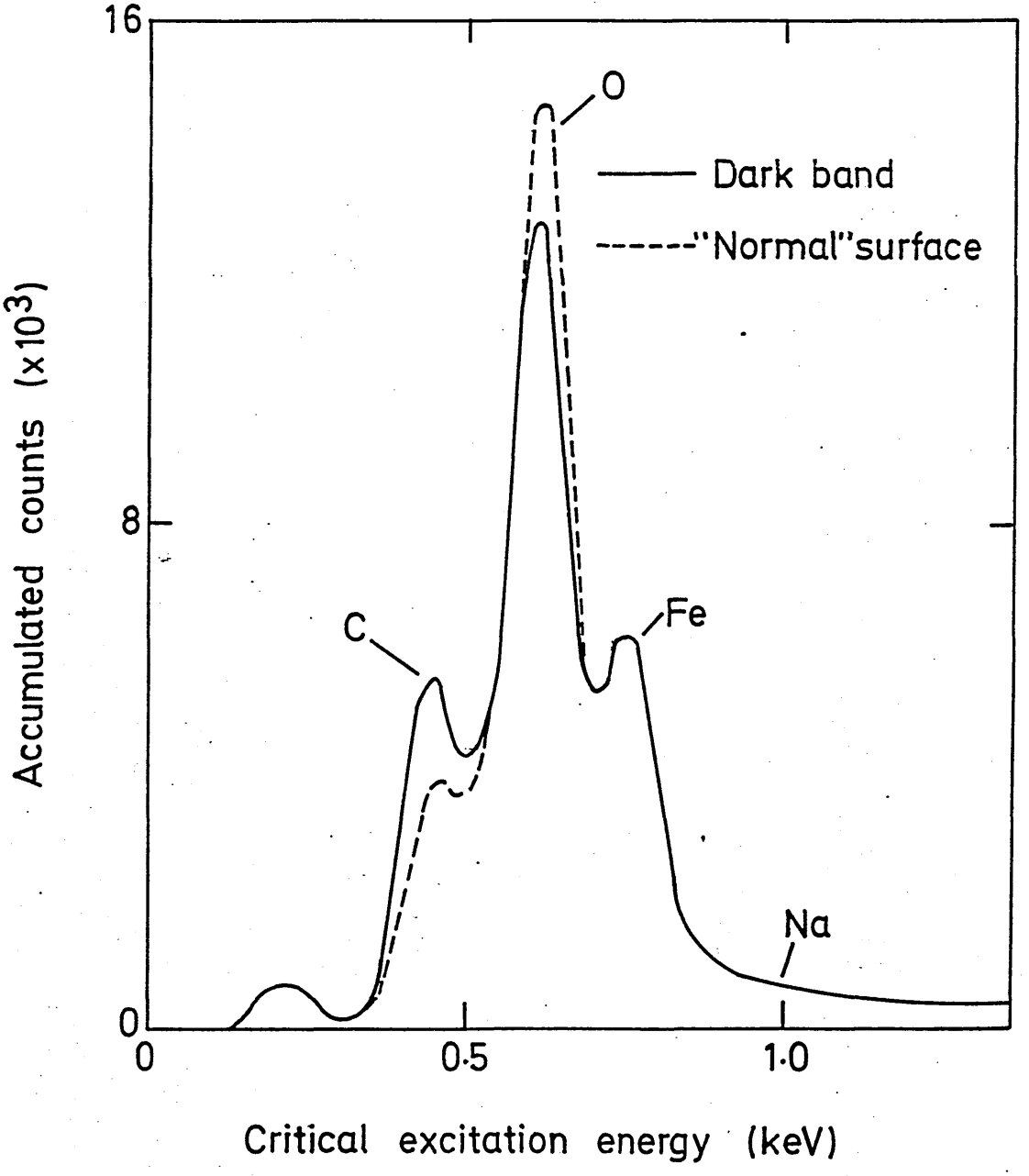
16
8
0
0
0·5
1·0
O
C
Fe
Na
Dark band
"Normal" surface
Accumulated counts (x10³)
Critical excitation energy (keV)

FIGURE 89: Comparison of calculated and experimentally measured film boiling surface heat transfer coefficients in the case of a quench in water.

I - Cess and Sparrow[109] model.

II - Nishikawa and Ito[112] model.

III - Nishikawa, Ito and Matsumoto[114] model.

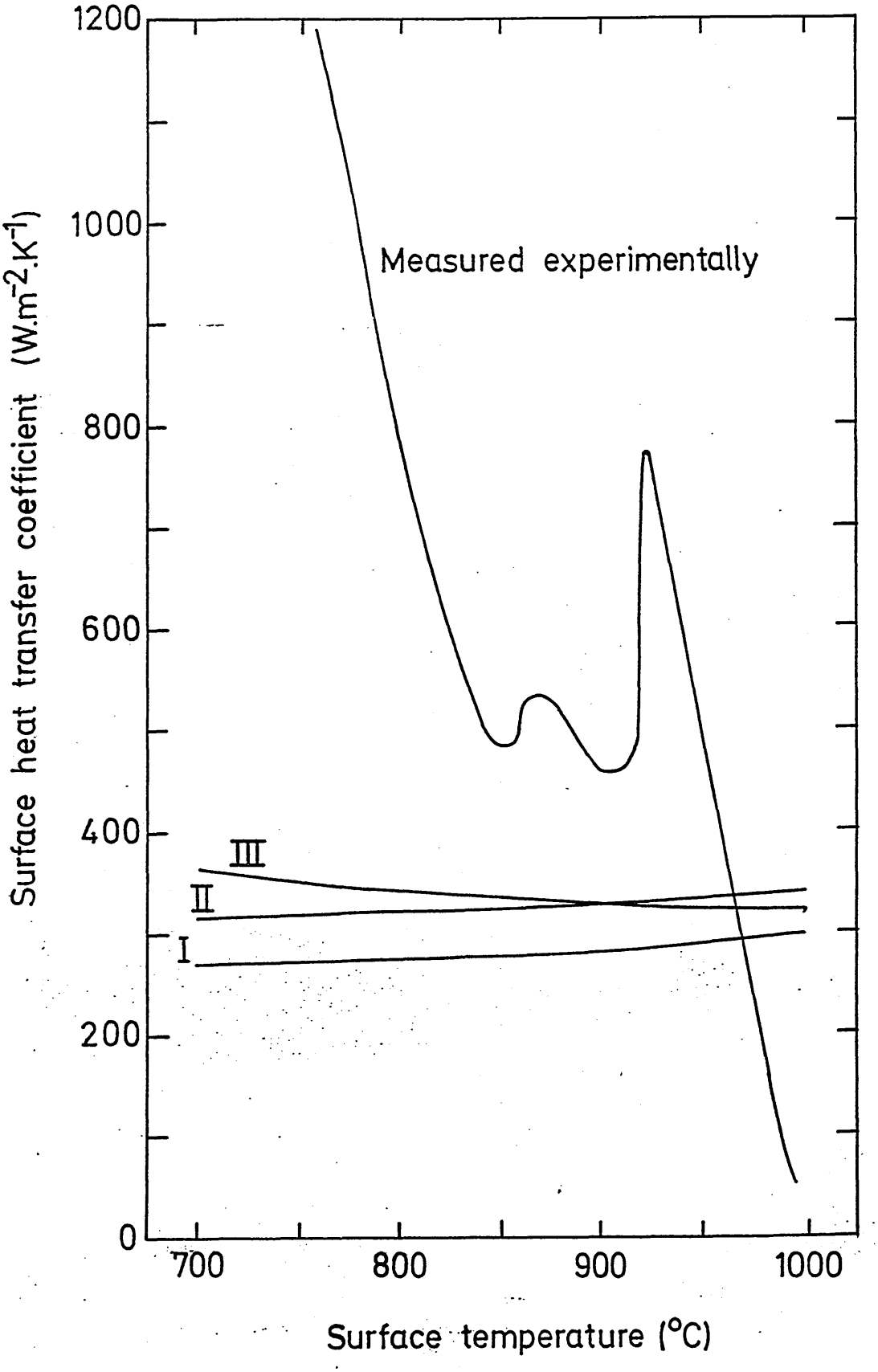
1200
1000
800
600
400
200
0
700
800
900
1000
Surface heat transfer coefficient (W.m-2.K-1)
Surface temperature (°C)
Measured experimentally
III
II
I

FIGURE 90: Comparison of calculated and experimentally measured film boiling surface heat transfer coefficients in the case of a quench in an unagitated solution of 25% Aquaquench ACR.

I - Cess and Sparrow[109] model.

II - Nishikawa and Ito[112] model.

III - Nishikawa, Ito and Matsumoto[114] model.

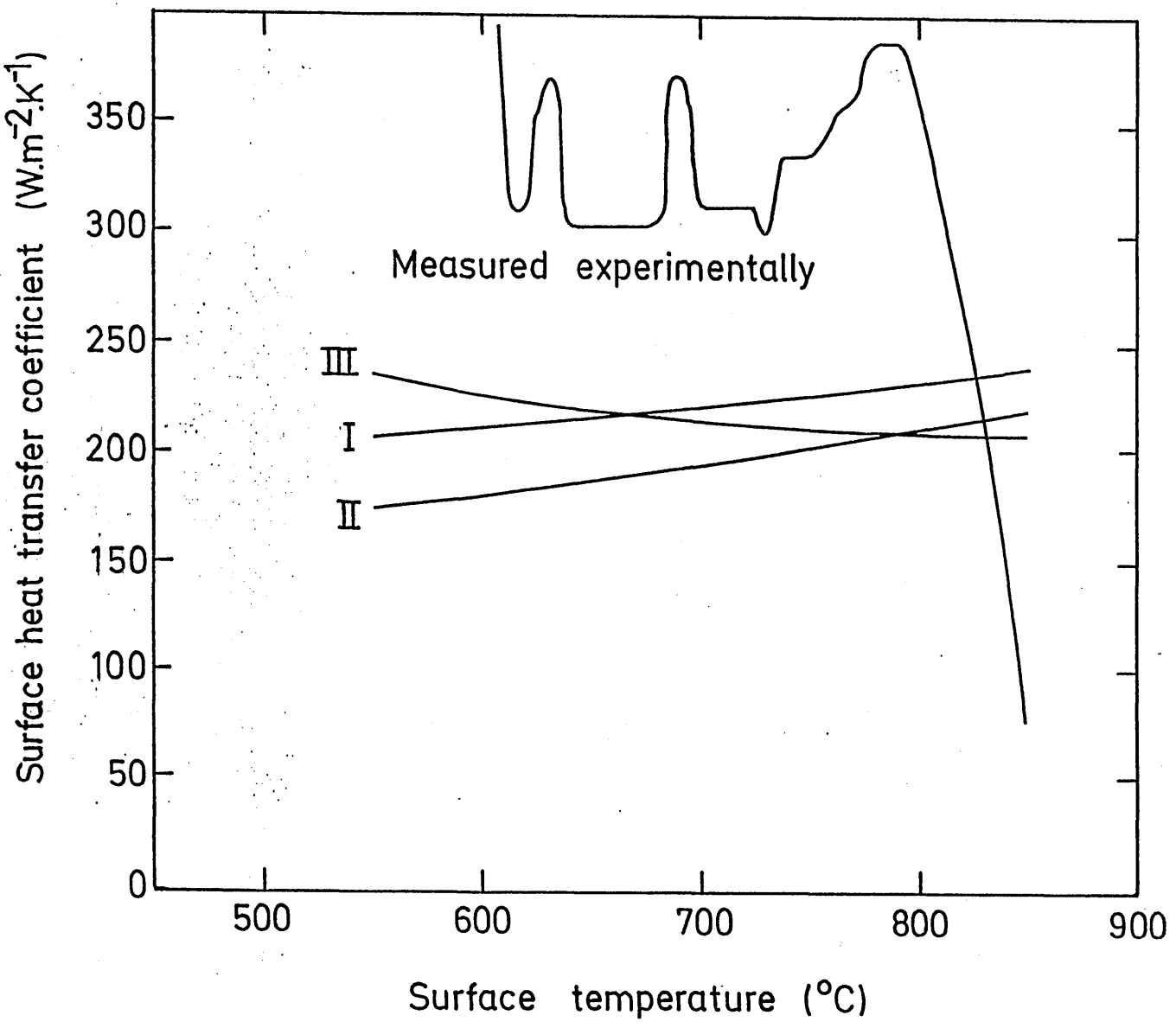
Surface heat transfer coefficient (W.m⁻².K⁻¹)
350
300
250
200
150
100
50
0
500
600
700
800
900
Surface temperature (°C)
Measured experimentally
III
I
II

FIGURE 91: Comparison of calculated and experimentally measured film boiling surface heat transfer coefficients in the case of a quench in water. Calculated surface heat transfer coefficients obtained using the turbulent interface model with the critical Reynolds number for transition from laminar to turbulent flow assumed to be 22,500.

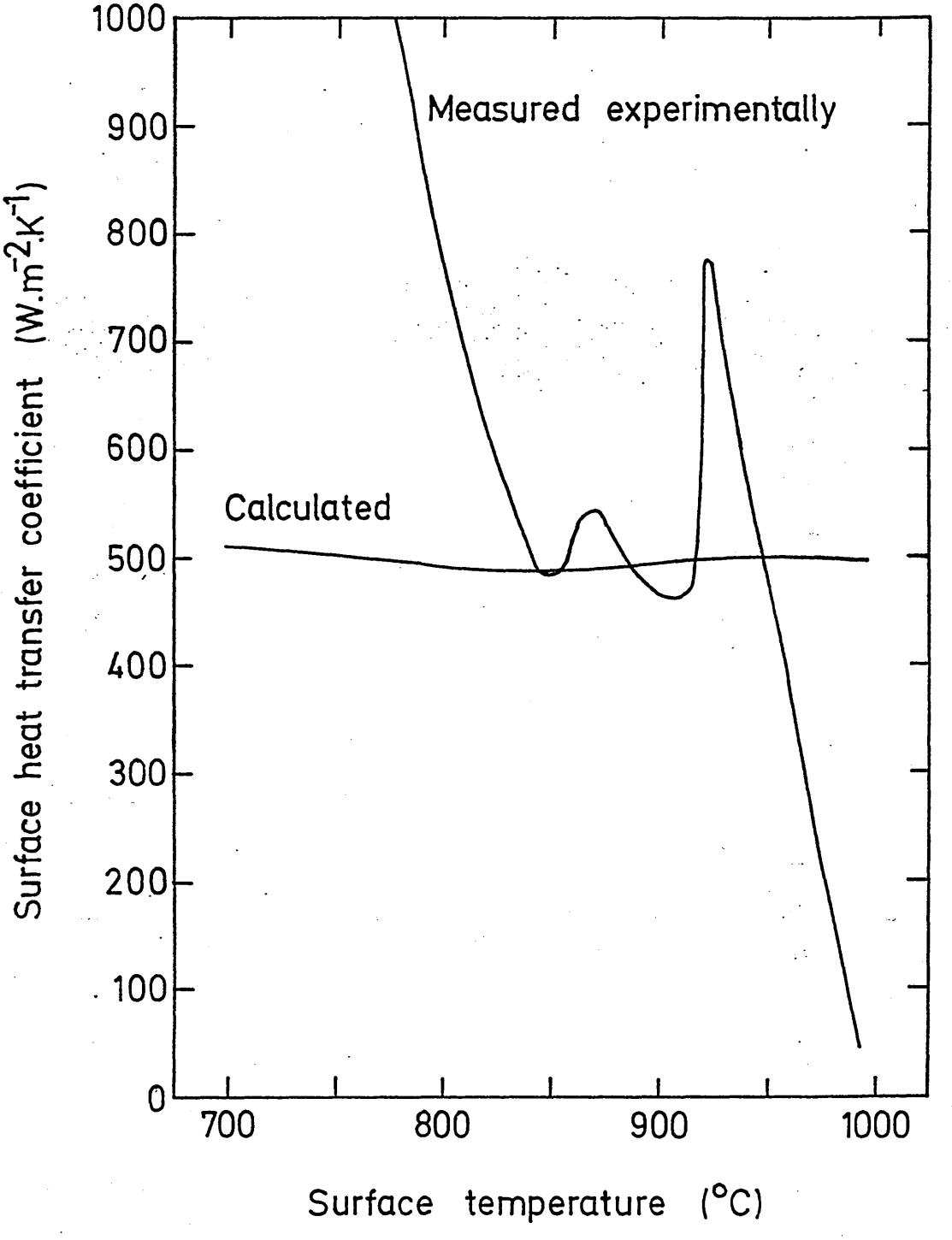
Measured experimentally
Calculated
Surface heat transfer coefficient (W.m^{-2}.K^{-1})
Surface temperature (°C)
1000
900
800
700
600
500
400
300
200
100
0
700
800
900
1000

FIGURE 92: Comparison of calculated and experimentally measured film boiling surface heat transfer coefficients in the case of a quench in an unagitated solution of 25% Aquaquench ACR. Calculated surface heat transfer coefficients obtained using turbulent interface model with the critical Reynolds number for transition from laminar to turbulent flow assumed to be 250.

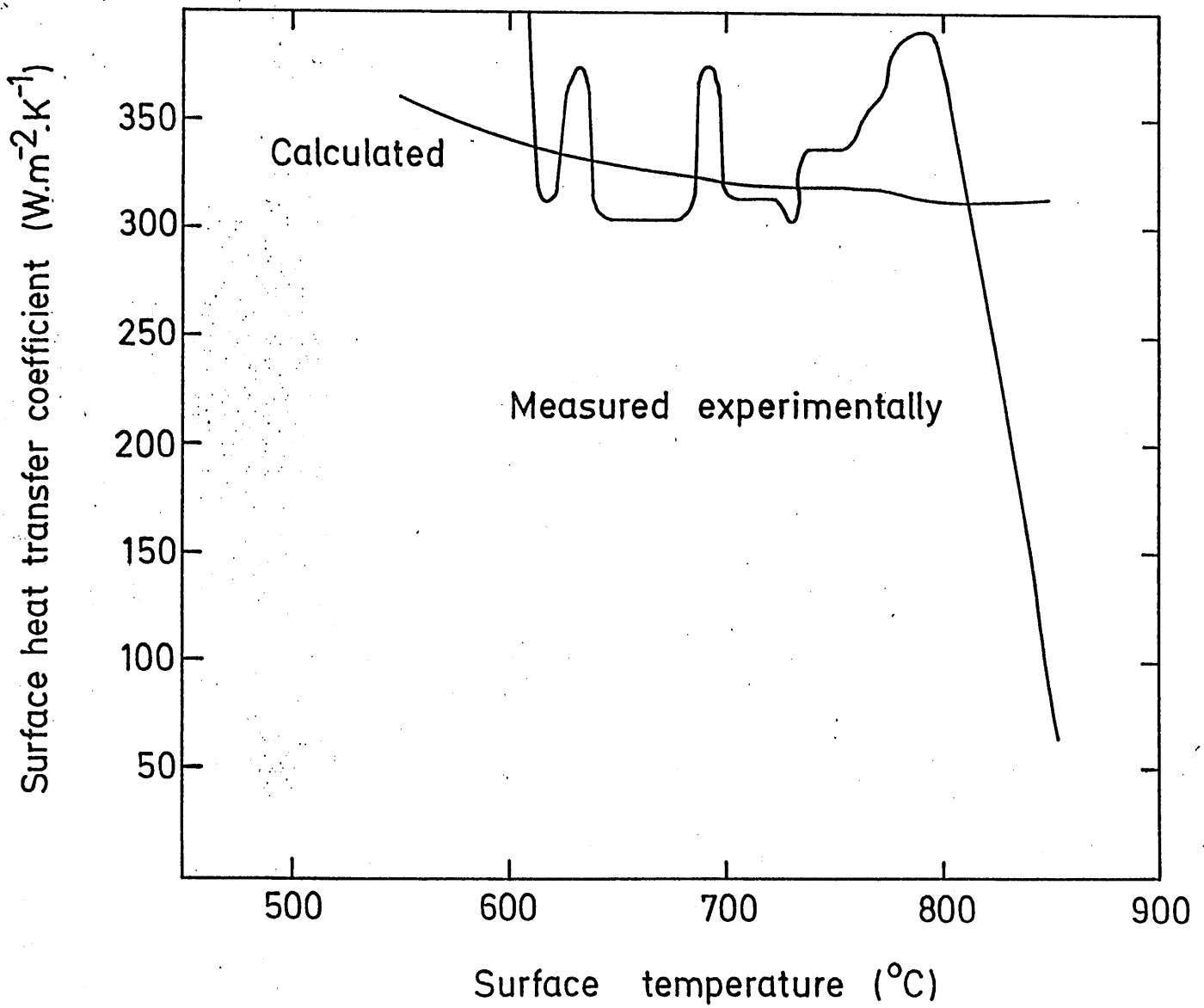
Surface heat transfer coefficient (W.m^{-2}.K^{-1})
350
300
250
200
150
100
50
Calculated
Measured experimentally
500
600
700
800
900
Surface temperature (°C)

FIGURE 93: Comparison of calculated and experimentally measured surface heat transfer coefficients at surface temperatures of 420°C and below in the case of a quench in an unagitated solution of 25% Aquaquench ACR.

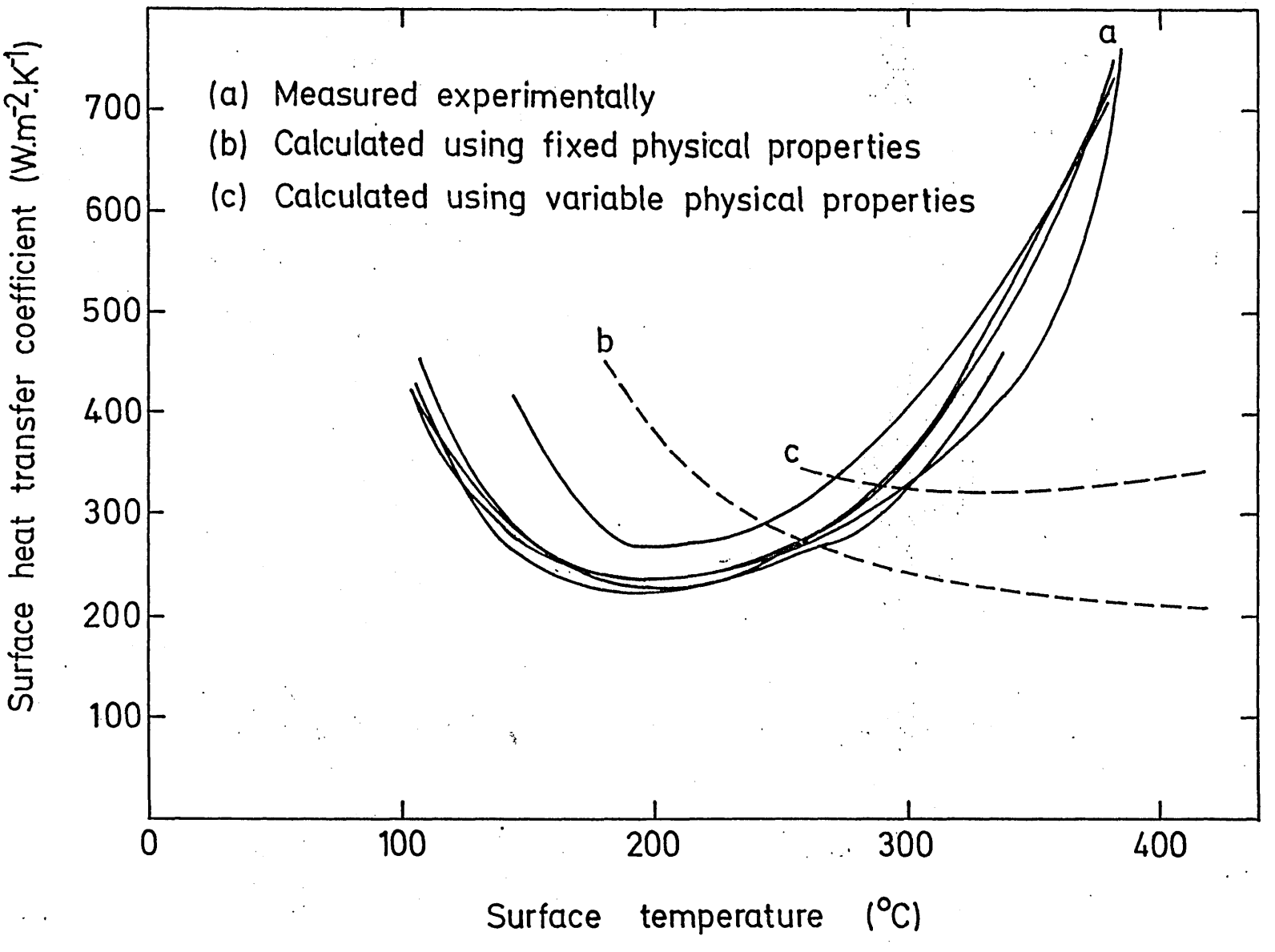
(a) Measured experimentally
(b) Calculated using fixed physical properties
(c) Calculated using variable physical properties
a
b
c
Surface heat transfer coefficient (W.m-2.K-1)
700
600
500
400
300
200
100
0
100
200
300
400
Surface temperature (°C)

FIGURE 94: Examples of changes in gradient, (denoted a), in the vapour transport stage of cooling curves measured during quenching in aqueous polyalkylene glycol solutions.

Diagram (i) - 25% Aquaquench 1250.

Diagram (ii) - 10% Aquaquench 1250.

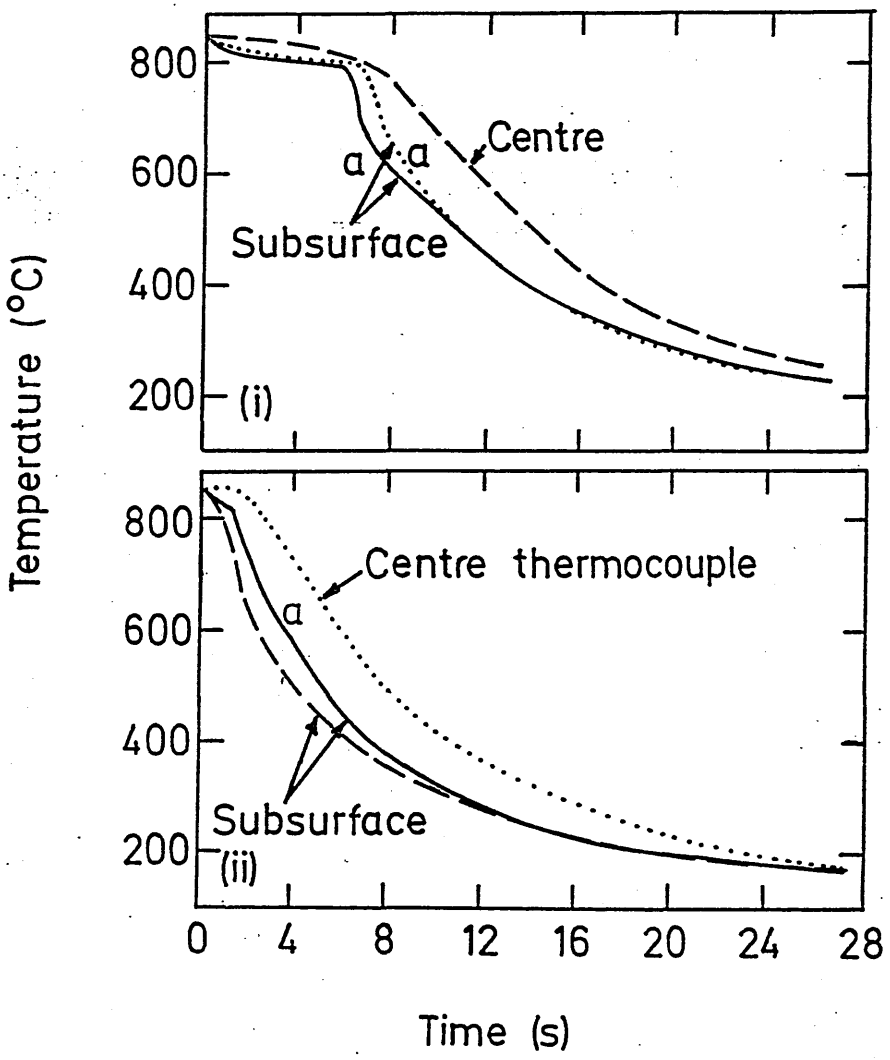
Temperature (°C)
800
600
400
200
Centre
a
a
Subsurface
(i)
800
600
400
200
Centre thermocouple
a
Subsurface
(ii)
0
4
8
12
16
20
24
28
Time (s)

FIGURE 95: Relationships between time and temperature measured during quenching in an unagitated solution of 15% Aquaquench ACR.

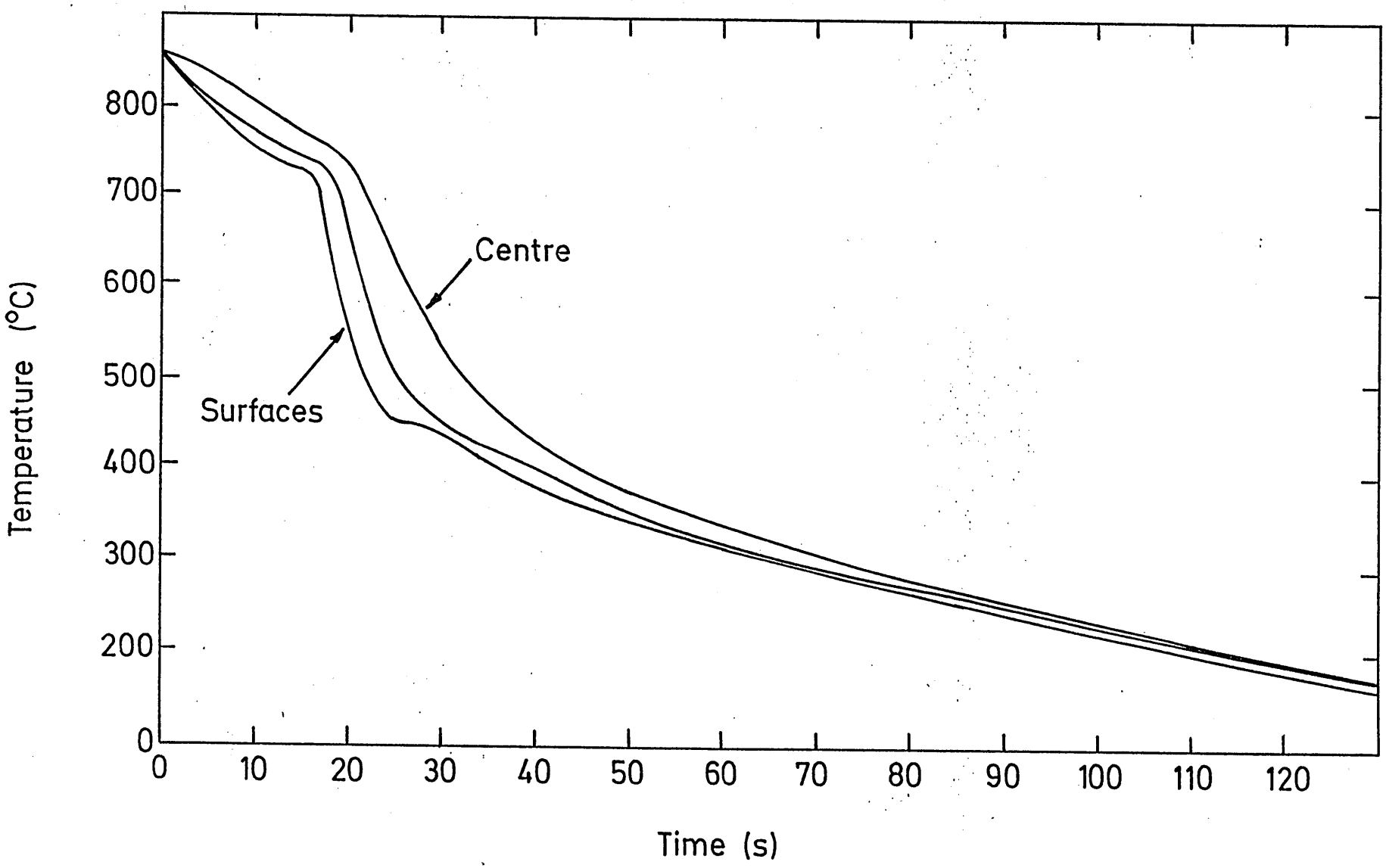
Temperature (°C)
800
700
600
500
400
300
200
0
Centre
Surfaces
0
10
20
30
40
50
60
70
80
90
100
110
120
Time (s)

PLATE 1: Face of a plate quenched in an unagitated solution of 10% Aquaquench ACR showing the film boiling stage.

Time = 2 s

Surface temperature = 808^{o}C

Surface heat transfer coefficient = 490 W.m^{-2}.K^{-1}

PLATE 2: Face of a plate quenched in an unagitated solution of 10% Aquaquench ACR showing the film boiling stage.

Time = 4 s

Surface temperature =792^{o}C

Surface heat transfer coefficient = 400 W.m^{-2}.K^{-1}

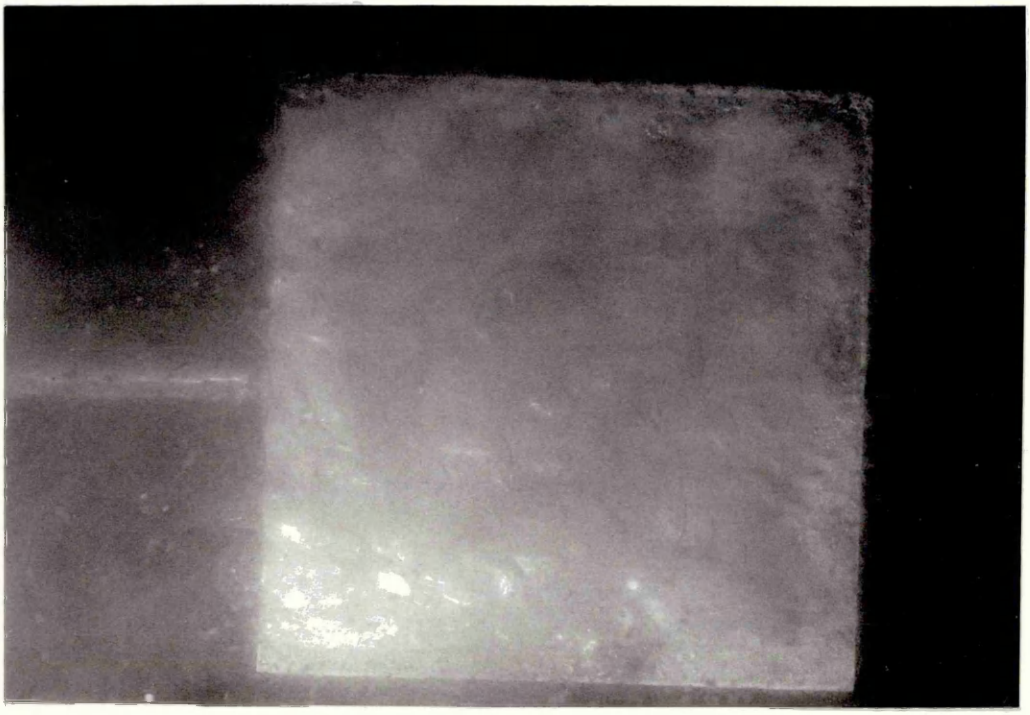

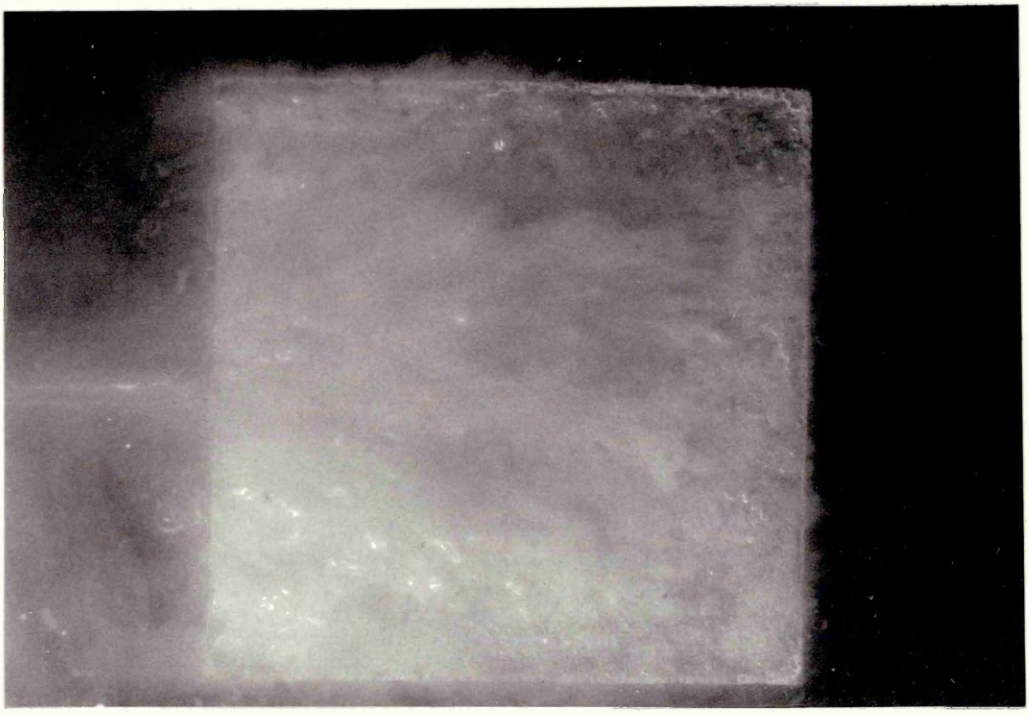

PLATE 3: Face of a plate quenched in an unagitated solution of 10% Aquaquench ACR showing the appearance of the transition boiling stage.

PLATE 4: Face of a plate quenched in an unagitated solution of 10% Aquaquench ACR showing the appearance of the surface at about the period of the maximum surface heat transfer coefficient.

Time = 14 s

Surface temperature = 514^{o}C

Surface heat transfer coefficient 3150 $W.m^{-2}.K^{-1}$

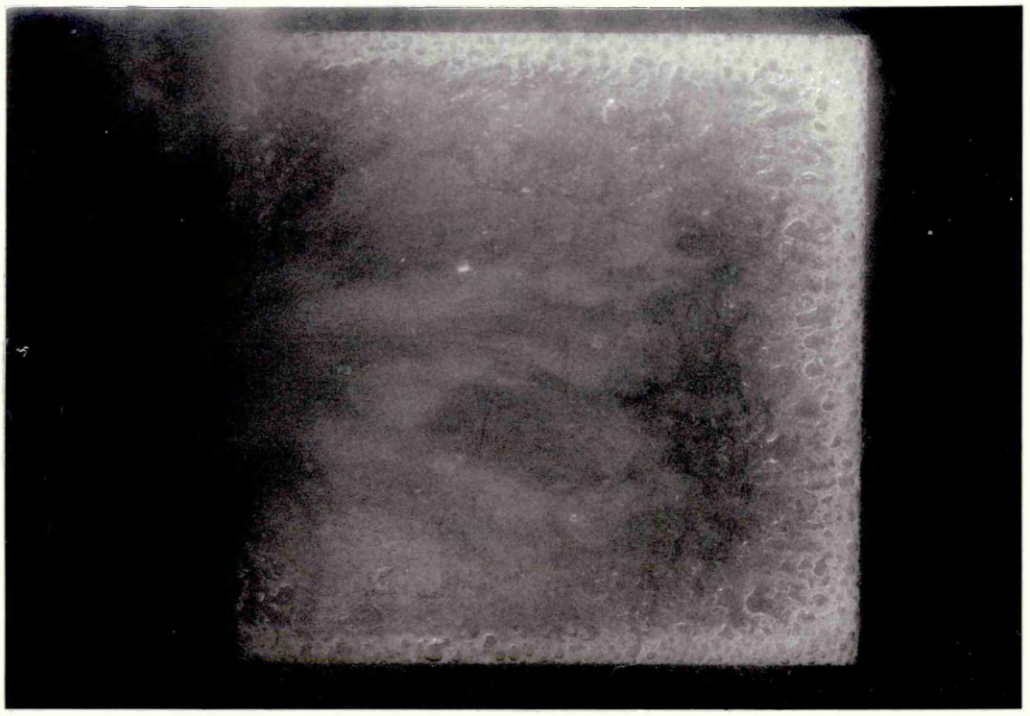

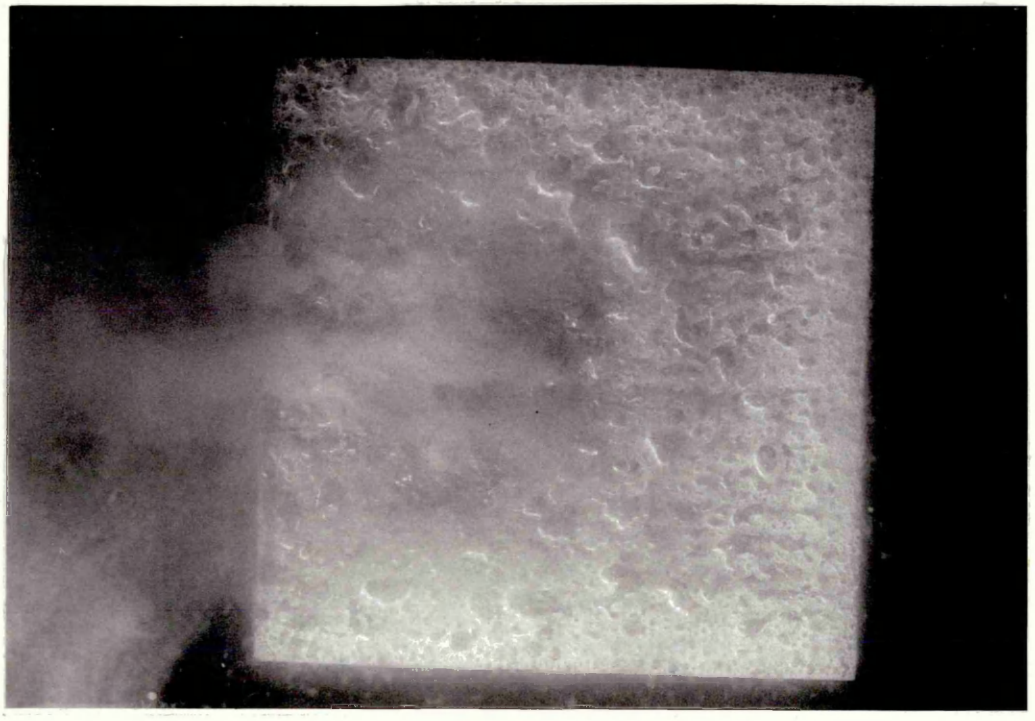

PLATE 5: Face of a plate quenched in an unagitated solution of 10% Aquaquench ACR.

Time = 16 s

Surface temperature = 434^{o}C

Surface heat transfer coefficient = 3010 W.m^{-2}.K^{-1}

PLATE 6: Face of a plate quenched in an unagitated solution of 10% Aquaquench ACR.

Time = 32 s

Surface temperature = 374^{o}C

Surface heat transfer coefficient = 781 W.m^{-2}.K^{-1}

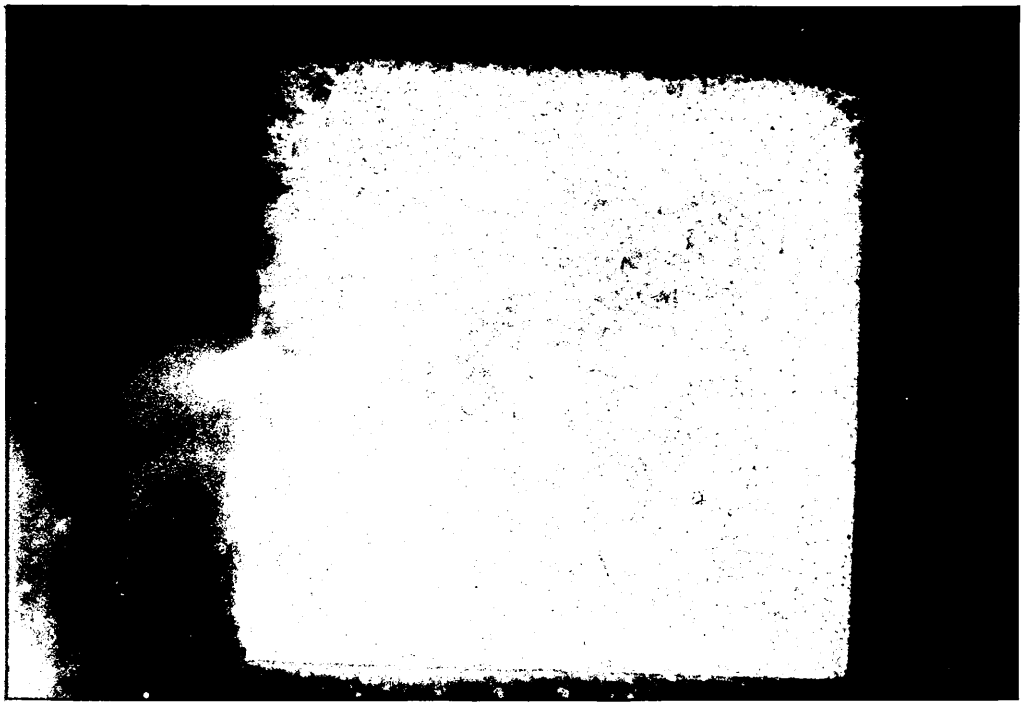

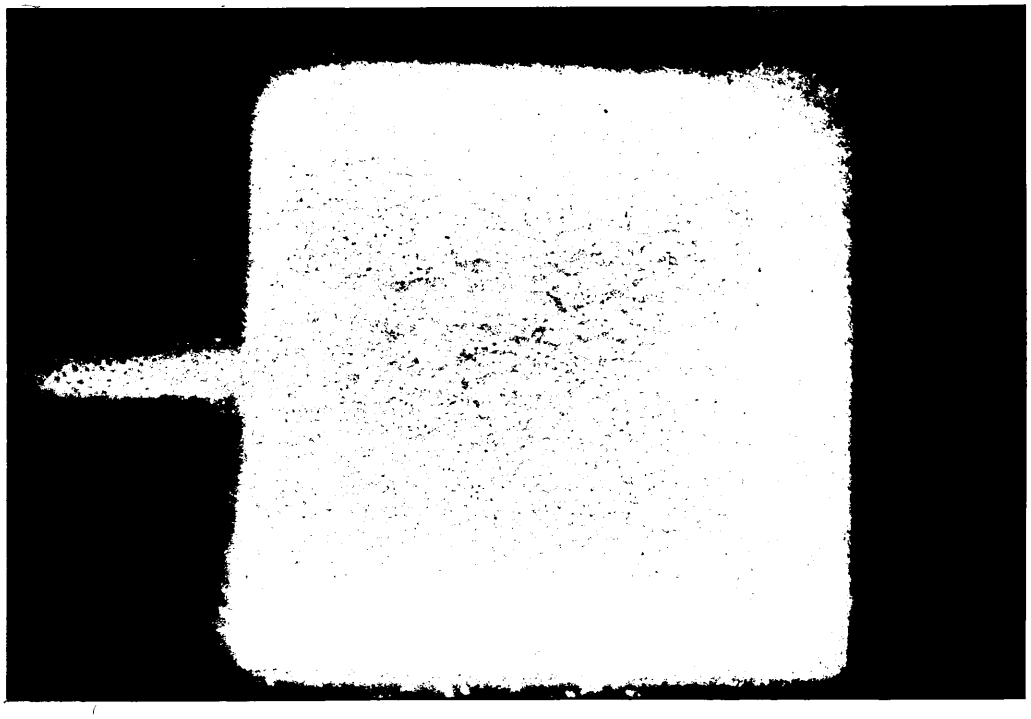

PLATE 7: Face of a plate quenched in an unagitated solution of 10% Aquaquench ACR.

Time = 40 s

Surface temperature = 348^{o}C

Surface heat transfer coefficient = 640 W.m^{-2}.K^{-1}

PLATE 8: Face of a plate quenched in an unagitated solution of 10% Aquaquench ACR.

Time = 60 s

Surface temperature = 279^{o}C

Surface heat transfer coefficient = 530 W.m^{-2}.K^{-1}

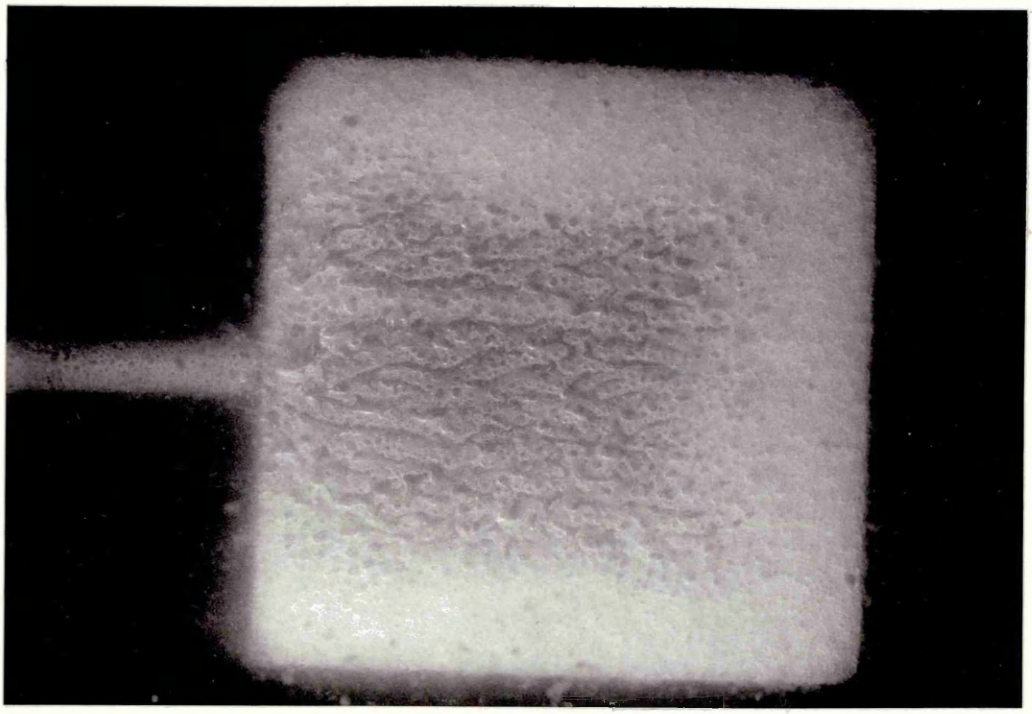

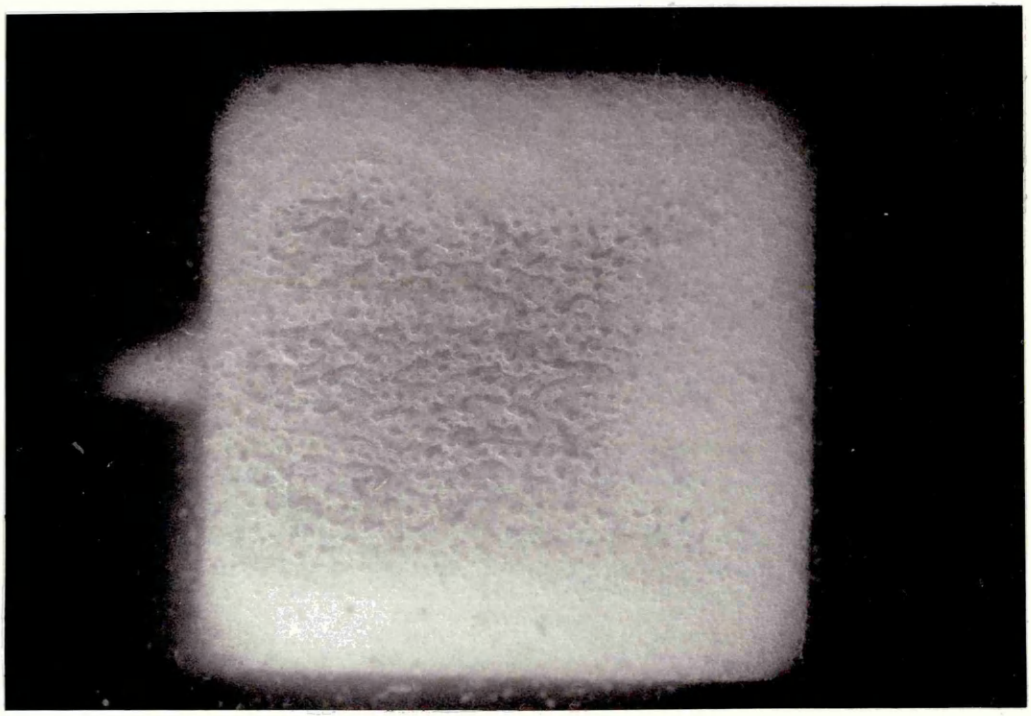

PLATE 9: Face of a plate quenched in an unagitated solution of 10% Aquaquench ACR.

Time = 76 s

Surface temperature = 217^{o}C

Surface heat transfer coefficient = 680 W.m^{-2}.K^{-1}

PLATE 10: Face of a plate quenched in an unagitated solution of 10% Aquaquench ACR.

Time = 88 s

Surface temperature = 184^{o}C

Surface heat transfer coefficient = 680 W.m^{-2}.K^{-1}

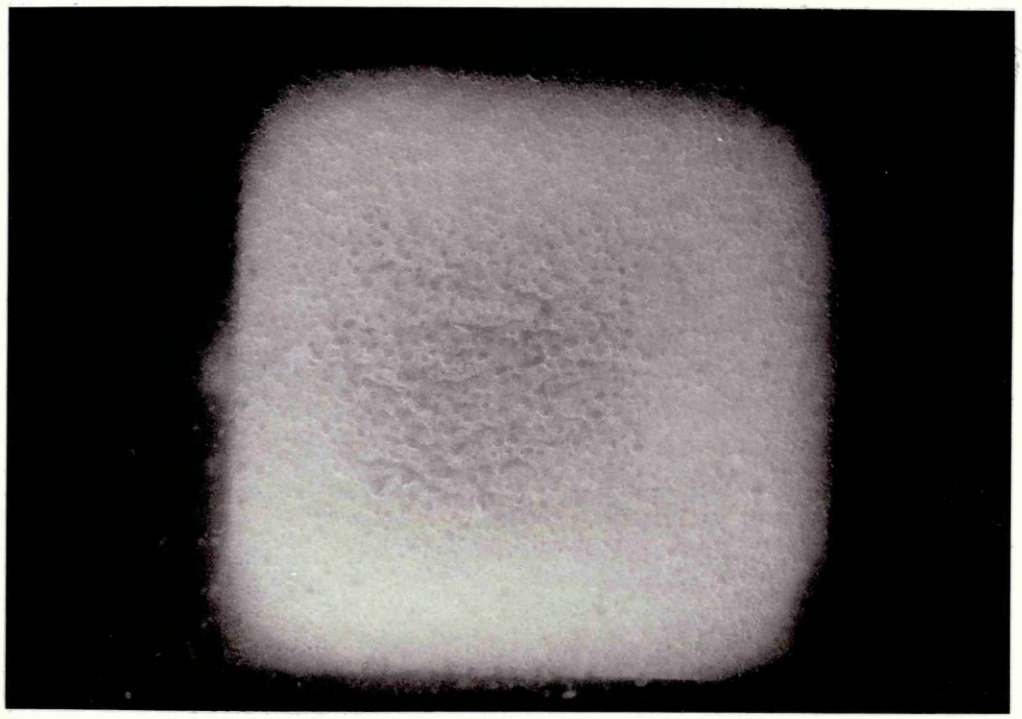

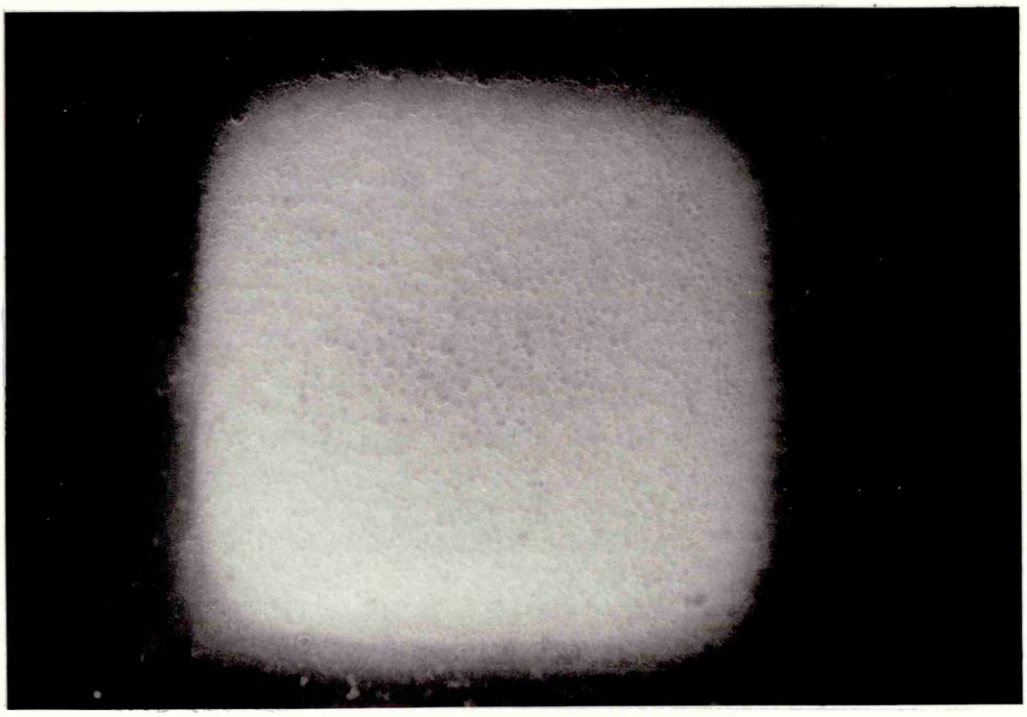

PLATE 11: Face of a plate quenched in an unagitated solution of 10% Aquaquench ACR.
Time = 112 s

PLATE 12: Face of a plate quenched in an unagitated solution of 10% Aquaquench ACR.
Time = 120 s

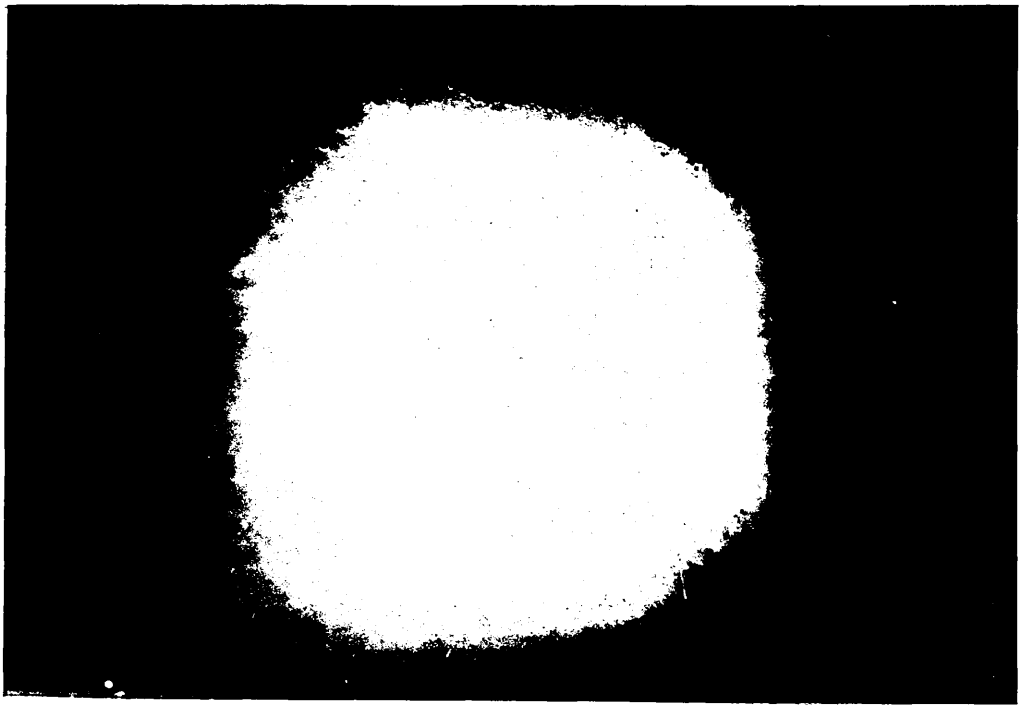

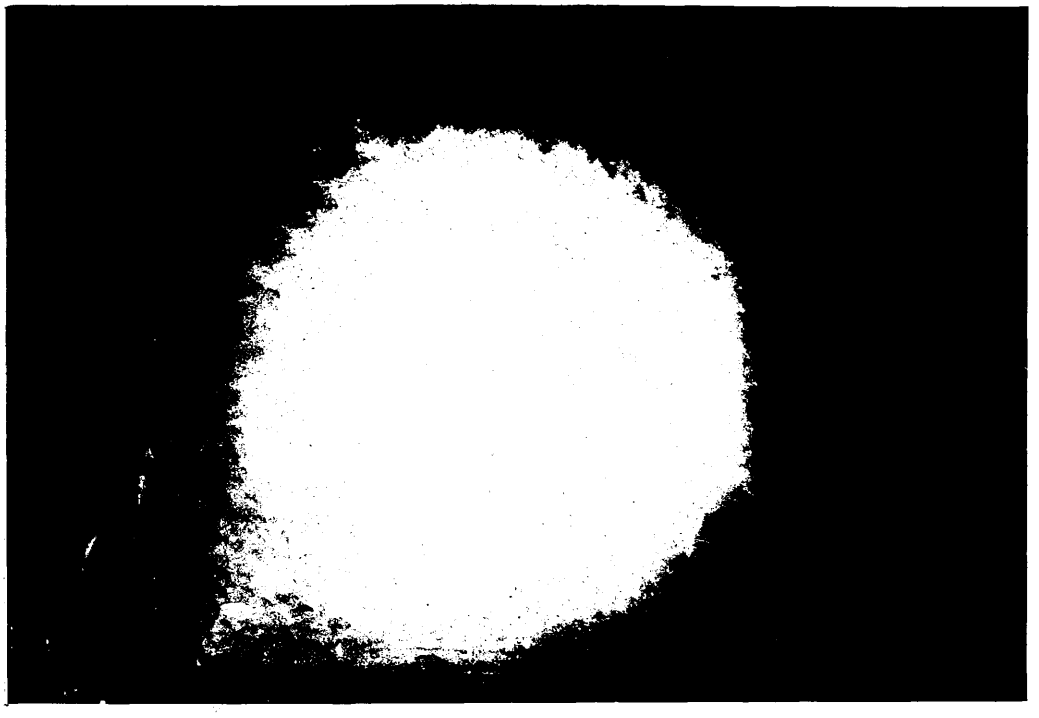

PLATE 13: Face of a plate quenched in an unagitated solution of 5% Aquaquench ACR showing the film boiling stage.

Time = 0 s

Surface temperature = 840^{o}C

PLATE 14: Edge of a plate quenched in an unagitated solution of 20% Aquaquench ACR showing Taylor waves in the vapour blanket.

Time = 2 s

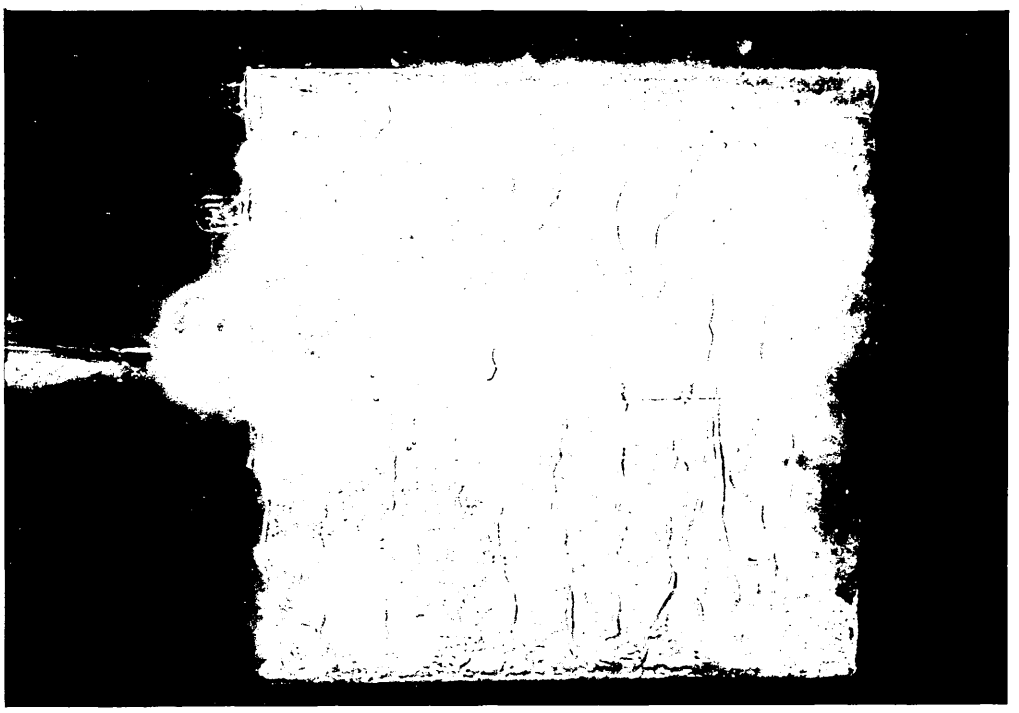

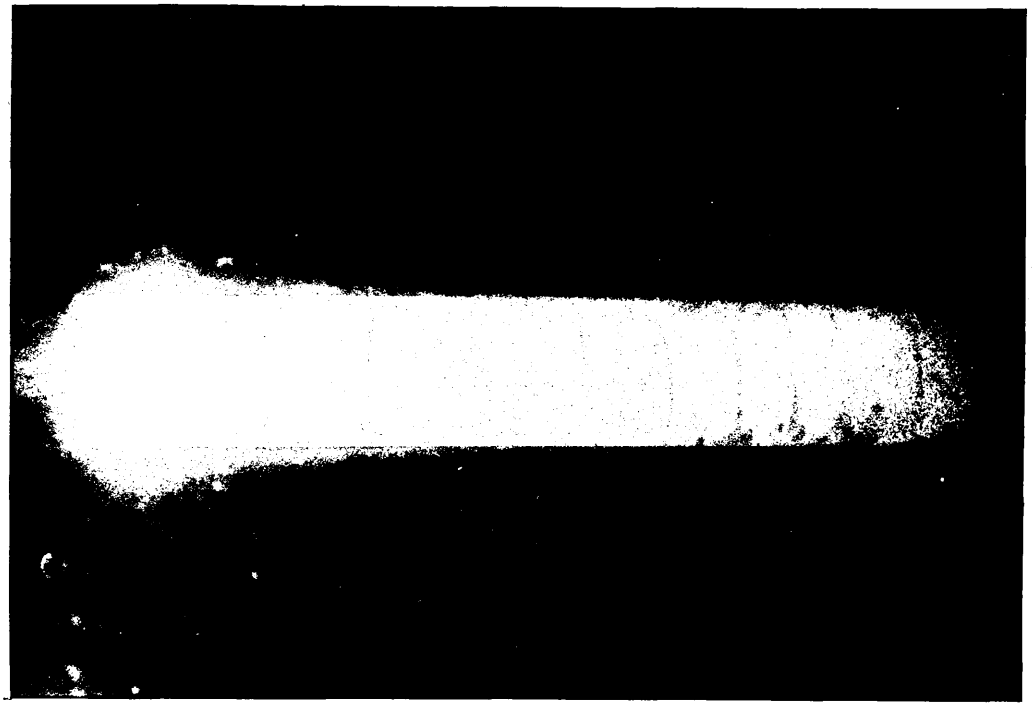

PLATE 15: Edge of a plate quenched in an unagitated solution of 20% Aquaquench ACR showing Taylor waves in the vapour blanket.

Time = 12 s

PLATE 16: Face of a plate quenched in an unagitated solution of 5% Aquaquench ACR showing both film and transition boiling stages.

Time = 4 s

Surface temperature = 784^{o}C

Surface heat transfer coefficient = 575 $W.m^{-2}.K^{-1}$

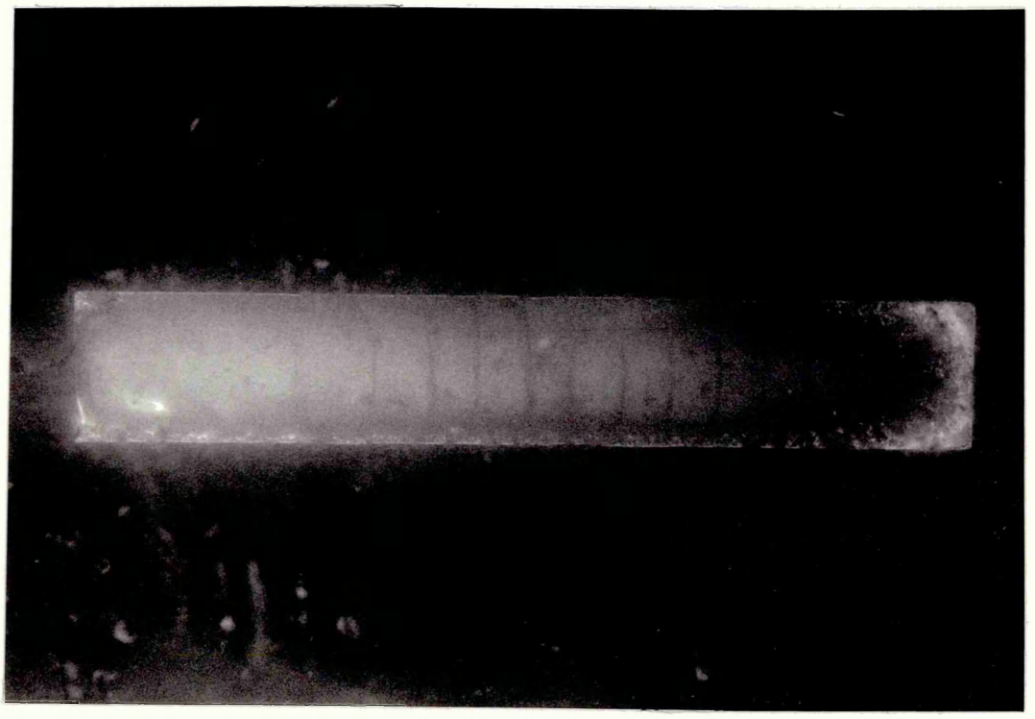

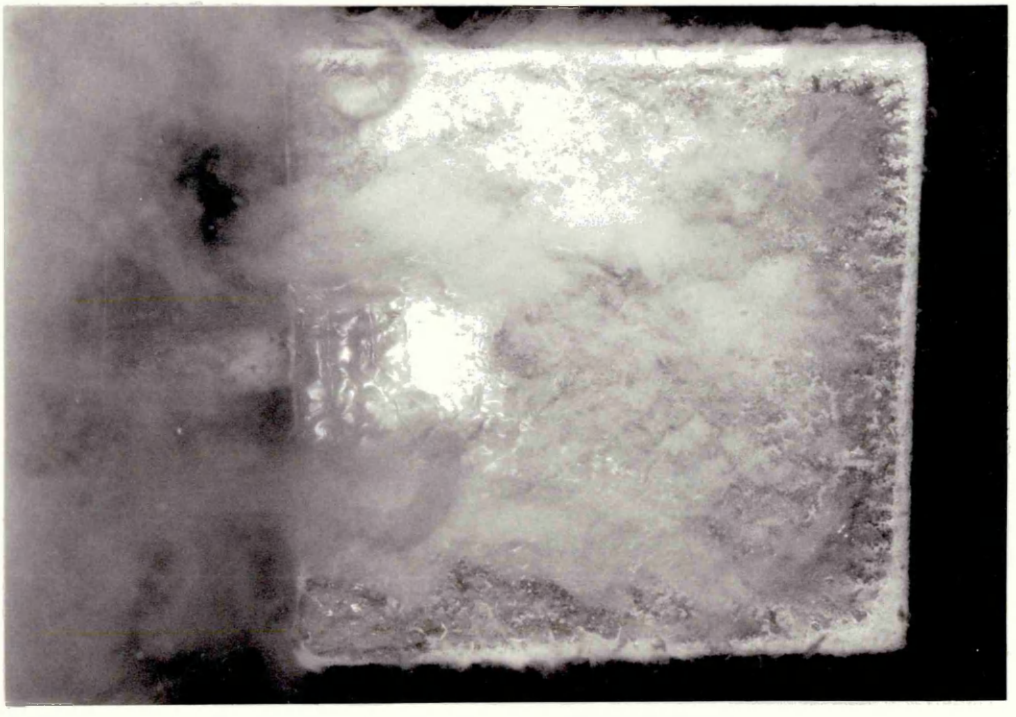

PLATE 17: Face of a plate quenched in an unagitated solution of 5% Aquaquench ACR showing the appearance of the dendritic stage.

Time = 14 s

Surface temperature = 450^{o}C

Surface heat transfer coefficient = 1500 W.m^{-2}.K^{-1}

PLATE 18: Face of a plate quenched in an unagitated solution of 5% Aquaquench ACR showing both the dendritic and frothy stages.

Time = 28 s

Surface temperature = 370^{o}C

Surface heat transfer coefficient = 450 W.m^{-2}.K^{-1} PLATE 19:

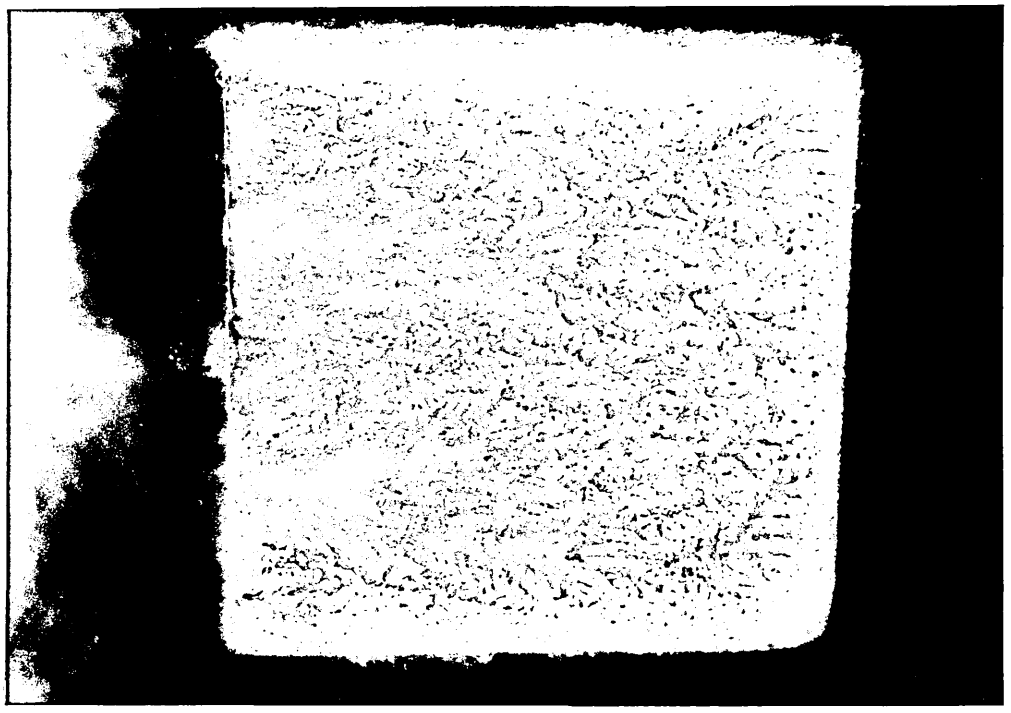

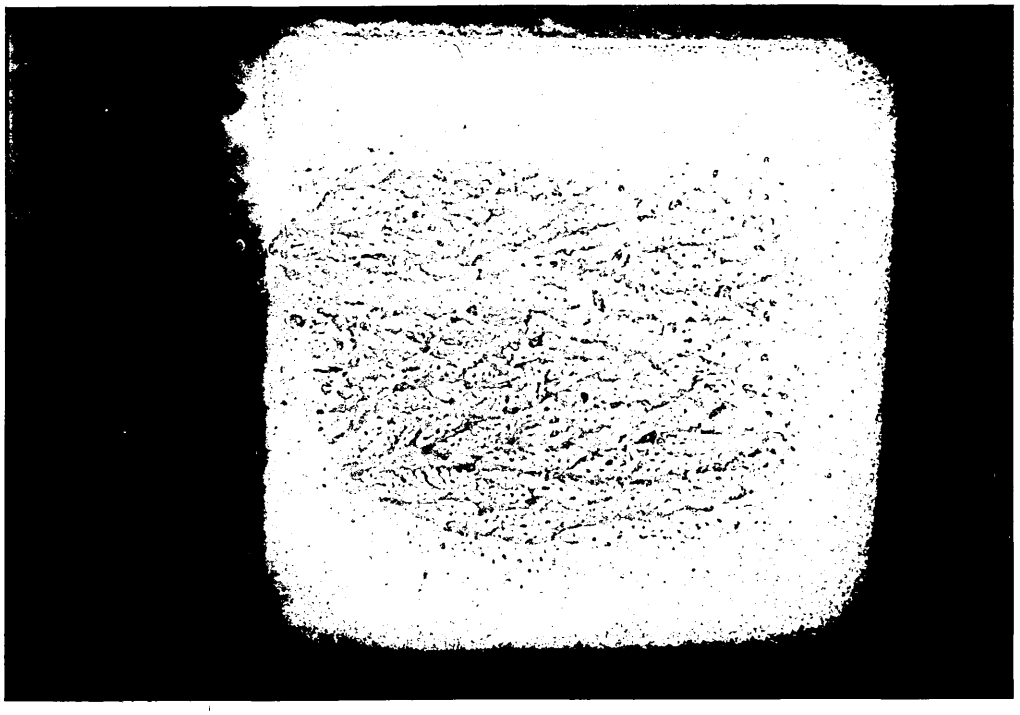

PLATE 19: Appearance of the face of a plate after quenching in an unagitated solution of 5% Aquaquench ACR.

PLATE 20: Appearance of the edge of a plate after quenching in an unagitated solution of 5% Aquaquench ACR.

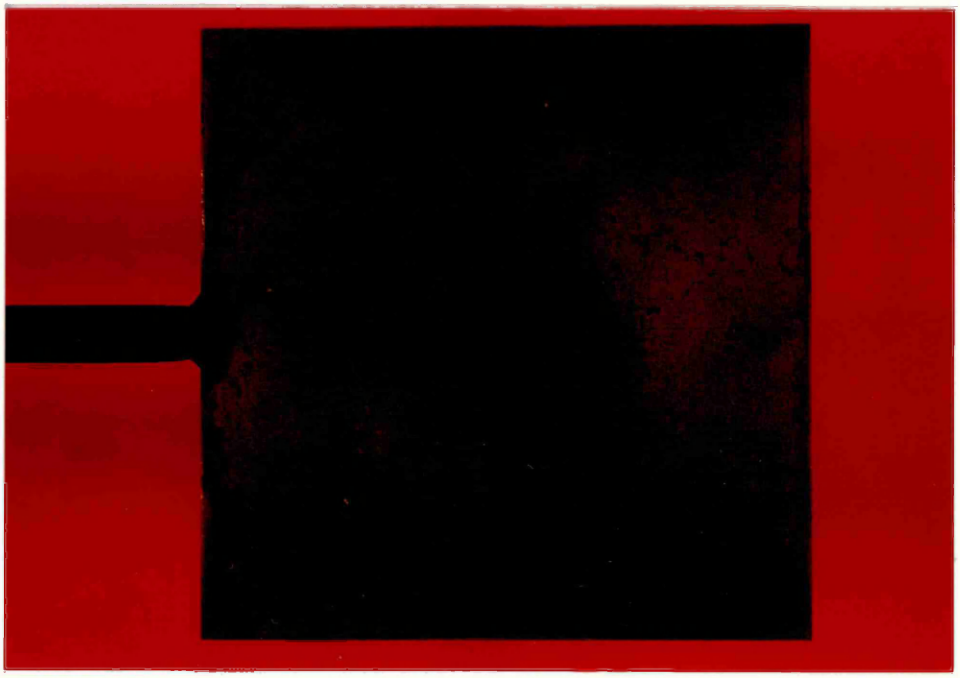

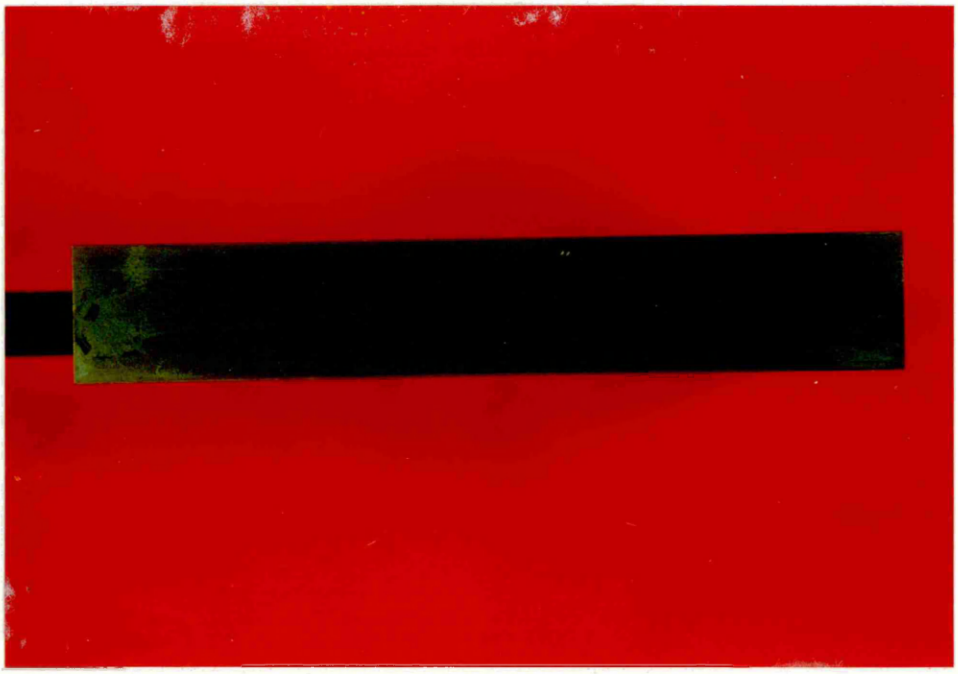

PLATE 21: Appearance of the face of a plate after quenching in an unagitated solution of 15% Aquaquench ACR.

PLATE 22: Appearance of the edge of a plate after quenching in an unagitated solution of 15% Aquaquench ACR.

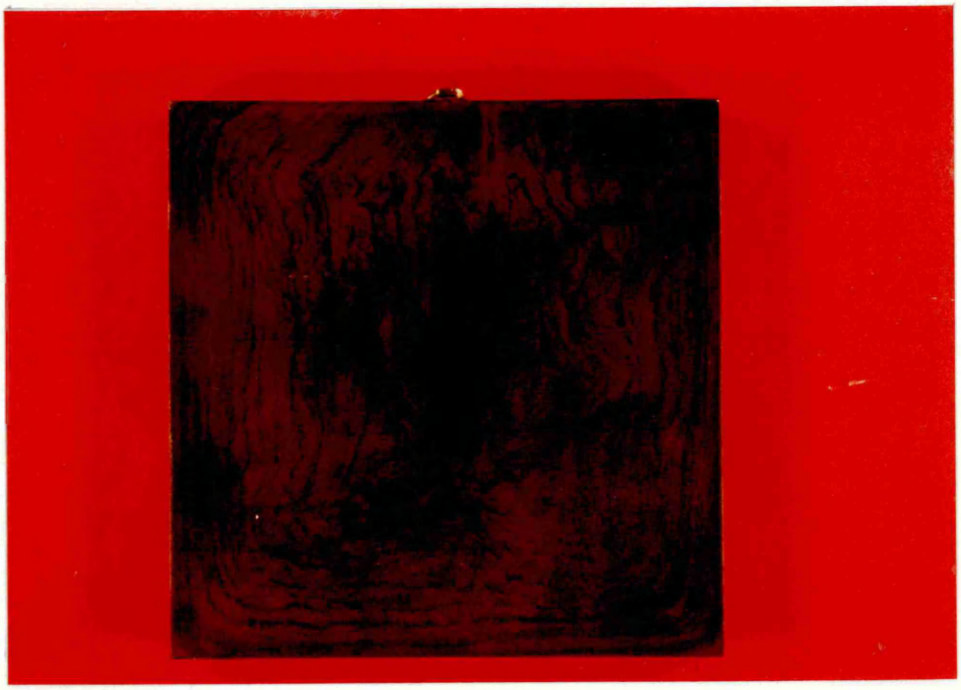

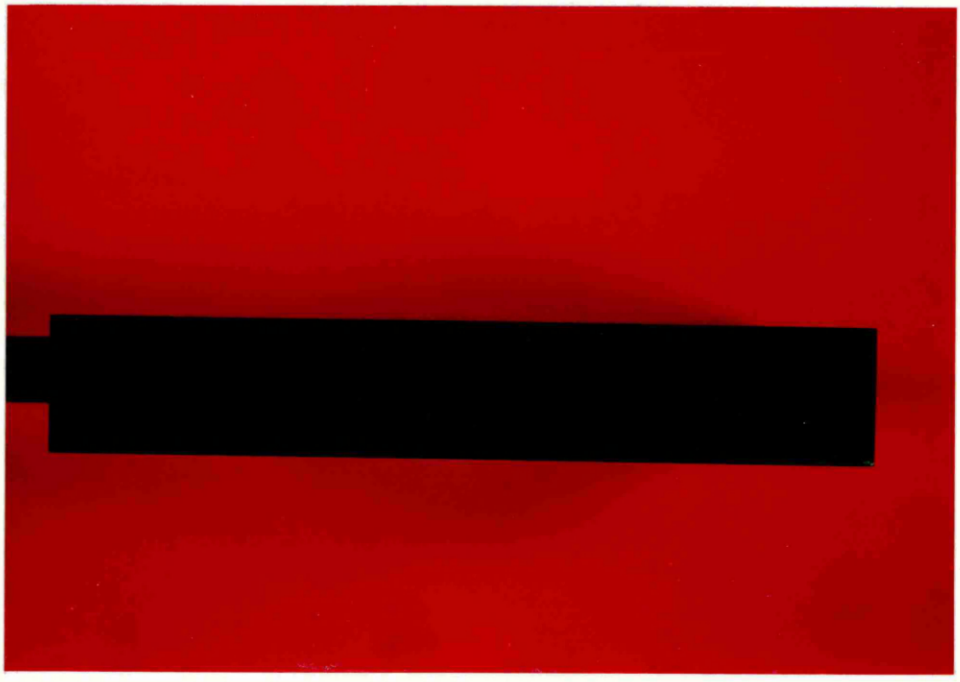

PLATE 23: Photograph taken from a cine film of a quench performed in an unagitated solution of 10% Aquaquench ACR.
Time = 14.8 s

PLATE 24: Photograph taken from a cine film of a quench performed in an unagitated solution of 10% Aquaquench ACR.
Time = 33.2 s

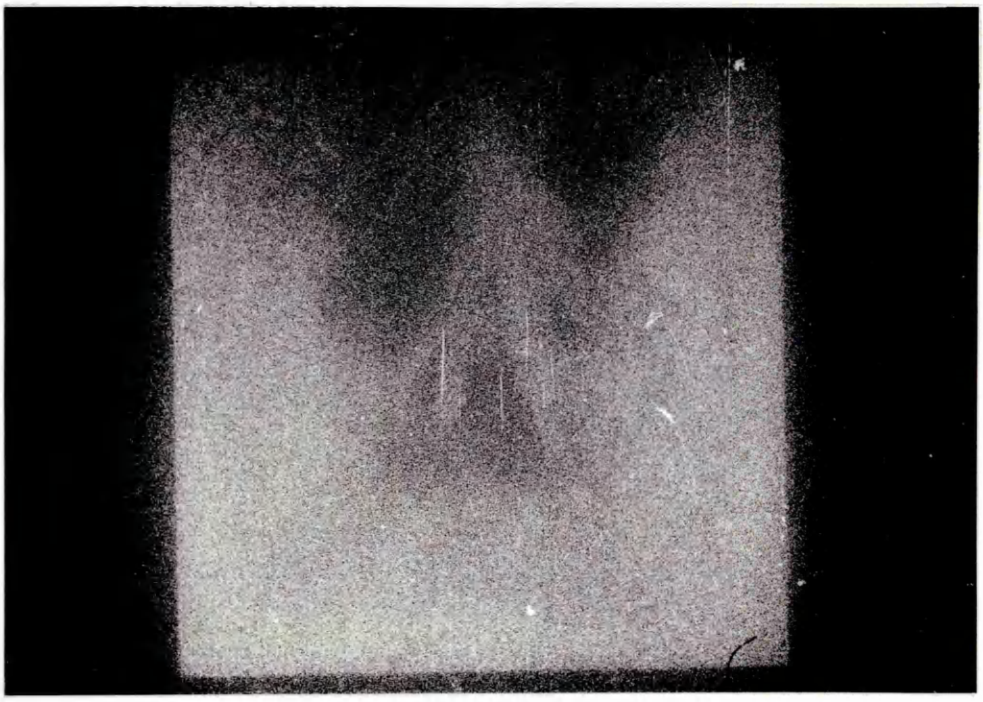

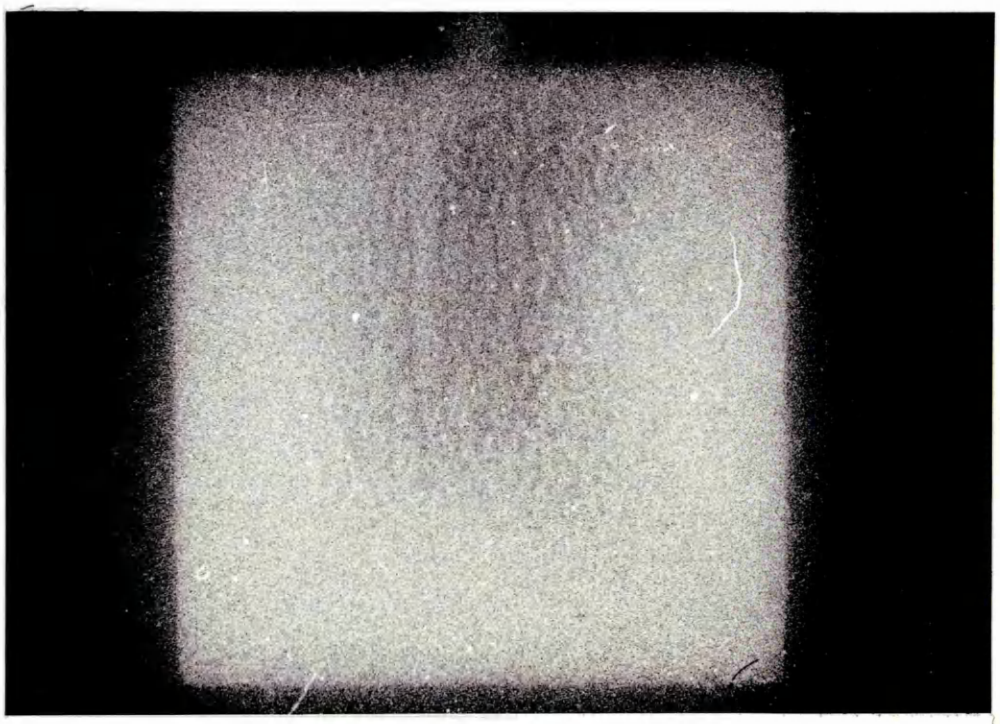

PLATE 25: Photograph taken from a cine film of a quench performed in an unagitated solution of 10% Aquaquench ACR. Time = 39.8 s

PLATE 26: Micrograph of the surface of a plate quenched in 15% Aquaquench ACR at an area between the dark markings.

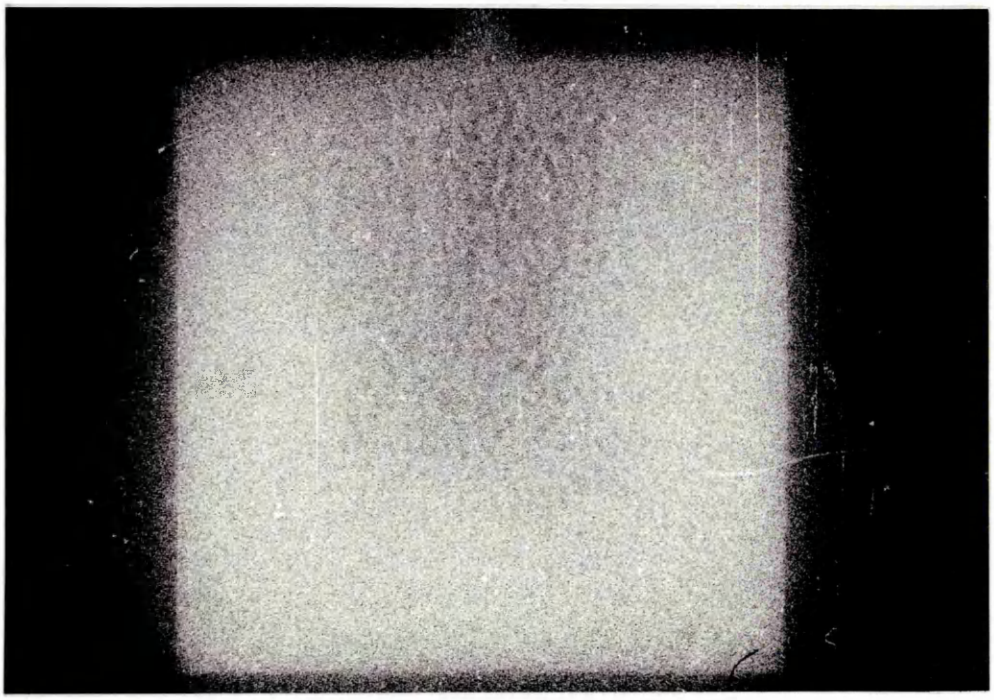

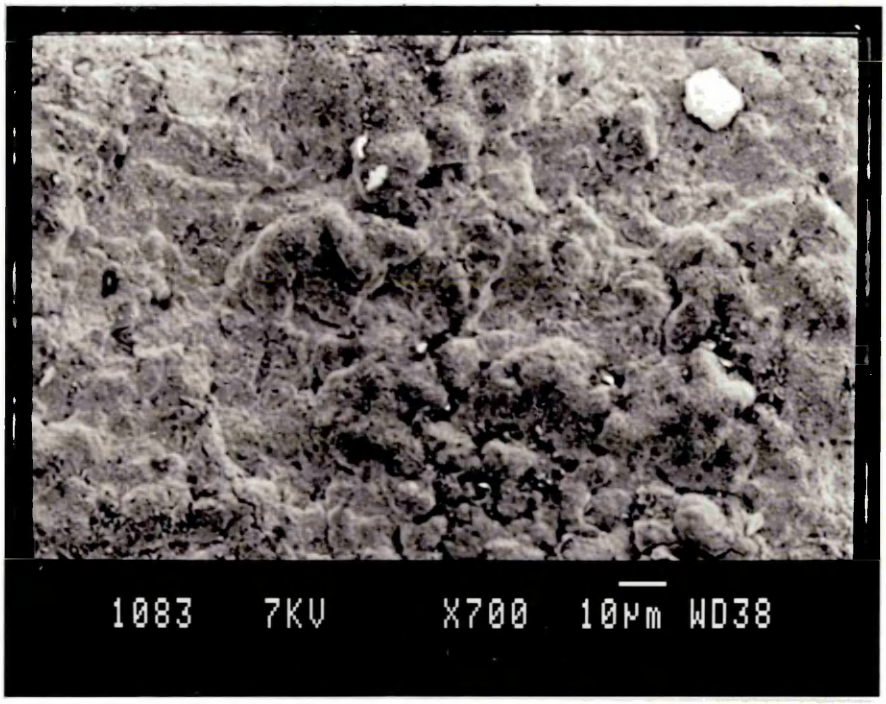
1083 7KV X700 10µm WD38

PLATE 27: Micrograph of the surface of a plate quenched in 15% Aquaquench ACR at an area containing a dark marking.

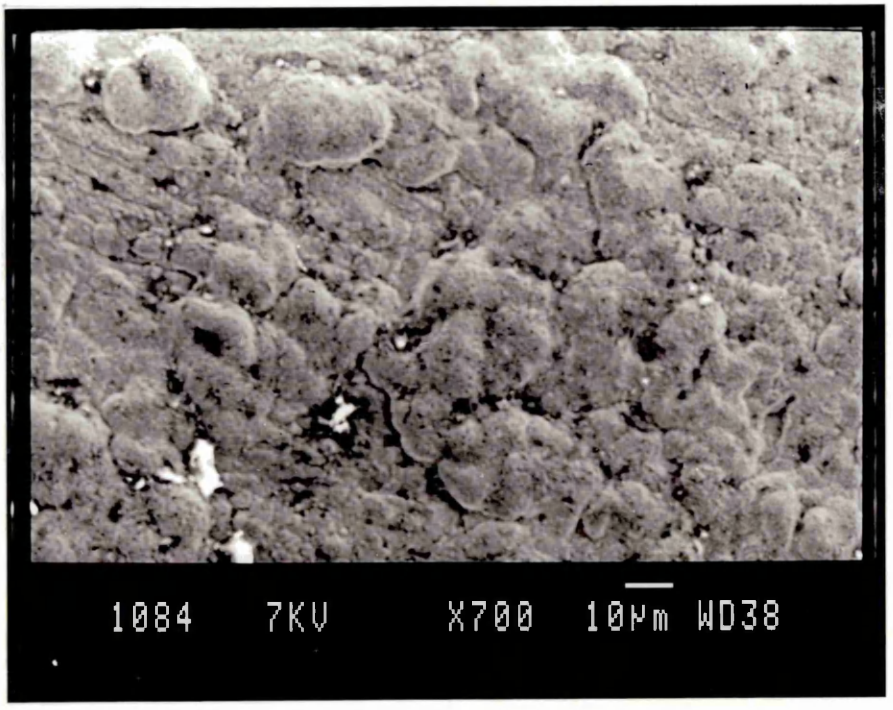
1084 7KV X700 10µm WD38

APPENDIX A

AN EVALUATION OF POLYMER QUENCHANTS AS ALTERNATIVES TO QUENCHING OILS

CASE STUDY

MSc MODULE THREE

W D GRIFFITHS

29 September 1989

Introduction

Quenching in water produces a relatively high cooling rate and this can generate thermal stresses which may be sufficiently high to cause the quenched part to crack, either during quenching or after, or create an unacceptable level of distortion. An oil quench may be used to produce lower thermal stresses but at the cost of some reduction in mechanical properties. In addition the use of an oil quench involves increased health and safety costs.

In recent years polymer quenchants have been marketed under a variety of tradenames. Two main types of quenchants are commercially available consisting of aqueous concentrates of either polyalkylene glycol or sodium polyacrylate. In use these concentrates are further diluted with water to a required concentration.

Polymer quenchants have been claimed to offer advantages over the use of quenching oils because the former are aqueous based and therefore incombustible. Ignition of quenching oils can occur and can lead to destruction and financial loss. An additional advantage is claimed in that the smoke and fume produced during oil quenching is avoided and working environments are greatly improved.

However, for polymer quenchants to be considered as competitors to quenching oils it must be shown that they are capable of providing a quench of similar severity and at an equal or lower cost. Also it must be shown that polymer quenchants have no special disadvantages inherent in their use, for example, corrosion or disposal problems.

The Comparison Of Quenchants By The Calculation Of Thermal Stress And Strain

A problem that has arisen with the introduction of polymer quenchants is that of demonstrating satisfactorily that the new product is capable of producing the quenched properties achieved with a quenching oil. Various methods of measuring the quenching severity of a liquid have been proposed. These methods have included the comparison of cooling curves obtained in the different quenchants, the observation of the effects of quenching on standard samples and the measurement and comparison of cooling rates.

However, the use of the results obtained to predict the performance of a polymer quenchant in an industrial application is difficult. In addition these methods are of only slight assistance in aiding understanding of the quenching mechanisms involved.

A more informative procedure has recently become available. Models of the generation of thermal stress and strain during heat treatment have been developed in recent years and one in particular has been applied to quenching in solutions of polymers.[3 4 17 21]

The model initially[3] consisted of an elastic-plastic model of an infinite plate of a high hardenability steel. Plane stress conditions were assumed and the stress and strain were calculated in the through thickness direction of the plate. The temperature distribution, stress and strain assumed to be symmetrical about the centre-line of the plate.

The temperature distribution in the half-section of the plate was calculated from an explicit finite difference solution to Fick's Law of transient heat conduction. The relationship between surface temperature and surface heat transfer coefficient was determined separately and used in the model to give an accurate temperature distribution in the specimen throughout the period of the quench.

For the calculation of stress and strain the half-section was divided into ten elements. The values of elastic stress and strain in each element were calculated from the contraction which occurred due to the reduction in temperature over a specified time step. The high hardenability steel, (835M30), experienced a martensitic transformation only and, where the temperature of an element was between M_s and M_f, the change in dimension caused by transformation and the consequent stress and strain were included.

Where the calculated stress exceeded the yield stress plastic deformation was assumed to have occurred. The Von Mises criterion was applied and values of stress greater than the yield stress were corrected to equal the yield stress. The model required that no net force exist on the section of the plate and this was not obeyed when plastic deformation occurred. Therefore, after the aplication of Von Mises criterion the forces on the plate were rebalanced to meet the above requirement. Further details on the calculation procedure can be found in reference 3.

The effect of temperature on the yield stress of the material was obtained experimentally and included in the model. This was particularly important when the steel was in the austenitic stage

as the yield stress of this phase was relatively low. The effect of work hardening on the yield stress was also included in the model.

This model was subsequently made more accurate[11 12] by the inclusion of viscous processes and transformation plasticity. The former, comprising creep and stress relaxation were included by using the standard linear solid.

Transformation plasticity has been observed when a transformation occurs under the influence of an applied stress. A plastic deformation occurs even though the applied stress is lower than the yield stress of the material. A relationship to describe this was derived from dilatometry experiments performed under both tensile and compressive applied streses. These results indicated that transformation plasticity occurred between M_s and M_s-40^{o}C and above a threshold stress of 40 MPa.

This visco-elasticplastic model has been applied to quenching in both polalkylene glycol and sodium polyacrylate solutions and also to a variety of quenching oils including RDN 175, a medium speed oil.

Polyalkylene Glycol

The quenching characteristics of polyalkylene glycol solutions have been examined by many workers.[1-10] In several cases a reduction in residual stress or distortion in quenched specimens, (compared to water quenching), has been noted. The generation of thermal stress and strain during quenching, and hence residual stress and strain, has also been calculated in the case of this

quenchant.

Price and Fletcher[3] examined a 25% solution of Aquaquench 1250, a commercially available concentrate of polyalkylene glycol supplied by Edgar Vaughn & Co. Limited, using a plane stress elastic-plastic model of an infinite steel plate in which stress and strain were calculated in the through-thickness direction in the plate. In the case of a 20 mm thick plate of a low alloy steel quenched in 25% Aquaquench 1250 the calculated residual stress distribution consisted of a low surface tensile stress which rose to a maximum tensile stress at a distance of about 2.5 mm from the plate face. The residual stress then decreased to reach a compressive minimum value at the centre of the plate. The level of residual stress predicted were greater than those predicted in the case of a quench in a medium speed oil. However, the model used was incomplete in that it did not include the effects of creep and stress relaxation and transformation plasticity.

A more accurate model was developed which included transformation plasticity and viscous effects.[11 12] The relationships between stress and strain during quenching in a still solution of 25% Aquaquench 1250 were re-examined with this model.[4] The absolute levels of both residual stress and strain were significantly reduced in the case of the improved model compared to the values predicted by Price and Fletcher[3] but the qualitative distributions were similar, (figure 1). Experimental measurements of residual stress and strain produced a good agreement with the predicted values.

The levels of predicted residual strain with this model were of the order of those measured after quenching in RDN175, a medium speed quenching oil, but the residual stresses produced were much higher than in the quenching oil, particularly at points just below the surface. Therefore, while quenching in 25% Aquaquench 1250 solution may produce a level of distortion similar to that achieved by quenching in some oils, this would be at the expense of an increased risk of quench cracking.

The quenching characteristics of a series of polyalkylene glycol solutions have been examined and this information used to calculate the relationship between stress and strain during quenching. Solutions of 5, 10, 15, 20 and 25% Aquaquench 1250 were studied.[5]

Little variation in the relationships between surface temperature and surface heat transfer coefficient was noted in these solutions and this was reflected by the predicted residual stresses which were similar in each solution, figure 2.[21]

The predicted residual stresses were tensile at the surface, rose to a maximum just below the surface and fell to a compressive minimum at the centre as predicted in the case of the 25% solution previously.[15] [16] There was some indication that an increase in concentration decreased the value of the surface tensile stress. The relationship between concentration and residual strain was more complex and no clear trends were apparent.

Since there were only slight differences in the predicted residual stress with variations in concentration this suggested that their was no advantage to be gained in using solutions of

polyalkylene glycol greater in concentration than about 5% Aquaquench 1250. However, experience in their use has suggested otherwise with low concentrations producing quench cracking in some applications. The suppliers have recommended the use of Aquaquench 1250 in concentrations of 15% as a replacement for accelerated quenching oils.[13] At this concentration the bulk quenchant costs of the oil, (50-75 p per litre), would be about two to three times the bulk quenchant costs of the polyalkylene glycol solution.

Sodium Polyacrylate

Sodium polyacrylate solutions have been presented as a new generation of polymer quenchants compared to polyalkylene glycol solutions.[14] Studies of this quenchant have suggested that it may be capable of replacing a wider range of oils than polyalkylene glycols.[2 6 7 14 15 16]

A study has been performed of the residual stresses and strains generated during quenching in a range of solutions of Aquaquench ACR, a commercially available concentrate of sodium polyacrylate also supplied by Edgar Vaughn & Co. Limited.[17] The residual stresses and strains in 20 mm thick plates of a low alloy high hardenability steel were calculated using the visco-elasticplastic model applied in the case of quenching in polyalkylene glycol solutions. The results showed that increasing the concentration of sodium polyacrylate decreased the absolute value of predicted residual stress at any point in the specimen. The relationship between concentration and predicted residual

strain was more complex. These calculations were validated by experimental measurement of the residual stress and strain.

The residual stress predicted in the case of a quench performed in a still solution of 15% Aquaquench ACR showed a strong similarity to the level and distribution of residual stress predicted in the case of a quench performed in a medium speed quenching oil, RDN175, (figure 3). A similar degree of agreement between value and distribution was obtained when the predicted residual stresses in the case of quenching in 5% Aquaquench ACR and 25% Aquaquench 1250 were compared, (figure 4).

The low residual stresses predicted in the case of quenching in sodium polyacrylate solutions were attributed to the formation of a viscous phase which caused a rapid reduction in vapour velocity, and hence heat transfer, at a surface temperature of about 420^{o}C, ie, above the temperature of M_s in the steel. This reduced the temperature gradient in the specimen at M_s to values equivalent to those recorded during oil quenching and produced similar levels of residual stress.

These results indicated that some solutions of sodium polyacrylate were capable of replacing some quenching oils with no increased risk of quench cracking. However, residual strain and hence distortion would probably be greater. The suppliers recommended the use of a 20% Aquaquench ACR solution as a replacement for normal speed quenching oils[13] at an approximately equal cost of about 44 p per litre.

Bulk Quenchant Costs

The following costs were obtained from the suppliers of the polymer quenchants;[13]

CONCENTRATE	COST (per litre)	RECOMMENDED DILUTION	TO REPLACE OIL	DILUTE COSTS
Aquaquench 1250	170 p	15%	Accelerated	26 p
Aquaquench ACR	220 p	20%	Normal speed	44 p

The costs of the two concentrates are only approximate since prices are frequently negotiated and can therefore be dependent on the order size, application and customer.

The replacement of the normal speed oil with a 20% Aquaquench ACR solution can be supported by the results of the mathematical model of the generation of thermal stress and strain during quenching. The model also predicted that polyalkylene glycol solutions produced residual stresses greater than those produced in a medium speed quenching oil and therefore their use as replacements of accelerated quenching oils can be considered feasible. The cost of the normal speed quenching oil and the polymer alternative, (sodium polyacrylate), were approximately equal but substantial savings appear to be offered in changing from an accelerated oil to a solution of 15% Aquaquench 1250.

Additional savings in bulk quenchant costs could, however, be possible. The results of the model suggested the possibility of using a 5% Aquaquench ACR solution, (rather than a 25% Aquaquench 1250 solution), to replace an accelerated quenching oil, (cost

50-75 p per litre). Figure 4 shows the predicted residual stresses in the case of the two polymer solutions to be equivalent. The dilute cost of a 5% Aquaquench ACR solution would be significantly lower at 11 p per litre.

The suppliers of both mineral oils and polymer quenchants recommend that their products be used at temperatures above ambient, generally 40°C in the case of polymer quenchants and from 80°C up to 200°C in the case of an oil, (depending on the type of oil).[7] The size of the quenching bath should be sufficiently large that the rise in temperature of the quenchant during the operation be insufficient to significantly alter the physical properties of the quenchant. For example, for an oil quench, the following bath size is recommennded;[7]

$$\text{bath size} = \frac{\text{mass of steel x temperature decrease}}{\text{2.6 x permissible rise in oil temperature}}$$

However, quenching oils and polymer quenchants have different specific heat capacities therefore, for the same throughput of steel, the temperature rise of the same volume of quenchant would be significantly different;

QUENCHANT	OPERATING TEMPERATURE	SPECIFIC HEAT CAPACITY
Polymer	35 - 50°C	3975 $J.kg^{-1}.K^{-1}$
Oil	up to 200°C	2092 $J.kg^{-1}.K^{-1}$

The specific heat capacity of steel, (assuming the property is independent of temperature), is about 711 $J.kg^{-1}.K^{-1}$. The rise in

temperature of the bath can be calculated by;

$$\Delta\theta_Q = \frac{(\theta_s - \theta_Q) m_s C_{ps}}{m_Q C_{pQ}}$$

where $\Delta\theta_Q$ = temperature rise of quenchant

θ_s = initial temperature of steel

θ_a = initial temperature of quenchant

m_s = mass of steel

C_{ps} = specific heat capacity of steel

m_Q = mass of quenchant

C_{pQ} = specific heat capacity of quenchant

Since the specific heat capacity of the polymer quenchant is larger than that of oil then, in quenching baths of equal volume and with equal throughput, the quenching oil would experience a greater rise in temperature. Therefore a smaller bath of polymer quenchant could be employed which, for the same throughput, would experience the same temperature rise as a larger oil bath. This decrease in size may be calculated by;

$$\frac{(\theta_s - \theta_a) m_s C_{ps}}{\rho_{PQ} V_{PQ} C_{pPQ}} = \frac{(\theta_s - \theta_a) m_s C_{ps}}{\rho_O V_O C_{pO}}$$

$$V_{PQ} = \frac{\rho_O V_O C_{pO}}{\rho_{PQ} C_{pPQ}}$$

where ρ = density

V = volume

subscript PQ = polymer quenchant

subscript O = quenching oil

For example, an oil quenching bath of 1000 litres could be replaced by a polymer bath, (in which equal throughputs would cause equal rises in temperature), of 474 litres representing an approximately 50% decrease in bulk quenchant costs. This assumes that the recommended applications were followed and that the polymer solutions produced the required quenched properties. Variations in the concentration of polymer used would produce variations in the cost of the bulk quenchant. Generally, the optimum concentration of the polymer solution will become known with experience in its use. The table below shows the bulk quenchant costs of a bath when filled with quenching oil and the alternative polymer solutions.

QUENCHANT	TANK SIZE (l)	BULK COST
Accelerated oil	1000	500-750
Normal speed oil	1000	40.00
5% Aquaquench 1250	474	40.29
10% Aquaquench 1250	474	80.58
15% Aquaquench 1250	474 A	120.87
20% Aquaquench 1250	474 A	161.16
25% Aquaquench 1250	474 A	201.45
5% Aquaquench ACR	474 A	52.14
10% Aquaquench ACR	474	104.28
15% Aquaquench ACR	474	156.42
20% Aquaquench ACR	474 N	208.56
25% Aquaquench ACR	474 N	260.70

KEY A - may replace accelerated quenching oils

N - may replace normal speed quenching oils

This shows that each concentration of the polymer solutions considered is significantly cheaper than their quenching oil alternatives when the possibility of using a reduced bath size is considered.

However, whether the use of a small bath is feasible will depend on many other factors. An operator that replaced a quenching oil with a polymer quenchant would already have equipment, particularly the quenching tank, suitable for the established product range. It might therefore not be feasible to reduce the bath size. Crankshafts, for example, require a certain depth of bath and therefore volume of quenchant independent of the nature of the quenchant used. In cases where the size of the bath rather than the temperature rise of the quenchant is the limiting factor on the quenching operation then a lower quenchant volume would, of course, be a disadvantage in that it would reduce quenching loads.

Insurance And Safety Costs

The use of aqueous based polymer quenchants in preference to quenching oils represents a decrease in the fire risk involved in quenching. With oil quenching a part may be trapped at the surface of the bath during entry and cause its ignition. This may ultimately lead to the complete destruction of the heat treatment shop. The use of an incombustible quenchant might therefore be

reasonably expected to lead to a reduction in insurance costs commensurate with the reduced risk of fire. The suppliers state that some users have been able to negotiate a reduction in insurance premiums on changing to polymer from oil quenching.[7]

Generally speaking a quenching tank and its associated fire risk must be viewed within the context of its position within the heat treatment operation which can contain many fire hazards in itself. An insurer may therefore not decrease the insurance premium on the grounds that the reduction in the overall fire risk was negligible. However, the use of a polymer quenchant would probably reduce the number of insurance claims made over a future period of time and would therefore cause a reduction in future premiums since claims and premiums are usually linked.

The fire risk involved in the use of oil also requires expenditure on safety equipment not associated with the use of polymer quenchants. For example, expenditure on, and maintenance of, gravity drop systems, snuffer plates and inert gas curtains, (all equipment designed to reduce the fire hazard), would become unnecessary.

Other Savings Associated With The Use Of Polymer Quenchants

There are other advantages, and therefore savings, which accrue from the use of polymer quenchants, but which are difficult to cost.

Polymer quenchants do not produce mist and fume during quenching and therefore working environments are significantly improved.

Prolonged skin contact with oil may cause dermatitis; no health problems associated with the use of polymer quenchants have yet been reported.

Degreasing of quenched components becomes unnecessary.

Polymer quenchants are less susceptible to changes in quenching severity caused by water contamination than are quenching oils. Contamination of the latter by water significantly increases their quenching severity and therefore monitoring techniques may be required. Polymer quenchants are also tolerant of oil contamination of the order of 1 or 2%.

Drag-out losses, (ie, the amount of quenchant removed from the bath upon removal of the quenched part), have been shown to be reduced with polymer quenchants.[15] (However, drag-out losses are also dependent on application; the viscosity of the quenchant, (ie, concentration), and the geometry of the quenched part are particularly important).

Polymer quenchants are reported to have a longer life, for equal throughputs, than quenching oils,[7] though the latter can be reclaimed. Reclamation costs for oils are high, compared to their original cost, being of the order of about 18 p per litre. Polymer quenchants can also be restored but this can involve an expensive ultrafiltration treatment, (though this can be performed in situ).[18]

Alternatively advantage can be taken of the phenomenom of inversion in polyalkylene glycol solutions contaminated by salts, a relatively cheap process involving only heating and labour costs.[19] Upon heating inversion of the polymer solution occurs causing a separation into an uncontaminated, polymer-rich phase

and a denser, salt-rich phase. The latter may be easily drained.

Spillage of a polymer quenchant is more easily dealt with than oils as the former quickly dries to a non-slippery residue.

Most polymer quenchants are biodegradable therefore disposal costs should be cheaper. In practice however, disposal methods for oils and polymer solutions are identical - dumping on land fill sites - and therefore disposal costs should be similar though possibly reduced in the case of the polymer quenchant if a smaller volume is involved. (This comparison may not be valid in the future if the heat treatment industry becomes more environmentally aware. In this event one would expect the biodegradable polymer quenchants to be much cheaper to dispose of).

Finally, the more dilute solutions of polymer quenchants, for example, polyalkylene glycol, are less viscous than oil and therefore quenching scale tends to fall to the bottom of the tank from where it may be easily removed. In a more viscous quenching oil this scale may be carried into the agitation system to cause damage and increased maintenance costs.

Disadvantages Associated With The Use Of Polymer Quenchants

The use of polymer quenchants is also accompanied by some disadvantages and their associated costs.

Polymer quenchants require a much greater expenditure on maintenance and control than quenching oils. Control must be maintained over concentration, temperature, agitation rate, chemical contamination, bacterial contamination and corrosion

inhibitor level.

Control over concentration can be achieved by measuring either the refractive index, the viscosity or the cooling curve of the solution. Each method requires the purchase of equipment and the determination of the relationship between concentration and the property measured. These relationships are also affected by the amount of chemical contamination, (for example, ammonia or salt), and therefore methods of determining the level of contamination and its effect on the measurement of concentration would have to be established. Contamination of the polymer solution by oil based hydraulic fluid may occur and this may necessitate a switch to the use of water-glycol hydraulic fluids. Some bacterial contamination can occur but there has been no evidence that this affected the quenching characteristics of the polymer solutions. Bacterial contamination may, however, affect the working environment by the production of hydrogen sulphide. Some polymer concentrates contain biocide packages and it may be necessary to monitor the biocide levels present in the bath.[20] Since the polymer solutions are aqueous based higher levels of corrosion on tank fittings may be expected compared to the use of oil. This has been compensated for, to some extent, by the inclusion of corrosion inhibitor packages in the supplied polymer concentrates. Therefore their concentration in the quenching bath should also be monitored by a suitable titration technique.[20]

In short, whereas quenching oils require control over temperature, water and chemical contamination and agitation the use of a polymer quenchant may require the purchase of a certain

amount of specialised equipment, (for example, a refractometer), and the more extensive quality checks required, performed on a periodic basis, would mean increased labour costs.

Since polymer quenchants are aqueous based and therefore comparatively faster than oils there is a greater risk of quench cracking. However, an opposite effect may occur in some applications, for example, there may be a decrease in mechanical properties in quenched aluminium alloys as the polymer quench may be slightly slower than the quenchant it replaced, (for example, nitrogen or boiling water).

More efficient quenchant cooling systems may be required as polymer quenchants are generally used at lower operating temperatures than quenching oils. If a polyalkylene glycol solution is used the bath temperature may quickly rise above the inversion temperature, (about 80^{o}C), and cause bulk inversion of the bath. Polymer quenchants also require a more powerful and hence more expensive agitation system than quenching oils.

Finally, it should be borne in mind that upon changing from a quenching oil to a polymer quenchant the quenching bath should be thoroughly cleaned and degreased to prevent contamination of the new quenchant.

Conclusions

The polymer quenchants commercially available have been shown to be capable of producing similar residual stress distributions to some quenching oils. The suppliers recommendations of 15% Aquaquench 1250 to replace accelerated quenching oils and 20%

Aquaquench ACR to replace normal speed quenching oils have been shown to be feasible by the calculation of the generation of thermal stress and strain during quenching. These applications, however, gave diluted polymer quenchant costs which were approximately the same as the cost of the quenching oils, per litre, in the case of the sodium polyacrylate solution, but which were significantly lower in the case of the polyalkylene glycol solution.

The specific heat capacities of the polymer quenchants are about twice the specific heat capacities of the quenching oils. This suggests that the former can be used at about half the volume of the latter, (thus further reducing bulk quenchant costs by about half), while the quenching bath would still experience the same temperature rise for the same mass of steel quenched. Whether this can be taken advantage of depends on individual applications and would be dependent on such factors as throughput of quenched parts and also their geometry. In favourable applications it might be possible to achieve the same throughput by quenching more often in a smaller bath. An operator, changing from a quenching oil to a polymer quenchant, would probably already posess a range of equipment suitable for quenching a specific range of parts in the former medium. The volume of polymer quenchant required may therefore be fixed. New installations, however, could be designed to take advantage of this by being smaller and therefore cheaper to fill.

Polymer quenchants offer considerable advantages over quenching oils in that they are incombustible and therefore the risk of fire can be greatly reduced. Working environments can

also be enhanced. These reasons may be sufficient in themselves to change to polymer quenchants. The reduction in fire risk would probably result in a long term reduction in insurance premiums while the improved working environment would result in improved industrial relations and a reduction in employee sickness.

Polymer quenchants have one significant disadvantage in that their use requires the exercise of greater quality control than has been necessary with quenching oils. The quality control procedures for both quenchants are not, however, greatly dissimilar. Polymer quenchants require additional control over their concentration, level of corrosion inhibitor and level of biological contamination. The other areas of control, over quenching characteristics and chemical contamination, should not be more expensive to maintain than with quenching oils.

References

1. Blackwood, RR and Cheesman, WD, Us patent no. 3,220,893, November 30,1965.
2. Metals Handbook, 9 th edition, American Society of Metals, Nov. 1981, vol. 4, 54-58.
3. Fletcher, AJ and Price, RF, Met. Technol., Nov 1981, 8, (11), 427-446.
4. Fletcher, AJ and Soomro, AB, Mat. Sci. Eng., 91, 1987, 153-160.
5. Allen, FS, Fletcher, AJ and King, S, Mat. Sci. Eng., 93, 1987.
6. Hilder, NA, Heat Treat. Met., 1987.2, 31-46.
7. "Quenching Principles and Practice", pamphlet, Edgar Vaughn &

Co. Limited.

8. Hasson, JA, Met. Prog., Sep. 1985, 128, (4), 67, 69-70, 72.
9. Kopietz, k-H, Heat Treat., Sept. 1984, 16, (9), 20-24, 26.
10. Burgdorf, EH, Ind. Heat., Oct. 1981, 18-25.
11. Abbasi, F, PhD thesis, Sheffield City Polytechnic, 1983.
12. Soomro, AB, PhD thesis, Sheffield City Polytechnic, 1986.
13. von Bergen, RT, private communication.
14. von Bergen, RT, proc. conf., Heat treatment '84, London, England, 2-4 May, 1984, Institute of Metals, 17.1-17.4.
15. Segerberg, S, proc. conf., 4th International Congress on Heat Treatment of Materials, vol. 2, Federal Republic of Germany, 3-7 June, 1985, Institut fur Werkstofftechnik TU Berlin, 1254-1265.
16. Segerberg, S and Bodin, J, Metallurgia, Sep. 1986, 53, (9), 425-426.
17. Fletcher, AJ and Griffiths, WD, proc. conf., 2nd International Conference on Residual Stresses, Nancy, France, 22-25 Nov, 1988.
18. Anderson, K, Croucher, T and Butler, D, Met. Prog., May, 1983, 37-40.
19. Croucher, T, Heat Treat., Nov. 1982, 14, (11), 18-19.
20. Technical Information, BP Lubricants plc..
21. Allen, FS, PhD thesis, Sheffield City Polytechnic, 1987.

FIGURE A1: Comparison of the calculated residual stresses produced by two different models in the case of a quench in a polyalkylene glycol solution, (25% Aquaquench 1250).
After Fletcher and Soomro.[4]

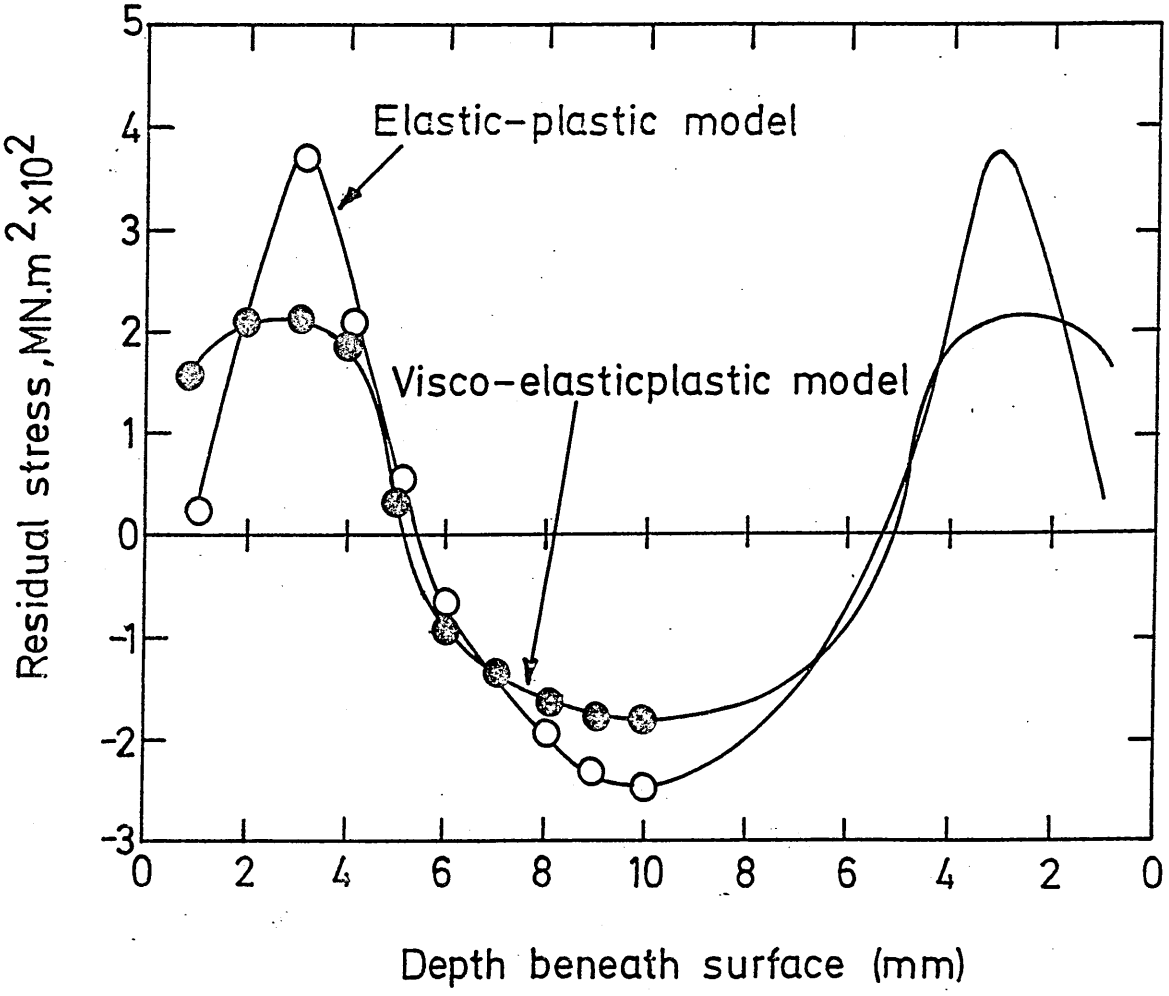
Elastic-plastic model
Visco-elasticplastic model
Residual stress, MN.m^{-2} x10^{2}
Depth beneath surface (mm)
5
4
3
2
1
0
-1
-2
-3
0
2
4
6
8
10
8
6
4
2
0

FIGURE A2: Calculated residual stresses after quenching in a range of polyalkylene glycol solutions, (after Allen[21]).

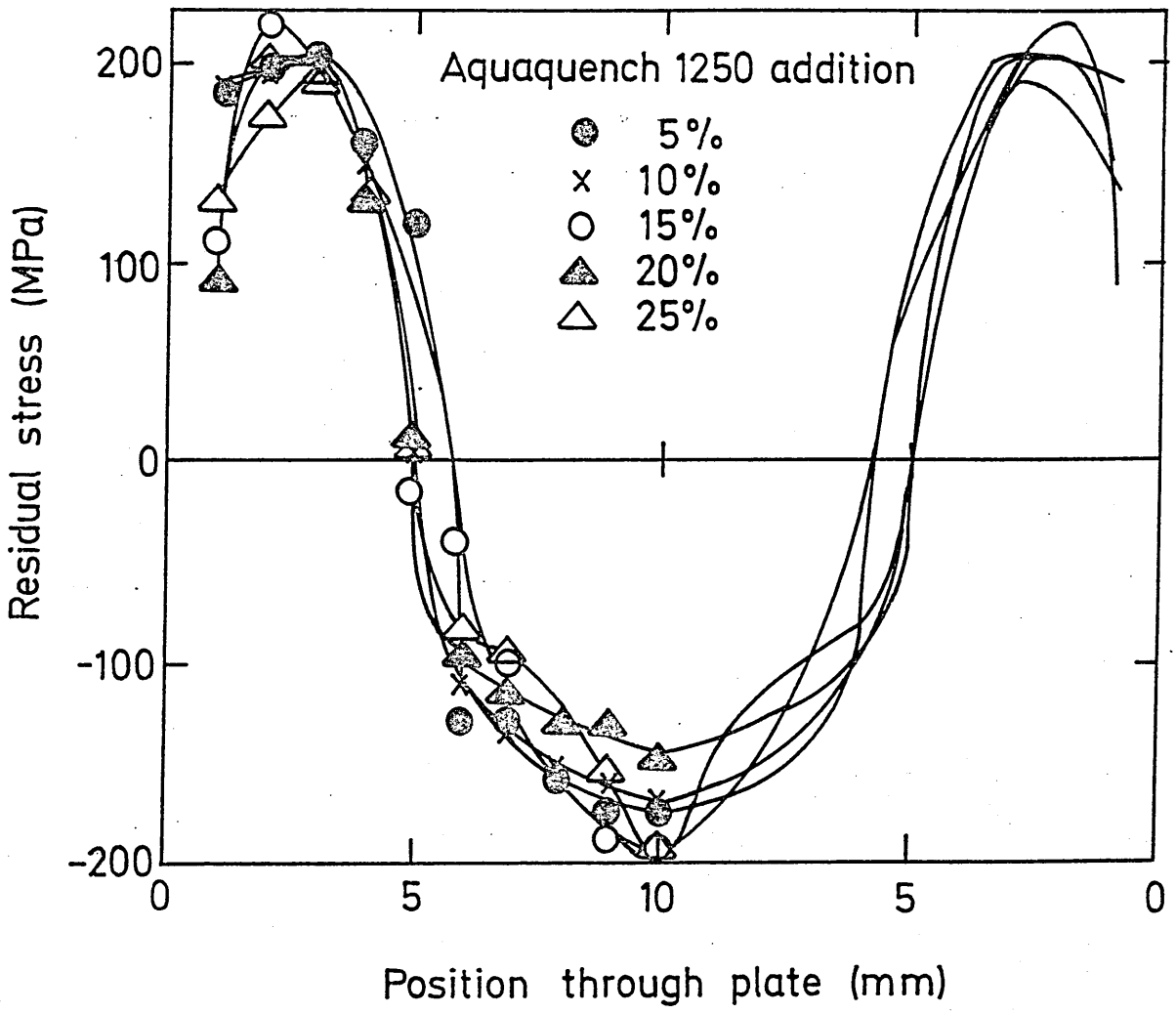
Aquaquench 1250 addition
5%
10%
15%
20%
25%
200
100
0
-100
-200
0
5
10
5
0
Residual stress (MPa)
Position through plate (mm)

FIGURE A3: Comparison of calculated residual stresses in the case of quenching in a sodium polyacrylate solution, (15% Aquaquench ACR), and a medium speed quenching oil, (RDN 175).

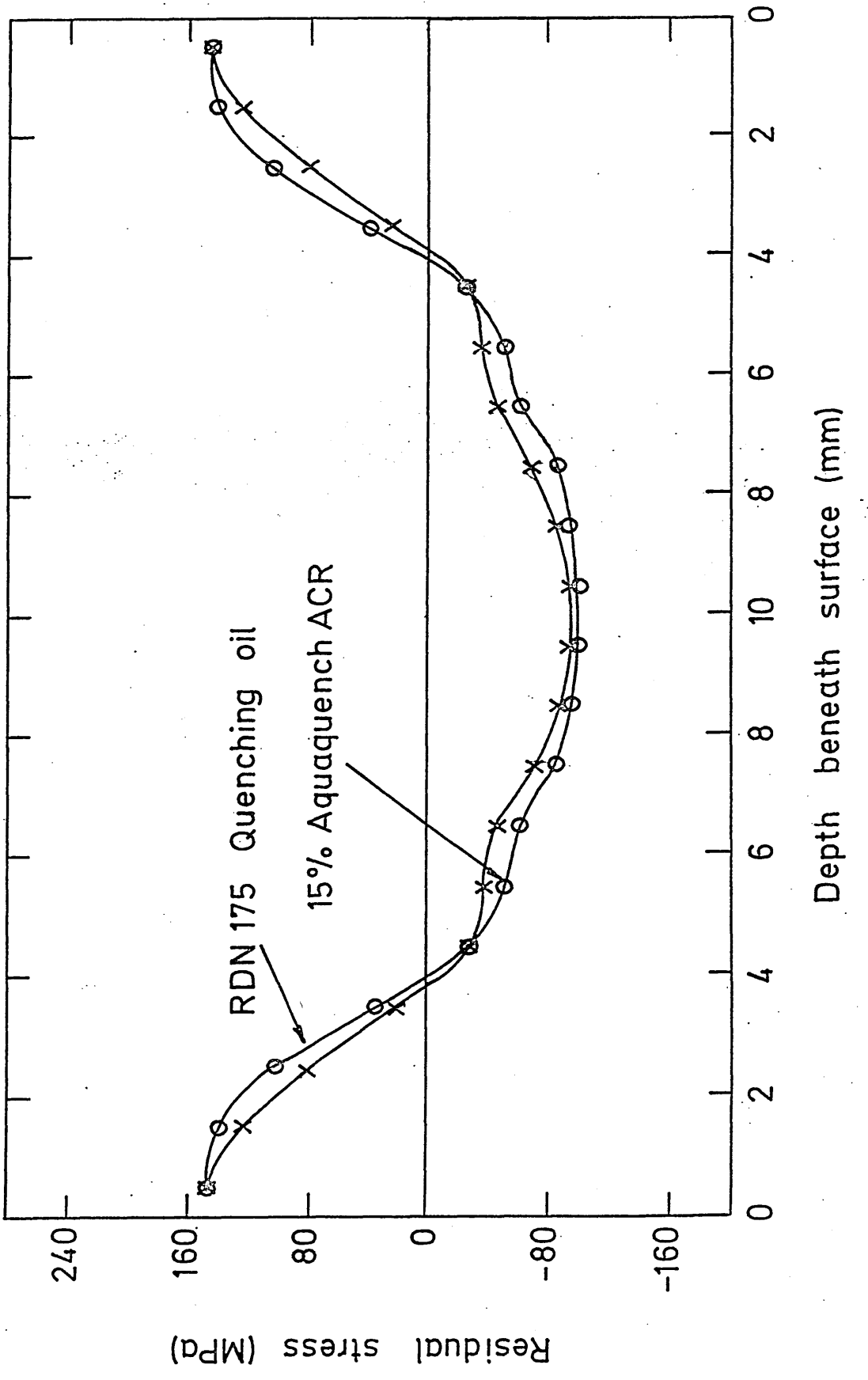
RDN 175 Quenching oil
15% Aquaquench ACR
Residual stress (MPa)
240
160
80
0
-80
-160
Depth beneath surface (mm)
0
2
4
6
8
10
8
6
4
2
0

FIGURE A4: Comparison of calculated residual stresses in the case of quenching in a polyalkylene glycol solution, (25% Aquaquench 1250), and a sodium polyacrylate solution, (5% Aquaquench ACR).

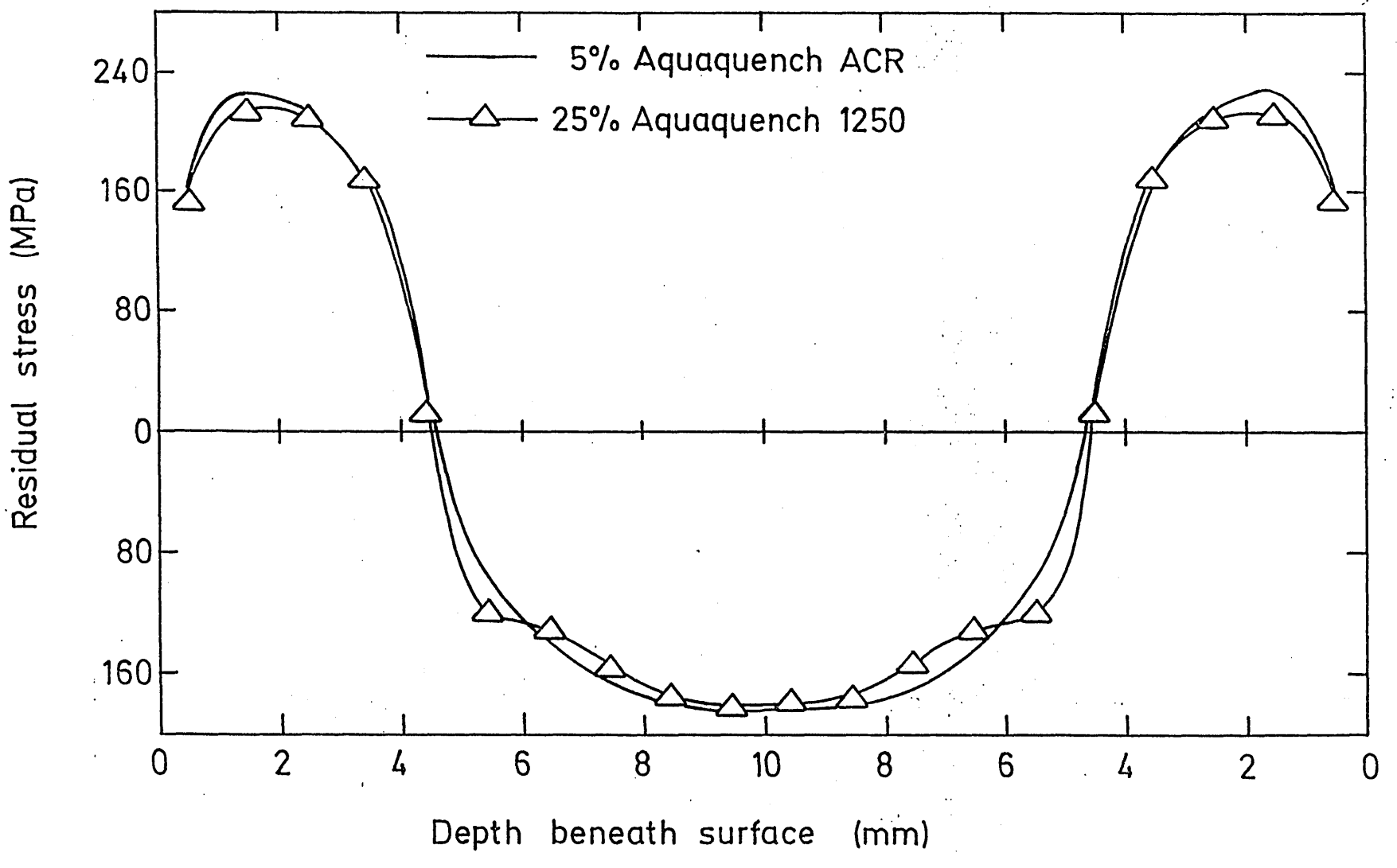
5% Aquaquench ACR
25% Aquaquench 1250
Residual stress (MPa)
240
160
80
0
80
160
0
2
4
6
8
10
8
6
4
2
0
Depth beneath surface (mm)

APPENDIX B

The following FORTRAN 77 program was written to ennable the the residual stresses in a quenched plate to be quickly determined from the results of the layer removal experiment. It was based on the method given by Price.[136]

Program Listing

```
      DIMENSION ZA(10),ZB(10),SIGMA(10),DELTA(9,10),SIGMAB(9),
     !DELTAZ(10), DEB(10)
      E=210700.0
      V=0.3
      T=0.02
      DO 10 N=1,10
      READ(5,*)DELTAZ(N)
      READ(5,*)DEB(N)
      SIGMAB(N)=(E/(1.0-V))*DEB(N)
      SIGMA(N)=(SIGMAB(N)*((T-DELTAZ(N))**2.))/((2.*T+DELTAZ(N))*
     !DELTAZ(N))
      ZA(N)=(T-DELTAZ(N))*(4.*T-DELTAZ(N))/(6.*T)
      ZB(N)=T-ZA(N)-DELTAZ(N)
      IF (N.EQ.1.0) GO TO 10
      DO 20 M=1,N-1
      DELTA(M,N)=(SIGMAB(M)/ZB(M))*(ZA(M)-((N-M)*0.001)+(0.001/2.))
      SIGMA(N)=SIGMA(N)-DELTA(M,N)
   20 CONTINUE
   10 CONTINUE
      DO 30 Y=1,10
```

```
      WRITE (6,40)DELTAZ(Y),DEB(Y),SIGMA(Y)
   40 FORMAT(5X,F5.3,5X,E11.5,5X,F8.3)
   30 CONTINUE
      STOP
      END
```

Explanation Of Variables

DEB	Strain recorded by strain gauge on the base of the plate.
DELTA	Change in calculated residual stress due to presence of the stresses in the remainder of the plate.
DELTAZ	Thickness of material removed.
E	Youngs Modulus.
M	Number of layers previously removed.
N	Number of layers.
T	Thickness of the plate.
SIGMA	Residual stress.
SIGMAB	Stress determined independently of the stresses in the remainder of the plate.
V	Poissons ratio.
ZA	Distance from the neutral plane to the face of the plate.
ZB	Distance from the neutral plane to the base of the plate.

"The Generation Of Thermal Stress
And Strain During Quenching In
Sodium Polyacrylate Solutions"

This paper was presented at the 2nd
International Conference on Residual Stresses
held at Nancy, France, on the 23-25 November, 1988.

THE GENERATION OF THERMAL STRESS AND STRAIN DURING QUENCHING IN SODIUM POLYACRYLATE SOLUTIONS

A J FLETCHER AND W D GRIFFITHS
Department of Metals and Materials Engineering
Sheffield City Polytechnic,
Sheffield, United Kingdom

ABSTRACT

The relationships between surface temperature and surface heat transfer coefficient were determined in a series of aqueous solutions of sodium polyacrylate. These relationships were used in a viscoelastic-plastic model to simulate the generation of stress and strain during quenching. Shortly after the passage of the maximum surface heat transfer coefficient a polymer-laden viscous gel was observed to form which reduced heat transfer during the nucleate boiling stage. The generation of thermal stress and strain followed the same pattern in all concentrations but the residual stress produced at any point in the plate was reduced by the increase in sodium polyacrylate concentration. Concentrations of 15% or more Aquaquench ACR, (a commercially available solution of sodium polyacrylate), produced residual stresses and quenching characteristics similar to a medium quenching oil, RDN175.

INTRODUCTION

In recent years a range of aqueous solutions of polymers, (chiefly polyalkylene glycol, sodium polyacrylate and polyvinylpyrrolidone), have become available to heat treaters. Certain concentrations of these may be seen as replacements for conventional quenching oils since they are able to produce cooling rates, and thereby residual stresses and strains, similar to those associated with normal speed mineral quenching oils [1]. Evidence for this is largely confined to cooling curve and cooling rate tests [2]. These tests have suggested that cooling rates at certain temperatures of particular significance, (such as M_s), are similar in some oils and some polymer quenchants. Comparable levels of residual stress and strain are therefore inferred. However a detailed examination of the generation of thermal stress and strain in polymer quenchants has been confined to polyalkylene glycol solutions [3]. This paper investigates the generation of residual stress and strain in solutions of Aquaquench ACR, (a proprietary solution of sodium polyacrylate and corrosion inhibitors in

water supplied in a pre-blended form by Edgar Vaughan UK). Concentrations stated in this paper are solutions by volume of this mixture. Sodium polyacrylate is characterised by a lengthy, stable film boiling stage [4] and is a strong candidate as a competitor to established oils.

EXPERIMENTAL PROCEDURE

The surface heat transfer coefficients and their relationship with surface temperature were determined in unagitated solutions of 5,10,15,20 and 25% Aquaquench ACR at 20°C ± 2° using a stainless steel plate, (grade 316, dimensions 120x120x20 mm), quenched from 850°C [5]. The plate surface was ground to a 400 finish for each quench. The relationships between time and temperature were measured at a point in the plate 1.5mm below the surface adjacent to the centre of the plate face, (see figure 1).

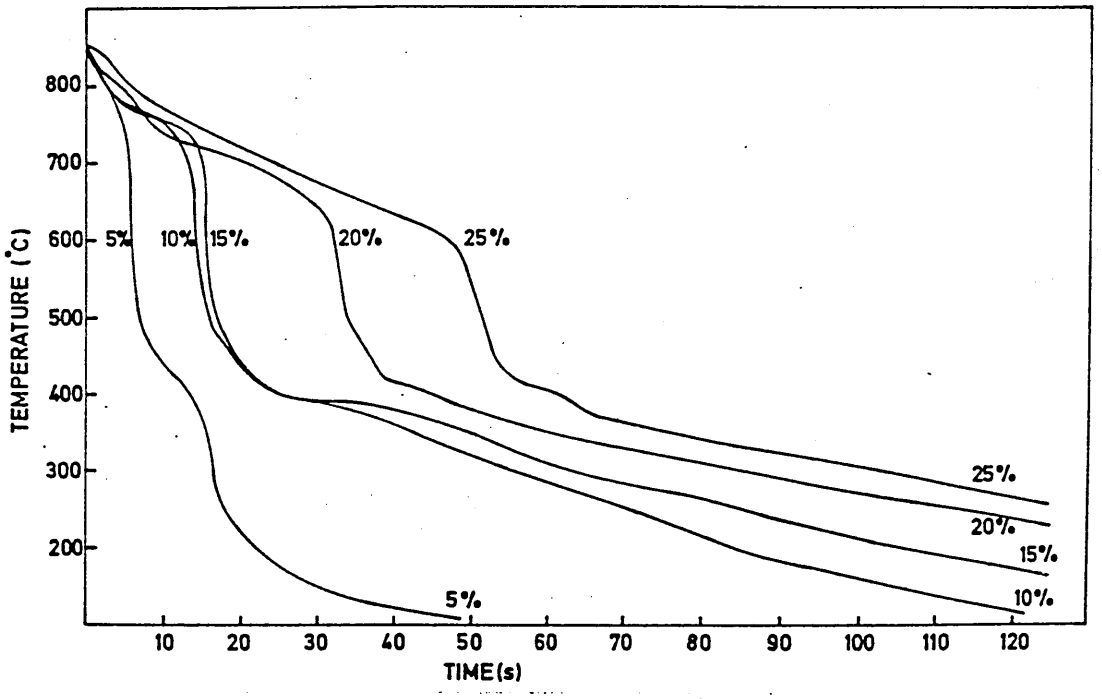

Figure 1 The relationships between time and surface temperature during quenching in Aquaquench ACR solutions

This information was used in conjunction with an explicit finite difference technique to obtain the surface heat transfer coefficients during the quench by a method of successive approximation. These are given in figure 2, each curve representing an average of at least three quenches, (the results from both plate faces being evaluated in each quench).

The relationships thus obtained were used in a viscoelastic-plastic model to simulate the generation of stress and strain in an infinite plate of a low alloy, high hardenability steel, (835M30). This model has been formulated to describe the effects of material property temperature dependence, differential cooling rate, the martensite transformation, creep and stress relaxation and transformation plasticity while quenching in various media [6,7].

QUENCHING CHARACTERISTICS OF SODIUM POLYACRYLATE SOLUTIONS

The relationships between time and temperature during quenching display the same essential characteristics as water and oil with typical film, transition and nucleate boiling stages, (figure 1). Increasing the concentration of sodium polyacrylate increased the duration of the film boiling stage, (from 4.9 s in the 5% to 48.1 s in the 25% solution). Simultaneously the minimum film boiling point fell from 779°C in 5% to 592°C in 25% Aquaquench ACR. Mean surface heat transfer coefficients, (figure 2), in this stage varied only slightly, (3-400 $W.m^{-2}.K^{-1}$). There is some indication that they decline slightly as surface temperatures fall.

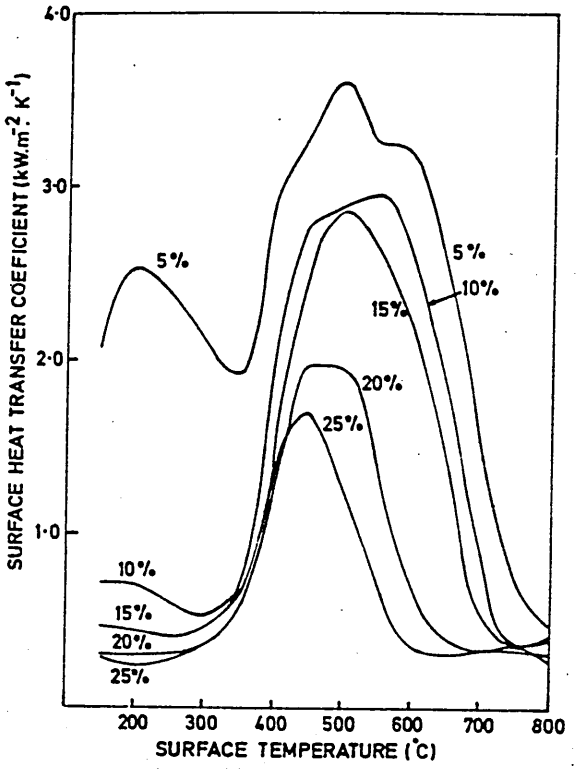

Figure 2 Surface heat transfer coefficients in Aquaquench ACR solutions

Photography revealed the presence of Taylor waves in the liquid/vapour interface. The maximum surface heat transfer coefficient fell from 4225 $W.m^{-2}.K^{-1}$ to 1807 $W.m^{-2}.K^{-1}$ as the concentration of Aquaquench ACR increased from 5% to 25% while the temperature at which it occurred fell from 519°C in 10% to 429°C in 25% ACR, (the 5% result was anomalous in this respect). The cooling curves displayed a change in gradient shortly after the passage of the maximum surface heat transfer coefficient which occurred consistently, in concentrations greater than 10%, at a mean surface temperature of 421°C. This corresponded to a rapid fall in the value of the surface heat transfer coefficient and appears to be associated with the formation of a viscous gel. Hence at typical M_s temperatures, surface heat transfer coefficients are confined to values below 600 $W.m^{-2}.K^{-1}$, these values decreasing with rising concentration, (figure 2). This is at least an order of magnitude less than the level produced in a water quench and is comparable to a medium speed quench oil. Towards the end of the quench the surface heat transfer coefficients showed a tendency to rise slightly.

THE GENERATION OF THERMAL STRESS AND STRAIN

The mechanism by which the residual stresses and strains arise is demonstrated in figure 3 which shows the relationship between the calculated stress and strain at the surface and centre of an En30B plate quenched in 15% Aquaquench ACR.

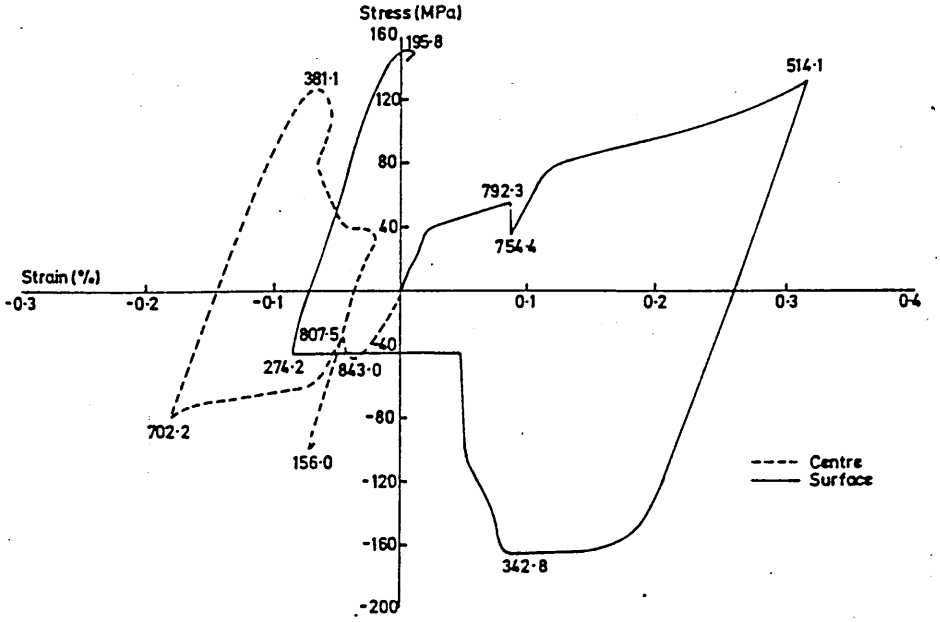

Figure 3 Relationship between stress and strain during quenching in 15% Aquaquench ACR

Similar relationships were obtained during the cooling of the plates in each of the quenchant concentrations considered. The surface, which initially cooled faster than the centre, experienced a tensile stress while the centre experienced a compressive stress. The low yield stress of austenite at this temperature led to substantial amounts of plastic deformation. At 792°C the surface stress unloaded slightly as the cooling rate rose in the interior and exceeded that of the surface. This continued until 754°C when the surface cooling rate rose with the passage of the minimum film boiling point. (In the centre the compressive stresses unloaded at 843°C, becoming more tensile, until at 808°C the compressive loading began again). At the onset of transition boiling the rate of cooling at the surface rose abruptly and the generation of tensile stress in this part of the specimen returned. This continued until the temperature reached 514°C. The maximum surface heat transfer coefficient occurred at 527°C and thereafter the surface heat transfer coefficient fell abruptly. At this point the surface stress unloaded until it became compressive at 444°C. Plastic deformation again occurred at the surface hereafter. The centre stress unloaded at 702°C and became increasingly tensile as the centre temperature fell to 381°C. At 343°C and 381°C respectively the surface and centre unloaded again. This was quickly followed at 300°C by the start of the martensite transformation at the surface. This would be expected to cause the resumption of the generation of compressive stress as the surface expanded relative to the austenite region in the interior of the specimen. However, the simultaneous onset of transformation plasticity caused a reduction in the compressive stress,

(to -40 MPa), at which level the stress was maintained until transformation plasticity was complete, (at 260°C). By this stage the transformation front had moved towards the centre of the specimen and the consequent expansion there led to a reversal of the compressive stress in the surface, where the transformation was in a more advanced stage. Finally, after completion of the transformation in all parts of the specimen there was a very small reduction in the surface and centre stress as the temperature gradient in the specimen was finally eliminated.

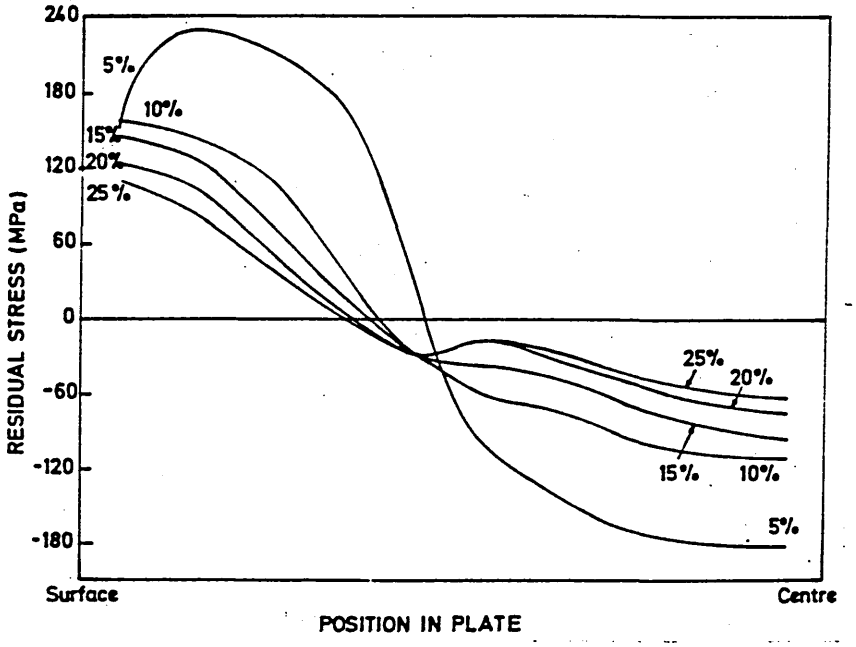

Figure 4 Residual stress distributions in Aquaquench ACR solutions

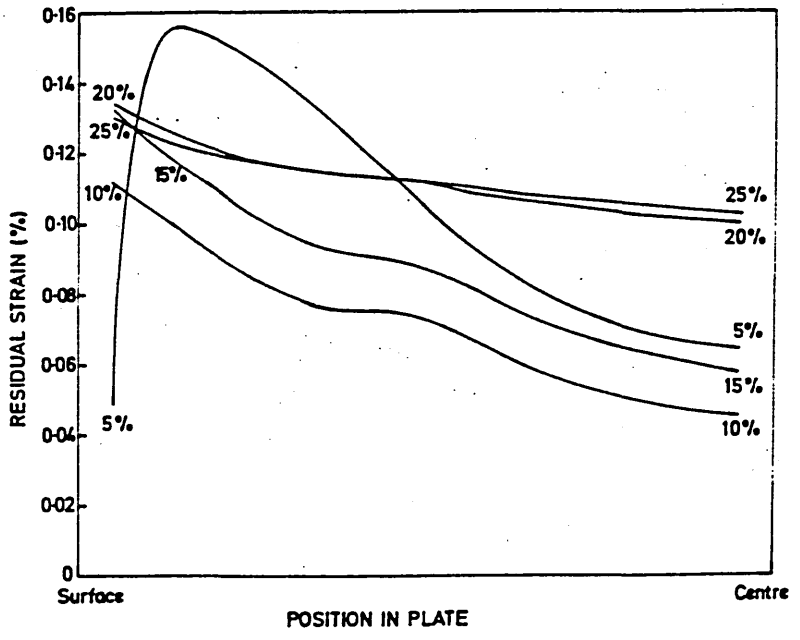

Figure 5 Residual strain distributions in Aquaquench ACR solutions

The residual stress distributions in the plate show that as the concentration of the polymer was increased the levels of absolute residual stress at a specific point in the plate decreased, (figure 4).

The surface stress was always tensile and the centre stress always compressive. The point of reversal from tensile to compressive stress remained in approximately the same position at about halfway between the surface and centre. The residual strain distributions, (figure 5), were less clear but showed that strains are tensile throughout the plate at the end of the quench and displayed a tendency to rise with increasing concentration. However the results obtained for the 5% Aquaquench ACR solution were inconsistent with this trend. (The residual strains shown in figure 5 contain a uniform addition of 0.127% tensile strain to account for the change from a ferrite and carbide structure before heat treatment to a martensitic structure after quenching).

DISCUSSION

The viscous gel which formed at a surface temperature of about 420°C occurred as the surface stress was in the process of unloading after the passage of the maximum surface heat transfer coefficient. It caused a reduction in the mean temperature gradient in the plate as it began to transform at 300°C. The overall effect was a gradual reduction in the final stress as the concentration of Aquaquench ACR increased. The residual strain was largely dependent upon the magnitude of the first plastic deformation relative to those that came later in the quench. The influence of the polymer concentration on these quantities was complex and led to the complex relationships between residual strain and quenchant composition.

The residual stress distributions produced by solutions that contained 15% or more Aquaquench ACR were comparable to those produced by RDN175 quenching oil. The solution that contained 5% Aquaquench ACR produced quenching characteristics comparable to a 25% solution of Aquaquench 1250, (a proprietary blend of polyalkylene glycol from the same source). Therefore, as far as residual stress generation is concerned, solutions based on sodium polyacrylate show considerable promise.

ACKNOWLEDGEMENTS

Thanks are due to Edgar Vaughan (UK), plc for the supply of the Aquaquench solutions.

REFERENCES

1. von Bergen, R.T., proc. conf., Heat Treatment '84, London, England, 2-4 May, 1984, Institute of Metals, 17.1-17.4.
2. Hilder, N.A., Heat Treat. Met., 1987.2, 31-46.
3. Fletcher, A.J. and Soomro, A.B., Mat. Sci. Eng., 91, 1987, 153-160.
4. Kopietz, K-h and Munjat, F.S., US Patent no. 4087290, May 2, 1978.
5. Price, R.F. and Fletcher, A.J., Met. Technol., May 1980, 203-211.
6. Fletcher, A.J. and Soomro, A.B, Mat. Sci. Eng., 82, 1986, 101-115.
7. Fletcher, A.J. and Price R.F., Met. Technol., Nov. 1981, 427-446.